FINAL REPORT

Caltech
Multidisciplinary University Research Initiative (MURI)

INVESTIGATIONS OF NOVEL ENERGETIC MATERIALS TO STABILIZE ROCKET MOTORS

ONR Contract No. N00014-95-1-1338
1 OCTOBER 1995 – 30 SEPTEMBER 2001

~ ~ ~

California Institute of Technology
Jet Propulsion Center

30 April 2002

Report Documentation Page

Form Approved
OMB No. 0704-0188

1. REPORT DATE	2. REPORT TYPE	3. DATES COVERED
30 APR 2002	**N/A**	**-**

4. TITLE AND SUBTITLE	5a. CONTRACT NUMBER
Investigations of Novel Energetic Materials to Stabilize Rocket Motors, Final Report	**N00014-95-1-1338**
	5b. GRANT NUMBER
	5c. PROGRAM ELEMENT NUMBER
6. AUTHOR(S)	5d. PROJECT NUMBER
	5e. TASK NUMBER
	5f. WORK UNIT NUMBER
7. PERFORMING ORGANIZATION NAME(S) AND ADDRESS(ES) **California Institute of Technology, Jet Propulsion Center, 1200 East California Blvd., Pasadena, CA 91125**	8. PERFORMING ORGANIZATION REPORT NUMBER
9. SPONSORING/MONITORING AGENCY NAME(S) AND ADDRESS(ES)	10. SPONSOR/MONITOR'S ACRONYM(S)
	11. SPONSOR/MONITOR'S REPORT NUMBER(S)

12. DISTRIBUTION/AVAILABILITY STATEMENT
Approved for public release, distribution unlimited

13. SUPPLEMENTARY NOTES
The original document contains color images.

14. ABSTRACT

15. SUBJECT TERMS

16. SECURITY CLASSIFICATION OF:			17. LIMITATION OF ABSTRACT	18. NUMBER OF PAGES	19a. NAME OF RESPONSIBLE PERSON
a. REPORT	b. ABSTRACT	c. THIS PAGE			
unclassified	**unclassified**	**unclassified**	**UU**	**275**	

Contributors to this Report

Principal Investigators

Merrill W. Beckstead (Technical Director)	Brigham Young University
Fred E. C. Culick (Program Director)	California Institute of Technology
Thomas B. Brill	University of Delaware
Thomas A. Litzinger	Pennsylvania State University
Vigor Yang	Pennsylvania State University
Gary A. Flandro	University of Tennessee Space Institute
Robert A. Frederick	University of Alabama at Huntsville
M.C. Lin	Emory University
E.W. Price, R. Sigman, J. Seitzman	Georgia Institute of Technology

Sub-Contractor

Robert A. Beddini	University of Illinois, Urbana-Champagne

UIUC MURI

M. Quinn Brewster	University of Illinois, Urbana-Champagne
Charles Wight	University of Utah

Consultants

Robert Brown
Norman S. Cohen
Joseph Flanagan
Woodward Waesche

ACKNOWLEDGMENTS

This document is the final report of the Caltech Multidisciplinary University Research Initiative (MURI), a five-year program lasting from 1 October 1995 to 30 September 2000, with a one-year no-cost extension. Nine universities collaborated in this program.

Brigham Young University
California Institute of Technology
Emory University
Georgia Institute of Technology
Pennsylvania State University
University of Alabama at Huntsville
University of Delaware
University of Tennessee Space Institute
University of Illinois at Urbana-Champagne

Four consultants, retired from positions in the U.S. rocket industry, provided advice and guidance throughout the program, including review of this report.

During the first three years of the Caltech MURI, the participants also served as technical monitors and collaborators with seven research groups in Russia: two each at the Institute of Chemical Physics in Moscow and at the Institute for Chemistry and Kinetics; one each at the Institute for Chemical Physics in Chernogolovka, Mendeleev University, Moscow, and Baltic State University, St. Petersburg. Their contributions to the technical content of the Caltech MURI Program are considerable.

Dr. Leonard Caveny originated the MURI Program and arranged financial support from the Ballistic Missile Defense Office. Program Management was provided by the Office of Naval Research. Dr. Richard Miller was Program Manager for two years, followed by Dr. Judah Goldwasser to the end of the program. Dr. Fred Blomshield, NAWC, China Lake, has been Technical Monitor and Coordinator throughout the program.

Most of this report is a collection of pieces prepared by the authors noted in the text. I greatly appreciate their cooperation in this task extending over many months. I am particularly indebted to the MURI consultants (Brown, Cohen, Flanagan and Waesche) for their multiple readings of the opening pages of the report and their many useful suggestions. Norm Cohen was particularly diligent and offered many additions that I have included.

During the first three years of the program I was assisted by Ms. Marionne L. Epalle (née Kirk). She was succeeded by Ms. Melinda A. Kirk who ultimately brought forth this report. Everybody involved in the Caltech MURI is greatly indebted to both for their endless patience and superb management of the many administrative details.

F.E.C. Culick
Richard L. and Dorothy M. Hayman Professor of
Mechanical Engineering and Professor of Jet Propulsion

ABSTRACT

This document is the final report of the Caltech Multidisciplinary University Research Initiative (MURI), "Investigations of Novel Energetic Materials to Stabilize Rocket Motors," ONR Contract No. N00014-95-1-1338. With a one-year no-cost extension, the program covered the period 1 October 1995 to 30 September 2001 and involved Principal Investigators at nine Universities. In addition, for three years, funds from another source supported research by seven Russian research groups. Participants in the Caltech MURI provided technical oversight of that work.

A second MURI devoted to the same general subject was carried out at the University of Illinois at Urbana-Champaign (UIUC). The two programs were largely complementary. Some of the sections in this report have been co-authored by representatives of both MURIs. Similarly, the final report of the UIUC MURI will contain some duplication of material covered in this document.

The Caltech MURI was a multidisciplinary program devoted to research on fundamental problems of the chemistry, combustion and gasdynamics of novel energetic propellants and their unsteady behavior in rocket motors. This program achieved significant progress towards the ultimate overall objective of research in this field, to identify and quantify the influences of propellant composition on the stability of motions in a solid propellant rocket motor. To attain that objective it is essential to support cross-disciplinary effort between propellant chemists and researchers; combustion researchers; and researchers concentrating on the dynamics of solid rocket combustors. This MURI program was the first sustained effort to accomplish the necessary collaborations among faculty and students in universities, with participation by representatives of government laboratories and industry; in the many respects described in this report the program has been highly successful. Failure to continue support of university research in selected areas identified by the conclusions of the Caltech MURI will have two serious consequences: research related to problems of both steady combustion and dynamics in solid rockets will practically come to an end in U.S. universities; and the supply of new graduates educated at the forefront of the field will dry up.

Consistent with the requirements of its overall technical objective, the Caltech MURI was organized into three tasks having the following objectives:

OBJECTIVES

Task I — Fundamental Chemistry and Chemical Dynamics

The objective of Task I was to investigate the pathways and kinetics of pyrolysis of solid rocket propellant ingredients and the unimolecular and exothermic bimolecular reactions of the resulting gaseous products. The temperatures in the experiments were representative of the burning surface and the flame zone, and the pressures were atmospheric and higher. The ingredients of interest were selected in accord with the overall objective to understand advanced formulations of conventional materials and novel energetic materials that might offer as yet unknown opportunities to gain better control of the combustion processes.

Task II — Combustion Dynamics

The objective of Task II was to develop a mechanistic understanding of the steady and unsteady combustion characteristics of advanced ingredients/propellants, both theoretically and experimentally. This understanding will allow the identification of critical energy release paths in an ingredient's combustion. The three-fold objective of this task was (1) to identify and develop an understanding of the aspects of combustion that contribute most significantly to unstable combustion; (2) to develop methods to potentially modify either the ingredient's chemical structure or the combustion path, so as to improve the combustion stability characteristics; and (3) to evaluate several techniques for measuring the combustion response.

Task III — Combustor Dynamics

The objective of Task III was to construct a unified framework accommodating propellant chemistry, combustion mechanisms, and motor dynamics to study the mutual coupling between unsteady flow motions and transient combustion responses of propellants in practical motor environments. Both analytical and numerical methods were pursued in this work. The results obtained will provide motor designers with specific guidelines for developing a stable rocket motor, and assist propellant chemists and combustion researchers in optimizing ingredient formulations for curing stability problems at the molecular level.

Reports of progress and results of research in the Caltech MURI have appeared in more than 350 documents, presentations and annual reviews. Thirty students have received degrees, including 21 Ph.D.s with full or partial support by MURI funding. Major progress has been accomplished in all three tasks. A large number of papers (more than 300) have either appeared already, have been accepted for publication in archival journals, or are in the review process.

ACCOMPLISHMENTS

Task I

Laboratory experiments have quantified the infrared inactive molecules from flash pyrolysis of energetic materials and have characterized flash pyrolysis of complex material; have evaluated fast decomposition mechanisms of high nitrogen compounds; and have investigated the role of TiO_2 in the pyrolysis behavior of AP-HTPB pseudo propellants to clarify the plateau mechanism. Theoretical work has developed the kinetics and pathways for gas phase radical reactions of C, H, O and N compounds essential to nitramine, ADN, AP and azide combustion. Based on previous work carried out in a different context, a theoretical method has been developed to compute reaction kinetics generally for systems of interest for solid propellants.

Task II

Experimental results have been obtained for species and temperature profiles in the gas and condensed phases during combustion of RDX, HMX, BAMO, BAMO/RDX and BAMO/AMMO. With these data and other results, kinetic mechanisms and models have been developed for combustion of RDX, HMX, AP, AP/HTBP, GAP,

GAP/HMDI, GAP/RDX and ADN. The modeling has established the importance of certain endothermic condensed phase reactions and vaporization on reducing the temperature sensitivity and depressing the peaks of the response function for pressure coupling. The numerical model predicts all major characteristics of a burning propellant. The major problem with advanced energetic ingredients is likely to be high-frequency instabilities, which can often be remedied by additives. Lower frequency instabilities in motors using AP propellants can be treated by careful selection of AP particle size distributions or by developing plateau/bi-plateau propellants. A detailed model of aluminum combustion has been developed and applied to aluminum droplets burning under realistic conditions existing in motors. Scanning electron micrographs were obtained for quenched samples of bi-plateau propellants, helping to determine the mechanism due to binder melt layer interference causing the plateau behavior, and the influences of TiO_2. Various test devices were used to measure the response functions of three classes of MURI propellants. The results of those measurements have confirmed that energetic ingredients modify the pressure-driven response of AP-based propellants.

Task III

Substantial progress has been accomplished in the application of LES (large-eddy simulations) methods to simulate steady and unsteady flows in solid rockets, including simplified models of propellant combustion. An approximate method based on spatial averaging has been extended to include the effects of combustion noise; and has shown that triggered or pulsed instabilities occur only if the gasdynamics in the chamber is nonlinear, and the combustion dynamics is nonlinear due to velocity coupling with a threshold velocity. An essential mechanism in this velocity-coupling has been found to be the frequency-dependence of turbulence penetration in the combustion zone. Formal analysis of vorticity generation at the surface of a burning propellant has clarified the process of flow-turning and related phenomena important to the stability. Subscale tests have shown clearly the existence of pulsed instabilities and have demonstrated the stability to pulses of motors operating with AP/HTPB aluminized propellants. The last result is consistent with measured low response functions due to the plateau mechanism.

The contributions to this document are relatively short summaries of the work accomplished during the six-year program. Attachment E to the report is a complete bibliography of journal and conference papers covering work supported entirely or in part the Caltech MURI. A CD-ROM containing nearly all of those documents is available from CPIA.

TABLE OF CONTENTS

CONTRIBUTORS I
ACKNOWLEDGMENTS II
ABSTRACT III
EXECUTIVE SUMMARY 1
INTRODUCTION 9
I.1 Observed Characteristics of Combustion Instabilities 10
I.2 Chief Justification for the Caltech MURI: The Primary Mechanism for Combustion Instabilities in Solid Rockets 13
I.2.1 Identification of the Mechanism; The Combustion Response Function 13
I.2.2 Qualitative Description of the Mechanism 17
I.3 Accomplishments of the Caltech MURI 19
I.3.1 Task I. Chemical Kinetics and Dynamics 19
I.3.2 Task II. Combustion Dynamics 22
I.3.2.1 Steady State Modeling 22
I.3.2.2 Experimental Studies 24
I.3.2.3 Modeling the Unsteady Nature of Ingredients 25
I.3.2.4 Modeling the Unsteady Nature of Propellants 26
I.3.2.5 Numerical Simulation of Aluminum Particle Combustion 26
I.3.3 Task III. Combustor Dynamics and Motor Tests 28
I.3.3.1 Extensions of the Approximate Analysis 29
I.3.3.2 Analysis of Generation of Unsteady Vorticity 30
I.3.3.3 Large Eddy Simulations (LES) 30
I.3.3.4 Analysis of the Turbulent Compressible Flow Adjacent to the Combustion Zone 31
I.4 The Future 32
References 36
1 TASK I — FUNDAMENTAL CHEMISTRY AND CHEMICAL DYNAMICS 38
1.1 Survey of Propellant Ingredients (Flanagan and Waesche) 38
1.2 Decomposition of Energetic Materials and Formulations 40
1.2.1 Low Heating Rates (Wight) 40
1.2.2 High Heating Rates (Brill) 42
1.3 Effects of Temperature and Pressure on Exothermic Reactions near Propellant Surfaces (Lin) 44
1.4 Modeling Kinetic Mechanisms Within the Combustion Process (Beckstead) 46
1.4.1 Utilization of Condensed Phase Kinetics and Mechanisms 47
1.4.2 Utilization of Gas Phase Mechanisms 48
References 52
2 TASK II — COMBUSTION DYNAMICS 60
2.1 Experimental Testing Methods for Combustion of Energetic Ingredients and Propellants (Beckstead) 60
2.1.1 Burning Rate Measurements 60
2.1.2 Measurement of Chemical Species 61
2.1.3 Measurement of Temperatures 63
2.1.4 AP/HTPB Laminate Flames 64
References 66
2.2 Measurements of the Chemical and Thermal Structure of Propellants and Ingredients (Litzinger) 68
2.2.1 Experimental Approach 68
2.2.2 Energetic Binders 68
2.2.3 Pseudo-Propellants 73
(a) Effect of Azide Polymer Structure 73
(b) Effect of Oxidizer Structure 74
(c) Effects of Heat Flux on Pseudo-Propellant Combustion 74
(d) Closure 75
References 81
2.2.4 Ultrasonic Measurement of Propellant Ballistics (Frederick) 81
(a) Ultrasonic Measurement Uncertainty [11-14] 83

References 83
2.3 Measurements of the Dynamical Response of Burning Solid Propellants 85
2.3.1 T-Burner Response Measurements of MURI Propellants (Blomshield, NAWC) 85
(a) Propellants 86
(b) T-Burner Response Measurements 88
(c) Results for Bi-Plateau Propellants 90
(d) Results for Mono-Modal AP Metallized Propellant 92
(e) Conclusions 93
References 93
2.3.2 Pressure and Heat Flux Driven Response Measurements (Litzinger) 94
(a) Results for HMX 95
(b) Results for AP/HTPB 99
(c) Results for AP/Energetic Binder 100
(d) Results for AP/AN/HTPE 103
References 106
2.3.3 Pressure-Coupled Response Measurements of Aluminized and Non-Aluminized Solid Propellants Using the Magnetic Flowmeter (Micci) 107
(a) Results 107
2.3.4 Response Function Measurement in an Oscillatory Burner Employing an Ultrasonic Technique (Krier) 109
(a) Technical Approach 109
(b) Results 110
2.3.5 Ultrasonic Measurement of Propellant Response Functions (Frederick) 116
2.4 Modeling the Dynamical Response of Burning Solid Propellant (Beckstead) 117
2.4.1 Modeling Unsteady Solid Propellant Combustion with Simplified Kinetics (Brewster, Loner and Tang, UIUC) 118
2.4.2 Modeling Combustion Instability of RDX and HMX with Detailed Chemistry (Erikson and Beckstead) 121
2.4.3 A Theoretical Pressure-Driven Response Function for Composite Solid Propellants (Rasmussen, Frederick and Moser) 123
References 125
2.4.4 Modeling the Effects of Velocity Coupling on the Global Dynamics of Combustion Chambers (Culick) 127
(a) The Model Framework 127
(b) Models of the Surface Layer 129
(c) Models of the Gas Phase 130
(d) Some Results for the Combustion Response Function 130
(i) Influence of Gas Phase Dynamics 131
(ii) Combined Influences of the Dynamics of the Surface Layer and the Gas Phase 131
2.4.5 Velocity Coupling, the Combustion Response, and Global Dynamics (Isella, Culick) 133
References 140
2.5 Extension of the QSHOD Model to AP Composite Propellants (Culick) 141
1) Heterogeneities 142
(2) Unsteady Heat Transfer in the Condensed Phase 142
(3) Matching Conditions at the Interface; The Response Function 143
(4) Extension of the QSHOD Model to Composite Propellants 144
(5) Influences of the Downstream Flow; Velocity Coupling 145
References 145
2.5.1 Interactions Between Acoustically Induced Turbulence and Surface Combustion (Beddini) 146
References 151
2.6 Behavior of Metals in Solid Propellant Combustion Instability (Price , Sigman, Seitzman) 152
2.6.1 Ignition and Sintering 152
2.6.2 Residual Oxide Size Analysis 153
References 157
2.6.3 Extinguished Surface Studies (Price, Sigman, Frederick, Moser and Cohen) 157
2.7 Numerical Simulation of Aluminum Particle Combustion (Beckstead) 160

References 164
2.8 Stability Additives—A Brief Tutorial (Cohen) 166
2.8.1 History and Controversy 166
2.8.2 Particle Damping 167
2.8.3 Combustion Stabilization Mechanisms in General Terms 168
2.8.4 Some Special Cases 170
2.8.5 Some Speculation 171
2.8.6 Concluding Remarks 172
References 173
3 TASK III — CHAMBER DYNAMICS 175
3.1 Numerical Simulation of Motor Internal Flow Evolution and Combustion Dynamics (Yang, Penn State) 176
3.1.1 Unsteady Motor Flow Evolution with Acoustic Excitation 177
3.1.2 Propellant Combustion Dynamics in Rocket Motors 178
3.1.3 Numerical Simulations with Experimental and Model Boundary Conditions (Culick) 180
References 180
3.1.4 Two-Phase Flow Interactions in Rocket Motors 181
References 181
3.2 Linear and Nonlinear Analyses of Motor Dynamics (Culick, Caltech) 182
3.2.1 Analysis of the Global Dynamics of a Combustor 183
3.2.2 Acoustic, Vorticity and Entropy (Temperature) Waves 185
3.2.3 The Wave Equation for Unsteady Flow in a Combustor 186
3.2.4 Spatial Averaging; Combustor Dynamics as a Collection of Oscillators 186
3.2.5 Linear Stability 188
3.2.6 Nonlinear Behavior in Combustion Instabilities 190
3.2.7 Noise and Forced Oscillations 190
3.3 Unsteady Motor Flowfields and Interactions with Flame Zone Gas Dynamics (Flandro) 192
3.3.1 Improved Motor Stability Calculations 193
3.3.2 Interactions with Other Tasks 197
3.3.3 Recommendations for Future Work 198
References 199
3.4 Pulsed Motor Firings (Blomshield) 202
3.4.1 Motor Firing Details 202
3.4.2 Firing Results and Analysis of Motors No. 3 Through 5 203
(a) Linear Stability 206
3.4.3 Firing Results and Analysis of Motors No. 6 Through 10 207
3.4.4 Conclusions 210
References 211
3.5 Pulsed Tests of Motors Using Bi-plateau Propellants (Blomshield) 213
References 219
Attachment A MURI Propellants 221
Attachment B Caltech-sponsored MURI Workshops 226
Attachment C A Workshop Report: Mechanisms for Plateau Behavior in AP/HTPB Propellants (Cohen) 227
Attachment D Thoughts on Oscillatory Vorticity Models Contributions to Combustion Stability of Solid Propellant Rocket Motors 243
Attachment E List of Caltech MURI Publications 251

EXECUTIVE SUMMARY

Combustion instabilities occupy a distinctive position in the development of rockets. They are entirely unwanted, but nevertheless are nearly inevitable in new designs; and not uncommonly, they persist in operational motors. Unplanned for, they can cause large added costs if they suddenly appear late in development. The very fact that instabilities do occur, often as surprises, suggests what is true: there is a certain lack of basic understanding at all levels and, it seems also, failure occasionally to put into practice what is understood. Continuing progress in improved capabilities (more energy, higher pressure, higher propellant loadings, extremes of burn rates, etc.…) and imposition of new requirements (insensitivity, smokeless, exhaust, environmentally friendly combustion products, etc.…) will cause new conditions to be encountered. The possibilities for instabilities will expand as well.

Quite generally, combustion instabilities exist as consequences of interactions among three classes of phenomena: chemistry and chemical dynamics; combustion dynamics; and combustor dynamics. These dynamical processes take place simultaneously in widely different spatial scales characterized by lengths roughly in the ratios $(10^{-3} - 10^{-6}):1:(10^{3} - 10^{6})$. However, due to the wide differences in the associated characteristic velocities, the corresponding time scales are all close. The instabilities in question are observed as oscillations having a time scale in the range of natural acoustic oscillations of the combustor in question. The apparent dominance of that single macroscopic time scale must not be permitted to obscure the fact that the relevant physical processes occur on three disparate length scales. Hence, understanding combustion instabilities at the practical level of design and successful operation is ultimately based on understanding three distinct sorts of dynamics.

The primary practical objective is to avoid combustion instabilities by proper design during development of new motors. If combustion instabilities occur, then some means must be found to eliminate them. Currently the only ways to cure problems of instability involve changes of internal geometry or modifications of propellant composition, the second being the more common approach. Experience has shown that revisions of composition (*e.g.* changing the distribution of oxidizer particle sizes, or introducing small amounts of 'stability additives') can be effective. The MURI program has led to deeper understanding of the fundamental reasons for success of those methods. Hence our abilities to avoid instabilities in new motor designs have been improved.

It was a basic premise of the MURI program that elimination of combustion instabilities in future motors will be accomplished almost always by appropriate choice of propellant characteristics consistent with the basic performance requirements. The problem of doing so becomes evermore difficult as propellants become increasingly energetic. Hence the attention of the MURI program was directed to understanding the behavior of high-energy ingredients and propellants. We have identified the central importance of specific contributions to the dynamic sensitivity of propellant combustion. Notably, endothermic and exothermic reactions in the condensed phase, and their influences on the burn-rate sensitivity, are characteristics to be examined carefully in advanced propellant formulations.

Attention and support have been given to research in this area for more than fifty years, albeit usually not in sustained fashion. Considerable progress has in fact been achieved. In addition to what is known and understood, a few important practical tools exist. At least as importantly, the classes of problems that must be solved to bring the subject to a satisfactory level for practical purposes are now well defined. The major difficulties are associated

chiefly with developing methods to solve those problems; almost all of those methods are associated with experimental requirements.

The MURI programs, one directed by the University of Illinois at Urbana-Champaign (UIUC) and one by Caltech, have provided the first opportunities for true collaborations among researchers working with all of the disciplines relevant to combustion instabilities. In a broad sense, the two MURI programs differ chiefly in the following respects: the UIUC MURI had no efforts in combustor dynamics; and the Caltech MURI had no work in ingredient and propellant synthesis. Otherwise, there was coincidence of general areas of research, but not in emphasis. For further details, consult the websites: http://www.its.caltech.edu/~culick/muri.html and http://www.mie.uiuc.edu/content/asp/research/research_centers/muri_consortium.asp.

The Caltech MURI was organized as three tasks: I, ***Chemical Dynamics***; II, ***Combustion Dynamics***; and III, ***Combustor Dynamics***. That structure is reflected in the three main sections of this document. This final report is intended to provide a broad summary of the content of the Caltech MURI program with particular attention to those aspects most closely related to the requirements of industrial and governmental organizations. For that reason the following remarks are organized in a top-down fashion. Figure E-1 shows the scheme of this report, essentially a flow chart for the disciplines and content of the MURI programs. The arrows connecting the various boxes indicate that the subjects cited are mutually influential. In reality, the connections are fairly well understood at the research level but have yet to produce extensive consequences in practical applications. Part of the purpose of this report and earlier papers (Blomshield, 2000; Culick 2000; Flanagan, 2000; Brewster, 2000; Beckstead, 2000; Yang, 2000) is to improve that situation. Much can be done early in development programs to reduce the probabilities of combustion instabilities appearing later in full-scale motors.

It is helpful to view the subject from the top down, as defined in Figure E-1. Success achieved in the research discussed here must be measured partly by the extent to which the results of the research contribute to treating the problems of dynamics encountered in full-scale motors. In any event, observations of the behavior of full-scale motors have motivated the form of the analyses comprising Task III concerned with combustor dynamics. The term 'combustor dynamics' refers generally to unsteady motions in a combustor. The various forms of combustion instabilities form a subset of combustor dynamics. Global analysis of combustor dynamics in particular has been constructed intentionally to be easily applicable in practice. Although still in early stages of development, numerical simulations also are based on formulations of realistic problems. Task III also included motor tests at the Naval Air Warfare Center and at Thiokol.

Quantitative numerical results for the flow field and dynamical behavior in a combustor cannot be obtained without quantitative specifications of the dynamical behavior of the combustion processes, the subject of Task II. In the present context, 'combustion dynamics' refers to the responsiveness of the combustion processes to changes in the local values of the flow properties, mainly pressure, velocity and temperature. That responsiveness provides a feedback path connecting the ***combustion*** dynamics with the ***combustor*** dynamics.

Whether they are associated with residual combustion within the volume or with combustion processes at the surface of a burning propellant, the ***combustion*** dynamics take place at length scales of the order of a millimeter or so and less, down to as small as a few microns. But the ***combustor*** dynamics evolve on the scale of the chamber, a

factor of 10^3–10^6 larger than the scale of the combustion processes. This wide separation of scales implies that in some sense one should be able to average spatially over the smaller scales to produce models of the ***combustion*** dynamics more appropriate to macroscopic scales of the ***combustor*** dynamics.

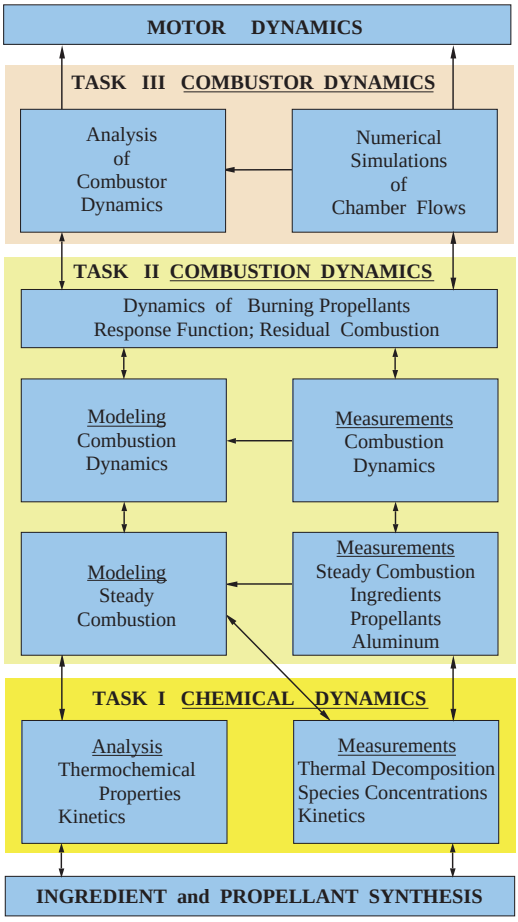

Figure E-1. Intellectual Organization of the MURI Programs

The results of such averaging procedures (which are only implicit in most analyses) are usually represented as *response* or *admittance functions*. We must emphasize that spatial averaging in the manner suggested need *not* rid the model of dependence on heterogeneities on a small scale. For example, just as the case is for the characteristics of steady burning, response functions should be functions of the average oxidizer size in a propellant and possibly higher order moments of the distribution as well. Spatial averaging causes those dependencies to appear as contributions to the values of a relatively small number of global parameters. Despite the various works in the past including some significant progress made recently in the University of Illinois CSAR program, the process of spatial averaging has not been properly worked out for the dynamical behavior of burning heterogeneous solid propellants.

Introduction of response functions therefore creates the essential and fundamental connection between combustor dynamics and combustion dynamics, the main subjects addressed in Task II. In fact, the work in Task II also included many projects concerned only with matters of steady combustion. The reason is basic. However we

may represent the combustion dynamics, the central idea is that we are trying to model the dynamical behavior, here its response to an imposed disturbance. Much of the dynamical behavior actually depends on characteristics of the steady combustion field. Hence it is essential to construct accurate models for the steady combustion of propellants.

Much continuing effort before and during the MURI program has been directed to modeling the response function for combustion dynamics. Results currently available remain incomplete, particularly for practical applications. That dynamical system, a burning propellant or an aluminum drop, say, is defined in the first instance by complete specification of its steady combustion behavior. Hence knowledge of the steady process—burning rate, pressure exponent, temperature sensitivity, distribution of temperature, dependence on particle size distribution, chemistry, and chemical kinetics—is prerequisite to analysis of the dynamics. It is at that level that the results of Task I become necessary.

Steady combustion of any material is the macroscopic consequence of the collective action of an enormous number of microscopic processes. Those include convective, conductive and radiative transfer of energy; and physical and chemical kinetics. Representation of the modes of energy transfer is accomplished as part of combustion analysis. The required information about the kinetic processes must be supplied independently; that is a chief purpose of the work in Task I.

In fundamental respects, then, we may choose to view in reverse the overall scheme just described and illustrated in Figure E-1. We can conceive of the ideal world in which for given ingredients and propellants the appropriate experimental and analytical methods could be directed from the bottom up within the three levels or tasks, and emerge with predictions of the dynamics of a specified motor design. We cannot presently carry out such a program. A reasonable question is: how far are we from the ideal success, and what are the obstructions? It is a fair assessment that the MURI programs have produced significant advances, but there have been failures with respect to expectations held six years ago, and serious deficiencies remain in this field.

There should be no doubt that we have a much clearer understanding now of the problems that must be solved, and of the deficiencies of methods available, than we did when the MURIs began. Perhaps the best justification for this conclusion is that, with the benefit of what has been learned in these programs, we can now in retrospect quite easily recognize where the original programs were flawed. That is not intended so much as a criticism in hindsight, as a remark that several negative results (unobtainable other than by actually carrying out the research) enable us now to dismiss as useless several methods that appeared to some to have good possibilities at the time. We have learned much in six years.

Chief Accomplishments of the Caltech MURI Program

Task I. Chemical Kinetics and Dynamics

The research in Task I was concerned with chemical activity extending from the sub-surface region at the interface into the gas phase. This continues to be one of the most daunting tasks of all research efforts in energetic materials. At the outset the decision was made to focus on experimental studies of fast thermolysis of novel

energetic materials and on computational studies of near surface, gas-phase, exothermic, radical recombination reactions. The findings in both of these programs were actively used by Task II participants in the development of new combustion models that are required for understanding combustion sources of instability.

In addition to the existing T-jump/FTIR method for vibrational spectroscopy in fast thermolysis work, a new T-jump/Raman spectroscopy method was developed at the University of Delaware. A computational method new to the combustion field was applied at Emory University to determine rate constants for gas phase radical-radical reactions relevant to near-surface chemistry during propellant combustion. In the computational program dozens of new or improved rate constants were calculated for the unimolecular and bimolecular surface driving reactions in HMX, RDX, AN, ADN, AP and GAP. Many of these results were incorporated in the combustion modeling carried out in Task II.

With the opportunity to explore new lines of chemical thinking, several novel efforts were pursued, including pyrolysis studies of complex mixtures such as the use of energetic metal salts as a means to attenuate high-frequency acoustic modes; and exploration of the condensed-phase chemistry of AP-HTPB to help understand bi-plateau behavior.

Task II. Combustion Dynamics

Work in Task II comprised four main areas: steady-state modeling; experimental studies (both steady and unsteady combustion); modeling unsteady behavior; and numerical simulation of aluminum particle combustion. The chief concern of Task II was development of mechanistic understandings of the steady and unsteady combustion characteristics of advanced ingredients/propellants. The approach to accomplish this was primarily focused on modeling, with the experimental work designed to support the modeling efforts. At the start of the MURI program in 1995, the Yetter Mechanism for RDX had been developed based on previous ONR funding by Dick Miller. This mechanism consists of 232 fundamental reaction steps and 44 species, and has become a "standard" for modeling the combustion of RDX. Work was also in progress to use the Yetter mechanism within the framework of a detailed kinetics model for the combustion process. This work was pioneered by Yang and co-workers, Beckstead and co-workers, and Yetter, Smooke and co-workers. These models provided the foundation for the MURI program to build upon. These models have been applied to describe various aspects of RDX combustion and then extended to other ingredients (HMX, AP, GAP and ADN) and to two mixtures of ingredients (AP/HTPB, RDX/GAP).

Experimental procedures and hardware were developed to measure species profiles through the flame using an MPMS at Penn State. Measurements of gas phase species and temperature profiles as well as condensed phase temperature profiles were made for RDX, HMX, BAMO, BAMO/RDX, and BAMO/AMMO. Variations in the burning behavior of the various mixtures have been documented and published in various journal articles. The effect of an externally imposed heat flux on the combustion process has also been made and evaluated. These data were used for modeling validation.

A test facility was developed at Penn State to measure the combustion response of ingredients and propellants for both pressure and radiation driven unsteady combustion. The differences between the response to the two

different stimuli has been measured and reported. In addition, procedures and hardware have been developed to measure species during unsteady combustion using an MPMS. Measurements of response functions and species oscillations during radiation-driven combustion have been completed for HMX, and several of the MURI propellant formulations.

A numerical model for unsteady combustion of a monopropellant has been developed which includes detailed chemical kinetics. This is the first model to accomplish this. The code was applied to both RDX and HMX and tested under a variety of simulated steady-state conditions. Calculations show that pressure coupled responses obtained from model simulations matched experimental T-burner trends quite well for both RDX and HMX, including the prediction of higher responses with increased mean pressure. Ranges of validity of the quasi-steady assumption, which in normally made in most models, were evaluated.

A two-dimensional unsteady state numerical model for aluminum particle combustion has been developed at BYU. The current model solves the conservation equations, while accounting for the species generation and destruction with a 15 reaction kinetic mechanism. Most previous models have only assumed infinite kinetics. The kinetic mechanism in the model consists of surface reactions and gas phase reactions for the formation of the aluminum sub-oxides. The aluminum sub-oxides later react and condense to form the normal liquid aluminum oxide product.

Task III. Combustor Dynamics and Motor Tests

By its nature, the research in Task III was planned to provide the connection between the results of Task II to applications in motor design and development. Put another way, it is a central purpose of Task III to establish, as far as possible, guidelines or 'rules of thumb' relating the dynamical behavior of motors—in fact combustion chambers generally—to characteristics of the response function. Hence, through the modeling and representations of response functions (Task II) which must be based on the fundamental behavior exposed in Task I, we have in principle the framework for understanding the dynamical behavior of full-scale motors in terms of the propellant composition. This grand objective has yet to be achieved, but the Caltech MURI has successfully achieved impressive progress towards eventual success.

Apart from the motor tests at NAWC, China Lake and at Thiokol, the research in Task III comprised three types of work:

1) application and further development of an approximate method based on spatial averaging;
2) analysis of the unsteady vorticity field and its effects in an unstable motor;
3) large eddy simulations (LES) of steady and unsteady flows in solid rockets, including reduced order models of propellant combustion.

The approximate analysis has been developed over more than two decades, with continually improving numerical methods and examination of more processes. During the MURI program almost all the work has been concerned with nonlinear behavior. Two processes not previously treated can now be investigated routinely with the available code:

(i) velocity coupling; a simplified ad hoc model is being used;
(ii) influences of noise on linear behavior.

Investigation of velocity coupling has led to three significant results:

1) Pulsed instabilities apparently exist only if nonlinear gasdynamics is included, with nonlinear velocity coupling having a threshold velocity;
2) Apparently only velocity coupling (not pressure coupling) will account for the sensitivity of combustion instabilities to small changes of propellant composition.
3) The frequency dependence of turbulence penetration of the combustion zone provides a credible mechanism for the driving of higher harmonics necessary to support nonlinear waves.

Thus the approximate method now contains explicitly all processes dominant in a solid propellant rocket motor. The ideas and special results are being incorporated in a large code being developed by SEA, Inc. to give the capability of applications to arbitrary grain geometries.

Special problems arise when oscillations are present in a solid rocket, associated with the flow inward at the boundary. Interactions between that flow, and fluctuations of the velocity and pressure gradient parallel to the boundary, generate unsteady vorticity. The vorticity is converted into the chamber, eventually in actual flows to be dissipated by the action of viscous forces and interactions with turbulence. This process first appeared in approximate form as a result found in one-dimensional analysis of stability in a solid rocket; it came to be known as "flow-turning." Rigorous analysis of the phenomenon was initiated by Flandro prior to the MURI program and has continued to the present.

Relative to other types of chemical propulsion, the solid rocket community was for many years slow to develop methods of large-scale simulations (*i.e.* applications of computational fluid dynamics (CFD)). Fortunately that situation has changed considerably in the past fifteen years. Especially during the MURI program much progress has been made with simulations of both steady and unsteady flows at Pennsylvania State University. Indeed, only ONERA in France has paid serious attention to numerical analysis of unsteady flows, but their emphasis has been different. No group elsewhere has achieved the level of accomplishment reached at Penn State during the MURI program for simulations of unsteady compressible flows with representation of the combustion of the solid propellant.

Large-scale computations of the internal flow, including some (simplified) representation of the combustion processes, have two basically important roles in this field:

1) To provide numerical results as accurately as possible for 'real' flows, that is, containing all the processes present in motors, as a tool in the design process; and
2) To provide results serving as the basis for assessing the accuracy of predictions obtained from the approximate method and other analyses.

Several examples of the second purpose of numerical calculations existed before the MURI programs started. During the Caltech MURI, a new important example was completed, demonstrating remarkable agreement between analytical (necessarily containing some approximations) and numerical results for generation of unsteady vorticity. The results were obtained with finite difference analysis of a non-reacting flow, but the general principle is applicable: good comparison between numerical results and those obtained with analysis is an extremely important step to building confidence in our understanding, and ability to predict, the flows internal to a solid rocket motor—steady and unsteady.

Two subscale 30-pound motor tests funded partly by Thiokol demonstrated the stability, including stability to pulses of aluminum bi-plateau propellants operating in both high-pressure booster and low-pressure sustainer phases on both plateaus. This demonstrated stability aggregated and validated the fundamental steady-state and unsteady combustion data acquired on the program, the mechanism of the bi-plateau behavior, the forecasted and measured low combustion responses at axial mode frequencies, and the predicted stability of the motors. We have shown the credibility of our research approach in this MURI. As propulsion requirements will continue to expand in the future, this research must continue in order to improve our capabilities and apply them to more advanced systems.

INTRODUCTION

The Caltech MURI was a multidisciplinary program devoted to research on fundamental problems of the chemistry, combustion and gasdynamics of novel energetic propellants and their behavior in rocket motors. While the program was the first of its kind at the university level, the overall long-term objective is ultimately practical: to identify and quantify the influences of propellant composition on the stability of motions in full-scale motors, with a view to providing guidelines for design and development.

To appreciate the context in which the MURI programs were conducted, it is essential to have some acquaintance with problems encountered in practice. The widespread concern with combustion instabilities, due to their occurrence in all types of propulsion systems, is apparent from the abbreviated chronology given in Figure I-1. It is important to understand that much is to be learned by understanding problems of instabilities as they arise in different types of propulsion systems. In addition to the generic influences and the particular examples cited in Figure I-1, there are many tens of unacceptable instabilities in solid rockets alone; *e.g.* see a partial compilation by Blomshield (2000).

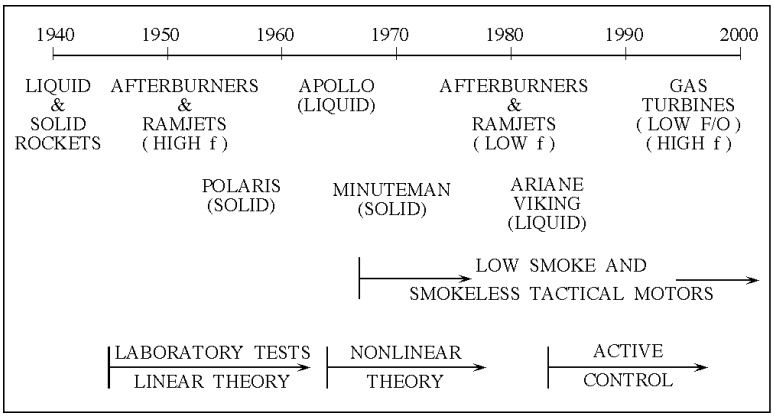

Figure I-1. A Brief Chronology of Combustion Instabilities

Increased performance of solid rockets requires higher energy propellants operating at higher propellant loadings and chamber pressures. The higher power densities provide an environment more favorable to the conversion of combustion energy to energy of unstable motions growing to unacceptable levels. There are primarily two strategies for reducing and preventing combustion instabilities: increase the losses in the system; or reduce the tendency for the combustion processes to drive the instabilities. The Caltech MURI program was devoted largely to the second.

Although the source of all serious combustion instabilities—the 'mechanism'—is ultimately related to the combustion processes, the problem of combustion instabilities is not one of propellant combustion alone. In fact, a combustion instability arises due to coupling between the dynamical behavior of the propellant combustion and the dynamics of the chamber. The block diagram in Figure I-2 illustrates this fundamental idea.

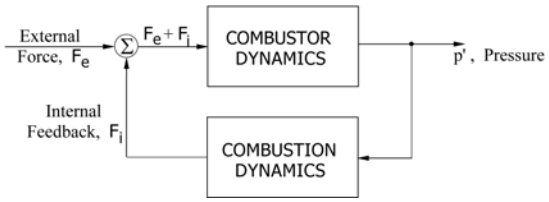

Figure I-2. Simplified Block Diagram for the Dynamics of a Combustion System

The observed behavior of the system is precisely analogous to the well-known situation in electronics: feedback (in this case the combustion processes[1]) added to an amplifier (in this case the chamber dynamics or acoustics) will, under suitable condition, convert the amplifier to an oscillator.

Consequently, the conditions under which instabilities occur, and their characteristics, depend on the dynamics of both the chamber (*i.e.* the geometry and certain processes, largely dissipative, within the chamber) and the dynamics of the combustion processes. The chamber behaves essentially as a resonant system containing damping: it is characterized by many modes of oscillation having discrete frequencies whose values are determined principally by the acoustics of the volume. The source of the energy contained in instabilities, and the cause of the feedback, is the combustion processes. Hence it is there that one should look to determine the real causes of instabilities and for possible basis for avoiding or eliminating them.

I.1 Observed Characteristics of Combustion Instabilities

The greatest obstacle to understanding the causes of combustion instabilities, and hence to working out effective means for treating them in practice, has been the problem of obtaining reliable quantitative data at all levels. Even under controlled laboratory conditions, the high temperatures and pressures preclude the use of ordinary instrumentation and techniques of measurement, a serious constraint still existing. When certain kinds of anomalous behavior were first observed in rocket firings (*e.g.* enhanced heat transfer rates, unexplained increases of mean pressure, excessive burning rates and occasional failures) the causes were unknown. An important reason was the inability of early instrumentation to detect oscillations in the acoustic frequency range. That situation changed in the mid-forties and early fifties. It is from that era that the idea of unstable motions in a combustor date, and hence the term "combustion instability". The notion of 'instability' is commonly realized as a growing dynamical motion in a linear system. Thus, understanding combustion instabilities begins with the idea that they arise as the consequences of linearly unstable motions growing out of small disturbances. Figure I-3 is a reproduction of a pressure trace in a motor illustrating well that sort of behavior. The average ('DC') part of the pressure has been removed by filtering. However, in many cases, it is essential to examine the total time-dependent pressure. The example in Figure I-4 makes the point: a significant rise of mean pressure, and therefore thrust, accompanies the growing oscillations.

[1] There are some important examples (the Space Shuttle booster motors and the ARIANE booster motors) in which vortex shedding associated with average flow past an obstacle, or induced in the boundary region near the burning surface, is coupled to the acoustic field in the chamber. Some aspects of that problem have been addressed in Task III but that effort constitutes a small part of the MURI program.

Figure I-3. An Unstable Motion Growing Out of Noise

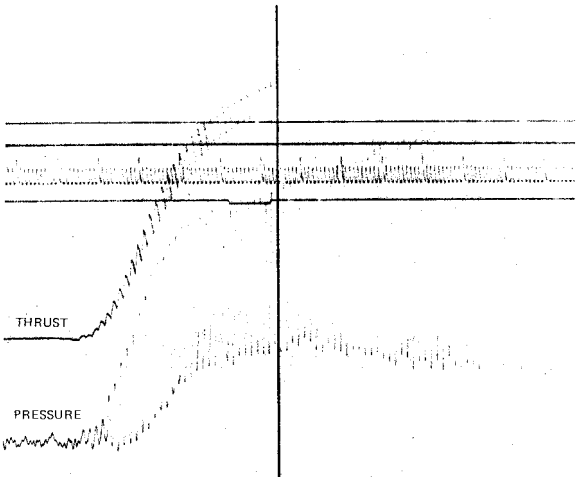

Figure I-4. An Instability Accompanied by Increases in the Average Pressure and Thrust

Perhaps the best known case of an unacceptable linear instability occurring in a large operational system, is the problem encountered in the Stage 3 motor of the Minuteman II vehicle, in the late 1960's. Most of the understanding of the problem was summarized in several papers given in a special session of the 7th Joint Propulsion Meeting (1971). A pressure record of flight data is reproduced in Figure I-5. Owing to the low sampling rate and the compressed time scale, the oscillations are revealed as a swelling of the trace of mean pressure. The unsteady motions are true linear instabilities and were remarkably reproducible, both in flight tests and in ground tests.

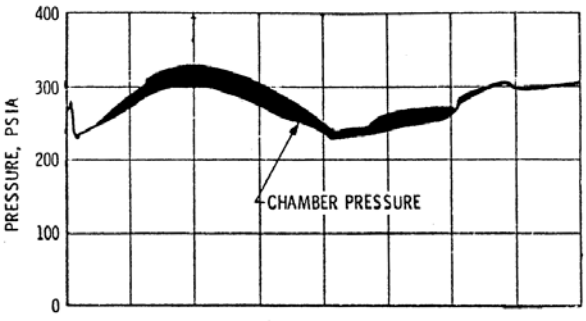

Figure I-5. A Typical Pressure Trace from the Minuteman II, Stage 3 Motor (Flight Test)

The preceding examples are all true linear instabilities formally classified as 'Hopf' or *supercritical bifurcations* in the field of dynamical systems. An unstable motion of this sort occurs when a small disturbance is unstable in the sense that however small it is, the energy flow to the motion depends on the motion itself and exceeds the energy loss, an example of feedback causing a system to become unstable. The instability exists when some parameter assumes a value greater than some 'critical' value. The term 'supercritical' derives from the phenomenon of unstable fluid motion when the Reynolds number exceeds its critical value for the particular flow in question. A second important class of unstable motions comprises *subcritical bifurcations*[2]. In this case a linearly stable system will nevertheless support an unstable motion if it is exposed to a sufficiently large initial disturbance. This behavior has been known for more than four decades to exist in liquid and solid propellant rockets. Subcritical bifurcations in rockets have commonly been called "triggered" or "pulsed" instabilities. Alternative labels, favored in the Russian literature, are *soft excitations* (linear instabilities, supercritical excitations) and *hard excitations* (nonlinear or pulsed instabilities, subcritical bifurcations)

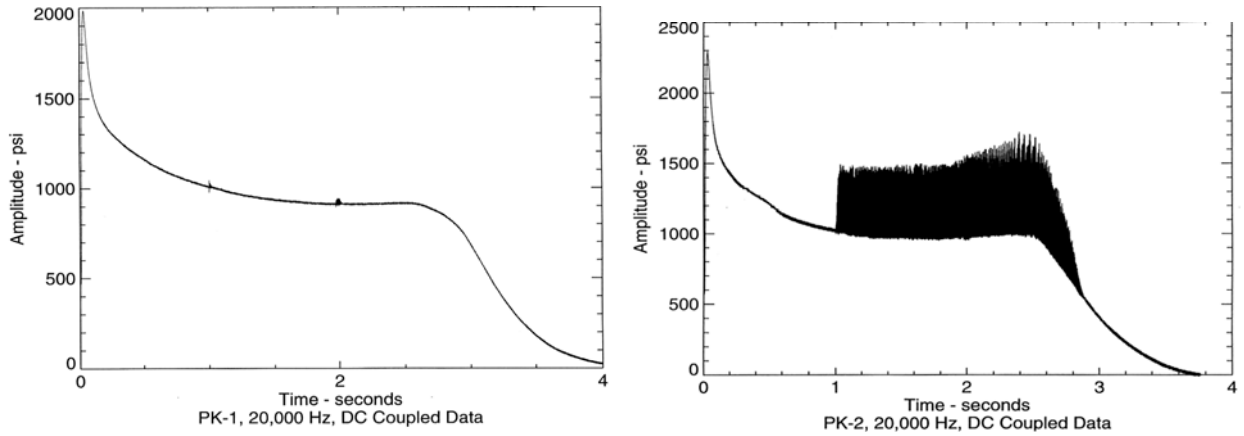

(a) Pulse Amplitude 40 psi. **(b) Pulse Amplitude 100 psi.**

Figure I-6. Example of a Nonlinearly Unstable Motor

Experimentally, the simplest situation is that displayed in Figure I-6 reproducing the results of two recent firings of identical motors (Blomshield, 2000). The motor is evidently stable to small disturbances (pulses) having amplitudes below 40 psi but it is unstable to pulses 100 psi and larger. There are no data to establish the precise limits. This behavior fits exactly the definition of a subcritical bifurcation quoted above. Pulsed instabilities can occur in marginally stable motors if a sufficiently large object—*e.g.* a piece of insulation or slag passes through the exhaust nozzle, generating a pressure pulse. For example, small (and harmless) pressure pulses occur commonly in the solid rocket booster motors on the Space Shuttle. The amplitudes of the pulses are less than 2% of the mean pressure and last about a second. They are produced by masses of slag passing through the nozzle after having been ejected from a pool of slag accumulated in the nozzle cavity.

[2] Strictly, the existence of pulsed instabilities evolving to stable oscillations (stable limit cycles) requires a subcritical bifurcation accompanied by a turning point.

Observations of the sort just described—and there are indeed vast numbers of others—provide the context in which the MURI programs have been conducted. The chief questions to be addressed are:

- What are the basic causes or mechanisms for the presence of coherent oscillations in solid propellant rockets?
- How can one reduce, eliminate and avoid combustion instabilities in full-scale systems?

Both questions require a broad range of knowledge ranging from the fundamental steady and unsteady combustion of propellants to the intricacies of linear and nonlinear oscillations in solid rocket combustion chambers.

The primary mechanism for the overwhelming number of combustion instabilities, including all severe (*i.e.* high amplitude) cases is the coupling or interaction between unsteady combustion dynamics at the burning surfaces, and the gasdynamics of the chamber. Consequently, that part of the overall problem has been the focus of a large part of the research carried out in the MURI programs.

I.2 Chief Justification for the Caltech MURI: The Primary Mechanism for Combustion Instabilities in Solid Rockets

Since the 1960s it has been generally recognized that the primary mechanism for combustion instabilities resides in the dynamics of the combustion processes associated with the conversion of the cold solid propellant to hot combustion products. To treat and, in the best case, avoid instabilities, it is essential to understand how those processes respond to changes of their environment, mainly pressure and temperature, imposed by changing conditions in the combustion chamber. With the introduction of advanced high-energy propellants operating at higher pressures, the requirements become increasingly pressing for understanding details of the mechanism. The time scale of oscillations is in the range of less than one tenth to perhaps ten milliseconds, the periods of natural acoustic resonances in solid rocket combustors. Frequencies of instabilities in tactical and strategic motors normally lie in the range from about 100 Hertz to tens of kilohertz. That characteristic sets the bandwidth required of laboratory diagnostics as well as instrumentation for full-scale tests. To appreciate the special organization of the Caltech MURI, it is helpful to understand the physico-chemical context in which the primary mechanism resides.

I.2.1 Identification of the Mechanism; The Combustion Response Function

For convenience we can view the combustion of a solid as a sequence of processes taking place in four regions: (1) inert solid; (2) a sub-surface reactive region in the condensed phase; (3) the interface region in which transformation of the propellant from condensed material to gasses take place; and (4) the gas phase near the interface, where most of the energy release occurs, in chemical reactions of gaseous species. Downstream of the gas phase combustion zone lies the main chamber. To keep the explanation simple we ignore the presence of aluminum combustion. Figure I-7 is a sketch showing those regions and roughly the ranges of responsibilities of the three tasks in the Caltech MURI. Thus, by far most of the work on the basic mechanisms has been the responsibility of Tasks I and II.

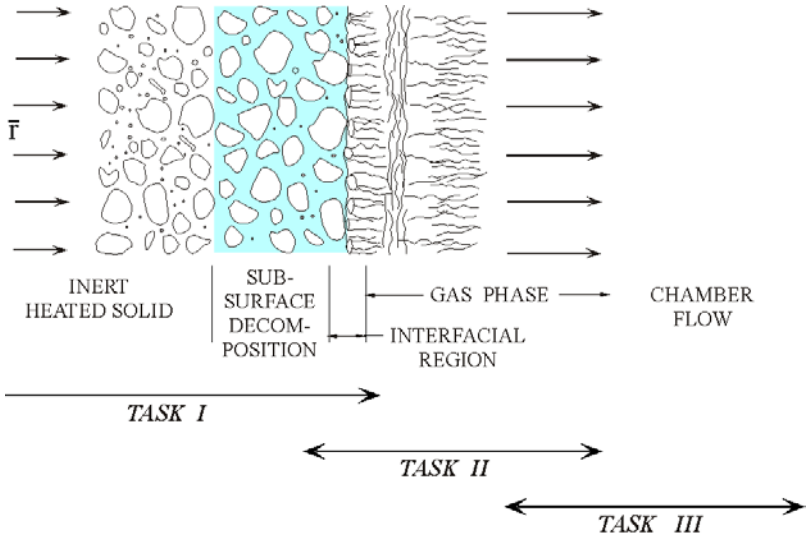

Figure I-7. Various Regions Contributing to the Basic Mechanism of Combustion Instabilities

Part of the objective of Task III was to begin with the results of Tasks I and II for the mechanisms; cast them in the form required for the purposes at hand; and incorporate them in analyses constructed to interpret and predict combustion instabilities. Task III also included[3] pulse motor tests carried out at NAWC, China Lake.

The mechanism in question here is, broadly speaking, primarily a matter of combustion dynamics. It has become customary to represent the mechanism quantitatively as an admittance or response function. We use the latter here, defined generally as the fluctuation of mass flow rate of gases departing the combustion zone to the imposed fluctuation of either the pressure or the velocity. Thus the response function for pressure fluctuations (referred to as the "response to pressure coupling") is defined in dimensionless form as R_p,

$$R_p = \frac{m'/\overline{m}}{p'/\overline{p}} \tag{I.1}$$

where $(\,)'$ means fluctuation and $\overline{(\,)}$ is an average value. The average value $\overline{m}$ represents the average inflow of mass due to the propellant burning. In almost all applications, the fluctuations are steady sinusoidal oscillations, written as

$$\frac{m'}{\overline{m}} = \frac{\hat{m}}{\overline{m}} e^{-i\omega t} \quad , \quad \frac{p'}{\overline{p}} = \frac{\hat{p}}{\overline{p}} e^{-i\omega t} \tag{I.2 a,b}$$

and

$$R_p = \frac{\hat{m}/\overline{m}}{\hat{p}/\overline{p}} \tag{I.3}$$

where $\hat{(\,)}$ denotes the amplitude of the oscillation, including both magnitude and phase. Because generally the oscillations of mass flux rate are not in phase with the pressure oscillations, the function R_p is complex, the real part representing that part of $m'/\overline{m}$ that is in phase with the pressure oscillation.

[3] A second series of motor tests completed by Thiokol, Inc. using plateau propellants was funded jointly by Thiokol and the UIUC MURI.

Although the response function for pressure coupling is most commonly used, and dominated the research in both the Caltech and UIUC MURIs, there is a second response function, that associated with velocity coupling, which under some practical circumstances is far more important. This matter was addressed in Tasks II and III, discussed in Sections 2 and 3 of this report. Several conclusions, significant for practical applications, reached in the Caltech MURI program relate to velocity coupling. At this point we confine our remarks to the response function for pressure coupling.

A simple interpretation of the response function explains its importance to combustion instabilities. According to the definition (I.3), a pressure oscillation having amplitude $\hat{p}/\overline{p}$ produces the oscillation $\hat{m}/\overline{m}$ of mass flow into the chamber

$$\frac{\hat{m}}{\overline{m}} = R_p \frac{\hat{p}}{\overline{p}} \tag{I.4}$$

Viewed from the chamber, the boundary appears then to oscillate. The apparent motion is entirely analogous to that of a speaker or piston mounted at the boundary. Thus pressure waves are generated in a fashion similar to that of a loudspeaker in a room. Through a complicated sequence of processes whose details are not germane here, those waves coalesce and combine with the original pressure waves causing the fluctuations of mass flux. Whether or not that merging process augments or subtracts from the existing wave system in the chamber depends on the phase between $\hat{m}$ and $\hat{p}$. The part of $\hat{m}$ in-phase with $\hat{p}$ increases the amplitude of the wave system and is therefore destabilizing. Consequently, in this context, the most important consequence of the research in Tasks I and II is determination of the amplitude and phase of $\hat{m}/\overline{m}$, *i.e.* the magnitude and phase (or real and imaginary parts) of R_p, and their dependencies on propellant composition. For a particular motor, the tendency for combustion dynamics to drive instabilities is proportional to the integral of R_p over the entire area of burning surface. Hence it is clearly essential to know the response function for the propellant used.

Both experimental and theoretical determinations of R_p involve two bodies of information: the characteristics of steady combustion of the propellant in question; and the dynamics. The processes involved in steady combustion must be known first because the dynamics are the time variations of those processes. In one sense, the dynamics are in any event better known at the levels of Tasks II and III than in Tasks I. The reason is that presently there are no methods for direct accurate experimental measurement of the fundamental processes forming the behavior which is the subject of Task I. Measurements of dynamical behavior while still in unsatisfactory states, become successively less difficult and more accurate in the areas covered by Tasks II and III.

Consequently, the research in Task I has mainly to do with steady processes, or with behavior taking place on relatively slow time scales. Moreover, much of the experimental and modeling effort in Task II was concerned with steady behavior for the reason cited: the essential need for knowledge of steady-state combustion as the basis for working out the dynamics. In contrast, virtually all of the research in Task III was concerned with dynamical behavior, including applications to instabilities in full-scale motors.

For both steady combustion and combustion dynamics, the dominant processes in all regions identified in Figure I-7 are heat transfer and energy release or absorption. Those processes are of course strongly coupled because the rate at which energy is released affects the temperature profile; and both the local rate of heat transfer and the temperature influence the rate of energy release. The details are important, a fact explaining much of the character of the research carried out in Task I and part of Task II.

Traditional composite propellants using ammonium perchlorate as oxidizer, as well as advanced propellants using higher energy oxidizers and binder, burn in qualitatively similar fashion. The interface between the condensed and gas phases is fairly well defined, may be dry or wet, and may exhibit local dynamical activity owing to the presence of solid particles and responsive collections of liquid pools or drops. The dynamics of the interfacial region is particularly noticeable in microcinematography when the propellant contains aluminum. The metal collects in molten droplets, mobile and ignitable on the surface; those not fully consumed are carried away by the gaseous products of the interface.

The high temperature at the surface is sustained by a balance between heat flow away from the interface, required to heat the cool propellant advancing to the surface; energy required to effect the phase changes at and near the interface; and the heat transfer supplied to the interfacial region from the combustion zone in the gas phase. It's a delicate balance, easily disturbed by changes in the chemical processes in the interfacial region, particularly within the subsurface region in the condensed phase. Figure I-8 is a sketch of the temperature field, showing also the possible consequences of additional exothermic reactions in the sub-surface condensed phase. Note that in this figure we imagine that the temperature exists in a spatially averaged sense. Local variations on the scale of oxidizer particles are smeared out in the averaging procedure and explicit effects of inhomogeneities are absent.

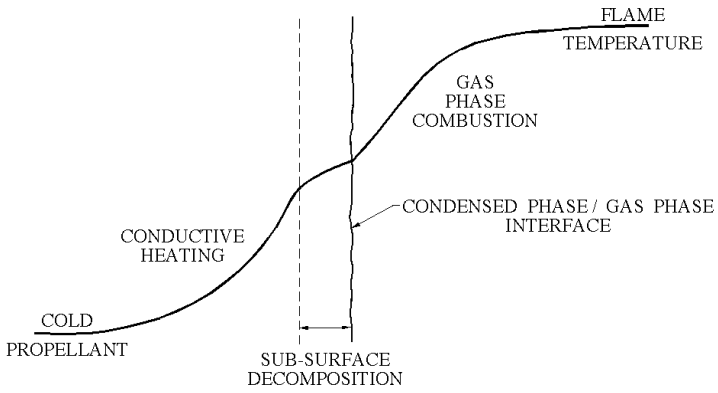

Figure I-8. Representation of the Temperature Field in a Burning Solid Propellant

Measures of success of the research must be based on at least three criteria:

1) Progress in understanding the fundamental processes participating in the combustion dynamics;
2) The extent to which advances in understanding fundamental behavior lead to deeper understanding of the mechanism and its practical consequences; and
3) Direct application of the results of research to practical problems.

I.2.2 Qualitative Description of the Mechanism

The essentials of the behavior represented macroscopically by response functions can be described as a sequence of elementary steps, described here in simplified form with reference to Figure I-7:

(i) Suppose that for some reason the rate of reactions in the combustion zone increases—perhaps due to a fluctuation of pressure, or temperature, or to increased local mixing associated with greater intensity of turbulence locally in the chamber.

(ii) Increased reaction rates produce a rise in the rate of energy release and an increase of temperature of the combustion zone.

(iii) Due both to radiation and heat conduction, the heat transfer from the combustion zone to the interfacial region increases, having at least two possible consequences: the temperature at the surface is increased; and the rate at which condensed material is converted to gas is also increased.

(iv) Because the temperature in the interfacial region rises, so also does the heat flow to the subsurface region and further into the solid, tending to cool the interface.

(v) If there are subsurface reactions, the heat flow will tend to increase their rate, with consequences depending on the associated energy release (or absorption) rate.

(vi) Exothermic subsurface reactions will act to maintain higher temperature locally, thereby encouraging the conversion of condensed material to gas at the interface, but also tending to increase the heat flow to the cooler solid.

(vii) The net result may be that if the fluctuation of heat flow, and reduction of temperature, at the interface does not happen too quickly, the enhanced reaction rate assumed in Step (i) may produce a fluctuation of mass flow leaving the surface, that is in phase with the initial perturbation. Hence in this event the entire process is destabilizing in the sense that the initial disturbance has the result that the disturbed mass flow into the chamber tends to augment that initial disturbance.

Whether or not the preceding sequence will be destabilizing depends entirely on details of the processes involved. Notably, if sub-surface reactions are endothermic, then the sequence (v) – (vii) leads to the conclusion that the reactions may cause the propellant combustion to be less sensitive to disturbances. That is why the Caltech MURI was planned, and carried out, in the manner described above and in the remainder of this report. The tasks and projects within the tasks were intended to investigate details of the various parts of the overall problem.

Many years ago, the simplest representations of the mechanism were worked out by several researchers, giving apparently different results. However, it turned out subsequently that at the level of practical applications, the results were almost the same, because all of the analyses were based on the same fundamental assumptions. “Same results” means here the same combustion dynamics; that is, the *form* of the dependence of the response function (equivalent to a transfer function in the language of controls) is identical for all the results. The reason for that surprising result is fundamental to the MURI program because it succinctly captures the essence of the state of the subject when the MURI work began.

The reason why so many analyses of the combustion dynamics produce the same behavior is that all assumed quasi-steady (*i.e.* not truly dynamical) behavior throughout the regions sketched in Figure I-7 except in the condensed phase. It’s a reasonable approach because the characteristic response time for thermal fluctuations are much faster in the gas phase than in the condensed phase and, under many conditions, the dynamics of the interfacial

region are also fast. Thus the dynamics of the response are dominated by unsteady heat transfer in the condensed phase. As a result, the response of a burning solid typically has the form shown in Figure I-9. Although details have been worked out only for pressure coupling, there is reason to believe that unsteady heat transfer is always a significant contributing process to the dynamics of burning solid propellants.

$$\left|R_p\right| = \frac{\left|m'/\overline{m}\right|}{p'/\overline{p}}$$

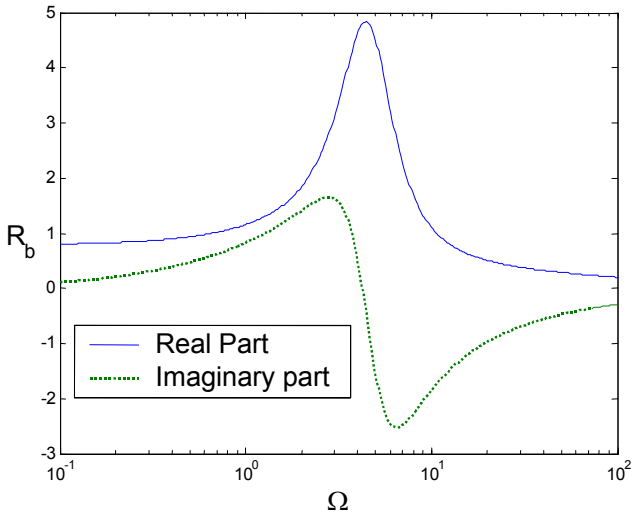

Reference Case: QSHOD Result with A = 6.0, B = 0.60

Figure I-9. Typical Form of the Simplest Model for the Combustion Response Function

It's an interesting—but not surprising—fact that the result sketched in Figure I-9 was established independently in the U.S., where it has come to be known as the QSHOD[4] response function, and much earlier in Russia, where it is known (also now in the West as well) as the Z-N[5] response function. Those two results follow from different approaches to the quasi-steady part of the problem and therefore suggest different ways of evaluating various parameters arising in the representation of the *steady* combustion processes.

Experimental results, even with the large uncertainties associated with the methods available, have long shown that the QSHOD/Z-N model contains the dominant feature of the response of real propellants, namely a broadband peak as shown in Figure I-9. The variation of the phase with frequency has been roughly confirmed, but it is much more difficult to measure than is the magnitude. Such measurements, most of which have been done with various forms of a device called a T-burner, allow evaluation of the two parameters A and B in the QSHOD/Z-N form of the response function,

$$R_p = \frac{nAB}{\lambda + \frac{A}{\lambda} - (1 + A) + AB} \tag{I.5}$$

where n is the index in the burn rate law $r \sim p^n$ and λ is a function of the complex frequency of oscillations.

[4] QSHOD stands for **Q**uasi-**S**teady **H**omogeneous **O**ne-**D**imensional.
[5] Z-N stands for **Z**el'dovitch-**N**ovozhilov.

The accuracy of existing experimental methods prevents determination of the values of A and B with sufficient precision to assess whether or not the models of the combustion processes are good representations of actual behavior. Moreover, the models are simplified to the extent that they are incapable of predicting the dynamical consequences of small changes of propellant composition. Experimental data combined with the models have not produced useful information about the dependence of A and B on propellant composition, particularly for heterogeneous composite propellants.

Even at the present level of experimental methods, it is evident that unsteady heat transfer in the condensed phase is certainly not the only dynamical process contributing to the response of a burning solid. The most persuasive evidence is the common observation of multiple peaks in the response, or larger values of response than the formula (I.5) predicts for frequencies above the broad peak.

Owing to limitations of both analysis of the combustion dynamics and the experimental methods of measuring response functions, it is essential to carry out theory and experiment in close coordination. That structure has been followed throughout the Caltech MURI. Fundamental results of Task I have rapidly become incorporated in the modeling activities in Task II. Ideas and modeling of the response function have been used in the analyses of global behavior and motor dynamics carried out in Task III. One interesting novel aspect of that activity has been the use of predicted behavior—mainly nonlinear features of instabilities—to infer certain properties that the combustion response function must have. Probably the most important result in that respect is the conclusion that the response to velocity coupling seems now to be even more crucial to understanding combustion instabilities than previously recognized. It's a conclusion clearly directing where substantial future work should be directed.

I.3 Accomplishments of the Caltech MURI

Throughout the duration of the program, close contact was maintained between the participants, through personal contacts, annual program reviews at the JANNAF Combustion Meeting, and with nineteen workshops, an average of four per year. Thus the accomplishments cannot all be ascribed uniquely to particular tasks since they depend on cooperative efforts. However, for this report it is convenient to categorize the work and the accomplishments into the three tasks.

I.3.1 Task I. Chemical Kinetics and Dynamics

The research in Task I was concerned with chemical activity extending from the sub-surface region at the interface into the gas phase. This continues to be one of the most daunting tasks of all research efforts in energetic materials. At the outset the decision was made to focus on experimental studies of fast thermolysis of novel energetic materials and on computational studies of near surface, gas-phase, exothermic, radical recombination reactions. The findings in both of these programs were actively used by Task II participants in the development of new combustion models that are useful for understanding combustion sources of instability.

Research on fast thermolysis using vibrational spectroscopy requires that both infrared and Raman spectroscopy be used if mass balances are to be closed. The T-jump/Raman spectroscopy method was therefore developed at the University of Delaware to complement the T-jump/FTIR method. This is the main new diagnostic method

developed in Task I. In addition, an attempt was made to determine if the shape and magnitude of the control voltage trace of the T-jump/FTIR spectroscopy experiment could be quantified well enough to determine kinetics and heat flow in very fast heating experiments. It could, but only under ideal conditions of heat transfer. Determination of the absolute rate constants for gas phase radical-radical reactions that are relevant to near-surface chemistry during propellant combustion at elevated pressure require the use of elaborate quantum mechanical methods (modified Gaussian-2), variational transition state theory as opposed to simple transition state theory, and statistical mechanical methods. This was a computational approach new to the combustion field and was implemented at Emory University for determination of the details of reaction kinetics.

We took the title of this program "Novel Energetic Materials to Stabilize Rockets" to heart in the experimental part of Task I in that it presented the opportunity to explore several new lines of chemical thinking that could prove fruitful for tailoring combustion. Underlying this effort were our first pyrolysis studies into complex mixtures as opposed to pure materials. For example, we explored the use of energetic metal salts of nitrotriazolone (NTO) as a means to produce gaseous metal salt particles which might dampen high-frequency acoustic modes in the motor combustion chamber. The use of an energetic additive as opposed to the inert additive would help maintain the energy density of the formulation. We explored the condensed phase chemistry of AP-HTPB with TiO_2 and melamine additives to try to understand bi-plateau behavior. We determined that the additives do affect the decomposition chemistry to some extent and are not only affecting the physical properties of the surface. We engaged in a thorough study of high nitrogen compounds, e.g., amino tetrazole salts, azo and hydrazo furazans and azides for their possible use as combustion additives. The condensed phase chemistry was investigated, but the absence of a parallel formulation program in the MURI prevented testing of any of the materials. The cured GAP/RDX/BTTN propellants formulated at China Lake were pyrolyzed and characterized. The pure components as well as the mixtures were studied, and insights were gained regarding interactions of the components with one another during fast decomposition.

In the computational program, a new approach to calculating rate constants for barrierless, exothermic free radical reactions occurring in the near field of the burning propellant under high pressure and temperature conditions was established. The new method is based on state-of-the-art *ab initio* molecular orbital and statistical reaction rate theories. Dozens of new or improved rate constants were calculated, many with previously unrecognized pathways, for the unimolecular and bimolecular surface driving reactions in HMX, RDX, AN, ADN, AP, and GAP. The reactions involve C, H, O, N, and Cl containing radicals. The temperature range was 300-2000K and the pressure used was typically 200 atm. Many of the absolute rate constants listed in Tables 1 and 2 and their pathways were incorporated into the combustion modeling in Task II.

Table 1. Rate Constants Predicted for Unimolecular and Related Reverse Reactions.

Reaction	T/K	P/Atm	k
$HN(NO_2)_2 \rightarrow HNNO+NO_2$	300-1000	200	6.9×10^{16} exp(-18,300/T)
$HNNO_2 \rightarrow NH+NO_2$	500-2000	200	7.3×10^{44} $T^{-9.3}$exp(-24,100/T)
$CN_2NNO_2 \rightarrow CH_2N+NO_2$	500-1500	200	7.3×10^{57} $T^{-11.0}$ exp(-26,100/T)
$\rightarrow HCN+HONO$			1.5×10^{11} exp(-14,200/T)
$\rightarrow CH_2O+N_2O$			2.9×10^{9} exp(-16,400/T)
$CH_2NO \rightarrow HCN+OH$	200-2000	200	1.8×10^{10} exp(-25,600/T)
$CH_2N \rightarrow HCN+H$	500-2000	200	1.5×10^{12} exp(-14,000/T)
$CH_2N+M \rightarrow HCN+H+M$	500-2000	0[a]	3.8×10^{11} $T^{1.0}$ exp(-10,800/T)
$NH+NO \rightarrow H+N_2O$	300-3000	200	7.1×10^{9} $T^{0.83}$ exp(1,100/T)
$\rightarrow OH+N_2$			1.8×10^{9} $T^{0.83}$ exp(1,100/T)
$NH+NO_2 \rightarrow HNNO_2$	300-3000	∞ [b]	1.4×10^{16} $T^{-0.73}$ exp(-617/T)
		0	0
$\rightarrow N_2O+OH$	300-3000	0	2.1×10^{13} $T^{-0.49}$ exp(360/T)
		∞ [b]	0
$NH+NO_2 \rightarrow HNO+NO$	300-3000	<200	1.3×10^{6} $T^{2.0}$ exp(1,180/T)
$CH_2N+NO \rightarrow CH_2NNO$	300-3000	200	1.1×10^{38} $T^{-8.1}$ exp(-330/T)
$\rightarrow HCN+HNO$			4.2×10^{2} $T^{2.7}$ exp(-3,400/T)
$CH_2N+NO_2 \rightarrow CH_2NNO_2$	500-1500	200	1.0×10^{33} $T^{-6.5}$ exp(-2,800/T)
$\rightarrow HCN+HONO$			3.6×10^{6} $T^{1.4}$ exp(-1,050/T)
$\rightarrow CH_2O+N_2O$			1.5×10^{4} $T^{1.7}$ exp(-3,700/T)
$CH_2N+OH \rightarrow H_2CNOH$	300-3000	200	2.4×10^{22} $T^{-2.9}$ exp(-2,100/T)
$\rightarrow HCN+H_2O$			1.7×10^{19} $T^{1.8}$ exp(-1,500/T)
$NCO+NO \rightarrow N_2O+CO$	300-3000	<200	4.0×10^{19} $T^{-2.2}$ exp(-877/T)
$\rightarrow N_2+CO_2$		<200	1.5×10^{21} $T^{-2.7}$ exp(-918/T)[d]

Unimolecular rate constants at the pressure indicated are given in s^{-1} [a]Low pressure limit. [b]High pressure limit.

Table 2. Rate Constants Predicted for Bimolecular Reactions.

Reactions	T/K	k (cm^3/mole.sec)
$NO+HN_3 \rightarrow HNO+NH_2$	300-5000	$1.0\times10^{7}\ T^{1.7}\ exp(-28{,}500/T)$
$NO_2+ NH_3 \rightarrow HONO+NH_2$	300-5000	$1.2\times10^{1}\ T^{3.4}\ exp(-11{,}300/T)$
$HNO+NO_2 \rightarrow HONO+NO$	300-5000	$4.4\times10^{1}\ T^{2.6}\ exp(-2{,}034/T)$
$H+HONO \rightarrow H_2+NO_2$	300-3500	$2.0\times10^{8}\ T^{1.6}\ exp(-3{,}300/T)$
$\rightarrow OH+HNO$		$5.6\times10^{10}\ T^{0.86}\ exp(-2{,}500/T)$
$\rightarrow H_2O+NO$		$8.1\times10^{6}\ T^{1.9}\ exp(-1{,}900/T)$
$OH+HONO \rightarrow H_2O+NO_2$	200-500	$4.1\times10^{12}\ (T/300)^{-0.8}$
	500-2000	$1.8\times10^{7}\ T^{1.5}\ exp(1{,}260/T)$
$H+HNO_3 \rightarrow H_2+NO_3$	300-3000	$5.6\times10^{8}\ T^{1.5}\ exp(-8{,}200/T)$
$\rightarrow OH+HONO$		$3.8\times10^{5}\ T^{2.3}\ exp(-3{,}500/T)$
$\rightarrow H_2O+NO_2$		$6.1\times10^{1}\ T^{3.3}\ exp(-3{,}200/T)$
$OH+HNO_3 \rightarrow H_2O+NO_3$	750-1500	$8.7\times10^{1}\ T^{3.5}\ exp(839/T)$
$HNO+HONO \rightarrow H_2O+2NO$	300-3000	$1.7\times10^{-3}\ T^{4.2}\ exp(-8{,}350/T)$
$HONO+HCl \rightarrow H_2O+ClNO$	300-3000	$1.1\times10^{2}\ T^{3.0}\ exp(-5{,}120/T)$
$HONO+NO_2 \rightarrow HNO_3+NO$	300-5000	$2.0\times10^{2}\ T^{3.3}\ exp(-15{,}400/T)$
$HONO+HONO \rightarrow NO+NO_2+H_2O$	300-5000	$3.5\times10^{-1}\ T^{3.6}\ exp(-6{,}100/T)$
$HONO+NH_3 \rightarrow H_2O+NH_2NO$	300-3000	$1.0\times10^{-3}\ T^{3.3}\ exp(-14{,}800/T)$
$HNO_3+HN_3 \rightarrow H_2O+NH_2NO_2$	300-3000	$4.3\ T^{3.5}\ exp(-22{,}140/T)$

bimolecular and second order decomposition in cm^3/mol-s

I.3.2 Task II. Combustion Dynamics

I.3.2.1 Steady State Modeling

The research in Task II was concerned with developing mechanistic understanding of the steady and unsteady combustion characteristics of advanced ingredients/propellants. The approach to accomplish this was primarily focused on modeling, with the experimental work designed to support the modeling efforts. At the start of the MURI program in 1995, the Yetter Mechanism for RDX had been developed, based on previous ONR funding by Dick Miller. This mechanism consists of 232 fundamental reaction steps and 44 species, and has become a "standard" for modeling the combustion of RDX. Work was also in progress to use the Yetter mechanism within the framework of a detailed kinetics model for the combustion process. This work was pioneered by Yang and co-workers, Beckstead and co-workers, and Yetter, Smooke and co-workers. These models provided the foundation for the MURI program to build upon. These models have been applied to describe various aspects of RDX combustion and then extended to other ingredients (HMX, AP, GAP and ADN) and to two mixtures of ingredients (AP/HTPB, RDX/GAP). The basic approach is applicable to other advanced ingredients.

There were two or three major developments that allowed the development of these models. The most obvious is the speed of modern computers, which had allowed the solution of the differential equations required to describe the many chemical reactions. The better computers also have allowed the solution of quantum mechanical models leading to the definition of chemical reaction paths, that was not previously possible. The other is the development of diagnostic experiments, which have allowed the measurement of fundamental chemical reactions, and the

generation of detailed species concentrations of products leaving the propellant surface. Some of these developments have been the topic of Task 1 and are discussed in the previous section.

The models calculate the burning rate, pressure exponent, and temperature sensitivity as functions of pressure and initial temperature. The calculated results are within the data scatter of the experimental data, providing good checks of internal consistency. Calculations were performed for pressures from one atm up to 100 atm, and there is no reason why the calculations couldn't be extended to higher pressures. The detailed models also predict the temperature and species profiles at the various conditions. The corresponding experimental data have been obtained at low pressures (usually atmospheric pressure) because the flame zone is sufficiently spread out to allow the diagnostic probes to have a viable control volume at low pressures. At high pressures the flame zone is on the order of tens of microns which is prohibitively small, precluding the possibility of obtaining diagnostic data at pressures of interest. Thus, the models are validated by comparing results with experimental data obtained at one atmosphere. Then model calculations can be made at pressures of interest.

The model has also been validated by comparing to detailed combustion data such as the temperature and species profiles. Figure I-10 shows the calculated temperature profile for RDX burning at one atm compared to Parr's experimental data. Similar results have been generated for the various species generated by the combustion process. Agreement with the experimental data is very reasonable.

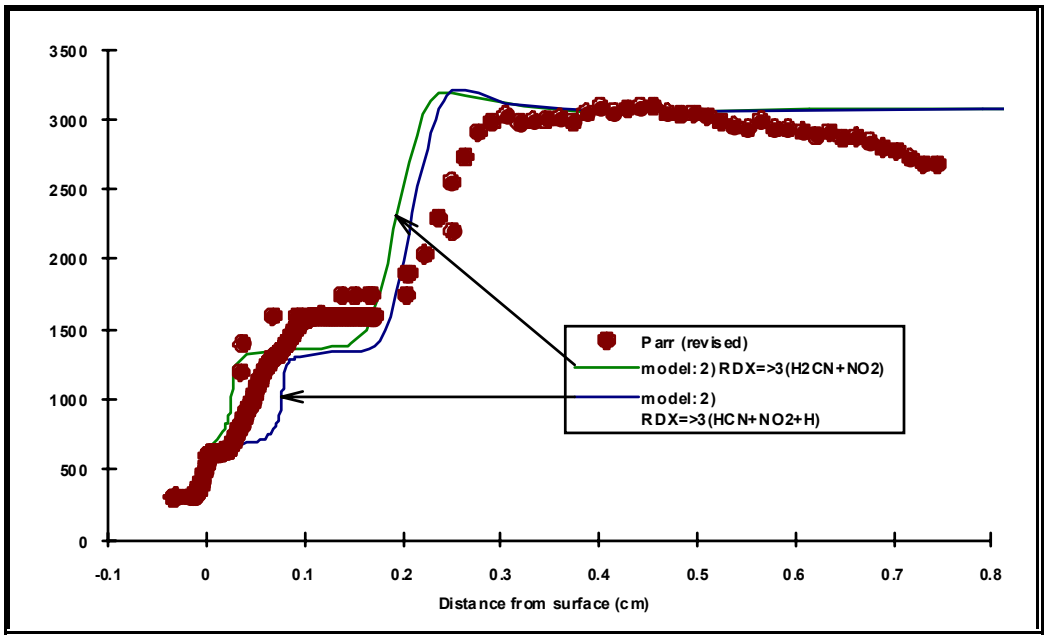

Figure I-10. Calculated temperature profile for RDX burning at one atm (with laser augmentation) compared to Parr's experimental data

Initial results showed that the temperature sensitivity of both RDX and HMX were essentially identical and varied little with pressure. These results are not in agreement with the experimental; data. The RDX temperature sensitivity is ~0.001 K^{-1} and does not vary much with pressure. In contrast, the temperature sensitivity of HMX is ~0.004 K^{-1} at 1-2 atm and decreases to ~0.001 K^{-1} at about 30-40 atm. Extensive efforts were expended to determine

the differences in the σ_p values of RDX and HMX. Chemically they are very similar, and their flame temperatures and burning rates are essentially identical. However Parr has observed that at low pressures, 1-2 atm, the flame standoff distance of HMX is much greater than RDX, and the HMX flame is much less stable than that of RDX. These differences were attributed to a greater condensed phase exothermic energy release with HMX than with RDX. Subsequent modifications in the model have shown that this is indeed the case. The reason is the higher melt vaporization and surface temperatures of HMX. Those effects permit a greater degree of reactivity in the condensed phase, a process more significant at low pressure. This determination is in keeping with the original objective of Task II to develop a mechanistic understanding of the steady combustion characteristics of propellant ingredients.

As part of the MURI program a review paper was written summarizing the unsteady combustion characteristics of typical propellant ingredients. One of the conclusions of the paper was that the magnitude of the unsteady propellant response increases with increasing temperature sensitivity. Thus, the results of these studies have shown that a measure of a propellant's unstable response can be related to the exothermicity of the condensed phase reactions of the propellant. This understanding will help in evaluating the instability tendencies of new, advanced ingredients. Again, this result is in direct alignment with the original objectives of the program.

I.3.2.2 Experimental Studies

Experimental procedures and hardware were developed to measures species profiles through the flame using an MPMS by Litzinger at Penn State. Measurements of gas phase species and temperature profiles as well as condensed phase temperature profiles were made for RDX, HMX, BAMO, BAMO/RDX, and BAMO/AMMO. Variations in the burning behavior of the various mixtures have been documented and published in various journal articles. The effect of an externally imposed heat flux on the combustion process has also been made and evaluated. These data were used for the modeling validation.

A test facility was developed at Penn State to measure the combustion response of ingredients and propellants for both pressure and radiation driven unsteady combustion. The differences between the response to the two different stimuli has been measured and reported. In addition, procedures and hardware have been developed to measures species during unsteady combustion using an MPMS. Measurements of response functions and species oscillations during radiation-driven combustion have been completed for HMX, and several of the MURI propellant formulations.

As part of another program, Penn State researchers also applied the Z-N method to their measurements of steady-state data in order to compute response functions for bi-plateau propellants. They measured burn rate, pressure exponent, temperature sensitivity, surface temperature and activation energy. Results forecast very favorable stability properties that were subsequently verified in subscale motor tests. Burn rate, exponent and temperature sensitivity were also measured at Thiokol, NAWC, UAH and UIUC with very good agreements.

A facility was also developed at the University of Alabama at Huntsville (UAH) to measure instantaneous burn rates by ultraoxonic reflections from moving surfaces. The technique was checked out for steady-state burning and, by using a closed chamber, for measuring burn rates vs. pressure in a single test. Agreements with conventional strand data were excellent. Considerable effort was made to characterize the sources of uncertainly and error in the

method. Further developments succeeded in measuring transient burning rates during rapid monotonic pressure transients, observing effects of dP/dt, and during oscillatory pressure transients to measure response functions of interest for combustion instability. A rotating valve system was devised to impose pressure oscillations on burning samples. However, at present, good quality and credibility of data are limited to frequencies below 100 Hz. More work is needed to improve signal strength and instrumentation response in order to increase the range of frequencies for this very promising alternative to the T-burner. A parallel effort was conducted at UIUC.

The group at UAH also studied extinguished surfaces of bi-plateau propellants with optical and scanning electron microscopes at pressures in the plateau and non-plateau regimes. Results helped to verify the plateau mechanism as involving binder melt layer interference with the normal combustion of very fine AP at the propellant surface and the influence of the TiO_2 additive on this interference. It is believed that binder melt layer interference can bring about a low combustion response. A parallel extinguished surface study was carried out at Georgia Tech.

I.3.2.3 Modeling the Unsteady Nature of Ingredients

An unsteady numerical monopropellant combustion model has been developed which includes detailed chemical kinetics. This is the first model to accomplish this. The code was applied to both RDX and HMX and tested under a variety of simulated steady-state conditions. Calculations show that pressure coupled responses obtained from model simulations matched experimental T-burner trends quite well for both RDX and HMX, including the prediction of higher responses with increased mean pressure. Ranges of validity of the quasi-steady assumption, which in normally made in most models, were evaluated. The quasi-steady assumption was determined to be valid for RDX and HMX below about 200 Hz at 1 atm and below about 1000 Hz at 68 atm. Somewhat higher limiting frequencies were reported in the literature for nitrate esters used as double-base binders. Heat flux responses obtained from transient calculations matched experimental laser-recoil results reasonably well for RDX, but not for HMX. The discrepancies were attributed to inadequacies in the HMX combustion model, particularly with respect to condensed phase and near surface gas phase chemistry. Finally, modeling results for species concentrations under oscillatory conditions achieved reasonable agreement with experimental trends. The phase characteristics of the species were attributed to spatial concentration gradients and flame motion. This capability is also a first.

A similar modeling approach was successfully accomplished with GAP, making use of experimental data acquired by our Russian colleagues. The Russians also acquired considerable data with ADN. Concerned about GAP and ADN stem from their high temperature sensitivities associable with their high condensed phase exothermicities. In the case of ADN, dynamic instabilities produce a regime of erratic burning in strands at intermediate pressures. It has been shown that a very high condensed phase exothermicity leads to intrinsic instabilities.

A physico-chemical model for AP, but using global kinetics, was developed in order to examine the relative importance of the various processes to stability. A unique stability criterion was derived relating the dependence of condensed phase heat release to the dependence of heat feedback from the flame on burn rate. This criterion is applicable to energetic monopropellants generally, and therefore provides a basis for evaluating their propensity for

instability. This AP model provided excellent agreement with experimental data for burn rate, exponent and temperature sensitivity, and good agreement with NAWC data obtained for response functions.

I.3.2.4 Modeling the Unsteady Nature of Propellants

Numerical and mathematical solutions were derived from a comprehensive model for the response function of AP composite propellants. Important effects of AP particle size were explained in terms of the competing flame structure (AP flame and interactive AP/binder diffusion flame), and agree with known trends respecting axial and tangential mode instabilities. Binder decomposition and the diffusion flame are stabilizing influences. AP condensed phase reactions and the AP flame are destabilizing. Axial mode stability is improved by avoiding very coarse AP sizes, as demonstrated from experience on Sidewinder, THAAD and other programs. Tangential mode stability is improved by avoiding very fine AP sizes, as demonstrated from the ATR, Maverick and other programs.

The numerical code is ready for incorporation into a gasdynamics code (Task III) that would describe the stability of the rocket motor/propellant system. A modular approach is envisioned so that families of advanced propellants (represented by models) can be attached to or selected by the code like loading propellants into a motor.

The mathematical solution for a response function is a first in composite propellant combustion modeling, and has the advantage of highlighting mechanisms. Numerical solutions require many parametric computations to discern trends and mechanistic significance. The comparisons of computed response functions made with standard data for monomodal AP propellants showed fairly good agreement.

I.3.2.5 Numerical Simulation of Aluminum Particle Combustion

Aluminum combustion can be an important mechanism in driving an instability, and the formation of its oxide smoke plays a key role in particle damping of instabilities. A two-dimensional unsteady state numerical model for aluminum particle combustion has been developed at BYU under MURI sponsorship. The current model solves the conservation equations, while accounting for the species generation and destruction with a 15 reaction kinetic mechanism. Most previous models have only assumed infinite kinetics, relying upon a diffusion-controlled mechanism. The kinetic mechanism in the model consists of surface reactions and gas phase reactions for the formation of the aluminum sub-oxides. The aluminum sub-oxides later react and condense to form the normal liquid aluminum oxide product.

Model calculations have been made for a variety of conditions, to help validate the model and to explore the effects of different gases and conditions. The calculations show that the flame temperature profiles for combustion in O_2, H_2O and CO_2 are significantly different. The flame temperature with CO_2 is over a thousand degrees less than the flame temperature with either O_2 or H_2O, because the enthalpy of the reaction and hence the heat released is significantly less. The flame temperature for reacting with either O_2 or H_2O is much greater and the oxidizing species have much higher diffusivities which also influence the resultant diffusion flame. This calculation is a significant achievement as the gases prevalent in propellants are H_2O and CO_2, and not O_2.

The model was used to explore the effect of pressure on aluminum combustion. Most experimental measurements have been made at low pressures, usually one atmosphere, while typical rocket motor conditions are

in the range of 30 to 100 atmospheres. Figure I-11 shows the predicted dependence of the distribution of temperature on pressure, showing a gradual increase in flame temperatures as the pressure is increased. This is reasonable because the aluminum and aluminum oxide boiling (dissociation for aluminum oxide) points increase with ambient pressure. This increase in flame temperature is very important and has not been accounted for in most previous investigators.

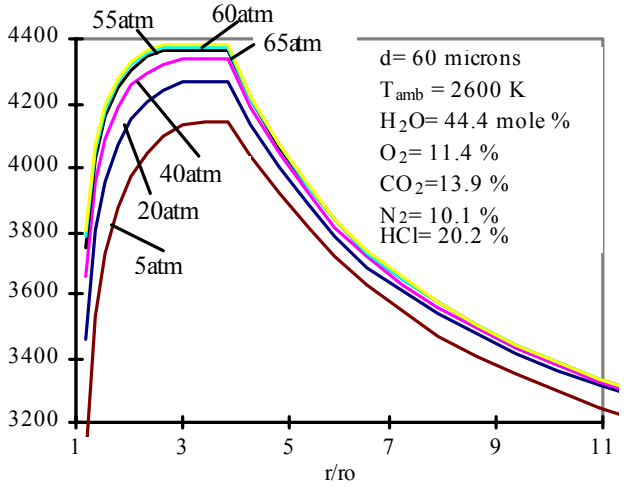

Figure I-11. Predicted temperature profiles vs. non-dimensional radius for various pressures.

The calculations from the model have been compared with recent experimental data. Some of the latest and best experimental measurements of temperature and species distributions around a burning aluminum particle have been performed by Bucher et al at Princeton (as part of the UIUC MURI contract). In one of their experiments, they burned aluminum particles in an O_2/Ar atmosphere and measured the temperature profile extending outward from the particle surface in very small increments. Figure I-12 shows a comparison of Bucher's data with the temperature profile calculated by the model. Very good agreement between predictions and measurements was achieved.

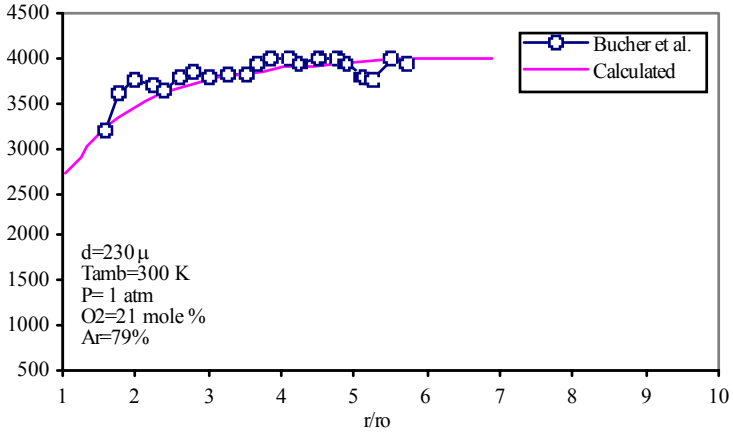

Figure I-12. Calculated temperature profile vs. non-dimensional radius compared with experimental data from Bucher et al.

Calculated burning times for Al particles show that the exponent of the particle diameter dependence of burning time is not a constant. It changes from about 1.2 for larger diameter particles to 1.9 for smaller diameter particles, approaching the D^2-law for very small particles. The calculations also show effects of deposition of the aluminum oxide on the particle surface. The partial pressures of the key oxidizing species were found to correlate the available data on burn times as a function of aluminum particle size. An oxidation index was thus derived as the coefficient in the particle burn-time/diameter relation.

Studies of the combustion of aluminum agglomerates formed in propellant combustion were carried out at UIUC and by our Russian colleagues. Although the nature of large agglomerates was found to be very different from the parent aluminum mixed into propellants, it appears that the essential features regarding particle burn times are the same. Valuable data were acquired on the specific gravities of large agglomerates and on their residual burnout sizes, which are necessary ingredients for slag formation computations. Fractions of fine oxide smoke yielded by the combustion of large agglomerates were also quantified for use in particle damping calculations.

I.3.3 Task III. Combustor Dynamics and Motor Tests

By its nature, the research in Task III was planned to provide the connection between the results of Task II to applications in motor design and development. Put another way, it is a central purpose of Task III to establish as far as possible guidelines or 'rules of thumb' relating the dynamical behavior of motors—in fact combustion chambers generally—to characteristics of the response function. Ultimately, a comprehensive model developed in Task II can be incorporated in the flow-field model constructed in Task III for detailed computations. This general procedure has been carried out and verified for steady flows but has not yet been completed for unsteady flows except for simple combustion models. Hence, through the modeling and representations of response functions (Task II) which must be based on the fundamental behavior exposed in Task I, we have in principle the framework for understanding the dynamical behavior of full-scale motors in terms of the propellant composition. This grand objective has yet to be achieved, but the Caltech MURI has successfully achieved impressive progress towards eventual success.

The process described in the preceding paragraph is not a new idea, but prior to the Caltech MURI, it has not been so clearly formulated and preserved for the entire range of possible dynamic behavior. Until the MURI program began, the simplest—arguably the only—application of these ideas was linear stability. In practice, there are two main strategies for reducing or eliminating combustion instabilities: modify the propellant composition; or revise the geometry of the propellant grain. The latter has been successful often because motors tend typically to be linearly unstable relatively early in a firing when the geometry is still not greatly different from its initial form. On the other hand, nonlinear or pulsed instabilities have been encountered later in firings and notably in slender motors having uniform ports. The advantage of addressing the problem by modifying the composition is that stabilizing process is likely to be active throughout a firing, persisting independently of changes of the internal geometry.

Changes of composition have long been known to have at least two consequences in this context: the energy dissipation associated with the condensed combustion products (mainly aluminum oxide) may be increased; and the

response function may be favorable affected. The reasons for the latter are often not known, but some guidelines based on experience have been formulated.

Thus there are already important reasons for understanding the connections between changes of propellant composition and observable characteristics of the motor dynamics. The justification is even stronger with the introduction of advanced high-energy propellants likely to be operated at pressures higher than has been customary.

Prior to full-scale motor tests, it is not possible to know how a particular propellant/motor design will behave dynamically without analyzing the configuration. It is necessary **but not sufficient** to know the combustion dynamics—the response function—of the propellant. As we emphasized with Figure I-2, instabilities arise as a consequence of the combined dynamics of the propellant combustion and the chamber itself. Hence the analyses and computations of Task III not only serve as a means of assessing the influences of propellant response functions, but also belong to the motor designer's tool kit.

Apart from the motor tests at NAWC, China Lake and at Thiokol, the research in Task III comprised three types of work:

1) Application and further development of an approximate method based on spatial averaging;
2) Analysis of the unsteady vorticity field and its effects in an unstable motor;
3) Large eddy simulations (LES) of steady and unsteady flows in solid rockets, including reduced order models of propellant combustion.

I.3.3.1 Extensions of the Approximate Analysis

The approximate analysis has been developed over more than two decades, with continually improving numerical methods and examination of more processes. During the MURI program almost all the work has been concerned with nonlinear behavior. Two processes not previously treated can now be investigated routinely with the available code:

(i) Velocity coupling; a simplified ad hoc model is being used;
(ii) Influences of noise on linear behavior.

Investigation of velocity coupling has led to two significant results:

1) Pulsed instabilities apparently exist **only** if nonlinear gasdynamics in the chamber is included, with nonlinear velocity coupling having a threshold velocity;
2) Apparently **only** velocity coupling (not pressure coupling) will account for the sensitivity of combustion instabilities to small changes of propellant composition.

These conclusions imply that future work should emphasize modeling and measurement of the response function for velocity coupling.

Given the significant levels of noise in solid rockets, questions have long been raised in respect to the possible effects of random (stochastic) motions, or noise, on dynamical behavior generally, and combustion instabilities in particular. With the approximate method it has been shown that noise is incapable of driving oscillations of significant amplitude. Although noise will excite the acoustic modes in a chamber, the values of the damping characteristics (*i.e.* the "Q" for the oscillations) inferred from experimental data carry uncertainties too large to be of general value. Moreover, the "Q" found in this way involves the effects of driving (the combustion dynamics) and damping. Hence it is not possible in this way to gain unambiguous information about the driving and damping

processes separately. A diagnostics method based on these ideas yields some limited information but does not get at the real problem of determining the response function.

Thus the approximate method now contains explicitly all processes dominant in a solid propellant rocket motor. The ideas and special results are being incorporated in a large code being developed by SEA, Inc. to give the capability of applications to arbitrary grain geometries.

I.3.3.2 Analysis of Generation of Unsteady Vorticity

Special problems arise when oscillations are present in a solid rocket, associated with the flow inward at the boundary. Interactions between that flow, and fluctuations of the velocity and pressure gradient parallel to the boundary, generate unsteady vorticity. The vorticity is converted into the chamber, eventually in actual flows to be dissipated by the action of viscous forces and interactions with turbulence. The details of the generation process are complicated but are important because this process requires work by the acoustic field in the chamber, and therefore contributes to the losses in the balance of energy gains and losses governing the stability of small amplitude motions.

This process first appeared in approximate form as a result found in one-dimensional analysis of stability in a solid rocket; it came to be known as "flow-turning." Rigorous analysis of the phenomenon was initiated by Flandro prior to the MURI program and has continued to the present. At least two other groups not participating in the MURI program have also spent considerable time on solving problems related to that arising in solid rockets. However, the methods and results obtained at UTSI and Caltech (by a student, S. Malhotra, who began his Ph.D. program with Flandro) remains the standard by which other works are to be measured.

Some controversial details of this matter remain, but eventually the results will be incorporated in the computer code being developed by SEA, Inc. That code will replace the Standard Stability Prediction Program (SSPP) which has long been the standard means for analyzing linear stability of flows in solid rockets.

I.3.3.3 Large Eddy Simulations (LES)

Relative to other types of chemical propulsion, the solid rocket community was for many years slow to develop methods of large-scale simulations (*i.e.* applications of computational fluid dynamics (CFD)). Fortunately that situation has changed considerably in the past fifteen years. Especially during the MURI program much progress has been made with simulations of both steady and unsteady flows at Pennsylvania State University. Indeed only ONERA in France has paid serious attention to numerical analysis of unsteady flows, but their emphasis has been different. No group elsewhere has achieved the level of accomplishment reached at Penn State during the MURI program for simulations of unsteady compressible flows with representation of the combustion of the solid propellant.

Probably the main reason for the slow development of CFD in solid rocketry has been the lack of motivation at the design level. Quite simple one-dimensional calculations combined with accumulated experience and full-scale tests have been adequate for satisfactory design and development. Empirical corrections, based on test data, serve well to correct deficiencies—but without improving understanding. That strategy is likely not optimal, either in

respect to performance or, in the long run, cost. With higher energy propellants operating at higher pressures, the traditional approach to design may prove much less effective.

What is certainly true is that expensive problems of combustion instabilities continue to appear during development programs. At about the time the MURI programs began, the THAAD motor exhibited a serious instability, serious enough to threaten the success of the program. Consultation with experts (most were subsequently involved in the Caltech MURI program) led to a 'fix' that was apparently successful. However, the reasons for that success remain somewhat obscure. That program, and of course all others since and in the future, could benefit from a mature approach to treating instabilities. Despite the considerable research and advances during the past forty years, the strategy to treat instabilities contains an unnecessarily large ad hoc component.

With the development of LES applied to solid rockets, the situation just described could be improved considerably. Large-scale computations of the internal flow, including some (simplified) representation of the combustion processes, have two basically important roles in this field:

1) To provide numerical results as accurately as possible for 'real' flows, that is, containing all the processes present in motors, as a tool in the design process; and
2) To provide results serving as the basis for assessing the accuracy of predictions obtained from the approximate method and other analyses.

Reaching the first goal requires considerable further development, mainly for two reasons: extension to truly three-dimensional flows (only two-dimensional and axisymmetric have been treated to date); and accurate representation of the combustion processes is either unknown or causes the problem to become too large for computations with computers currently available.

Several examples of the second purpose of numerical calculations existed before the MURI programs started. During the Caltech MURI, a new important example was completed, demonstrating remarkable agreement between analytical (necessarily containing some approximations) and numerical results for generation of unsteady vorticity. The results were obtained with finite difference analysis of a non-reacting flow, but the general principle is applicable: good comparison between numerical results and those obtained with analysis is an extremely important step to building confidence in our understanding, and ability to predict, the flows internal to a solid rocket motor—steady and unsteady.

With the successes of the Caltech MURI program, we have attained new levels of capability in this field.

I.3.3.4 Analysis of the Turbulent Compressible Flow Adjacent to the Combustion Zone

This work (Beddini, UIUC) was added during the third year of the Caltech MURI program. Although it is concerned with certain aspects of the flow internal to the chamber, its real purpose is to investigate some important aspects of the combustion response function. Penetration of turbulent motions into the combustion zone increases the burn rate, a phenomenon that is particularly important under unsteady conditions.

Results obtained to date suggest that this process may explain the existence of a threshold velocity in velocity coupling. Moreover, the frequency-dependence of turbulence penetration in the combustion zone explains the ability of velocity-coupling to drive higher harmonics, a key feature of previous ad hoc models that explained

nonlinear driving and triggering. Planned merging of this analysis with an analytical model of the response function remains incomplete. The research lies at the interface of Tasks II and III, and is another example of the strong connections and collaborations among the three tasks of the Caltech MURI.

I.4 The Future

Unlike many other fields capturing headlines and imaginations with dizzying advances and apparent breakthroughs, combustion generally, and solid rocketry in particular has for many years seemed relatively slow moving. But what has happened are remarkable gains in solid rocket motor capabilities due to improvements in propellant mechanical properties and ranges of burn rates with favorable ballistics properties, achievements in low smoke/signature and low hazards (intensive munitions, IM). Moreover, environmental safety has improved for field personnel and the public. These developments have perhaps been more important than the slow but steady gains in performance from formulating higher energy propellants, increasing propellant mass fractions, operating at higher design pressures and increasing motor length/diameter ratios.

Progress in the latter respects is generally achieved by designing higher energy propellants to be operated at higher pressures. Experience of a half-century has repeatedly established that with improvements in other capabilities, such as smokelessness, inevitably come problems with combustion instabilities. The potential existence of instabilities has rarely been anticipated so that when oscillations occur in development programs, they are unanticipated, becoming expensive surprises. Why is that the case? Have the MURI programs contributed to improve this situation? Where are the gaps in understanding? What should be done at the research level in the future? We consider briefly those questions in order.

Why are Combustion Instabilities Unanticipated in Development Programs?

A key factor has been a lack of familiarity with and confidence in the existing predictive capabilities, by program managers and project engineers.

The complete answer to this question is complicated because it is necessarily connected to the strategies and tactics of development programs as formulated both by the customers and by the suppliers. Short of those activities, and the capabilities of design staffs, the matter of being able to predict instabilities rests on three prerequisites: the capabilities and state of research; preparation of the achievements of research in a form suitable for practical applications (i.e., the ‘transition’ of research to practice); and conveyance of the results, a process requiring mainly involvement of the responsible people.

Transfer of research in universities to practice has traditionally occurred through meetings, publications, consultants, and employment of recent graduates. The latter is particularly important to sustain and increase the capabilities of engineering staffs in industry and government. In recent years, appropriate use of the SBIR program has become increasingly apparent. This is and will continue to be a significant factor in making available the results of this MURI program. Many of the results of Task III are being incorporated in a computer program being developed by SEA, Inc., expressly for use by industrial and government organizations. Properly used and maintained, the result should go far to help reduce the expensive surprises of combustion instabilities.

In fact, while those surprises have continued to arise, the capability of experts in the field to treat the problems has grown considerably as advances have been made in research. Nevertheless, the ability to *predict* occurrences remains limited by technical problems solvable only by continued research. The necessary research is possible, principally in universities, given the current and foreseeable state of the industry. Continuations of research, new graduates entering the field, and future applications, will serve to improve and bolster confidence in the predictive capabilities so that they will be used to greater effect in respect to cost, schedule, and program success.

How Has the Caltech MURI Contributed to Improving the Capabilities for Addressing Combustion Instabilities in Practice?

Because the Caltech MURI has been a research program, much of the work, even in Task III, may superficially appear somewhat distant from the applications most important to practice. It is important to understand that the more obviously useful results flowing from Task III to practice are achieved only with the foundations existing in Tasks I and II.

The basic results obtained in Task I have flowed directly to the modeling work in Task II. Relevant experimental results as well have been provided by the University of Delaware to an SBIR project developing a combustion model of azido-based propellants such as GAP propellants. Theoretical results obtained at Emory University for rate constants have been distributed throughout the propellant community for computer simulations of combustion of nitramine, nitrato, ADN and AP-based propellants. In all cases, the development of methods has been at least as important as the particular results.

All of the research in the MURI program has been reported at JANNAF meetings as well as published in the appropriate archival journals. Special results have been conveyed privately as well. For example, experience with ultrasonic instrumentation imported from France to the University of Alabama has been shared with Thiokol, Inc. Industry collaborated by providing propellants and supplemental data for research in the MURI Program, and expressed interest in the research, as reflected by their participation in MURI Workshops. The modeling activities in Task II have advanced our mechanistic understandings that will be important for future propellant R&D, and have advanced generally the state of the art. Those successes fit immediately in the corresponding activities carried out in industry and in government laboratories. Particularly noteworthy is work on aluminum combustion carried out at Brigham Young University, and (with funding from other sources) at Baltic State University and the Institute of Chemical Physics in Russia.

Within the next two to three years, substantial impact on industrial capability will be made by a large computer program being developed by SEA, Inc. under an SBIR program. The result will be a greatly expanded and extended version of the Standard Stability Prediction Program (SSPP) currently used throughout the industry. The advances will involve much of the progress achieved in Tasks II and III of the Caltech MURI and will include, among other features, extension to three-dimensional configurations; nonlinear behavior; and provision for accommodating new results for modeling combustion dynamics and response functions as they may become available in the future. All of that means a much superior capability for realistic prediction and interpretation of combustion instabilities in motors. We anticipate that this capability will be received favorably by users in industry, especially as a new

generation of scientists and engineers who are more comfortable with advanced capabilities rise to high positions of responsibility.

Where are the Gaps in Understanding and Capabilities?

As an extended research program coordinating the multidisciplinary work in nine universities (plus seven Russian research groups during the initial three years) the Caltech MURI has had unique success both in advancing the field and in defining clearly where future work should be focussed. Significant progress was achieved both in methods and in producing specific results in all three areas of chemical kinetics and dynamics (Task I); combustion dynamics and modeling (Task II); and in combustor dynamics, for predicting and interpreting combustion instabilities in motors (Task III).

The experimental and modeling work of Tasks I and II have been particularly successful for steady combustion of energetic ingredients and propellants. Together, the analytical methods and the numerical simulations carried out in Tasks II and III have provided an impressively strong and deep foundation for understanding all aspects of the macroscopic dynamical behavior observed in motors.

Then what is incomplete or missing? It is a significant qualitative achievement of the Caltech MURI that we can identify unambiguously those areas of the field that not only merit, but require, continued investigation to provide the complete basis required for efficient design and development of advanced solid propellant propulsion systems in the future.

- The experimental and theoretical methods in Task I have demonstrated their crucial roles in providing fundamental results required for modeling combustion of ingredients and propellants. Their value both in research and eventually as part of practical development activities is clear. Continued support must not be denied.
- Modeling for steady combustion of ingredients, propellants and of aluminum has been advancing steadily and must continue for at least two reasons: 1) to accommodate the results of improved experimental methods as they are developed; and 2) to generate specific results for new materials.

It seems that three areas must be particularly emphasized in future research programs:

1) Heterogeneities of Propellants

Theory, experiment and modeling directed to understanding the consequences of heterogeneities of propellants is clearly an important area for future research. This subject has been receiving growing attention, in other programs whose futures are uncertain. The research is directed not merely to oxidizer particles or energetic powders incorporated as solids in propellant formulations, but also to additives used for ballistic modification (e.g. catalysis) and so-called "stability additives." Stability additives which are thought to work by acoustic damping may actually be working by affecting combustion processes, a matter that warrants further investigation. The additive TiO_2 investigated in the MURI appeared to be both a ballistic modifier and combustion stabilizer, and showed that appropriate research could uncover the mechanism by which these remarkable effects are brought about. More work is needed to broaden the

scope of usable additives for advanced energetic propellants, since additives generally provide a powerful and convenient approach to combustion modifications.

In the Caltech MURI, energetic powder heterogeneities (e.g. due to AP or HMX particles) were treated in spatially averaged fashion in some of the modeling work. However, it is likely that much can be gained from investigation of the statistical nature of propellant compositions, both for steady combustion and for dynamical behavior. A variety of statistical methods are available for applications in future works. Advanced experimental methods, notably laser-based diagnostics, should be developed and applied, but coordinated with theoretical work.

2) Measurement of Response Functions

There seems no doubt that the most important deficiency directly affecting both theoretical and practical treatment of combustion instabilities is the complete inability to obtain *accurate* measures of combustion dynamics—i.e., propellant response functions—for realistic frequencies and pressures. This deficiency clearly has two enormously damaging consequences:

- It is impossible to confirm or deny the results of modeling; and
- It is impossible to carry out with confidence a test program to screen propellants for practical applications.

We cannot over-emphasize the practical importance of the second item. Together, the Caltech MURI and the UIUC MURI programs covered all existing methods for measuring response functions. All have been found wanting in one respect or another.

The most promising course for future research on this problem seems to lie with laser-based diagnostics: **p**lanar **l**aser-**i**nduced **f**luorescence (PLIF); **p**article **i**maging **v**elocimetry (PIV); and **l**aser **D**oppler **v**elocimetry (LDV). The first is receiving very limited short-term support at Caltech for development intended for applications to combustion instabilities. Applicability to acoustically driven atmospheric flames has been proven with the results of the initial tests. The last (LDV) was tried briefly at Princeton University in the early 1980's. The results were promising, but the method was not pursued for reasons largely non-technical.

Laser-based diagnostics of combustion dynamics merits the most serious consideration for new research related to combustion instabilities. Successful results will benefit all chemical propulsion systems.

3) Velocity Coupling

For nearly forty years, velocity coupling has been a troublesome matter in the area of combustion instabilities in solid rockets. The term refers generally to the response of a burning propellant to fluctuations of velocity parallel to the surface. It is therefore a phenomenon peculiar to solid rockets, clearly being involved in the excitation and maintenance of oscillations having velocity components parallel to the surface. Velocity coupling has also been long suspected as a significant, if not essential, factor in the occurrences of pulse instabilities.

Theoretical work in Tasks II and III of the Caltech MURI has established definitely that velocity coupling:

i) is required for existence of pulsed instabilities;

ii) is likely responsible for the greatest sensitivity of combustion instabilities to small changes of propellant composition; and

iii) is the likely mechanism for driving the higher harmonics necessarily part of nonlinear instabilities.

Thus, further investigation of velocity coupling must be a central matter in future work on combustion instabilities. However, modeling of the phenomenon without supporting experimental work would be a vacuous exercise. Therefore we must conclude that the single most important subject for future work on combustion instabilities in solid propellant rockets is development of diagnostics for measuring response functions, for pressure coupling, and especially for velocity coupling. We have considerable qualitative and some quantitative understanding of both pressure and velocity coupling, their common features and their differences. Models exist, but the experimental basis for sorting out true behavior is extremely weak. What is needed is a diagnostic method that is both accurate and flexible. Laser-based diagnostics appear to offer the solution to this impasse and critical need. Funding for their development is not merely merited, but essential to maintaining healthy foundations and hence further advances of solid-propellant rocketry in the U.S.

References

1. Beckstead, M.W. (2000) "An Overview of Combustion Mechanisms anad Flame Structures for Advanced Solid Propellants," *36th AIAA/ASME/SAE/ASEE Joint Propulsion Conference & Exhibit*, AIAA Paper No. 2000-3325 also published in *29th JANNAF Propellant Development & Characterization Meeting*, CPIA #698, 2000, pp 371-397.
2. Beckstead, M.W. Meredith, K.V. and Blomshield, F.S. (2000) "Examples of Unstable Combustion as Measured in T-Burners," *36th AIAA/ASME/SAE/ASEE Joint Propulsion Conference*, AIAA Paper No. 2000-3696.
3. Blomshield, F. (2000) "Summary of Multidisciplinary University research Initiative in Solid Propellant Combustion Instability," *36th AIAA/ASME/SAE/ASEE Joint Propulsion Conference & Exhibit*, AIAA Paper No. 2000-3172.
4. Brewster, M.Q. (2000) "Unsteady Combustion of Solid Propellants—Simplified Kinetics Modeling," *36th AIAA/ASME/SAE/ASEE Joint Propulsion Conference & Exhibit*, AIAA Paper No. 2000-3174.
5. Culick, F.E.C. (2000) "Combustion Instabilities: Mating Dance of Chemical, Combustion, and Combustor Dynamics," *36th AIAA/ASME/SAE/ASEE Joint Propulsion Conference & Exhibit,* July 2000, Huntsville, AL., Paper No. AIAA 2000-3178.
6. Flanagan, J. (2000) "Fundamental Chemistry Studies: MURI – CIT & UIUC," *36th AIAA/ASME/SAE/ASEE Joint Propulsion Conference & Exhibit*, AIAA Paper No. 2000-3171.
7. Yang, V. (2000) "Combustion Dynamics of Solid Rockets," *36th AIAA/ASME/SAE/ASEE Joint Propulsion Conference & Exhibit*, AIAA Paper No. 2000-3177.

TASK I

FUNDAMENTAL CHEMISTRY AND CHEMICAL DYNAMICS

Thomas B. Brill, Team Leader

1
TASK I — FUNDAMENTAL CHEMISTRY AND CHEMICAL DYNAMICS

1.1 Survey of Propellant Ingredients (Flanagan and Waesche)

The development of modern solid propellants can be linked to chemical advancements of the middle-to-late 19th century, in particular nitration of hydroxyl groups to form nitrate esters such as nitroglycerin (NG) and nitrocellulose (NC). Double-base (DB) propellants derived from this process now include cast (CDB), extruded (EDB), composite-modified (CMDB), elastomer-modified CMDB (EMCMDB), and cross-linked (XLDB) propellants. The original double-base formulations were produced by extrusion, the diameter of grains being limited by the presses available. During the 1940's, a gelation/slurry process was developed[1] that allowed casting of grains and thereby eliminated the massive presses needed to prepare high-density propellants. The CMDB formulations incorporate oxidizers and high-energy additives as a means of increasing propellant performance, while the EMCDB formulations incorporate an elastomer into the propellant matrix as a means of improving low-temperature physical properties.

Composite propellants incorporating a binder-fuel, an oxidizer or monopropellant, and various additives were developed in the second half of the 20th Century. The earliest such propellants were asphalt-based developed at GALCIT with oxidizers such as potassium perchlorate and potassium nitrate. The same team also employed polysulfide binders, such as LP-33, to enable higher solids loading. More useful propellants (i. e., higher performance, improved physical properties) evolved, once polyester- and polyether-based polyurethanes became available for use in conjunction with oxidizers such as ammonium nitrate and, especially, ammonium perchlorate (AP). AP is still the most widely used oxidizer owing to its availability, cost, and high oxygen content. Carboxyl-terminated materials, such as the copolymer of acrylic acid and butadiene (PBAA) and the copolymer of acrylonitrile and butadiene (PBAN), were developed next; these are still employed in certain systems, such as the Space Shuttle boosters. The polybutadienes are the basis of most modern composite solid propellants; hydroxyl-terminated polybutadiene (HTPB) being currently the most widely used owing to its low viscosity and attendant ability to produce propellants with high solids contents and excellent physical properties. Davenas[2] and Singh[3] discuss these classes of solid propellants and many of the topics that follow.

Metallic fuels are added to increase specific impulse (I_{sp}). The focus is primarily on aluminum because it yields the second highest volumetric heat release through Al_2O_3 formation behind beryllium and the attendant formation of BeO.[4] Beryllium propellants are now generally not viable because of the extremely toxic combustion products, in addition to the reduced density of such propellants. Although boron appears to be an attractive energetic candidate, its oxidation does not yield B_2O_3 alone, owing to the equilibrium with gaseous HBO_2 and an attendant decrease in heat release. Zirconium, which yields ZrO_2, may be employed in systems that require higher overall propellant density, because zirconium powder is nearly 2.5 times denser than Al powder. For some applications, this density increase may overcome the lower energy release associated with the production of ZrO_2 relative to the formation of Al_2O_3. Magnesium has been considered as a partial replacement for Al, owing to environmental factors mentioned below; in addition, it has been found that complete combustion of Mg is relatively easy to achieve. Metal hydrides such as AlH_3, BeH_2, and ZrH_2 appear to be promising fuels owing to their high heat release, but virtually all metallic

hydrides are incompatible with the polymers and/or the curing agents employed in present-day binders. Their application to propellants is severely limited without further developments in coating technology.

Most of the currently utilized solid propellants are based on C-H-O-N materials or the perchlorate ion (ClO_4^-) and Al, as mentioned above. The theoretical I_{sp} of these propellants along with certain propellants that contain fluorine is discussed by Lempert and co-workers.[5,6]

High media visibility of the Space Shuttle Booster has raised environmental questions about the use of AP-based systems. Discussion of these issues is available.[7] Elimination of HCl as a product is a major environmental objective. If needed, this goal might eventually be achieved by the use of alternative primary oxidizers[8] or by chemically binding the HCl by a 1:1 molar substitution of AP by sodium nitrate to form NaCl upon combustion. Another method under consideration is to bind Cl as $MgCl_2$ through the partial substitution of Al by Mg.

Finally, small amounts of additives are sometimes incorporated to influence a specific ballistic effect. The a priori identification of such additives was a major goal of this MURI program. For instance, catalysts may accelerate (but sometimes suppress) the overall combustion rate of the base propellant. In addition, catalysts often reduce the sensitivity of combustion rate to changes in combustion pressure or propellant temperature. These catalysts or suppressants can be solids, such as fine Fe_2O_3, or liquids, such as *n*-butyl ferrocene and selected carboranes. Atwood and co-workers[9] overviewed the characteristics of the mostly widely utilized catalysts on the combustion of solid oxidizers. Another important use of additives is to eliminate the phenomenon known as "combustion instability", which is characterized by high-amplitude oscillations in the chamber pressure. It has been demonstrated[10] that incorporation of a small amount of the appropriate size of Al can suppress such instability.

Advanced solid propellant ingredients incorporate new oxidizers and/or use new binder/plasticizers. Some of these are shown in Fig. 1. Both double-base and composite propellants currently in use sometimes incorporate the two well-known cyclic nitramines, RDX and HMX. Their primary value is to optimize oxygen balance, while increasing the heat of formation, thereby maximizing the formulation I_{sp}. In the past decade hexanitrohexazaisowurtzitane (HNIW), a cage nitramine, has attracted much attention.[11,12] In addition to an improved oxygen balance, HNIW possesses a higher density (2.02 g/cm^3) than HMX (1.908 g/cm^3), and a higher energy content based upon the heat of formation. The oxidizer attracting the second most attention as a new propellant ingredient is ammonium dinitramide (ADN). ADN was first described by Pak.[13] Tartakovsky, et al.,[14] surveyed the synthesis of dinitramide salts. However, the utility and long-term viability of ADN is debatable, owing to questions regarding control of the burning rate and impact sensitivity of propellants containing significant amounts of ADN. Hydrazinium nitroformate (HNF)[15] has resurfaced after forty years as a candidate oxidizer.[16] Considerable progress has been made largely by producing desirable crystal properties and attendant reduced sensitivity to impact and friction, but it is still too early to declare HNF to be a viable propellant ingredient. For instance, the high sensitivity of burning rate to pressure[17] remains an issue. Octanitrocubane (ONC) was recently achieved Eaton, et al.[18] The density (1.99 g/cm^3) was lower than predicted and additional work will be required to determine if the energy release is close to theoretical predictions.[19] The largest volume of research on high-energy ingredients in the past decade has been centered upon high-nitrogen heterocyclics, such as triazoles, tetrazoles, and furazans, some of which are discussed in the next section. The liquid and solid furazans have drawn the greatest

attention. These compounds demonstrate a relation of burning rate to molecular structure that could be quite valuable.[20-22] Sheremetev[23] and Tselinskii, et al.,[24] have summarized these areas. Another new oxidizer, diaminodintroethylene (DADNE), has potential for many applications.[25] The incorporation of the difluoroamino (-NF_2) group, a focus of extensive research in the 1960s[26], has resurfaced in syntheses of cyclic[27] and linear[28] nitramines. Possible combinations of –NF_2 with other energetic moieties have been reported.[29]

Many families of new advanced oxidizers are represented by the structure, $R[CH_2X]_2$, where X can be: a) -$C(NO_2)_3$; b) -$C(NO_2)_2NF_2$; c) -$C(NO_2)_2CH_2N_3$; d) -$C(NO_2)_2N_3$; e) -$C(NO_2)_2C(NO_2)_3$; and f) -$C(NO_2)_2F$. The literature is rich with information on these compounds, but the most recent work is on types (c) and (d).[30-32] The pentanitro-terminated materials (e) have been described.[33] Agrawal[34] recently surveyed this area.

A considerable effort has been devoted for two decades to develop new energetic polymers. Glycidyl azide polymer (GAP)[35] has been most thoroughly investigated as a result of its high density (1.3 gm/cm^3), positive heat of formation, and unique ability to desensitize NG.[36-38] GAP has been employed both as a binder and as an energetic plasticizer.

Many other promising energetic materials are now reaching scale-up status and D'Andrea[39] has broadly described several polymers in terms of systems. The two main categories of polymers are: a) H-$[O\text{-}CH_2\text{-}CR_1R_2\text{-}CH_2]_x$-OH {oxetanes}, where R_1=R_2= CH_2N_3 {BAMO}, R_1=CH_3, R_2=CH_2N_3 {AMMO}, and R_1= CH_2ONO_2, R_2= CH_3 {NMMO}; and b) H-$[O\text{-}CR_1R_2\text{-}CH_2]_x$-OH where R_1=H, R_2= CH_2N_3 {GAP}, R_1=H, R_2= CH_2ONO_2 {PGLYN or PGN}, and R_1= CN, R_2= NF_2 {PCDE}. The status of category (b) was recently given.[40] Two additional -NF_2 polymers of note are category (a)[41] where R_1=R_2= CH_2NF_2 and (b), where R_1=H and R_2= $CH_2\text{-}O\text{-}CH_2\text{-}CH_2\text{-}CH_2\text{-}C(NF_2)_2\text{-}CH_3$.[42] The utilization of polymers that contain substantial fluorine facilitates the use of boron, because BOF will be formed instead of the mixture of B_2O_3 and HBO_2 discussed earlier. Additionally, the reduction in two-phase flow losses in the nozzle, resulting from the formation of gaseous AlF rather than solid Al_2O_3, yields a higher overall I_{sp}.

New opportunities to advance the field of rocket propulsion are possible when the important combustion characteristics can be predicted from the composition of the propellant. Understanding the relation between the decomposition of energetic materials and their combustion characteristics is central to this goal.[43] The tendency to form particular species in suitable amounts in the surface reaction zone is required knowledge in the model of combustion and combustion stability. Thus, detailed studies of the condensed phase kinetics and mechanism, which is discussed next, forms a molecular foundation for the initiating processes.

1.2 Decomposition of Energetic Materials and Formulations

1.2.1 Low Heating Rates (Wight)

The decomposition chemistry of energetic materials and their formulations is an essential component of the combustion process. Nitramines primarily will be used to illustrate the main points. Experiments carried out at slow heating rates provide information at a moderate level of detail. For example, it is possible to make detailed reaction rate measurements because the temperature of the sample is well known. Also, it is possible to use species-

selective detection methods so that reaction rates for specific product channels can be measured independently. These types of studies are well-suited to determining reaction rates in hazards situations such as under slow cookoff conditions. This is the type of accident scenario that represents the highest danger of violent reaction, including the possibility of a deflagration-to-detonation (DDT) transition as the reaction wave propagates through thermally damaged material. A disadvantage of the slow heating techniques is that the reaction mechanism may be different for slow and fast heating events (discussed below), so that reaction kinetics determined under slow heating conditions might not be able to predict the rates of fast reactions that occur under combustion conditions.

Numerous authors have investigated the rates and mechanisms of decomposition of RDX and HMX under slow heating conditions.[44-48] Of particular note is the simultaneous thermogravimetric modulated beam mass spectrometry (STMBMS) technique. This instrument allows the rate of selected gas phase product formation to be measured as a function of time. Detailed descriptions of the apparatus and data collection procedures have been described by Behrens, et al.[49-51] The results of the STMBMS analysis show that RDX and HMX have similar decomposition mechanisms as well as similar degradation products.[49,50,52-57] The common degradation products for both RDX and HMX observed via STMBMS are N_2O, CH_2O, NO, H_2O, and CH_3NHCHO. Behrens et al., have also carried out experiments on isotopically labeled materials in order to gain additional mechanistic information about which reaction products arise from labeled functional groups in the starting material.[53,55,56]

Evidence suggests that the first observable product is N_2O. Detecting the degradation products during decomposition is vital because it allows one to determine the specific bonds that are breaking as well as the order in which they occur. From this data, one can make kinetic assignments to specific bonds, which aids in determining the overall degradation mechanism. Using model-fitting techniques, for example, Behrens calculated an activation energy of 48 Kcal mol^{-1} for the initial decomposition region in HMX.[58] Since N_2O is the first observable product, this suggests that the N-N bond is the weakest in the molecule and that approximately 47.5 Kcal mol^{-1} are needed to begin decomposition at this site.

One of the challenges of studying reaction kinetics of solid materials is that the reaction rate laws frequently do not obey simple order-n kinetic expressions. This is because unlike the gas phase, elementary steps of the reaction sequence do not take place in isolated binary collisions. Moreover, the reaction environment may be altered dramatically at the ending stages of reaction compared with the starting material.

In order to address this issue, model-free kinetic methods have been developed to describe rates of reactions without making assumptions about the functional form of the reaction model. Thus far, the applications of these kinetic analysis methods have been applied to globally measured reaction rates, such as measurements of gas formation rate by thermogravimetric analysis (TGA) or heat production by differential scanning calorimetry (DSC). The TGA method utilizes a sensitive balance mechanism that monitors mass loss as a function of temperature. The DSC, in turn, measures heat flow either into or out of a sample during the degradation process, thereby providing information on the endo/exothermicity of the sample. One of the big advantages of the model-free methods of kinetic analysis is that they can be used to determine the kinetics of composite explosives and propellants, which are usually mixtures of oxidizers, fuels, polymeric binders, plasticizers and cross-linking agents. These chemically

complex mixtures can exhibit several successive stages of reaction that may overlap one another and therefore be difficult to analyze using traditional model-fitting methods.

One specific propellant sample that was studied by Peterson and Wight[59] consisted of 83% HMX and 17% binder,[60] of which HTPB was a major component. This analysis showed that the propellant degraded in a three-step process. The first step was attributed primarily to the binder material. The second step was the HMX degradation, and the third step was due to the HTPB binder additive. It was also noted that the addition of these specific binder materials caused some of the HMX to degrade at a lower than normal temperature.

Kinetic analysis was conducted on the propellant using a model-free isoconversional method that allows one to determine activation energies as a function of degradation.[61-63] This method is particularly useful in that it permits one to track the activation energy changes during the entire decomposition process. This ultimately allows for a more kinetically accurate assignment to degradation steps and processes. The results showed a nearly constant energy value of 6 Kcal mol^{-1} for the first degradation step. The HMX section had an average value of 29 Kcal mol^{-1}, while the final HTPB step showed values near 60 Kcal mol^{-1}. These HTPB energies were compared to those for a pure HTPB sample and found to be in excellent agreement.

The slow heating methods can provide a high degree of detailed information about both the mechanisms and rates of reaction of chemically complex composite propellants and explosives. The results can be used to make predictions of accident scenarios that involve slow heating, and in some cases may also be extrapolated to high temperature to predict combustion behavior.

1.2.2 High Heating Rates (Brill)

The combustion-like pyrolysis chemistry of energetic materials liberates products, which initiated the flame zone. High rate pyrolysis studies, which emphasize the condensed phase, can be grouped according to the method of heating: infrared laser and hot surface. A number of variations of these two methods have been developed so this focus here will be on the developments in the past ten years aimed at understanding the mechanisms and kinetics of combustion of energetic materials.

The CO_2 laser can be used in the pulsed or continuous wave mode to decompose the surface layer at heating rates on the order of 10^7 K/sec. Two advantages of this method are that very fast heating can be achieved and chemical diagnostic techniques can be use in conjunction to determine the products that are formed. A disadvantage is that independent specification of the heating rate and final temperature is not achieved so that kinetic determinations are difficult. Litzinger's group has discussed the chemical and physical processes during laser heating of RDX.[64]

Wight, et al.,[65,66] employed a single laser pulse to heat a film of RDX sandwiched between two transparent windows at 77 K. By the use of FTIR spectroscopy, this work demonstrated that cleavage of the $N\text{-}NO_2$ bond is the initial step in fast decomposition of RDX. The same method has been applied to determine the products of GAP and PGN.[67] Likewise, Haas, et al.[68,69] used a used a high power, pulsed CO_2 laser to shock heat GAP. Post-reaction determination of the solid and gaseous products was made by FTIR and GC-MS methods. Litzinger, et al.,[70,71] employed a CW CO_2 laser to assist the decomposition and combustion of RDX and HMX while using a triple

quadrupole mass spectrometer and a thermocouple to perform species and temperature measurements. Their data are particularly helpful for comparing the products of pyrolysis to those from laser assisted combustion.

Hot surface or filament heating methods offer the advantage of fast pyrolysis with independent control over the heating rate and final temperature. The sacrifice is that the heating rates are lower than are possible with the CO_2 laser. To date the most widely applied method of this type is T-jump/FTIR spectroscopy.[72] The analogous technique with Raman spectroscopy has recently been reported.[73] Modeling of the platinium filament, sample, and surroundings as a system reveals that heating rates up to 600 K/sec are achievable while stopping and holding at a known and adjustable temperature.[74,75] The control voltage of the filament can be recorded simultaneously with rapid-scan FTIR spectra of the evolved products to obtain thermochemical information, product sequencing, and formation rates. Catalytic effects of the filament have been shown to be negligible.[76] Kim and Thynell[77] devised an variation on this method in which a heated cavity is employed in place of the filament. This approach improves the heat transfer to the sample but sacrifices on the opportunity to detect the earliest quenched products.

T-Jump/FTIR spectroscopy has provided mechanistic information, for example, on HMX and RDX,[78] AP,[76] ADN,[79] DNNC,[80] EDDN,[81] HNF,[82] metal salts of NTO,[83] aminotetrazoles,[22] and substituted furazans.[84] It has been applied to obtain kinetic information on HMX and RDX,[85] poly(styrene peroxide),[86] HTPB,[87] polyethylene glycol,[88] cellulose acetate butyrate (CAB),[89] and GAP.[90] Mixtures of energetic materials are among the more difficult systems to study, but results have been obtained on AP/HTPB,[91] RDX/CAB,[92] and RDX/GAP.[93] The products are quantified by multivariate analysis[94] enabling complex mixtures of products to be resolved. Good elemental atom balances can be obtained by combining the IR and Raman methods.[73]

Insight has been gained on RDX and HMX by the use of T-Jump/FTIR spectroscopy.[75,78,89,96] The decomposition channels for at flash heating conditions appear to be represented by the global reactions 1 and 2, which together are approximately thermally neutral.[78] The reaction 1 is favored at lower temperatures whereas reaction 2 dominates at higher temperatures. Consistent with lower heating rate results,[52,54] the nitrogen oxides are liberated before the other products.

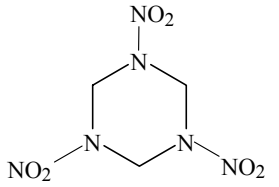

$$\rightarrow [N_2O + CH_2O] \times 3 \qquad (1)$$

$$\rightarrow [NO_2\,(HONO) + HCN] \times 3 \qquad (2)$$

The Arrhenius parameters for reactions 1 and 2 have been extracted from these data[85] and used in combustion models in which detailed chemistry has been incorporated. Heat was proposed to be generated in bubbles by reaction 3 with a heat of reaction of about –44 Kcal mol^{-1}.

$$CH_2O + NO_2 \longrightarrow NO + CO + H_2O \qquad (3)$$

In addition to the "major" products from RDX (NO_2, NO, N_2O, CO, CO_2, CH_2O, HCN, H_2O, etc.), the approximate identity and temperature dependence of volatile "minor" products (defined as <4% mole fraction) from thermal decomposition RDX have been determined by multivariate regression in the 265–325°C range.[95] The gaseous phase products include HNCO, HONO, hexahydro-1-nitroso-3,5-dinitro-*s*-triazine, a triazine modeled as *s*-

triazine, C-hydroxyl-N-methylformamide, and both RDX vapor and RDX aerosol. The relation between this work and previous studies of slower decomposition of RDX[49,52-57] and on quenched burning of RDX-containing propellants[96,97] enables the description of products from RDX decomposition to be unified over a wide range of heating and temperature conditions.

The identity of the species liberated by slow and fast decomposition of the condensed along with details, such as the temperature and pressure dependencies of their concentrations and rates of liberation to the primary reaction zone of the flame, are essential to modeling steady and transient combustion. The field of condensed phase decomposition kinetics and mechanisms is, however, far from a satisfactory state in terms of the necessary details. The phase heterogeneity, spatially small reaction zone, and temperature and concentration gradients complicate the acquisition of detailed information. By contrast, the gas phase chemistry is more tractably investigated, both experimentally and computationally.

1.3 Effects of Temperature and Pressure on Exothermic Reactions near Propellant Surfaces (Lin)

Pyrolysis and evaporation leads to liberation of gaseous products from the propellant surface. The reactions involving these large and mid-size free radicals and molecules dominate the early stages of propellant flame zone. The rates of some of these reactions can be determined experimentally. For example, a laser provides an intense tunable light source between 200 and 800 nm applicable for millisecond to nanosecond chemical kinetic methods including discharge-flow,[98] high-temperature fast flow,[99] and dual flash pump-probe.[100] The various methods for generation and detection of reactive intermediates in the gas phase are described by Setzer.[101] The availability of the broadly tunable CW ring dye laser and broad-beam, rare-gas excimer lasers has reinvigorated the shock tube as the most effective high-temperature reactor. Various free radicals can be selectively generated by pulsed photolysis behind incident or reflected shock waves at practically any temperatures above 800K using diagnostic methods such as atomic resonance and resonant laser absorption,[102] laser induced fluorescence and, potentially, the ultra-sensitive cavity ringdown absorption technique.[103]

Unfortunately, most of the radicals, such as $HNNO_x$ and CH_2NNO_x (x=1,2) from nitramines, do not fluoresce from their excited states (which are also unknown experimentally and theoretically). Accordingly, they cannot be readily detected by optical diagnostics under combustion conditions. In addition, these reactive intermediates are difficult to prepare neatly in the laboratory for kinetic studies. Theoretical prediction of their thermal energetics and decomposition mechanisms becomes the only means to obtain their kinetic parameters over a wide range of temperature and pressure useful for computer simulation of burning and stability characteristics.

The focus of this section is on recent calculations of the potential energy surfaces using the modified Gaussian-2 (G2M) method.[104] The method employed a series of calculations to improve electron correlation and the expansion of basis sets using the geometry optimized with a hybrid density function theory (typically the B3LYP method with the 6-311G(d,p) Gaussian basis set). The predicted G2M energies for systems containing as many as 8-heavy atoms approximate the values one would obtain at the CCSD(T)/6-311+(3df,2p) level of theory.[104] The

G2M method predicts the heats of atomization for the 32 first and second row compounds employed in the original G2 method by Pople and coworkers[105] with about 1 kcal/mol absolute deviation from experimental values.

The major reaction paths for all radical-radical reactions take place via long-lived intermediates, usually without well-defined transition states. Accordingly, the computationally simple transition-state theory (TST),[106] which is quite useful in predicting direct metathetical (or exchange) reaction rates, is no longer applicable in this case. In order to circumvent the difficulty, the "transition state" for a barrierless radical-radical reaction was defined canonically for each temperature at the separation with maximum Gibbs free energy calculated with the geometry and vibrational frequencies of the association complex predicted with a full quantum calculation.

These molecular parameters including energy, 3N-7 (or 3N-6 for a linear complex) vibrational frequencies and moments of inertia, were then employed for multichannel statistical theory (such as Rice-Ramsperger-Kassel-Marcus or RRKM)[106] calculations to predict rate constants for all individual product channels. A detailed description of this approach is available.[107-111]

Elementary processes relevant to RDX, HMX and ADN decomposition reactions near the burning surfaces are briefly summarized in two subsections; one for the unimolecular decomposition reactions and related reverse radical association reactions and the other for bimolecular processes not directly related to unimolecular reaction systems.

Unimolecular and related reverse reactions illustrated by 4–6 commonly take place in high-temperature combustion reactions:

$$AB \underset{+M}{\overset{+M}{\rightleftharpoons}} AB^{\surd} \longrightarrow A + B \qquad \text{(unimolecular decomposition)} \qquad (4)$$

$$A + B \rightleftharpoons AB^{\surd} \longrightarrow AB\,(+M) \qquad \text{(association/stabilization)}$$

$$\longrightarrow C + D \qquad \text{(association/decomposition)} \qquad (5)$$

or

$$A + B \rightleftharpoons BA^{\surd} \longrightarrow BA\,(+M)$$

$$\longrightarrow E + F \qquad (6)$$

where "√" represents internal excitation resulting from collisional activation (AB + M) or chemical activation (A + B). AB and BA are two structural isomers. A specific example of 4–6 is given below for the decomposition of the first radical intermediate produced by the decomposition of dinitramidic acid 7–9

$$HNNO_2 \underset{+M}{\overset{+M}{\rightleftharpoons}} HNNO_2^{\surd} \longrightarrow NH + NO_2 \qquad (7)$$

$$HN + NO_2 \rightleftharpoons HNNO_2^{\surd} \longrightarrow HNNO_2\,(+M)$$

$$\longrightarrow NN(O)OH^{\surd} \longrightarrow N_2O + OH \qquad (8)$$

$$NH + NO_2 \rightleftharpoons HNONO^{\surd} \longrightarrow HNONO\,(+M)$$

$$\longrightarrow HNO + NO \qquad (9)$$

These reactions are pivotal to the initiation of the ADN combustion reaction.

The rate constants calculated with canonical variational RRKM theory for the unimolecular decomposition of $HN(NO_2)_2$ and $HNNO_2$, and the bimolecular NH + NO_2 reactions given above are listed in Table 1. These rate constants have been employed for kinetic modeling of ADN decomposition (*e.g.* Fig. 2) under low-pressure conditions.[112]

Similar calculations have been performed for the unimolecular decomposition of CH_2NO_x (x=1,2) and related bimolecular reactions, CH_2N + NO_x, as well as the CH_2N + OH reaction. The results of these calculations are also summarized in Table 1.

Many bimolecular reactions involving HNO, HONO and HNO_3 are key reactive intermediates in nitramine and AP combustion reactions. Many of these reactions not only take place by the simple metathetical (*i.e.*, direct exchange) mechanism but also by multiple indirect complex-forming mechanisms. For example, the reaction of H with HONO was found to occur primarily by indirect addition/decomposition processes,[113] instead of the commonly assumed direct abstraction process 10–12.

$$H + HONO \longrightarrow H_2 + NO_2 \qquad \text{(direct abstraction)} \qquad (10)$$

$$\rightleftharpoons HON(O)H^{\surd} \longrightarrow HNO + OH \qquad \text{(addition/decomposition)} \qquad (11)$$

$$\rightleftharpoons N(OH)_2{}^{\surd} \longrightarrow NO + H_2O \qquad \text{(addition/decomposition)} \qquad (12)$$

In the above mechanism, both isomers of HONO (cis and trans) are involved, but the cis-isomer generally provides lower energy paths to the products listed above. Similar complex mechanisms were found to hold for several other reactions: HNO + NO_2,[113] OH + HONO,[114] OH + HNO_3,[115] HONO + HONO,[116] and HONO + HCl,[117] among others. The results for these and other reactions computed with TST (for direct reactions) and RRKM (for complex-forming reactions) are summarized in Table 2 for kinetic modeling applications. Currently the NIST kinetics database is an important source of other elementary reaction rate constants.[121]

This section is intended as a brief introduction to the power of computational methods to sort out near surface gas phase flame reactions of energetic materials. Obviously the subject is complex and the number of flame reactions in large. As this field expands the rate constants can be used in chemically based flame zone models of combustion.

1.4 Modeling Kinetic Mechanisms Within the Combustion Process (Beckstead)

This Section describes the approaches to explore, utilize and model the different kinetic mechanisms that are used in modeling the combustion of a propellant ingredient. The combustion process in solid ingredients is a complex combination of reactions occurring below the burning surface (see Section 1.2) and above it in the gas phase (see Section 1.3). General observations are that many propellant ingredients melt during combustion, forming a thin liquid layer on the burning surface. Condensed phase reactions can occur in that liquid layer forming bubbles, in which gas reactions can also subsequently occur. Figure 3 is a schematic of the process showing the non-reacting solid on the left, and progressing through the liquid melt layer and finally the gas. The process generates a very frothy mixture of liquid, bubbles, gas and droplets, making the division between gas and condensed phases (*i.e.* the

burning "surface") difficult to define or measure. Also, the dimensions of the phases vary with pressure. For example at one atm, the liquid layer is ~ 70μm thick for HMX and ~130 μm for RDX, while the gas phase reaches equilibrium within ~4mm for HMX and ~1 mm for RDX.[122,123] At higher pressures (70 to 100 atm) the melt layer is less than 20 μm and the equilibrium temperature is reached within ~100–200 μm.

Developing a mathematical model to describe the process in Fig. 3 is a challenge. As previously discussed, experimental data relating to the kinetics of the reactions occurring in the liquid layer along with the physical properties are very difficult to obtain due to the small size of the layer and the inherent transient nature of species in that layer. The reactions in the gas phase are more amenable to diagnosis as many of them can be measured independently. Also, *ab initio* calculations of reaction paths offer considerable promise.

1.4.1 Utilization of Condensed Phase Kinetics and Mechanisms

Both HMX and RDX have a relatively well-defined melting temperature (~553-556 K for HMX and ~478 K for RDX). Below the melting point it is usually assumed that solid phase reactions can be neglected because the gas and liquid phase reactions will be much faster than those in the solid phase. Above the melting point, it is assumed that decomposition reactions begin, which is the start of the combustion process. Thus, in modeling the condensed phase reactions, the process is normally first started by an initial bond breaking reaction. This is generally true, but in the case of AP, one modeling study concluded that solid phase reactions had to be accounted for[124] to determine the observed combustion behavior. Also, in the case of an energetic polymer, such as GAP, the melting point is not well defined. Thus, an arbitrary, low temperature must be selected for modeling purposes to correspond to the onset of reactions and below which reactions will be negligible.

The condensed phase processes discussed in Section 1.2.2 for HMX and RDX are described in more detail by Brill[83] and involve primarily reactions 1–3. The final step added to Brill's condensed phase mechanism was the evaporation of the pure liquid propellant (reaction 13). This overall formalism has been used extensively in recent combustion models.

$$\mathrm{HMX(RDX)_{(l)} \quad \Rightarrow \quad HMX(RDX)_{(g)}} \tag{13}$$

Determining appropriate kinetic parameters for reaction steps is usually much more difficult than Proposing reaction steps. To help define the kinetic parameters for reaction 2, Brill proposed using kinetic data from a simple linear nitramine, dimethylnitramine (DMN),[85] which decomposes to form NO_2 and HCN, similar to what is proposed for reaction 2. The rate parameters reported by Lloyd, *et al.,*[125] were reasoned by Brill to represent the best estimate of the N-NO_2 homolysis rate.

To evaluate the rate parameters for reaction 1 Brill used his T-Jump/FTIR experiment to measure the species evolving from heated RDX and HMX samples.[78] This was necessary as there are no known simple nitramines that form just N_2O and CH_2O. From his data he was able to determine a N_2O/NO_2 ratio for both RDX and HMX. In order to get the temperature dependence of reaction 1, Brill proposed that the measured N_2O/NO_2 ratio should closely follow the ratio of the kinetic rate constant for reaction 1 to that of reaction 2. Therefore, Brill used the rate expression for reaction 2 and the measured N_2O/NO_2 ratio to determine the kinetic parameters for reaction 1.

Kinetic rate constants for reaction 3 (the heat-generating $CH_2O + NO_2$ reaction) have been determined by three different sources,[126,127,128] again, with relatively large differences in the reported values. Brill chose the kinetic rate parameters from Lin, *et al.,*[128] because their data covered the largest temperature interval in their experiments. How to apply a gas phase reaction within the condensed phase is a concern. If the decomposition products are treated as bubble forming gases in the liquid phase, then the pressure inside the bubbles would be greater than the ambient pressure. It is not certain how great a pressure difference exists in these bubbles, so the pressure is generally approximated as that of the ambient pressure.

The final step in the Brill mechanism is the evaporation of the liquid RDX or HMX. Because both RDX and HMX begin reacting once they melt, it is very difficult to get experimental vapor pressure data. However, solid-vapor equilibrium data (*i.e.* sublimation data) are reported for RDX[129-131] and HMX.[129,130,132] Using the heat of sublimation and the Van't Hoff equation, the vapor pressure of HMX and RDX can be approximated for conditions above the melting point.[133] The sublimation data and the extrapolated vapor pressure curves for both RDX and HMX. The vapor pressure of RDX is observed to be several orders of magnitude higher than that of HMX, and thus can be expected to vaporize much more readily than HMX. Within the calculations using the condensed phase mechanism, the evaporation step is much more predominant in RDX than in HMX.

Analogous condensed phase mechanisms have been developed in conjunction with models for AP, GAP, ADN and various combinations of ingredients as described in Section 1.2.

1.4.2 Utilization of Gas Phase Mechanisms

During the past two decades extensive progress has been made in the development of detailed gas phase mechanisms for combustion processes[134] So much so, that a standard mechanism for hydrocarbon (methane or natural gas) combustion with 325 steps and 53 species can be downloaded from the web. This is the GRI (Gas Research Institute) mechanism[135] that has become a standard. Parallel to the development of the hydrocarbon mechanism, work has proceeded to develop analogous mechanisms for propellant ingredients. The most extensive is work that was initiated by Melius[136-138] during 1986–1990 for RDX. His work was expanded by Yetter and Dryer[139] culminating in a "standard" mechanism for RDX published and distributed in 1995, consisting of 232 reaction steps and 45 species.[140] The Yetter mechanism has provided the basis for most of the work reported in this document. Both the hydrocarbon and the propellant work utilize the CHEMKIN format and libraries,[141-143] which have become standards for analyzing multi-step gas phase chemical reactions.

The reaction species leaving the burning surface are usually relatively complex, *i.e.* three or more atoms. Further from the surface, as the reactions start to approach equilibrium, the reactants and reactions become typical of combustion in general, *i.e.* species such as NO, OH, N_2O, CO, etc. Reactions involving many of these species are also involved in hydrocarbon combustion and many can be found in the GRI mechanism. Thus, the difficult work is in characterizing the near surface reactions. This has been part of the MURI focus and was discussed by Lin in Section 1.3 above. As part of the current program a sensitivity analysis was done for the RDX mechanism, identifying the most sensitive reactions within the mechanism. These in turn were the focus of study as part of the

MURI program. In addition to expanding the Yetter RDX mechanism, mechanisms were developed for HMX, AP, GAP, ADN and some combinations of ingredients.

Table 1. Rate Constants Predicted for Unimolecular and Related Reverse Reactions.[a]

Reaction	T/K	P/Atm	k
$HN(NO_2)_2 \rightarrow HNNO+NO_2$	300-1000	200	6.9×10^{16} exp(-18,300/T)
$HNNO_2 \rightarrow NH+NO_2$	500-2000	200	7.3×10^{44} $T^{-9.3}$exp(-24,100/T)
$CN_2NNO_2 \rightarrow CH_2N+NO_2$	500-1500	200	7.3×10^{57} $T^{-11.0}$ exp(-26,100/T)
$\rightarrow HCN+HONO$			1.5×10^{11} exp(-14,200/T)
$\rightarrow CH_2O+N_2O$			2.9×10^{9} exp(-16,400/T)
$CH_2NO \rightarrow HCN+OH$	200-2000	200	1.8×10^{10} exp(-25,600/T)
$CH_2N \rightarrow HCN+H$	500-2000	200	1.5×10^{12} exp(-14,000/T)
$CH_2N+M \rightarrow HCN+H+M$	500-2000	0[b]	3.8×10^{11} $T^{1.0}$ exp(-10,800/T)
$NH+NO \rightarrow H+N_2O$	300-3000	200	7.1×10^{9} $T^{0.83}$ exp(1,100/T)
$\rightarrow OH+N_2$			1.8×10^{9} $T^{0.83}$ exp(1,100/T)
$NH+NO_2 \rightarrow HNNO_2$	300-3000	∞ [c]	1.4×10^{16} $T^{-0.73}$ exp(-617/T)
		0	0
$\rightarrow N_2O+OH$	300-3000	0	2.1×10^{13} $T^{-0.49}$ exp(360/T)
		∞ [c]	0
$NH+NO_2 \rightarrow HNO+NO$	300-3000	<200	1.3×10^{6} $T^{2.0}$ exp(1,180/T)
$CH_2N+NO \rightarrow CH_2NNO$	300-3000	200	1.1×10^{38} $T^{-8.1}$ exp(-330/T)
$\rightarrow HCN+HNO$			4.2×10^{2} $T^{2.7}$ exp(-3,400/T)
$CH_2N+NO_2 \rightarrow CH_2NNO_2$	500-1500	200	1.0×10^{33} $T^{-6.5}$ exp(-2,800/T)
$\rightarrow HCN+HONO$			3.6×10^{6} $T^{1.4}$ exp(-1,050/T)
$\rightarrow CH_2O+N_2O$			1.5×10^{4} $T^{1.7}$ exp(-3,700/T)
$CH_2N+OH \rightarrow H_2CNOH$	300-3000	200	2.4×10^{22} $T^{-2.9}$ exp(-2,100/T)
$\rightarrow HCN+H_2O$			1.7×10^{19} $T^{1.8}$ exp(-1,500/T)
$NCO+NO \rightarrow N_2O+CO$	300-3000	<200	4.0×10^{19} $T^{-2.2}$ exp(-877/T)[d]
$\rightarrow N_2+CO_2$		<200	1.5×10^{21} $T^{-2.7}$ exp(-918/T)[d]

[a]The original publications can be found in Ref. 118. Unimolecular rate constants at the pressure indicated are given in s^{-1} and bimolecular and second order decomposition in cm^3/mol-s. [b]Low pressure limit. [c]High pressure limit. [d]Ref. 119.

Table 2. Rate Constants Predicted for Bimolecular Reactions.[a]

Reactions	T/K	k (cm^3/mole.sec)	Reference
$NO+HN_3 \rightarrow HNO+NH_2$	300-5000	$1.0\times10^{7}\ T^{1.7}\ exp(-28,500/T)$	a
$NO_2+ NH_3 \rightarrow HONO+NH_2$	300-5000	$1.2\times10^{1}\ T^{3.4}\ exp(-11,300/T)$	a
$HNO+NO_2 \rightarrow HONO+NO$	300-5000	$4.4\times10^{1}\ T^{2.6}\ exp(-2,034/T)$	a
$H+HONO \rightarrow H_2+NO_2$	300-3500	$2.0\times10^{8}\ T^{1.6}\ exp(-3,300/T)$	111
$\rightarrow OH+HNO$		$5.6\times10^{10}\ T^{0.86}\ exp(-2,500/T)$	111
$\rightarrow H_2O+NO$		$8.1\times10^{6}\ T^{1.9}\ exp(-1,900/T)$	111
$OH+HONO \rightarrow H_2O+NO_2$	200-500	$4.1\times10^{12}\ (T/300)^{-0.8}$	114
	500-2000	$1.8\times10^{7}\ T^{1.5}\ exp(1,260/T)$	a
$H+HNO_3 \rightarrow H_2+NO_3$	300-3000	$5.6\times10^{8}\ T^{1.5}\ exp(-8,200/T)$	a
$\rightarrow OH+HONO$		$3.8\times10^{5}\ T^{2.3}\ exp(-3,500/T)$	a
$\rightarrow H_2O+NO_2$		$6.1\times10^{1}\ T^{3.3}\ exp(-3,200/T)$	a
$OH+HNO_3 \rightarrow H_2O+NO_3$	750-1500	$8.7\times10^{1}\ T^{3.5}\ exp(839/T)$	115
$HNO+HONO \rightarrow H_2O+2NO$	300-3000	$1.7\times10^{-3}\ T^{4.2}\ exp(-8,350/T)$	120
$HONO+HCl \rightarrow H_2O+ClNO$	300-3000	$1.1\times10^{2}\ T^{3.0}\ exp(-5,120/T)$	117
$HONO+NO_2 \rightarrow HNO_3+NO$	300-5000	$2.0\times10^{2}\ T^{3.3}\ exp(-15,400/T)$	117
$HONO+HONO \rightarrow NO+NO_2+H_2O$	300-5000	$3.5\times10^{-1}\ T^{3.6}\ exp(-6,100/T)$	a
$HONO+NH_3 \rightarrow H_2O+NH_2NO$	300-3000	$1.0\times10^{-3}\ T^{3.3}\ exp(-14,800/T)$	120
$HNO_3+HN_3 \rightarrow H_2O+NH_2NO_2$	300-3000	$4.3\ T^{3.5}\ exp(-22,140/T)$	a

[a]The original publications can be found in Ref. 118.

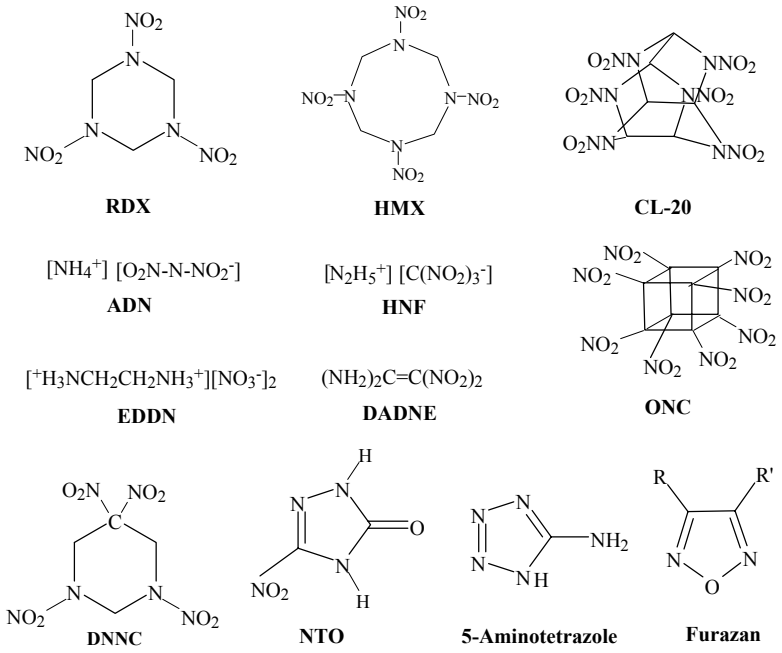

Figure 1. Structures of selected compounds.

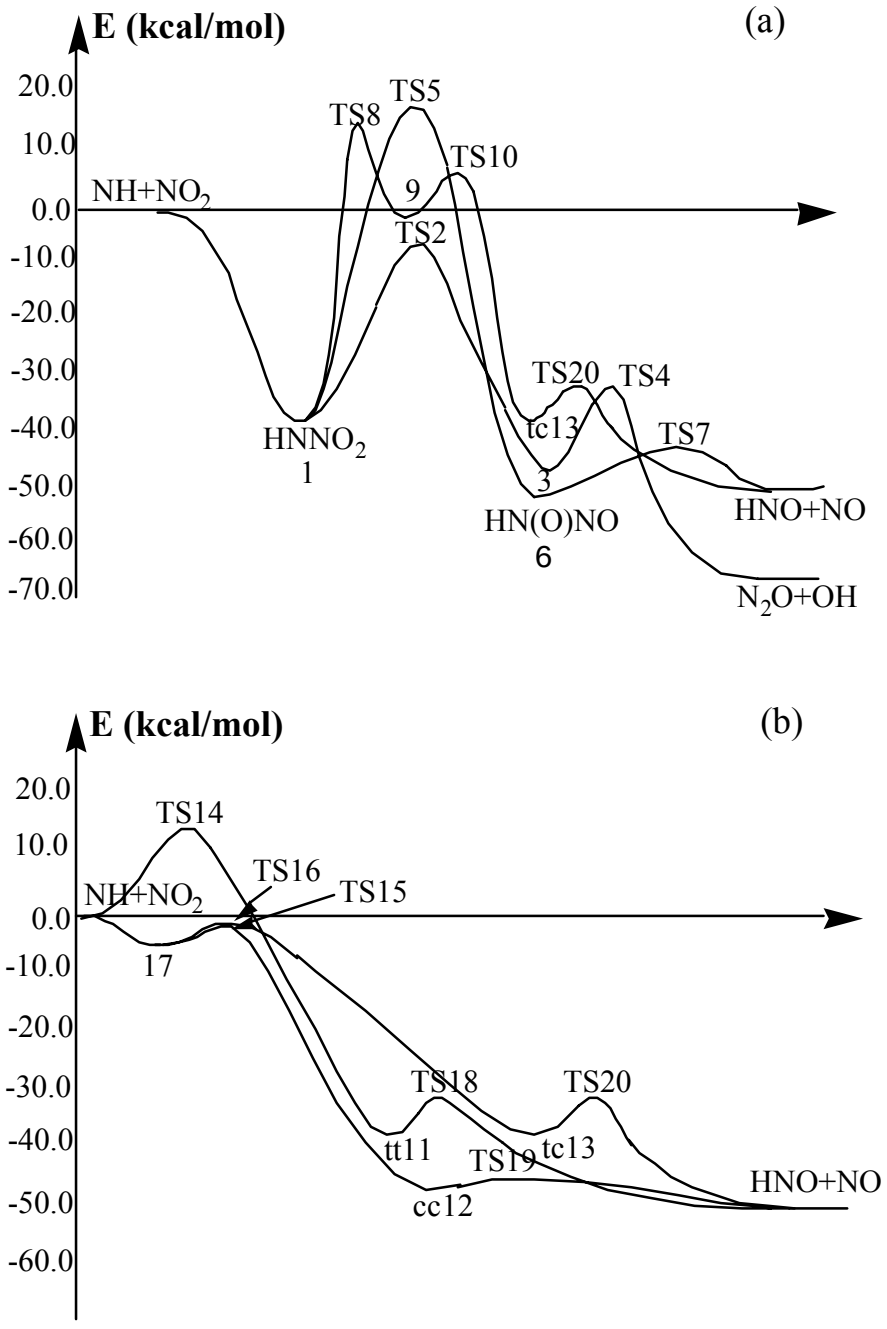

Figure 2. Potential energy profiles for the reaction NH + NO_2 via $HNNO_2$ (a) and HNONO (b) based on G2M calculation.

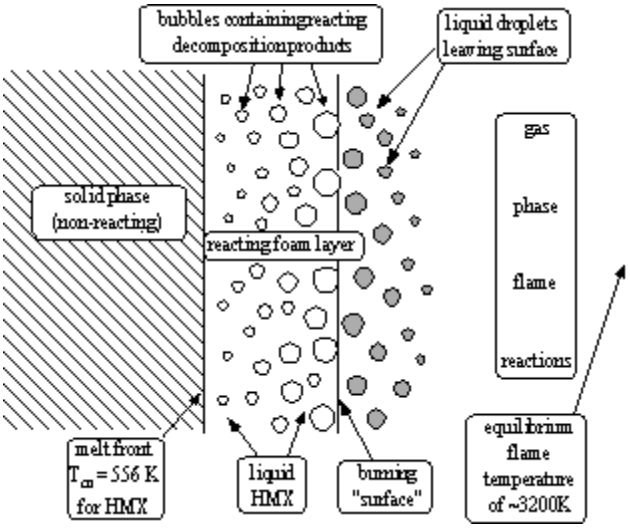

Figure 3. Schematic of the physical processes occurring at the surface of a burning propellant ingredient.

References

1. Moore, T. "Solid Rocket Development at Allegany Ballistics Laboratory", *AIAA paper 99-2931,* 35th Joint Propulsion Conference, Los Angeles, CA. 20-23 June 1999.
2. Davenas, A., *Solid Propellant Propulsion Technology*, Pergamon Press, Oxford, UK 1993.
3. Singh, H., "Advanced Solid Propellants For Propulsion of Futuristic Missiles", *Proceedings of the 1st International Seminar on Force Multiplier Technology*, New Delhi, 1999, pp. 91-103.
4. Cohen, N. S., "Combustion in Fuel-Rich Propellant Systems", *AIAA Journal*, Vol. 7, No. 7, 1969, pp. 1345-1351.
5. Lempert, D. B., Nechiporenko, G. N., Dolganova, G. P., and Stesik, L. N., "Specific Impulse of Optimized Solid Propellants (Binder + Metal + Oxidizer) as a Function of the Metal and Oxidizer Properties", *Chemical Physics Reports*, Vol. 17, No. 8, 1998, pp. 1547-1556.
6. Lempert, D. B., Nechiporenko, G. N., Soglasnova, S. I., and Stesik, L. N., "On Some Peculiarities of the Specific Impulse Dependency of CHONF Compositions on the Oxygen-to-Fluorine Ratio", *Chemical Physics Reports*, Vol. 18, No. 9, 2000, pp. 1739-1750.
7. McDonald, A. J., and Bennett, R. R., "Environmental Impacts From Launching Chemical Rockets", *Proceedings of AGARD Conference on Environmental Aspects of Rocket and Gun Propulsion*, AGARD Proceedings 559, Norway, Paper No.1, 1994.
8. Beckman, C., "Clean Propellants For Space Launch Boosters", *Proceedings of AGARD Conference on Environmental Aspects of Rocket and Gun Propellants*, AGARD Proceedings 559, Norway, Paper No. 6, 1994.
9. Atwood, A. I., Boggs, T. L., Curran, P. O., Parr, T. P, Hanson-Parr, D. M., Price, C. F., and Wiknich, J., "Burning Rate of Solid Propellant Ingredients, Part 1: Pressure and Initial Temperature Effects", *Journal of Propulsion and Power*, Vol. 15, No. 6, 1999, pp. 740-747.
10. Waesche, R. H. W., "Mechanisms and Methods of Suppression of Combustion Instability by Metallic Additives", *Journal of Propulsion and Power,* Vol 15, 1999, pp. 919-922.
11. Nielsen, A. T., Chafin, A. P., Christian, S. L., Moore, D. W., Gilardi, R. D., George, C. F., and Flippen-Anderson, J. L., "Synthesis of Polyazapolycyclic Caged Polynitramines", *Tetrahedron*, Vol. 54, 1998, pp. 11793-11812.
12. Latypov, N. V., Wellman, U., Goede, P., and Bellamy, A. J., "Synthesis and Scale-up of 2,4,6,8,10,12-Hexanitro-2,4,6,8,10,12-hexaazaisowurtzitane from 2,6,8,12-Tetraacetyl-4,10-dibenzyl-2,4,6,8,10,12-hexaazaisowurtzitane (HNIW, CL-20)", *Organic Process Research and Development*, Vol. 4, No. 3, 2000, pp. 156-158.
13. Pak, Z. P., "Some Ways to Higher Environmental Safety of Solid Rocket Propellant Applications", *AIAA Paper 93-1755,* 1993.

14. Luk'yanov, O. A. and Tartakovsky, V. A., "Synthesis and Characterization of Dinitramidic Acid and its Salts", *Solid Propellant Chemistry, Combustion, and Motor Interior Ballistics*, Yang, V. Brill, T. B., Ren, W-Z, eds., Vol. 185, *Progress in Aeronautics and Astronautics*, AIAA, Reston, VA, pp. 207-219.
15. Schoyer. H. F. R., Schnorhk, A .J., Korting, P. A. O. G., van Lit, P. J., Mul, J. M., Gadiot, G. M. H. J. L., and Meulenbrugge., "High-Performance Propellants Based on Hydrazinium Nitroformate", *Journal of Propulsion and Power,* Vol. 11, No. 4, 1995, pp. 856-869.
16. Schöyer, H. F. R., Korting, P. A. O. G., Veltmans, W. H. M., Louwers, J., v. d. Heijden, A. E. D. M., Keizers, H. L. J., and v. d. Berg, R. P., "An Overview of the Development of HNF and HNF-based Propellants", *AIAA Paper 2000-3184*, 2000.
17. McHale, E. T. and Von Elbe, G., "The Deflagration of Solid Propellant Oxidizers", *Combustion Science and Technology,* Vol. 2, 1970 pp. 227-237.
18. Zhang, M-X., Eaton, P. E., and Gilardi, R .D., "Hepta- and Octanitrocubanes", *Angewante Chemie International Edition*, Vol. 39, No. 2, 2000, pp. 401-404.
19. Eremenko, L. T., and Nesterenko, D. A., "Energetics of Decomposition of Poly-nitrocubanes", *Chemical Physics Reports*, Vol. 16, No. 9, pp. 1675-1683, 1997.
20. Sinditskii, V. P., Fogelzang, A. E., Egorshev, V. Yu., Serushkin, V. V., and Kolesov, V. I. "Effect of Molecular Structure on Combustion of Polynitrogen Energetic Materials", *Solid Propellant Chemistry, Combustion and Motor Interior Ballistics*, Yang, V. Brill, T. B., Ren, W-Z, eds., Vol. 185, *Progress in Aeronautics and Astronautics*, AIAA, Reston, VA, pp. 99-127.
21. Sinditskii, V. P., "Mechanism of Modifying the Burning Rate of Compositions Containing Nitro- and Nitrato Groups by High-Energy Polynitrogen Compounds", *Fifth International Symposium on Special Topics in Chemical Propulsion*, June 2000 Stresa, Italy, in press.
22. Brill, T. B. and Ramanathan, H.,"Thermal Decomposition of Energetic Materials 76. Chemical Pathways that Control the Burning Rate of 5-Aminotetrazole and its Hydrohalide Salts," *Combustion and Flame*, Vol. 122, Nos. 1/2, 2000, pp. 165-171.
23. Sheremetev, A. B., "Nitro and Nitroaminofurazanes", *Journal of the Russian Chemical Society*, Vol. 41, No.1, pp.43-53, 1997.
24. Tselinskii, I. V., Mel'nikova, S. F., Romanova, T. V., Pirogov, S. V., Khisamutdinov, G. Kh., Mratkhuzina, T. A., Korolev, V. L., Kondyukov, I. Z., Abdrakhmanov, I. Sh., and Smirnov, S. P., "4H-8H-Difurazano[3,4-b:3',4'-e]pyrazine and some of its Derivatives," *Russian Journal of Organic Chemistry*, Vol.33, No.11, 1997, pp. 1739-1748.
25. Latypov, N. V., Bergman, J., Langlet,, A., Wellmar, U., and Bemm, U., "Synthesis and Reactions of 1,1-Diamino, 2,2-dinitroethylene", *Tetrahedron*, Vol. 54, 1998, pp. 11525-11536.
26. Miller, R. S. "Research on New Energetic Materials" in *Decomposition, Combustion, and Detonation Chemistry of Energetic Materials*, eds. Brill, T. B., Russell, T. P., Tao, W. C., and Wardle, R. B., *Materials Research Society Symposium Proceedings*, Vol. 418, 1996, pp. 3-14.
27. Chapman, R. D., Gilardi, R. D., Welker, M. F., and Kreutzberger, C. B., "Nitrolysis of a Highly Deactivated Amide by Protonitronium. Synthesis and Structure of HNFX", *Journal of Organic Chemistry*, Vol. 64, 1999, pp. 960-965.
28. Litvinov, B. V., Fainzil'berg, A. A., Pepekin, V. I., Smirnov, S. P., Loboiko, B. G., Shevelev, S. A., and Nazin, G. M., "Enhancement of Efficiency of High-Energy Substances: High-Energy Compounds Containing Active Fluorine and Active Oxygen in Molecules", *Doklady Chemistry*, Vol. 336, Nos. 1-3, 1994, pp.86-87.
29. Feng Z., "Renewed Interests in Difluoramino and its Compounds", *Progress in Chemistry* Vol. 12, 2000, pp. 171-177.
30. Yan, H., Chen, B-R, and Guan, X-P, "Synthesis of High Density Azidonitramines", *Proceedings of the 27th ICT Conference*, Karlsruhe, Germany, Paper No.135, 1996.
31. Weber, J. F, and Frankel, M. B., "Synthesis of Novel Energetic Compounds. 8. Electrosynthesis of Azidodinitromethyl Compounds", *Propellants, Explosives, Pyrotechnics,* Vol.1 5, 1990, pp. 26-29.
32. Khisamutdinov, G.Kh., Slovetsky, V.I., Golub, Yu M., Shevelev, S.A., and Fainzil'berg, A.A., "α-Azidopolynitroalkanes. Synthesis and Vibrational Spectra", *Russian Chemical Bulletin*, Vol. 46, No. 2, 1997, pp. 324-327.
33. Stepanova, O. P., Poryadkova, M. A., and Golod, E. L., "Destructive Nitration of Polynitrocarbonyl Compounds", *Russian Journal of Organic Chemistry*, Vol. 30, No. 10, 1994, pp. 1533-1537.
34. Agrawal, J. P., "Recent Trends in High-Energy Materials", *Progress in Energy and Combustion Science*, Vol. 24, 1998, pp. 1-30.

35. Kishore, K., and Ganesh, K. "High Energy Glycidyl Azide Polymer (GAP): A Review," *Journal of Propulsion and Power*, in press.
36. Frankel, M. B., Grant, L. R., and Flanagan, J. E., "Historical Development of GAP", *Journal of Propulsion and Power*, Vol. 8, No. 4, 1992, pp. 560-563.
37. Kubota, N., Sonobe, T., and Yamamoto, A., "Burning Rate Characteristics of GAP Propellants", *Journal of Propulsion and Power,* Vol. 6, 1990, pp. 686-689.
38. Oyumi, Y. "Reactivity of Azide Polymer Propellants", *Solid Propellant Chemistry, Combustion and Motor Interior Ballistics*, Yang, V. Brill, T. B., Ren, W-Z, eds., Vol. 185, *Progress in Aeronautics and Astronautics*, AIAA, Reston, VA, pp. 73-95.
39. D'Andrea, B., Lillo, F., and Marcelli, G., "High-Speed Mechanical Characterization and Temperature Constraints of Propellants with Energetic Binders", *AIAA Paper 2000-3183*, 2000.
40. Cliff, M. D. and Cunliffe, A. V., "Plasticised PolyGLYN Binders for Composite Energetic Materials", *30th International Conference of the ICT*, Karlsruhe, Germany, 1999, paper 85.
41. Manser, G., "Difluoroamino Oxetanes and Polymers Formed Therefrom for use in Energetic Formulations", *U. S Patent 5,272,249*, 1996.
42. Zhirong, J., Guilin, X., and Yuanfa, C., "A New Energetic Polymer Containing Difluoroamino Group", *Proceedings of the 21st ICT Meeting*, Karlsruhe, Germany, 1990, Paper No. 52.
43. Brill, T. B. "Connecting the Chemical Composition of a Material to its Combustion Characteristics," *Progress in Energy and Combustion Science*, Vol. 18, 1992, pp.91-116
44. Kimura, J., Kubota, N., "Thermal Decomposition Process of HMX," *Propellants and Explosives*, Vol. 5, 1980, pp. 1-8.
45. Cosgrove, J.D., Owen, A. J., The Thermal Decomposition of 1,3,5-Trinitro Hexahydro 1,3,5-Triazine (RDX)—Part I: The Products and Physical Parameters," *Combustion and Flame*, Vol. 22, 1974, pp. 13-18.
46. Cosgrove, J.D., Owen, A. J., The Thermal Decomposition of 1,3,5-Trinitro Hexahydro 1,3,5-Triazine (RDX)—Part II: The Effects of the Products," *Combustion and Flame*, Vol. 22, 1974, pp. 19-22.
47. Boggs, T. L., "The Thermal Behavior of Cyclotrimethylenetrinitramine (RDX) and Cyclotetramethylenetetranitramine (HMX)," *Fundamentals of Solid-Propellant Combustion*, AIAA Inc., New York, NY, 1984, pp. 121-175.
48. Fifer, R. A., "Chemistry of Nitrate Ester and Nitramine Propellants," *Fundamentals of Solid-Propellant Combustion*, AIAA Inc., New York, NY, 1984, pp. 177-237.
49. Behrens, Jr., R., "The Application of Simultaneous Thermogravimetric Modulated Beam Mass Spectrometry and Time-of-Flight Velocity Spectra Measurements to the Study of the Pyrolysis of Energetic Materials," *Chemistry and Physics of Energetic Materials*, Vol. 309, Kluwer Academic Publishers, Netherlands, 1990, pp. 327-346.
50. Behrens, Jr., R., "Thermal Decomposition of HMX and RDX: Decomposition Processes and Mechanisms Based on STMBMS and TOF Velocity-Spectra Measurements," *Chemistry and Physics of Energetic Materials*, Vol. 309, Kluwer Academic Publishers, Netherlands, 1990, pp. 347-368.
51. Behrens, Jr., R., "New Simultaneous Thermogravimetry and Modulated Molecular Beam Mass Spectrometry Apparatus for Quantitative Thermal Decomposition Studies," *Reviews of Scientific Instruments*, Vol. 58, 1987, pp. 451-461.
52. Behrens, Jr., R., "Thermal Decomposition of Energetic Materials: Temporal Behaviors of the Rates of Formation of the Gaseous Pyrolysis Products from Condensed-Phase Decomposition of Octahydro-1,3,5,7-tetranitro-1,3,5,7-tetrazocine," *Journal of Physical Chemistry*, Vol. 94, 1990, pp. 6706-6718.
53. Behrens, Jr., R., Bulusu, S., "Thermal Decomposition of Energetic Materials. 2. Deuterium Isotope Effects and Isotopic Scrambling in Condensed-Phase Decomposition of Octahydro-1,3,5,7-tetranitro-1,3,5,7-tetrazocine," *Journal of Physical Chemistry*, Vol. 95, 1991, pp. 5838-5845.
54. Behrens, Jr., R., Bulusu, S., "Thermal Decomposition of Energetic Materials. 3. Temporal Behaviors of the Rates of Formation of the Gaseous Pyrolysis Products from Condensed-Phase Decomposition of 1,3,5-Trinitrohexahydro-*s*-triazine," *Journal of Physical Chemistry*, Vol. 96, 1992, pp. 8877-8891.
55. Behrens, Jr., R., Bulusu, S., "Thermal Decomposition of Energetic Materials. 4. Deuterium Isotope Effects and Isotopic Scrambling (H/D, $^{13}C/^{18}O$, $^{14}N/^{15}N$) in Condensed-Phase Decomposition of 1,3,5-Trinitrohexahydro-*s*-triazine," *Journal of Physical Chemistry*, Vol. 96, 1992, pp. 8891-8897.
56. Behrens, Jr., R., "Identification of Octahydro-1,3,5,7-tetranitro-1,3,5,7-tetrazocine (HMX) Pyrolysis Products by Simultaneous Thermogravimetric Modulated Beam Mass Spectrometry and Time-of-Flight Velocity-Spectra Measurements," *International Journal of Chemical Kinetics*, Vol. 22, 1990, pp. 135-157.

57. Behrens, Jr., R., "Determination of the Rates of Formation of Gaseous Products from the Pyrolysis of Octahydro-1,3,5,7-tetranitro-1,3,5,7-tetrazocine (HMX) by Simultaneous Thermogravimetric Modulated Beam Mass Spectrometry," *International Journal of Chemical Kinet.ics*, Vol. 22, 1990, pp. 159-173.
58. Behrens, Jr., R., Bulusu, S., "Thermal Decomposition of HMX: Low Temperature Reaction Kinetics and their use for Assessing Response in Abnormal Thermal Environments and Implications for Long-Term Aging," *Materials Research Society Symposium Proceedings*, Vol. 418, Materials Research Society, 1996, pp. 119-126.
59. Peterson, J. D., Wight, C. A. "Thermal Decomposition of Composite HMX/HTPB Propellant," *Proc. NATAS Annu. Conf. Therm. Anal. Appl*., 28th, 2000, pp. 121-126
60. Binder composition: R-45M (HTPB): 7.52%, dioctyladipate (DOA): 8.12%, lecithin: 0.7%, isophorone diisocyanate (IPDI): 0.62%, and triphenyl bismuth (TPB): 0.04%.
61. Vyazovkin, S., "Advanced Isoconversional Method," *Journal of Thermal Analysis*, Vol. 49, 1997, pp. 1493-1499.
62. Vyazovkin, S., Wight, C. A., "Kinetics in Solids," *Annual Reviews of Physical Chemistry*, Vol. 48, 1997, pp. 125-149.
63. Vyazovkin, S., Wight, C. A., "Isothermal and Non-isothermal Kinetics of Thermally Stimulated Reactions of Solids," *Int. Rev. Phys. Chem.* Vol. 17, 1998, pp. 407-433.
64. Lee, Y. J., Tang, C. J., and Litzinger, T. A. "A Study of the Chemical and Physical Processes Governing CO_2 Laser Pyrolysis and Combustion of RDX." *Combustion and Flame*, Vol. 117, No. 3, 1999, 600-628.
65. Botcher, T. R. and Wight, C. A., "Transient Thin Film Laser Pyrolysis of RDX," *Journal of Physical Chemistry*, Vol. 97, No. 36, 1993, pp. 9149-9153.
66. Botcher, T. R. and Wight, C. A., "Explosive Thermal Decomposition Mechanism of RDX," *Journal of Physical Chemistry*, Vol. 98, No. 26, 1994, pp. 5441-5444.
67. Ling, P. and Wight, C. A., "Laser Photodissociation and Thermal Pyrolysis of Energetic Polymers," *Journal of Physical Chemistry B*, Vol. 101, No. 12, 1997, pp. 2126-2131.
68. Haas, Y., Ben Eliahu, Y., and Welner, S., "Infrared Laser Induced Decomposition of GAP," *Combustion and Flame*, Vol. 96, Nos. 1/2, 1994, pp. 212-220.
69. Ben Eliahu, Y., Haas, Y., and Welner, S. "Laser Initiation of the Decomposition of Energetic Polymers: Shock Wave Formation," *Journal of Physical Chemistry,* Vol. 99, No. 16, 1995, pp. 6010-6018.
70. Litzinger, T. A., Fetherolf, B. L.; Lee, Y. J., and Tang, C. J., "Study of the Gas-Phase Chemistry of RDX: Experiments and Modeling," *Journal of Propulsion and Power*, Vol. 11, No. 4, 1995, pp. 698-703.
71. Tang, C. J., Lee, Y. J., Kudva, G., and Litzinger, T. A., "A Study of the Gas-Phase Chemical Structure During CO_2 Laser Assisted Combustion of HMX," *Combustion and Flame*, Vol. 117, Nos. 1/2, 1999, pp. 170-188.
72. Brill, T. B., Brush, P. J., James, K. J., Shepherd, J. E., and Pfeiffer, K. J. "T-Jump/FTIR Spectroscopy: A New Entry into the Rapid Pyrolysis of Solids and Liquids," *Applied Spectroscopy*, Vol. 46, No. 6, 1992, pp. 900-911.
73. Roos, B. D. and Brill, T. B. "Thermal Decomposition of Energetic Materials 75. T-Jump/Raman Spectroscopy and its Application to High-Nitrogen Compounds," *Applied Spectroscopy*, Vol. 54, No. 7, 2000, pp. 1019-1026.
74. Shepherd, J. E. and Brill, T. B. "Interpretation of Time-to-Explosion Tests," *Tenth International Symposium on Detonation*, Naval Surface Warfare Center, White Oak, MD, 1993, pp. 849-855.
75. Thynell, S. T., Gongwer, P. E., and Brill, T. B. "Condensed-Phase Kinetics of Cyclotrimethylenetrinitramine by Modeling the T-Jump/Infrared Spectroscopy Experiment," *Journal of Propulsion and Power*, Vol.12, No. 6, 1996, pp. 933-939.
76. Brill, T. B., Brush, P. J., and Patil, D. G., "Thermal decomposition of Energetic Materials 60. Major Reaction Stages of a Simulated Burning Surface of NH_4ClO_4," *Combustion and Flame*, Vol. 94, Nos. 1/2, 1993, pp.70-76.
77. Kim, E. S. and Thynell, S. T. "Condensed-Phase Kinetic Rates of RDX from Confined Rapid Thermolysis/FTIR Spectroscopy**,"** Proceedings of the JANNAF 35th Combustion Subcommittee and 17th Propulsion Systems Hazards Subcommittee Meeting, Joint Sessions, CPIA Publication 685, 1998, pp. 145-159.
78. Brill, T. B. and Brush, P. J. "Condensed Phase Chemistry of Explosives and Propellants at High Temperature: HMX, RDX and BAMO," *Philosophical Transactions of the Royal Society of London, Series A*, Vol. 339, 1992, pp. 377-385.

79. Brill, T. B., Brush, P. J., and Patil, D. G., "Thermal Decomposition of Energetic Materials 58. Chemistry of Ammonium Nitrate and Ammonium Dinitramide at the Burning Surface Temperature," *Combustion and Flame*, Vol. 92, Nos. 1/2, 1993, pp. 178-186.
80. Brill, T. B., Patil, D. G., Duterque, J. and Lengelle, G.,"Thermal Decomposition of Energetic Materials 63. Surface Reaction Zone Chemistry of Simulated Burning 1,3,5,5-Tetranitrohexahydropyrimidine (DNNC or TNDA) Compared to RDX," *Combustion and Flame*, Vol. 95, Nos. 1/2, 1993, pp. 183-190.
81. Maiella, P. G. and Brill, T. B., "Spectroscopy of Hydrothermal Reactions III. The Water Gas Reaction, "Hot Spots", and Formation of Volatile Salts of NCO- from Aqueous $[NH_3(CH_2)_2NH_3]NO_3$ at 720 K and 276 Bar by T-Jump/FTIR Spectroscopy," *Applied Spectroscopy*, Vol. 50, No. 7, 1996, pp. 829-835.
82. Williams, G. K. and Brill, T. B. "Thermal Decomposition of Energetic Materials 67. Hydrazinium Nitroformate (HNF) Rates and Pathways under Combustion-like Conditions," *Combustion and Flame*, Vol. 102, No. 3, 1995, pp. 418-426.
83. Brill, T. B., Zhang, T. L., and Tappan, B. C."Thermal Decomposition of Energetic Materials 74. Volatile Metal Isocyanates from Flash Pyrolysis of Metal-NTO and Metal-Picrate Salts and an Application Hypothesis," *Combustion and Flame*, Vol. 121, No. 4, 2000, pp. 662-670.
84. Beal, R. W. and Brill, T. B. **"**Thermal Decomposition of Energetic Materials 77. Behavior of N-N Bridged Bifurazan Compounds on Slow and Fast Heating*," Propellants, Explosives, Pyrotechnics,* vol. 25, 2000, pp.241-246.
85. Brill, T. B. "Multiphase Chemistry Considerations at the Surface of Burning Nitramine Propellants," *Journal of Propulsion and Power*, Vol. 11, No. 4, 1995, pp. 740-751.
86. Williams, G. K. and Brill, T. B. "Thermal Decomposition of Energetic Materials 70. Kinetics of Organic Peroxide Decomposition Derived from the Filament Control Voltage of T-Jump/FTIR Spectroscopy," *Applied Spectroscopy*, Vol. 51, No. 3, 1997, pp. 423-427.
87. Arisawa, H. and Brill, T. B. "Flash Pyrolysis of Hydroxyl-terminated Polybutadiene (HTPB) II: Implications of the Kinetics to Combustion of Organic Polymers," *Combustion and Flame*, Vol. 106, Nos. 1/2, 1996, pp. 144-154.
88. Arisawa, H. and Brill, T. B. "Flash Pyrolysis of Polyethylene Glycol II. Kinetics Determined by T-Jump/FTIR Spectroscopy," *Combustion and Flame*, Vol. 109, Nos. 1/2, 1997, pp. 105-112.
89. Gongwer, P. E., Arisawa, H. and Brill, T. B. "Kinetics and Products from Flash Pyrolysis of Cellulose Acetate Butyrate (CAB) at 465-600° C," *Combustion and Flame*, Vol. 109, No. 3, 1997, pp. 370-381.
90. Arisawa, H. and Brill, T. B. "Thermal Decomposition of Energetic Materials 71. Structure-Decomposition Relationships in Flash Pyrolysis of Glycidyl Azide Polymer (GAP)," *Combustion and Flame*, Vol. 112, No. 4, 1998, pp. 533-544.
91. Brill, T. B. and Budenz, B. T. "Condensed Phase Issues for AP-HTPB Pseudopropellant and the Effect of Burning-Rate Additives," *Progress in Astronautics and Aeronautics*, Vol.185, V. Yang, T. B. Brill, W. Z. Ren, eds., American Institute of Aeronautics and Astronautics, Reston, VA, 2000, pp. 3-32.
92. Brill, T. B., Gongwer, P. E., and Budenz, B. T. "Oxidizer-Binder Interactions from T-Jump/FTIR Flash Pyrolysis," *Proceedings of the 28th International Conference of the ICT*, Karlsruhe, Germany, June, 1997, p. 14-1 to 14-11.
93. Roos, B. D. and Brill, T. B. "Flash Pyrolysis of GAP/RDX Mixtures, Cured GAP-Diol, and the Curing Agent," to be published.
94. Arisawa, H. and Brill, T. B. "Flash Pyrolysis of Polyethyleneglycol I: Chemometric Resolution of FTIR Spectra of the Volatile Products at 370-550° C," *Combustion and Flame*, Vol. 109, Nos. 1/2, 1997, pp. 87-104.
95. Gongwer, P. E. and Brill, T. B. "Thermal Decomposition of Energetic Materials 73. The Identity and Temperature Dependence of "Minor" Products from Flash-Heated RDX," *Combustion and Flame*, Vol. 115, No. 3, 1998, pp. 417-423.
96. Schroeder, M. A., Fifer, R. A., Miller, M. S., Pesce-Rodriguez, R. A. "Condensed-Phase Processes during Solid Propellant Combustion I. Preliminary Chemical and Microscopic Examination of Extinguished Propellant Samples," *BRL-MR-3845*, Aberdeen Proving Ground, MD, June 1990.
97. Schroeder, M. A., Fifer, R. A., Miller, M. S., Pesce-Rodriguez, R. A., Singh, G. "Condensed-Phase Processes during Solid Propellant Combustion Part II. Preliminary Chemical and Microscopic Examination of Conductively Quenched Samples of RDX, XM39, JA2, and HMX-Binder Compositions," *BRL-TR-3337*, Aberdeen Proving Ground, MD, May 1992.
98. Clyne, M. A. A. and Nip, W. S., "Generation and Measurement of Atom and Radical Concentrations in Flow Systems," *Reactive Intermediates in the Gas Phase: Generation and Monitoring*, Setzer, D. W. ed., Academic Press, N.Y., 1979, pp.2-50.

99. Fontijn, A. and Felder, W. "High Temperature Flow Tubes. Generation and Measurement of Refractory Species," *Reactive Intermediates in the Gas Phase: Generation and Monitoring*, Setzer, D. W. ed., Academic Press, N.Y., 1979, pp. 59-142.
100. Lin, M. C. and McDonald, J. R. "Production and Detection of Reactive Species with Lasers in Static Systems," *Reactive Intermediates in the Gas Phase: Generation and Monitoring*, Setzer, D. W. ed., Academic Press, N.Y., 1979, pp. 233-294.
101. D. W. Setzer, ed., Reactive Intermediates in the Gas Phase: Generation and Monitoring, Academic Press, N.Y., 1979.
102. Hanson, R. K., "The Role of Lasers in Shock Tube Studies of Chemical Kinetics," in *Shock Waves*, Marsceille, W., Brun R., and Dumitrescu, L. Z. eds., Springer-Verlag, Berlin, 1995, pp. 7-14.
103. Busch K. W. and Busch, M. A.,eds., "Cavity Ringdown Spectroscopy: An Ultratrace-Absorption Measurement Technique," *ACS Symposium Series 720*, American Chemical Society, Washington D.C., 1999.
104. Mebel, A. M., Morokuma, K., and Lin, M. C., "Modification of the Gaussian-2 Theoretical Model: The Use of Coupled-Cluster Energies, Density Functional Geometries and Frequencies," *Journal of Chemical Physics*, Vol. 103, No. 17, 1995, pp. 7414-7421.
105. Curtiss, L. A., Redfern, P. C., Raghavachari, K., and Pople, J. A., "Assessment of Gaussian-2 and Density Functional Theories for the Computation of Enthalpies of Formation," *Journal of Chemical Physics*, Vol. 106, No. 3, 1997, pp. 1063-1079.
106. Laidler, K. J., *Chemical Kinetics*, 3rd ed. Harper and Row, N. Y., 1987.
107. Hsu, C. C., Mebel, A. M., and Lin, M. C., "Ab Initio Molecular Orbital Study of the HCO + O_2 Reaction. Direct Versus Indirect Abstraction Channels," *Journal of Chemical Physics*, Vol. 105, No. 6, 1996, pp. 2346-2352.
108. Chakraborty, D., Park, J., and Lin, M. C., "Theoretical Study of the OH + NO_2 Reaction: Formation of Nitric Acid and the Hydroperoxy Radical," *Chemical Physics*, Vol. 231, No. 1, 1998, pp. 39-49.
109. Mebel, A. M., Diau, E. W. G., Lin, M. C. and Morokuma, K. "Ab Initio and RRKM Calculations for Multichannel Rate Constants of the C_2H_3 + O_2 Reaction", *Journal of the American Chemical Society*, Vol. 108, 1996, pp. 9759-9768.
110. Chakraborty, D., Hsu, C.-C., Lin, M. C., "Theoretical Studies of Nitroamino Radical Reactions. Rate Constants for the Unimolecular Decomposition of HN(NO_2) and Related Bimolecular Processes," *Journal of Chemical Physics*, Vol. 109, No. 20, 1998, pp. 8887-8896.
111. Hsu, C. -C., Lin, M. C., Mebel, A. M., and Melius, C. F., "*Ab Initio* Study of the H + HONO Reaction: Direct Abstraction Versus Indirect Exchange Processes," *Journal of Physical Chemistry A*, Vol. 101, No. 1, 1997, pp. 60-66.
112. Park, J., Chakraborty, D., and Lin, M. C., "Thermal Decomposition of Gaseous Ammonium Dinitramide at Low Pressure: Kinetic Modeling of Product Formation with Ab Initio MO/cVRRKM Calculations," *Twenty-Seventh Symposium (International) on Combustion*, The Combustion Institute, Pittsburgh, PA, 1998, pp. 2351-2357.
113. Mebel, A. M., Lin, M. C., and Morokuma, K., Ab Initio MO and TST Calculations for the Rate Constant of the HNO + NO_2 $\rightarrow$ HONO + NO," *International Journal of Chemical Kinetics*, Vol. 30, No. 9, 1998, pp. 729-736.
114. Xia, W. S. and Lin, M. C., "Ab Initio MO/Statistical Theory Prediction of the OH + HONO Reaction Rate: Evidence for the Negative Temperature Dependence", *Physics and Chemistry Communications*, submitted.
115. Xia, W. S. and Lin, M. C., "A Multifacet Mechanism for the OH + HNO_3 Reaction: An Ab Initio MO/Statistical Theory Study", W. S. Xia and M. C. Lin, *Journal of Chemical Physics*, submitted.
116. Mebel, A. M., Lin, M. C., and Melius, C. F., "Rate Constant of the HONO + HONO $\rightarrow$ H_2O + NO + NO_2 Reaction from Ab Initio MO and TST Calculations," *Journal of Physical Chemistry A*, Vol. 102, No. 10, 1998, pp. 1803-1807.
117. Lu, X., Park, J. and Lin, M. C., " Gas-Phase reactions of HONO with NO_2, O_3 and HCl: An Ab Initio MO/TST Study" *Journal of Physical Chemistry A,* Vol 104, No. 38, 2000, pp. 8730-8738.
118. Chakraborty, D. and Lin, M. C., "Gas-Phase Chemical Kinetics of [C,H,N,O] Systems Relevant to Combustion of Nitramines", *Progress in Astronautics and Aeronautics*, eds. V. Yang, T. B. Brill and W.-Z. Ren, AIAA, Washington, DC, Vol. 185, 2000, pp.33-71.
119. Zhu, R. and Lin, M. C., "The NCO + NO Reaction Revisited: Ab Initio MO/VRRKM Calculations for Total rate Constant and Product Branching Ratios" *Journal of Physical Chemistry A*, Vol.104, No. 46, 2000, pp. 10807-10811.

120. Lu, X., Musin, R. N., Lin, M. C., "Gas-Phase Reactions of HONO with HNO and NH_3: An *Ab Initio* MO/TST Study", *Journal of Physical Chemistry A*, Vol. 104, No. 21, 2000, pp. 5141-5148.
121. *NIST Chemical Kinetics Database,* National Institute of Standards and Technology, Gaithersburg, MD, 1998, Version 2Q98.
122. Parr, T. P. and Hanson-Parr, D. M., "Optical Diagnostics of Solid-Propellant Flame Structure", *Chapter 2.5 in Solid Propellant Chemistry, Combustion, and Motor Interior Ballistics*, Vol. 185, editors V. Yang, T. B. Brill, and W. Z. Ren, AIAA Progress in Astronautics and Aeronautics, 2000, pp. 381-412.
123. Wilson, S. J., Fetherolf B. L., Brown, P. W. and Kuo K. K., "Surface Microstructure Resulting from Laser-Induced Pyrolysis and Combustion of M43 and XM39", *30th JANNAF Combustion Mtg.*, Vol. II, CPIA No. 606, 1993, pp. 167-182.
124. Jing, Q. and Beckstead, M. W. "Influence of AP Solid Phase Decomposition on Temperature Profile and Sensitivity." AIAA-98-0488 (1998).
125. Lloyd, S. A., Umstead, M. E. and Lin, M. C. "Kinetics and Mechanism of Thermal Decomposition of Dimethylnitramine at Low Temperatures" *Journal of Energetic Materials*, Vol. 3, 1985, pp187-210.
126. Pollard, F. H. and R. M. H. Wyatt. "Reactions Between Formaldehyde and Nitrogen Dioxide." *Transactions of the Faraday Society,* Vol. 45, 1949, pp 760-767.
127. Fifer, R. A. and Holmes, H. E., "Kinetics of Nitramine Flame Reactions." *16th JANNAF Combustion Meeting*, CPIA-PUB-308-VOL-II, 1979, pp.35-50.
128. Lin, C. Y., Wang, H. I., Lin, M. C., and Williams, C. F., "A Shock Tube Study of the CH_2O +NO_2 Reaction at High Temperature." *International Journal of Chemical Kinetics,* Vol. 22, 1990, pp.455-482.
129. Rosen, J. M. and Dickenson, C. "Vapor Pressures and Heats of Sublimation of Some High Melting Organic Explosives." *Journal of Chemistry and Engineering Data,* Vol. 14 1969, pp. 120-124.
130. Maksimov, Y. Y., Apal`kova, V. N.,. Braverman, O. V. and Solov`ev, A. I. "Kinetics of Thermal Decomposition of Cyclotrimethylenetrinitramine and Cyclotetramethylene-Tetranitramine in the Gas Phase." *Russian Journal of Physical Chemistry*, Vol. 59, 1985 pp. 201-204.
131. Edwards, G. "The Vapour Pressure of Cyclotrimethylene Trinitramine (Cyclonite) and Pentaerythritoltetranitrate." *Transactions of the Faraday Society,* Vol. 49, 1953, pp. 152-154.
132. Taylor, J. W. and Crooks, R. J. "Vapour Pressure and Enthalpy of Sublimation of 1,3,5,7-Tetranitro 1,3,5,7-Tetraazacyclooctane (HMX)." *Journal of the Chemical Society, Faraday Transactions I,* Vol. 72, 1976, pp. 723-729.
133. Maksimov, Y. Y. "Boiling Point and Enthalpy of Evaporation of Liquid Hexogen and Octogen." *Russian Journal of Physical Chemistry,* Vol. 66, 1992, pp. 280-281.
134. Westbrook, C. K. and Dryer F. L., "Chemical Kinetic Modeling of Hydrocarbon Combustion", *J. Progress in Energy Combustion Science*, Vol. 10, 1984, pp. 1-57.
135. Frenklach, M., Bowman, T., Smith, G., and Gardiner, B., "GRI-MECH 3.0", http://www.me.berkeley.edu/gri_mech/, 2000.
136. Melius, C. F. and Binkley J. S., "Thermochemistry of the Decomposition of Nitramines in the Gas Phase", *21st Symposium (Int'l) on Combustion*, The Combustion Institute, 1986, pp. 1953-1963.
137. Melius, C., "Thermochemical Modeling: I. Application to Decomposition of Energetic Materials", *Chemistry and Physics of Energetic Materials*, edited by S. N. Bulusu, Kluwer Academic. The Netherlands, 1990, pp. 21-49.
138. Melius, C. F. "Thermochemical Modeling: II, Application to Ignition and Combustion of Energetic Materials." *Chemistry and Physics of Energetic Materials*, edited by S. N. Bulusu, Kluwer Academic. The Netherlands, 1990, pp. 51-78.
139. Yetter, R. A., Dryer F. L., Allen M. T. ,and Gatto J. L., "Development of Gas-Phase Reaction Mechanisms for Nitramine Combustion", *Journal of Propulsion and Power*, Vol. 11, No. 4, 1995, pp. 683-697.
140. Prasad, K., Yetter R. A. and Smooke M. D., "An Eigenvalue Method for Computing the Burning Rates of RDX Propellants", *Combustion Science and Technology*, Vol. 124, (No.1-6), 1997, pp. 35-43.
141. Kee, R. J., Rupley F. M. and Miller, J. A., "CHEMKIN II: A Fortran Chemical Kinetics Package for the Analysis of Gas Phase Chemical Kinetics", SAND89-8009B•UC-706, 1993.
142. Kee, R. J., Rupley F. M., and Miller, J. A. "A Fortran Program for Modeling Steady Laminar One-dimensional Premixed Flames", SAND85-8240•UC-401, 1992.
143. Kee, R. J. Dixon-Lewis G., Warnatz, J., Coltrin, M. E., and Miller, J. A., "A Fortran Compute Code Package for the Evaluation of Gas-Phase Multicomponent Transport Properties", SAND86-8246•UC-401, 1991.

TASK II

COMBUSTION DYNAMICS

Merrill W. Beckstead, Team Leader

2
TASK II — COMBUSTION DYNAMICS

2.1 Experimental Testing Methods for Combustion of Energetic Ingredients and Propellants (Beckstead)

To support the modeling efforts of the dynamic response of propellants by analytical models and detailed numerical models, steady state testing was performed to obtain key parameters required for analytical modeling and detailed data for validation of the numerical models. Experiments were conducted on a variety of propellants with and without aluminum, and also on pure ingredients, "pseudo" propellants, and binder/AP sandwiches. This section of the report provides on overview of the experimental methods used in these tests and the data that were developed from them.

2.1.1 Burning Rate Measurements

Among the most basic characteristics that must be determined for any propellant are its burning rate at different initial conditions of temperature and pressure. This data is important for validation of numerical models for steady state burning, and also yields important information required for the analytical modeling of dynamic response. Specifically, two parameters related to the dynamic response derived from the data are the temperature sensitivity and the pressure exponent of the burning rate. The temperature sensitivity is a measure of the effect of the initial temperature of the propellant on its steady state burning rate; it is an important input parameter to the classical models of propellant dynamic response. The pressure exponent of the burning rate represents the response of the propellant to low-frequency excitation.

In the MURI program, testing for burning rate was performed using the ultrasound technique. The temperature sensitivity of several MURI Phase II propellants have been measured using the ultrasonic burning rate measurement technique including two Thiokol Phase II BAMO/AMMO propellants and the two Alliant baseline propellants. One propellant from each set was metallized. The BAMO/AMMO propellants contained ammonium perchlorate (AP). The Alliant propellants had HTPE binders and AP and AN as oxidizers. The BAMO/AMMO propellants exhibited higher temperature sensitivities that the HTPE/AP/AN propellants.

The ultrasonic technique is utilized in these propellant tests. This technique is highly effective for measuring the instantaneous thickness of the propellant. The ultrasonic pulse-echo technique has been developed by ONERA in the 80's [1] and utilized at several other places [2-5]. It has been used at UAH for several years to measure steady state burning rate [6], temperature sensitivity [7], and propellant response function [8]. The ultrasonic transducer emits a sound pulse that propagates through the propellant to the propellant surface where it is then reflected back down to the transducer. The same transducer then detects the returning pulse. By measuring this propagation time and knowing the speed of sound through the propellant, the instantaneous thickness can be determined for each pulse emitted by the ultrasonic transducer. The burning rate is determined by taking the time derivative of the instantaneous thickness.

The process is shown schematically in the Figure 1 along with a typical waveform. The ultrasonic transducer sends a pulse through the coupling material, which is typically epoxy, and to the propellant. Wherever an impedance mismatch exists an echo is produced. Care is taken to match the impedance of the coupling material and

propellant to minimize this echo. The propellant/burning gas interface produces the strongest echo that is returns and is detected by the ultrasonic transducer. The propagation time is measured an electronic instrument at 1000, 5000 or 10,000Hz. Most of the data presented here were recorded at 1000 Hz.

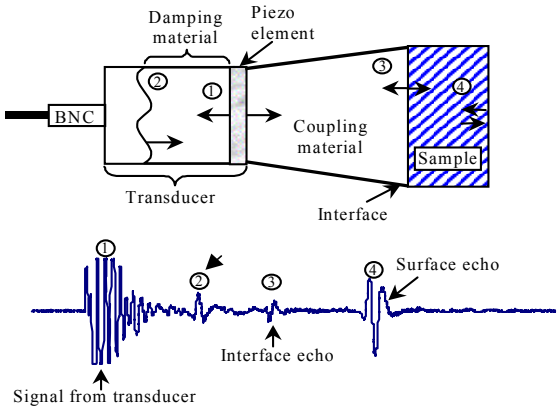

Figure 1. Typical ultrasound set-up

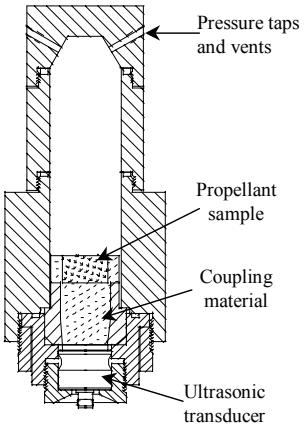

Figure 2. Closed bomb for burning rate tests

The test is performed in a closed bomb, Figure 2, and therefore the pressure increases during the test. Therefore, data for a large range of pressures can be obtained from one test producing burning rate measurements for a wide range of pressures from a single test.

The burning rates for the metallized Thiokol propellant are shown in the Figure 3. The ultrasonic data are higher than the Thiokol data for low pressures but matches better at high pressure. The temperature sensitivity is fairly constant. The great utility of the technique developed is that data over pressure ranges that correspond to operational systems is obtained with small quantities of ingredients. This allows screening of new ingredients and formulations in the laboratory.

2.1.2 Measurement of Chemical Species

Measurements were made of the chemical species that leave the surface of reacting propellants as well as the change of these species from the surface through the flames formed above the surface. The objective of this work was to obtain species data for novel energetic materials and new propellants under steady state conditions to better understand the physical and chemical processes involved and to contribute to model development and validation. In this work, individual propellant ingredients and "pseudo" propellants were also studied; pseudo-propellants refer to propellants that contain the major components, *i.e.* oxidizer and fuel, but are not all of the typical minor ingredients or additives.

The experimental facility used in these studies consisted of a high-power CO_2 laser used as the heat source for ignition and sustaining combustion, visual diagnostics for the examination of flame behavior and species sampling height, a triple quadrupole mass spectrometer (TQMS) for gaseous product analysis, and a data acquisition and

analysis system. Only a brief discussion of the facility will be given here; detailed features of the experimental setup have been described elsewhere [9].

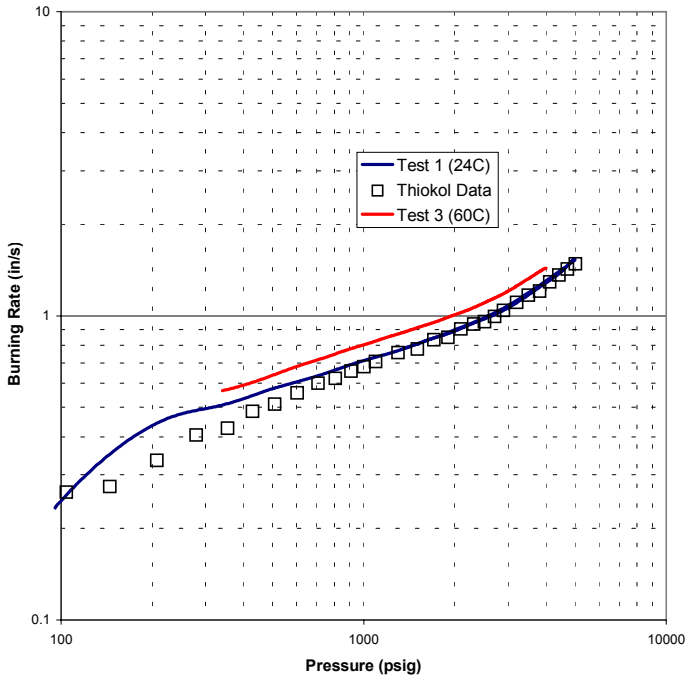

Figure 3. Burning rate vs. pressure for metallized propellant with energetic binder. Top curve is 60°C; other curves are for 24°C. The open symbols are strand data from Thiokol.

Experiments were typically conducted at 0.1 MPa (1 atm) in an argon environment, with heat fluxes ranging from 50 to 400 W/cm^2. Gaseous products evolved from the propellant surface were extracted through the use of quartz microprobes (with sampling orifice sizes of approximately 25 micron) and analyzed by the TQMS. In the mass spectrometer, the samples gases are ionized by electron impact and the ions then flow into the first quadrupole mass filter, where a specific ion of interest is selected, *e.g.*, a mass to charge ratio (m/z) of 28, which might contain diatomic nitrogen, carbon monoxide, and ethylene. When the first quadrupole mass filter is set for an m/z of 28, only species with this m/z will exit from the filter. The 28 m/z ions then pass into the second mass filter which is set to hold them on axis as they collide with argon atoms. The collision process causes the 28 m/z ions to fragment into lower mass fragments, some of which are charged. These smaller fragments, referred to as "daughter" ions, then flow into the third quadrupole mass filter where they are detected. Based upon the fragments that are detected the amounts of each species with 28 m/z can be determined quantitatively. Thus, the TQMS permits identification and quantification of all of the major products from the combustion process. This operation of the TQMS is illustrated schematically in the Figure 4.

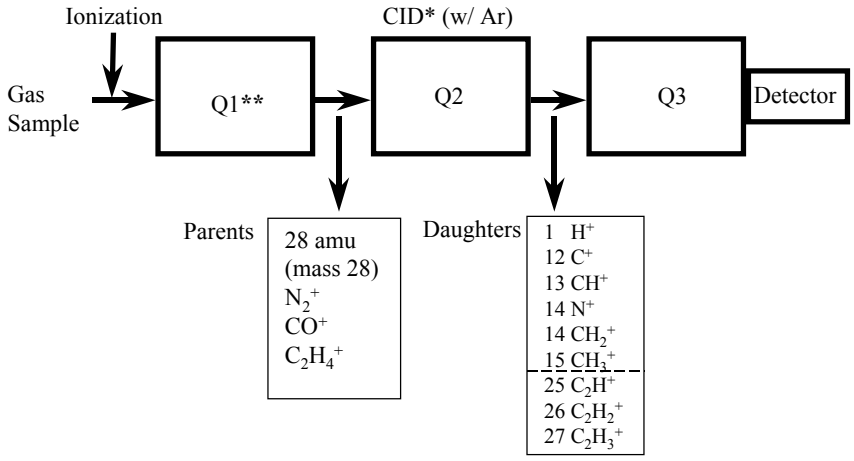

***CID = Collision-Induced Dissociation**
****Q1, Q2, Q3 : first, second, and third single quadrupole mass filters, respectively.**

Figure 4. Operation of triple quadrupole mass spectrometer

In order to obtain species variation above the reacting surface, samples must be collected at various heights. This sampling is accomplished by pushing the sample toward the microprobe that is held in a fixed location. Samples are continuously collected with the microprobe and analyzed to provide the variation in species above the reacting surface. These species "profiles" provide insight into the types of reactions that are occurring in the gas-phase above the sample and provide a benchmark for the validation of the numerical models of propellant combustion developed as part of the overall program.

Representative results for the species detected above a pseudo-propellant of HMX and GAP [10, 11] are presented in the Figure 5. The results show the major reactions that occur in propellants with nitramine as the oxidizer, and the presence of three reaction zones: a primary reaction zone, a dark zone, and the secondary reaction zone. In the primary zone, NO_2 and H_2CO are consumed near the surface to form NO and CO. The dark zone is the region of fairly constant species mole fractions, which is followed by the reactions of NO and HCN to form CO and N_2, and then the conversion of CO to CO_2. Results for pure HMX [12] under similar conditions show that the same major species are present, but that the dark zone is much longer.

2.1.3 Measurement of Temperatures

To complement the chemical species measurements made in the experiments described above, temperature measurements were made. Temperature profiles from the surface into the gas-phase were measured using the micro-thermocouple technique. Both tungsten/rhenium (W/Re) and platinum/rhodium (Pt/Rh) type thermocouples of 25-μm diameter were used for the measurement. The temperature and species measurements were used to check for consistency in the data sets and to investigate for energy release in the gas-phase. Together the species and temperature measurements were provided rigorous test cases for the development of numerical models. For conditions similar to those under which the species measurements were obtained, the temperature profile shows a

rapid rise near the surface and then a region of relatively constant temperature corresponding to the primary and dark zone regions. The secondary region could not be probed due to the high temperatures involved. [11]

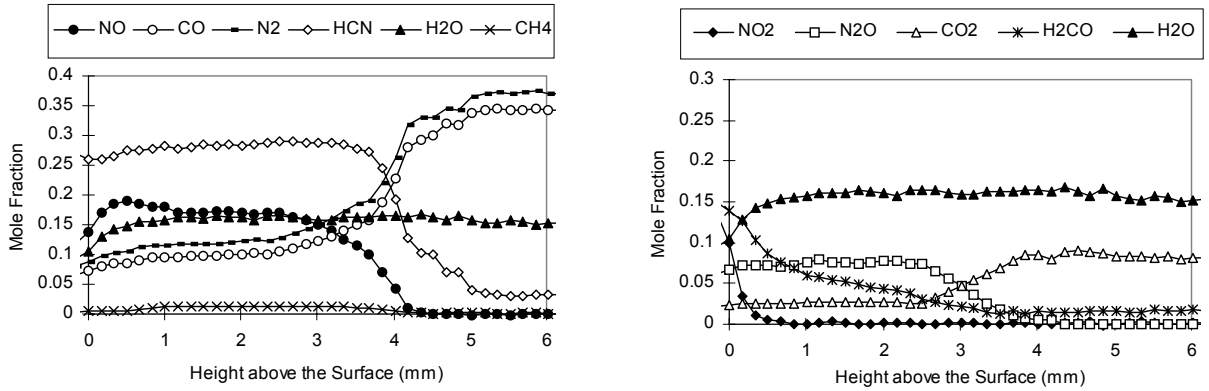

Figure 5. Typical species measurement results: HMX/GAP at 1 atmosphere in argon [10, 11]

2.1.4 AP/HTPB Laminate Flames

In trying to understand the complex combustion processes of AP composite propellants much can be learned from the simpler physical model of a two-dimensional laminate or sandwich configuration. A laminate propellant consists of a thin layer of material, usually binder, laminated between two thicker slabs of a different material, usually AP, as shown in Fig. 1. Previous work on AP/HC-binder laminates by Price and co-workers [13] has illuminated the effects of pressure, binder width, and other variables on surface geometry and burning rate by observing the surface condition of quenched samples. Other work using PLIF and emission imaging by Parr and Hanson-Parr [14] has provided understanding about the ability of various energetic materials to form diffusion flames with hot leading edges by observing the gas-phase flame structure. Both parts of the problem, the gaseous flame zone and the regressing surface, are important since heat release from the gaseous reaction zone drives decomposition and pyrolysis of the solid via conductive heat feedback at the surface. The information obtained from previous work has focused on one region or the other, gas flame or solid surface.

Under the MURI program further advancement was made with development of an optical method for obtaining information about both the flame structure in the gas and the condition of the burning surface of AP/binder laminates simultaneously. Ultraviolet emission and transmission imaging were used to obtain nearly simultaneous images of both gas-phase flame structure and the burning surface profile. By imaging flame emission and surface topography at nearly the same time it was possible to see the important spatial relationship and interaction between gas-phase combustion and surface decomposition.

Figure 6 shows a set of composite emission/transmission images obtained by this technique illustrating the effect of increasing binder thickness. The top images in Fig. 1 are experimental [15] and the bottom figures are computational [16]. Within each image the bottom portion is the unburned solid region. The thin rectangle at the center of the solid region represents the approximate location of the IPDI-cured HTPB binder layer (thickness between 50 and 450 μm). The outer regions are pressed slabs of AP. The top portion of each image is the gaseous flame zone and combustion product region. The interface between the gas and solid regions shows the profile of the

burning surface as obtained from the transmission image. The emission image, which is due primarily to OH* chemiluminescence and broadband emission at 310 nm, is superposed on the surface profile image to give an indication of the gas-phase flame structure in relation to the burning surface.

Although the detailed flame structure and chemistry of AP/HC combustion is still a topic of research [18] it is generally agreed that there are at least two flame zones, a lean premixed AP flame and a stoichiometric diffusion flame. The AP flame forms near and is parallel to the AP surface. It liberates heat primarily by forming N_2 and H_2O, reaching about 1300 K at equilibrium. The diffusion flame forms near AP-binder interfaces between oxidizing species from the AP flame (*e.g.*, ClO_x, O_2) and hydrocarbon species from the binder. It reaches about 2800 K at equilibrium through formation of CO, CO_2 and additional H_2O. It extends downstream from the surface somewhat such that its influence on the decomposing surface through conductive heat feedback is localized in the vicinity of AP-binder interfaces.

The results from simultaneous emission/transmission imaging elucidate some key features about the combustion of AP and HC-binder. It can be seen in Fig. 1 that the diffusion flames actually do not form right at the AP-binder interface. In fact calculations indicate that the stoichiometric level surface does not intersect the burning surface at the fuel-oxidizer interface but outside the interface, on the AP side. This is due to two effects. One is the large stoichiometric ratio for AP/HC (approximately 9:1 by mass) and the other is the effect of finite Peclet number.

The two primary variables investigated in the laminate experiments were pressure and binder width. Binder width is important because it is the length scale for diffusive transport and represents the effects of both AP particle size and AP loading in a particulate composite propellant. The effect of binder width on flame structure and surface profile can be seen in Fig. 1. Both experimental and computational results show that for thicker binder layers the binder surface protrudes into the gas phase above the neighboring AP. The diffusion flame height (at least its stoichiometric surface template) also increases with binder width. It was found that while the diffusion flame height is strongly influenced by binder width it is only weakly affected by pressure, in agreement with simple Shvab-Zeldovich (SZ) theory [18].

Limited investigation of the effects of other laminate propellant variables was also conducted. Oxygenating the binder with fine AP (simulating the binder/fine-AP region of a bimodal composite propellant) was found to cause the diffusion flame height to decrease and the leading edges of the diffusion flame to shift toward the AP-binder interface, in accordance with SZ theory. The effect of curative (DDI vs. IPDI) was also considered. DDI curing tended to produce flickering flames whereas IPDI produced more steady flames. This may be a clue to eventually explaining the distinctive differences between IPDI- and DDI-cured propellant burning rates. More extensive observations of fine-AP doped binder and DDI curing are needed.

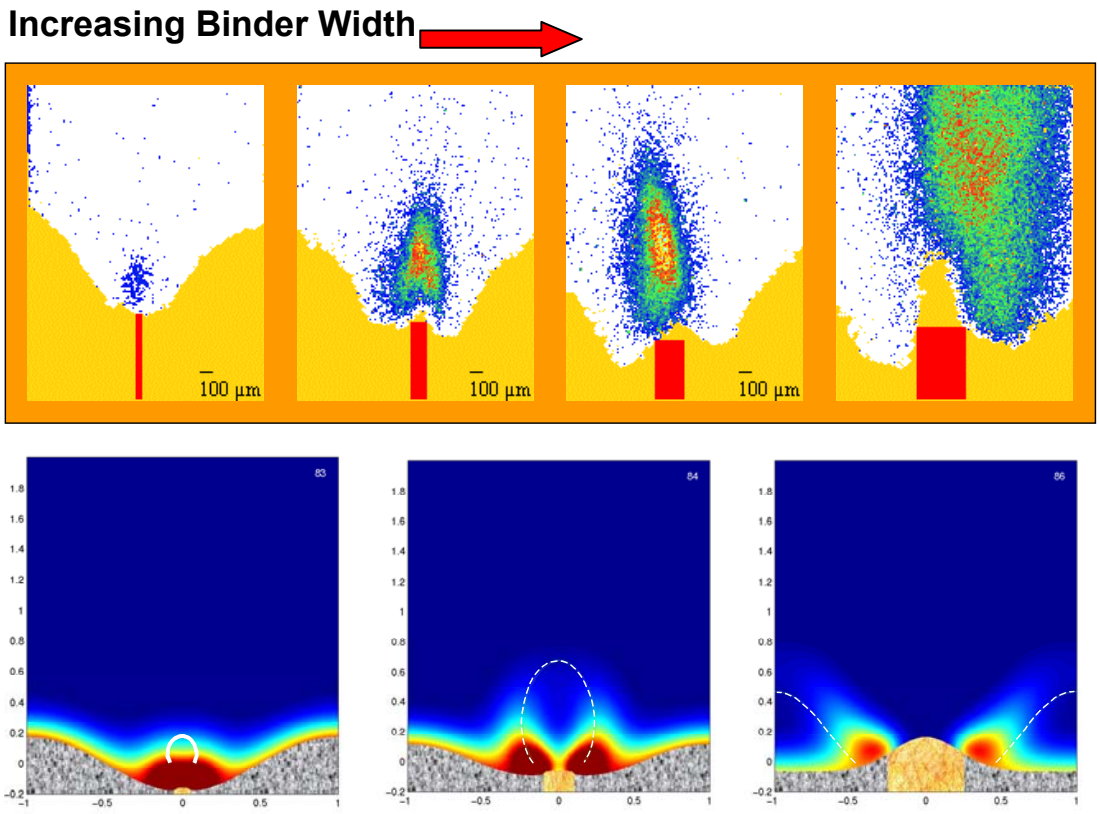

Figure 6. AP/HTPB laminate flame structure and surface profile. Center lamina: IPDI-HTPB binder. Outer laminae: AP. Top row: ultraviolet (310 nm) composite emission-transmission image at 4 atm pressure with 100 W/cm^2 CO_2 laser augmentation. Bottom row: computational simulations. Dotted line is stoichiometric level surface.

References

1. Traineau, J., and Kuentzmann, P., "Some Measurements of Solid Propellant Burning Rates in Nozzleless Motors," *Journal of Propulsion and Power*, Vol. 2, May-June 1986, pp. 215-222.
2. Murphy, J. J., and Krier, H., "Ultrasound Measurements of Solid Propellant Burning Rates: Theory and Application," AIAA Paper No. 98-3556, July 1998.
3. Korting, P. A. O. G., den Hertog, E. H. and Schöyer, H. F. R., "Determination of the Regression Rate of Solid Fuels in Solid Fuel Combustion Chambers by Means of the Ultrasonic Pulse-Echo Technique. Part I. The Measurement Technique," Report LR-453, Delft University of Technology, Delft, The Netherlands, April 1985.
4. Dijkstra, F., Korting, P., and Van der Berg, R., "Ultrasonic Regression Rate Measurement in Solid Fuel Ramjets," AIAA Paper No. 90-1963, July 1990.
5. J. Louwers, G. Gadiot, M. Versluis, AJ. Landman, T. van der Meer, and D. Roekaerts, "Measurement of Steady and Non-Steady Regression Rates of Hydrazinium Nitroformate with Ultrasound," *Proceedings of the International Workshop on Measurement of Thermophysical and Ballistic Properties of Energetic Materials*, Milano, Italy, 22-24 June 1998.
6. Chiyyarath, K., Moser, M. D., and Frederick, R. A., Jr., "Ballistic characteristics of Bi-Plateau Solid propellants," 1997 JANNAF Combustion Subcommittee/Propulsion Systems Hazards Subcommittee/ and Airbreathing Propulsion Subcommittee Joint Meeting, 27-31 October 1997.
7. Moser, M. D., Chiyyarath, C. U., Rasmussen, B. M., Rochford, E. E., and Frederick, R. A., Jr., "Ballistic Characterization of MURI Propellants," 1998 JANNAF Combustion Joint Meeting, Tuscon AR., December 1998.

8. Di Salvo, R., Frederick, R. A., Jr., and Moser, M. D., "Experimental Determination of Pressure Coupled Response Functions." 1998 JANNAF Combustion Joint Meeting, Tuscon AR., December 1998.
9. Y.J. Lee, C.-J. Tang, and T. A. Litzinger, A Triple Quadrupole Mass Spectrometer System for Studies of Gas-Phase Combustion Chemistry of Energetic Materials, *Measurement Science and Technology* v. 9, 1576-1586 (1998)
10. Litzinger, T. A., Y. Lee and C.-J. Tang, An Experimental Study of Nitramine/Azide Propellant Combustion, in Solid Propellant Chemistry, Combustion, and Interior Ballistics edited by Vigor Yang, Thomas Brill, and Wu-Zhen Ren, Progress in Aeronautics and Astronautics, Volume 85, AIAA, Chapter 2.4, pp. 355-379. (2000)
11. Tang, C. J., Y. J Lee, and T. A. Litzinger, The Chemical and Thermal Processes of GAP/Nitramine Pseudo-propellants under CO_2 Laser Heating, *34th JANNAF Combustion Meeting*, 1997.
12. Tang, C.-J., Y. Lee, G. Kudva and T. Litzinger, A Study of the Gas-phase Chemical Structure during Laser-assisted Combustion of HMX, *Combustion and Flame* v. 117, p. 170-188 (1999)
13. Price, E. W., "Review of sandwich burning," 30th JANNAF Combustion Subcommittee Meeting, CPIA Publ. 606, v. 2, 259-279, 1993.
14.] Parr, T. P. and Hanson-Parr, D. M., "Solid Propellant Diffusion fFame Structure," *Twenty-Sixth Symposium (International) on Combustion*, The Combustion Institute, Pittsburgh, 1981-1987, 1996.
15. Chorpening, B. T., G. M. Knott, and M. Q. Brewster, "Flame Structure and Burning Rate of AP/HTPB Propellant Sandwiches," Proceedings of the Combustion Symposium, Vol. 28, 847-853, 2000.
16. Knott, G. M. and M. Q. Brewster, "A Two-Dimensional Model of Composite Propellant Flame Structure and Burning Rate," 36th AIAA/ASME/SAE/ASEE Joint Propulsion Conference, Huntsville, AL, AIAA Paper No. 2000-3460, July 16-19, 2000, submitted to *Combustion Science and Technology*
17. Smooke, M. D., R. A. Yetter, T. P. Parr, D. M Hanson-Parr, "Experimental and Modeling Studies of Two-Dimensional Ammonium Perchlorate Diffusion Flames," *Proceedings of the Combustion Institute*, Vol. 28, 329-846, 2000
18. Brewster, M. Q. and B. T. Chorpening, 2000 "Combustion of Solid Propellant Sandwiches: Effect of Binder Oxygenation and Finite Peclet Number," 5th International Symposium on Special Topics in Chemical Propulsion: Combustion of Energetic Materials, 18-22 June, Stresa, Italy (to be published by Begell House).

2.2 Measurements of the Chemical and Thermal Structure of Propellants and Ingredients (Litzinger)

Information on the chemical and thermal structure of propellant flames and also on the decomposition processes of individual ingredients were required to conduct the modeling of propellant response. As a result a series of studies were conducted to obtain this data using microprobe sampling to obtain species information and micro-thermocouples to determine the thermal structure. This section of the report summarizes the experimental approaches used and then presents major results; details of the various studies can be found in references 1-9. The results are presented for two types of studies – energetic binders and pseudo-propellants, consisting of a nitramine oxidizer and an energetic binder.

2.2.1 Experimental Approach

The experimental apparatus is composed of a high-power CO_2 laser used as the heat source for ignition and sustaining combustion, visual diagnostics for the examination of flame behavior and species sampling height, a triple quadrupole mass spectrometer (TQMS) for gaseous product analysis, and a data acquisition and analysis system. Experiments were conducted at 0.1 MPa (1 atm) in an argon environment, with heat fluxes of 50 to 400 W/cm^2. Gaseous products evolved from the sample surface were extracted by quartz microprobes and analyzed in the TQMS. Using parent and daughter modes of the TQMS and careful calibration, it was generally possible to differentiate and quantify species at the same mass-to-charge (m/z) value. For each m/z value selected, the parent mass was fragmented using the process of collision-induced dissociation (CID) in daughter mode operation. Then, the most probable chemical structures for the parent mass were deduced from the observed daughter ion masses, a library of mass spectra, and available results in the literature. Temperature profiles were measured using the micro-thermocouple technique to investigate gas-phase reaction zones identified by the species measurements and to determine the surface temperatures. Both tungsten/rhenium (W/Re) and platinum/rhodium (Pt/Rh) type thermocouples of 25-μm diameter were used for the measurements. Flame structure and surface behavior were observed using a high-magnification video system.

2.2.2 Energetic Binders

Over the course of the MURI program three different energetic binders were studied: BAMO, BAMO/AMMO and GAP. In addition experiments were performed to determine the effects of TiO_2 on the decomposition of BAMO/AMMO since TiO_2 is an important ingredient in bi-plateau propellants. The major results for the binder studies were the identification and quantification of species. Major findings of the binder studies include:

1) For all three energetic binders direct measurement of nitrogen confirmed that its formation was the first step in decomposition.
2) Subsequent decomposition processes showed evidence of decomposition of the side chain and backbone of the polymers.
3) Large molecular weight species from the backbone decomposition were identified in these studies, which had not been reported by earlier researchers

For the BAMO/AMMO TiO_2 study, the major conclusion was that the effects observed were largely due to changes in physical characteristics rather than chemical characteristics, although some small shifts in chemical composition were observed. The effects observed are believed to be related to the effect of the TiO_2 on the absorption of the incident laser flux. Typical results from the BAMO/AMMO studies are presented in a series of figures in this section.

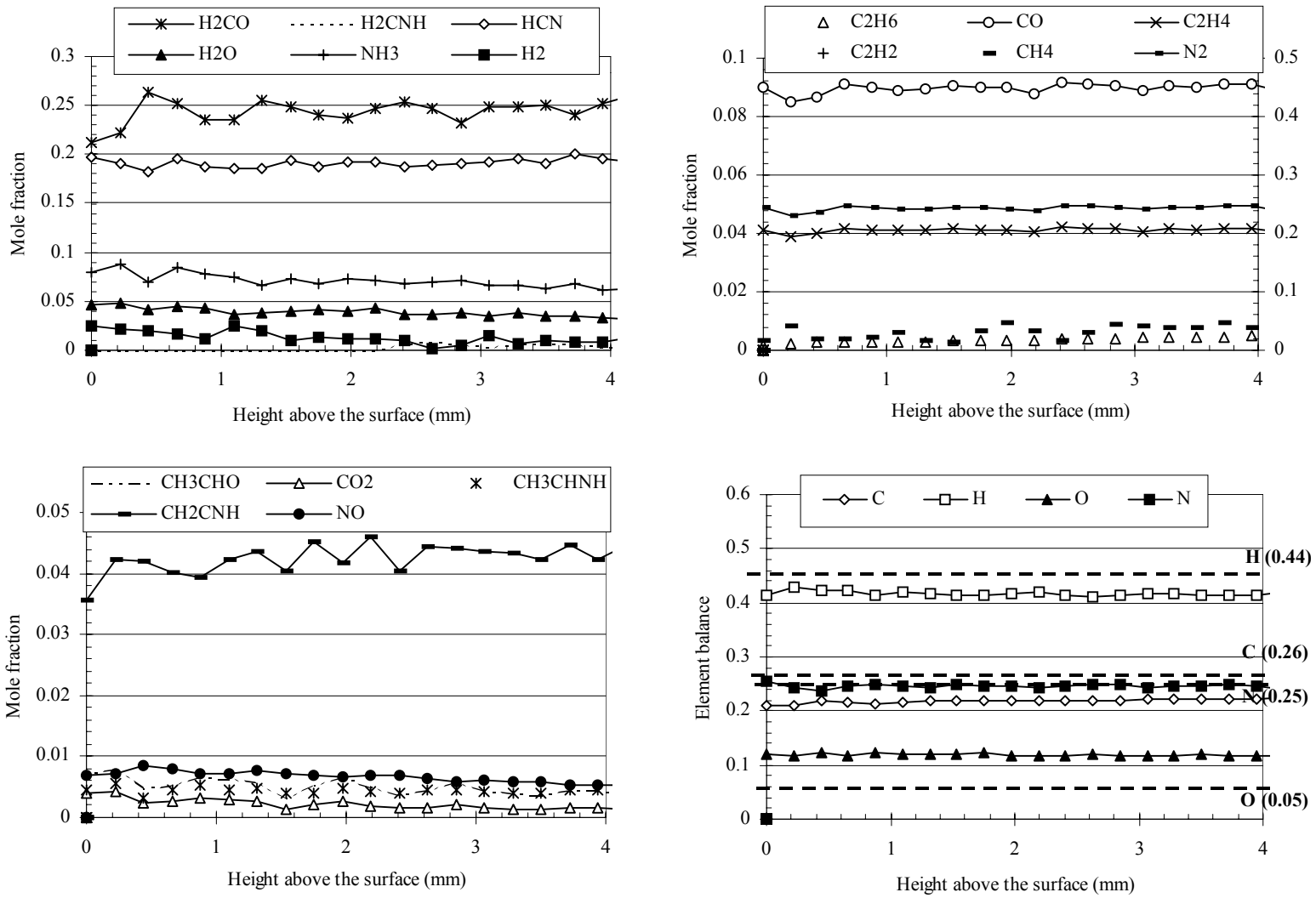

Species profiles and element balance for BAMO/AMMO at 400 W/cm^2

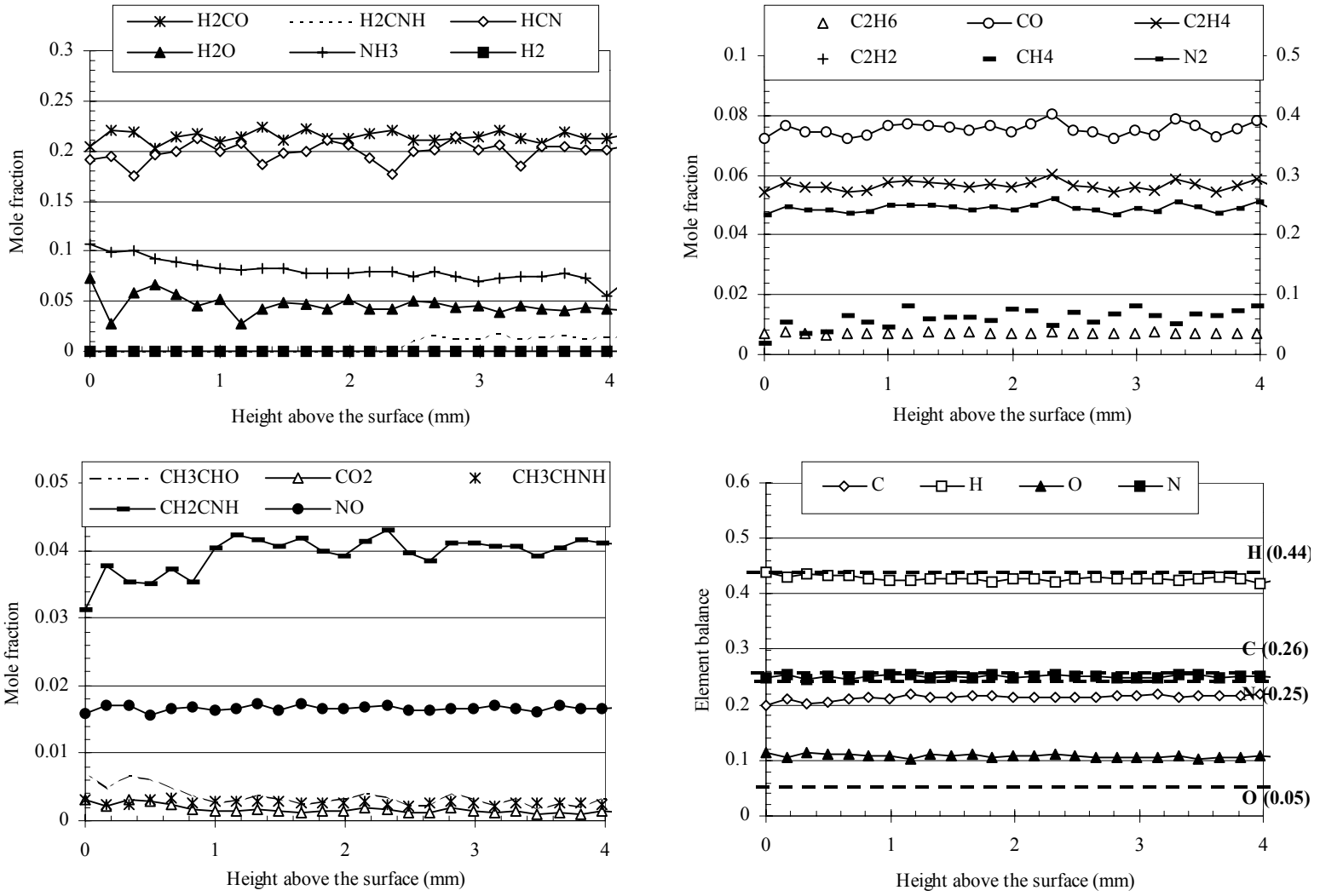

Species profiles and element balance for BAMO/AMMO with 1% TiO_2 at 400 W/cm ^{2}

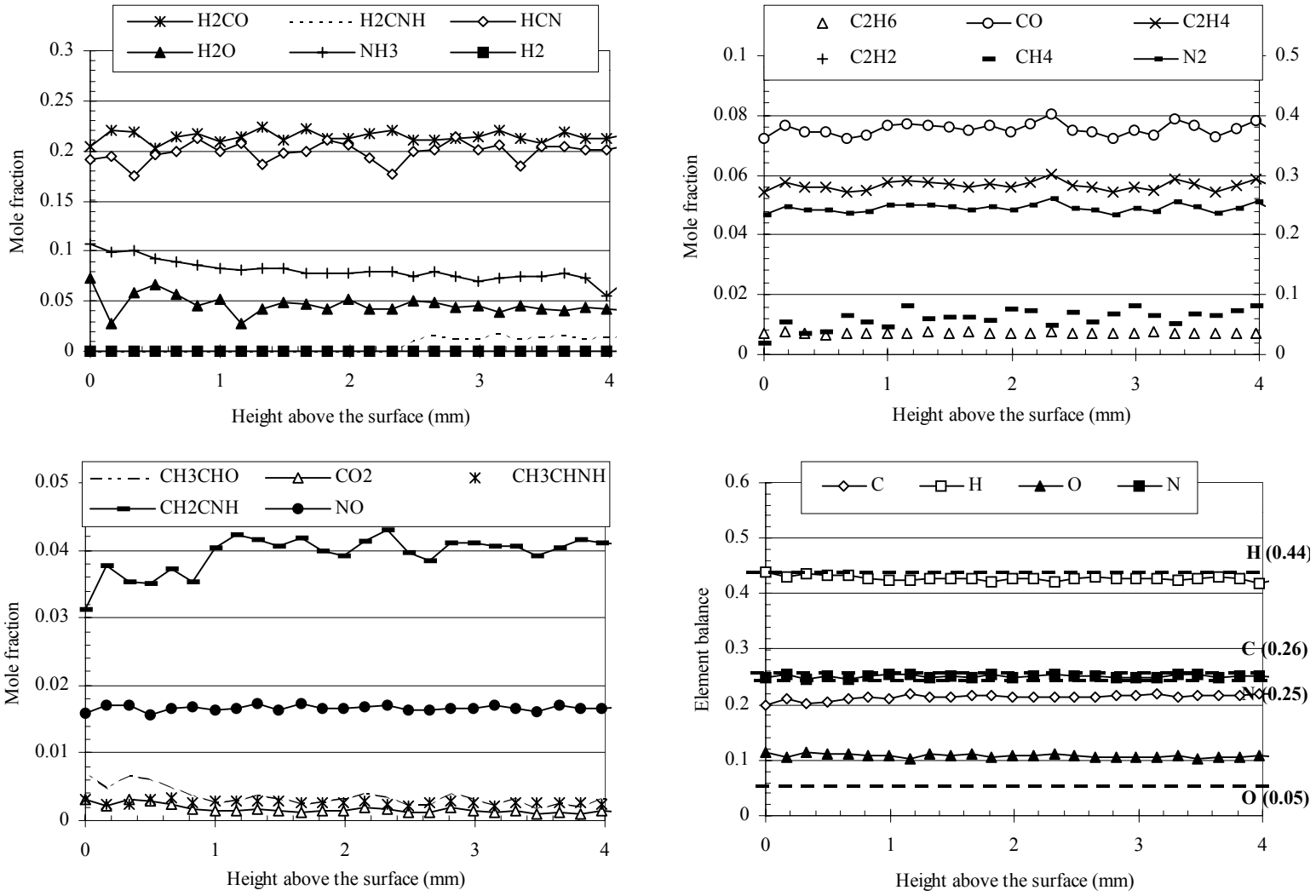

Species profiles and element balance for BAMO/AMMO with 5% TiO_2 at 400 W/cm ^{2}

2.2.3 Pseudo-Propellants

In order to understand the behavior of nitramine propellants, RDX and HMX, in conjunction with energetic binders a series of experiments were performed with pseudo-propellants, which were prepared simply by mixing the nitramine and binder without curing the propellant. All tests were done with laser-supported combustion at 1 atm in Argon. The RDX and HMX used were not modified in any manner to control particle size, which was later found to cause some of problems in the testing. Later work by Parr and Hanson-Parr resolved this matter. Major findings of the work are summarized in remainder of this section.

(a) Effect of Azide Polymer Structure

A comparison of the results for RDX/BAMO and RDX/GAP presents some interesting insight into the effect of the structure of the azide polymer on the chemical and physical processes involved in combustion process. Table 1 presents a summary of the results for key parameters for the three pseudo-propellants tested along with those of the neat nitramines at 100 W/cm^2. Listed in the table are the length of the primary reaction zone, which is estimated from the NO_2 profile, the height above the sample surface at which secondary reactions begin along with surface regression rates and measured surface temperatures. Choosing the point at which the secondary reactions begin was somewhat arbitrary because the species data often showed a region of gradual increase of CO and N_2 followed by a region where they increased with a much greater slope. The tables show the locations corresponding to the beginning of the larger slope.

RDX/GAP had a much higher regression rate than RDX/BAMO, 0.8 versus 0.35 mm/s; however, the two materials had similar surface temperatures. Even with the much higher regression rate, GAP did not affect the length of the primary reaction zone, while the addition of BAMO caused a significant change in the primary reaction zone length as well as the surface concentration of NO_2 and the shape of the NO_2 profile. Clearly, BAMO had a much greater impact on the near surface reaction zones and "stretched" it substantially.

The location where secondary reactions begin was changed substantially by the addition of GAP to RDX; and the secondary reactions occurred over a larger distance, suggesting that the final reactions occur in a distributed fashion, rather than in a thin "sheet" observed for neat RDX. (The effect of GAP on the secondary reaction zone of HMX was similar, and a simple 1-D model of this portion of the flame showed that the products entering the dark zone of the HMX/GAP resulted in a distributed secondary reaction zone.) The addition of BAMO to RDX again had a more dramatic effect than that of GAP. It pushed the beginning of the secondary reactions beyond 4mm from the surface where the species measurements ended. The video recordings of the combustion of RDX/BAMO at this condition showed no luminosity characteristic of the secondary flame, suggesting that it was "blown off" by the addition of BAMO at these experimental conditions.

Additional differences among the propellants can be seen in the near surface mole fractions of the major products. The surface mole fractions for tests at 100 W/cm^2 are summarized in Table 2 along with those for the neat materials. Products associated with the initial decomposition of nitramines, NO_2, HCN, N_2O and H_2CO are listed in the first four columns of the table. Of the three pseudo-propellants RDX/BAMO shows the greatest impact on these species with substantial increase in NO_2 and H_2CO relative to neat RDX, as well as a significant reduction in HCN.

The increase in H_2CO can be partially explained by the fact that it is a product of BAMO. The reduction in HCN is not easily explained because both BAMO and RDX produce it at similar levels, so its reduction may indicate a chemical interaction in the condensed-phase. For RDX/GAP, only the increase of H_2CO appears to be significant.

The very different impact of BAMO and GAP on RDX clearly raises the question of what are the key physical and chemical processes causing them. The structure of the gas-phase reaction zone can be affected by a number of factors including:

- Increased velocity of products leaving the surface
- Increased surface temperatures
- Increased subsurface heat release resulting from the energetic binder
- Addition of inert N_2 at the surface by the azide binder that could lower reaction rates through dilution effects
- Changes in the mole fractions of major reactive species leaving the surface
- More fuel-rich stoichiometry that will lower reaction rates and lower the final flame temperature.

However, all of these factors are present for both GAP and BAMO, and it is not possible to argue from the present data what interplay of these factors caused the observed trends.

(b) Effect of Oxidizer Structure

More interesting questions are raised by comparison of the results for RDX/GAP with those of HMX/GAP to illustrate differences caused by the structure of the nitramine. Previous work with neat nitramines under experimental conditions similar to those used in this study showed distinct differences in their gas-phase chemical structure. Some of these difference are clear in Tables 1 and 3 including the fact that the primary reaction zone length of HMX was much greater than that of RDX at the same experimental conditions. When GAP was added to HMX it resulted in a *shortening* of the primary reaction zone at both heat fluxes, whereas the primary reaction zone for RDX/GAP was unchanged relative to that for neat RDX. The effect on the location of the beginning of the secondary reactions was to move it farther from the surface for both nitramines with the addition of GAP. Also the effect of GAP on the burning rate of RDX was much greater than that for HMX at both heat fluxes, even though the surface temperatures increased by approximately the same amount, 40 to 50K, in each case.

(c) Effects of Heat Flux on Pseudo-Propellant Combustion

The arrows included in Table 4 illustrate the direction of the change of a each table entry when heat flux was increased. The number of arrows is an attempt to visually indicate the magnitude of the change; an increase of approximately three times was used to delineate the use of one and two arrows. A horizontal arrow indicates that a quantity was unchanged within the uncertainly of the experiments.

For the two nitramine/GAP propellants, the effect of increasing heat flux on burning rate was of approximately the same order; the burning rate increased by slightly more than a factor of 2. For RDX/BAMO, however, the effect of increasing heat flux was nearly a factor of 4. Even considering the fact that the high heat flux for RDX/BAMO was 400 W/cm^2 as opposed to 300 W/cm^2 for the propellants containing GAP; this is a more substantial effect of

heat flux on regression rate. For all of the pseudo-propellants, an increase in heat flux resulted in higher measured surface temperatures, in contrast to the neat nitramines, for which surface temperature was independent of heat flux.

The effect of increasing heat flux on the reaction zones was complex, showing some consistent trends and some opposing trends. For all three propellants, increasing the heat flux caused the primary reaction zone length to increase by a factor of 2 or more. On the other hand the start of secondary reactions showed opposite trends for the two GAP based propellants. Increasing heat flux caused the start of secondary reactions to move closer to the surface for RDX/GAP, while it pushed them beyond 8mm for HMX/GAP. The effect of increasing heat flux on RDX/BAMO is not entirely clear because of the limited spatial extent of the measurements that were taken only to approximately 3mm at the high heat flux. The changes in reaction zone structure and burning rate cannot be explained with simple phenomenological arguments.

(d) Closure

The species and temperature data for three nitramine/azide pseudo-propellants presented in this paper must be considered in light of the very challenging nature of the experiments. While the element balances are not as good as desired, indicating that some species may have been missed, the experiments are among the few in the literature that attempt mass closure in propellant studies. Measurements of surface temperature are notoriously difficult due to the challenge of identifying the surface and problems with residue. Independent experiments to confirm the species and temperature data would be very useful to the overall effort to understand and model the behavior of the nitramine/azide propellants. Even so, the data show many fascinating similarities and differences among the three materials in terms of nitramine/azide polymer interactions and also on the effects of increasing heat flux. The trends are too complex to explain with phenomenological arguments and point to the need for detailed numerical modeling of the pseudo-propellants. The experimental results presented in this paper provide many challenging cases for model validation.

Table 1. Combustion Characteristics for Nitramines and Pseudo-propellants at 100 W/cm^2

	Surface regression rate (mm/s)	Length of Primary Reaction Zone (mm)	"Dark Zone" Present	Beginning of secondary reactions (mm above surface)	$T_{surface}$ (K)	$T_{dark\ zone}$ (K)
RDX	0.2	~0.5	No	~0.5	610	NA
HMX	0.9	~2.5	No	~2.5	650	NA
RDX/GAP	0.8	~0.5	Yes	~3.5	650	1250
HMX/GAP	1.1	~0.5	Yes	~3.5	700	1300
RDX/BAMO	0.35	~1	Yes	No final flame	640	1200

NA – not applicable

Table 2. Mole Fractions of Species at Sample Surface for 100 W/cm^2

	NO_2	HCN	N_2O	H_2CO	NO	N_2	NH_3	CO	CO_2	H_2O
RDX	0.04	0.23	0.09	0.03	0.21	0.06	0	0.08	0	0.22
HMX	0.10	0.20	0.09	0.18	0.14	0.08	0	0.06	0	0.15
GAP	0	0.16	0	0.10	0	0.35	0.08	0.10	0	0.01
BAMO	0	0.22	0	0.15	0	0.42	0.05	0.02	0	0.05
RDX/GAP	0.05	0.19	0.06	0.08	0.14	0.10	0.04	0.09	0.02	0.20
HMX/GAP	0.10	0.26	0.07	0.14	0.14	0.08	NM	0.07	0.02	0.10
RDX/BAMO	0.13	0.14	0.08	0.10	0.13	0.10	NM	0.06	0	0.17

NM – not measured

Table 3. Effect of Increasing Heat Flux on Combustion Characteristics

(Arrows indicate change relative to corresponding case at 100 W/cm^2; all results for 300 W/cm^2 except RDX/BAMO at 400)

	Surface regression rate (mm/s)	Length of Primary Reaction Zone (mm)	"Dark Zone" Present	Beginning of secondary reactions (mm above surface)	$T_{surface}$ (K)	$T_{dark\ zone}$ (K)
RDX	0.7 ↑↑	~1 ↑	No	~1.5 ↑	610 →	NA
HMX	1.2 ↑	~2.5 →	No	~4 ↑	650 →	NA
RDX/GAP	1.9 ↑	~1 ↑	Yes	~2.5 ↓	700 ↑	1250 →
HMX/GAP	2.4 ↑	~1.5 ↑↑	Yes	> 8 ↑↑	750 ↑	1400 →
RDX/BAMO	1.4 ↑↑	~2 →	Yes	~ 3	670 ↑	1500 ↑

NA – not applicable

Table 4. Mole Fractions of Species at Sample Surface for High Heat Flux

	NO_2	HCN	N_2O	H_2CO	NO	N_2	NH_3	CO	CO_2	H_2O
RDX	0.12	0.23	0.08	0.03	0.16	0.05	0	0.07	0	0.22
HMX	0.12	0.18	0.12	0.10	0.10	0.06	0	0.03	0	0.19
GAP	0	0.16	0	0.11	0	0.36	0.10	0.11	0	0.01
BAMO	0	0.22	0	0.15	0	0.42	0.05	0.02	0	0.05
RDX/GAP	0.12	0.18	0.04	0.07	0.10	0.12	0.04	0.10	0.02	0.16
HMX/GAP	0.03	0.26	0.08	0.15	0.13	0.10	NM	0.10	0.03	0.12
RDX/BAMO	0.14	0.19	0.09	0.02	0.13	0.17	NM	0.06	0.01	0.21

NM – not measured

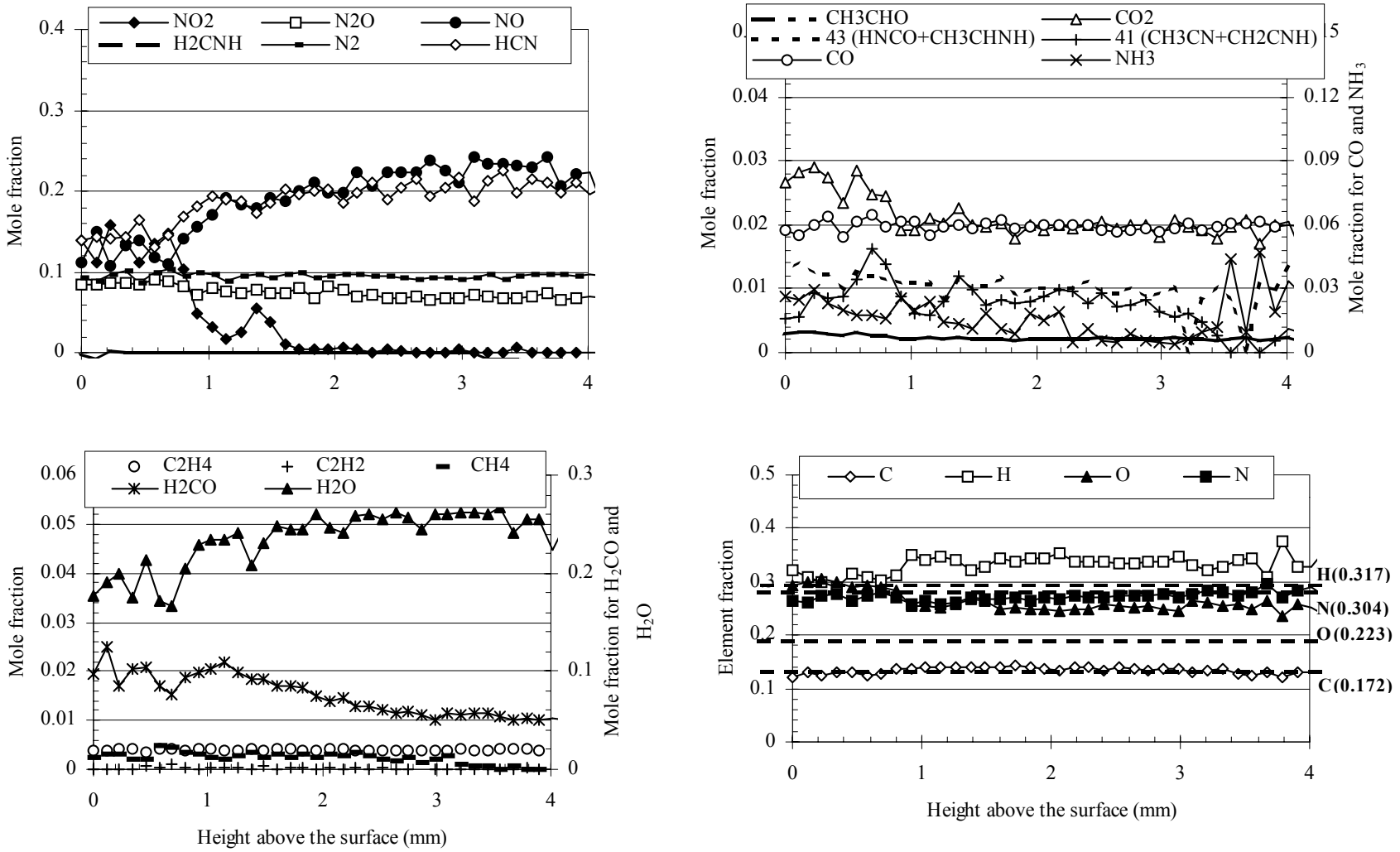

Species and element fraction profiles for deflagration of RDX/BAMO pseudo-propellants at heat flux of 100 W/cm2 in argon at 1 atmosphere.

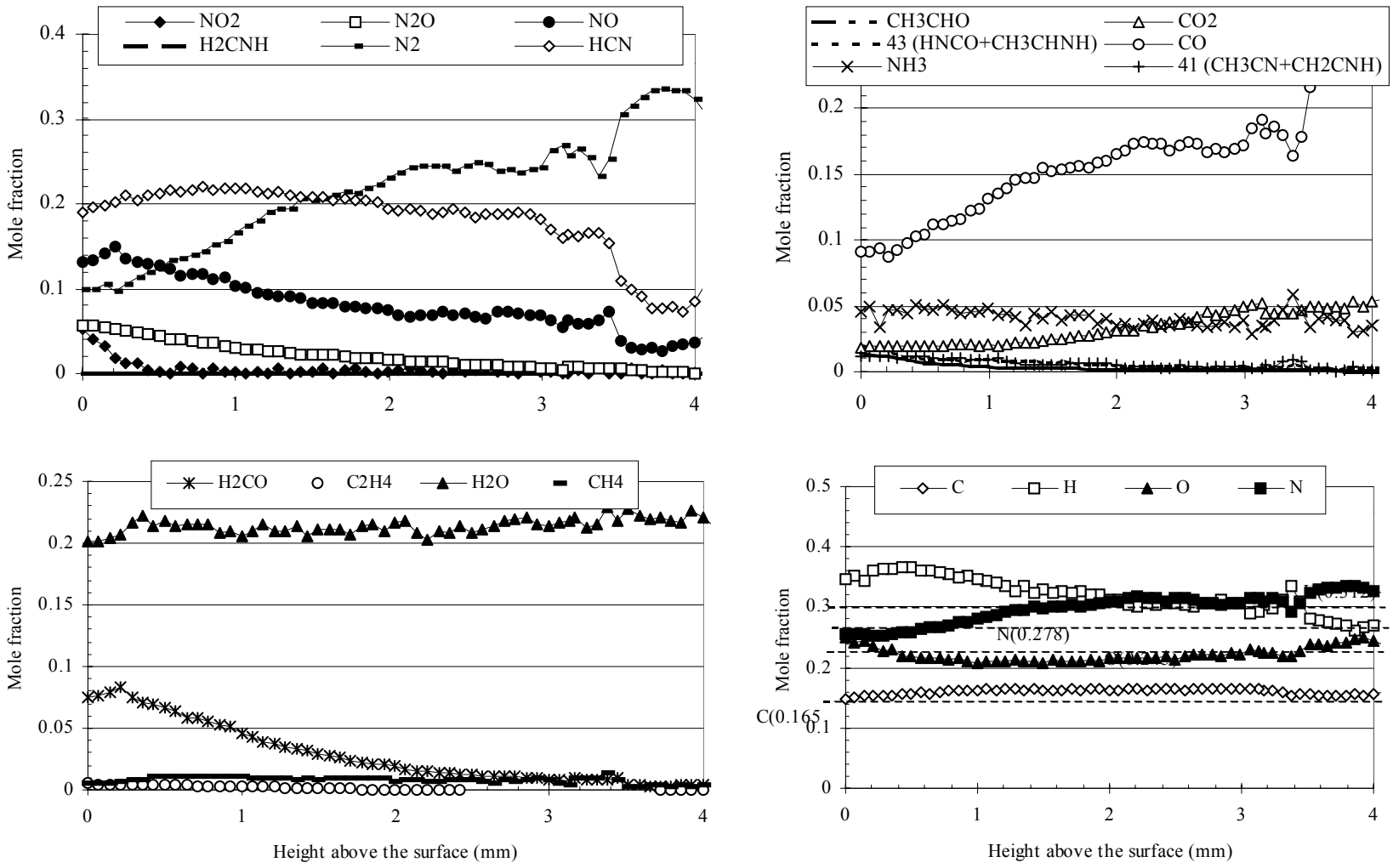

Species and element fraction profiles for deflagration of RDX/GAP pseudo-propellants at heat flux of 100 W/cm2 in argon at 1 atmosphere.

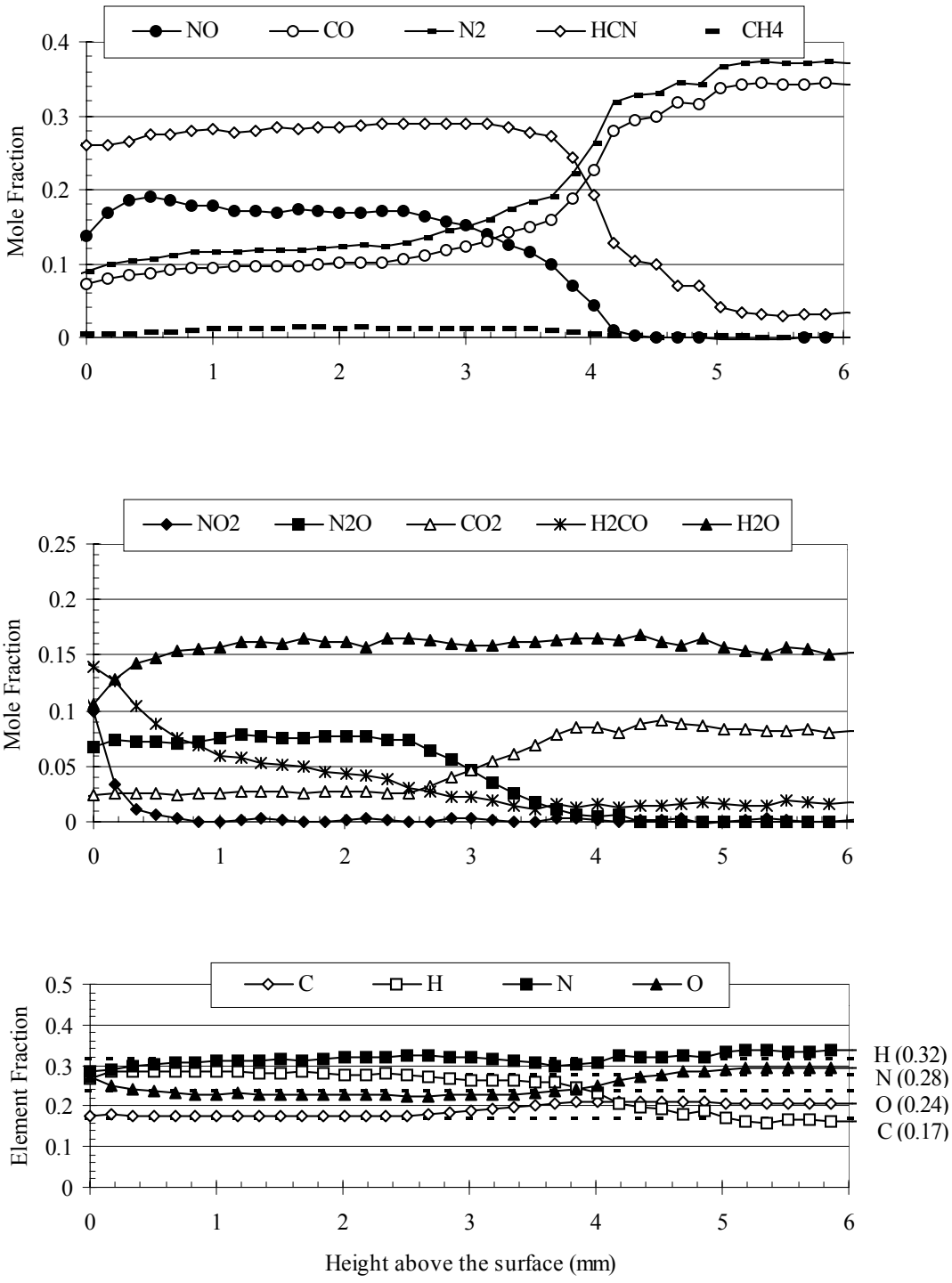

Species and element fraction profiles for deflagration of HMX/GAP pseudo-propellants at heat flux of 100 W/cm^2 in argon at 1 atmosphere.

References

1. Litzinger, T. A., Y. Lee and C.-J. Tang, An Experimental Study of Nitramine/Azide Propellant Combustion, in Solid Propellant Chemistry, Combustion, and Interior Ballistics edited by Vigor Yang, Thomas Brill, and Wu-Zhen Ren, Progress in Aeronautics and Astronautics, Volume 85, AIAA, Chapter 2.4, pp. 355-379. (2000)
2. Tang, C.-J., Y. Lee, G. Kudva and T. Litzinger, Simultaneous Species and Temperature Measurements during Laser-assisted Combustion of GAP, *Combustion and Flame* v. 117, 244-256 (1999)
3. Tang, C.-J., Y. Lee, G. Kudva and T. Litzinger, A Study of the Gas-phase Chemical Structure during Laser-assisted Combustion of HMX, *Combustion and Flame* v. 117, p. 170-188 (1999)
4. Lee, Y., C.-J., Tang and T. Litzinger, A Study of the Chemical and Physical Processes Governing the during CO_2 Laser-assisted Pyrolysis and Combustion of RDX, *Combustion and Flame*, 117:600-628 (1999)
5. Lee, Y. J., C.-J. Tang and T. Litzinger, Thermal Decomposition of RDX/BAMO Pseudo-Propellants, *Combustion and Flame*, 117:795-809 (1999)Lee, Y., C.-J. Tang, G. Kudva and T. Litzinger. 1996. Thermal Decomposition of BAMO and RDX/BAMO Pseudo-propellants. *33rd JANNAF Combustion Meeting*
6. Lee, Y. J., G. Kudva and T. Litzinger, "Thermal Decomposition of BAMO/AMMO and BAMO/AMMO/TiO_2," *36th JANNAF Combustion Meeting*, 1999.
7. Lee, Y. , C.-J. Tang , G. Kudva and T. Litzinger. The Thermal Decomposition of 3,3'-Bis-Azidomethy-Oxetane *Journal of Propulsion and Power*. 14: 37-44 (1998)
8. Y.J. Lee, C.-J. Tang, and T. A. Litzinger, A Triple Quadrupole Mass Spectrometer System for Studies of Gas-Phase Combustion Chemistry of Energetic Materials, *Measurement Science and Technology* v. 9, 1576-1586 (1998)
9. Tang, C. J., Y. J Lee and T. A. Litzinger, The Chemical and Thermal Processes of GAP/Nitramine Pseudo-propellants under CO_2 Laser Heating, *34th JANNAF Combustion Meeting*, 1997.

2.2.4 Ultrasonic Measurement of Propellant Ballistics (Frederick)

The quasi-steady ballistics of solid propellant samples were measured using ultrasonic instrumentation.[1-5] This included measuring the burning rates at pressure from 100 to 5000 psia and initial temperatures from 24 to 60C. This technique is highly effective for measuring the instantaneous thickness of the propellant. The ultrasonic pulse-echo technique has been developed by ONERA in the 80's [6] and utilized at several other places.[7-10] UAH participated in an AGARD working group that made an assessment of the international applications of ultrasonic instrumentation to laboratory burners and motors for steady state applications.[4,5] UAH also held an international workshop on this topic as part of the program. The technique has been used and extended at UAH to measure steady state burning rate[1], temperature sensitivity, and propellant response function (discussed below). The ultrasonic transducer emits a stress wave that propagates through the propellant to the combustion surface where it is then reflected back down to the transducer. The same transducer then detects the returning pulse. By measuring this propagation time and knowing the speed of sound through the propellant, the instantaneous thickness can be determined for each pulse emitted by the ultrasonic transducer. The burning rate is determined by taking the time derivative of the instantaneous thickness.

The measurement process is shown schematically in Figure 1 along with a typical waveform. The ultrasonic transducer sends a pulse through the epoxy coupling material and to the propellant. Care is taken to match the impedance of the coupling material and propellant to minimize the echo produced at the interface of the coupling and the propellant. The propellant/burning gas interface produces the strongest echo that is returned and detected by the ultrasonic transducer. The propagation time of the burning surface echo is measured by an electronic instrument at 1000, 5000 or 10,000 Hz. Special care has been taken to characterize the effect of pressure on the acoustic properties of the propellant and coupling material. An analogue electronic device automatically interprets the

waveform to determine the return time of the surface reflection. The complete waveform is also digitized for post-test analysis. All of the data were recorded at 1000 or 5000 Hz.

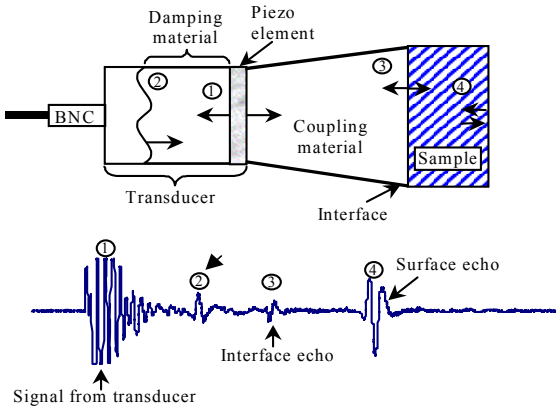

Figure 1. Ultrasonic Transducer, Propellant, and Sample Signal

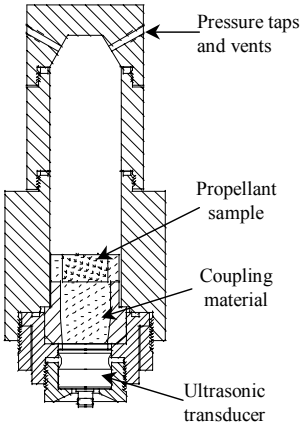

Figure 2. Schematic of Closed Bomb with Sample

The quasi-steady test is performed in a closed bomb, shown in Figure 2. As the sample burns, the internal pressure of the combustion bomb increases. Therefore, burning rate for a large range of pressures can be obtained from one test. A typical test uses 25 grams of propellant and covers pressure ranges from 500 to 5000 psia. The pressurization level and pressurization rate are dependent on the propellant burning rate, mass of the propellant, initial chamber pressure, and the initial volume of the chamber. For the elevated temperature tests, the entire propellant sample and the sample holder are preconditioned to an elevated temperature before testing occurs. Example burning rates for the metallized Thiokol propellant are shown in the Figure 3 below. The ultrasonic data are higher than the Thiokol data for low pressures but match better at high pressure. The temperature sensitivity is fairly constant. The great utility of the technique developed is that data over pressure ranges that correspond to operational systems is obtained with small quantities of ingredients. This allows screening of new ingredients and formulations in the laboratory.

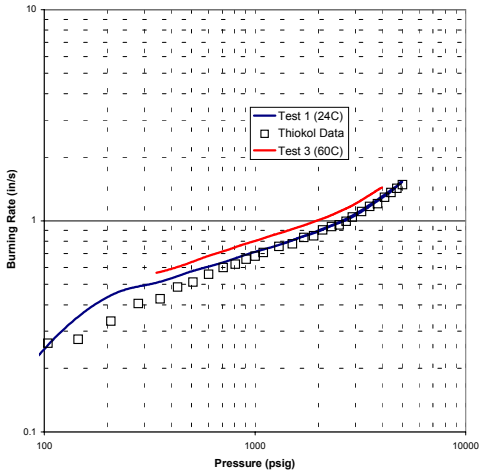

Figure 3. Burning rate vs. pressure for BAMMO/AMMO/GAP propellant with 18% aluminum.

(a) Ultrasonic Measurement Uncertainty [11-14]

The pulse-echo ultrasonic technique has been successfully applied to solid propellant for burning rate measurement. However, no one has ever performed an uncertainty analysis of this technique. This study presents a detailed uncertainty assessment of the technique and shows the results for a set of three selected propellants. Direct Monte-Carlo simulations were performed to determine the uncertainty in the burning rate. The total uncertainty was shown to range between 0.01 in/sec and 0.035 in/sec and the relative uncertainty from 3.5 to 5%. In general, when propellant burns faster, the total uncertainty is larger and the relative uncertainty is smaller. The total uncertainty in the burning rate tends to follow the same variation with pressure as the burning rate and the relative uncertainty stays pretty much constant during an entire test. A sensitivity analysis shows that the parameters which have the most influence on the uncertainty in the burning rate are the propagation time of the ultrasonic pulses through the propellant and the initial thickness of the propellant. The thicker the initial length of the propellant sample is, the lower the uncertainty will be.

Figure 4 shows the effect of initial temperature on the burning rate of propellant #2. This propellant was tested at two different initial temperatures (20°C and 55°C). The graph clearly shows that burning rate increases as the initial temperature increases. Figure 14 shows the effect of the initial temperature on the relative uncertainty in the burning rate of this propellant. However, the relative uncertainty in the test fired at 55°C is much higher than the other one (5% compare to 3.6%) even though the burning rate is higher. This is due to the fact that the initial thickness of the propellant was 0.5 in for the test fired at 55°C and 0.75 in for the test fired at 20°C. The initial thickness of the propellant has an important effect on the value of the uncertainty in the burning rate. The higher the initial thickness, the lower the relative uncertainties in the burning rate.

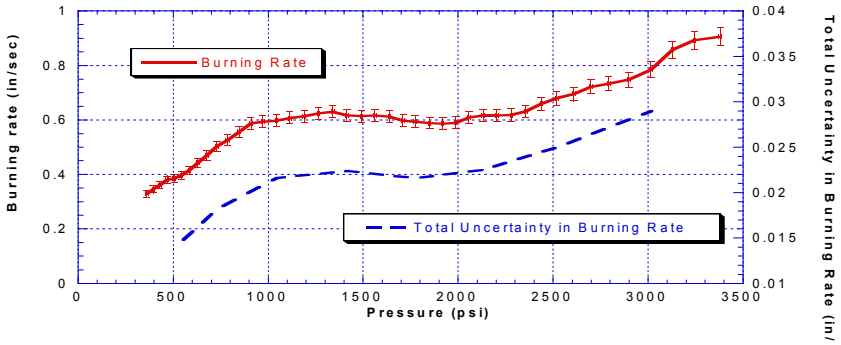

Figure 4. Burning Rate of Propellant #2 at 20°C and 55°C

References

1. Chiyyarath, K., Frederick, R.A., Jr. and Moser, M., Ballistic Characterization of Bi-Plateau Solid Propellants," CPIA Pub 662, Vol. IV, pp 73-81, Oct 1997. (Limited Distribution)
2. Moser, M., "Ultrasonic Instrumentation for Solid Propellants," International Workshop on Advanced Combustion Diagnostics, Huntsville, AL, January 1998.
3. Moser, M.D., Chiyyarath, C. U., Rasmussen, B. M., Rochford, E. E., and. Frederick, R. A, Jr., "Ballistic Characterization of MURI Propellants", CPIA Pub 680, Vol. II, pp. 397-406, Dec 1998. (Limited Distribution)
4. Frederick, R.A., Jr., Traineau, J-C, and Popo, M., "Review of Ultrasonic Technique for Steady State Burning Rate Measurements," AIAA Paper 2000-3801, 36th AIAA/ASME/SAE/ASEE Joint Propulsion Conference and Exhibit, July 16-19, 2000.

5. Frederick, Robert, and Traineau, J-C, *Evaluation of Methods for Solid Propellant Burning Rate Measurements*, Chapter 5, "Non-Intrusive Techniques," NATO/RTO Advisory Report, AVT Working Group 016, edited by Ronald S. Fry, JHU/CPIA, In Press, January 2002
6. Traineau, J., and Kuentzmann, P., "Some Measurements of Solid Propellant Burning Rates in Nozzleless Motors," *Journal of Propulsion and Power*, Vol. 2, May-June 1986, pp. 215-222.
7. Murphy, J. J., and Krier, H., "Ultrasound Measurements of Solid Propellant Burning Rates: Theory and Application," AIAA Paper No. 98-3556, July 1998.
8. Korting, P. A. O. G., den Hertog, E. H. and Schöyer, H. F. R., "Determination of the Regression Rate of Solid Fuels in Solid Fuel Combustion Chambers by Means of the Ultrasonic Pulse-Echo Technique. Part I. The Measurement Technique," Report LR-453, Delft University of Technology, Delft, The Netherlands, April 1985.
9. Dijkstra, F., Korting, P., and Van der Berg, R., "Ultrasonic Regression Rate Measurement in Solid Fuel Ramjets," AIAA Paper No. 90-1963, July 1990.
10. J. Louwers, G. Gadiot, M. Versluis, AJ. Landman, T. van der Meer, and D. Roekaerts, "Measurement of Steady and Non-Steady Regression Rates of Hydrazinium Nitroformate with Ultrasound," *Proceedings of the International Workshop on Measurement of Thermophysical and Ballistic Properties of Energetic Materials*, Milano, Italy, 22-24 June 1998.
11. Dauch, F., Moser, M.D., Frederick, Jr., R.A., and Coleman, H.W., "Uncertainty Assessment of Ultrasonic Measurement of Propellant Burning Rate." CPIA Pub 680, Vol. I, pp. 293-304, Dec 1998, public release
12. Dauch, Frederic*, Uncertainty Analysis of the Ultrasonic Technique Applied to Solid Propellant Burning Rate*, Master of Science in Engineering, The University of Alabama in Huntsville, Huntsville AL, March 22, 1999, Advisor: M.D. Moser.
13. Dauch, F., and Moser, M.D., Frederick, R.A., Jr., and Coleman, H.W., "Uncertainty Assessment of the Pulse-Echo Ultrasonic Burning Rate Measurement Technique," AIAA Paper No. 99-2224, 35th AIAA/ASME/SAE/ ASEE Joint Propulsion Conference Joint Propulsion Conference, Los Angeles, CA, June 20-23, 1999
14. McQuade, W., Ultrasonic Instrument Development for Solid Propellant Burning Rate Measurement, March 1998, Chairman: M. D. Moser.

2.3 Measurements of the Dynamical Response of Burning Solid Propellants

One of the major objectives of the MURI program was to develop mechanistic understandings and techniques to determine the dynamic response of a solid propellant to a disturbance. It was hoped that the achievement of such an objective would help assure the combustion stability of future solid rocket motors employing advanced energetic propellants.

The standard device to measure the response has been the T-burner. Response data were acquired by Blomshield (NAWC) with the T-burner, to serve as a frame of reference for comparing and evaluating the new methods and to assure having data for stability analyses. His results and participation are summarized in Section 9.1.

Ultrasound and dynamic recoil techniques formed the basis of investigating novel methods for combustion response measurements. Extensive data were obtained by Brewster (UIUC) and by Litzinger (PSU). Unfortunately, the dynamic recoil method is limited to very low pressures and controlling mechanisms at very low pressures are not necessarily relevant to the pressures of interest. However, good and interesting data were obtained as long as the frequencies were kept low and constant during a test, as shown by Litzinger (PSU) and Brewster (UIUC). High frequencies gave inadequate signals and were too rapid for a meaningful response at the very low burn rates associated with very low pressures. The attempt to sweep a large frequency range in a single test turned out to give meaningless data because the thermal wave did not have enough time to adjust to the rapid frequency changes. Another problem with the method, when using an oscillatory laser heat flux as the driver, is accurately relating heat flux with oscillatory pressure responses; they are not the same, nor does a radiant flux at lower pressure properly represent a higher pressure in the energy balance. These results are summarized in Sections 9.2 and 9.3

Another technique, attractive because of its capabilities to high frequencies at practical pressures of interest, is the MHD burner. This method was developed by Micci at PSU. However, results indicated that more interpretive work is needed to extract meaningful results from the raw data. His results are summarized n Section 9.4.

The ultrasound method was validated by steady-state and quasi-steady burn rate and σ_p measurements at UAH (Moser) and UIUC (Krier), which agreed with more conventional techniques employed by NAWC (Atwood), PSU (Kuo) and the Thiokol supplier of first-round propellants (Campbell). Response function measurements that combined ultrasound with an oscillatory driven burner were limited to low frequencies, <150Hz, because of signal and accuracy limitations. These limitations were studied extensively, both analytically and experimentally, as part of the work by Moser and Krier. Data at low frequencies are nevertheless valuable to show how the response varies from the pressure exponent as we move off of zero frequency, and accurately define the start of the response function curve which can then be picked up by analytical computations for higher frequencies. It is a promising method which deserves more future work.

2.3.1 T-Burner Response Measurements of MURI Propellants (Blomshield, NAWC)

This section describes the experimental T-Burner response testing results of two bi-plateau propellants and one metallized mono modal ammonium perchlorate propellant. The combustion instability behavior is always of interest when new propellants are obtained. These new propellants can be made up of new oxidizers, binders or additives. It is often of interest how changes in formulation and new ingredients affect the propellant combustion response.

The only standardized method to determine the response is the T-Burner. In this study the T-burned at China Lake was used. It has a pressure range from atmospheric to 4000 psi and a frequency range of 300 to 4000 Hz.

(a) Propellants

Thiokol Corporation in Utah cast the two bi-plateau propellants used in this study. Although Thiokol, as part of this research effort cast eleven bi-plateau propellants, only two were cast in sufficient quantity for pressure coupled response testing. The propellants are designated No. 1a, Mix 0304/0305, and No. 4, Mix 209-96-064. No. 1a was the aluminized baseline propellant and No. 4 was the non-aluminized baseline propellant. Both were AP (ammonium perchlorate) based HTPB (Hydroxyl Terminated PolyButadine) propellants. The other nine propellants cast in this program varied ammonium perchlorate size, plasticizer, coarse to fine ratio and solid additives. They will not be discussed in this section. These propellants were unique because certain additives and binder components were found to provide very interesting burning rate behavior. The observed and controllable behavior was the formation of two distinct low-pressure exponent regions of the burning rate versus pressure curve. Hence, the name for this class of propellants is called bi-plateau propellants. The ballistic properties make them very suitable for boost and sustain applications. An explanation for the plateau behavior can be found in Reference 1. Table 1 shows the approximate formulations and the three test conditions for each propellant. One of these contained aluminum and one was a non-aluminized analog. Each be-plateau propellant was tested at the two plateau pressures and at one pressure in-between. Figures 1 and 2 show the burning behavior. The two plateau regions for each propellant are clearly seen.

Table 1. Propellants

Ingredients	No. 1a			No. 4		
HTPB	12.0			12.0		
AP (2 and 200 μm distributions)	71.0			86.0		
TiO_2	2.0			2.0		
Aluminum (H-95)	15.0			0		
Burning Characteristics	Pressure (psi)					
	300	1000	2200	300	1000	2000
Rate (in/sec)	0.23	0.36	0.61	0.22	0.38	0.60
Exponent	0.19	0.71	0.0	0.28	1.00	0.0

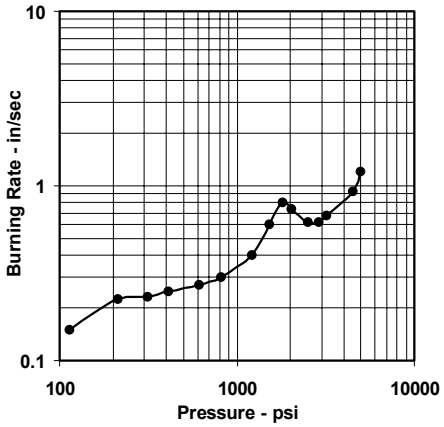

Figure 1. No. 1a, Metallized Bi-Plateau Propellant

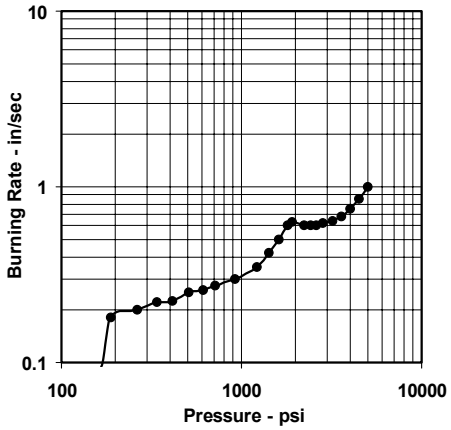

Figure 2. No. 4, Non-Metallized Bi-Plateau Propellant

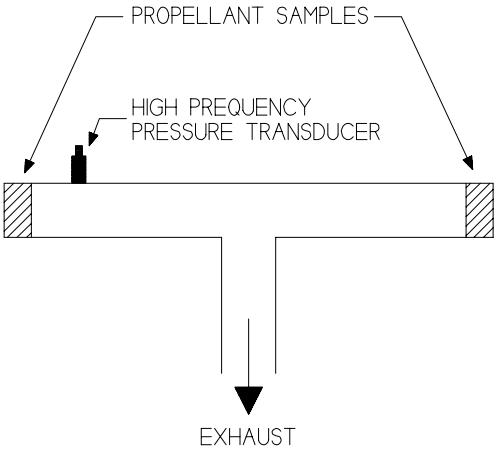

Figure 3. T-Burner

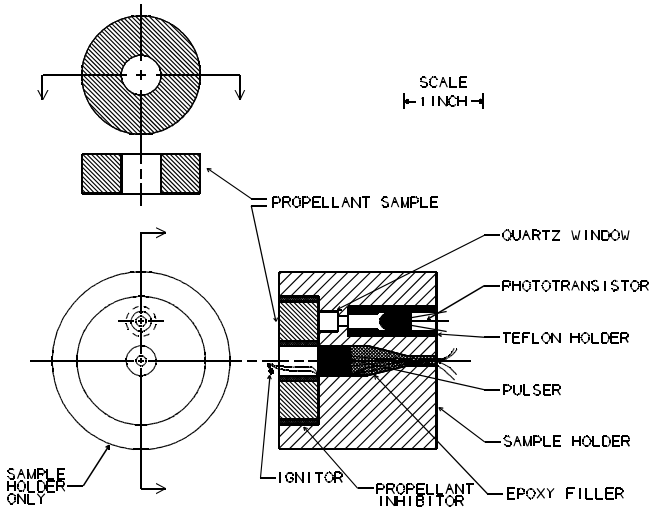

Figure 4. T-Burner Propellant Sample and Holder

United Technologies Chemical Systems Division in San Jose, CA developed the mono-modal metallized propellant. This propellant was unique in that it only had one distribution of AP versus two or three unique distributions for conventional AP based propellants. This propellant had a more conventional burning rate curve. The mono modal AP propellant was evaluated at only one pressure. The approximate formulation is 68 percent 200 mm AP, 19 percent Al and 12 % HTPB. The 200 mm AP was basically "as delivered" from the manufacturer and, hence, had a rather wide distribution.

Three other propellants were to be tested in the T-Burner as part of this program. But, unfortunately, due to budget cuts during the second half of the program, these were not tested. The first was a Thiokol propellant containing a 62% bimodal blend of AP, 18% aluminum 20% BAMO/AMMO plasticized with GAP. Three additional propellants in this family were cast but not in sufficient quantities for T-Burner response characterization. The second two were from Alliant Techsystems based on a HTPE binder system and containing Ammonium Nitrate

(AN). A metallized version contained 20% AN, 10% aluminum, 50% AP and 20% HTPE. The reduced smoke version contained 10% AN, 70% AP and 20% HTPE. In this case 5 additional formulations were cast based on AN/HTPE but, again, not in sufficient quantities for T-Burner characterization. It is hoped that future funding will allow the testing of these three propellants.

(b) T-Burner Response Measurements

The pressure-coupled response is the amplification or attenuation of acoustic pressure waves by the combustion zone of a burning solid propellant. The higher the response at a particular frequency the more a propellant will drive and couple with acoustic oscillations in a motor. It is desirable to know the response so that predictions can be made on the stability of potential solid propulsion systems.

The standard way to measure the combustion response is by the T-burner.[2] The T-burner shown in Figure 3 requires two disks of propellant of equal thickness mounted as shown in Figure 4. One sample is placed on each end of a 1.5-inch diameter pipe combustor and they are ignited simultaneously. Ideally, they will also burn out simultaneously. Data is obtained by pulsing the burner during the burn and after burn out. For some propellants, pulsing is not required and the T-burner acoustic oscillations grow spontaneously. In either case, the difference between the alpha during sample burn, α_1, and the decay alpha after burnout, α_2, is known as the combustion alpha, α_c. The pressure amplitude rate of change of each alpha is measured by a piezoelectric quartz pressure transducer. The combustion alpha is directly related to the pressure coupled response. The combustion driving alpha, α_c, and the damping alpha, α_d, can be determined from:

$$\alpha_c = \frac{\left[\alpha_1 - \alpha_d\right]}{S_b / S_c} \tag{1}$$

and

$$\alpha_d = \alpha_2\left(f_1\right) \tag{2}$$

Where: α_1 pressure decay rate constant during burn
$\alpha_2(f_1)$ pressure decay constant after burning with correction to frequency of α_1
S_b/S_c propellant burning surface area to channel area ratio

From the computed α_c, burner length and propellant properties, the combustion response can be computed with:

$$R_{pc} = \frac{\alpha_c \bar{p}}{4 f a \rho_p \bar{r}_b \left(S_b / S_c\right)} \left(\frac{a_m}{a}\right) \tag{3}$$

Where: $\bar{p}$ mean pressure
$\bar{r}_p$ measured burning rate
f frequency
a theoretical speed of sound of the gases
ρ_p propellant density
a_m measured speed of sound
$a_m = 2fL$, L = burner length

The test frequency depends on the burner length and the combustion gas temperature. Currently at NAWCWPNS, burners of lengths 50 to 4 inches, corresponding to a frequency range of 300 to 4000 Hz are used. The NAWCWPNS High Pressure T-burner is capable of evaluating the response at pressures up to 4200 psi. The measurement of α_2 requires the triggering of the second pulse at burnout of the two propellant samples. In order to determine burnout for proper timing of the second pulse, a phototransistor is mounted behind each sample.[3] See Figure 4. The detector sees a burst of light as the sample burns out. It is desired that outputs of each phototransistor mounted on each sample occur at the same time. Ideally, the two samples should burn out simultaneously. However, if the samples do not burn out simultaneously then the analysis of the second pulse must be delayed until after the slowest sample has burned out.

Figures 5 and 6 show sample data traces for a test of a reduced smoke propellant and the metallized propellant, respectively. From top to bottom, the traces shown are the AC pressure, DC pressure and the two phototransistor outputs. The pulse and oscillations to determine α_1 can be seen in the top AC pressure trace around 0.3 seconds. The decay pulse and oscillation to determine α_2 can be seen around 0.7 seconds. The exact pulse times are different for each propellant due to the burning rate variations between the two propellants. Phototransistor outputs often have different characteristics as shown. For the reduced smoke propellant, which is often slightly translucent, the phototransistor actually saw the ignition flash through the propellant. The top burn out trace shows a spike where the second pulse occurred, while the bottom burn out trace barely shows the first pulse. Metallized propellants are more opaque and the phototransistor shows this in Figure 6. Only the second pulse is observed by the burn out detectors. In both cases, sample burnout is evident and that is where the second pulse was fired. Although somewhat subjective, the point where the burnout trace rolls over is where burnout occurs. In both these test cases, burnout occurred simultaneously for both samples. If the traces show uneven burnout, that test is suspect and usually not used.

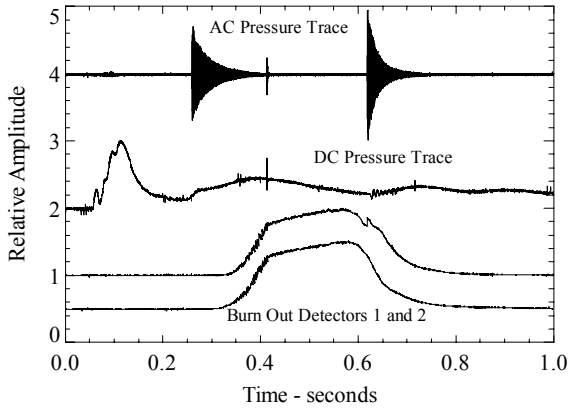

Figure 5. Sample Data for a Reduced Smoke Propellant

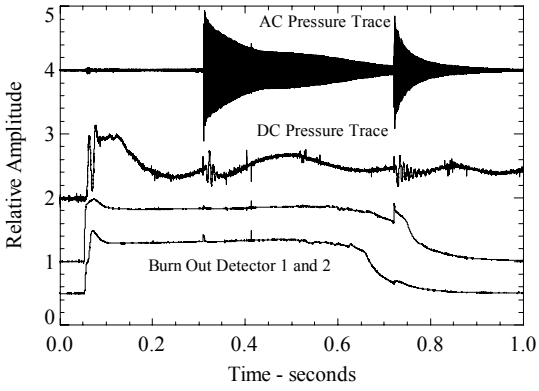

Figure 6. Sample Data for a Metallized Propellant

For both tests shown in Figures 5 and 6, the burner length was 15 inches, which corresponds to a nominal frequency of 1200 Hz. The test pressure was 1000 psi. For the reduced smoke example in Figure 5 the alpha 1, alpha 2 and combustion alphas were computed to be -9.1, -26.8 and 17.4 sec^{-1}, respectively, and the computed response function for this test was 1.63. For the metallized example in Figure 6 the alpha 1, alpha 2 and combustion

alphas were computed to be -23.7, -51.5 and 29.1 sec^{-1}, respectively, and the computed response function for this test was 2.30.

(c) Results for Bi-Plateau Propellants

Figures 7–10 show the measured alphas for all the tests performed on the Bi-Plateau propellants. Figure 7 show the alpha during sample burn, α_1, for all three pressures versus frequency for the aluminized baseline propellant, No 1a. Figure 8 shows the same for the reduced smoke propellant, No. 4. Figure 9 and 10 are a similar plot showing the damping alphas, or α_2, measured after the samples burn out. One thing that is quickly apparent is the increased magnitude for the alphas for the aluminized propellant at all three pressures, Figures 7 and 9, compared to the reduced smoke propellant curves, Figures 8 and 10. This is due the presence of aluminum particles and their oxides that greatly increases the damping in the T-burner. Unfortunately, since the pulsed during / pulsed after T-burner technique looks for small differences between the two alphas, the errors introduced are larger when determining the response of metallized propellants due to the larger magnitude of the decay alphas. Figures 11 and 12 show the computed combustion alpha α_C, from Equation (1). This is the alpha value used in Equation (3) to determine the pressure coupled response function.

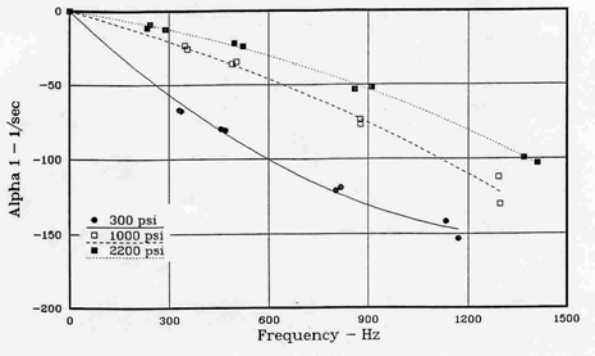

Figure 7. Alpha During Burn at 300, 1000 and 2200 psi for the Metallized Propellant, Mix No. 1a

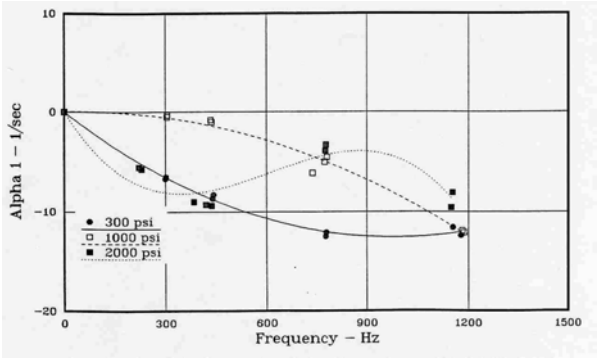

Figure 8. Alpha During Burn at 300, 1000 and 2000 psi for the Reduced Smoke Propellant, Mix No. 4

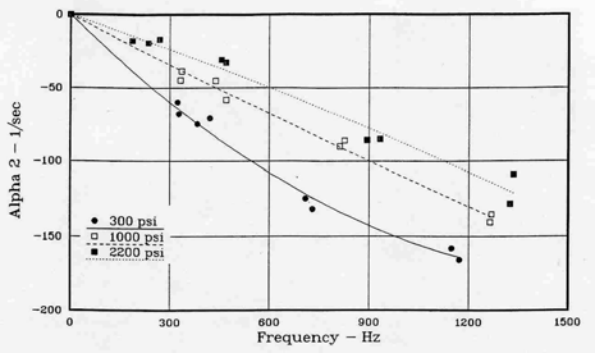

Figure 9. Damping Alpha at 300, 1000 and 2200 psi for the Metallized Propellant, Mix No. 1a

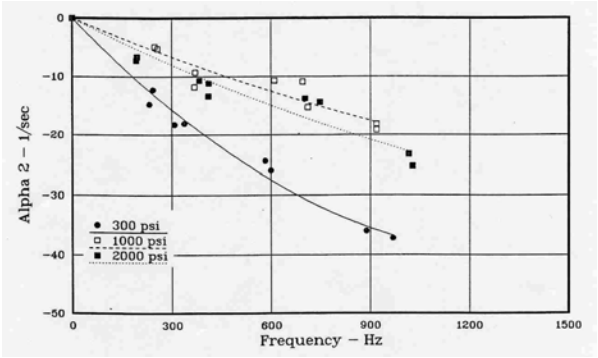

Figure 10. Damping Alpha at 300, 1000 and 2000 psi for the Reduced Smoke, Mix No. 4

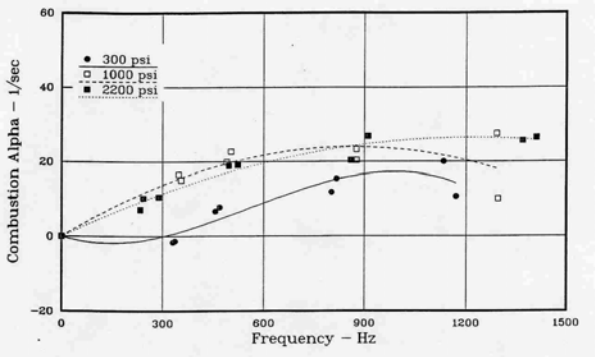

Figure 11. Combustion Alpha at 300, 1000 and 2200 psi for the Metallized Propellant, Mix No. 1a

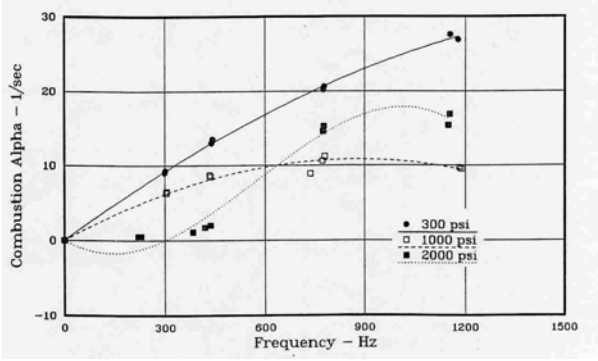

Figure 12. Combustion Alpha at 300, 1000 and 2000 psi for the Reduced Smoke, Mix No. 4

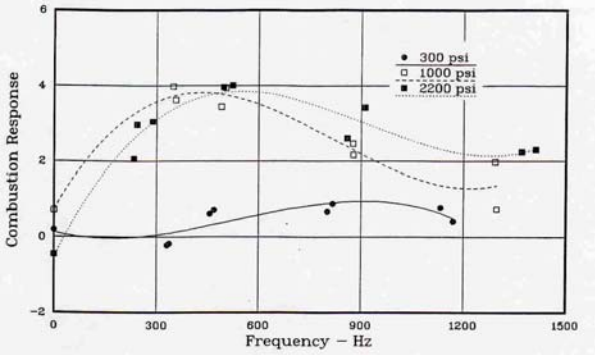

Figure 13. Combustion Response at 300, 1000 and 2200 psi for the Metallized Propellant, Mix No. 1a

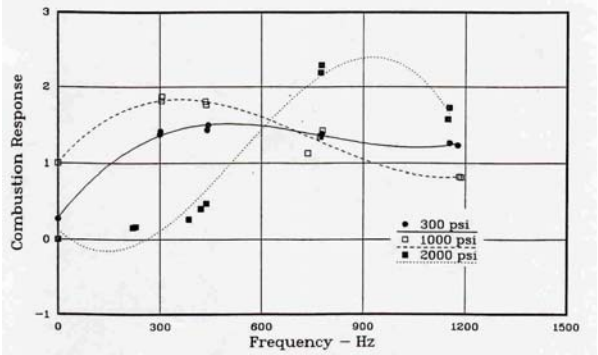

Figure 14. Combustion Response at 300, 1000 and 2000 psi for the Reduced Smoke, Mix No. 4

The response function versus frequency is plotted in Figures 13 and 14 for both propellants at the three testing pressures. For all the curves presented, second or third order polynomial curve fit was used to fit the data, which ever worked best. The upward pointed curve at the far right of some of the curves is a result of the third order fit and does not indicate an increasing trend in the data.

Theoreticians to understand the nature of the instability often use the non-dimensional frequency, omega-•. Many composite propellants whose pressure coupled response has been evaluated by the T-burner have a response peak with an omega value of between 5 and 30.[4] Omega is the ratio of the acoustic time to the thermal conduction time and it is computed by the following:

$$\Omega = \frac{2\pi f \eta}{\bar{r}^2} \tag{4}$$

Where: f frequency in cycles per second
η thermal diffusivity
r burning rate in units of in/sec

In this expression, η/r^2 is the characteristic time of the thermal wave. Figures 15 and 16 plot the pressure-coupled response versus Omega for the two propellants, respectively, at the three test pressures.

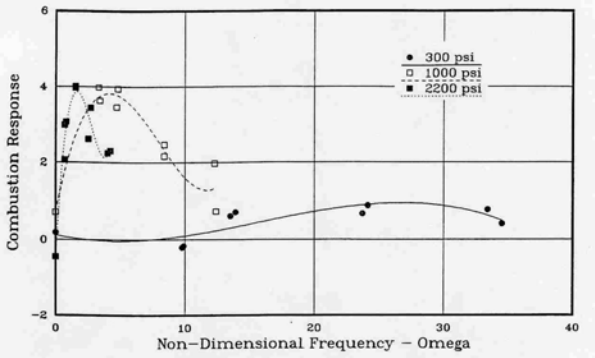

Figure 15. Combustion Response versus Omega at 300, 1000 and 2200 psi for the Metallized Propellant, Mix No. 1a

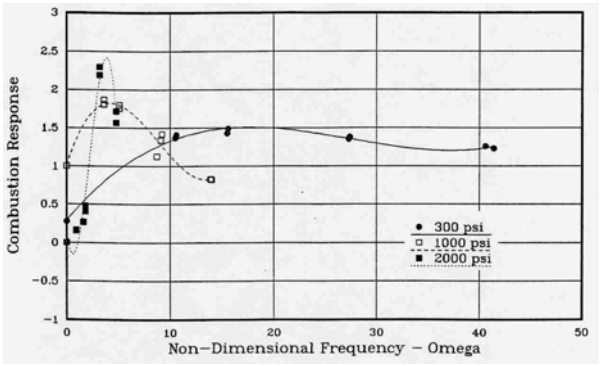

Figure 16. Combustion Response versus Omega at 300, 1000 and 2000 psi for the Reduced Smoke, Mix No. 4

From the data and the above plots, several observations can be made:

1) The most interesting observation was the low response at low frequency for the metallized propellant at the low-pressure plateau and a similar low response for the reduced smoke propellant at the high-pressure plateau. See Figures 13 and 14. From this it may be implied that when the exponent is low near zero in this case, a propellant is not subject to any pressure-coupled response driving at low frequencies. Once the frequency increases to a point where quasi-steady state burning rate behavior is no longer present, then the pressure coupled response begins to increase. Why this observed behavior is not apparent for the metallized propellant at 2200 psi and for the reduced smoke propellant at 300 psi is not known.

2) Another observation dealing with the metallized propellant can be seen in Figures 7 and 9 that show the measured alpha 1 and alpha 2. The magnitude of the alphas at 300 psi is substantially higher than the alphas for 1000 and 2200 psi. Since these differences were not seen with the reduced smoke propellant, Figures 8 and 10, it is postulated that a change in the aluminum combustion / agglomeration occurs at 300 psi.

3) In general, the response of the metallized propellant was higher than that of the reduced smoke propellant at the middle pressure and at the high-pressure plateau. This was particularly true at low frequencies. At 300 psi, the reduced smoke propellant had a higher response than the metallized propellant. As frequency increases these differences are not as apparent.

(d) Results for Mono-Modal AP Metallized Propellant

Figures 17–19 show the results of the mono-modal AP metallized propellant from United Technologies. Figure 17 shows the three alphas, alpha 1 during combustion, alpha 2 after sample burn out and the combustion alpha used to determine the response function. Figures 18 and 19 shows the response function plotted versus frequency and omega, respectively. The response curves show the classic shape first rising to a response of around 4 then falling off as frequency increases. The response curve peak is around 10 on the Omega scale that is typical. This response curve shape is typical of conventional composite propellants. The peak value is slightly higher than expected, however.

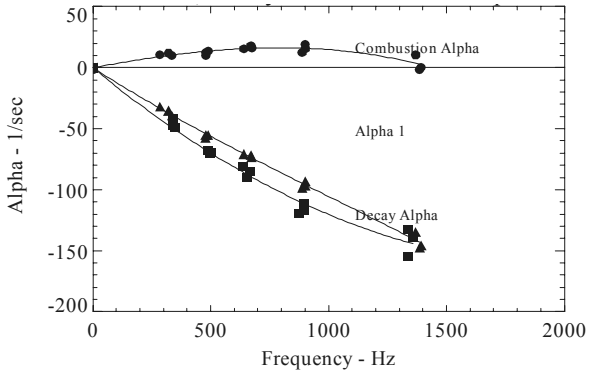

Figure 17. Decay Alpha During Burn, After Burn and the Combustion Alpha for the Mono-Modal AP Metallized Propellant

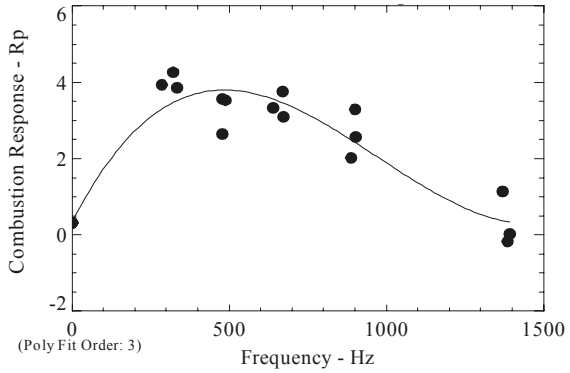

Figure 18. Response of Mono-Modal AP Metallized Propellant

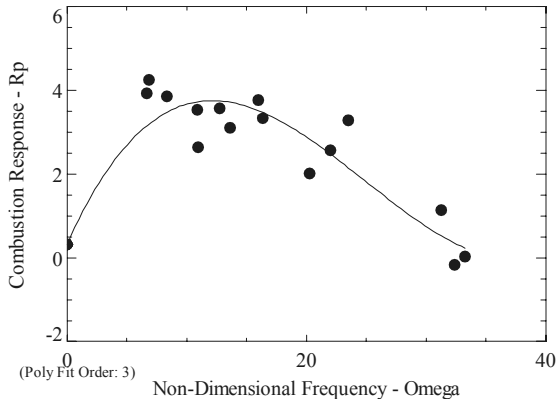

Figure 19. Response of Mono-Modal AP Metallized Propellant Plotted versus Non-Dimensional Frequency

(e) Conclusions

In this study, the pressure coupled response of two bi-plateau propellants, one metallized and one not, and one mono-modal AP aluminized propellant was determined. The response of both bi-plateau propellants was determined by the T-burner at 3 pressures between 300 and 1200 Hz. The three pressures corresponded to the two plateaus and a region in between. The results indicate substantial difference between the propellants and among the three pressures tested. The response of the mono-modal AP aluminized propellant was determined from 300 to 1500 Hz at 1000 psi. It had a very traditional composite propellant response curve, however the response peak was slightly high with a value of 4 around 400 Hz.

References

1. C.J. Hinshaw and N.S. Cohen, "Achievement of Plateau Ballistics in AP/HTPB Propellants," *32nd JANNAF Combustion Meeting*, CPIA Publication No. 631, Vol. III, October 1995.
2. "T-burner Manual," CPIA Publication No. 191, November 1969.
3. F.S. Blomshield, J. C. Finlinson and R. Stalnaker, "Photoelectric Detection of T-Burner Grain Burnout," 26th *JANNAF Combustion Meeting*, CPIA Publication No. 529, Vol. II, pp. 153-160, October 1989.

4. F.S. Blomshield, "Lessons Learned in Solid Rocket Combustion Instability," *29th JANNAF Combustion Meeting*, CPIA Publication No. 593, Vol. IV, pp. 177-196, NASA Langley Research Center, Hampton, Virginia, 1992.

2.3.2 Pressure and Heat Flux Driven Response Measurements (Litzinger)

This work was part of a larger program aimed at understanding and modeling propellant combustion and its interaction with changes in pressure and velocity in a typical rocket motor. The primary objective of the work was to obtain pressure-driven response data for a family of propellants to understand the effects of propellant composition on response. A secondary objective was to compare the pressure-driven response to laser-driven response to determine the extent to which the laser and pressure-driven propellant responses are analogous to each other, as hypothesized by earlier investigators.

In order to perform the pressure-driven response studies, a pressure-driven combustion facility was developed that could measure thrust response, which was used to determine the amplitude and phase response during combustion of propellant samples at low pressure (1, 2, and 3 atm). [1,2] Additional experiments were performed at atmospheric pressure in a different test facility to obtain the propellant response to an oscillating radiant heat flux. A CO_2 laser was used to ignite the propellant, and in some cases to sustain combustion, when propellants would not sustain burning at low pressure. The laser also served as a source of oscillatory laser flux during laser-driven response measurements. Families of heterogeneous propellants were tested to determine composition effects on response, and HMX was studied to compare the pressure and laser-driven response results, because the relevant theories have been developed for homogeneous propellants.

Pressure-driven response amplitudes measured in the new facility for traditional HTPB-AP, non-aluminized propellants exhibited trends as a function of frequency consistent with a condensed-phase response. In parametric studies, the response decreased with an increase in pressure and mean laser flux. An energy balance based on steady-state thermocouple measurements indicated that the observed trend with pressure was due to increased condensed phase heat release, with little change in gas-phase heat feedback to the surface. The analytical model of Culick [3] showed qualitative agreement in trends for the pressure-driven response function but under-predicted the experimentally measured values for the pressure-driven response function. The physical effects underlying the trend with mean heat flux were more complex and appeared to be due to an increase in the condensed-phase heat release and a decrease in the unsteady components of the net flux and gas-phase heat feedback incident on the propellant surface.

Laser-driven response amplitudes for the AP/energetic propellants showed no change with the increase in laser flux, while the pressure-driven response amplitudes decreased with the increase in laser flux. The changes in mean laser flux had different effects on the laser and pressure-driven response amplitudes, which suggests different driving mechanisms. Laser-driven response amplitudes for the HTPE propellants increased with the increase in laser flux, while the pressure-driven response amplitudes decreased with the increase in laser flux.

The pressure-driven response amplitudes of HMX were found to increase with the increase in pressure, consistent with the expectation that increasing the unsteady gas-phase heat feedback, would increase the response

with increasing pressure. Laser-driven response experiments on HMX showed that the response amplitude decreased with an increase in pressure. The unsteady component of the laser flux induces an unsteady component of the gas-phase heat feedback that is out of phase with the laser flux. The laser-driven experiments measured the response of the propellant to this net unsteady flux that is incident on the propellant surface. The increase in pressure increased the unsteady gas-phase heat feedback and hence decreased the net unsteady flux on the propellant surface and resulted in the lower response amplitudes. Thus, the laser and pressure-driven responses were not found to be analogous for HMX.

Comparison of the pressure and laser-driven response data with the theoretical transfer function of Son *et al.* [4] showed that the transfer function under-predicted the experimental data at two and three atmospheres and slightly under-predicted the experimental data at one atmosphere. Comparisons of the experimental results for HMX with the modeling results of Erikson [5] showed that the numerical model predicted a laser-driven response that is three times lower than the measured laser-driven response and a pressure-driven response that is 50-70% lower than the measured pressure-driven response. Erikson attributed this relatively poor agreement to the quality of the condensed-phase kinetics and temperature sensitivity data. The analytical model of Iribicu and Williams, [6] which requires experimental inputs for the condensed-phase heat release and the gas-phase heat feedback, was applied and provided reasonable agreement with the experimental values for pressure-driven response amplitude. Clearly the difficulties in obtaining such experimental data reinforce the need for rigorous models that capture the appropriate physics.

Detailed discussion of the results of the various studies can be found in references 7–16.

(a) Results for HMX

For HMX laser and pressure-driven response experiments were conducted at 1, 2 and 3 atm in argon. At these conditions a mean laser flux was necessary to sustain combustion. In addition micro-thermocouple measurements were performed to obtain information required to interpret the results and to estimate condensed phase heat release. Modeling of the gas-phase region was used to estimate the heat feedback from the flame to the surface. Non-dimensional response function results are presented in this section. The major conclusions from this work are as follows:

1) Due to the presence of the laser heat flux, the flame was significantly "stretched" resulting in heat feedback to the surface that is substantially less than that without the laser flux.
2) As a result of the lower heat feedback to the sample surface the steady and unsteady laser fluxes dominate over the steady and unsteady heat feedback in the laser-driven testing, so the laser flux is not simply a perturbation on the steady heat feedback.
3) The variation of laser-driven response with mean laser flux was found to be different than that of the pressure-driven response, which can be explained in terms of the heat feedback to the surface in the two cases.
4) As pressure was increased the non-dimensional pressure-driven response of HMX was found to increase. This trend is a result of the increasing steady heat feedback to the surface as pressure increases, which leads to an increase in the unsteady heat feedback as pressure increases.
5) Variation of the laser and pressure-driven responses with increasing pressure were found to be different, which is again related to the difference in the role of heat feedback from the flame in the two sets of experiments.

Burning rates and Surface temperatures for HMX at various pressures and heat fluxes.

	101 kPa			202 kPa		303 kPa	
Heat fluxes (W/cm^2)	35	60	90	35	60	35	60
Burning rates	0.55	0.74	0.87	0.8	1.0	1.05	1.25
Surface temperature	630	635	645	650	660	655	670

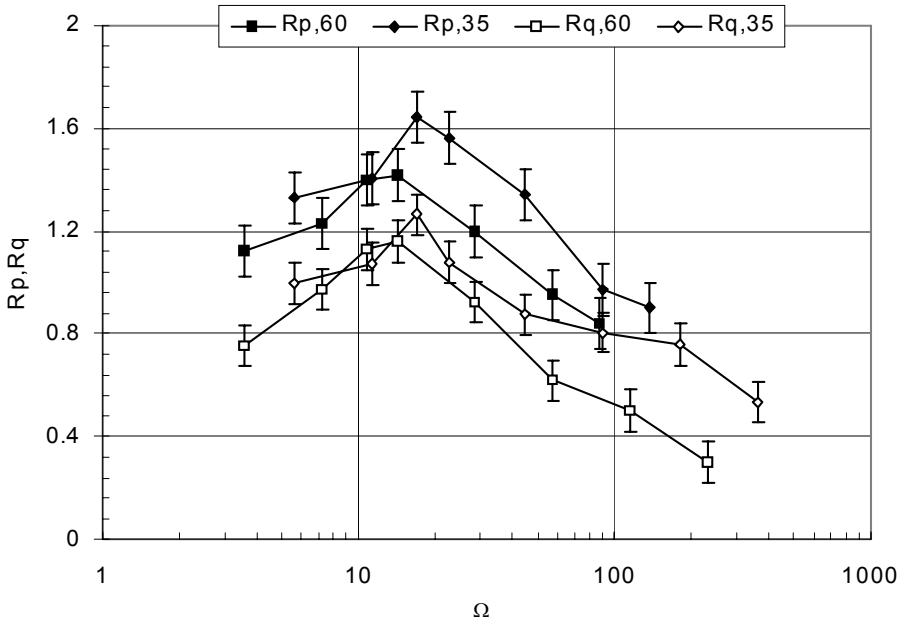

Figure 1. Comparison of Thrust Response Amplitudes versus Ω during Laser and Pressure-Driven combustion of HMX at 101 kPa at mean heat fluxes 35 and 60 W/cm^2 with unsteady flux of $\pm$ 15 W/cm^2.

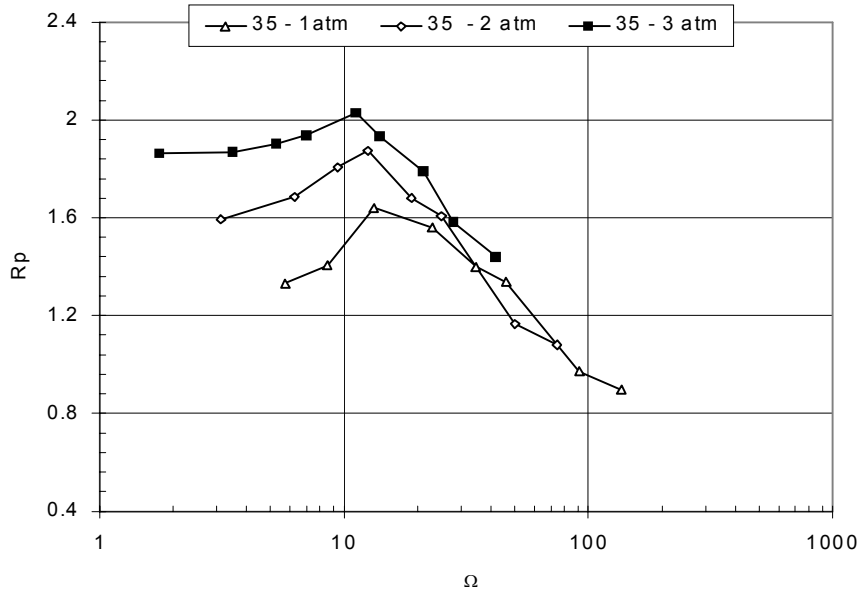

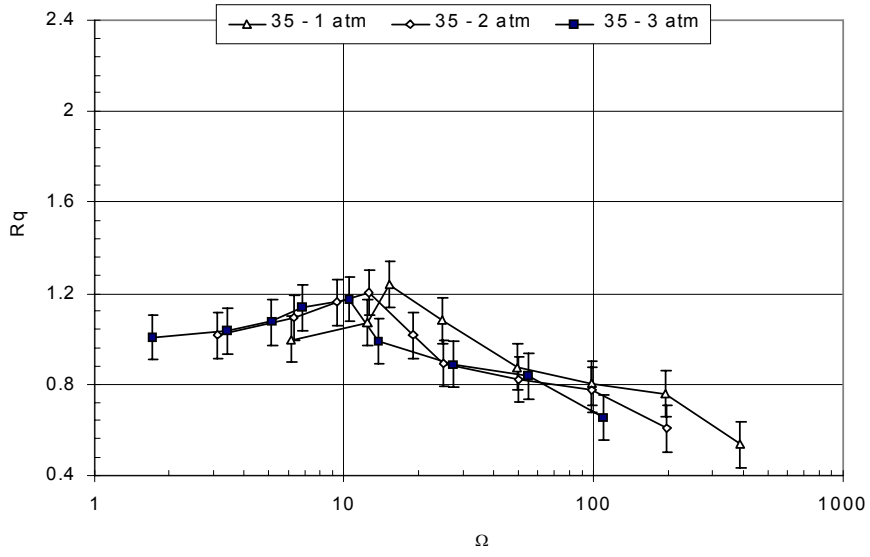

Figure 2. Response Amplitudes for HMX at 35 W/cm^2 and 101, 202 and 303 kPa.

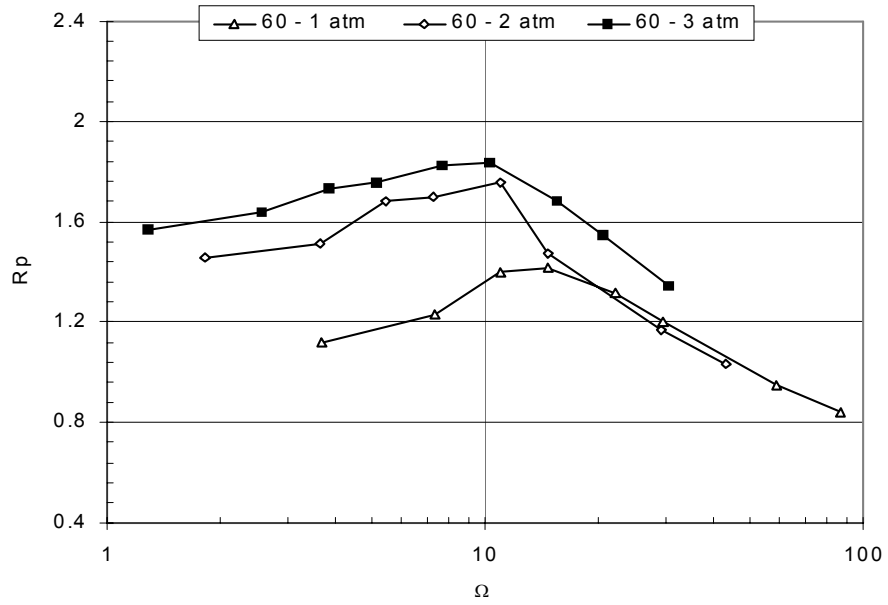

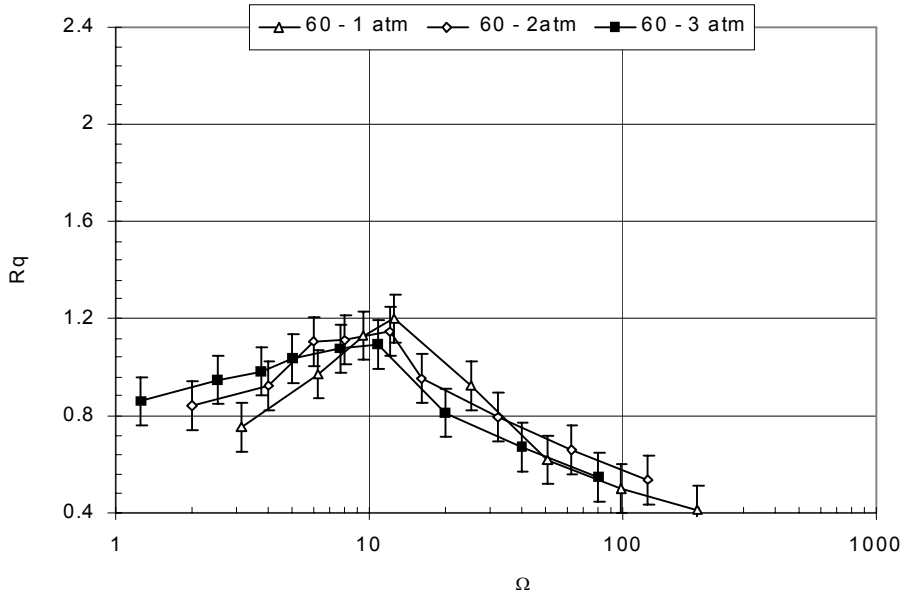

Figure 3. Response Amplitudes for HMX at 60 W/cm^2 and 101, 202 and 303 kPa.

(b) Results for AP/HTPB

Testing of two AP/HTPB propellants, designated MURI 4 and 5, were conducted to determine laser and pressure-driven responses at 1 atm. Pressure-driven tests were performed with and without a mean laser flux; they were also carried out at 2 and 3 atm. Steady-state tests were conducted to determine mean burning rate and also surface temperature of these materials; results for MURI 4 are listed below. Major observations from these experiments are

Comparison of laser and pressure-driven response for laser-supported combustion shows that the responses have similar behavior with frequency, but that the pressure-driven response amplitude is substantially greater.

- For pressure-driven response under conditions of self-sustained burning, the following observations can be made:
- The response amplitudes are higher than those measured with a mean laser flux.
- The response amplitudes decrease with an increase in pressure – in contrast to HMX.
- The response amplitude becomes nearly constant at low frequency with an increase in pressure.

Burn rate and surface temperature data for MURI 4 at one, two and three atmospheres.

	101 kPa	202 kPa	303 kPa
Burning rate (mm/s)	1.35±0.10	1.8±0.15	2.1±0.20
Surface Temperature (K)	720±60	770±70	805±70
N	0.42		
n_{Ts}	0.1		

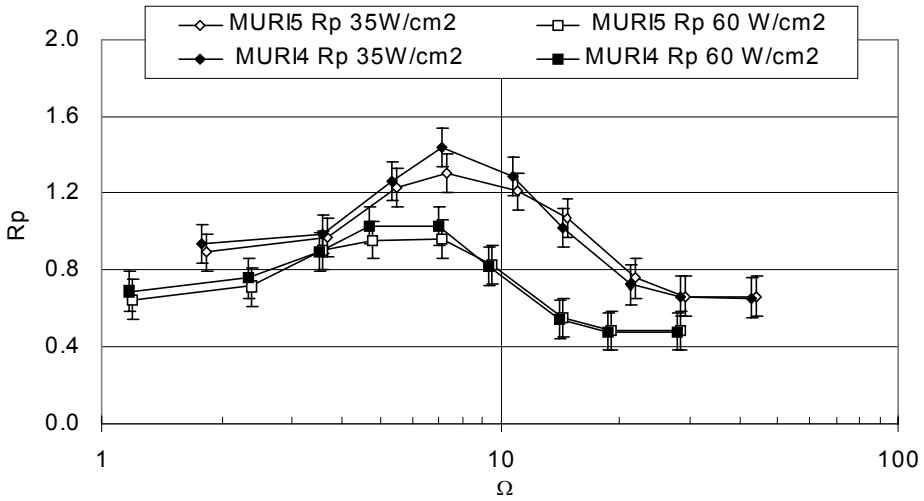

Figure 4. Pressure-driven response versus Ω for MURI 4 at 1 atm.

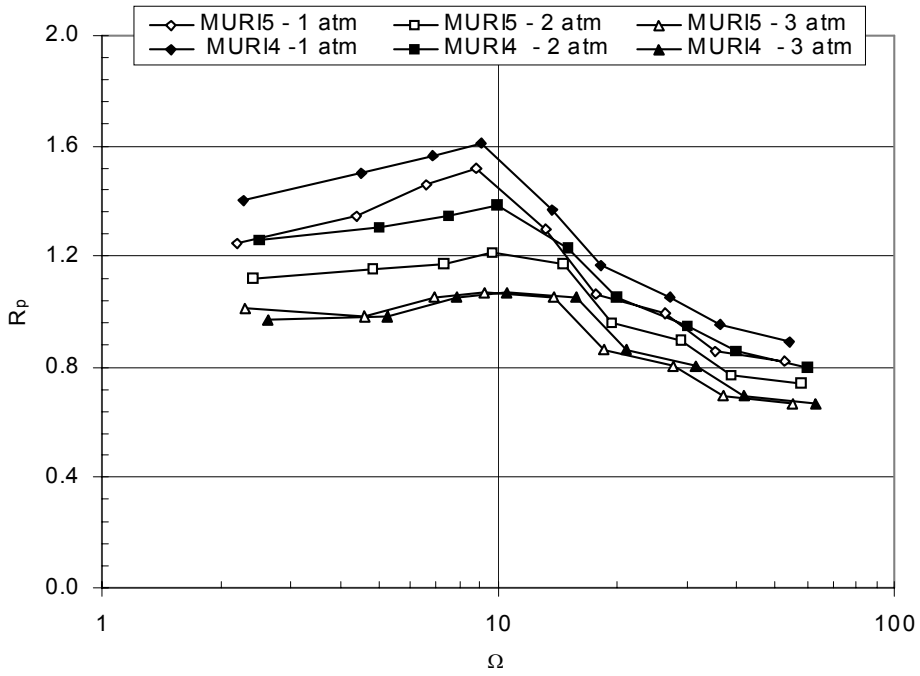

Figure 5. Pressure-driven Response for self-deflagration at 1, 2, and 3 atmospheres.

(c) Results for AP/Energetic Binder

Testing of an AP/energetic binder propellant was conducted to determine laser and pressure-driven responses at 1 atm. In addition, pressure-driven tests were performed with and without a mean laser flux; they were also carried out at 2 and 3 atm. Steady-state tests were conducted to determine mean burning rate and also surface temperature of this propellant material; results for are listed below. Major observations from these experiments are:

Under conditions of laser-supported combustion, the behavior of the laser and pressure-driven responses was similar, but the pressure-driven results had higher amplitudes. This trend is similar to that found for the AP/HTPB propellants.

1) For the pressure-driven response under self-sustained conditions, response amplitude was found to decrease with increasing pressure, again consistent with the results for the AP/HTPB propellants.

2) A comparison of the results for the AP/energetic binder propellant to that for the AP/HTPB propellant shows that the AP/energetic binder propellant exhibits a much less distinct peak in its response. This difference is consistent with the increase in condensed phase heat release with the energetic binder.

3) A one-dimensional energy balance at the surface of the propellants confirmed that the energetic binder increased the condensed-phase heat release. For self-sustained combustion, the heat release with the energetic binder was approximately 50% greater than that of the AP/HTPB propellant for all three pressure tested.

Burn rate and surface temperature data for AP/energetic binder propellant at 1, 2 and 3 atm.

	101 kPa	202 kPa	303 kPa
Burning rate (mm/s)	1.75±0.15	2.35±0.25	2.9±0.25
Surface Temperature (K)	920±80	980±80	1010±80
N	0.45		
n_{Ts}	0.08		

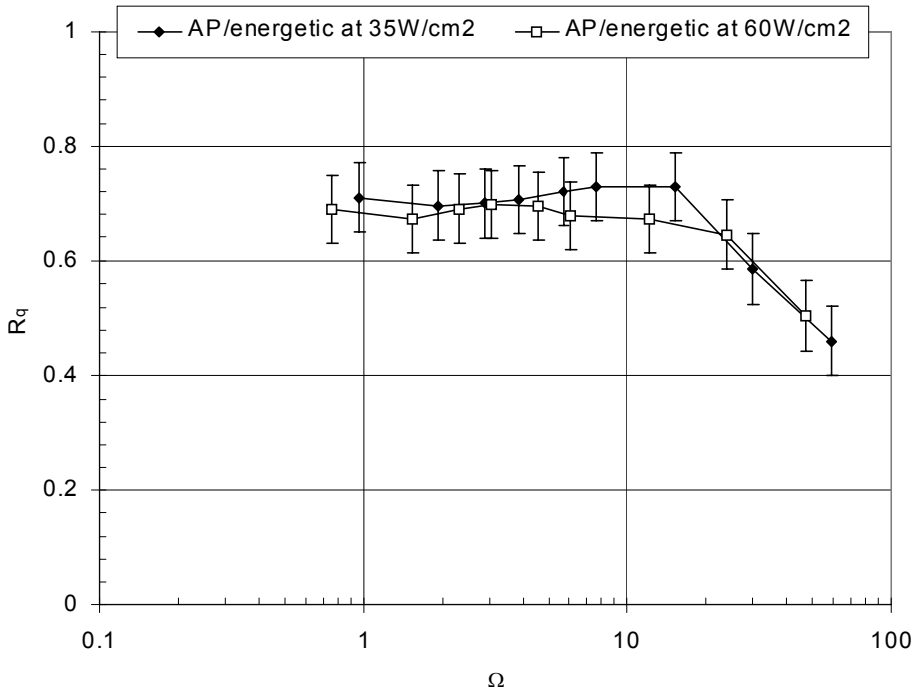

Figure 6. Laser-driven Thrust Response Amplitude versus Ω for the AP/energetic propellant.

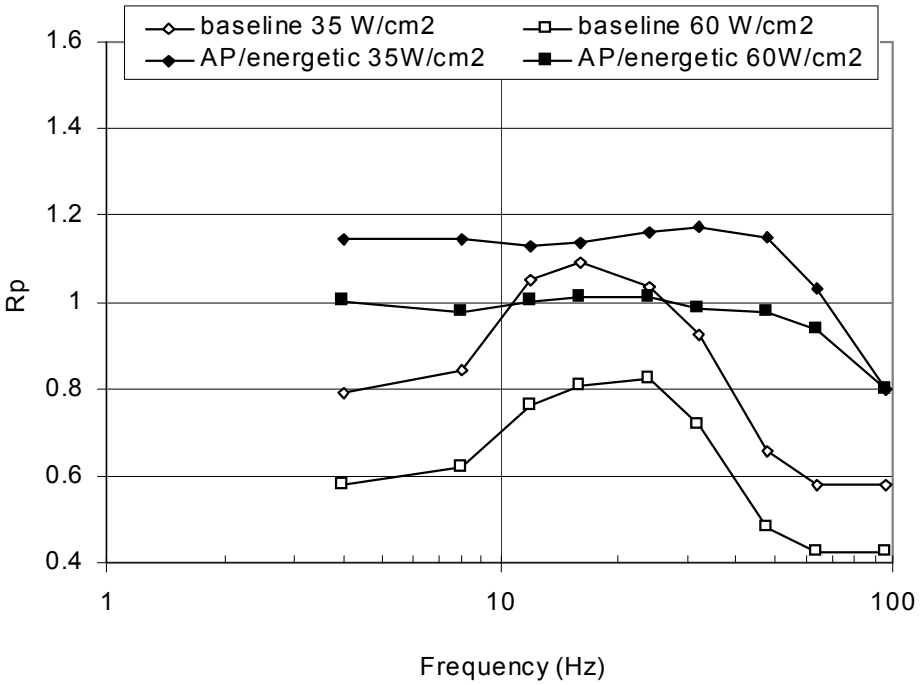

Figure 7. Pressure-driven Thrust Response Amplitudes for an AP/energetic propellant compared to base line propellant.

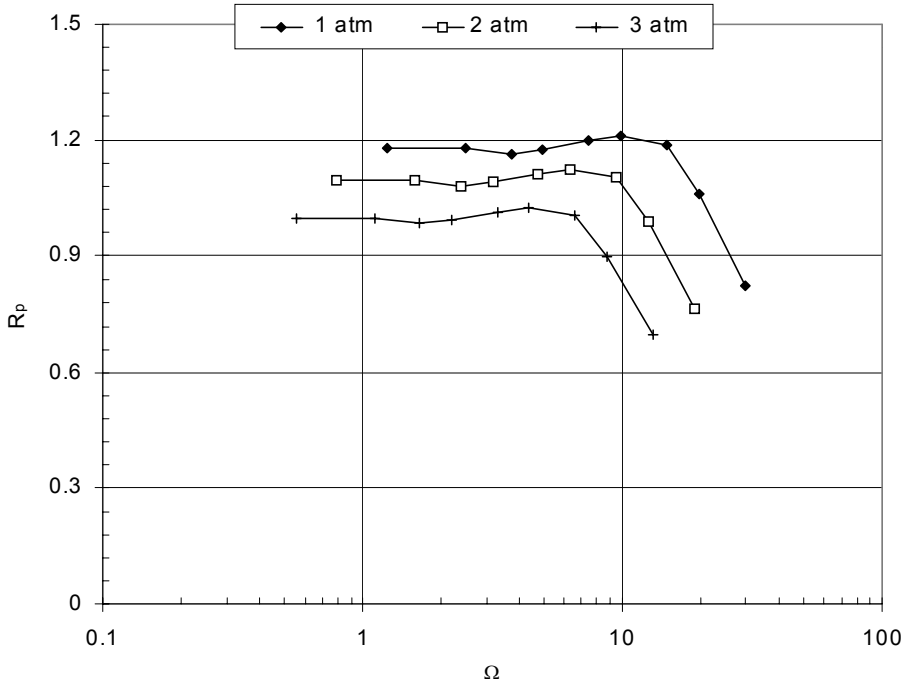

Figure 8. Response Amplitudes for AP/energetic propellant at 1,2 and 3 atmospheres during self-deflagration.

(d) Results for AP/AN/HTPE

This family of three propellants was tested to determine the effects of the HTPE binder and also the effects of AN addition. Response tests for laser and pressure-driven conditions were conducted at 1 atm. The major observations for these tests are as follows:

1) Overall the behavior of the HTPE propellant shows behavior similar to the energetic binder/AP propellant, which is consistent with increased condensed phase heat release.

2) The addition of AN reduces the response amplitude for both laser and pressure-driven testing.

3) These propellants had the lowest response amplitudes for all those tested.

Burn rate and surface temperature for the HTPE propellants at 1, 2, and 3 atm.

Propellant Type		**101 kPa**		**202 kPa**		**303 kPa**	
	n	T_s (K)	r_b (mm/s)	T_s (K)	r_b (mm/s)	T_s (K)	r_b (mm/s)
AP	0.42	1025	1.4	1050	1.8	1070	2.15
AP+AN high rate	0.4	1000	1.4	1035	1.75	1075	2.15
AP+AN low rate	0.45	900	0.95	930	1.25	950	1.55

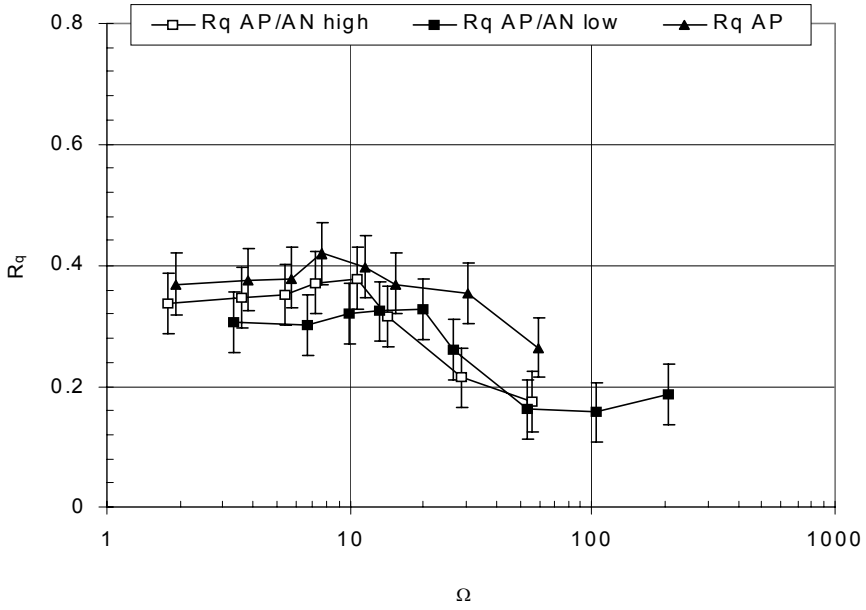

(a)

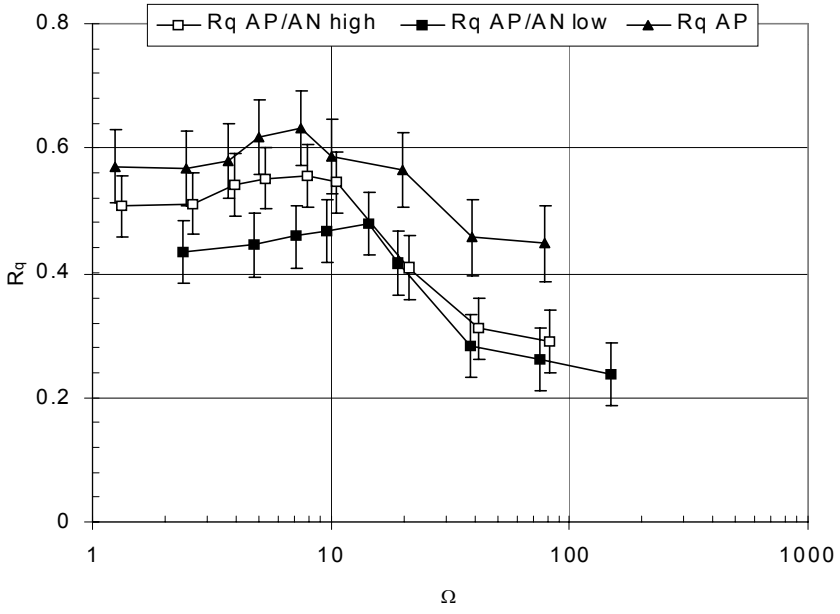

(b)

Figure 9. Laser-driven Response Amplitudes at 35±15 (a) and 60±15 (b) W/cm^2.

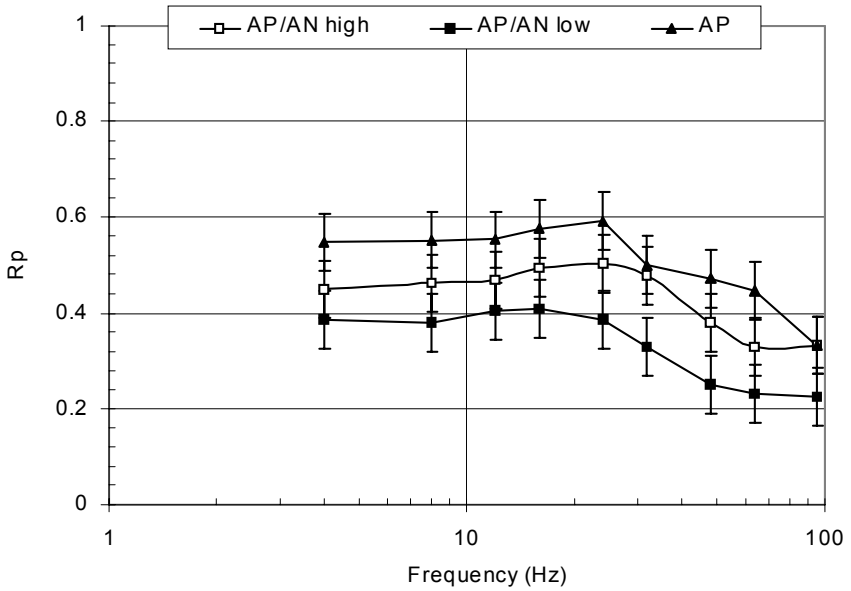

Figure 10. Pressure-driven Thrust amplitude for pressure-driven combustion in air at 60 W/cm^2.

The results in Figure 11 are illustrative of the trends observed in pressure-driven response as the propellant composition was varied and indicate that the composition of the binder can have a substantial effect on the basic character of the response.

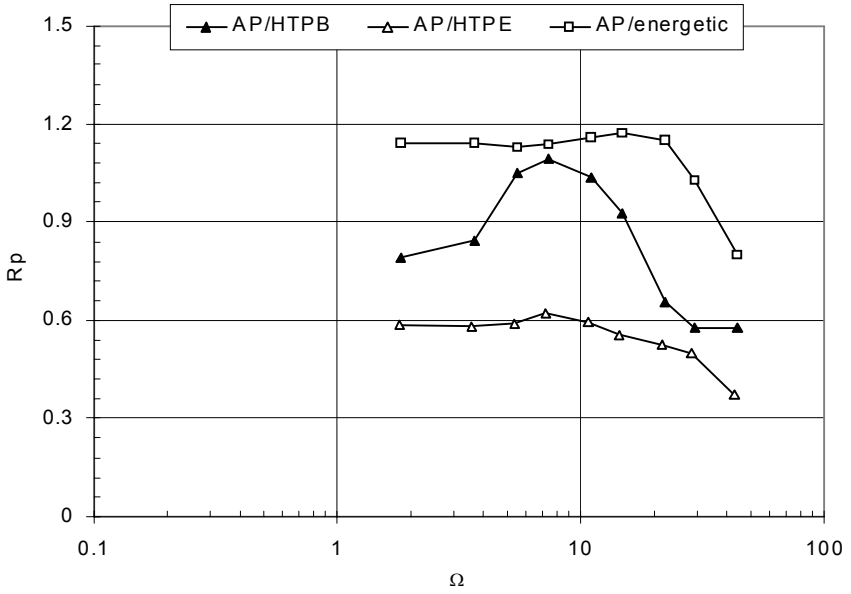

Figure 11. Comparison of Pressure-driven Response Amplitude for Three Propellants.

References

1. Lee, Y. J., G. Kudva and T. Litzinger, Development of a Thrust Response Measurement System for Pressure-driven Combustion Studies, *35th JANNAF Combustion Meeting*, 1998.
2. Lee, Y., G. Kudva and T. A. Litzinger, Development of a Facility for Measurement of the Response of Solid Propellants under Pressure-driven Conditions, *Journal of Measurement Science and Technology*, 11:51-58 (2000).
3. Culick, F.E.C., Calculation of the Admittance Function for a Burning Surface, *Astronautica Acta*, 13:221-237, 1967.
4. Son, S.F., Burr, R.F., Brewster, M.Q., Finlinson, J.C., and Hanson-Parr, D., "Nonsteady Burning of Solid Propellants with an Externally Radiated Heat Flux: A Comparison of Model with Experiment," AIAA91-2194, 27th Joint AIAA/SAE/ASEE/ASME Joint Propulsion Conference, Sacramento, CA 1991.
5. Erikson, W. W., Modeling of the Unsteady Combustion of Solid Propellants with Detailed Chemistry, Ph.D. Thesis, Brigham Young University, 1999.
6. Iribicu, M.M., and Williams, F.A., "Influence of Externally Applied Thermal Radiation on the Burning Rates of Solid Propellants," *Combustion and Flame*, Vol. 24, 1975, pp. 185-198.
7. Tang, C., Y. Lee, G. Kudva and T. Litzinger. 1996. A Study of the Combustion Response of HMX Mono-propellant to Sinusoidal Laser Heating. *33rd JANNAF Combustion Meeting*.
8. Lee, Y. J., C. J. Tang and T. A. Litzinger, Comparison of Laser-driven and Acoustically-driven Combustion of HMX, *34th JANNAF Combustion Meeting*, 1997.
9. Lee, Y. J., C. J. Tang and T. A. Litzinger, An Experimental Study of Acoustically-driven Combustion Instabilities of Solid Propellants, *34th JANNAF Combustion Meeting*, 1997.
10. Lee, Y. J., G. Kudva and T. Litzinger, Development of a Thrust Response Measurement System for Pressure-driven Combustion Studies, *35th JANNAF Combustion Meeting*, 1998.
11. Kudva, G., Y. J. Lee, and T. Litzinger, Comparison of Laser and Pressure-driven Thrust Measurements in the Combustion of MURI Propellants, *35th JANNAF Combustion Meeting*, 1998.
12. Kudva, G., Y. J. Lee and T. Litzinger, Comparison of Laser and Pressure-driven Thrust Measurements in the Combustion of an AP/Energetic Binder Propellant," *36th JANNAF Combustion Meeting*, 1999.
13. Study of Pressure and Heat Release Effects on Laser and Pressure-driven Response Amplitudes for HMX, G.K. Kudva and T.A. Litzinger, *37th JANNAF Combustion Meeting* 2000.
14. Low Pressure Laser and Pressure-driven Response of AP/HTPE and AP/AN/HTPE Propellants, G.K. Kudva and T.A. Litzinger, *37th JANNAF Combustion Meeting*, 2000.
15. Kudva, G., Y. J. Lee and T. Litzinger, Comparison of Laser and Pressure-driven Thrust Measurements of HMX, AIAA Joint Propulsion Conference, 1999.
16. Lee, Y., G. Kudva and T. A. Litzinger, Development of a Facility for Measurement of the Response of Solid Propellants under Pressure-driven Conditions, *Journal of Measurement Science and Technology*, 11:51-58 (2000).

2.3.3 Pressure-Coupled Response Measurements of Aluminized and Non-Aluminized Solid Propellants Using the Magnetic Flowmeter (Micci)

The purpose of this work was to measure the pressure-coupled response function of several different solid propellants, both aluminized and non-aluminized. The magnetic flowmeter burner, a device that directly measures the one-dimensional acoustic gas velocity of a sufficiently ionized combustion flow was used in this study. The pressure-coupled combustion response can be obtained when this velocity measurement is combined with an acoustic pressure measurement. Additionally, the regression rate of the propellant is measured using an ultrasound transducer. A rotating gear above the exhaust nozzle produces an acoustic wave inside the chamber at the desired frequency. The pressure-coupled response functions of six different solid propellant formulations have been obtained at mean chamber pressures of 300 psi (2.1 MPa) and 1000 psi (6.9 MPa). These response functions were then compared and conclusions were drawn regarding the effects of the propellant formulation on the pressure-coupled combustion response.

(a) Results

Six different propellant formulations were tested using this method. Propellant formulation 4 was designed as an HTPB-AP composite baseline in order to study the effects of individual composition changes on the pressure-coupled response. For instance, formulation 5 uses a different curing agent (IPDI instead of DDI) and propellant formulation 9 has a higher coarse-to-fine ammonium perchlorate ratio. Formulation 1a is an aluminized propellant and UTP-31665 is a mono-modal propellant that is also aluminized. The tests were performed at several frequencies ranging from 300 Hz to 2000 Hz, with mean chamber pressures around 300 psi or 1000 psi. The experimental data points are fit to a curve using the Denison and Baum A and B model[6]. The pressure-coupled response functions for the non-aluminized propellants 4, 5, and 9 at mean chamber pressures of 300 and 1000 psi are shown in Figures 1 and 1 respectively. These results indicate that IPDI (in propellant 5) causes a much higher response function at a higher frequency when compared to the baseline formulation (propellant 4). Likewise, comparing propellant 9 to propellant 4 reveals that the higher coarse-to-fine ratio produces a lower response peak at a lower frequency.

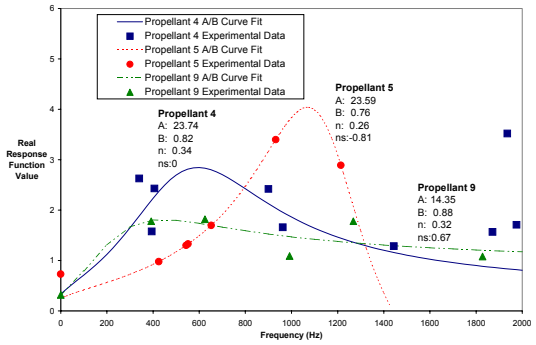

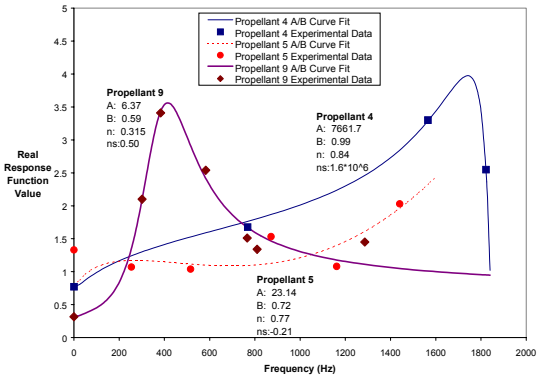

Figure 1. Response Functions at 300 psi **Figure 2. Response Functions at 1000 psi**

[6] Novozhilov, B. V., "Theory of Nonsteady Burning and Combustion Stability of Solid Propellants by the Zeldovich-Novozhilov Method," Nonsteady Burning and Combustion Stability of Solid Propellants, *Progress in Astronautics and Aeronautics,* Vol. 90, AIAA, NY, 1992, p. 601.

The pressure-coupled response function results for propellants 1a and UTP-31665 are shown below in Figure 3. Comparing these aluminized propellants to the non-aluminized shows that the presence of aluminum causes a decrease in the peak pressure-coupled response. However, propellant 1a has a higher coarse-to-fine AP ratio, which helps to offset this result. Additionally, the acoustic frequency of the peak for propellant 1a, at 700 Hz or a non-dimensional frequency of 14 Ω, is slightly higher than the peak frequency for propellant 4, 400 Hz (12Ω). Similarly, the UTP-31665 propellant shows a lower peak response at a higher acoustic frequency as well. Figure 7 shows a comparison of the response function of UTP-31665 at mean chamber pressures of 300 psi and 1000 psi. Though the frequency at which the responses peak is very close, the effect that the chamber pressure has on the magnitude of the response can easily be seen. The 1000 psi curve peaks at a real response value of 4.3 as opposed to the 300 psi curve that peaks at 1.86.

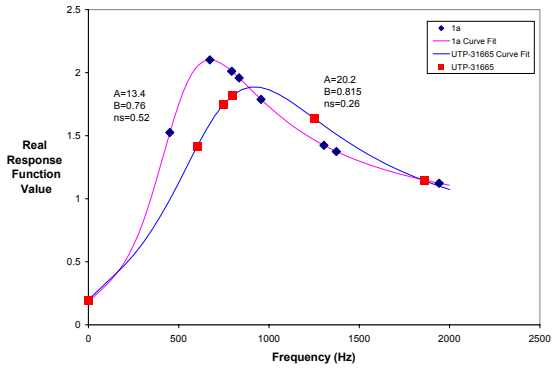

Fig. 3. Response Functions for Propellants 1a and UTP-31665 at 500 psi.

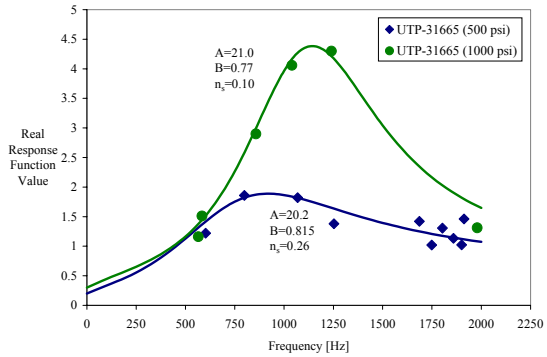

Fig. 4. Response Functions for Propellant UTP-31665 at 500 and 1000 psi.

A reduced smoke propellant with a poly BAMO-AMMO binder was also tested. Figure 5 shows the results of these tests at 300 and 1000 psi. The 300 psi response is flat while the 1000 psi response is at a value of 4 and still rising at a frequency of 1750 Hz.

Finally, data obtained by the magnetic flowmeter method was compared to the Naval Air Warfare Center (NAWC) T-burner data[7]. Figure 6 shows propellant 1a data with T-burner points taken at both 300 psi and 1000 psi. The magnetic flowmeter data was obtained at 500 psi showing a good transition between the T-burner points.

[7] Blomshield, F., personal correspondence, January 2000.

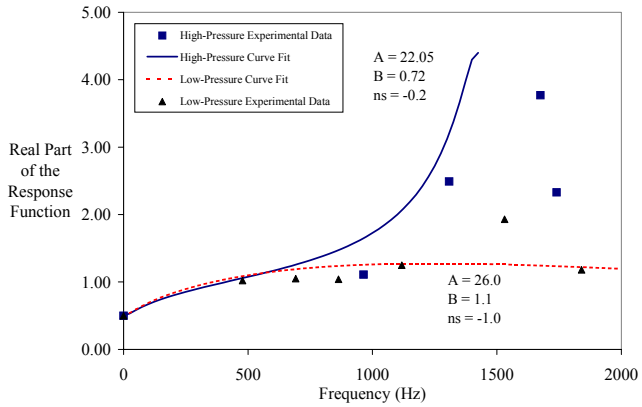

Fig. 5. Response function for BAMO-AMMO propellant at 300 and 1000 psi.

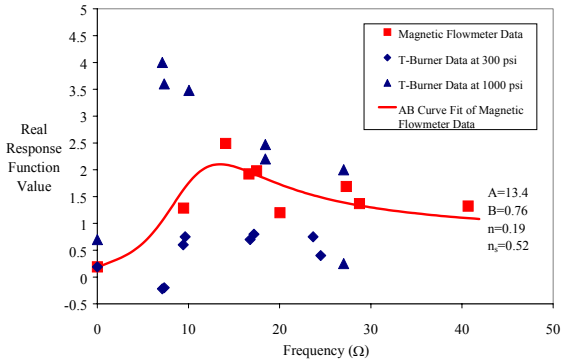

Fig. 6. Propellant 1a response functions comparing NAWC T-burner data to magnetic flowmeter data.

2.3.4 Response Function Measurement in an Oscillatory Burner Employing an Ultrasonic Technique (Krier)

The primary motivation behind this research was to obtain a better understanding of solid propellant burning behavior under oscillatory conditions. To this end we sought to determine the effects of different additives (such as aluminum, ammonium nitrate, coarse to fine ratio of AP, etc.) on the burning rate and burning response of a propellant. An extension of this work included a study focused on the frequency dependence of propellant burning rates. In addition, experimental procedure improvement was a central objective throughout our work. This led to a reanalysis of the transducer selection for our ultrasound system in an effort to increase the intensity and reliability of the ultrasound signal used to make thickness measurements.

(a) Technical Approach

The design of our test chamber is based upon the rotating valve burner developed at United Technologies Chemical Systems Division (CSD). It consists of two nozzles: the first is a steady state nozzle and the second is an oscillatory nozzle which is opened and closed by a rotating shaft controlled by a variable speed 2 hp electric motor. The chamber is designed for a maximum pressure of 3000 psi, with a safety factor of five. The pedestal is secured underneath the chamber and contains both the test sample as well as the ultrasound transducer. The various test pressures are obtained through the manipulation of nozzle sizes and helium pre-pressurization. Two piezoelectric pressure transducers record the pressure time history of each experiment. Test conditions typically range from 300 to 2000 psi in pressure with frequencies between 20 and 300 Hz. For tests specifically performed for response function purposes, target pressures of 300 and 1000 psi are used.

Propellant thickness measurements are made employing an ultrasound echolocation technique. A pulse is sent into the propellant sample by means of an ultrasonic transducer coupled to its surface. This pulse returns to the transducer after it travels through the sample and reflects off the burning surface. A Ritec RAM-10000 ultrasound system is used to both pulse the transducer—with a typical pulse repetition rate of 2.5 kHz—and receive the reflected echoes. These echoes are sampled at 25 MHz and are recorded digitally using a Gage Systems CS8500

high-speed data acquisition board. The data is post-processed using Matlab and various digital signal-processing techniques. These tools ascertain the relative movement of the propellant surface echo and thus, determine the propellant thickness. Taking the time derivative of this result gives the instantaneous burning rate, which can be coupled with pressure data to calculate the response function.

(b) Results

A list of the propellants tested and their respective formulations is given in Table 1.

Table 1: Propellant formulations tested.

Designation	AP (%) (200/90/2-20 □m)	Al[α] (%)	Binder	Curative	Miscellaneous	
Thiokol #1a	39/ 0/31	15	HTPB	DDI	TMO[β]	(2%)
Thiokol #2	44/ 0/26	15	HTPB	IPDI	TMO	(2%)
Thiokol #4	53/ 0/33	—	HTPB	DDI	TMO	(2%)
Thiokol #5	53/ 0/33	—	HTPB	IPDI	TMO	(2%)
Thiokol #10	55/ 0/33	—	HTPB	DDI		—
UTP #5	69/ 0/ 0	19	HTPB	DDI		—
UTP #6	59/ 0/ 0	19	HTPB	DDI	HMX	(10%)
UTP #7	52/ 0/17	19	HTPB	DDI		—
UTP #8	41/ 0/28	19	HTPB	DDI		—
Alliant #1	46/ 0/ 5	20	HTPE[χ]	—	AN	(10%)
Alliant #2	9/16/25	20	HTPE	—	AN	(10%)
Alliant #3	28/12/20	20	HTPE	—		—
Alliant #4	20/ 0/23	20	HTPE	—	Bi_2O_3	(21%)
Alliant #5	54/ 0/16	—	HTPE	—	AN	(10%)
Alliant #6	28/16/25	—	HTPE	—	AN	(10%)
Alliant #7	38/16/25	—	HTPE	—		—

α aluminum sizes are: Thiokol (95 μm), UTP (17 μm), Alliant #1 (15 μm), Alliant #2-7 (4 μm).
β transition metal oxide ballistic additive
χ consists of TPEG polymer

One of the recent major accomplishments of this research has been the implementation of a focused ultrasound transducer as an alternative to the planar (unfocused) transducer. This change was made for two principle reasons. First, signal intensity is significantly increased within the focal tube of a focused transducer. Therefore, a properly focused transducer will produce a signal of greater amplitude within the area of interest, yielding a more reliable and easier to track signal. Second, the increased signal amplitude eliminates the need for amplification (increasing the gain), thus, reducing the noise in the signal. Burning rate measurements taken with the focused transducer exhibit better agreement with manufacturer data as well as less scatter than its planar counterpart. This reduced scatter is also evident in response function measurements, especially at higher frequencies where signal noise is significant. The following propellant studies were performed exclusively with the focused transducer unless otherwise noted.

A burning rate study was performed with Thiokol #5, a plateau propellant. Tests were run under steady state and oscillatory conditions both at and below the plateau region as shown in Figure 1. The UIUC steady state and oscillatory data show excellent agreement with Thiokol data *below* the plateau region; however, the data differ

within the plateau region. This is evident with data taken at the University of Alabama at Huntsville as well, as seen in Figure 2. Additionally, the UIUC data exhibits a frequency dependence within this region, which is shown in Figure 3. Experiments are planned at frequencies above 100 Hz to determine the upper limit of this dependence.

A plot comparing steady state burning rate data for Thiokol #4 from UIUC, Huntsville and Thiokol is given in Figure 4. Both the UIUC and Huntsville data indicate a burning rate roughly five percent higher than measured by Thiokol. When measurements were made with the ultrasound system under oscillatory conditions, it was found that the burning rate was frequency dependent. This relationship is shown in both Figures 5 and 6. The burning rate increases at lower frequencies and returns to steady state values near 100 Hz. Response function plots for Thiokol #4 are given in Figure 7 and 8. The data suggest that Thiokol #4 has a dampening effect on the response under these conditions evidenced by the persistent negative real part.

Results, including response function plots, of the compositional study performed with the planar transducer prior to January 2001 can be found in Reference 5 (2000). A summary of key findings is provided below. It is important to note that typically only 2-4 experiments have been performed at each test condition (*i.e.* 50 Hz at 300 psi). Therefore, general trends in the data are discussed, which may not be statistically significant.

Thiokol #1a was chosen for a comparison study with data taken using a magnetic flowmeter at the Pennsylvania State University (PSU) and T-burner measurements made at the Naval Air Warfare Center in China Lake, CA. The response function magnitude and phase measured with our ultrasound technique shows good agreement with similar data taken with the magnetic flowmeter. The real and imaginary parts, however, are more ambiguous. The ultrasound measurements show evidence of a negative excursion in the real part of the response near Ω=12.5, which is not observed with either the magnetic flowmeter or T-burner.

The effects of composition on the response function were studied based upon propellant comparisons. A trend was suggested from the relationship between UTP propellants #5,7 and 8 that the presence of fine AP reduces the driving potential at the upper end of frequencies tested (*i.e.* 200-300 Hz). Thiokol #4 and #10 were examined to determine the influence of a transition metal oxide ballistic modifier. Within relative error and data scatter, the response functions are very similar, indicating no effect of the modifier under the tested conditions. Aluminum was shown to have a damping effect on the response function through comparison of Alliant propellants #1,3,5 and 7. The oxidizer ammonium nitrate was shown to produce no distinguishable difference in the response function over the range of frequencies investigated for Alliant #2 and #3. Finally, the high-density oxidizer, Bi_2O_3, was found to have little effect on the combustion response when the relationship between Alliant #3 and #4 was examined. Several of these propellant comparisons are targeted for future exhaustive research in order to provide meaningful statistical conclusions.

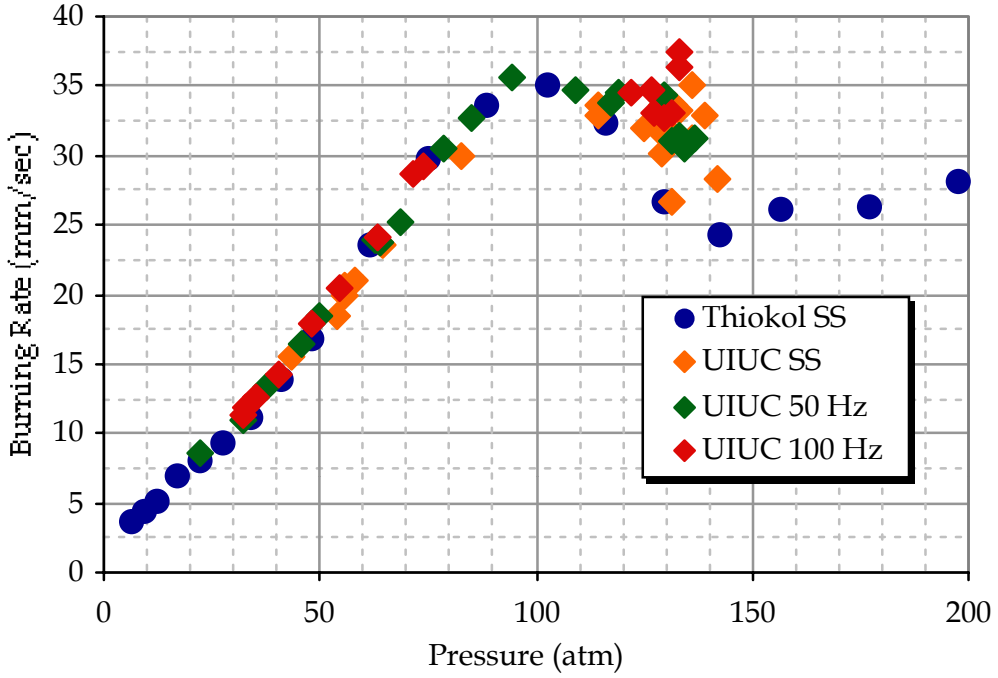

Figure 1. Burning rate versus pressure plot of UIUC steady state and oscillatory data for Thiokol #5.

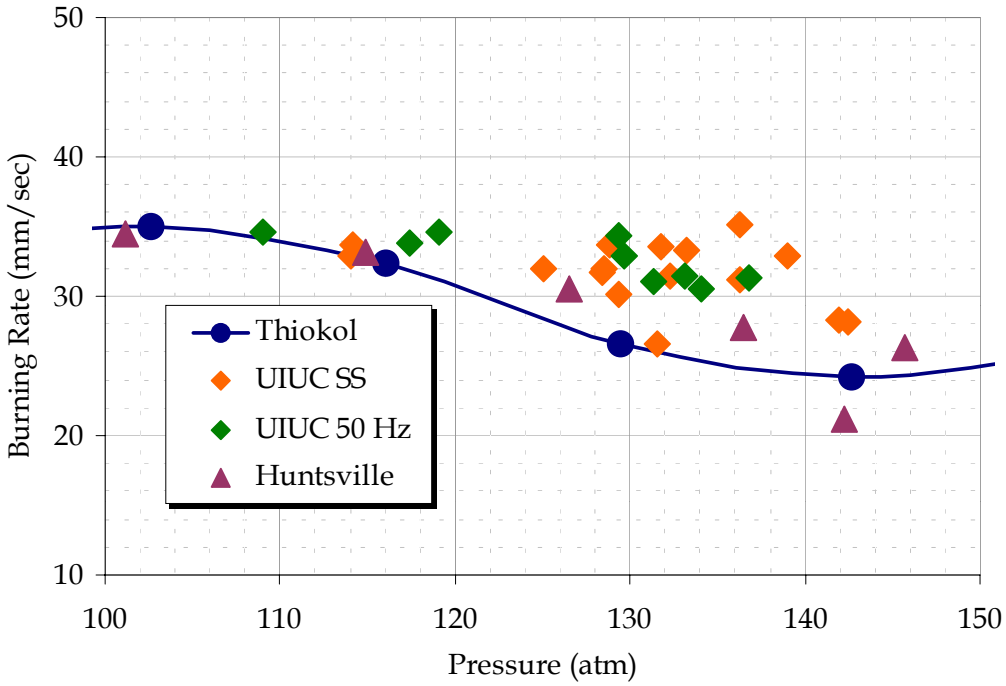

Figure 2. Plot of Thiokol, UIUC and Huntsville burning rate data within the plateau region for Thiokol #5.

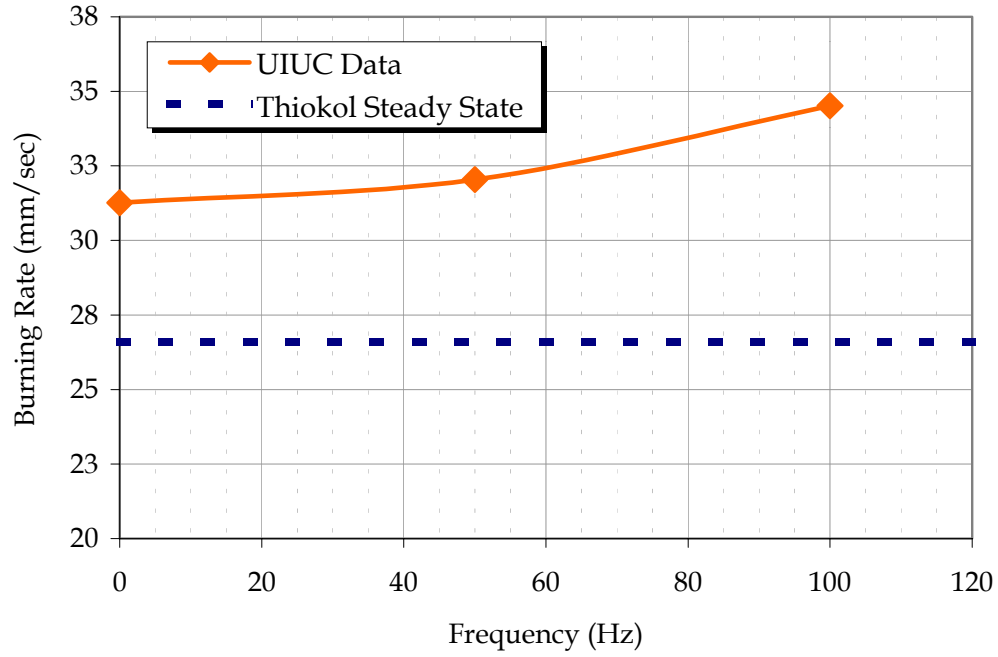

Figure 3. Plot of average burning rate versus frequency for Thiokol #5 at 1900 psi (~130 atm).

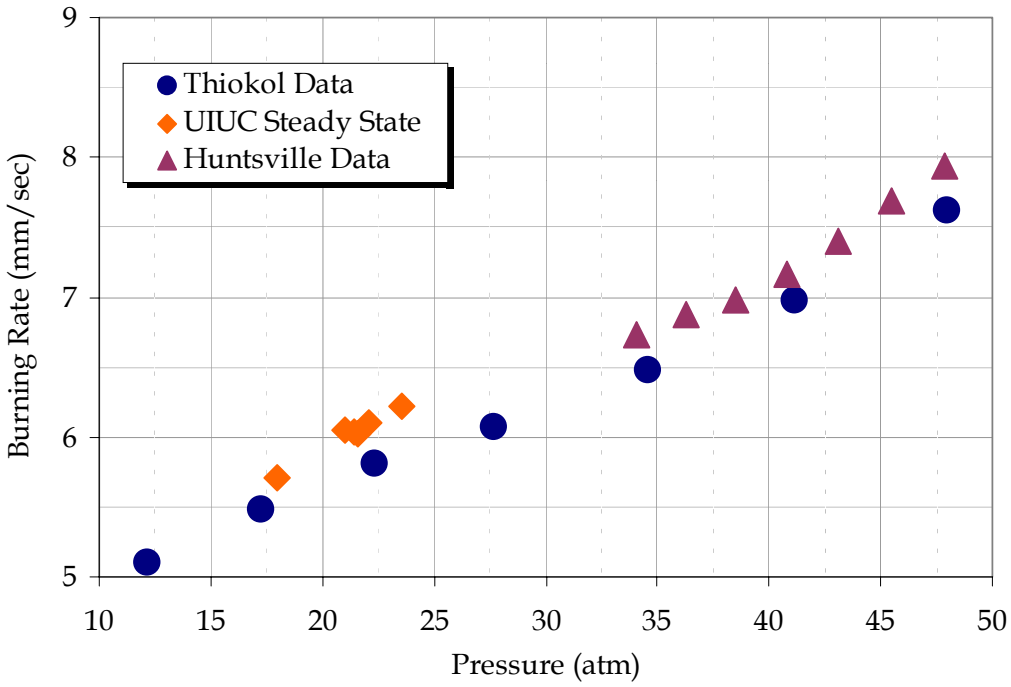

Figure 4. Plot of UIUC steady state burning rate data with Thiokol and Huntsville measurements for Thiokol #4.

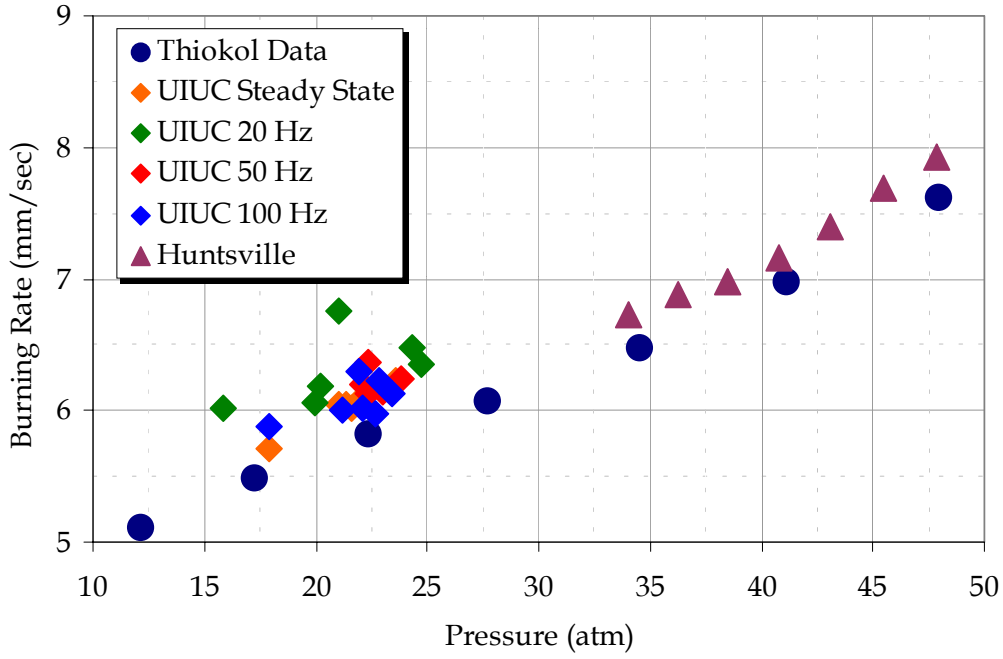

Figure 5. Plot of UIUC steady state and oscillatory data compared with Thiokol and Huntsville data for Thiokol#4.

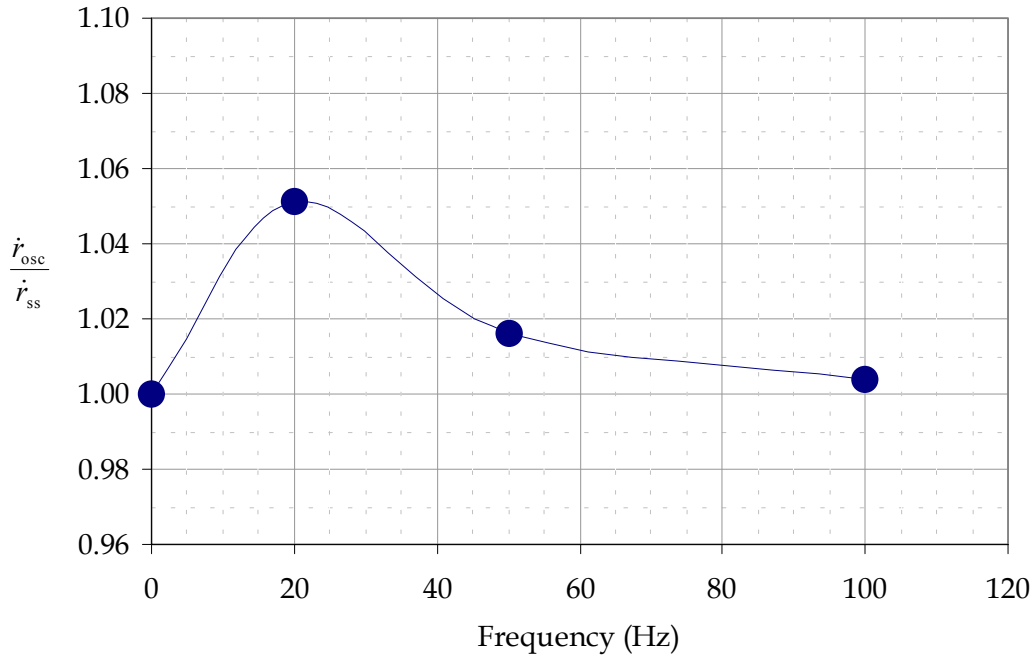

Figure 6. Plot of average burning rate versus frequency for Thiokol #4 at 300 psi (~21 atm).

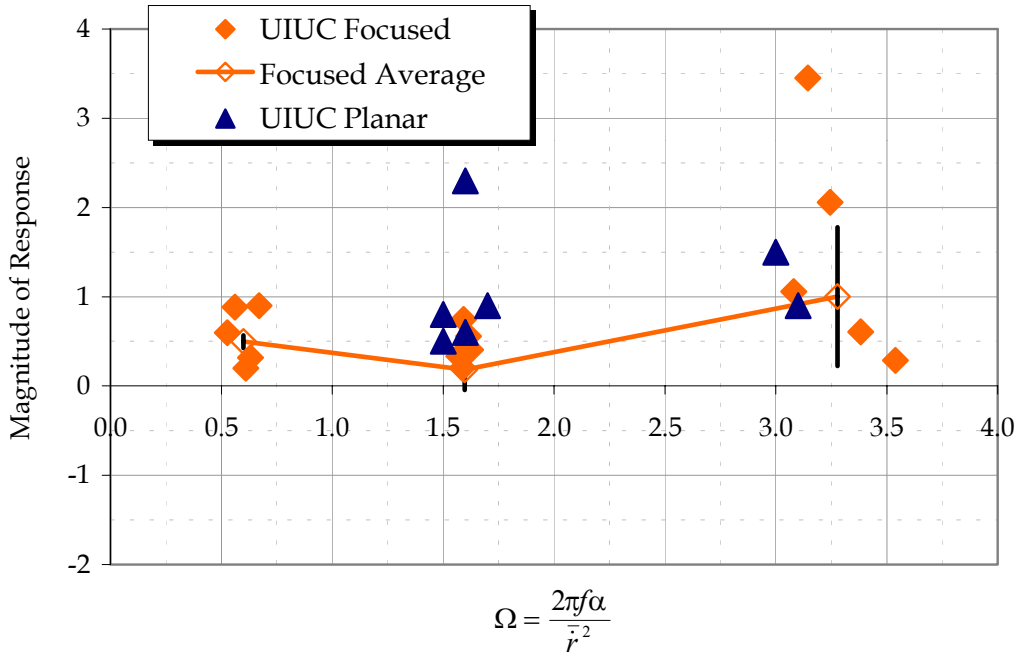

Figure 7. Response function magnitude for Thiokol #4 at 300 psi (~21 atm).

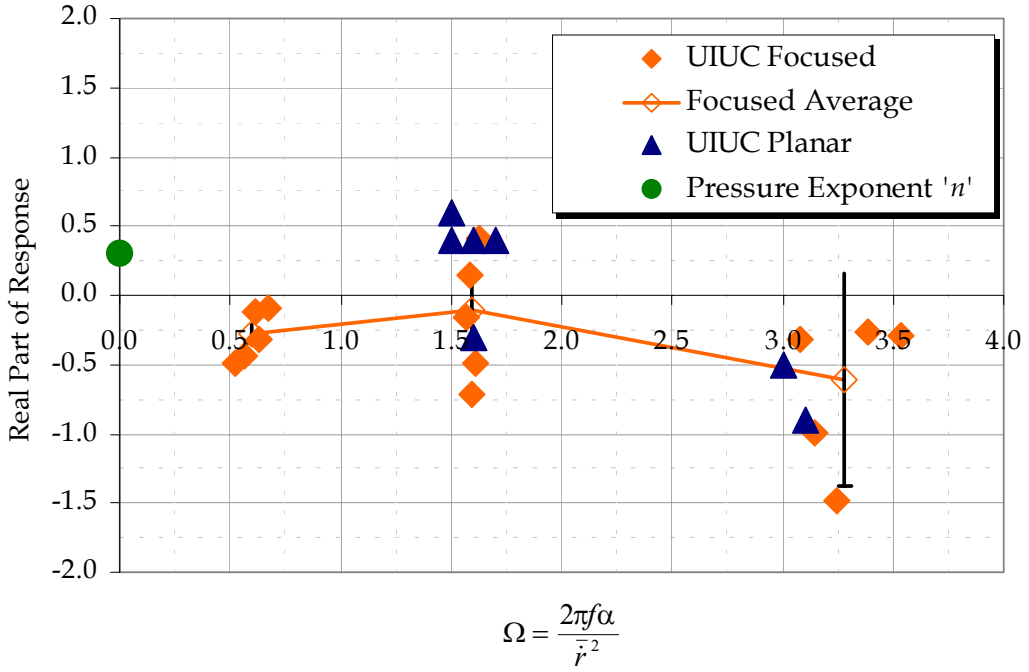

Figure 8. Real part of response for Thiokol #4 at 300 psi (~21 atm).

2.3.5 Ultrasonic Measurement of Propellant Response Functions (Frederick)

The pressure coupled response function was measured for a composite non-metallized propellant in a vented bomb. The technique described is unique in the manner in which the pressure oscillations are generated. An inert gas is injected into the throat of a venting nozzle to generate the necessary pressure oscillations as shown in Figure 1. The burning rate was measured using the ultrasonic technique. Testing was done at various frequencies from 10-75 Hz and pressures from 600-1200 psig. The pressure coupled response function was evaluated for each test together with the random error. An analytic model of the conditions within the combustion chamber has also been developed to aid in determining the settings needed to obtain the desired conditions in the test. These results seem to be reasonable. The data at high frequency approaches the signal to noise limit.

Four propellants were specifically formulated and tested to develop and evaluate the burner. The first was the MURI 064 baseline propellant. It is composed of 86 % AP, 12 % HTPB, and 2% is catalyst. The three other propellants were specifically formulated at UAH and prepared by AMCOM to interpret the effect of AP particle size on the characteristics of the propellants. These propellants were all composed of 75% AP and 25% HTPB. The first was a bimodal 17/200 μm propellant whereas the second and third were mono-modal 200 μm and 17 μm propellants. Table 1 below summarizes the composition of these propellants.

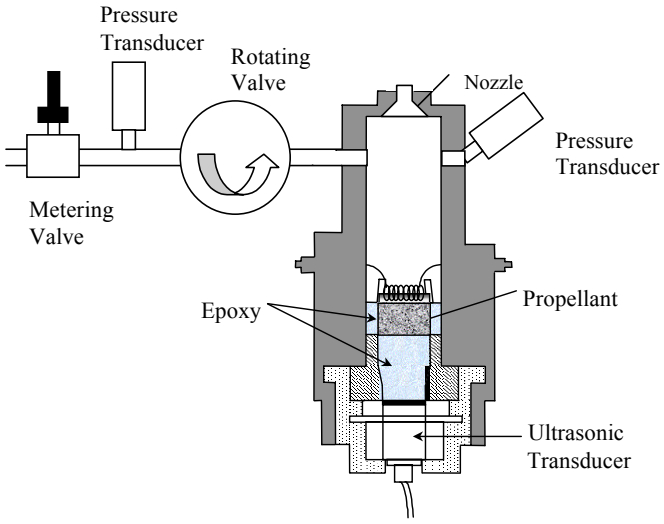

Figure 1. Modulated Gas Injection Bomb

Table 1. Propellant Formulation Matrix

Propellant	AP %	HTPB %	% Catalyst Additives	% by weight of AP 17 μm	% by weight of AP 200 μm
064	86	12	2	N/A	N/A
98-37	75	23.2	1.8	30	45
98-38	75	23.2	1.8	0	75
98-39	75	23.2	1.8	75	0

Figure 2 is a graphic summary of the R_p data. It is plotted as a function of non-dimensional frequency, Ω. For most propellant formulations, the first peak is contained within the initial ten units of non-dimensional frequency. This range was achieved at the low frequencies of these tests because of the relatively slow burning rate of these laboratory propellants. For ease of visual identification, the tests were lumped in three pressure categories. The first category comprised tests whose pressure was between 370 and 392 psig (Low Pressure). The second was between 613 and 692 psig (Medium Pressure), and the third between 803 and 982 psig (High Pressure).

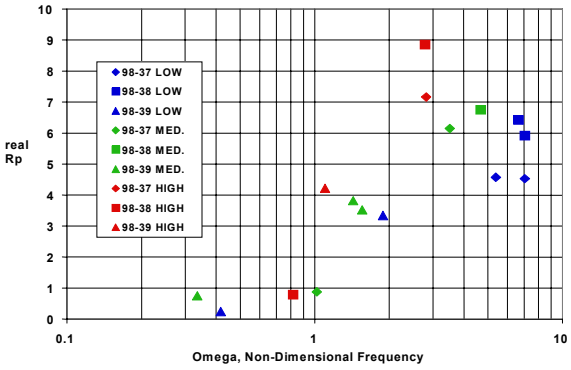

Figure 2. Response values as function of non-dimensional frequency.

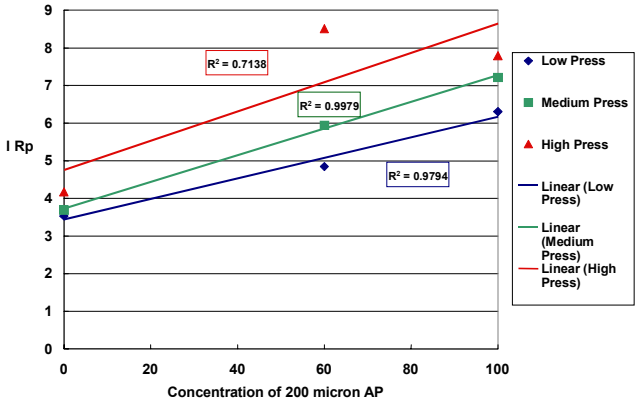

Figure 3. Pressure-Coupled Response vs. AP modality.

If the groups of data at similar pressure and frequency are plotted as a function AP modality concentration, the result is apparent. Observing the results in Figure 3 it can be seen that the bi-modal propellant behaves as a mixture of the two mono-modal AP compositions. This result is well within the uncertainty of the measurement. The results proved to be quite good nonetheless. From this group of data the following empirical rule was obtained.

$$R_p = \sum_i \alpha_i \cdot R_p^i(f_0, p_0)\Omega \geq 1 \qquad (1)$$

The response of a mixed modality propellant is given by the weighted average in AP concentration of the response of the constituent propellants at constant pressure and frequency.

2.4 Modeling the Dynamical Response of Burning Solid Propellant (Beckstead)

A burning solid propellant is a chemically reacting, dynamic system. As such it can be characterized by parametric measures developed for dynamic systems analysis such as frequency response functions. Although a burning propellant is inherently a nonlinear dynamic system, linear behavior can be approached in both experimental behavior and theoretical modeling; hence, the utility of frequency response functions. The dynamic response function of most interest in solid propellant combustion (for obvious practical reasons) is the response to

pressure perturbations. Response to radiation (*e.g.*, laser energy) has also attracted interest recently as a laboratory diagnostic. The linear pressure- and radiation-frequency response functions are defined as follows.

$$R_p = \frac{r_b'/\bar{r}_b}{P'/\bar{P}} \qquad\qquad R_q = \frac{r_b'/\bar{r}_b}{q_r'/\bar{q}_r}$$

The dynamical response of burning solid propellants is important for two fundamental reasons. (1) Combustion instability in motors, where the propellant is coupled to an acoustic chamber, is still a difficult unsolved problem in practice. (2) Dynamic behavior offers opportunities for testing postulated mechanisms and discovering fundamental behavior that are unavailable if just steady burning is considered. In fact, dynamic burning can be considered a convincing test of fidelity for a combustion model. Whereas steady burning rate data, for example, can usually be nicely fit by even unphysical models if enough free parameters are included, dynamical burning rate data usually cannot. Thus there are both practical and fundamental reasons for considering the dynamic burning behavior of solid propellants.

Solid propellant combustion modeling can be categorized according to the physical state of the system (*e.g.*, premixed vs. non-premixed) as well as its mathematical description (*e.g.*, linear vs. nonlinear). For the purposes of this section a convenient breakdown is as follows:

Reactant Mixedness:	Premixed	vs.	Nonpremixed
Kinetics:	Simple	vs.	Detailed
Gas-phase inertia:	Quasi-steady	vs.	Unsteady
Linearity:	Linear	vs.	Nonlinear

This section describes in order of generally increasing mathematical complexity a summary of the work of three groups within the MURI consortia who developed models of dynamic solid propellant combustion. The various efforts differ according to the type of propellant considered (homogeneous-premixed or composite-nonpremixed), the complexity of kinetics used (simple or detailed), the inertia of the gas-phase zone (quasi-steady or unsteady) and the mathematical character (linear or nonlinear). The first group (Brewster, UIUC) considers premixed (homogeneous) propellants using simplified kinetics with quasi-steady gas and both linear and nonlinear behavior. The second group (Beckstead, BYU) considers premixed (homogeneous) propellants using detailed kinetics, quasi-steady and fully unsteady gas, and focussing on linear behavior. The third group (Frederick/Moser, UAH) considers nonpremixed (heterogeneous) propellants using simplified kinetics, quasi-steady gas, with both linear and nonlinear behavior.

2.4.1 Modeling Unsteady Solid Propellant Combustion with Simplified Kinetics (Brewster, Loner and Tang, UIUC)

Advances in simulating unsteady solid propellant combustion were made under the MURI program using simplified kinetics models. A new model was developed and used to make predictions *a priori* of oscillatory unsteady burning. The results confirmed the basic correctness and utility of the approach and represent a step in the

direction of being able to make predictions of energetic solids combustion performance without knowing the answer beforehand.

The new approach is based on a low activation energy (low-E_g) assumption for the gas-phase reaction zone. This model demonstrated the ability to predict not only the first derivatives but also the second derivatives of steady burning rate with respect to initial temperature, pressure, and radiant flux ($\partial^2 r_b/\partial T_o \partial P$, $\partial^2 r_b/\partial T_o^2$, $\partial^2 r_b/\partial T_o \partial q_r$, etc.)[1]. After showing promise with steady-state data the model was tested against the more difficult challenge of unsteady combustion. Initially, linear behavior was addressed. Since laser-recoil data for HMX were readily available the frequency response of burning rate to oscillatory laser radiation, R_q, was modeled and compared with those data as shown in Figure 1[2,3]. The R_q comparison was used to determine kinetic and thermochemical properties that cannot yet be predicted from first principles. Based on the combustion parameters obtained from the unsteady radiation response, blind predictions of the pressure-coupled response function R_p were then made[3,4]. At that time there were no reported measurements of R_p for HMX. The R_p predictions were published and presented at the Joint Propulsion Conference at Seattle in July 1997[2].

Later that same year (1997) the first HMX T-burner measurements were conducted at China Lake and compared with the earlier predictions as shown in Figure 2[4,5]. Considering the difficulty of this kind of prediction the agreement in Figure 2 is promising. Not only did the new simple kinetics model match the measurements reasonably well over the appropriate range of validity, the quasi-steady breakdown frequency was also predicted (at non-dimensional frequency $\Omega_{QSC} \sim 25$). That the quasi-steady assumption should fail at a sufficiently high frequency was not a new result; but the mechanism of failure, namely, condensed phase reaction layer relaxation—as opposed to gas phase—was a new (or at least mostly forgotten) idea that came out of this work. A formula for predicting quasi-steady breakdown also resulted: $\Omega_{QSC} \sim (\pi/2)E_c/2RT_s^6$. Similar results for both pressure- and radiation-response functions were also subsequently demonstrated with other materials such as NC/NG[7] and HNF[8].

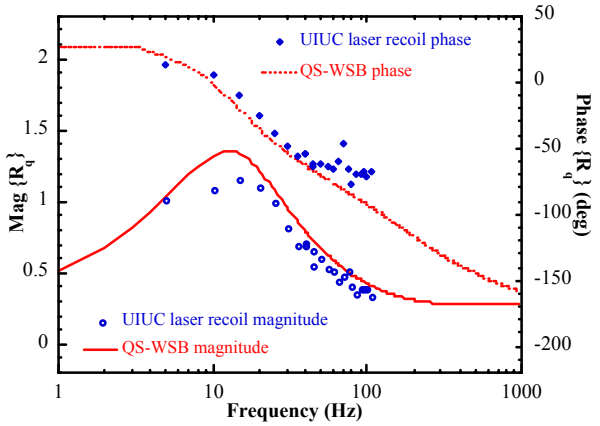

Figure 1. Radiation response function for HMX (1 atm, 35 W/cm^2); CO_2 laser-recoil measurements[3]. Quasi-steady theory with simplified kinetics model (WSB)[2,3]. Quasi-steady assumption should hold for f < 32 Hz (f_R = 130 Hz).

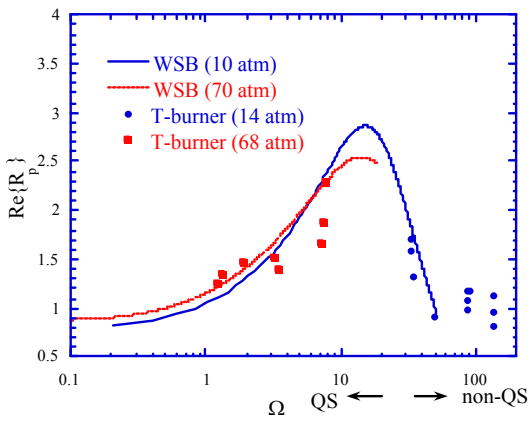

Figure 2. In-phase component of pressure-coupled response function for HMX. Data points represent T-burner measurements[5]; lines are simplified kinetics model predictions made before measurements[2,4]. Quasi-steady assumption was predicted to hold for Ω < 25.

In addition to the low-E_g gas-phase development, theoretical advances in representing condensed phase decomposition also contributed to this new modeling approach. It is generally agreed that the condensed phase reaction zone of most energetic solids can be characterized by a high activation energy, thermal decomposition process ($E_c/RT >> 1$) and that the Activation Energy Asymptotics (AEA) branch of combustion theory should therefore apply. However, instead of a mathematically rigorous implementation of AEA theory, usually an approximate, partially *ad hoc* expression has been employed, both for steady and unsteady burning: $r_b = A_s P^{ns} \exp(-E_c/2RT_s)$. In correlating steady burning rate over limited parameter space (*e.g.*, for a fixed initial temperature) this simple Arrhenius expression with $n_s = 0$ is adequate. But when the parameter space is expanded (such as variations in initial temperature or radiant flux or for unsteady burning) the inadequacy of the simple Arrhenius pyrolysis expression with $n_s = 0$ becomes apparent. The new approach employs a decomposition description that is simplified in the kinetics (zero order reaction), but mathematically rigorous (AEA). A significant result that came out of this approach was that the n_s parameter (shown[9,10] to be equivalent to the ZN parameters δ/r) is not usually zero but negative, as shown in Eq. 1[6,10].

$$n_s = \frac{\delta}{r} = \frac{-n}{\sigma_p \left[2(T_s - T_o) - \frac{Q_c}{C} - \frac{f_r q_r}{mC} \right] - 1} < 0 \text{ (except plateau/mesa)} \qquad (1)$$

When pressure sensitivity is positive ($n > 0$, the usual case), Eq. 1 shows that n_s is negative, usually $n_s \sim -1$. Before 1995[10] no published study had suggested negative n_s values as being physically plausible, only zero or positive values. Since Eq. 1 is based on the simplest of possible kinetics (zero order, unimolecular decomposition), more detailed kinetics have since been employed to calculate n_s or δ (the ZN Jacobian parameter); the results have confirmed negative values[4].

Toward the end of the MURI program, after linear dynamic burning results had been validated to a degree, an effort was begun to address nonlinear combustion issues, particularly those pertinent to motor performance. One preliminary finding was that the "ignition spike" observed in certain rocket motors, which is usually attributed to erosive burning, could be replicated by nonlinear dynamic burning. This class of motors usually has large L/D_{bore} and small A_{bore}/A_{throat} and thus high internal gas velocities. However, this means that the motors also usually have small L* (= V/A_{throat}) values, which makes them susceptible to pressurization-rate-dependent dynamic burning effects in addition to erosive burning. Figure 3 shows a calculated "ignition spike" for typical tactical motor conditions (L* = 2.6 m)[11]. The pressure spike in Figure 3 is a result of nonlinear pressurization-rate-dependent dynamic burning only (no erosive burning or igniter mass flux). Confirming this effect will have significant positive implications for the use of simulation in motor design. Large boosters with L* values up to 30 m usually do not show an over-pressure spike (either experimentally or computationally) but modeling results do suggest that the pressurization rate even in large motors can be influenced by nonlinear pressurization-rate-dependent dynamic burning. Since ignition transient modeling is still a difficult problem it is important to continue research in this area. At the University of Illinois (Center for Simulation of Advanced Rockets) simplified kinetics models are being used

to address ignition transient as well as acoustic instability behavior. This approach is also being adapted to non-premixed combustion of composite propellants.

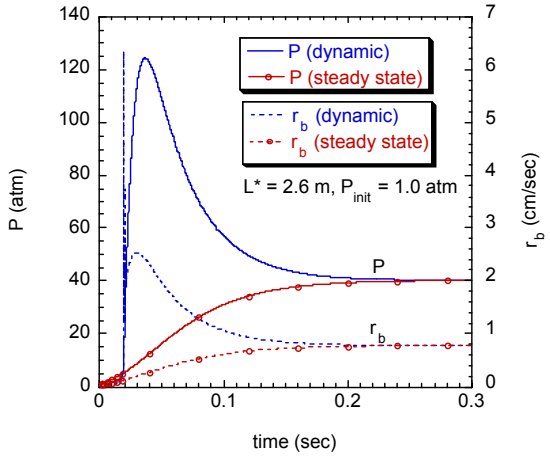

Figure 3. "Ignition spike" as simulated by nonlinear pressurization-rate-dependent dynamic burning (no igniter mass flux or erosive burning) with simplified kinetics model[11].

2.4.2 Modeling Combustion Instability of RDX and HMX with Detailed Chemistry (Erikson and Beckstead)

To aid in developing a more fundamental understanding of unstable combustion, a numerical model of unsteady solid monopropellant combustion has been developed. The model allows three distinct modes of simulations to be performed within the framework of a single code: (1) steady-state, (2) quasi-steady gas phase, and (3) fully unsteady gas phase. Detailed gas phase chemistry for both RDX and HMX is included using the same basic mechanisms discussed on steady state modeling.

Reasonable agreement with experimental data was obtained for many steady state combustion parameters including burning rate, surface temperature, melt layer thickness, and low pressure temperature and species profiles. Modeled temperature profiles at high pressures showed a steeper gradient near the surface region than did experimental data. This was attributed to inadequacies in the chemical reaction mechanisms. Temperature sensitivity results from the RDX model agreed quite well with experimental data. However, the HMX model, failed to adequately match experimental temperature sensitivity at low pressures.

A series of calculations were made to evaluate the relationship between burning rate and surface temperature. The calculations reinforce the idea that the burning rate is not just a simple Arrhenius function of surface temperature. Changes in pressure, initial temperature, and radiant flux level appear to have different effects on burning rate and surface temperature. This also implies that the Jacobian parameter, δ, used in the ZN theory is non-zero, as has been suggested by others.[3,10,12,13] The model has been used to calculate the ZN parameters for RDX and HMX for varying pressures and heat fluxes. These results show that the δ parameter is indeed non-zero, and typically has a value on the order of 0.01, usually negative.

The magnitude of the pressure-coupled response function, R_p, was calculated by the quasi-steady model for RDX and HMX and compared to the experimental T-burner data from Finlinson[14] (see also similar results in Section 9). Due to the large amount of scatter in the experimental data, particularly for RDX, generalizations are difficult.

However, the T-burner data for both RDX and HMX appear to show an increase in response magnitude with pressure—a trend consistent with the modeling results.

Ranges of validity of the quasi-steady assumption were evaluated by performing simulations for RDX and HMX using both the quasi-steady and corresponding fully unsteady models. At low frequencies, the fully unsteady calculations coincide with the quasi-steady, but at higher frequencies, deviations between the two calculations occur. The characteristic times for gas phase processes are typically much shorter than for condensed processes (*e.g.* thermal relaxation for the gas phase may be ~ 100x faster than for the condensed phase, and reaction times may be still faster[15]). As the frequency increases, the oscillatory time scales approach that of the gas phase thermal relaxation and chemical reaction time scales, eventually yielding deviations from the quasi-steady theory. The quasi-steady assumption was determined to be valid up to about 200 Hz at 1 atm and up to about 1000 Hz at 68 atm.

Heat flux responses obtained from transient calculations matched experimental laser-recoil results reasonably well for RDX, as shown in Figure 1. Simulations were performed at three different incident radiant flux levels and yielded peak response values of ~0.5 at low frequencies in excellent agreement with laser-recoil data from Brewster and Schroeder[16]. In addition to the low-frequency peak, the experimental data also exhibit high-frequency amplification, with R_q values reaching around 1.0 at several hundred Hz. The fully unsteady RDX model simulations also show similar high-frequency amplification, with amplitudes increasing with higher heat flux levels. The prediction of high-frequency amplification by the fully unsteady model illustrates a limitation of a quasi-steady analysis.

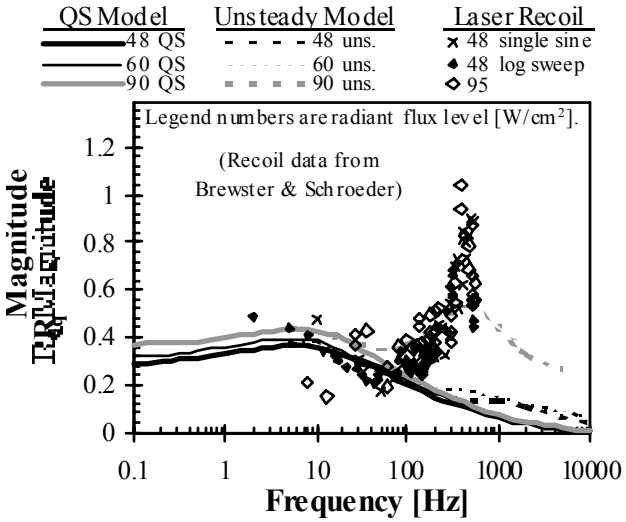

Figure 1. RDX R_q from quasi-steady and fully unsteady models compared with experimental laser recoil data.

For HMX, the heat flux response curves obtained from simulations failed to adequately match experimental laser-recoil data.[3,17] Simulated peak responses under-predicted laser-recoil results by a factor of 2 to 3.

The differences between the HMX and RDX heat flux responses are striking, but not unexpected. The model predicts a steady state σ_p value of ~0.001 K^{-1} for RDX for a range of pressures, which is in good agreement with experimental data. The model predicts a similar value of σ_p for HMX. However experimental values of σ_p for

HMX are a strong function of pressure with large values (>0.005 K^{-1}) at low pressure decreasing to smaller values (~0.001 K^{-1}) at high pressures. Since σ_p is a parameter which correlates strongly with combustion responses in traditional theories[18] higher experimental values of R_q for HMX are expected. Because the HMX steady-state model failed to adequately predict σ_p at low pressures, it is not surprising that the corresponding unsteady model did not predict R_q well at low pressures. These discrepancies were attributed to inadequacies in the HMX combustion model, particularly with respect to condensed phase and near surface gas phase chemistry.

The model was also used to explore the physical effects of an imposed radiant heat flux on the pressure-coupled response. Two major effects were observed as the radiant flux level was increased. First, the peak amplitude diminishes, and second, the location of the peak response shifts to slightly higher frequencies. As the radiant flux level increases, it becomes a greater portion of the *total* heat flux (conductive plus radiant) incident on the propellant surface. Hence the fluctuations in *conductive* heat feedback to the surface caused by pressure oscillations would be comparatively decreased, reducing the response. This effect is accentuated by the burning rate augmentation due to the added radiant energy. This tends to blow the flame away from the surface—further reducing the influence of conduction and conductive flux oscillations.

Lee, *et al*.[19] have measured chemical species concentrations for RDX burning under oscillatory conditions with mass spectrometry. The concentrations of CO_2, N_2, and H_2O (major species) appear to be in phase with each other, but very close to 180° out of phase with NO. When the model was used to simulate the same conditions, the calculated results were very similar to the experimental results within ~0.03 cm from the burning surface. Further from the surface the phase relationship of H_2O changed, as the concentrations changed. Unfortunately experimental data were not gathered as a function of distance from the surface. These results are evidence of overall flame movement. During pressure oscillations, the flame zone (and hence the associated concentration profiles) moves alternately toward and then away form the propellant surface.

These results show that the utility of having a detailed model allows one to interpret results in greater detail, and extrapolate to conditions that are awkward for experimental measurements.

2.4.3 A Theoretical Pressure-Driven Response Function for Composite Solid Propellants (Rasmussen, Frederick and Moser)

Composite propellant combustion is a very complicated phenomenon that does not yield easily to pure analytical approaches. One of the first true composite steady-state models was the Beckstead-Derr-Price (BDP) multiple flame model[20], introduced in 1970. It inspired many similar models and improvements[21], and most composite models today still follow the same basic example. Some notable improvements have been inclusion of separate surface temperatures for binder and oxidizer,[22,23] and new techniques for modeling multi-modal propellants[24] (*i.e.* different AP particle diameters in the same propellant).

While such models have become better at predicting steady-state properties, there has been some difficulty extending the heterogeneous framework to nonsteady models[25]. Most nonsteady models since the 1950's have relied on Quasi-Steady gas phase, Homogeneous solid phase, One-Dimensional (QSHOD) assumptions. The

assumption of a homogeneous solid phase, in particular, greatly simplifies the final form of the response function, so the heterogeneity of composite propellants makes them poor subjects for QSHOD models.

There have been several approaches to accounting for heterogeneity in nonsteady models[25]. One tactic is to use a steady-state model to calculate physical parameters, which in turn plug into QSHOD models.[26,27] Another approach is to perturb and linearize a steady-state model.

The study competed here is a different approach based on direct simulation. The first part of the study is a steady-state model that predicts reasonable burning rate vs. pressure curves. The second part is a nonsteady model based on the steady-state description. The nonsteady model is almost identical to the steady-state model, but it does include some additional terms to account for thermal lags and conductive "capacitance" in the solid phase. Simpler versions of this method for heterogeneous propellants have created reasonable non-linear response predictions.[28]

The "pre-mixed" flame is a kinetics flame that emerges due to the exothermic decomposition of AP. The most reactive product of this flame is the approximately 30% O_2 that results from AP decomposition. The "reaction" flame is also a kinetics flame, but it receives its chemical energy through a reaction between perchloric acid from the AP flame and gaseous decomposition products from the polymer binder. Finally, the "diffusion" flame occurs above the kinetics region where the products of the previous two flames diffuse into each other and form the final decomposition products. Figure 1 is an illustration of the multiple flame model framework.

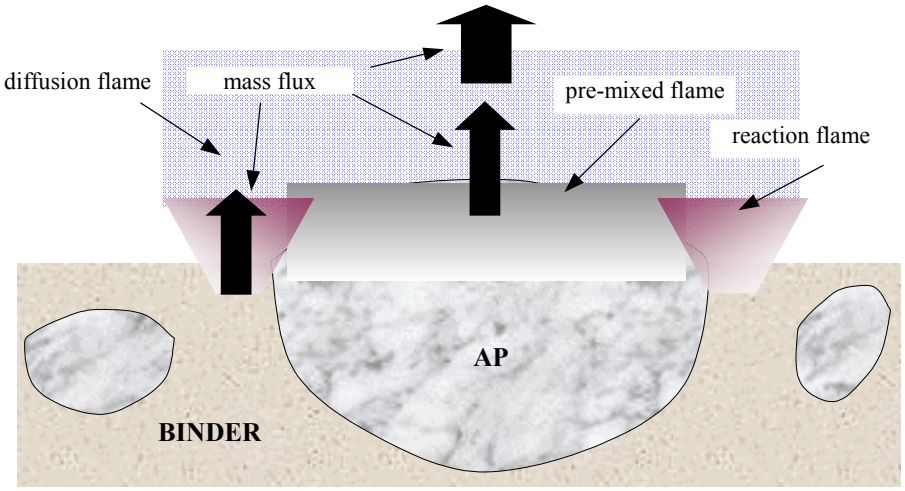

Figure 1. Physical Model.

Full-calculation results in the nonsteady regime are interesting, because they required the imposition of a gas-phase pressure-dependent-heat flux term to be consistent with linear methods. No one has yet attempted a nonsteady, nonlinear model of this complexity, so any result is encouraging. Nevertheless, it seemed odd that when more realistic assumptions were applied, they lead to less realistic results.

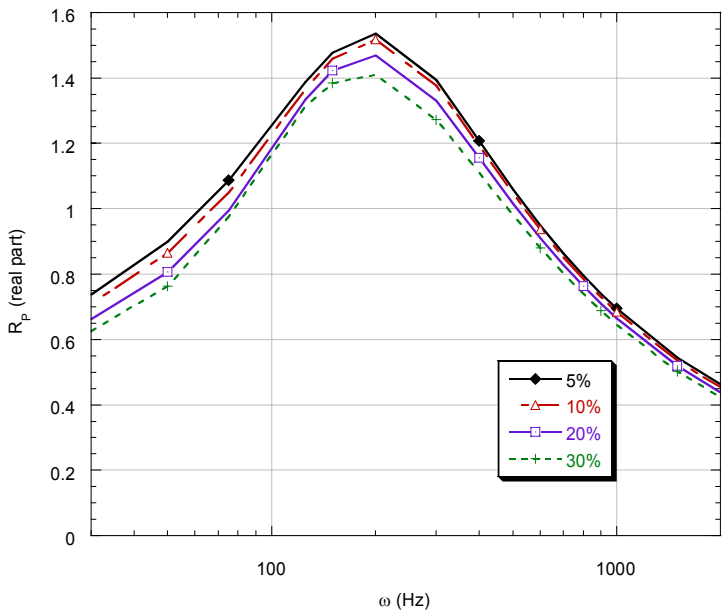

Figure 2. Effect of Oscillation Magnitude on Response Function.

Nonlinear effects should show up most profoundly through the oscillation magnitude. In a linear system, the response to a harmonic input is itself harmonic, so the oscillation magnitude is completely irrelevant. In nonlinear systems, however, the response becomes "less harmonic" as the input magnitude goes up. Thus, one should see a definite trend of some sort as the driving pressure magnitude goes from 5% to 30%. Figure 2 shows the result.

A basic problem encountered is that the definition of R_P is inherently linear, so any R_P taken from a nonlinear simulation will be somewhat contrived and arbitrary. The effect of oscillation amplitude could differ greatly, depending on how one takes the non-linear burning rate prediction and abstracts a linear value of the propellant response function.

References

1. Ward, M. J., S. F. Son, and M. Q. Brewster, "Steady Deflagration of HMX with Simple Kinetics: A Gas Phase Chain Reaction Model," *Combustion and Flame*, 114, 556-568, 1998.
2. Brewster, M. Q., M. J. Ward, and S. F. Son, "New Paradigm for Simplified Combustion Modeling of Energetic Solids: Gas Chain Reaction," *33rd AIAA/ASME/SAE/ASEE Joint Propulsion Conference*, Seattle, WA, AIAA Paper No. 97-3333, July 6-9, 1997.
3. Loner, P. S. and M. Q. Brewster, "On the Oscillatory Laser-Augmented Combustion of HMX," 27th International Symposium on Combustion, The Combustion Institute, Pittsburgh, PA, 1998, pp. 2309-2318.
4. Brewster, M. Q., "Workshop Report on Flame Structure and Combustion Modeling of HMX and RDX," *34th JANNAF Combustion Meeting*, West Palm Beach, FL, CPIA Publ. No. 662, II, 123-140, Oct. 1997.
5. Finlinson, J. C. and R. A. Stalnaker, "Pure Oxidizer T-Burner Pressure Coupled Response for AP, HMX, RDX from 200 to 1000 PSI," 34th JANNAF Comb. Mtg., CPIA Pub. 662, Vol. II, 1997, pp. 39-47.
6. Brewster, M. Q., "Solid Propellant Combustion Response: Quasi-Steady (QSHOD) Theory Development and Validation," Chapter 2.16 in *Solid Propellant Chemistry, Combustion, and Motor Interior Ballistics*, Progress in Astronautics and Astronautics, V. Yang, T. B. Brill, and W. Z. Ren, eds., AIAA, Reston, VA, Vol. 185, 607-638, 2000.

7. Brewster, M. Q., M. J. Ward, and S. F. Son, “Simplified Combustion Modeling of Double Base Propellant: Gas Phase Chain Reaction Vs. Thermal Decomposition,” *Combustion Science and Technology*, 154, 1-30, 2000.
8. Louwers, J., G.M.H.J.L. Gadiot, M.Q. Brewster, S.F. Son, T. Parr, and D. Hanson-Parr, “Steady-State Hydrazinium Nitroformate (HNF) Combustion Modeling,” *Journal of Propulsion and Power*, 15:6, 772-777, 1999.
9. Son, S. F. and M. Q. Brewster, "Linear Burning Rate Dynamics of Solids Subjected to Pressure or External Radiant Flux Oscillations," *Journal of Propulsion and Power*, 9:2, 222-232, 1993.
10. Brewster, M. Q. and S. F. Son, "Quasi-Steady Combustion Modeling of Homogeneous Solid Propellants," *Combustion and Flame*, 103:1/2, 11-26, 1995.
11. Tang, K. C. and M. Q. Brewster, “Nonlinear Dynamic Combustion in Solid Rockets: L*-Effects,” AIAA 2000-3572 and *Journal of Propulsion and Power*, 14:4, 909-918, 2001.
12. DeLuca, L., "Frequency Response Function of Burning Solid Propellants," *Meccanica*, Dec. 1980, pp. 195-205.
13. DeLuca, L., Di Silvestro, R., and Cozzi, F. "Intrinsic Combustion Instability of Solid Energetic Materials," *Journal of Propulsion and Power*, Vol. 11, 1995, pp.804-815.
14. Finlinson, J. C., Stalnaker, R. A., and Blomshield, F. S., "HMX and RDX T-Burner Pressure Coupled Response From 200 to 1000 psi," *36th Aerospace Sciences Meeting*, AIAA paper 98-0556, January, 1998.
15. Culick, F. E. C., "A Review of Calculations for Unsteady Burning of a Solid Propellant," *AIAA Journal*, Vol. 6, 1968, pp. 2241-2255.
16. Brewster, M. Q., and Schroeder, T. B., "Unsteady Combustion of Homogeneous Energetic Solids," *Challenges in Propellants and Combustion, 100 Years After Nobel*, edited by K. K. Kuo, Begell, New York, 1997, pp. 1082-1092.
17. Tang, C.-J., Kudva, G., Lee, Y., and Litzinger, T. A., "A Study of the Combustion Response of the HMX Monopropellant to Sinusoidal Laser Heating," CPIA Publication 653, Vol. II, 1996, pp. 159-168.
18. Beckstead, M. W. and Erikson, W. W., Combustion Instability of Solid Monopropellants, 33rd JANNAF Combustion Meeting, 1996, Vol. II, CPIA No. 653, pp 145–157.
19. Lee, Y. J., Tang, C.-J., and Litzinger, T. A. "An Experimental Study of Acoustically-Driven Instabilities for Solid Propellants," *34th JANNAF Combustion Subcommittee Meeting*, Vol. II, CPIA Publication 662, 1997, pp. 79-91.
20. Beckstead, M.W., Derr, R. L., and Price, C.F. “A Model of Composite Solid-Propellant Combustion Based on Multiple Flames” *AIAA Journal* Vol. 8, Dec 1970, pp.2200-22078.
21. Cohen, N.S. “Review of Composite Propellant Burn Rate Modeling” *AIAA Journal* Vol. 18 March, 1980. P.277-293.
22. Beckstead, M.W., “A Model for Solid Propellant Combustion” *Eighteenth Symposium (International) on Combustion*. The Combustion Institute, Pittsburgh, PA, 1981, pp. 175-185.
23. Cohen, N. S., and Strand, L. D., “An Improved Model for the Combustion of AP Composite Propellants” *AIAA Journal*, Vol. 20 No. 12 December, 1982, pp. 1739-1746.
24. Renie, J. P., Condon, J. A., and Osborn, J. R. “Oxidizer Size Distribution Effects on Propellant Combustion” *AIAA Journal* August, 1979, pp. 877-883.
25. Cohen, N. S. “Response Function Theories That Account for Size Distribution Effects— A Review” *AIAA Journal* Vol. 19 No. 7 July, 1981. pp. 907-912.
26. Beckstead, M. W., “Combustion Calculations for Composite Solid Propellants” *13th JANNAF Combustion Meeting*, CPIA Publication 281, Vol. II, 1976, pp.299-312.
27. Condon, J. A., Osborn, J. R., and Glick, R. L., “Statistical Analysis of Polydisperse, Heterogeneous Propellant Combustion” *13th JANNAF Combustion Meeting*, CPIA Publication 281, Vol. II, 1976, pp. 209-223.
28. Galfetti, L., Riva, G., and Bruno, C. “Numerical Computations of Solid-Propellant Nonsteady Burning in Open or Confined Volumes,” *Nonsteady Burning and Combustion Instability of Solid Propellants*, Deluca, L., Price, E. and Summerfield, M. ed. AIAA Progress in Astronautics and Aeronautics, Vol. 143, 1992 pp. 643-687.

2.4.4 Modeling the Effects of Velocity Coupling on the Global Dynamics of Combustion Chambers (Culick)

The research summarized in this section has been reported in a Ph.D. Thesis (Isella, 2001) and in three publications (Culick, Isella and Seywert, 1998; Isella and Culick, 2000a; 2000b). Chiefly two general problems have been addressed:

1) develop a simple general analysis of the combustion dynamics of a solid propellant that will conveniently accommodate models of the relevant chemical and physical processes, especially those in the interfaced region; and
2) investigate the influences of changes in the combustion response function on observable features of the combustor dynamics, particularly properties of limit cycles.

Both of these problems were chosen to try to determine answers to the question: what properties of a solid propellant are responsible for the often observed sensitivity of the dynamics of a solid rocket to apparently small (sometimes not well-known) changes in the composition of the propellant. The main conclusions are:

(i.) small changes in the composition and thermodynamic properties of a propellant have significant consequences for dynamical behavior due to pressure coupling only if the propellant is burning near its intrinsic instability boundary; and
(ii.) on the contrary the dynamics due to velocity coupling is evidently significantly sensitive to small compositional changes.

If these conclusions are true, then future work in the area of combustion instabilities must include intensive attention to modeling and measuring the combustion dynamics—*i.e.* the response function—associated with velocity coupling.

(a) The Model Framework

One important purpose of the work cited above was to construct a framework within which it should be possible easily to investigate the consequences of various processes participating in the combustion of a solid. Representation of the combustion dynamics must be in a form required for analyzing the global dynamics (Section 3.2). The simplest approach is an extension of the well-known one-dimensional analysis producing the QSHOD response function for pressure coupling (Culick, 1968; Beckstead et al, 1969; T'ien, 1972; among many works). Others have followed a similar tack (*e.g.* Louwers, 1999); the main novel aspect of this work is inclusion simultaneously of surface physical dynamics (*e.g.* due to mobility of liquid or solid particles); dynamics, rather than quasi-steady behavior, of the gas phase; and an elementary representation of velocity coupling.

On the submillimeter scale, a burning solid is heterogeneous both in the region adjacent to the interface and in the gas phase where much of the conversion to products takes place. The flow field in the chamber, in particular the unsteady acoustic field, has spatial variations normally the order of centimeters and larger. The dynamics of the combustion processes at the surface are formally accommodated as a boundary condition, a response function of some sort, in the analytical framework for the global dynamics. Hence the vast difference in characteristic scales is accommodated, in principle, by spatially averaging the combustion dynamics. The averaging is done over a surface in some sense far from the interface so far as the propellant combustion is concerned, but practically at the interface

so far as the field within the chamber is concerned. In that way, the results of solution to the "inner" problem of combustion dynamics in the surface region are used as the boundary conditions for solution to the "outer" problem of the unsteady flow field in the chamber.

We are not concerned here with the matter of spatial averaging: we assume it can be done, not necessarily an easy or obvious process. It's an important part of the general problem. Therefore we proceed from the beginning with a one-dimensional analysis. The spatial framework for the model shown in Figure 1.

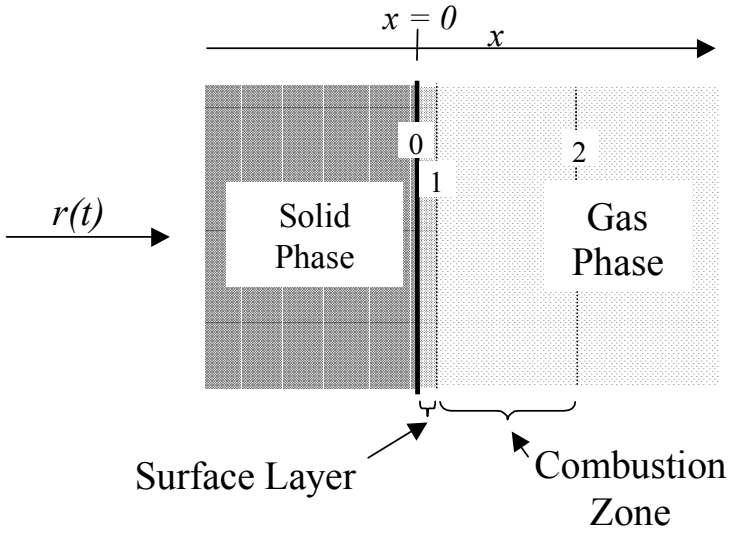

Figure 1. Spatial Definition of the Model

The strategy of the analysis is not novel and has been used in many previous works: solve the relevant equations, or postulate a model, governing the behavior in each of the three regions: solid phase; surface layer; and gas phase, including the region called 'combustion zone' in Figure 2.1. A major purpose of the analysis has been to determine the quantitative effects of the dynamics in the surface layer and gas phase in the response function found from the QSHOD model. Hence throughout the work we assume the same model for the solid phase: the dynamics is due to unsteady heat transfer in a homogeneous material having uniform and constant properties.[8]

Separate solutions or representations are obtained for each of the three regions. Unspecified constants or functions are then eliminated by satisfying boundary conditions and applying matching conditions at the two interfaces. Initially we intended, or hoped, to find such a form for the general behavior that different models for the surface layer and gas phase could easily be substituted and their consequences assessed. That goal has not been realized and probably is unattainable. Results require detailed numerical calculations before interesting information is obtained.

[8] Some departures from this model are discussed in the following section covering another part of the Caltech work by Shusser and Cohen.

(b) Models of the Surface Layer

From the beginning of this work we anticipated, because the dynamics of the gas phase are fast (owing to the relatively low material density), that the dynamics of the surface region should have greater effect on the combustion response function. We investigated two models of the region:

(i) first order dynamics represented by a constant time lag; and
(ii) unsteady heat transfer, with material properties different from those in the solid phase.

The idea of using a time lag is of course an old one, having been used by Grad (1949) in the first analysis of combustion instabilities, and later by Cheng (1982) as part of the Princeton group's extensive investigations (nearly a technical love affair) of time lag representations of unsteady combustion. The result in the present work, for the fluctuation of mass flux is

$$\frac{m'/\overline{m}}{p'/\overline{p}} = R_p \frac{e^{-i\Omega\tau}}{\sqrt{1+(\Omega\tau)^2}}$$

where R_p (sometimes written as R_b) is the response function found in the QSHOD theory. Thus R_p has the familiar two-parameter (A,B) representation. The dimensionless frequency is $\Omega = \omega\kappa/F^2$ κ is the thermal diffusivity and $\overline{r}$ is the linear burning rate and τ is the dimensionless time lag, equal to the physical time lag divided by $\kappa/\overline{r}^2$. Figure 2 shows a typical result (A = 14; B = 0.85; τ = 1.5). The graphs illustrate clearly a basic problem with a time lag theory: if the time lag is assumed constant (*i.e.* independent of frequency) the response (in this case the real part) possesses an oscillatory behavior with period increasing with frequency. Such behavior has never been observed.

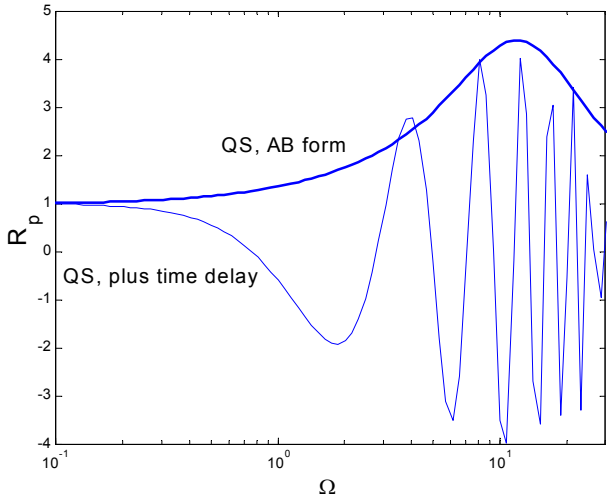

Figure 2. QSHOD Response Function with a Time lag: Thick Line, QSHOD Theory; Thin Line, QSHOD Model Including a Surface Layer Having First Order (time lag) Dynamics.

It is true that any response function can be written in a form showing a time lag behavior, but in general the time lag varies with frequency (Culick, 1968). If the physical model is sufficiently detailed, the dependence of τ on frequency is found as part of the solution. In particular, the QSHOD theory gives τ (Ω) such that the amplitude of the response function decays smoothly for frequencies higher than that at which the single peak occurs.

The second model for the surface is the only one considered for the following results. It is a simple representation of the dynamical behavior making use of the same solution as that for the homogeneous solid phase, with two differences:

(i) the uniform and constant properties are different from those of the condensed solid material;
(ii) the solution is forced to satisfy matching conditions of continuous temperature and heat transfer at the interfaces with the condensed phase and the gas phase.

(c) Models of the Gas Phase

In this analysis, all combustion processes are assumed to occur in the gas phase; upstream only phase changes are accounted for, assumed to take place at the interfaces. We assume distributed combustion of a simplified form, a single one-step reaction as previous treatments have used (T'ien, 1972; Huang and Micci, 1990; Lazmi and Clavin, 1992). Solutions must then be found numerically for the steady and linear unsteady temperature distributions, and subsequently matched to the solution for the surface layer.

(d) Some Results for the Combustion Response Function

Many experimental results exist suggesting that the responses of actual propellants tend often to be higher than that predicted by the QSHOD model for high frequencies. Initially the strongest motivation for this work on the response function was to determine in simple and relatively crude fashion what processes might have greatest effect on the values of the pressure-coupled response at frequencies greater than that at which the peak magnitude occurs. Roughly what that means, is finding one or more processes having 'resonant behavior' or characteristic times in the appropriate range. Unfortunately the analysis is sufficiently complicated that it has not been possible yet to deduce any explicit 'rules of thumb.' Therefore we present here a few plots of computed results to illustrate the behavior.

Figure 3 shows the basic or reference response function computed from the simple QSHOD model. The influences of dynamics in the surface layer and gas phase will be shown relative to that reference.

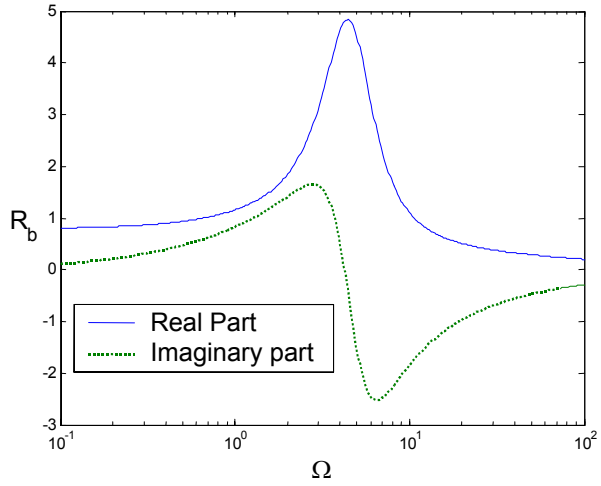

Figure 3. Reference Case: QSHOD Result with A = 6.0, B = 0.60.

(i) Influence of Gas Phase Dynamics

Figure 4 is the result when only the dynamics in the gas phase is added to the QSHOD model. The results are similar to those found by T'ien (1972) and Lazmi and Clavin (1992), not a surprising conclusion. As expected, the dynamics of the gas phase introduce a single additional peak at a frequency higher than that of the peak caused by unsteady heat transfer in the condensed phase.

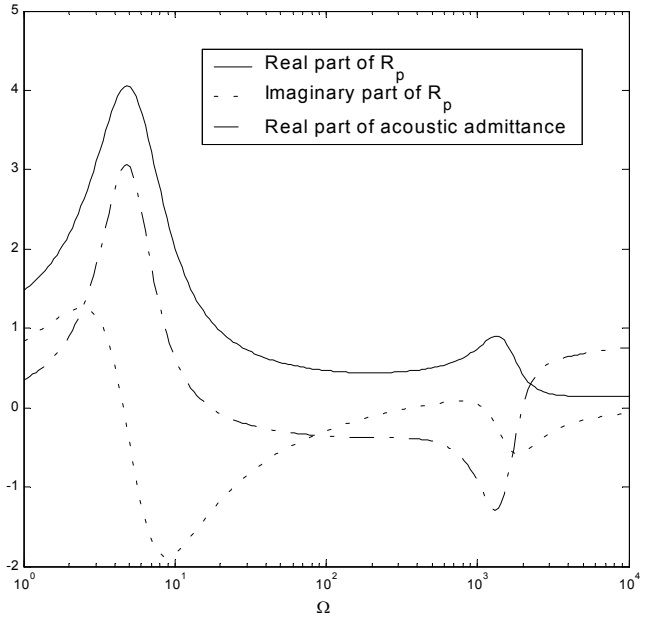

Figure 4. Combustion Response, QSHOD Model with Gas Phase Dynamics

(ii) Combined Influences of the Dynamics of the Surface Layer and the Gas Phase

The dynamics of the surface layer itself is the same as those of the condensed phase, but with different values of the defining parameters Figure 5 illustrates the effects of changing the surface activation energy and the material density on a function characterizing the response of heat transfer in the layer. The shape of this function differs from that (Figure 3) of the basic response function because it depends on the dependence of several flow variables on frequency.

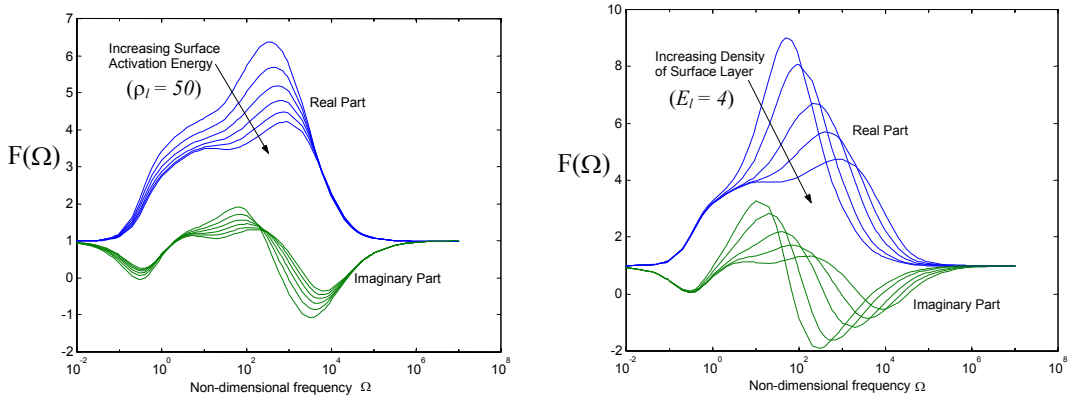

Figure 5. Effects of Activation Energy and Density on the Dynamics of the Surface Layer.

Finally, Figure 6 shows the result for one example of the response function with the dynamics of both the surface layer and the gas phase accounted for. Evidently for the conditions examined here the dynamics of the gas phase has more obvious influence on the response, in the higher frequency range, than does the surface layer.

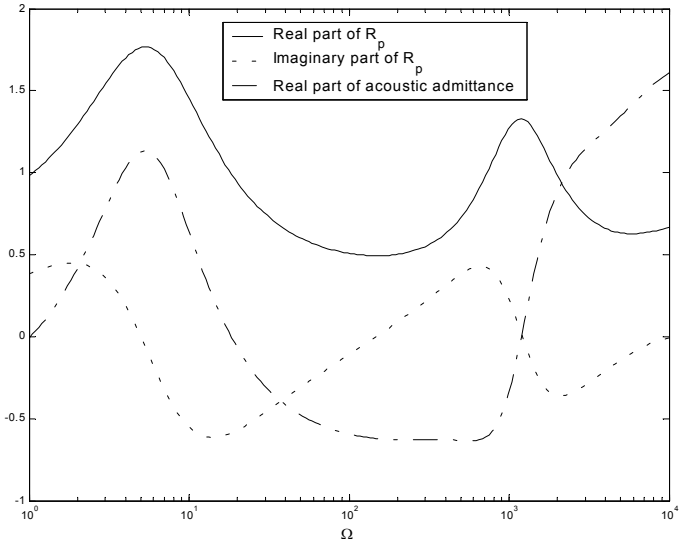

Figure 6. Combustion Response Function Including the Dynamics of the Surface Layer and the Gas Phase.

One way of summarizing the results is shown in Figure 7, showing the contributions to the response function by the solid (condensed) phase, the surface layer and the gas phase. The overall response function for the propellant is the product of the three contributions.

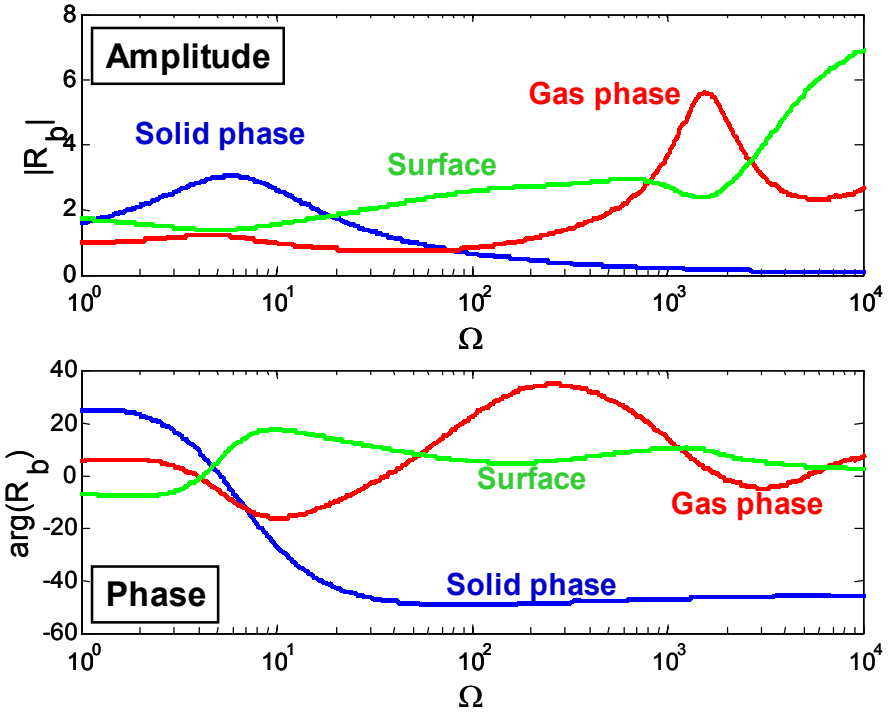

Figure 7. The Combustion Response Function Represented as Magnitudes and Phases of Individual Contributions.

2.4.5 Velocity Coupling, the Combustion Response, and Global Dynamics (Isella, Culick)

The work summarized in this section amounts to using some characteristics of the global combustor dynamics—the amplitudes and harmonic context of limit cycles—to draw some inferences about qualitative features of the combustion dynamics. At the beginning of the MURI program, during completion of his dissertation, Burnley (1996) showed that rectification associated with a velocity-coupled response function having also a threshold velocity, could be responsible for nonlinear or pulsed instabilities in a solid rocket motor. This result confirmed a conclusion reached several years previously by Levine and Baum (1983). That was the first example of using the behavior of the global dynamics as essentially a diagnostic tool to learn about the influences of the combustion dynamics on observable phenomena.

In the current work, the main questions at hand have to do with the apparent sensitivity of the global dynamics to small changes of propellant composition (see remarks (i) and (ii) in the introductory part of the section). We assume that small changes of composition likely have relatively small effects on the magnitude and phase of the response function. Therefore, we are really investigating the effects of small changes in the response function on the observable global dynamics. **Our main conclusion is that the sensitivity of the dynamics to changes in the response associated with velocity coupling is significantly greater than that for the response due to pressure coupling.** The implications for directions in future research are substantial.

Isella (2001) and Isella and Culick (2000) have reported the main results. Here we will only cite a couple of examples. The idea is to use the framework described in Section 3.2 below to compute the growth and limiting amplitudes for limit cycles. Essentially a modest parameter study has been done, the response function itself (*i.e.* the combustion dynamics) being the parameter. Following the tactic first introduced by Culick, Isella and Seywert (1998), it is helpful to display the response function, as a function of frequency, and the amplitudes of the modes forming a limit cycle, as two parts of the same figure, such as Figure 8 prepared for a typical case for the QSHOD response function. The chamber is cylindrical, 0.6 m long, 0.025 m in diameter, operated at a chamber mean pressure equal to 1.06×10^7 Pa. It is the same motor considered by Culick and Yang (1992).

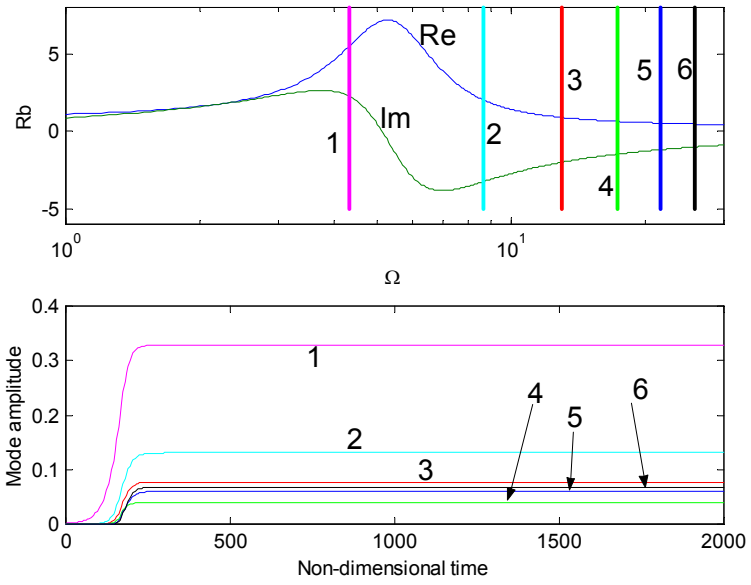

Figure 8. Results of a Simulation with a QSHOD Combustion Response (Pressure Coupling: A= 8.0, B = 0.6, n = 0.8).

Figures 9–11 show results obtained for the same motor and basic combustion response but including, respectively, a time delay; surface layer dynamics; and dynamics of both a surface layer and gas phase, all according to the analysis described above.

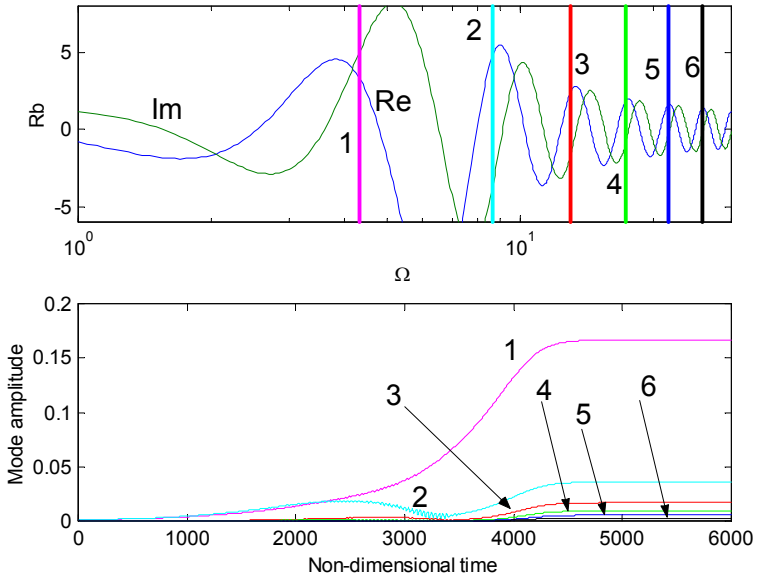

Figure 9. Results of a Simulation Including a Time Delay (τ = 1.5)

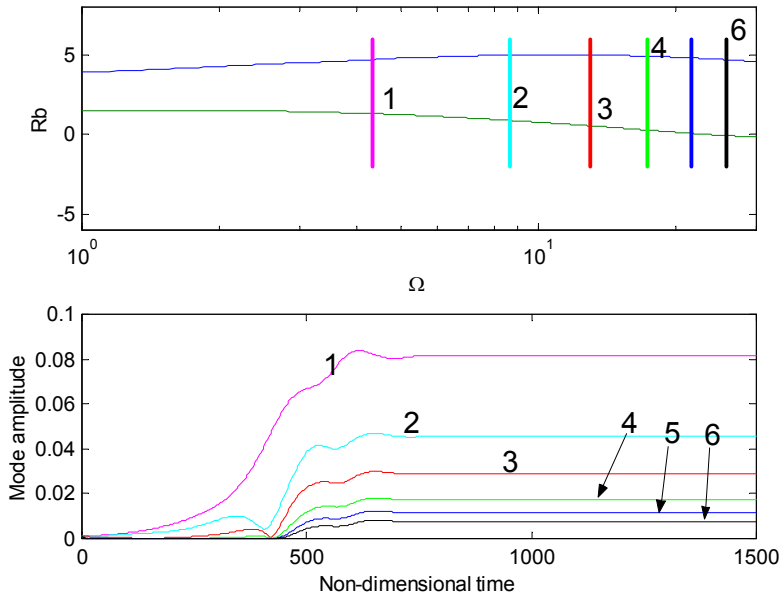

Figure 10. Results of a Simulation Including Dynamics of a Surface Layer

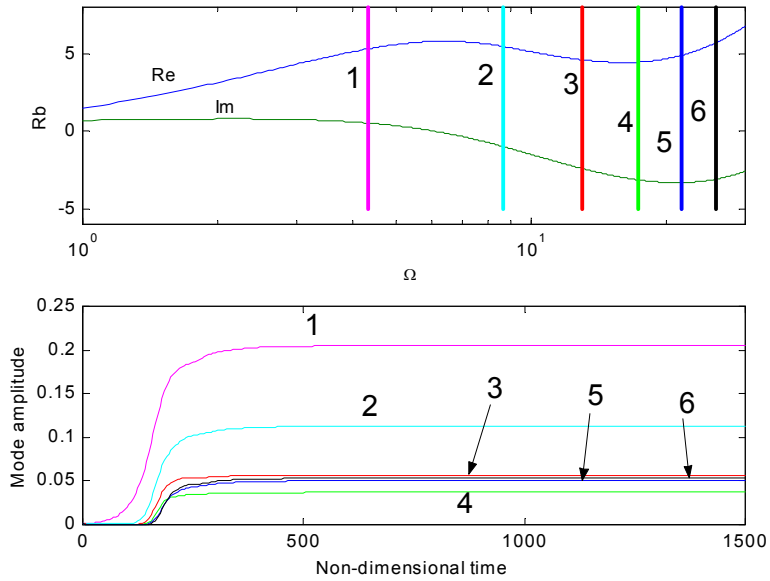

Figure 11. Results of a Simulation Including Dynamics of a Surface Layer and the Gas Phase

Owing to the significantly different dynamics added to the basic QSHOD model, the three examples illustrated in Figures 9–11 show quite different response functions—all, it must be emphasized—representing responses due to pressure coupling. The question here concerns the sensitivity of the response function to changes of composition (not the qualitative dynamics) and consequently the sensitivity of the global chamber dynamics.

For the examples chosen, the waveforms in the limit cycles are similar whether or not dynamics of the surface layer and gas phase are accounted for. This result is due mainly to the substantial attenuation of higher harmonics

due to particle damping (Culick and Yang, 1992). If the damping is reduced, the amplitudes and amounts of higher harmonics are substantially affected, as Figures 12 and 13 show.

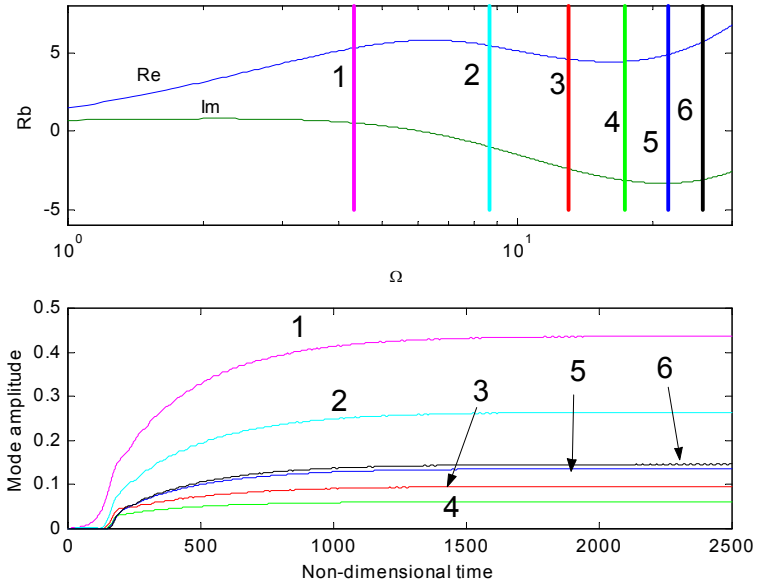

Figure 12. Simulations with Dynamics of the Surface Layer and Gas Phase Included, but with Reduced Particle Damping (10% Reduction Over the Entire Frequency Range)

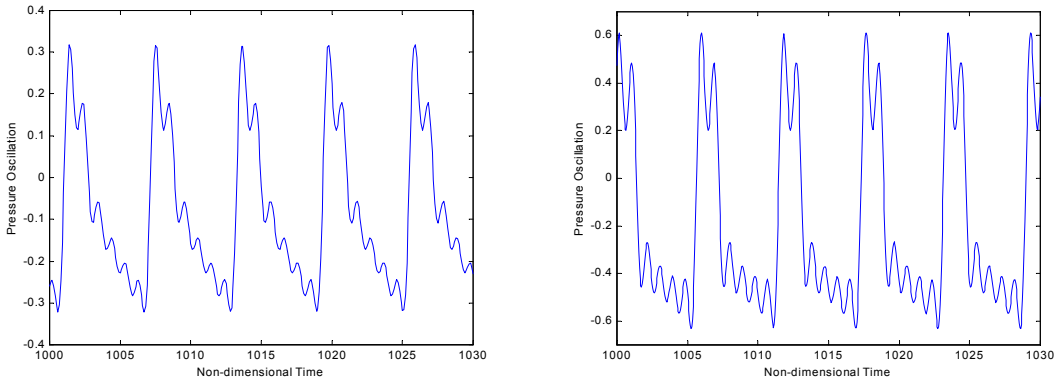

(a) **(b)**

Figure 13. Waveforms for the Limit Cycles (a) Figure 2.11; (b) Figure 2.12.

In general, models based on pressure coupling do not show dramatic sensitivity of the combustor dynamics to small changes of composition. Hence we investigated similar problems with a simple model of the response due to velocity coupling. The idea is based on the model introduced by Levine and Baum (1988).

Some recent work done on the dynamics resulting from functional form of the equations used in the analysis by Ananthkrishnan (2001) seems to prove that the absolute value function in itself, as it appears in a simple model of velocity coupling, is sufficient to produce a subcritical bifurcation (pitchfork) followed by a fold (saddle-node bifurcation).

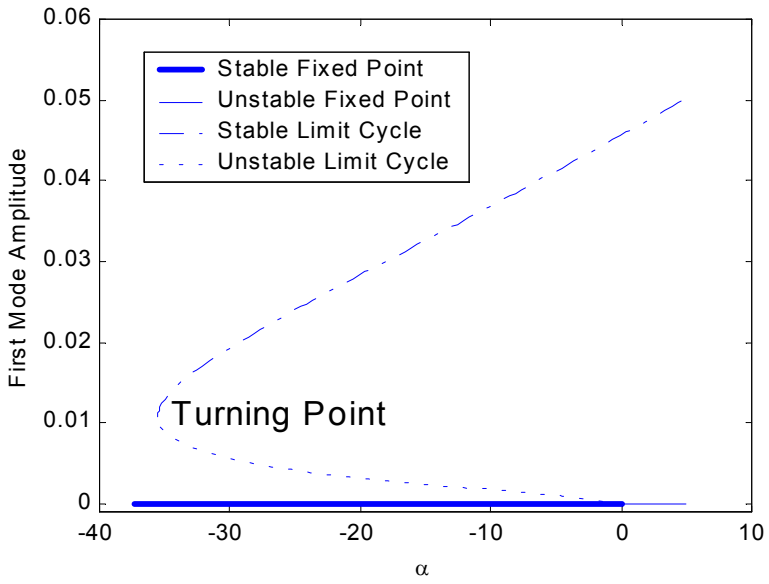

Figure 14. Bifurcation Diagram

In order to analyze the effect of velocity coupling on the overall dynamics, the following two relative sensitivities are defined:

$$S_{\tilde{R}_{vc}}^{A_{LC}} = \frac{1}{A_{LC}} \frac{\partial A_{LC}}{\partial \tilde{R}_{vc}} \tag{2.3}$$

$$S_{\tilde{R}_{vc}}^{\alpha_{BP}} = \frac{1}{\alpha_{BP}} \frac{\partial \alpha_{BP}}{\partial \tilde{R}_{vc}} \tag{2.4}$$

where A_{LC} is the amplitude of the limit cycle (defined at a fixed value of α), and α_{BP} is the value of the growth rate at which the unstable fold turns to a stable fold. Equation (2.3) defines the relative sensitivity of the amplitude of the limit cycle to variations in the velocity coupling coefficient; equation (2.4) refers to the sensitivity of the turning point to the same coefficient.

Figure 15 shows a plot of the sensitivities, calculated for the combustion chamber used in the examples of the previous section, and using a six mode approximation of the system. Note that the sensitivity of the turning point is very high, and also the sensitivity of the amplitude of the limit cycle is quite large in the range 0.15 to 0.25 of the coupling coefficient.

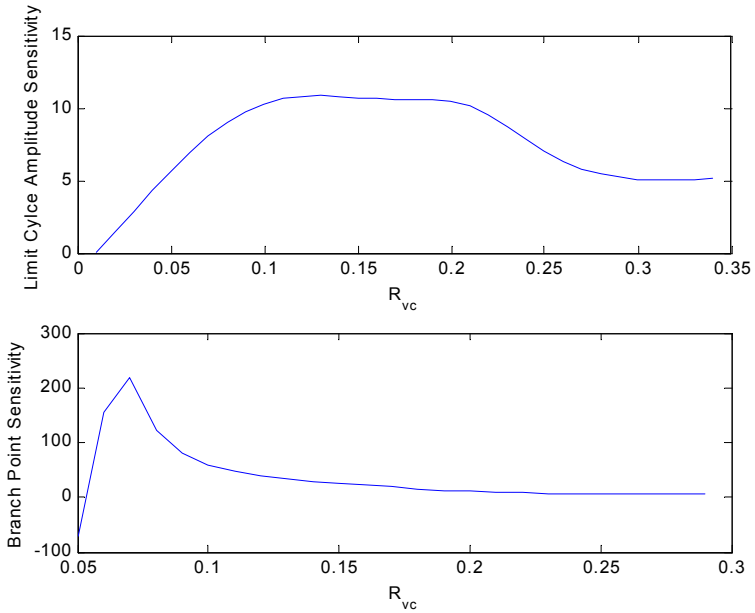

Figure 15. Sensitivity of Global Dynamics to Variations of the Coupling Coefficient

We now analyze the same combustor described in Section 2.4.5 with the introduction of the extra terms due to velocity coupling. For reference, Figure 16 presents the results of the simulation for the system with a combustion response based on the quasi-steady theory. The top section presents the combustion response function; the vertical lines mark the non-dimensional frequencies of the acoustic modes of the combustion chamber considered in the simulations. The bottom half shows the time evolution of the amplitude of each mode. The values of the parameters are: $A = 6.0$, $B = 0.55$, $n = 0.50$.

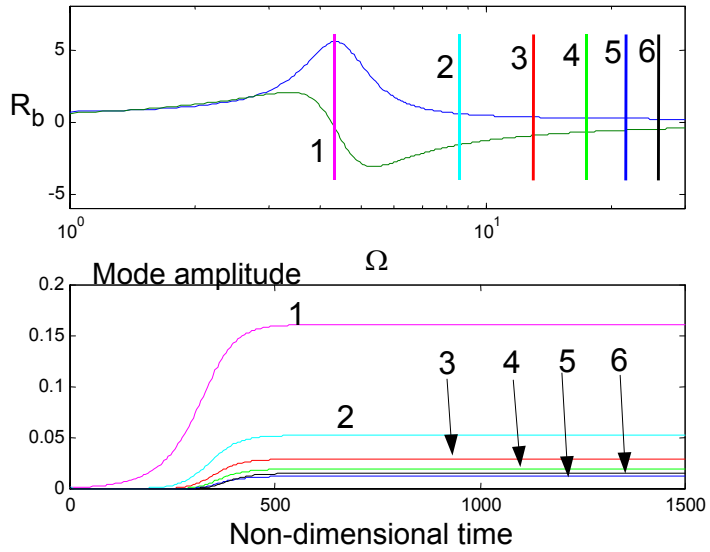

Figure 16. Simulation Results for QSHOD Combustion Response

The first mode is unstable and rapidly grows to a limit amplitude, while the other modes are all stable, and draw energy from the first mode (allowing the system to enter a limit cycle).

Figure 15 shows that there is a region of high sensitivity of the amplitude of the limit cycle for variations in the velocity-coupling coefficient. Figure 17 presents the global response for a small variation of the velocity coupling coefficient ($\widetilde{R}_{vc} = 0.15$ and $\widetilde{R}_{vc} = 0.165$).

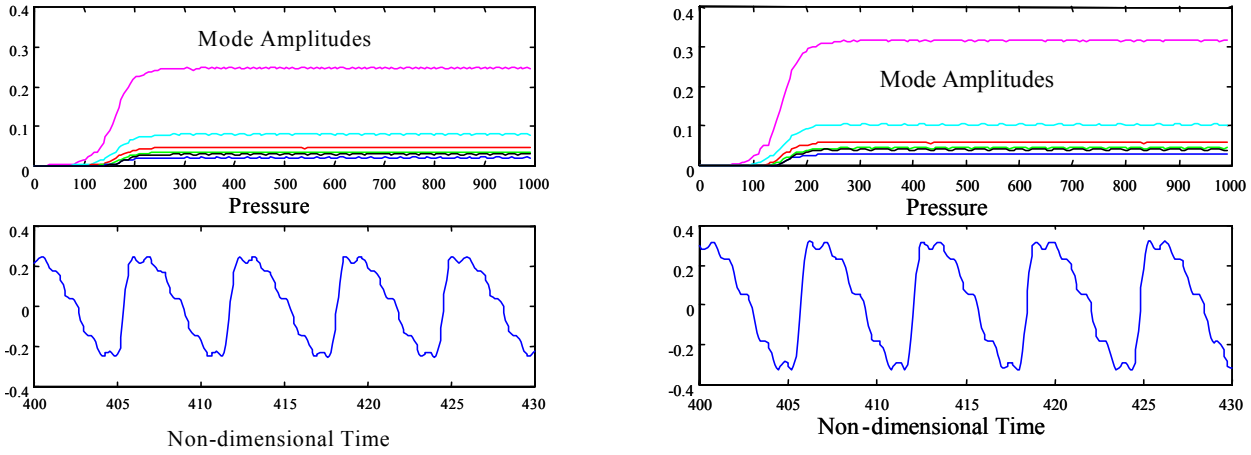

(a) **(b)**

Figure 17. Simulations with Velocity Coupling for: (a) $\widetilde{R}_{vc} = 0.15$, (b) $\widetilde{R}_{vc} = 0.165$.

The simulation uses the same coefficients for the pressure coupling as in the results of Figure 16, with the addition of the velocity coupling terms. Figure 18 and 19 show the pressure trace and the harmonic content for the same two cases.

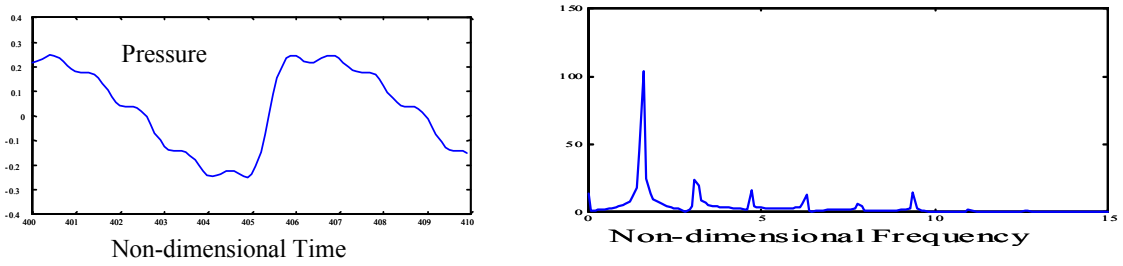

Figure 18. Pressure Trace and Harmonic Content for the Case $\widetilde{R}_{vc} = 0.15$

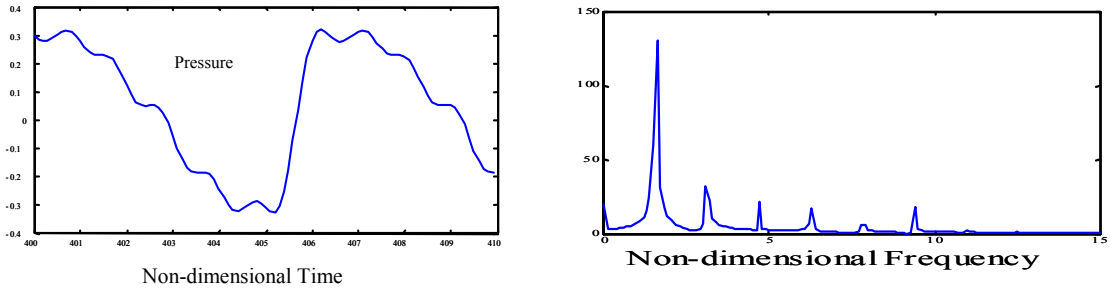

Figure 19. Pressure Trace and Harmonic Content for the Case $\widetilde{R}_{vc} = 0.165$

In summary, we have shown with these calculations that the global dynamics of a solid propellant motor seem to be affected more significantly by small changes in the combustion response to velocity coupling then in the combustion response to pressure coupling. We cannot claim at this time that this is a universal result but the possible implications are important. It appears in any case that to determine why small changes of propellant composition seem on a number of occasions to have relatively large effects in the chamber dynamics, one must investigate the phenomenon of velocity coupling. The most serious need is experimental. Attention must be paid to developing a method for measuring the combustion dynamics associated with velocity coupling.

References

1. Culick, F.E.C. (1968) "A Review of Calculations for Unsteady Burning of a Solid Propellant," *AIAA J.*, Vol. 6, No. 12 (pp. 2241–55).
2. Isella, G. and Culick, F.E.C. (2000) "Modeling Propellant Dynamics and Their Effects on the Global Dynamics of a Combustion Chamber, " (in preparation).
3. Isella, G. and Culick F.E.C. (2000) "Modeling the Combustion Response Function with Surface and Gas Phase Dynamics," *38th AIAA Aerospace Sciences Meeting*, AIAA-2000-0310.
4. Culick, F.E.C. Isella, G. and Seywert, C. (1998) "Influences of Combustion Dynamics on Linear and Nonlinear Unsteady Motions in Solid Propellant Rockets," AIAA-98-3704.
5. Beckstead, M.W., Mathes, H.B., Price, E.W. and Culick, F.E.C. (1969) "Combustion Instability of Solid Propellants," *12th Symposium (International) on Combustion*, (pp. 203–211).
6. T'ien, J.S. (1972) "Oscillatory Burning of Solid Propellants Including Gas Phase Time Lag," *Comb. Sci, and Tech.*, Vol. 5 (pp. 47–54).
7. Clavin, P. and Lazini, D. (1992) "Theoretical Analysis of Oscillatory Burning of Homogeneous Solid Propellant Including Non-Steady Gas Phase Effects," *Comb. Sci, and Tech.*, Vol. 83 (pp. 1–32).
8. Levine, J.N. and Baum, J.D. (1983) "A Numerical Study of Nonlinear Instability Phenomena in Solid Rockets," *AIAA J.*, Vol. 21, No. 4 (pp. 557–564).
9. Louwers, J. and Gadiot, G.M.H.J.L. (1999) "Model for Nonlinear Transient Burning of Hydrazine Nitroformate," *J. Propulsion and Power*, Vo. 15, No. 6, (pp. 778–782).
10. Burnley, V. (1996) "Nonlinear Combusiton Instabilities and Stochastic Sources," Ph.D. Thesis, Aeronautics, California Institute of Technology.
11. Culick, F.E.C. and Yang, V. (1992) "Prediction of the Stability of Unsteady Motions in Solid Propellant Rocket Motors," chapter in an AIAA Progress Series volume, *Nonsteady Burning and Combustion Stability of Solid Propellants*, 1992.

2.5 Extension of the QSHOD Model to AP Composite Propellants (Culick)

In a series of papers[1-6], Cohen and Shusser have investigated various elaborations of the QSHOD model, with the objective of representing the dynamical behavior of composite propellants. Because the QSHOD, or Z-N (Zel'dovich-Novozhilov) analysis applies strictly to homogeneous, one-dimensional propellants, it's extension to composite materials necessarily rests on suppositions and approximations that can be justified ultimately by the results. The approach has had considerable value in respect to qualitative interpretations, mechanistic understanding, and predictions of trends.

Although the MURI program was directed to investigation of high-energy propellants, we recognize the considerable continuing near-term interest in AP composite propellants and the need for better understanding of this dominant family of propellants as requisite for the more advanced materials. Moreover, the structure of modeling monopropellants such as AP is found to have much in common with the structure of advanced ingredient models: condensed phase decomposition, exothermic condensed phase reactions and distributed gas phase reactions in the flame zone. Generally, there are three problems to be addressed in constructing models of the dynamics of composite propellants:

i) non-steady behavior in the interfacial region and in the gas phase;
ii) accounting for the heterogeneities of composite propellants; and
iii) accommodating special properties and characteristics of high-energy propellants.

The works in question in this subsection considered each of these problems but placed more emphasis on the second. Unsteady behavior in the gas phase associated with penetration of turbulence into the combustion zone affects the threshold for the acoustic erosive burning, but was not fully incorporated into the formal analysis. Special characteristics of high-energy propellants involve components of the energy balance boundary condition and their dependence on the non-steady burning rate, but was not quantified beyond computations for AP. Essential assumptions built into the analyses were:

i) unsteady behavior is dominated by transient heat conduction in the condensed phases (AP and binder);
ii) interactions between oxidizer and binder occur only in the gas phase where the combustion processes are treated according to the model previously devised by Cohen and Strand[7-9] ; and
iii) statistical properties of the heterogeneous materials and their combustion are treated as averages—no rules are given to relate the average values to propellant composition.

Well after the work discussed here was begun, some significant progress has been reported by researchers at the University of Illinois at Urbana-Champagne[10] supported under the Department of Energy ASGI program. Their approach to analyzing the combustion of composite propellants is based on the idea of "random packing" of oxidizer particles in the binder. Apparently similar unreported work has been carried out at Thiokol, Inc. That method of accounting for heterogeneities seems not yet to have been applied to the problem of transient combustion. When it is, we expect that the method should give methods for computing the average values used in the works discussed here.

The idea that different transient behavior of the oxidizer (AP) and binder should be accounted for in modeling the response function is neither surprising nor novel, having apparently been first suggested by King[11,12]. One can imagine several possible consequences for dynamical behavior: fluctuations of compositional variables affecting the global response; dependence of the transient heat conduction, within the solid, on the distribution of particle sizes; influences arising from time-dependent interactions between the oxidizer and binder flames in the gas phase; and probably others. Needless to note, these are all very difficult to treat statistically and it seems wise at the present stage of development to continue using relatively simple models to determine if the more significant consequences of heterogeneities can be sorted out. Other possibilities exist—see works by Brewster and co-workers covered in the final report of the UIUC MURI, and §2.4.1 here, for example—but the model devised fifteen years ago by Cohen and Strand seemed a reasonable starting point.

That model began with the earlier treatments of the combustion of composite propellants by Beckstead, Derr and Price[13] and of AP and HMX by Price, Boggs and Derr[14]. Details of the extension by Cohen and Strand may be found in references 7-9 and are not central to the discussion here. What matters most in the work accomplished in the MURI program are the ideas involved in constructing the model with which computations are made of the response function. Broadly, the analysis may be divided into the following steps.

1) Heterogeneities

As in the previous models cited[7-12], the heterogeneous characteristics are accounted for by appropriate averaging of the flows of combustion products at the burning surface; of the heat feedback from the gas phase to the condensed phase; and of heat transfer within the solid. The three-dimensional geometry of the composite material consisting of oxidizer particles dispersed in the binder is effectively replaced by an average particle size, giving rise to an average surface area ratio (oxidizer/binder) at the burning surface. Correspondingly the heat transfer from the interface into the solid is also represented as an averaged process. The averaged areas of the oxidizer and binder carry with them models of the elementary flames constructed according to the previous works. Hence in the model of unsteady combustion the time-dependent behavior is treated quasi-statically according to the known model of steady combustion, including coupling between the oxidizer and binder flames, Figure 1.

(2) Unsteady Heat Transfer in the Condensed Phase

The well-known solution to the equation for unsteady heat transfer is used separately for the oxidizer and binder material. It is in this step that the different values of density, thermal conductivity and heat capacity of the solid oxidizer and binder enter the model. One can view the physical model as an effective columnar structure. The actual three-dimensional geometry of the solid phase is replaced by an array of rods of oxidizer material extending from the interface into the solid, accounting for unsteady heat transfer perpendicular to the interface. Heat transferred into the solid is weighted according to the volume fractions of material. Previous and contemporary works showed that lateral heat transfer between oxidizer particles and binder can be neglected on the spatial and time scales involved.

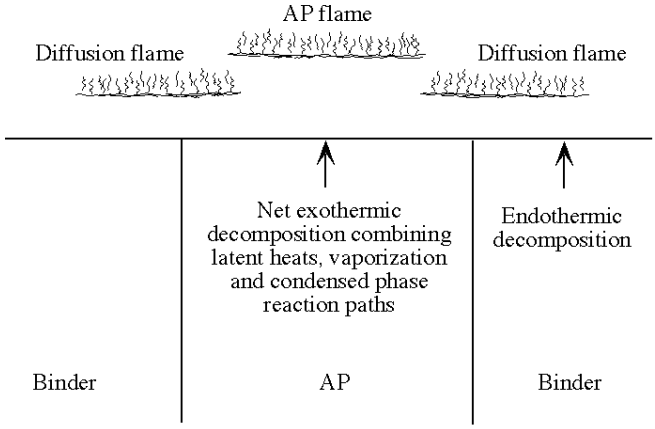

Flame positions and distribution of heat feedback depend on AP particle size and pressure

Figure 1.

(3) Matching Conditions at the Interface; The Response Function

The QSHOD model[15] and the Z-N model[16] of the combustion dynamics provide an interfacial condition, a formula relating the fluctuation of heat loss q'_{s-} into the condensed material to the heat flow q'_{s+} to the interface and the chemical activity, including energy absorption or release, at the interface. This matching condition has the form

$$q'_{+} = q'_{s-} + I_1 m' + I_2 p' \tag{1}$$

where I_1 and I_2 are function of the various thermochemical parameters and m' is the local fluctuation of mass flux, the fluctuation of the rate at which condensed material is converted to gases at the surface. Equation (1) is constructed initially for a smooth dry interface at which solid is converted to gas in an infinitesimally thin region. Several approaches exist to relaxing the several assumptions forming the basis of (1) at the expense of increasing complications. The form given here is adequate for the present discussion.

In applications to homogeneous propellants, (1) applies over the entire interface. The q'_{s-} is given by a familiar solution[15,16] having the dimensionless frequency $\Omega = \omega \kappa / \bar{r}^2$, where κ is the thermal diffusivity of the condensed material and $\bar{r}$ is the average burning rate. Other parameters appear in (1), notably the dimensionless surface activation energy *A*.

Some sort of model of the combustion process in the gas phase is required to give a representation of q'_{s+}, commonly called the 'heat feedback' from the gas phase. The simplest model is an infinitesimally thin flame standing some distance downstream of the interface. A major assumption in all the models discussed here is that the gas phase behavior 'quasi-statically.' Then q'_{s+} does not depend explicitly on frequency, but of course does contain parameters characterizing the particular model chosen. Fluctuations

for q_{s+} (*i.e.* q'_{s+}) are caused, in the QSHOD model for a homogeneous propellant, by p', m' and fluctuations of the temperature at both ends of the combustion zone.

After the formula for q'_{s+} and q'_{s-} are substituted in (1), possibly accompanied by further assumptions defined by the model used, the equation can be solved for m'/p', or better the dimensionless ratio called the response function for pressure coupling,

$$R_p = \frac{m'/\overline{m}}{p'/\overline{p}} \tag{2}$$

The remarkable property of R_p is that for the strict QSHOD model, R_p is a function of dimensionless frequency containing only two parameters; A, the dimensionless surface activation energy, and B, a dimensionless quantity whose form and value are set by the particular model used for combustion in the gas phase:

$$R_p = n\frac{AB}{\lambda + \frac{A}{\lambda} - (1+A) + AB} \tag{3}$$

where λ is a complex function of Ω.

Computed results for AP were in very good agreement with experimental response function data and showed the varying importance of both condensed phase exothermic reactions and gas phase flame reactions as functions of pressure. This work will be published in the *AIAA Journal.*

(4) Extension of the QSHOD Model to Composite Propellants

As in the pure QSHOD model, the key matter in extension of the preceding ideas to composite propellants is the interfacial matching condition (1). Consider a unit area of burning propellant, as sketched in Figure 1. There are two fundamental problems to be formulated and cast in such a form as to be used in (1):

i) averaging the contributions to q'_{s-} from the oxidizer and fuel in the condensed phase; and
ii) devising a model of heterogeneous combustion in the gas phase to serve as the basis for computing q'_{s+}, the heat feedback from the gas phase

Details of the approach taken in this work accomplished during the Caltech MURI program are given in references 1-6. We have already noted that q'_{s-}, the heat transfer from the interface into the solid, is given by a volume-averaged form constructed for the columnar model of oxidizer and binder, Figure 1.

The ideas developed in references 7-14 are used to construct a model for the combustion processes in the gas phase, eventually producing a formula for q'_{s+} representing a surface weighted average of heat feedback to the exposed surfaces of oxidizer and binder.

Then when (1) is used to construct the response function, the result depends on certain features of the combustion processes (*e.g.* flame stand-off distances) as well as the mass fractions of oxidizer and fuel. Thus, for example, there are two sets of parameters A, B for the two components of the propellant. Additional sets of values will appear if the oxidizer had a multi-modal distribution.

A unique feature of this work is that closed-form mathematical solutions were obtained for composite propellants, in addition to the numerical solutions. The mathematical solutions were able to show quite clearly how the inert binder component and the diffusion flame are stabilizing to the combustion, whereas numerical solutions required many parametric computations to uncover the important trends. There were good qualitative agreements with the limited experimental data available. The works will be published in the *Journal of Propulsion and Power*.

(5) Influences of the Downstream Flow; Velocity Coupling

Earlier work by King[12] and by Cohen and Strand [9] investigate possibilities for including erosive burning (*i.e.* the influence of flow parallel to the surface) in their models. When the ideas are extended to calculations of the response function, an additional term arises in the formulas for q'_{s+} , depending on the velocity fluctuations at the downstream edge of the combustion zone.

Consequently, the approach taken here offers an opportunity to construct formulas for the dynamical response for velocity coupling. We began this work in 1998 with the intention to incorporate concurrent work by Beddini[17,18] participating under a subcontract to the Caltech MURI program. We uncovered the important mechanism of turbulence penetration of the combustion zone as responsible for acoustic erosivity thresholds, and its frequency dependence as an explanation for the ability of the combustion response to drive the higher harmonics responsible for nonlinear behavior and triggering[1]. Moreover, Task III gasdynamics analysis showed the crucial importance of acoustic erosivity thresholds to nonlinear driving. Thus the collaboration offers considerable promise for important results, but the modeling is incomplete.

References

1. Cohen, N.S., Shusser, M., Culick, F.E.C. and Beddini, R.A., (1999) "Combustion Modeling of AP Composite Propellants for Stability Analysis," 36th JANNAF Combustion Meeting.
2. Shusser, M. Culick, F.E.C. and Cohen, N.S. (2000) "Combustion Response of Ammonium Perchlorate," 36th AIAA/ASME/SAE/ASEE Joint Propulsion Meeting, AIAA Paper No. 2000-3694, accepted for publication in *AIAA Journal*, 2001.
3. Shusser, M. and Culick, F.E.C., (2001) "Analytical Solution for Composite Solid Propellant Response Function," 37th AIAA Joint Propulsion Conference, Caltech Internal Document CI01-02, submitted to *AIAA Journal* 2001.
4. Shusser, M., Cohen, N.S. and F.E.C. Culick, (2000) "Combustion Response of AP Composite Propellants," 37th JANNAF Combustion Meeting, submitted to *AIAA J. Prop. and Power*.
5. Shusser, M., Culick, F.E.C. and Cohen, N.S., (2001) "Pressure Exponent of a Composite Solid Propellant," Caltech Internal Document CI01-03, submitted to *AIAA Journal*, 2001.
6. Shusser M., Cohen N.S., "Effect of Variable Thermal Properties of the Solid Phase on Composite Solid Propellant Combustion," Caltech Internal Document CI01-04, submitted to *Astronautica Acta*, 2001.
7. Cohen, N.S. and Strand, L.D. (1982) "An Improved Model for the Combustion of AP Composite Propellants," *AIAA Journal*, Vol. 20, No 12 (pp. 1739–1746).

8. Cohen, N.S. and Strand, L.D. (1985) "Combustion Response to Compositional Fluctuations," *AIAA Journal*, Vol. 23, No. 5 (pp. 760–767).
9. Cohen, N.S. and Strand, L.D. (1985) "Effect of AP Particle Size on Combustion Response to Crossflow," *AIAA Journal*, Vol. 23, No. 5 (pp. 776–780).
10. Kochevets, S. Buckmaster, J. and Jackson, T.L. (2000) "Random Propellant Packs and the Flames They Support," AIAA Paper No. 2000-3461.
11. King, M.K. (1980) "Composite Propellant Modeling," AIAA Paper No 80-1124.
12. King, M.K. (1979) "Erosive Burning of Composite Solid Propellants: Experimental and Modeling Studies," *J. Spacecraft and Rockets*, Vol. 16, No. 3 (pp. 154–162).
13. Beckstead, M.W., Derr, R.L. and Price, C.F. (1972) "A Model of Composite Solid Propellant Combustion Based on Multiple Flames," *AIAA Journal*, Vol. 8 (pp. 2200–2207).
14. Price, C.F., Boggs, T. and Derr, R.L. (1979) "The Steady-State Behavior of Ammonium Perchlorate and HMX," AIAA Paper No. 79-0164.
15. Culick, F.E.C. (1968) "A Review of Calculations for Unsteady Burning of a Solid Propellant," *AIAA Journal*, Vol. 6, No. 12 (pp. 2241–2255).
16. Novozhilov, B.V. (1992) "Theory of Nonsteady Burning and Combustion Stability of Solid Propellants by the Zel'dovich-Novozhilov Method," *Nonsteady Burning and Combustion Stability of Solid Propellants*, DeLuca, L., Price, E.W. and Summerfield, M. (Editors), AIAA Progress Series, Vol. 14-3 (pp. 601–641).
17. Beddini, R.A. (1998) "The Roles of Turbulence Interactions in Solid Propellant Combustion Instability," AIAA Paper No. 98-37-3.
18. Beddini, R.A. and Lee, Y. (1998) "The Treshold Condition of Propellant Velocity Response and its Relation to Local Turbulence Transition," 35th JANNAF Combustion Meeting.

2.5.1 Interactions Between Acoustically Induced Turbulence and Surface Combustion (Beddini)

A significant source of propellant response to solid rocket acoustics can result from the interaction between acoustically induced turbulence and combustion processes. The objective of the present investigation is to develop a model for prediction of the threshold condition of propellant response to a crossflow, as doing so may allow avoidance of unstable operating regimes. The threshold behavior involves transition from near-laminar to a turbulent flow as a prerequisite condition, and is thus a problem of hydrodynamic instability. A principal goal is to identify the key nondimensional parameters affecting these physical processes.

Linear stability theory is used to obtain the unstable flow regimes. To validate the approach, initial results were obtained for problems involving steady injection-induced flow, and oscillatory and modulated noninjected duct flows. These compare favorably with prior theoretical and experimental results for hydrodynamic stability behavior as a function of key parameters such as oscillatory flow Reynolds number and injection Reynolds number.

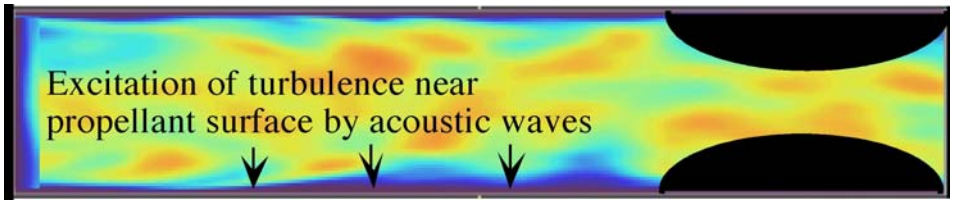

Figure 1. Schematic of flow disturbances caused by acoustic velocity components.

Figure 1 shows a schematic of the various processes involved. Longitudinal acoustic waves within the chamber core region create a flow near the surface with high vorticity gradients (the acoustic boundary layer). These disturbances, when reaching a certain threshold magnitude, can produce a secondary, near surface turbulence

distinct from that produced by the mean chamber flow. Turbulence directly produced by the acoustic waves near the surface can strongly enhance feedback with propellant gas-phase combustion mechanisms and create a propellant combustion - flow coupling process.

The results to be discussed here have been presented in various technical papers including Ref. 1–4, and the reader may wish to consult those articles for a more detailed discussion and bibliography. An approximation to the laminar acoustically induced velocity field is developed which is valid near the propellant surface. The predominant similitude parameters governing the acoustically-induced transition process are then obtained to be the injection Reynolds number based on angular frequency, $Re_{s\Omega} = V_s^{*2} / (\nu^* \Omega^*)$, Strouhal number $Sr = \Omega^* h^* / V_s^*$, and the relative maximum amplitude of the acoustic velocity, $A = \hat{u}^* / V_s^* = \Pi / (\gamma M_s)$, where Π is the acoustic pressure amplitude and M_S the injection Mach number. In these expressions, the dimensional reference parameters, indicated by an asterisk, are the surface injection velocity, V_S^*, the angular frequency Ω^*, kinematic viscosity ν^*, chamber half-height (radius) h^*, and acoustic velocity amplitude $\hat{u}^*$. Both the laminar acoustic velocity profile and the disturbance velocity field are found to depend on the mean chamber pressure p^*, the constant reference burning rate b^*, burning rate exponent, n, and the frequency by expressing the acoustic-injection Reynolds number as $Re_{s\Omega} \sim b^{*2} p^{*(2n-1)} / \Omega^*$.

Figure 2 shows a comparison between the near-surface analytical planar solution (solid curve), the numerical planar solution (circles), and the axisymmetric solution (dashed curve) of Majdalani & Van Moorhem[1] (1998) for $|\tilde{U}|$. The conditions correspond to $x/L = 0.5$, $\gamma = 1.2148$, $M_S = 0.00157$, $\Pi = 0.03$, and $Re_{s\Omega} = 169$. The abscissa, $\tilde{y}/h$, is the transverse distance measured from the surface normalized by the channel half-height. At these conditions, the near-surface approximate solution agrees well with the numerical solution within 15% of the half-channel, and is adequate for determining similitude parameter dependence for hydrodynamic stability. Additionally, the planar solution and the axisymmetric solution exhibit good agreement near the propellant surface, which supports the present assumption of planar flow used to investigate the near-surface phenomena in an axisymmetric geometry. The distance of the first maximum in the acoustic velocity (here defined as an effective acoustic boundary-layer thickness) is 2.66 *mm*, and analysis of the approximate solution shows that it varies as $(p^*)^{n-1}$, and thus decreases significantly with increasing chamber pressure.

Figure 3 presents the normalized amplitude of the streamwise velocities of the mean (long-dashed curve) and the oscillatory component (solid curve) of laminar flow together with that of disturbances (short-dashed curve) at the conditions approximating NAWC motor #2 pulse 2 (at a downstream distance $x/L = 0.5$). The estimated value of the acoustic-injection Reynolds number is $Re_{s\Omega} \approx 123$, and produces an acoustic boundary-layer thickness of approximately 0.8 mm. The significantly smaller magnitude of the mean flow compared with that of the oscillatory component provides an explanation of the negligible effect of the mean flow on hydrodynamic stability near the surface under conditions representative of those of combustion instability. The disturbance velocity amplitude was calculated and normalized at the approximately most unstable condition $kh = 125$ and $\tau = 0.04$. The eddies with this large velocity gradient near the surface could potentially interact with propellant combustion processes.

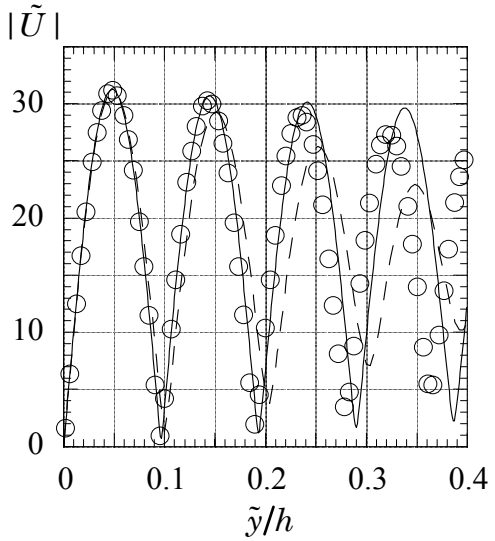

Figure 2. Amplitude of the *x*-component unsteady laminar velocity (*m* = 1, *x*/*L* = 0.5, γ = 1.2148, *Ms* = *0.00157*, Π = 0.03, and $Re_{s\Omega}$ = 169). Solid line; approximate near-surface planar solution. Circles; numerical planar solution. Dashed line; axisymmetric solution (Majdalani & Van Moorhem, 1998)

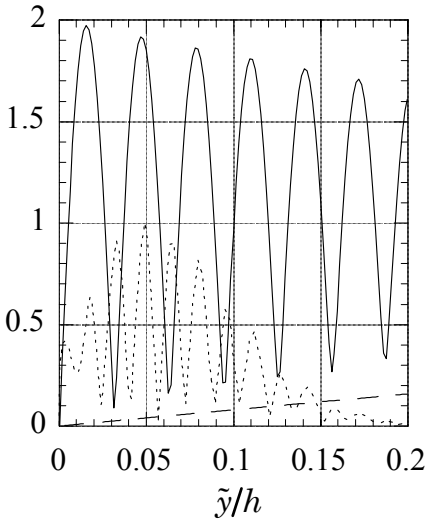

Figure 3. Amplitude of the mean flow, the oscillatory velocity, and disturbance velocity in planar geometry at the condition of NAWC motor #2 pulse 2 (*x*/*L* = 0.5). Solid line: oscillatory component. Long-dashed line: mean velocity. Short-dashed line: disturbance velocity

It is proposed that the sensitivity of the averaged neutral stability predictions to acoustic amplitude would provide a basis for the observed propellant response "threshold condition" discussed in the introduction. Calculations to obtain the neutral-stability amplitude have been performed at the velocity antinode of the first longitudinal mode (*x*/*L* = 0.5) of the chamber, where the maximum growth rates occur. Figure 4 presents the cycle-averaged growth rates (Im[$\overline{\omega}$]) at $Re_{s\Omega}$ = 123.01, *Sr* = 195.1, M_s = 5.22E-4, and γ = 1.2148. At 0.1% amplitude (Π = 0.001), the disturbance modes are slightly unstable only for the smaller wavenumbers associated with steady flow. The approximate theoretical amplitude for cycle-averaged neutral stability from the acoustic modulation is observed to be between 0.1% and 0.2% at the given conditions. The ability to interact with propellant combustion processes is likely to require a higher amplitude of acoustic oscillation, however. The results shown for an amplitude of 1% are viewed as potentially more indicative of a threshold value of acoustic response since peak values of growth rate greater than unity lead to burst behavior as well as lower height of the disturbances.

Figure 5 compares the average growth rates, $\overline{\omega}_I$, for varying chamber pressure. The average chamber pressures are increased in the direction of the arrow shown in the plot, and the values of the injection Reynolds number are presented for each curve. For the purpose of comparison of wavenumber independently of the pressure variation, the curves are presented in terms of the normalized wave number, $kh = k^* h^*$. As the chamber pressure increases, the disturbances exhibit higher growth rates, and the largest growth rate appears at higher relative wavenumber or smaller wavelengths. This exemplifies the trend that higher chamber pressures create instability in the flow for similar disturbance levels, and that these instabilities are closer to the propellant surface. Turbulent transition near the surface could enhance surface heat transfer and interact with propellant combustion processes.

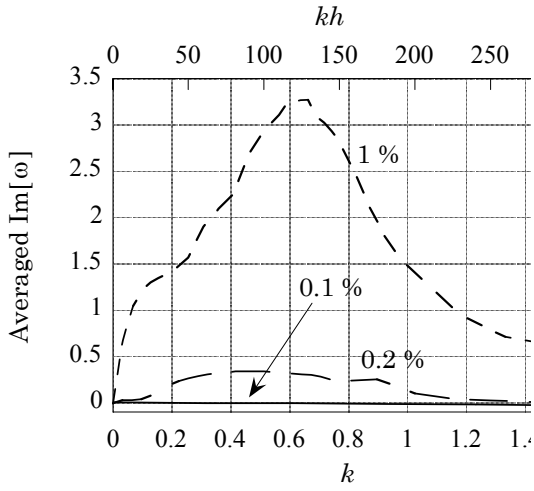

Figure 4. Growth rates of the disturbances for nearly steady and unsteady laminar flows.

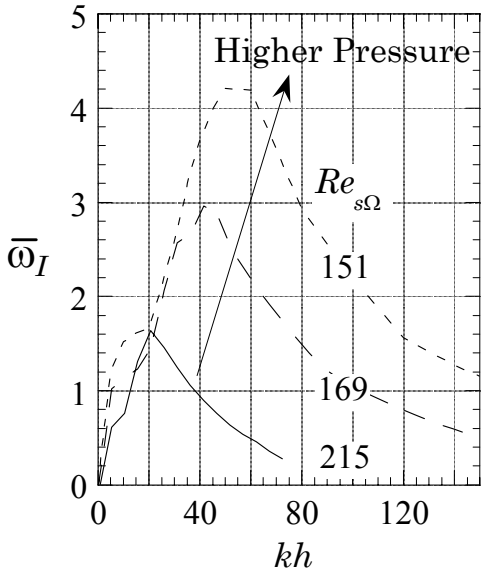

Figure 5. Growth rate of the disturbances for varying chamber pressure (x/L = 0.5, γ = 1.2148, Ms = *0.00157*, Π = 0.03)

Figure 6 compares the hydrodynamic stability maps showing the effect of chamber pressure. The dashed lines are cycle-averaged growth rates, Im[$\overline{\omega}$] and the solid lines are average frequency of disturbance, Re[$\overline{\omega}$] As described earlier, the disturbances have higher growth rates for higher chamber pressure, and the largest growth rate appears at higher wave number as the chamber pressure increases. It is expected from the magnitude of the growth rates that the flow is highly turbulent not only at the streamwise midpoint of the chamber, but also over a substantial fraction of the chamber length. The solid curves show that acoustic longitudinal mode frequencies can interact directly with high growth rate disturbances—leading to potential resonance behavior.

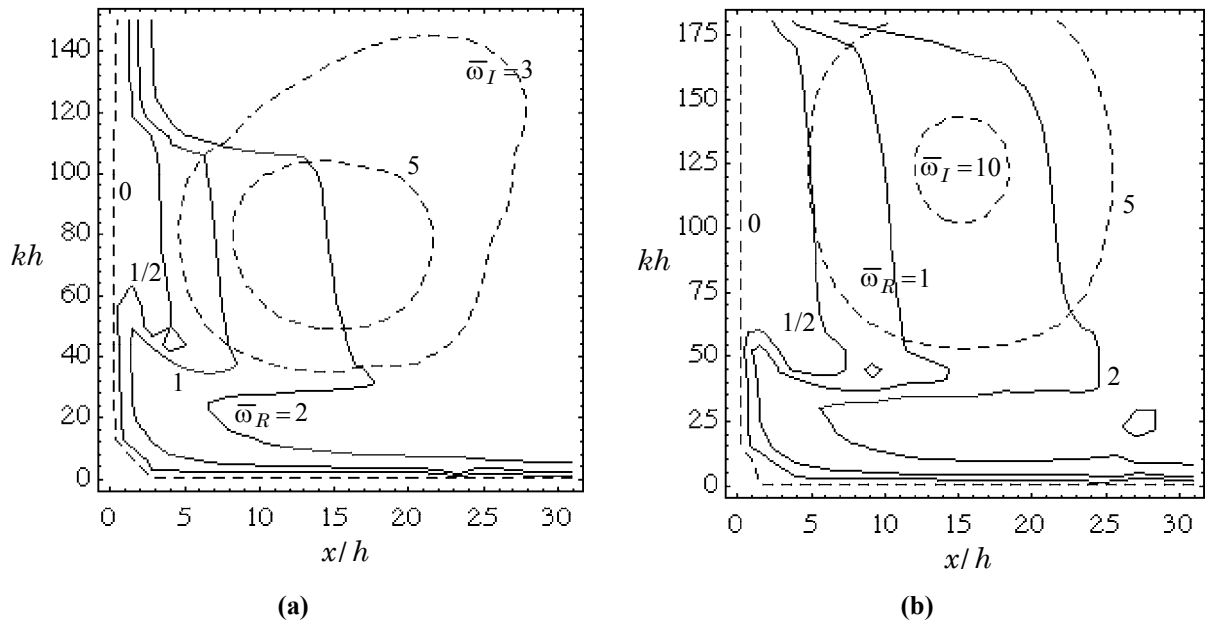

Figure 6. Stability maps for different chamber pressure (Π=0.03): (a) p^*=700 psi (47.632 atm), γ = 1.2180, M_S = *0.00081*, and $Re_{S\Omega}$ = 146. (b) 1450 psi (170.11 atm), γ = 1.2148, M_S = 0.00052, and $Re_{S\Omega}$ = 123.

The disturbance flowfield predicted by the present approach is actually a vortex array lying close to the surface and perpendicular to the acoustic and mean longitudinal motions, as shown in Figure 7. Both the height and axial wavelength of the vortices is an inverse function of wave number, *k*. There is generally a superposed broadband distribution of these disturbance eigensolutions. However, phenomena such as the predicted resonance and/or very high growth rate eigenvalues can produce a natural selection and emphasis of the disturbance flow for selected wave numbers or wavelengths of disturbance. The vortices might make themselves evident as a rippling pattern on the propellant surface, as heat transfer beneath the vortices could be enhanced if they were sufficiently close to the surface. E.W. Price had observed[2] a rippling pattern on the surface of extinguished grains of a homogeneous propellant—indications of significant combustion—flow interaction with a kind of flow generated by the present predictions.

Figure 6 shows a representative disturbance flowfield with color-scale indicating vorticity magnitude, together with velocity vectors superimposed, at a given instant of time. The vortices for this case meander back and forth slightly during the cycle, but remain stationary with respect to axial position when averaged over a cycle. They are also ejected away from the surface with time. The calculated dimensional wavelength for this case is approximately 2 mm. Figure 8 shows a photograph of the surface of the propellant extinguished during a longitudinal mode instability. (Tangential modes produce a similar pattern of shorter wavelength aligned perpendicularly to the tangential velocity). Though no specific quantitative comparison with the conditions of the experiment is conducted here, we note that the observed wavelength is approximately 1 mm, and is thus of the same order as the theory. The vortex field appears capable of transporting hot combustion gases down to the surface of the propellant much more effectively than a mere "sloshing" motion of the flow.

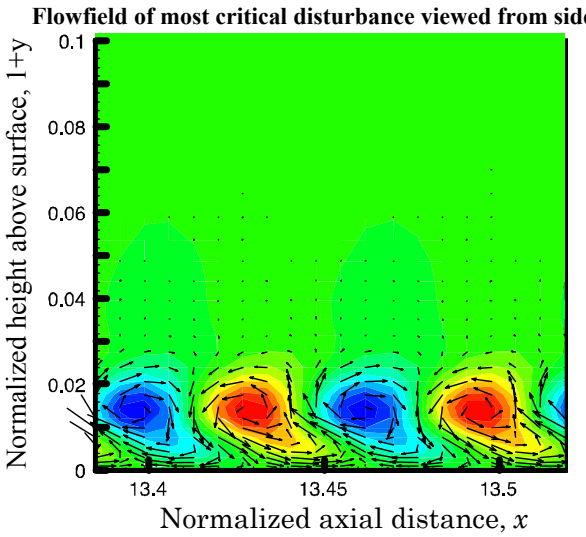

Figure 7. A representative disturbance flowfield predicted by the present theory (most highly amplified mode viewed from "side").

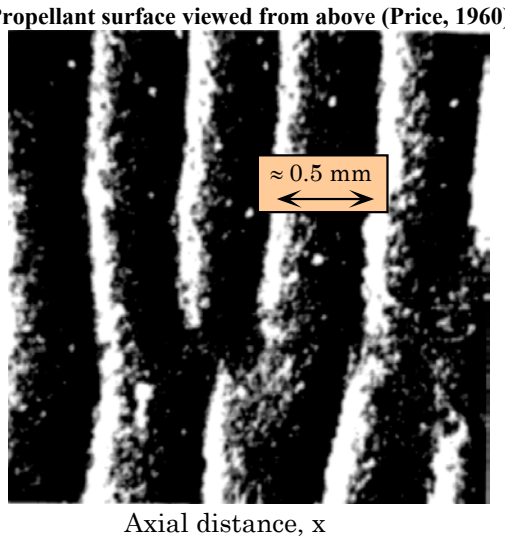

Figure 8. Photograph of extinguished propellant surface viewed from above (Price, 1960).

References

1. Majdalani, J. and Van Moorhem, W.K. (1998) "Improved Time-Dependent Flowfield Solution for Solid Rocket Motors", AIAA Journal, Vol. 36, No. 2, pp. 241-248.
2. Price, E.W. (1960) "Review of Experimental Research on Combustion Instability of Solid Propellants", In: Solid Propellant Rocket Research, Edited by Martin Summerfield, Progress in Astronautics and Rocketry, Vol. 1, Academic Press, New York, pp. 561-602.

2.6 Behavior of Metals in Solid Propellant Combustion Instability (Price , Sigman, Seitzman)

2.6.1 Ignition and Sintering

Initial investigations focused on the subignition heating behavior of the ingredient aluminum. The goal was to examine any significant differences in aluminum properties between different forms of aluminum that might lead to changes in combustion response and residual oxide particles that would then influence combustion instability. The different types of aluminum included: production powders, ultrafine (i.e., nanoaluminum – ALEX™), flake, and coated flake aluminum. Four methods were used: two based on visual observation of ignition behavior, and two that investigated the burning and sintering behavior of aluminum.

The first visual method employed a hot stage microscope, in which aluminum is heated from room temperature to 1000°C in a controlled-atmosphere and observed through an optical microscope. The second visual method employed a rapid heating apparatus, in which the aluminum was dropped onto a preheated plate and again observed through a microscope. The most notable findings of these test were: **1)** the ultrafine/nano aluminum (ALEX™) exhibits self-luminosity when dropped on a heated plate at temperatures at or above 664°C in air, and no such self-luminosity is observed when dropped at temperatures below 660°C or when production powders are substituted; and **2)** the luminosity with ultrafine aluminum generally begins at a point and spreads across the sample in either a slow irregular mode or a rapid high intensity mode of propagation, which also produces a significant amount of oxide smoke.

For combustion damping, an important mechanism leading to large residual oxide particles is agglomeration of aluminum on the propellant surface. An important step in the formation of an agglomerate is sintering. To study sintering effects, dry-pressed ammonium perchlorate (AP) and aluminum mixtures were burned in a window bomb. This also allowed investigation of the effects of different powders on burning rates. In addition, a novel device was constructed to measure the sintering temperature of aluminum powders. The device involves an electrical conductivity measurement of a sample of aluminum powder placed in a temperature-controlled oven. An added goal of this approach was development of a production tool to qualify ingredient powders. The most notable findings of these tests were as follows. **First**, dry pressed mixtures of AP/production aluminum powders burn at approximately the same rate as pure AP (it is somewhat difficult to discern the AP surface since the aluminum tends to sinter and retain the original shape of the sample. Samples using ultrafine aluminum burned at a rate several times the AP rate. The exact enhancement was beyond the capability of our video camera (30 fps) to capture. The results suggest a significant heat release close to or at the burning surface. **Second**, the aluminum sintering test measured distinct differences in the sintering temperatures between production and aluminum powders that were pretreated (primarily oxide coating changes). These seem to correlate with the significantly different agglomeration behavior seen in the combustion of propellant containing the pretreated aluminum. However, the test requires a significant amount of skill to operate with reproducible results. At this point, it was deemed not suitable for production line evaluation.

2.6.2 Residual Oxide Size Analysis

In the latter half of this effort, work shifted to studying the size of residual aluminum oxide particles produced during propellant burning. Again, the larger (nonsmoke) oxide particles can be an important source of damping for pressure oscillations A new facility[1] (Figure 1) was constructed for collection of the condensed phase residue, largely composed of residual aluminum oxide from solid propellant combustion. The propellant samples are burned in a high-pressure containment vessel with the plume confined within a steel tube so that the aluminum burns in an atmosphere of propellant products. The residue is collected in an ethanol bath and the oxide smoke is separated by repeated sedimentation. The larger residual oxide (>2-5 μm, denoted nonsmoke combustion residue - **NSCR**) is size graded using an air driven mechanical sieving system to sub-grade the residue. Then a large number of particles from these sub-grades (typically $>10^4$) were sized using an automated system based on an optical microscope, and a combination of commercial and in-house software.

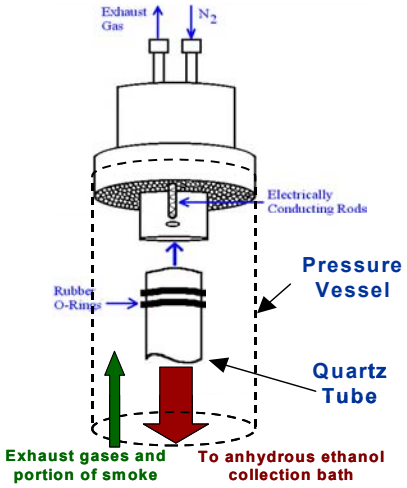

Figure 1. Oxide residual collection facility.

This system was used to collect and analyze the size distribution of condensed phase residue from an end burning charge of aluminized propellants supplied under the MURI program. Aluminized propellants provided by Thiokol, Pratt and Whitney CSD, and Alliant* were burned at 500, 1000, 1500 and 2000 psi. In all these propellants, the fine oxidizer is very fine and is beyond the limits of the pocket models.[2,3] From a mechanistic viewpoint, the matrix (fine AP and binder) probably burns with a cool fuel-rich, pre-mixed flame. In most cases the matrix would not burn on its own. In modelers terms,[3] it fails to meet the "encapsulation criterion" and the "thermal criterion". Thus, preconceived rules (agglomerate size is decreased by increasing the pressure and/or replacing some coarse AP by fine AP) may not hold true. In the figures below, the ratio of NSCR to total mass of residual oxide expected (assuming complete combustion of the aluminum and conversion to Al_2O_3) is shown on each graph.

*For compactness, the propellants are identified as follows: TCM*x* is Thiokol Corp. MURI mix-number *x*; TCM(2)52-2a is Thiokol propellant from Phase 2; UTP-*x* is P&W-CSD-United Technol. propellant-number *x*; and ALM*x* is Alliant Corp.-Special MURI mix-number *x*.

In addition, many of these propellants included other condensed phase particles that presumably do not react or otherwise change into a gaseous state, and thus contribute to the solid phase residue. While the ingredient additives are normally micron or submicron in size, microscopic examination of quenched propellants revealed surface accumulations of these additives (in addition to the aluminum). The additives were usually visually distinct from the aluminum oxide in the residue, but were not segregated during the sizing process. For comparison, the size distribution of condensed phase residue from an unaluminized sample of Thiokol propellant (TCM5) with condensed phase additives was also studied (Figure 2). For this propellant, NSCR increases with pressure, and the NSCR in the larger sizes (d>45μm) appears similar to the irregular accumulates of TiO_2 observed by scanning electron microscopy on the surface of samples of TCM5 quenched by rapid depressurization. They are light gray in color and very irregular in shape (nearer to planar than spherical). NSCR in the size range 5-45μm are mostly dark gray and perfectly spherical, leading to the conclusion that this TiO_2 has passed the melting point of 1850°C (100° less than the melting point of Al_2O_3) and melted into a spherical droplet. These spherical particles peaked in the 35-45μm range. These particles were also visible in residue from the aluminized Thiokol propellants.

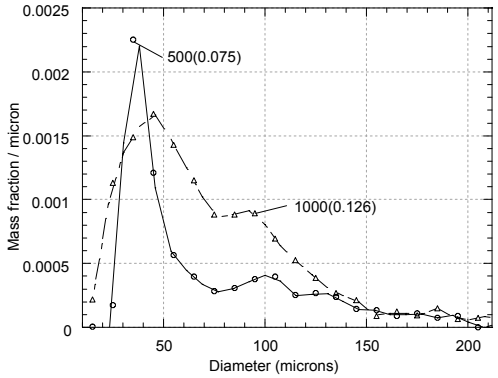

Figure 2. Size distribution of NSCR for TCM5, nonaluminized propellant with TiO_2 at 500 and 1000 psi.

The first round of aluminized propellants from Thiokol, containing nominally 95 μm Al, produced a large amount of NSCR, ~10-20% of the expected residue (Figure 3). The larger NSCR particles, which exhibited a peak in the mass weighted size distribution at about 100μm, contained a significant amount of unburned aluminum. This conclusion was based on: a) microscopic examination of the residue (much of it is gray as opposed to white, clear, or black for oxide); b) the ethanol at the base of the collection vessel (highly acidic due to the percolation of the exhaust plume) bubbles after the test; and c) separated residue also bubbles when placed in hydrochloric acid. The unburned Al occurred despite the long lengths and relatively low heat losses employed in the pressure combustor. The H-95 used in the Thiokol plateau propellants was still burning 23 inches from the burning surface. Average condensed phase particle size at this point is around 7.3μm. The amount of NSCR increased with pressure. There was little variation with respect to curing agent. There was very little difference in the amount of low-end (15μm) residue between samples, the greatest variation occurred with pressure. The slight increase in the amount of fine AP

(and decrease in coarse) contained in TCM1a versus TCM1 decreased the amount of NSCR at all pressures. In this case, replacing the coarse AP with fine (even very fine) AP appears to reduce the amount of surface agglomeration.

A phase 2 propellant from Thiokol propellants using an energetic binder (BAMO-AMMO/GAP) provided low agglomeration, with agglomeration decreasing with pressure. There was less overall NSCR (5-10% of the expected residue), with an increase in the mass of the smaller particles at 1000 psi compared to 500 psi (the actual peak appears to be in the 2-10μm range, which is at the edge of the system's collection efficiency range). These small sizes would be efficient in damping ~500 Hz instabilities.[4]

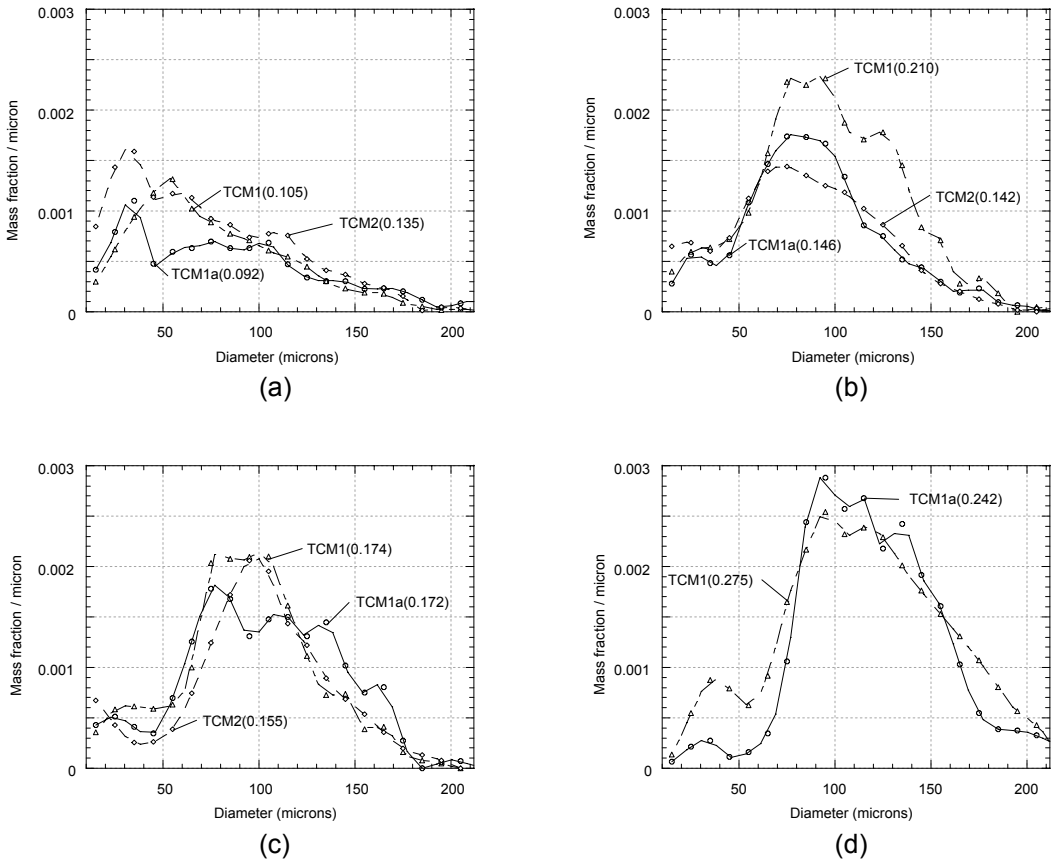

Figure 3. Variation of NSCR size distribution for Phase 1 TCM propellants as a function of formulation: (a) 500 psi (3.45MPa); (b) 1000 psi (6.9 MPa); (c) 1500 psi (10.35MPa); (d) 2000 psi (13.8 MPa).

The size distributions of the NSCR for the P&W-CSD propellants are seen in Figure 4. These propellants produced a reasonable amount of NSCR (5-9% of the expected residue). Although the finer aluminum used in the P&W-CSD propellants (compared to the TCM) agglomerates on the surface, the average particle size was found to be only 4.3μm. This is in good agreement with the value of 4.6μm obtained by Pratt & Whitney from residue collected outside of a small-scale rocket motor. The monomodal AP propellant with fine Al (31665) gave low NSCR (5-7%) with large amount of smaller particles. Replacement of some coarse AP with very fine HMX (31666) reduced the amount of NSCR (4-5%) and the low-end value. Replacement of coarse AP with fine AP (31667) produced more NSCR than the monomodal mix (6-7%) with good low-end values. Increasing the amount of very

fine AP even more (31668) increases the amount of NSCR while the low-end value remains about the same and the peak value at 25μm decreases. At 500 psi the peak appears to be in the 2-10μm range and in the 30-40μm range at 1000 psi for all propellants.

The aluminum used in the P&W-CSD propellants is much finer than that used in the TCM propellants, and is thus expected to reside within the pockets formed by the coarse AP and agglomerate during propellant burning. However (as with the TCM1,1a, and 2), the fine AP is too fine to satisfy either the "encapsulation" or "temperature criterion". The key here appears to be the requirement of a very hot leading edge diffusion flame for the ignition of accumulating aluminum[5]. A matrix of binder and very fine AP burns with a cool premixed flame which does not ignite the aluminum. Thus replacing a part of the coarse AP with fine AP does not necessarily reduce the size of the agglomerates.

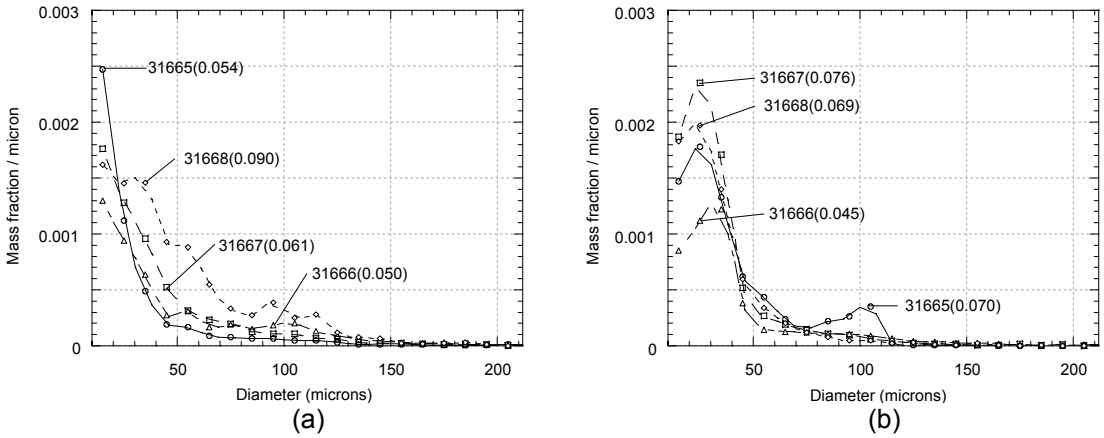

Figure 4. Size distributions of NSCR at (a) 500 psi (3.45MPa) and (b) 1000 psi (6.9 MPa) for 4 P&W-CSD propellants: 31665 (monomodal coarse AP); 31666 (fine HMX replacing some coarse AP); 31667 (fine AP replacing some coarse AP) and 31668 (more fine AP).

MURI propellants from Alliant Corporation used HTPE as a binder. The mix with bimodal AP (ALM1: coarse AP, very fine AP and AN) and regular aluminum produced a fairly uniform distribution of NSCR (3-8%) with fairly low low-end values. Introduction of medium sized AP and additional very fine AP/AN (ALM2) produced a large peak at 30μm with little change in overall NSCR or low-end values. Elimination of the AN and replacement with coarse AP (ALM3) decreased the amount of NSCR, lowered the peak at 30μm with slightly lower low-end values. Replacement of the intermediate AP with Bi_2O_3 (ALM4) increased the overall NSCR (8-10%) due to the Bi_2 now in the residue (it was assumed that the Bi_2O_3 is reduced to Bi_2 in computing the expected residue). The peaks at 23-30μm are higher as are low-end values.

For comparison, UTP31667 and ALM1, which differ in the binder (type and amount) and in the very fine oxidizer (AP versus primarily AN) produce very different NSCR distributions. ALM1 produces less NSCR with a wide size distribution at 500 psi while UTP 31667 is increasing at 15μm and presumably peaks just under 10μm. ALM1 presumably peaks between 2 and 10μm.

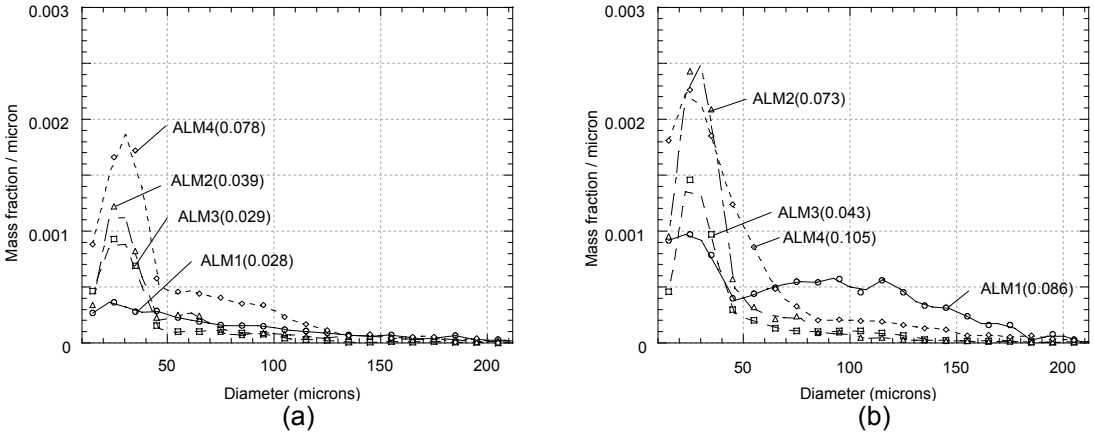

Figure 5. Size distributions of NSCR at (a) 500 psi (3.45MPa) and (b) 1000 psi (6.9 MPa) for 4 Alliant propellants.

References

1. Sigman, R. K., Lillard, R. P., Price, E. W., Seitzman, J. M., and Dokhan, A., "Size Distribution of Residual Oxide from MURI Propellants," presented at the 36th JANNAF Combustion Subcommittee Meeting, Cocoa Beach, FL, October, 1999.
2. Crump, J. E., "Aluminum Combustion in Composite Propellants," 2nd ICRPG Combustion Conference, (CPIA Publication 105, Vol. 1, May 1966) pp. 321-329.
3. Cohen, N. S., "A Pocket Model for Aluminum Agglomeration in Composite Propellants," AIAA-81-1585, AIAA-SAE-ASME 17th Joint Propulsion Conference, Colorado Springs, CO, July 27-29, 1981.
4. Culick, F. E. C., "Combustion Instabilities: Mating Dance of Chemical, Combustion, and Combustor Dynamics," AIAA Paper 2000-3178, 36th AIAA/ASME/SAE/ASEE Joint Propulsion Conference and Exhibit, Huntsville, AL, July 16-19, 2000.
5. Sambamurthi, J. K., Price, E. W., and Sigman, R. K., "Aluminum Agglomeration in Solid-Propellant Combustion," AIAA Journal, Vol. 22, No. 8, 1984, pp. 1132-1138.

2.6.3 Extinguished Surface Studies (Price, Sigman, Frederick, Moser and Cohen)

Series of plateau and bi-plateau propellant formulations were extinguished from combusiton at low, intermediate, high and very high pressures traversing the plateau and non-plateau pressure regimes. This work was carried out by Price and Sigman at Georgia Tech, and by Frederick and Moser at UAH with the help of consultant Cohen. The technique to obtain the surfaces was rapid decompression of the combustor containing the sample by rupture of a burst disc. High-speed microcinematography of the burning and extinguishment verified that the burning surfaces examined under the microscopes were representative of combustion conditions. Both optical and scanning electron microscopes were used. The EDAX capability of the SEM was utilized to distinguish coarse AP from coarse alunimum and very fine TiO_2 particles from the very fine AP in the formulation; the distinctions are by the elemental returns.

The observations were valuable to discern the mechanism by which the plateaus come about and are effected by the presence of the TiO_2 additive. The large differences between IPDI and DDI cure of the propellant were also studied. Examples of key micrographs are shown in Figures 1–4. Figure 1 is an example of a low-pressure surface, on the low pressure plateau. Figure 2 is an example of an intermediate pressure surface, at the end of the high

exponent region that precedes the high-pressure plateau. Figure 3 is on the high-pressure plateau. Figure 4 is at very high pressure, beyond the end of the high-pressure plateau.

Figyre 1 shows a flat surface, flat because the fine AP component of the propellant does not burn faster than the coarse AP component. The coarse AP is visible as flat discs, and the binder containing the fine AP is level with it. Clusters of the additive are in the middle of the coarse AP particles. Very high magnifications show the very fine AP to be somthered by the binder surface melt layer, indicating binder melt layer interference to be responsible for the flat surface and the low pressure plateau.

Figure 2 shows a highly irregular surface, because the very fine AP component is able to burn much faster than the coarse AP. The irregularities are the coarse AP sitting atop the binder containing the very fine AP which has been able to burn far ahead of it. The binder melt is not interfering with the very fine AP. This provides a high exponent region between the two plateaus, the high exponent because the propellant is trying to catch up to "normal" burning form the "abnormal" interfered-with burning.

Figure 3, on the high pressure plateau, shows a flattened surface once again as binder melt layer interference is able to set in once again. Figure 4, beyond the high-pressure plateau, show that the fine AP component is once again able to burn ahead of the coarse AP such that the binder plane is below the coarse AP surfaces. Very high magnifications show where the binder melt layer does and does not cover up the very fine AP.

Binder melt layer interference involves a tradoff between melt layer thickness and viscosity, which change with pressure and with the presence of TiO_2. The difference between IPDI and DDI cure was explained by the superior melt layer interference properties with DDI. The DDI cure provides a lower liquefaction temperature and a more fluid/mobile melt layer.

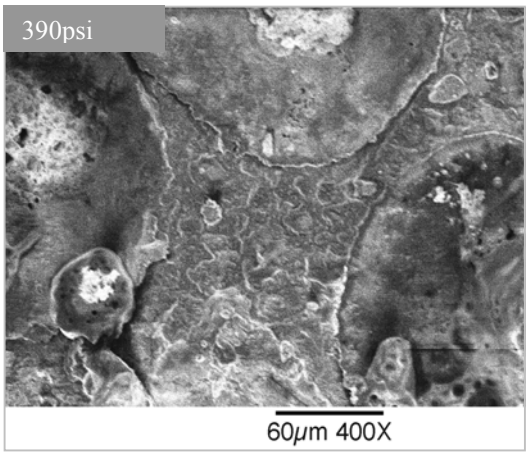

Figure 1.

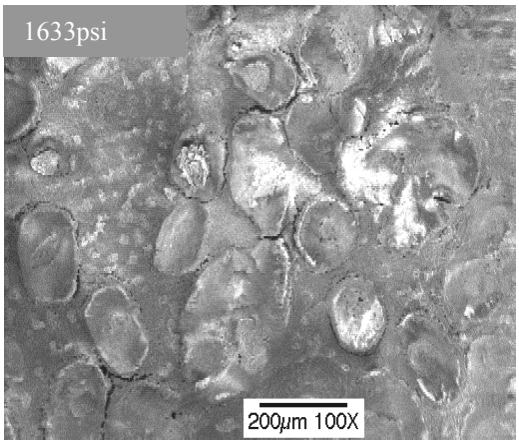

Figure 2.

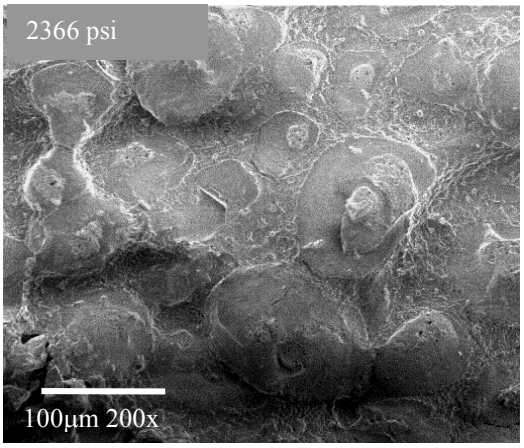

Figure 3.

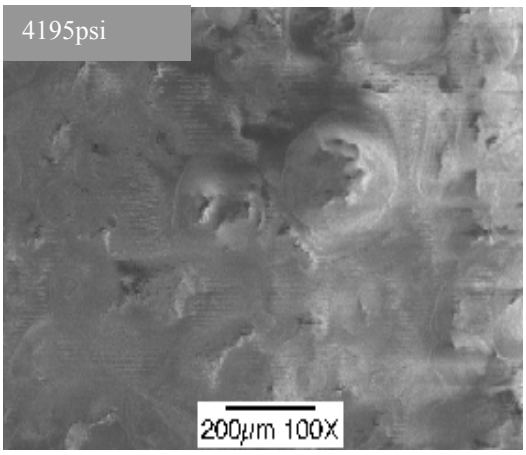

Figure 4.

2.7 Numerical Simulation of Aluminum Particle Combustion (Beckstead)

A two-dimensional unsteady state numerical model for aluminum particle combustion has been developed at BYU.[1,2,3,4,5,6] The current model solves the conservation equations, while accounting for the species generation and destruction with a 15 reaction kinetic mechanism. Most previous models have assumed infinite kinetics.[7,8] The kinetic mechanism in the model consists of surface reactions and gas phase reactions for the formation of the aluminum sub-oxides. The aluminum sub-oxides later react and condense to form liquid aluminum oxide.

Two of the major phenomena that differentiate aluminum combustion from hydrocarbon droplet combustion, namely the condensation of the aluminum oxide product and the subsequent deposition of part of the condensed oxide, are accounted for in detail with a sub-model for each phenomenon. The path to condensation consists of two steps; a homogeneous gas phase reaction, followed by homogeneous condensation. A seven-step combustion mechanism accounts for the kinetic process describing the formation of gaseous aluminum oxide from reactions of sub-oxides with oxygenated species. The second step is describes the homogeneous condensation of the gaseous aluminum oxide to liquid oxide based on classical nucleation theory. Most previous models have assumed that condensation only takes place in an infinitely thin zone, *i.e.* the flame zone. This model has relaxed that assumption and the condensation depends on factors such as species concentration, super-saturation of the sub-oxide vapors, temperatures, and hence, on the location within the environment around the burning particle. There has been little investigation done into the probable condensation paths for the aluminum oxide formation when the oxidizers are CO_2 or H_2O. Hence, the condensation paths in the presence of CO_2 and H_2O oxidizers are taken to be the same as the pure O_2 oxidizer case[6]. The effect of the oxide cap in the distortion of the profiles around the particle has also been included in the model. The oxide cap inhibits aluminum vaporization from the portion of the sphere it covers.

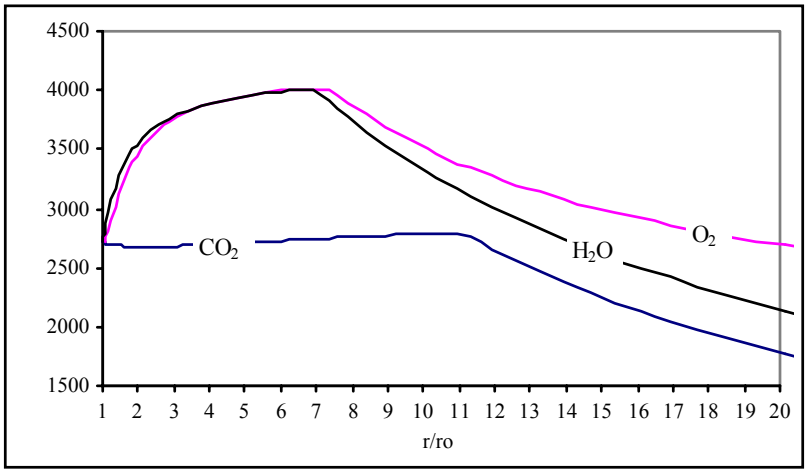

Figure 1 Temperature profiles for 21% O_2/Ar, 21% CO_2/Ar, and 21% H_2O/Ar cases, T_{amb}=300 K, P=1 atm.

Model calculations have been made for a variety of conditions, to help validate the model and to explore the effects of different gases and conditions. Figure 1 shows that the flame temperature profiles for the three oxidizers, O_2, H_2O and CO_2 are significantly different. The flame temperature of CO_2 is less than the dissociation temperature of aluminum oxide, because the enthalpy of the reaction and hence the heat released is not sufficient to raise the

flame temperature to the dissociation temperature[9]. The flame temperature for reacting with either O_2 H_2O is equal to the dissociation temperature of the oxide, which implies that some of the product liquid aluminum oxide gets dissociated to limit the flame temperature.

The flame zone for aluminum combustion includes the reaction zone and the condensation zone, both of which release a large amount of energy. The flame zone can be discerned from the plateau in the temperature profile, wherein the temperature is maintained at the dissociation temperature of the aluminum oxide. The flame zone location has been predicted to be farthest from the particle for the case of the CO_2 oxidizer, and closest to the particle in the case of the H_2O oxidizer. Turns et al observed in their experiments that the flame zone was closer to the particle surface in the presence of H_2O than without H_2O. One of the reasons attributable to this behavior is the value of the diffusivities. While H_2O has the highest diffusivity in Ar, CO_2 has the lowest diffusivity of the three oxidizers in Ar. The higher diffusivity results in the oxidizer diffusing relatively faster towards the particle than the aluminum diffusing outwards. In all the three cases, the aluminum diffuses through an almost similar mixture, dominated by argon. Another effect to be considered would be the evaporation rate of aluminum. In the case of CO_2-Ar, since the flame temperature is comparatively low, the evaporation rate should be lesser and hence the stoichiometric amount of fuel and oxidizer should be obtained at a relatively closer distance to the particle surface due to this effect.

The model shows that the main combustion product is Al_2O_3. It can be seen that some of the oxide diffuses outwards, which is the oxide smoke. This model does not attempt to determine the size of the oxide smoke, which is expected to be a function of the condensation. The concentration of the aluminum sub-oxides is negligible at distances far from the particle surface, which is to be expected considering their fast condensation and other kinetic reactions. AlO is seen to be main aluminum sub-oxide produced in the flame zone. Although any possible reaction between some of the products like H_2, CO & oxide cap with the aluminum has not been considered in this model due to the constraint of kinetic data availability, those reactions could have a role in the fragmentation and jetting of aluminum particles, which has been observed experimentally.[10,11]

The model was used to explore the effect of pressure on aluminum combustion. Most experimental measurements have been made at low pressures, usually one atm, while typical rocket motor conditions are in the range of 30 to 100 atm. The gas composition used in the calculations was the same as that by Davis[12], so that the results of the model could be compared with the experimental data. Figure 2 shows the predicted dependence of surface temperature and flame temperature on pressure, showing a gradual increase in surface and flame temperatures as the pressure is increased. This is reasonable because the aluminum and aluminum oxide boiling (dissociation for aluminum oxide) points have increased with ambient pressure. This increase in flame temperature is a very important concept which has not been treated by most investigators. Figure 3 shows the distribution of the calculated temperatures from the surface outward. It can be seen that the temperature profile of the flame zone is increasing in height as the pressure increases, and the flame zone is calculated to be more narrow and closer to the surface at high pressure than at low pressure.

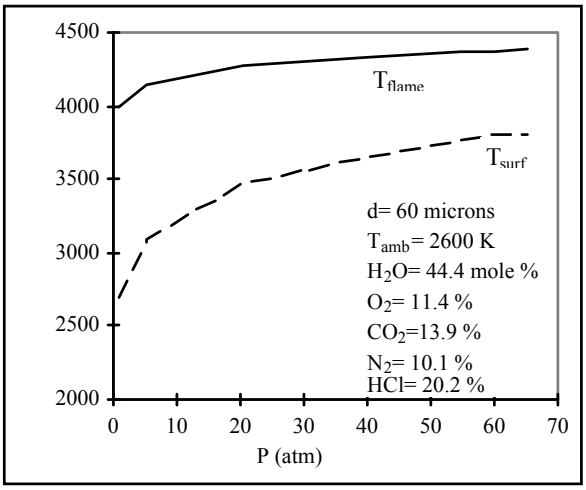

Figure 2. Predicted particle surface and flame temperatures as pressure is varied.

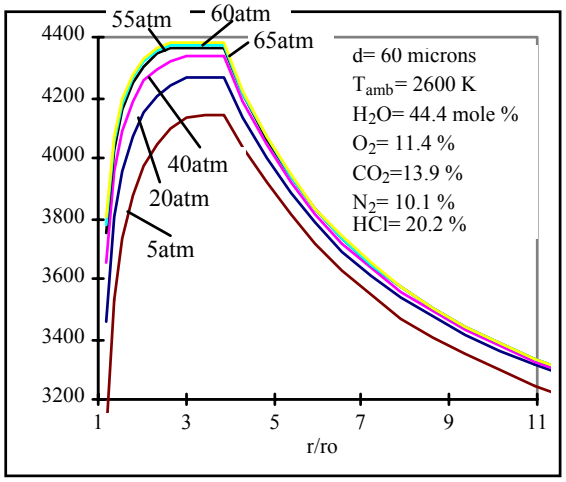

Figure 3. Predicted temperature profiles vs. non-dimensional radius for various pressures.

The calculations from the model have been compared with recent experimental data. Some of the latest and best experimental measurements of temperature and species distributions around a burning aluminum particle have been performed by Bucher et al[13,14,15] at Princeton. In one of their experiments, they burned aluminum particles in an O_2/Ar atmosphere and measured the temperature profile extending outward from the particle surface in very small increments. Figure 4 shows a comparison of Bucher's data with the temperature profile calculated by the model. Excellent agreement between predictions and measurements was achieved.

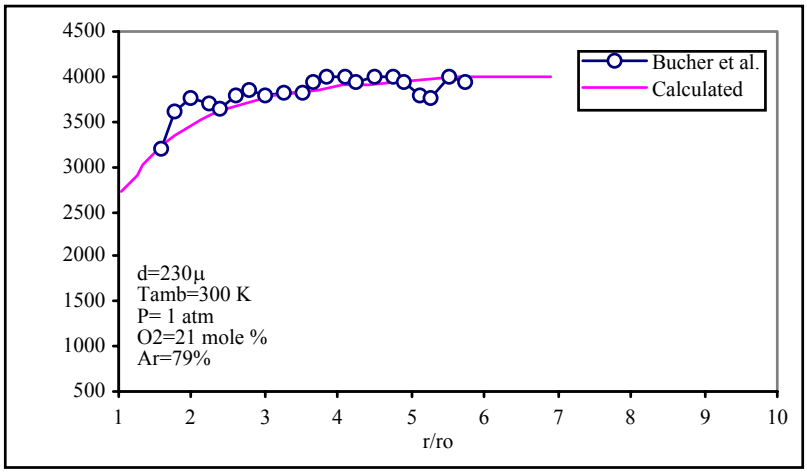

Figure 4. Calculated temperature (K) profile vs. non-dimensional radius compared with experimental data from Bucher et al.

Figure 5 shows the calculated relative AlO concentration profile compared with data from the same experiment. It can be seen that the profiles are very similar, although Bucher et al. observed a peak in AlO concentration at around r/r_o= 2.2, and the calculated peak value is at ~ 3.0. Figure 6 shows a comparison of Bucher's data with a calculated temperature profile for an N_2/O_2 atmosphere, similar to the Ar/O_2 case shown in Figure 4. It must be

noted that the dissociation of N_2 was not included earlier in these calculations, hence the disagreement between the earlier calculated values and experiment. However, very recent calculations, which take into account the N_2 dissociation, result in much better agreement between the two as shown in Figure 6. This is a very logical outcome since heat is required to dissociate N_2, thus lowering the calculated temperature of the system. In addition to looking at temperature and species profiles, the burn times calculated by this model were compared against experimental data, as well as against calculated values from an analytical model previously developed at BYU[16]. The calculated burning times compare well with the burning times from the modified analytical model, as well as with experimental data from Hartman[17] and Davis[18]. However, only a limited number of calculations were performed because of the time required for each calculation (about 12 cpu hours).

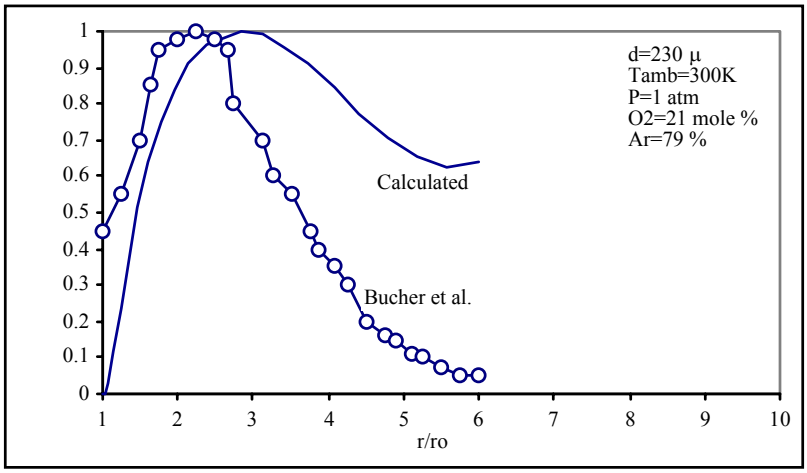

Figure 5. Calculated relative AlO concentration vs. non-dimensional radius compared with experimental data from Bucher et al.

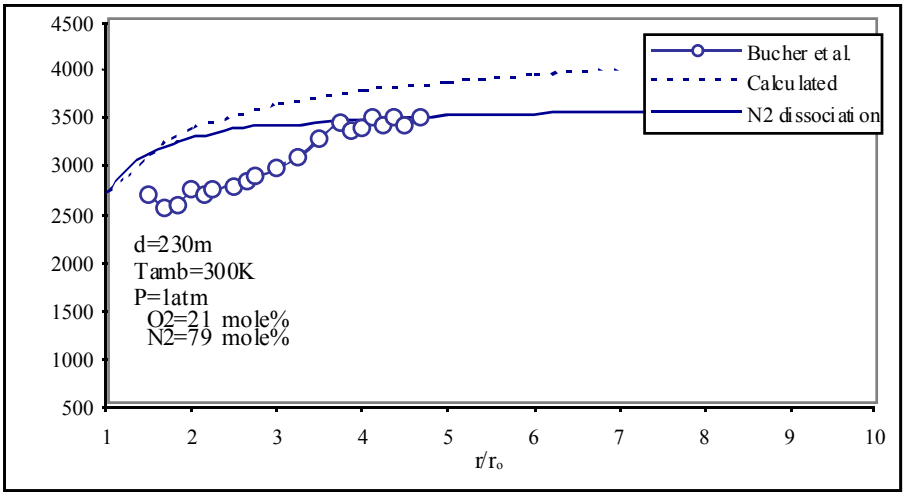

Figure 6. Calculated temperature profile vs. non-dimensional radius compared with experimental data from Bucher et al., with N2 replacing Ar as the inert gas.

A two-dimensional, unsteady state kinetic-diffusion-vaporization controlled numerical model for aluminum particle combustion has been developed. The model solves the conservation equations, while accounting for species generation and destruction with a 15 reaction kinetic mechanism. Parametric calculations were made to examine the flame structure for oxygen, water and carbon dioxide flames. Each of the three calculations was made for a mixture of 21% of the oxidizer mixed with 79% argon, all at one atm. The results show a dramatic difference for the CO_2 case. The flame temperature for the CO_2 case as~2700 K while for both O_2 and water the temperature is ~4000 K. These correspond to the thermodynamic equilibrium for the three oxidizers. There is much less energy in the CO_2 flame. The calculations also indicate that the flame for the CO_2 extends further from the surface than either O_2 or H_2O.

The calculated temperature profiles have been compared with recent experimental data by Bucher, et al, showing good agreement between the model and the available data.

The calculated burning times show that the exponent of the particle diameter dependence of burning time is not a constant and changes from about 1.2 for larger diameter particles to 1.9 for smaller diameter particles. The calculations also indicate that due to the deposition of the aluminum oxide on the particle surface, particle velocity oscillates. Calculations indicate that both the flame temperature and surface temperature increase with increasing pressure. Between 5 and 60 atm the flame temperature is calculated to increase by approximately 400 K. Calculations were also made for conditions corresponding to conditions that occur in a solid propellant rocket motor where little oxygen is present, and the principal oxidizers are water and CO_2.

References

1. Liang, Y. and Beckstead M. W., "Numerical Simulation of Single Aluminum Particle Combustion in Air", *34th JANNAF Combustion Meeting*, CPIA No. 662, Vol. IV, 1997, pp. 197-208.
2. Liang, Y. and Beckstead M. W., "Numerical Simulation of Quasi-Steady Single Aluminum Particle Combustion in Air", AIAA 98-0254, 1998.
3. Liang, Y. and Beckstead M. W., "Numerical Simulation of Unsteady Single Aluminum Particle Combustion in Air", AIAA 98-3825, 1998.
4. Widener, J. F., Liang, Y. and Beckstead, M. W., "Aluminum Combustion Modeling in Solid Propellant Environments", *35th JANNAF Combustion Meeting*, CPIA No 680, Vol I, 1998.
5. Liang, Y. Beckstead M. W. and Pudduppakkam K., "Numerical Simulation of Unsteady, Single Aluminum Particle Combustion", *36th JANNAF Combustion Meeting*, CPIA #691, Vol I, 1999, pp. 283-309.
6. Widener, J. F. Liang Y. and Beckstead M. W., "Aluminum Combustion Modeling in Solid Propellant Environments", AIAA 99-0049, 1999.
7. Law, C.K. "A Simplified Theoretical Model for the Vapor-Phase Combustion of Metal Particles," Combustion Science and Technology, Vol. 7, 1973, p. 197-212.
8. Brooks, K.P. and Beckstead, M.W. "Dynamics of Aluminum Combustion," Journal of Propulsion and Power, Vol. 11, No. 4, July-August, 1995, p. 769-780.
9. Bucher, P., Yetter, R.A. and Dryer, F.L. "Aluminum Particle Gas-Phase Flame Structure," 34th JANNAF Combustion Subcommittee Meeting, 27-31 Oct., 1997, p. 2-11.
10. Dreizin, E. L., "Experimental study of stages in aluminum particle combustion in air", Combustion and Flame 105, 1996, p.541-556.
11. Prentice, J. L. and Nelson,L.S. "Differences between the combustion of Aluminum particles in air and Oxygen-Argon mixtures", Journal of Electrochemical Society, Vol.115, 1968, p.809-812.
12. Davis, A. "Solid Propellants: The Combustion of Particles of Metal Ingredients," Combustion and Flame, Vol. 7, December 1963, p. 359-367.
13. Bucher, P. ,Yetter, R. A. ,Dryer, F. L., Vicenzi, E. P., Parr, T. P. and Hanson-Parr, D. M , "Observations on aluminum particles burning in various oxidizers", 33rd JANNAF Combustion Meeting, 1996.

14. Bucher, P.; Yetter, R.A.; Dryer, F.L. "Flame Structure Measurement of Single, Isolated Aluminum Particles Burning in Air," 26th Int'l Symposium on Combustion, Naples, Italy, July 28-August 2, 1996, p. 2-25.
15. Bucher, P., Yetter, R.A. and Dryer, F.L. "Aluminum Particle Gas-Phase Flame Structure," 34th JANNAF Combustion Subcommittee Meeting, 27-31 Oct., 1997, p. 2-11.
16. Brooks, K.P. and Beckstead, M.W. "Dynamics of Aluminum Combustion," Journal of Propulsion and Power, Vol. 11, No. 4, July-August, 1995, p. 769-780.
17. Hartman, K.O. "Ignition and Combustion of Aluminum Particles in Propellant Flame Gases," 8th JANNAF Combustion Mtg., Vol. 1, CPIA #220, Nov. 1971, p. 1-24.
18. Davis, A. "Solid Propellants: The Combustion of Particles of Metal Ingredients," Combustion and Flame, Vol. 7, December 1963, p. 359-367.

2.8 Stability Additives—A Brief Tutorial (Cohen)

2.8.1 History and Controversy

The ability to suppress combustion instability by the use of small concentrations of particulate additives was well-known by 1960. Good reviews of the experience acquired in the 1940s & '50s are contained in Lou et al (1958), Summerfield (1960) and Waesche (1999). At first, the additives were referred to as "chemical additives" on the belief that they stabilized the combustion by chemical means. As the experienced evolved, they became classified as "reactive additives" and "non-reactive additives" to distinguish the materials used. Still, the essential mechanism was thought to involve the chemical or physical properties of propellant combustion. It then became recognized that a suspension of particles in the combustion chamber gases could suppress instability by viscous dissipation of the wave motions, known as "particle damping". This led to two schools of thought, one advocating combustion stabilization and the other particle damping as the essential mechanism.

Developments in the 1960s emphasized aluminized propellants such that the use of additives for stabilization was not an issue. However, instances of instability that were encountered with the fully-aluminized propellants generated a re-thinking by both schools of thought (Price, 1971). On the chemical side, it was realized that aluminum could contribute to instability by its altering of the other ingredient proportions in the formulation or by its own combustion. The contributions of its own combustion evolved to what is now known as the "distributed combustion" mechanism. On the particle damping side, it was realized that particulates are not a panacea; they have to be selected carefully and there are regimes where even large amounts will not be adequate.

The interest in reduced-smoke and minimum-smoke propellants in the 1970s produced a resurgence in work with stability additives, which continued through the 1980s and to a lesser extent through the 1990s. The scope of work can be illustrated by a program in England which investigated 43 different supplies of additives (Evans and Smith, 1978) and one in the US which investigated 80 additive combinations (Rudy and Bain, 1981). Consistent with the work of the 1950s, aluminum and aluminum oxide emerged as two of the additives of choice (considering practical propellant requirements as well as stabilization effectiveness). Zirconium carbide emerged as a new additive of choice because it was not only effective but its high density served to minimize smokiness. However, the preferential use of these additives is not meant to preclude other additives which may be attractive for other reasons and effective under certain conditions.

The mathematical theory of particle damping was well-developed and verified for aluminum and aluminum oxide by the 1970s (Derr et al, 1975; Kraeutle et al, 1976). It was used for selecting the particle sizes of $A_{12}O_3$ and ZrC to be used. Aluminum burns to $A_{12}O_3$, which is usually but not always complete or in the range of particle sizes desired. There remained the school of thought that combustion alterations also played a role in stabilization, at least for the "reactive additives", and was supported by experiments with aluminum and ZrC (Wendelken, 1973; Rudy and Bain, 1981; Kubota and Yano, 1982; Blomshield and Stalnaker, 1996). However, the theories of combustion stabilization never went beyond verbal descriptions of ideas. To the extent that other additives were found to be effective, the precise mechanisms were never resolved.

2.8.2 Particle Damping

The classical relationships for particle damping are based on the theory of Temkin & Dobbins (1966), incorporated into the SSP code for motor stability predictions. For purposes of this discussion, the following approximate relationships are useful. Particle damping by a small concentration of additive may be given by (approximately):

$$\alpha = -(Cm\omega/2)(\omega\tau)/[1+(\omega\tau)^2 \quad (1)$$

where

$$\tau = \rho D^2/18\mu$$

Cm = particle concentration, ω = angular frequency, τ = particle relaxation time, D = particle size, ρ = particle density, μ = gas viscosity (typical value of 0.00065 poise).

Taking the derivative of α at $(\omega\tau)$ and setting it equal to zero results in the maximization of α at $(\omega\tau) = 1$. This yields an expression for the optimum particle size as:

$$Dopt = \sqrt{18\mu/\rho\omega} \quad (2)$$

and the maximum value of particle damping with that size is:

$$\alpha_{max} = -Cm\omega/4 \quad (3)$$

For convenience, a series of general parametric curves based upon Temkins & Dobbins has been published by Dehority (1970). It is quickly apparent from Eq. (2) that finer particle sizes are favored at higher frequencies and with higher-density materials. Eq. (3) then reveals that the finer sizes are more capable to produce greater maximum damping (at higher frequencies). It also shows that the damping is proportional to the particle concentration.

Examples of Dehority's curves help to frame the particle damping capabilities. For liquid $A_{12}O_3$ ($\rho \sim 3$ g/cc), the optimum particle size to damp 6000 Hz (multiply by 2π for ω) is 3.3μ and the damping by 1% at that frequency is 108/sec. However, its damping at 500 Hz drops all the way down to 1.6/sec. The optimum particle size to damp 500 Hz is 11μ, but the damping by 1% at that frequency is only 9/sec; at 6000 Hz it provides 18/sec. If we combined half of the two sizes, the damping at 6000 Hz would be 63/sec and at 500 Hz it would be 5.3/sec. Using a real size distribution, the damping at high frequencies is significantly reduced from potential maxima while the damping at low frequencies is improved by only a small amount. This helps to explain why 0.5% additive is usually insufficient to suppress high frequencies and why even aluminized propellants might not suppress an instability at low frequencies.

To put this in perspective, instabilities having a positive growth constant (α) less than 20/sec are referred to as "mild" or "weak", 20-50/sec as "moderate", 50-100/sec as "strong" and greater than 100/sec as "very strong". A reasonable amount of a sufficiently fine particle size distribution can suppress a very strong high-frequency tangential mode, and this has been observed in practice. Extrapolating Dehority's curves, 1% of 2μ $A_{12}O_3$ provides 270/sec worth of damping at 15 Khz so a real particle size distribution centered at 2μ could provide 150/sec. At low axial mode frequencies (hundreds of Hz), however, particle damping with an acceptable amount of additive can be effective only for mild instabilities.

2.8.3 Combustion Stabilization Mechanisms in General Terms

There are several ways in which additives can provide a mechanism to stabilize combustion, expressible in terms of reducing the combustion response function. When it comes to small additive levels, changes in propellant thermal properties or in the proportions of the other ingredients to accommodate the additive are too small to have a significant effect on the combustion dynamics or combustion response. Ideas which have been expressed in terms of "pilot flames at the propellant surface" or "hot melt layers" are really speaking to chemical or thermal stabilizations of the heat feedback from the gas phase or of the propellant surface by kinetic or thermal inertia.

This, too, can be into some perspective. An unstable growth constant of 70/sec, which can be characterized as strong, might be shown by an SSP motor stability analysis to result from a combustion driving gain of 400/sec reduced by system losses of 330/sec. Suppose the driving gain is associated with a combustion response function of 1.4. The driving gain is proportional to the response function. Thus if the response function can be reduced to 1.1, a very reasonable proposition, the driving gain is reduced to 314/sec and the motor becomes stable with a net α of -16/sec. The loss of 86/sec of driving is equivalent to some very good particle damping, based on the examples given in the previous section. Thus combustion stabilization can be a powerful alternative to particle damping…if not achieved with one type of additive, perhaps by another.

The combustion response function can be defined as:

$$Rp = (r'/\bar{r})/(p'/\bar{p}) \tag{4}$$

r' and $\bar{r}$ are the fluctuating and steady-state components of burn rate, respectively; p' and $\bar{p}$ are the fluctuating and steady-state components of the pressure. There can be a response to crossflow perturbations as well, but need not be included for purposes of this discussion.

Using a homogeneous propellant combustion model, suitable for the present discussion (and applicable to classical double-base propellants), an expression for the response function can be derived as (Culick 1968):

$$Rp = nAB/[AB - (1 + A) + A/\lambda + \lambda] \tag{5}$$

n is the steady-state pressure exponent, A is a parameter characteristic of the surface decomposition law, B is a parameter characteristic of the heat feedback law (*e.g.*, the heat transfer from the flame to the surface) and λ is a complex variable function of dimensionless frequency (known as Ω, which is ω multiplied by the characteristic response time of the solid). It is the real part of R_p which drives the instability in a motor.

For an Arrhenius decomposition law, $r \sim \exp(-E_s/R_u T_s)$, A becomes:

$$A = [E_s / R_u \bar{T}_s^2][\bar{T}_s - T_o] \tag{6}$$

E_s is the activation energy of surface of decomposition, R_u is the universal gas constant, $\bar{T}_s$ is the steady-state surface temperature and T_o is the bulk temperature of the solid (or conditioning temperature for Πk effects).

The form and content of B depends upon the particular flame model used. However, Zeldovich & Novozhilov showed that it is fundamentally related to burn rate temperature-sensitivity (σp):

$$B = 1/\sigma p(\overline{T}_s - T_o) \tag{7}$$

A study by Cohen (1985) showed that, for double-base propellants, a typical value for A is about 17 and for B about 1.0 (E_s ~ 40 Kcal/mol; $\overline{T}_s$ ~ 600K; σp ~ 0.003/K). Stability is promoted by decreasing values of A and increasing B. Decreasing A decreases the peak (resonant) value of R_p and the frequency at which the peak occurs. Note from Eq. (6) that lower values of A are promoted by low activation energies of decomposition and high surface temperatures. Increasing B tends to flatten response function curve more peaked with higher resonant values of R_p. From Eq. (7), high B is promoted by low σp with increasing surface temperature, but the weight of Eq. (7) favors a low σp by whatever means to achieve it. Cohen and Flanagan (1985) provide a good review of σp, low values being favored in general.

Of course, the pressure exponent n has a direct bearing on R_p. It is the value of R_p at zero frequency (steady-state or quasi-steady response), and R_p at any frequency is proportional to n. Thus response functions are often seen plotted as R_p /n. As low σp is a generally desired propellant property, so is low n. However, there is one note of caution of here. In cases where the low n is brought about by transitioning surface processes, as in plateau or mesa propellants, the dynamics of unstable burning can be too fast for the plateau mechanism to operate such that the effective n becomes characteristic of the underlying combustion process and much higher in value. It is for this reason that plateau or mesa propellants (negative or zero n) can be unstable (Cohen 1993).

We can now speak of combustion stabilization by additives in terms of increasing surface temperature (lower A), a reduced sensitivity of the heat feedback law to pressure (higher B), a lower σp (consistent with higher B) and a lower pressure exponent (in a way that continues to operate under dynamic conditions). We are ready to give content to ideas of thermal and reactive inertia. Hot spots at the propellant surface or hot melt layers on the surface can provide thermal inertia in terms of a higher surface temperature or reduced fluctuation in the surface temperature. Pilot flames from particles at or near the surface can provide a reactive inertia in terms of a reduced pressure-sensitivity in the heat feedback law.

The basis for the derivation of Eq. (5) for R_p is an energy balance at the propellant surface. The classical form is:

$$\left[\partial\theta/\partial z\right]o,\ gas = 1 + nB(P-1) + (1 - B + 1/A)(R-1) \tag{8}$$

The left-hand side is the instantaneous temperature gradient at the propellant surface, on the gas side, which must be matched to a transient heat conduction solution in the solid at the surface. θ is a dimensionless temperature, the value at the surface (θs) being $(T_s - T_o)/(\overline{T}_s - T_o)$. z is a dimensionless distance, normalized by the characteristic dimension of the solid (related to the characteristic time which converted ω to Ω in Eq. 5). P is the dimensionless instantaneous pressure, $p/\overline{p}$ (or 1 + $p'/\overline{p}$), and R is the dimensionless instantaneous burn rate, $r/\overline{r}$ (or 1 + $r'/\overline{r}$). We have from the surface decomposition law that:

$$(R-1) = A(\theta s - 1) \tag{9}$$

We see immediately from Eq. (9) that if A is low, any perturbations in θs will have a lower multiplicative effect on R. Thus R fluctuations will be lower in magnitude, resulting in lower R_p. That is one way in which a higher surface temperature can operate. If we substitute Eq. (9) into Eq. (8), the third set of terms on the right-hand side becomes $(\theta s - 1)[A(1 - B) + 1]$. This is where A appears. Thus a lower A serves to reduce the fluctuations in the temperature gradient (heat feedback) at the surface, adjusting to the lower R_p to satisfy the balance.

Eq. (8) also confirms that a lower n is desirable to reduce the temperature gradient fluctuations at the surface by the manner in which the pressure perturbations arrive (are seen) at the surface.

Increases in B in Eq. (8) tend to both increase and decrease the temperature gradient fluctuations at the surface by operation of the second and third group of terms. Taking the derivative of the gradient fluctuations with respect to B, the result is $[n(P - 1) - (R - 1)]$. Since n is less than 1 and R tends to be greater than P ($R_p > 1$), the derivative is negative so increases in B tend to reduce the temperature gradient fluctuations at the surface.

2.8.4 Some Special Cases

We can give substantive content to these effects in terms of a model that provides hot spots at the propellant surface or a hot melt layer on the propellant surface or pilot flames affecting the heat feedback to the surface. For example, we can think of a melt layer as a hot plate formed by an agglomeration of molten fine particles. A quasi-steady analysis is useful to illustrate. We can express the energy balance at the propellant surface in terms of the conventional steady-state burn rate law to contain the pressure-dependence of the underlying propellant and add a term to represent the thermal inertia of the hot plate due to the additive:

$$r = ap^n + \phi \tag{10}$$

where a is the burn rate coefficient and ϕ represents the effect of the hot plate. Taking the derivative with respect to p, dividing through by r and multiplying by p/p yields:

$$dr / r = [n /(1 + \phi / ap^n)]dp / p \tag{11}$$

Without the hot plate ($\phi = 0$), the quasi-steady response is simply n. With the hot plate, the value is less than n depending on the magnitude of ϕ in relation to the total heating. Even if small, the leverage attainable from a decrease in A or increase in B in the formal non-steady analysis could produce meaningful reductions in the response at frequencies of interest. It is not the purpose of this tutorial to develop the actual physical model, but to show the basics to illustrate the point.

Pilot flames at or near the surface can be represented by the heat feedback from burning fine metal particles. We know that aluminum and magnesium combustion are governed by the diffusion of metal vapor to react with oxidizing gases from the propellant such as H_2O. The reaction kinetics are much faster than the diffusion. Thus the combustion can be represented by a D^2 law that is not pressure-dependent at practical motor pressures (Widener and Beckstead, 1998; Beckstead, 2000). Other metals such as boron and zirconium, and carbides, burn by a surface-coupled reaction which is controlled by properties of the condensed phase. There is little pressure dependence. We can take yet another quasi-steady approach to the energy balance to show the effect on combustion response. The steady-state energy balance at the surface for a flame sheet model can be written as:

$$T_s = T_o + (1 - C_m)(Q_g / c_s)\exp(-\xi_g) + C_m(Q_m / c_s)\exp(-\xi_m) \tag{12}$$

with

$$\xi_i = k_i r / p^{m_i}$$

Q_g and Q_m are the heat release from the propellant (gas) flame and the metal combustion, respectively; ξ_g and ξ_m are the respective effective flame heights (dimensionless); c_s is the specific heat of the solid propellant. In the expression for $\xi_{i,}$ m_i is reaction order (taken to be $m_g = 2$ for propellant gas phase flames) and k_i is a constant (based on kinetics and/or diffusion, depending on the controlling process). For metal or metal carbide combustion, m_m is taken to be either 0 or 1. Substituting the steady-state burn rate law for r and assuming $m_m = 0$, Eq. (12) becomes:

$$T_s = T_o + (1 - C_m)(Q_g / c_s)\exp(-k_g a p^{n-2}) + C_m(Q_m / c_s)\exp(-k_m a p^n) \tag{13}$$

Taking the derivative with respect to pressure yields:

$$dT_s / dp = (n-2)k_g a p^{n-2}(1 - C_m)(Q_g / c_s)\exp(-k_g a p^{n-2}) - n k_m a p^{n-2} C_m (Q_m / c_s)\exp(-k_m a p^n) \tag{14}$$

For small flame heights (the propellant flame and pilot flames close to the surface), the exponentials reduce to unity. Taking $n = 0.5$, Eq. (14) becomes:

$$dT_s / dp = 1.5(1 - C_m)k_g (a / p^{2.5})(Q_g / c_s) - 0.5 C_m k_m (a / p^{0.5})(Q_m / c_s) \tag{15}$$

There are two ways of looking at this result. First, the pilot flame term is subtractive from the propellant (gas) flame term such that the surface temperature change with respect to pressure is reduced. Second, the pilot flame is much less pressure-sensitive than the propellant flame such that pressure perturbations are transmitted to the surface via the heat feedback law at a reduced level for $C_m > 0$. These are stabilizing effects.

2.8.5 Some Speculation

It is possible to speculate on why many of the obscure additives which have been explored were able to suppress oscillations in some cases but not in others.

Consider a non-reactive additive which may have been attempted in various particle sizes and in different propellants. Perhaps the wrong particle size was used for particle damping in the frequency range of interest. Perhaps it was too coarse to respond to the heating from a relatively cool, low energy propellant. Perhaps the situation came along where someone tried a very fine particle size in a propellant that was hot enough or burned slow enough so that the material was able to melt and fuse and form a hot layer on the surface to provide a stabilization in accordance with the mechanism of Eq. (11).

Consider a reactive additive. Perhaps it, also, was not of the correct size for particle damping. Perhaps it was too coarse, or its ignition temperature too high relative to the primary flame zone temperature of the propellant to enable the particles to ignite rapidly and form the pilot flames at or close to the propellant surface. Perhaps the burning rate of the propellant was too fast for an adequate particle thermal response. But then, as luck would have

it, the right combination of variables enabled the mechanism of Eq. (15) to become operative and achieve a successful result.

On the other hand, consider an additive that was effective in an R&D motor using a cylindrical grain but then failed to suppress the instability in the full-scale motor. Perhaps the higher L/D of the full-scale motor or greater concentrations of burn area in its special design enabled the instability to overpower the additive effect. Subsequent iterations to solve the problem relegated that additive to obscurity even though its damping may have been large.

The so-called preferred additives may have become so because of more forgiving properties and a more favorable history. The science of particle damping is now well-developed for $A_{12}O_3$ so that its sizes are properly selected. ZrC began to be used in an era of more energetic propellants, it has favorable ignition properties, and its surface reaction process enables its particle size to be selected on the basis of particle damping theory because its size doesn't change much in burning (Sambamurthi et al, 1984).

Aluminum combustion produces a broad range of $A_{12}O_3$ particle sizes, chiefly in the range suited to dampen high-frequency modes, and its combustion is generally highly efficient. But there are cases where its combustion is less efficient or less timely in the combustion zone. Combinations of variables which cause an extended ignition delay of the particles could impair the production of $A_{12}O_3$ for particle damping as well as the effectiveness of pilot flames for combustion stabilization. Excessive aluminum agglomeration could be detrimental in some cases, but beneficial in others where a hot metal plating on the surface might provide stabilization. Considering distributed combustion, there can be cases where aluminum increases the driving to promote an instability (Blomshield et al 1991). Trends in aluminum combustion and $A_{12}O_3$ damping might be complementary or opposed in certain cases. There have been cases where changing aluminum particle size stabilized motors, but the explanations were as speculative as those given here. The consideration of aluminum as one of the preferred additives, its history of general success, may be due to the forgiving nature of the balance of mechanisms it offers.

2.8.6 Concluding Remarks

The ideal stability additive would be of low density (for propellant insensitivity), would be available in desirable particle sizes, it would do its thing at or very near the burning surface to stabilize the motor (without disadvantage to steady-state ballistics and other practical propellant properties), and would then be transformed into gaseous products so as to release some energy without smoke. There may be instances where the currently-preferred additives are not desirable.

Our resource of open-minded and imaginative young people should be encouraged to explore new ideas or revisit old ones given new conditions or requirements. In doing so, maximum use should be made of the information, experience and analytical capabilities available because current budgets will not allow the scope of work and testing that was possible in an earlier era. Experiments aimed at characterizing mechanisms in a quantitative way combined with mathematical model representations can be an effective scientific approach to the desired results, and ought to be supported by the sponsoring agencies.

References

1. Lou, R.L., Kriger, R.C. and Wrightson, J.M. (1958) "Suppression of Unstable Burning in Solid Propellants", Report No. 1431, Aerojet-General Corp., Sacramento, CA.
2. Summerfield, M., editor (1960) *Solid Propellant Rocket Research*, Vol. 1 of the ARS (AIAA) Progress Series in Astronautics and Rocketry, Academic Press, New York.
3. Waesche, R.H.W. (1999) "Mechanisms and Methods of Suppression of Oscillatory Burning by Metallic Additives" *AIAA J. Prop. & Power*, Vol. 15, Nov-Dec. 1999, pp. 919-922. Also see 35th *JANNAF Combustion Meeting*, CPIA Pub. 680, Dec. 1998.
4. Price, E.W. (1971) "Comments on Role of Aluminum in Suppressing Instability in Solid Propellant Rocket Motors", *AIAA J*., Vol. 9, pp. 987-990.
5. Evans, G.I. and Smith, P.K. (1978) "The Suppression of Combustion Instability in Smokeless Solid Propellant Rocket Motors", AIAA Paper 78-1568, 14th AIAA/SAE Joint Propulsion Conference. Also see Paper #27, *AGARD Conference Proceedings No. 259, Solid Rocket Motor Technology*, National Technical Information Service (NTIS), Springfield, VA, July 1979.
6. Rudy, T.P. and Bain, L.S. (1981) "Chemical Control of Propellant Properties", Report AFRPL-TR-81-53, Chemical Systems Division, United Technologies, Sunnyvale, CA.
7. Derr, R.L. et al (1975) "Combustion Instability Studies Using Metalized Solid Propellants: Part 1, Experimental Verifications of Particle Damping Theory", 12th *JANNAF Combustion Meeting*, CPIA Pub. 273, Vol. II, pp. 155-166.
8. Kraeutle, K.J. et al. (1976) "Combustion Instability Studies Using Metalized Propellants: Additional Experimental Evidence for the Validity of Particle Damping Theory", 13th *JANNAF Combustion Meeting*, CPIA Pub. 281, Vol. II, pp. 155-166. Also see Paper #15, *AGARD Conference Proceedings No. 259, Solid Rocket Motor Technology*, National Technical Information Service (NTIS), Springfield, VA, July 1979.
9. Wendelken, C.P. (1973) "Combustion Stability Characteristics of Solid Propellants", Report AFRPL-TR-73-63, Air Force Rocket Propulsion Laboratory, Edwards AFB, CA.
10. Kubota, N. and Yano, Y. (1982) "Particulate Damping of Acoustic Instability in RDX/AP Composite Propellant" AIAA Paper 82-1223, 18th *AIAA/SAE/ASME Joint Propulsion Meeting*.
11. Blomshield, F.S. and Stalnaker, R.A. (1996) "Solid Propellant Combustion Instability Additive Investigations", 33rd *JANNAF Combustion Meeting*, CPIA Pub. 653, Vol. II, pp. 207-214.
12. Temkin, S. and Dobbins, R.A. (1966) "Attenuation and Dispersion of Sound by Particulate-Relaxation Processes", *J. Acoust. Soc. of America*, Vol. 40, No. 2, pp. 317-324.
13. Dehority, G.L. (1970) "A Parametric Study of Particulate Damping Based on the Model of Temkin and Dobbins", Report NWC TP 5002, Naval Weapons Center, China Lake, CA.
14. Culick, F.E.C. (1968) "A Review of Calculations for Unsteady Burning of a Solid Propellant", *AIAA J*., Vol. 6, Dec. 1968, pp. 2241-2255.
15. Cohen, N.S. (1985) "Combustion Response Functions of Homogeneous Propellants", AIAA Paper 85-1114, 21st *AIAA/SAE/ASME/ASEE Joint Propulsion Conference*.
16. Cohen, N.S. and Flanigan, D.A. (1985) "Mechanisms and Models of Solid Propellant Burn Rate Temperature Sensitivity: A Review", *AIAA J*., Vol. 23, pp. 1538-1547.
17. Cohen, N.S. (1993) "Why Negative Exponent Propellants Can Drive Combustion Instability", 30th *JANNAF Combustion Meeting*, CPIA Pub. 606, Vol. III, Nov. 1993, pp. 191-196.
18. Widener, J.F. and Beckstead, M.W. (1998) "Aluminum Combustion Modeling in Solid Propellant Combustion Products", AIAA Paper 98-3824, 34th *AIAA/ASME/SAE/ASEE Joint Propulsion Conference*.
19. Beckstead, M.W. (2000) "A Summary of Aluminum Combustion", *37th JANNAF Combustion Meeting*.
20. Sambamurthi, J.K. et al (1984) "Combustion of Zirconium Carbide", 21st *JANNAF Combustion Meeting*, CPIA Pub. 412, Vol. I.
21. Blomshield, F.S. et al (1991) "Aluminum Combustion Effects on Combustion Instability of High Burn Rate Propellants", 28th *JANNAF Combustion Meeting*, CPIA Pub. 573, Vol. III.

TASK III

CHAMBER DYNAMICS

Vigor Yang, Team Leader

3
TASK III — CHAMBER DYNAMICS

Results obtained from Tasks I and II provide a concrete basis for understanding the oscillatory combustion mechanisms of solid propellants in isolated environments. To extend these fundamental investigations to practical issues of combustion instabilities, it is important to study the propellant burning behavior at realistic rocket motor conditions. The purpose of this task is to establish a full physical understanding of all energy release processes and their interactions with flow oscillations that drive motor instability, as shown schematically in Figure 1.

All issues related to the fundamental physicochemical processes such as the mutual coupling among acoustic, vortical, and entropy disturbances arising from oscillatory combustion have been addressed systematically. Emphasis is placed on the interactions between chamber dynamics and combustion responses of propellants at both the fundamental level (*e.g.*, near-surface flame zone physiochemistry) and system level (*e.g.*, nonlinear motor stability characteristics).

The work addresses the following basic scientific issues of practical concern:

- How unsteady motor internal flow is established by propellant combustion;
- How local flow disturbances affect propellant burning characteristics;
- What sort of interactions exist between chamber dynamics and transient combustion responses of propellants; and
- How stability additives such as ZrC and metal particulates help improve motor stability behavior.

A unified approach comprising analytical analysis, numerical simulation, and experimental validation has been developed to study these issues. Detailed spatial distribution and temporal evolution of key heat-release processes responsible for driving combustion instabilities are identified in terms of thermochemical properties of propellants, local flow conditions, and motor oscillation characteristics. *Results obtained have not only provided motor designers with specific guidelines for developing a stable rocket motor, but also helped propellant chemists optimize ingredient formulations for curing stability problems at the molecular level.*

To accomplish this ultimate goal requires circumvention of two technical hurdles: (1) a thorough understanding of detailed flow characteristics in various parts of the chamber, including micro-scale processes near the propellant surface where major exothermic reactions occur and macro-scale processes in the core-flow region which dictate acoustic wave properties; and (2) a complete knowledge of propellant reaction mechanisms and combustion wave structures in motor environments under both steady and oscillatory conditions. Combination of these items offers a systematic, implementable, and unique guideline for attacking, motor instability problems which was not previously available. The present task involves the following four areas.

- Numerical Simulation of Motor Internal Flow Evolution and Combustion Dynamics (Yang, Penn State)
- Linear and Nonlinear Analyses of Motor Dynamics (Culick, Caltech)
- Unsteady Motor Flowfields and Interactions with Flame Zone Gas Dynamics (Flandro, UTSI)
- Subscale Motor Test Firings and Related Laboratory Tests (Blomshield, NAWC)

The major objectives, methods of approach, and research accomplishments in each of the above areas are summarized below.

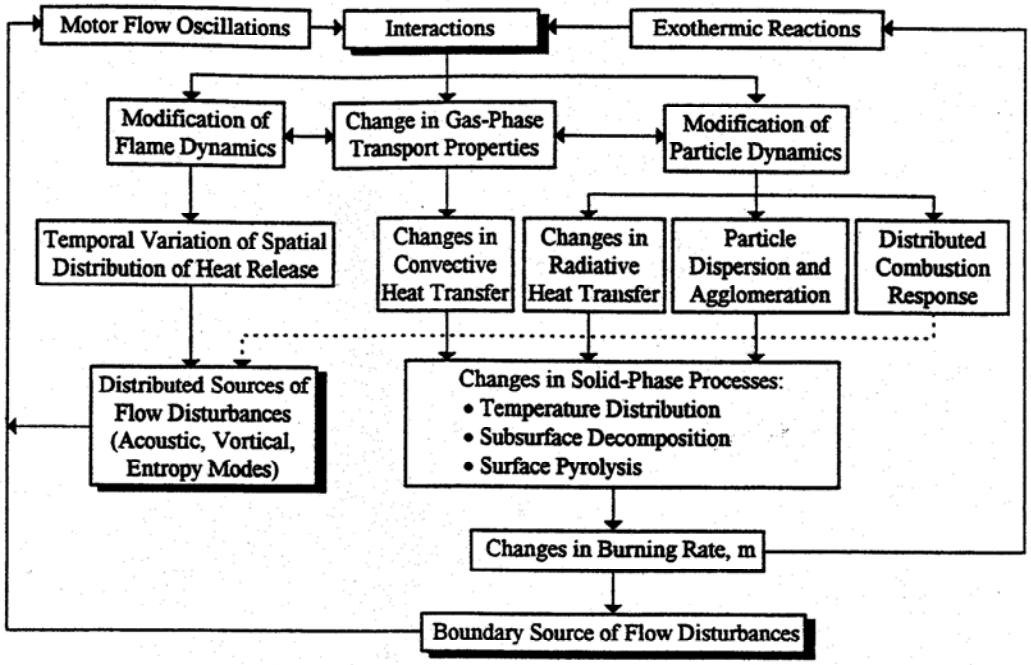

Figure 1. Interactions of motor flow oscillations and transient combustion responses of solid propellants.

3.1 Numerical Simulation of Motor Internal Flow Evolution and Combustion Dynamics (Yang, Penn State)

Since motor instability is a consequence of the transient combustion responses of propellants to local flow oscillations in a confined volume, any realistic investigation into this phenomenon requires a thorough understanding of the following two interactive processes: (1) *fluid dynamic processes* that dictate to the environment in which chemical reactions occur; and (2) *chemical processes* that provide the energy for driving instabilities. Combined, these two processes play a dominant role in determining the dynamical behavior of unsteady motions in a rocket motor.

Most previous research on motor internal flowfields and combustion processes has either focused on pure fluid dynamics (such as the cold-flow simulation work funded by AFAL, AFOSR, and NASA Marshall), or been based on simplified approaches with propellant burning mechanisms modeled by acoustic admittance functions. Very little effort has been made to investigate the intricate coupling between local fluid dynamics and chemical reactions in a rocket motor environment. The major obstacle lies in the lack of reliable experimental diagnostic and numerical

modeling techniques with accuracy sufficient to resolve the spatial distribution and temporal evolution of the heat release mechanisms in the near field of the propellant surface where rapid variations of flow properties of velocity, temperature, and entropy take place. With the advances in computational power and knowledge of propellant physiochemistry, the Penn State group has conducted a series of fundamental studies incorporating propellant chemical kinetics into motor flow analyses for both homogeneous and heterogeneous propellants. Detailed interactions between motor gas dynamics and nonsteady propellant combustion (including both gas-phase and subsurface reactions) were treated systematically. The instantaneous propellant burning characteristics such as surface regression and heat-release rates were obtained as part of the solution.

The objective of this subtask is twofold. The first is to establish a unified theoretical/numerical framework accommodating propellant chemistry, combustion mechanisms, and motor dynamics for predicting motor stability characteristics from first principles. The second is to identify the key mechanisms responsible for driving motor instabilities. Emphasis was placed on the following individual processes and their contributions to the global behavior of oscillations:

- motor internal flow development, including near-surface flow oscillations in laminar and turbulent regimes;
- gas-phase flame dynamics and heat-release mechanisms as well as subsurface degradation and surface regression phenomena;
- transient responses of propellant combustion to local flow oscillations;
- energy cascade from micro-scale flow disturbances in the flame zone to macro-scale acoustic motions in the chamber; and
- overall system dynamics such as limit-cycle and pulse-triggered instability phenomena.

Major results of this task can be summarized in three parts:

- unsteady motor flow evolution with acoustic excitation
- propellant combustion dynamics in rocket motors
- two-phase flow interactions in rocket motors

A brief summary of the research outcomes is given in the following paragraphs.

3.1.1 Unsteady Motor Flow Evolution with Acoustic Excitation

This study attempts to explore the fluid dynamic aspect of the internal flow development in rocket motors under conditions with and without externally imposed acoustic excitations. The physical model under consideration is a porous chamber with surface mass injection, simulating the evolution of combustion products from propellant surface. The analysis is based on a large-eddy-simulation (LES) technique in which the spatially filtered and Favre averaged conservation equations for large, energy-carrying turbulent structures are solved explicitly. The effect of the unresolved scales is modeled semi-empirically by considering adequate dissipation rates for the energy present in the resolved scale motions. Results show that the flowfield is basically governed by the balance between the inertia force and pressure gradient, as opposed to viscous effect and pressure gradient in channel flows without transpiration. Three successive regimes of development: laminar, transitional, and fully turbulent flow, are

observed. Transition to turbulence occurs away from the porous wall in the mid-section of the motor and the peak in the turbulence intensity moves closer to the wall further downstream as the local Reynolds number increases. Increase in pseudo-turbulence level at the injection surface causes early transition to turbulence. As the flow develops further downstream, the velocity profile transits into the shape of a fully developed turbulent pipe flow with surface transpiration. The flow evolution is characterized primarily by three non-dimensional numbers: injection Reynolds number, centerline Reynolds number, and momentum flux coefficient.

The second part of this study focuses on the effect of forced periodic excitations on the unsteady flowfield. Time-resolved simulations are performed to investigate the effects of traveling acoustic waves on large-scale turbulent structures for various amplitudes and frequencies of imposed excitations. The resultant oscillatory flowfield is decomposed into mean, periodic (or organized), and turbulent (or random) motions using a time-frequency localization technique. Emphasis is placed on the interactions among the three components of the flowfield. The primary mechanism for the transfer of energy from the mean to the turbulent motion is provided by the nonlinear correlations among the velocity fluctuations, as observed in stationary turbulent flows. The unsteady, deterministic component gives rise to an additional mechanism for energy exchange between the organized and turbulent motions, and consequently produces increased turbulence levels at certain acoustic frequencies. The periodic excitations lead to earlier laminar-to-turbulence transition than that observed in stationary flows. The turbulence-enhanced momentum transport, on the other hand, leads to increasede eddy viscosity and tends to dissipate the vortical wave originating from the injection surface. The coupling between the turbulent and acoustic motions results in significant changes in the unsteady flow evolution in a porous chamber.

Detailed results from this study are given in Refs. 1-4.

3.1.2 Propellant Combustion Dynamics in Rocket Motors

Interactions among the large-scale vortical structures, acoustic waves, and unsteady heat-release occurring within solid rocket motors have been investigated in depth. Emphasis is placed on the motor internal flow development and its influence on propellant combustion. The formulation is based on the Favre averaged, filtered equations for the conservation laws and takes into account finite-rate chemical kinetics and variable thermophysical properties. Only reduced chemical kinetics schemes were incorporated into the flow solver to render numerical calculations manageable. Turbulence closure was achieved using an LES technique with chemical source terms treated with state-of-the-art models for turbulence/combustion interactions. The governing equations and associated initial/boundary conditions were solved by means of an innovative preconditioning scheme in conjunction with the dual time-stepping integration method recently established at Penn State to overcome the numerical stiffness inherent in the studies of solid propellant combustion in motor environments.[5] The overall approach has been first applied to study the double-base homogeneous propellant combustion dynamics in a cylindrical rocket motor. The model included five global reactions in the gas phase and two decomposition pathways in the condensed phase. Figure 2 shows a typical snapshot of the temperature, heat release, and NO mass fraction distributions. The flow evolution and flame structures were thoroughly investigated, with the instantaneous propellant burning rate predicted as part of the solution. The work was the first of its kind and made a revolutionary breakthrough in

numerical simulation of rocket motor combustion dynamics. The entire motor interior ballistics was predicted from "first principles" for a given propellant composition and motor geometry. No adjustable parameters other than those originally used in the turbulence and chemistry sub-models were employed to match experimental data.

Detailed discussion of major research results were given in Ref. 6-9.

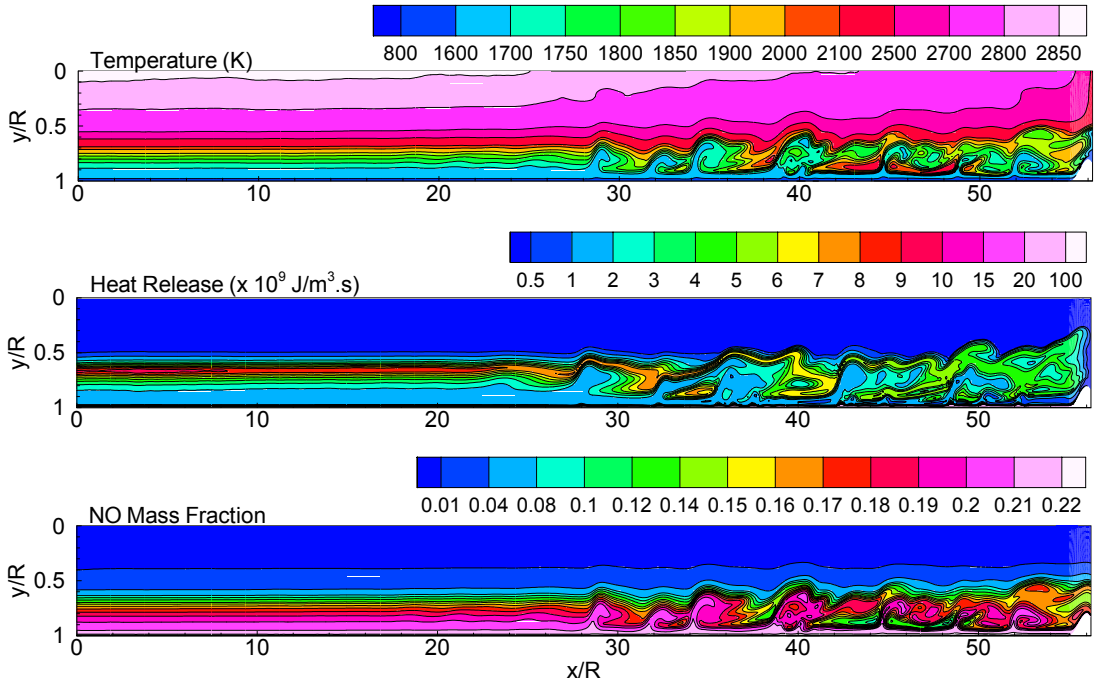

Figure 2. Snapshots of temperature, heat-release, and NO mass-fraction fields in rocket motor loaded with homogeneous double-base propellant.

In addition to homogeneous propellants, combustion of AP/HTPB composite propellants in rocket motors with acoustic oscillations has been carried out. This work consists of three parts. First, a combustion model of AP/HTPB composite propellant was established. Second, a parametric study was conducted to investigate the effects of pressure, AP particle size and cross flow on the AP/HTPB combustion wave structures and burning characteristics. Third, the gas-phase combustion response to acoustic oscillations was studied to explore motor stability behavior.

The physical model under consideration consisted of an axisymmetric chamber loaded with AP/HTPB propellant. A multiple flamelet model, containing fuel/oxidizer/fuel sandwich-type segment, was employed to investigate of the propellant flame structure which contains three parts, namely, primary diffusion, primary premixed and final diffusion flame. Since the flame standoff distances of the first two are of the order of 1 μm, attention was mainly focused on the final diffusion flame. The products of AP deflagration serve as the oxidizer in the final diffusion flame, which are modeled using the chemical kinetics mechanism proposed by Guirao and Williams. The major product in the deploymerization and pyrolysis of the HTPB fuel binder serves as fuel and was modeled with ethelene due to the similarity of the molecular structures. A two-step global chemical kinetics was employed to account for the final-stage diffusive combustion process. The formulation treats the complete

conservation equations of mass, momentum, energy, and species concentration, and accounts for finite-rate chemical kinetics. The numerical stiffness arising from chemical reactions and disparity of time and length scales was resolved be means of an additive semi-implicit method. A fourth-order central difference scheme along with matrix dissipation incorporated with TVD switches was used for spatial discretization.

Calculations have been carried out to investigate detailed combustion characteristics of AP/HTPB propellants and its interaction with local flow evolution in rocket. The effects of AP particle size and pressure were carefully studied. Results of burning rate show good agreement with experimental data in term of the pressure senstitivy, corss-flow conditions, and AP size effects. More importantly, the transient reponse of propellant combustion to impressed acoustic oscillations and the ensuing energy-relase fluctuations were examined systematically. Detailed discussions were given in Refs. 10-13.

3.1.3 Numerical Simulations with Experimental and Model Boundary Conditions (Culick)

In a series of works, Roh (Roh and Culick 1996, 1997, 1998, 1999) has made initial progress in extending previous work on numerical simulations to accommodate boundary conditions set by models of propellant combustion. Unlike the LES simulations described in the preceding sub-section, the somputational domain covers the volume of the chamber just short of the propellant at the boundary and does not include the combustion processes. Hence the boundart conditions must be specified independently of the numerical calculations. The idea is to provide the ability to introduce the results of modeling based either on analytical representations of the combutions processes or on experimental results. Success was shown for steady flow, but funding ceased before the formulation for unsteady flows could be completed. A particular difficulty with transient flows is constructing appropriate models including unsteady fluctuations of velocity parallel to the surface.

References

1. Jahnke C. and Culick, F.E.C., "An Application of Dynamical Systems Theory to Nonlinear Combustion Instabilities," AIAA 31st Aerospace Sciences Meeting (1993), AIAA Paper No. 93-0114. Published in *Journal of Propulsion and Power,* Vol. 10, No. 4 (1994) pp. 508–517.
2. Roh, T.-S. and Culick, F.E.C., "Applications of Various Methods of Analysis to Combustion Instabilities in Solid Propellant Rockets," JANNAF Combustion Meeting, November, 1996.
3. Roh, T.-S. and Culick, F.E.C., "Transient Combustion Responses of Homogeneous Propellants to Acoustic Oscillations in Axisymmetric Rocket Motors," 33rd AIAA/ASME/SME/ASEE Joint Propulsion Conference & Exhibit, Seattle, WA (July 1997) Paper No. AIAA 97-3325.
4. Roh, T.-S. and Culick, F.E.C., "Numerical Analysis of Transient Combustion Responses to Acoustic Oscillations in Axisymmetric Rocket Motors," 36th Aerospace Sciences Meeting & Exhibit, Reno, NV (Jan 1998), AIAA Paper No. 98-0253.
5. Roh, T.-S. and Culick, F.E.C., "Numerical Study of Acoustic Oscillations and Combustion Instabilities in Solid Propellant Rockets," 34th JANNAF Meeting, Tucson, AZ, December 1998.
6. Roh, T.-S., Cohen, N.S., Beddini, R.A. and Culick, F.E.C., "Numerical Analysis of Solid Rocket Motor Instabilities with AP Composite Propellants," 35th AIAA/ASME/SAE/ASEE Joint Propulsion Conference (June 1999) Los Angeles, CA, Paper No. AIAA 99-2804.

3.1.4 Two-Phase Flow Interactions in Rocket Motors

A numerical study on two-phase flow interactions in rocket motors with acoustic oscillations has been conducted. The gas phase was treated by means of the Eulerian approach which takes into account the complete conservation equations of mass, momentum and energy. The governing equations were solved numerically using a fully coupled implicit scheme based on the dual time-stepping integration algorithm. Particle phase was treated with the Lagrangian approach, and Runge-Kuta-Giles method was used to solve the particle-phase equations of motion. The attenuation and dispersion of traveling acoustic waves by suspended particles was studied first. Good agreement was obtained between the numerical and theoretical analysis. In particular, the optimum particle size for attenuating wave motions was obtained. The study on two-phase flow interactions with acoustic oscillations in rocket motors was then carried out. Results reveal that particle momentum and thermal relaxation times expressed in terms of particle size and acoustic wave properties play an important role in determining particle dynamics. The mutual couplings among acoustic oscillation, turbulent motion, and particle dynamics were also examined in depth. Strong interactions between periodic oscillations and turbulence suggest that acoustic oscillation provides additional mechanisms to transfer energy from periodic motions to turbulence, thereby enhancing turbulence intensity. On the other hand, the acoustic-wave induced vortical wave was effectively dissipated due to turbulence-enhanced momentum transfer. A comprehensive discussion of the subject is given in Refs 13 and 14.

References

1. Apte, S. and Yang, V., "Effect of Acoustic Oscillation on Flow Development in a Simulated Nozzleless Rocket Motor," *Solid Propellant Chemistry, Combustion, and Motor Interior Ballistics*, Progress in Astronautics and Aeronautics, Vol. 185, eds., V. Yang et al., 2000, pp. 791-822.
2. Flandro, G. A., Cai, W. D., and Yang, V., "Turbulent Transport in Rocket Motor Unsteady Flowfield," *Solid Propellant Chemistry, Combustion, and Motor Interior Ballistics*, Progress in Astronautics and Aeronautics, Vol. 185, eds., V. Yang et al., 2000, pp. 837-858.
3. Apte, S., and Yang, V., "Unsteady Flow Evolution in a Porous Chamber with Surface Mass Injection, I: Free Oscillation," *AIAA Journal*, Vol. 39, No. 8, 2001, pp. 1577-1586.
4. Apte, S., and Yang, V., "Unsteady Flow Evolution in a Porous Chamber with Surface Mass Injection, II: Acoustic Excitation," accepted for publication in *AIAA Journal*, 2001.
5. Hsieh, S. Y. and Yang, V., "A Preconditioned Flux-Differencing Scheme for Chemically Reacting Flows at All Mach Numbers," *International Journal of Computational Fluid Dynamics*, Vol. 8, 1997, pp. 31-49.
6. Roh, T. S. and Yang, V., "Transient Combustion Response of Homogeneous Solid Propellant to Acoustic Oscillations in a Rocket Motor," *Proceedings of the Combustion Institute*, Vol. 27, 1998, pp. 2335-2341.
7. Roh, T. S., Apte, S., and Yang, V., "Combustion Dynamics of Homogeneous Solid Propellant in a Rocket Motor with Acoustic Excitations," *Solid Propellant Chemistry, Combustion, and Motor Interior Ballistics*, Progress in Astronautics and Aeronautics, Vol. 185, eds., V. Yang et al., 2000, pp. 885-906.
8. Apte, S. and Yang, V., "Turbulent Flame Dynamics of Homogeneous Solid Propellant in a Rocket Motor," *Proceedings of the Combustion Institute*, Vol. 28, 2000, pp. 903-910.
9. Apte, S. and Yang, V., "Numerical Simulation of Unsteady Flow Evolution and Flame Dynamics in a Solid Rocket Motor," AIAA Paper 2001-0340, presented at the 38th AIAA Aerospace Sciences Meeting and Exhibit, January 2001.
10. Chu, W. W. and Yang, V., "Dynamic Responses of Diffusion Flames to Acoustic Oscillations in a Simulated Solid Rocket Motor," AIAA Paper 96-0883, presented at 34th Aerospace Sciences Meeting, January 1996.
11. Chu, W. W. and Yang, V., "Oscillatory Combustion of AP-Based Composite Propellant in a Rocket Motor Flow Environment," AIAA Paper 96-2885, presented at 32nd AIAA/ASME/SAE/ASEE Joint Propulsion Conference, July 1996.
12. Cai, W. D. and Yang, V., "A Model of AP/HTPB Composite Propellant Combustion," AIAA Paper 00-0311, presented at the 38th AIAA Aerospace Sciences Meeting & Exhibit, January 2000.

13. Cai, W. D., Two-Phase Flow Interactions and Combustion of AP/HTPB Composite Propellant in Rocket Motors with Acoustic Excitations, Ph.D. Thesis, The Pennsylvania State University, University Park, PA, 2001.
14. Cai, W. D. and Yang, V., "Two-Phase Turbulent Flow Interactions in a Rocket Motor with Acoustic Waves," AIAA Paper 98-0161, presented at 36th Aerospace Sciences Meeting, January 1998.
15. Yang, V., Brill, T., and Ren, W. Z. (eds.), *Solid-Propellant Chemistry, Combustion, and Motor Interior Ballistics*, AIAA Progress in Astronautics and Aeronautics, Vol. 185, June 2000.

3.2 Linear and Nonlinear Analyses of Motor Dynamics (Culick, Caltech)

The work carried out in this sub-task continued development of a general analytical framework for analyzing the dynamics of solid propellant rocket motors. While motivated by observations of the behavior of solid rockets, the results obtained are applicable to all types of combustion systems. In that sense, technology transfer is an intrinsic characteristic of the work.

We will refer to previous publications for details of the accomplishments during the Caltech MURI program, in particular, three Ph.D. theses (Burnley 1997; Isella 2000; and Seywert 2000) and the lengthy discussion by Culick (2000). The following remarks are very much in the nature of a tutorial, intended to motivate examination of the literature. The chief accomplishments during the past five years were related to nonlinear behavior, including the influences of noise.

Certain features of predicted nonlinear behavior have led to the conclusion that reliance of the combustion response to pressure fluctuations is likely inadequate, if not misleading. The basis for that assertion is the result that the amplitudes of limit cycles seem not to show the sensitivity to small changes of the response function that has often been observed. On the other hand, reinforcing previous suspicions expressed by many other workers in the field, it appears that the dynamical behavior is considerably more sensitive to small changes in the velocity-coupled combustion response. Results supporting this assertion have been discussed in Section 2.4.4. This conclusion has significant implications for interpretation of the dynamical behavior of motors and especially, in the near-term, for the sort of theory, modeling and laboratory tests that should be supported in future work.

In the context of the general theory of combustion instabilities, this use of the analysis of chamber dynamics with the combustion dynamics as a boundary condition in the feedback loop (see Figure I-7) demonstrates the remarkable power of the analytical framework. The methods will eventually be available for routine use in software currently being prepared (French 2001).

The analytical framework used in this work has its origins in the Principal Investigator's Ph.D. Dissertation in which spatial averaging was introduced by solving the problem of linear instability of liquid rockets by using a Green's function (Culick 1961; 1963). That work also included the first (incomplete) application of systematic expansion in two small parameters, the Mach numbers of the mean and unsteady flows. The approach based on spatial averaging was later extended to treat nonlinear dynamical behavior motivated by observational results for solid propellant rockets (Culick 1973; 1975). Subsequently, the approach has been developed further to investigate special characteristics of nonlinear behavior in combustion chambers and to widen the scope of applications, for example to systems with feedback control and to examine some influences of noise. The use of systematic expansion procedures has been followed in other works, as for example in the important investigations of vorticity

by Flandro and co-workers, some of which is reported in Section 3.3 here (see also the forthcoming dissertation by Malhotra (2002).

Probably the greatest deficiency in the framework as it presently exists is an apparent limitation to relatively small Mach numbers of the mean flow. Work in progress by Malhotra (2002) and at Penn State (Professor Yang, private communication) may help correct this matter.

The first works on nonlinear behavior in combustors was carried out at Princeton in the 1960's (Sirignano, Mitchell and Zinn, all students of Crocco). Several of the now well-known aspects of nonlinear behavior in combustion systems were first reported in those investigations, and later re-discovered by Culick and his students. However, the formulation and methods used by the Princeton group seems not to have developed, or even used, by others since that time. There are probably several reasons for that state of affairs. Among the reasons are: the analyses were based on methods of solving the partial differential equations of motion written for one-dimensional mean flows; the time-lag representation was used for the combustion response, in principle perfectly general for linear behavior but not for nonlinear behavior and as applied in the works cited, also implying a particular unrealistic dependence of the combustion response on frequency; and the analyses required very involved and tedious formal calculations before quantitative results could be computed. The last seems to have had at least two important consequences: the true meaning and generality, or lack of it, are sometimes obscure; and the extremely complicated and apparently particular nature of the analyses have discouraged others from pursuing the approaches further. Thus there are apparently no examples of applications by others.

Subsequently, Zinn and his students developed the first application of a form of Galerkin's method to problems of combustion instabilities, chiefly for liquid propellant rockets. Those were important works, again illustrating some features of nonlinear behavior for the first time (*e.g.* some aspects of the behavior of the amplitudes of acoustic modes in the formation of limit cycles). However, failure to respect systematic expansion procedures caused the analyses to be difficult to understand and in some cases results are misleading. Also, although the methods were applied to solid propellant rockets, no attention was paid to using realistic mean flow fields or to the role of vorticity (which was ignored in all those works). Again, the Georgia Tech analysis based on Galerkin's method seems to have been uniformly ignored by others, partly at least for the deficiencies noted. And there has been no further development at Georgia Tech since 1974. Seywert (2002) has initiated a more detailed comparison of the procedures favored by Georgia Tech and Caltech.

3.2.1 Analysis of the Global Dynamics of a Combustor

The combustion processes and flow in a combustion chamber are astonishingly complicated. Yet the pressure recorded is a simple, accurate observation and could be interpreted, for example, the recording of the displacement of a mass within a simple mechanical system such as that discussed in Section 3.2. It must therefore be possible, in some degree of approximation, to find a simple quantitative representation of the behavior behind such a pressure record. To be most useful and informative, such an approximation should not itself involve direct solutions of partial differential equations describing all chemical and physical behaviors defining the general problem.

For many years the approach summarized in this section has proven to be productive of basic understanding and of results having direct practical applications. The principal qualitative consequence has been stated at the end of Section 2, that the dynamics of a combustor can be expressed in terms of the simple oscillators described in the preceding paragraphs.

The following remarks constitute a superficial summary of the basis for this conclusion.

In the first instance the basic physical principles are formulated mathematically as partial differential equations. Those equations contain terms representing all processes and govern the total unsteady motions. If the necessary information is provided to allow quantitative representation of the processes, it is possible to carry out very useful numerical simulations described in a companion paper (Yang 2000). However, here we are concerned with application of some methods of analysis and for that purpose the equations must be approximated. The basis for doing so is an expansion of the dependent variables. In problems of combustor dynamics there are two small parameters characterizing the flow and suitable for formulating such an expansion: the Mach members of $\overline{M}_r$ of the mean flow and M'_r of the unsteady field. A two parameter expansion can then be worked out and used to define several classes of problems including linear stabilities and several sorts of nonlinear behavior (*e.g.* see Culick 1999). The details are irrelevant here: what is important to realize is that a systematic procedure exists to construct equations which experience has shown accurately describe observed behavior.

Because such a description based on partial differential equations is local in space, applications to macroscopic systems require that a considerable gap be spanned. One approach for doing so is spatial averaging. Several methods exist for spatial averaging, a general method that has been widely used for more than a century in many fields. The earliest forms of the method were developed for applications to structures; *e.g.* Rayleigh's method, Galerkin's method and others that can be viewed as forms of the *method of least residuals.* In general, spatial averaging has two great advantages: the partial differential equations are reduced to total differential equations; and the formulation is applicable to both linear and nonlinear problems.

As noted above it was the group at Georgia Tech who first applied a modified form of the method of least residuals to linear and nonlinear combustion instabilities in liquid and solid rockets (Powell 1970; Zinn and Powell 1970; Lopes and Zinn 1972; and other publications). Most of those works have technical restrictions intrinsic to particular details of the methods used, usually because the average velocity is taken to be uniform and the unsteady velocity is assumed to be derivable from a potential. The second is a serious matter partly, but not completely, overcome in the method used here[9].

Whatever procedure of spatial averaging is used, the starting point is the set of partial differential equations of conservation for a reacting mixture. Further modeling is required to represent combustion and other processes, but that task may be accomplished later in the analysis. Because observations are made of pressure waves, it is reasonable to seek a wave equation for pressure with perturbations—source terms in the volume and at the boundary that represent the distinctions between problems of combustion dynamics and classical acoustics. The derivation

[9] Seywert and Culick (1998) have given an incomplete discussion and comparison of some formal aspects of the two approaches to application of spatial averaging in this field. Further considerations of details are in progress.

follows the procedure used to obtain the classical acoustics equation, difficult only because of technical complications arising with the many terms in the equations.

3.2.2 Acoustic, Vorticity and Entropy (Temperature) Waves

The flow is viewed in the conventional way as the sum of an average or mean field and the unsteady fluctuations. All unsteady disturbances are accounted for, including those associated with the acoustic field, vorticity and entropy. It is fundamentally important to make the distinction between these three types of disturbances, referred to as waves because in combustion chambers, they all propagate, although with different speeds. The physical properties of those waves, and their contributions to observed behavior, are especialy noticeable in combustor flows for the following reasons.

Combustion instabilities have always been observed as anomalous behavior of the pressure field, appearing usually as reasonably well-defined oscillations. It seems now obvious that, given the frequencies observed, the oscillations in pressure records must betray the presence of acoustic waves. But that conclusion becomes less clear when one considers the medium in which the waves must propagate: there are variations of the average velocity and temperature; regions of separated flow are often present: and in full-scale combustors, the flow is inevitably turbulent, *i.e.* it is characterized by a broad spectrum of vorticity fluctuations. It should seem then surprising that well-defined acoustic waves are present: the reasons that acoustic waves are indeed identifiable under these conditions have been explained by Chu and Kovasznay (1956).

Taking advantage of previous special results, Chu and Kovasznay showed that, quite generally in the limit of small amplitudes, any disturbance in a compressible medium can be constituted of the three types or modes of waves: *acoustic, vorticity*, and *entropy* waves. Moreover, in a uniform average flow, those waves propagate independently of one another. Acoustic waves propagate at the speed of sound while vorticity and entropy waves 'propagate', or better, are convected, with the speed of the mean flow[10]. Entropy waves can be regarded as 'spots' of temperature different from the average value.

Thus, the first step to understanding the physical basis of combustion instabilities is to realize that there is scientific basis for the obvious presence of organized acoustic waves even within a complicated turbulent flow field. That they seem so often to dominate the unsteadiness observed in the pressure field is due chiefly to three reasons:

(i) the two other types of waves (vorticity and entropy) carry no pressure fluctuations in the limits of small amplitudes;
(ii) even in non-uniform flow the acoustic waves are only weakly affected by interactions with the vorticity and entropy waves; and
(iii) small local changes of pressure or in some circumstances, velocity, in a reacting flow can cause quite substantial changes in the rate of the energy released in chemical reactions; only a small fraction of that energy converted to mechanical energy may produce further significant local fluctuations of pressure.

[10] It is this difference in propagation speeds that is partly responsible for the difficulties in the current form of the averaging and expansion procedure described here.

It is the general process (iii) that is responsible for the internal feedback loop shown in Figure I-2 in the Introduction. Hence once again we conclude that the key to understanding, and controlling, combustion instabilities is associated with the coupling between combustion and combustor dynamics.

3.2.3 The Wave Equation for Unsteady Flow in a Combustor

The remarks in the preceding section describe the physical basis for modeling a broad class of unsteady notions, in any combustion chamber, with the equation for waves of pressure, but containing some additional forms not arising in classical acoustics. Those additional terms represent sources of mass, momentum and energy associated with combustion processes; interactions between the acoustic waves and the mean flow; and interactions among the three modes of motion, acoustic, vorticity and temperature waves. The details are unimportant here, so we simply quote the formal result, the perturbed wave equation for the pressure with its boundary condition on the pressure gradient:

$$\nabla^2 p' - \frac{1}{\bar{a}^2}\frac{\partial^2 p'}{\partial t^2} = h \tag{3.8}$$

$$\nabla p' = -f \tag{3.9}$$

Several points must be emphasized but without complete explanation:

(i) Equation (3.8) and its boundary condition (3.9) are valid only in an approximation, which is well defined and understood. The approximation has been shown by long experience to be valid for a wide variety of practical conditions.
(ii) The functions h and f contain formal representations of all relevant physical and chemical processes, constructed to the approximation cited in (i). However, to obtain explicit and quantitative results, those processes must be modeled, tasks outside the formal procedure.
(iii) Equations (3.8) and (3.9) are nonlinear, but in the limit of small amplitudes of motion, describe linear behavior, including stability.

3.2.4 Spatial Averaging; Combustor Dynamics as a Collection of Oscillators

In classical acoustics, with no combustion and flow, the functions h and f are missing unless there are other sources present, such as moving portions of the boundary. The idea now is to compare the two general problems, with and without the source functions. The second problem is the unperturbed classical problem defining the natural modes and frequencies described by the homogeneous wave equation and boundary condition:

$$\nabla^2 \psi_n + k_n^2 \psi_n = 0 \tag{3.10}$$

$$\hat{n} \cdot \nabla \psi_n = 0 \tag{3.11}$$

For some cases, the equation governing ψ_n is more complicated because the ψ_n must be calculated for the same geometry *and* distribution of average temperature as exists in the actual problem. Nonuniform temperature leads to additional terms in (3.10). In practical applications, determining the ψ_n may be an expensive procedure, but it can

always be accomplished. Work in progress will provide a convenient automated means of computing the Ψ_n and k_n for arbitrary configurations (French 2000).

The grand interpretation of the point of view taken here is founded in the basic idea discussed that any *small* disturbance can be regarded as a synthesis of three types of waves. For the matters in question here, experience has shown that the idea can be made even more precise: the dynamical motions called combustion instabilities consist chiefly of pressure perturbed by the influences of vorticity and entropy waves. Therefore, we take as the primary representation of the field a synthesis of acoustic waves, the ψ_n defined by the above two equations, having time-dependent amplitudes η_n:

$$p'(\vec{r};t) = \bar{p}\sum_{o}^{\infty} \eta_n(t)\psi_n(\vec{r}) \tag{3.12}$$

After the two problems defined above (the actual and the unperturbed problems) are compared (subtracted) and averaged with a weighting function (Ψ_n) over the volume of the chamber, we find the basic equations for the theory of global chamber dynamics:

$$\frac{d^2\eta_n}{dt^2} + \omega_n^2\eta_n = F_n \tag{3.13}$$

The forcing functions F_n are computed with the formula

$$F_n = -\frac{\bar{a}^2}{\bar{p}E_n^{\,2}}\left\{\iiint h\psi_n dV + \oiint f\psi_n dS\right\} \tag{3.14}$$

and

$$E_n^2 = \int \psi_n^{\,2} dV \tag{3.15}$$

Equation (3.13) is the basis for the statement emphasized at the beginning of this section. The left hand side represents the motion of a simple undamped oscillator, its 'displacement' being the amplitude of the corresponding natural mode of the chamber. Although not shown by the symbolic form (3.14), the force F_n contains linear parts—attenuation, frequency shifts and mode coupling—as well as nonlinear behavior, also including nonlinear coupling.

Thus we can split F_n into several meaningful parts and write the oscillator equations in the form

$$\begin{aligned}&\frac{d^2\eta_n}{dt^2} + D_{nn}\frac{d\eta_n}{dt} + (\omega_n^2 + E_{nn})\eta_n \\ &= -\sum^{i\neq n}\left[D_{ni}\dot{\eta}_i + E_{ni}\eta_i\right] + F_n^{\,NL}\end{aligned} \tag{3.16}$$

where $F_n^{\,NL}$ stands for all nonlinear contributions to the force. The left-hand side of (3.16) represents the behavior of a damped oscillator and is identical with (3.1); the summation on the right side contains all the linear coupling terms, and $F_n^{\,NL}$ is the nonlinear part. Thus equation (3.15) is the theoretical basis for the italicized assertion at the end of Section 2.

Remarks:

(i) It is especially important to understand that the function F_n defined by (3.14) contains *formal* representations of all relevant physical processes, but is by itself inadequate to give quantitative results. In passing from (3.12) to (3.16) we have written F_n

$$F_n = -D_{nn}\dot{\eta}_n - F_{nn}\eta_n - \sum^{i\neq n}\left[D_{ni}\dot{\eta}_i + E_{ni}\eta_i\right] + F_n^{\,NL}$$

thereby identifying the various coefficients D_{nn}, D_{ni}…etc. Comparison of (3.14) and (3.17) suggests what is true, that those coefficients are defined by integrals over the volume and on the surface of the chamber. The integrals are functions representing the various processes. Modeling, based either in theory or experimental results, is required to provide the necessary representations.

(ii) Each linear oscillator—*i.e.* each normal mode—is characterized by three parameters, of which two arise from perturbations to a classical undamped system:

(1) natural frequency, ω_n;
(2) growth or damping constant $D_{nn}=-2\alpha_n$, negative (*i.e.* $\alpha_n>0$) for unstable motions;
(3) the nonlinear physical processes contained in F_n^{NL} are those responsible for limiting linearly unstable motions, *i.e.* for forming limit cycles, and for producing subcritical bifurcation (triggered or nonlinear instabilities)
(4) parts of the coefficients shown and of F_n^{NL} follow from gas dynamics and hence are known; the remaining contributions must be found from models of the processes in question. In that regard, the combustion processes are the most important.

3.2.5 Linear Stability

The formalism described here has been widely used to investigate linear stability for more than thirty years. Linear problems are described by (3.16) with F_n^{NL} neglected:

$$\frac{d^2\eta_n}{dt^2}-2\alpha_n\frac{d^2\eta_n}{dt}+\left(\omega_n^2-2\omega_n\delta\omega_n\right)\eta_n = \sum^{i\neq n}\left[D_{ni}\dot{\eta}_i+E_{ni}\eta_i\right] \tag{3.17}$$

Almost all works dealing with linear stability concentrate on the stability of normal modes. If, as seems often to be the case, the coupling terms on the right hand side are small and can be ignored, (3.17) becomes

$$\frac{d^2\eta_n}{dt^2}-2\alpha_n\frac{d\eta_n}{dt}+\left(\omega_n^2-2\omega_2\delta\omega_n\right)\eta_n=0 \tag{3.18}$$

Use of (3.18) does not rest on ignoring the linear coupling. A well-known procedure in the theory of linear systems leads to the same form by a transformation of variables: that is the proper justification for using (3.18). In any case, the solution for η_n gives the time evolution of the amplitude of the n^{th} mode, following an initial disturbance $\hat{\eta}_n\cos\Phi_n$

$$\eta_n(t)=\hat{\eta}_n e^{\alpha_n t}\cos\left(\omega_n\sqrt{1-\zeta_n^2}\right)t \tag{3.19}$$

and

$$\zeta_n=-\frac{\alpha_n}{\omega_n} \tag{3.20}$$

In this field α_n is conventionally defined to be positive if the n^{th} mode is unstable. The stability boundary is therefore located by setting $\alpha_n=0$. This is far from the empty result it may appear to be, because α_n is a sum of several contributions arising from the linear processes contained in F_n, equation (3.14). Those contributions represent the effects of the linear processes accounted for in the functions k and f defined in (3.8) and (3.9). As a consequence of the spatial averaging, α_n contains integrals over the volume of the chamber and over the boundary

covering largely the burning surface, and closed by the area of the entrance to the nozzle. Schematically we can therefore express α_n as

$$\begin{aligned}\alpha_n &= [\alpha_n]_{nozzle} + [\alpha_n]_{particle\,damping} + [\alpha_n]_{mean\,flow/\,acoustics} \\ &+ [\alpha_n]_{surface\,combustion} + [\alpha_n]_{vortex\,shedding} + [\alpha_n]_{distributed\,\,combustion} \\ &+ [\alpha_n]_{other}\end{aligned} \tag{3.21}$$

Before discussing briefly the pieces of α_n, we note a useful interpretation. The envelope of the pressure oscillations varies as $e^{\alpha_n t}$, *i.e.*

$$[p']_{amp} = ke^{\alpha_n t} = |\eta_n|_{\max}$$

where k is independent of time. It is a result of classical acoustics that the time-averaged energy $\langle E_n \rangle$ of an oscillation is proportional to the square of the pressure amplitude, *i.e.* where k_1 is another constant in time. Differentiating this formula leads to

$$\alpha_n = \frac{1}{2}\left(\frac{1}{\langle E_n \rangle}\frac{\langle dE_n \rangle}{dt}\right) \tag{3.22}$$

The growth (or decay) constant is equal to one-half the fractional rate of change of time–averaged energy. Thus α_n given by (3.21) is most easily regarded as a sum of rates of energy losses and gains. It is fundamentally important to understand that the growth constant defined here, and normally observed experimentally, is related to the growth (or decay) of acoustic energy, **not** the total energy of unsteady motions. Then for linear problems, the growth or decay constant for the **acoustic** waves necessarily has the form (3.21), more terms appearing if additional processes are accounted for. Contributions from the exhaust nozzle and particle damping can be estimated sufficiently accurately, for most practical purposes, with well-known methods. The part due to mean flow/ acoustics interactions is determined within the procedure used to expand the basic partial differential equations. For most instabilities encountered in practice, the most important mechanism is associated with the dynamics of surface combustion, discussed in Section II here. This part of the growth constant is proportional to an integral of the combustion response function over the burning surface.

Vortex shedding enters the problem as three different phenomena: formation of large coherent vortices arising from unstable shear layers shed from edges and obstructions; growth of coherent vortices out of the region of high shear adjacent to the burning surface ("parietal vortex shedding"); and the creation of both steady and unsteady distributed vorticity due to interactions between the flow within the chamber and the flow entering from the burning surface. Parietal vortex shedding was discovered and explored by French researchers (Vuillot et al.) working on the instability found in the Ariane 5 booster motors. It was not a subject of the MURI program. Neither was the matter of shedding from obstacles, a problem first identified by Flandro and Jacobs and subsequently investigated by Flandro and his co-workers as well as Dunlap and others at the Chemical Systems Division (CSD) of United Technologies, Inc. Flandro summarizes recent work on distributed vorticity in the following section.

The actual contributions of distributed combustion to stability in solid propellant rockets remains an open question. In practical situations, the most likely origin is residual combustion of aluminum far from the burning surface. Although there exists suggestive evidence, and some attention has been given to the problem (Beckstead and students) the dynamics of distributed combustion was not treated in the MURI program.

3.2.6 Nonlinear Behavior in Combustion Instabilities

As noted in Section 3.2.1, certain basic features of nonlinear behavior in rocket motors were first reported by the Princeton group in the 1960s and early 1970s. Notable results were the discovery of limit cycles in systems described by nonlinear gasdynamics sustained by linear combustion dynamics (time-lag representation); and examples of nonlinear or pulse instabilities in linearly stable systems, although some confusion exists in respect to the stability or instability of the limit cycles produced.

Prior to the MURI program, the use of a continuation method had been introduced at Caltech to investigate the influences of various nonlinear processes on the properties of limit cycles (Jahnke and Culick, 1994). That approach has proven to be the most effective means of investigating limit cycles. It is especially important that unlike the previous works cited above, bifurcation points and the stability of limit cycles are unambiguously determined as part of the analysis. Further applications of the method have been reported in three Ph.D. theses (Burnley, 1996; Isella, 2001; and Seywert, 2001) and in various papers referenced elsewhere in this report.

An important aspect of the nonlinear analysis is that it provides a framework within which the influences of noise are easily included. Since investigations of noise formed a novel, though small, part of the MURI program, they merit a brief discussion here.

3.2.7 Noise and Forced Oscillations

Combustion processes and flow in all types of combustion chambers generate substantial noise. The precise origins are well-known and have received relatively little attention, partly because while the noise is an irritation, it contains very little energy, so changes in the noise-level—even its complete elimination—would have no measurable effect on the designed performance of the system.

From time-to-time questions have been raised concerning possible connections between the noise field, regarded as distributed stochastic sources, and the dynamics of the combustor, in particular stability. The observed ‘noise’ is really a part of the pressure recorded by transducers. Hence, like the entire pressure record itself, the properties of the noise must in fact somehow reflect also the properties of the chamber. Is it possible to learn something about the stability of a motor by suitable processing of pressure records?

It is assumed that the behavior of the system for which the data is given can be represented by a simple model, here a collection of damped simple oscillators. Then some sort of ‘curve-fitting’ procedure is used to extract values for the parameters characterizing the model. In our work (Seywert and Culick, 1999; 2000) we have used a ‘maximum entropy method’ suggested by Hessler and available as part of the MATLAB Toolbox. Figure 4 shows one result, the reconstruction of a smoothed spectrum for the trace shown in Figure 3.

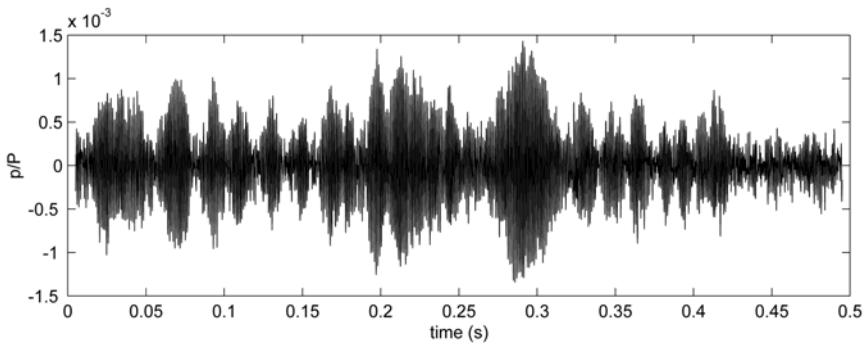

Figure 3.

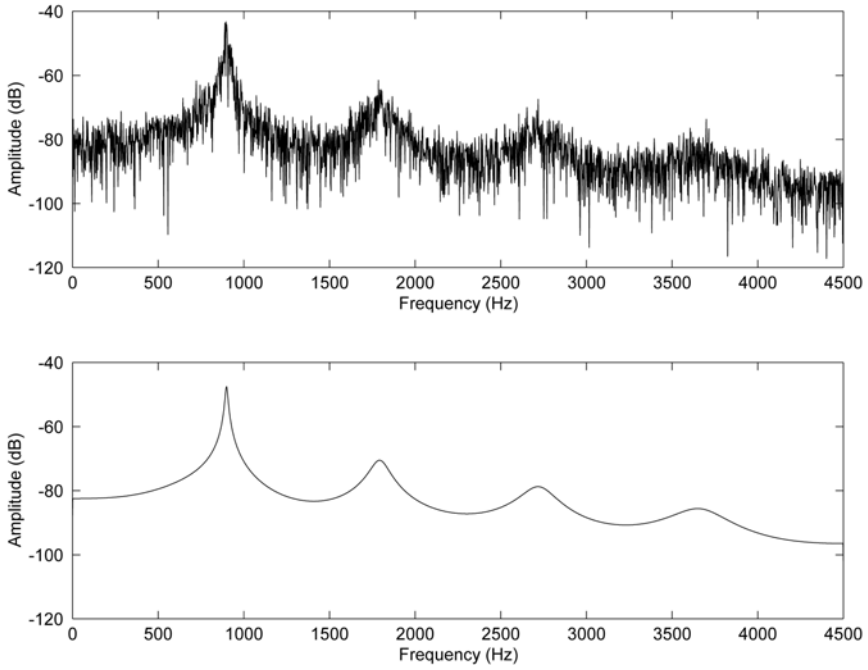

Figure 4.

Our conclusion is that, due to the randomness of the forcing function, the values of the α_n carry uncertainties varying from ten to more than thirty percent. Whether or not the method is useful in practice therefore will depend very much on the particular problem in question. However, several general remarks follow from the calculations and examples we have done:

(i) Some amount of noise must be present to excite the response of the chamber. For realistic levels, as far as we can estimate, the consequent uncertainties in the inferred values of the decay constants α_n are too large for quantitative work;
(ii) For practical applications, full-scale motors must be fired, an expensive procedure.
(iii) It is especially important to realize that this method can be applied only to stable motors.
(iv) Moreover, the values of α_n are of course net values, differences between the damping and driving: there is no possibility with this method alone to learn anything about the damping and driving themselves. To do so requires separate determinations of the contribution due, say, to the damping processes.

(v) Finally, any results obtained with this method are strictly valid only for the motor in question. It is conceivable that with a sufficiently large body of empirical information collected in this fashion, something could be learned of general behavior. However, it seems an expensive and tedious approach.

It's an interesting and possibly useful idea to apply methods of system identification. However, just as in the field of controls where most of the subject of system ID has been developed, there is no substitute for understanding the system from first principles—particularly in the long term.

3.3 Unsteady Motor Flowfields and Interactions with Flame Zone Gas Dynamics (Flandro)

A central theme in the combustion instability problem and its link to the chemistry elements of the MURI program is the dynamic behavior of the combustion zone and its coupling to the chamber unsteady fluid dynamics. Task 3.3 began as an in-depth study of the flame zone with the object of correcting limitations and errors in earlier models. In particular, there was a clear need to introduce multidimensional effects since the earlier one-dimensional treatments gave no information concerning the production and propagation of vorticity in the flame zone; a strictly multidimensional effect. Recent work had made it clear that predictive models of combustion instability must at minimum accommodate physically correct boundary conditions such as the no-slip constraint on solid surfaces. Standard analytical models are based on irrotational fluid dynamics (acoustics) assumptions, which preclude the satisfaction of the no-slip condition.

As the work on the combustion zone modeling proceeded, it became apparent that additional study of the chamber gasdynamics was needed. For example, attempts to extend the classical combustion instability theory by inclusion of rotational flow effects led always to the same result, namely that all rotational corrections, including the Culick flow turning effect cancelled. The reason for this became clear, when it was realized that all of the classical models for the system stability are based on an acoustic model. That is these calculations seek to estimate the rate of growth or decay of acoustic waves only. However, the unsteady flow field in a realistic rocket motor geometry is composed of both irrotational (acoustic) components and rotational corrections (vorticity waves) that naturally accompany the acoustic motions. The vorticity waves must be present in order that the no-slip constraint is satisfied both on inert surfaces and on burning propellant surfaces whenever there are gas motions parallel to such surfaces. With these observations in hand, a revised set of objectives was formulated during the last two years of the research program, and the work was redirected to accomplish the following:

- Reconstruct the basic rocket motor stability analysis to include *all* unsteady flow effects including acoustic (irrotational) and vortical (rotational) wave motions.
- Include all viscous forces in the stability analysis including the dilatational effects that are usually neglected.
- Formulate a method to integrate effects of turbulence directly into the stability calculations. The numerical work of Yang and his coworkers provides the required distributions of eddy viscosity and other required parameters in a given motor geometry.
- Dimensional effects related to the production and propagation of vorticity with all viscous effects included.
- Demonstrate the application of the improved models in a wide variety of motor geometries and flow field conditions.

These objectives were fully achieved; the results were tested by comparison to experimental rocket motor data of various types. One indication of success (to be detailed in the next section) is the prediction of new instability effects that do not appear in the traditional calculations. In particular, new terms were discovered that clarify the origins of unexplained instabilities that have been found in large solid rocket motors. These observations have been mainly from the French researchers who identified what they call the *parietal vortex shedding* effect which has led to important operational difficulties in the Ariane solid rocket boosters.

The results of the Task 3.3 study can be summarized in three parts: enhancements to stability modeling, clarification of some misunderstandings related to rotational flow effects, improved combustion zone analysis, and inclusion to turbulence effects in the combustion instability problem. These findings are summarized in the following paragraphs.

3.3.1 Improved Motor Stability Calculations

All current solid propellant rocket instability calculations (*e.g.* Standard Stability Prediction Program, SSPP) account only for the evolution of acoustic energy with time. However, the acoustic component represents only part of the total unsteady system energy; additional kinetic energy resides in the shear waves that naturally accompany the acoustic oscillations. Since most solid rocket motor combustion chamber configurations support gas oscillations parallel to the propellant grain, an acoustic representation of the flow does not satisfy physically correct boundary conditions. It is necessary to incorporate corrections to the acoustic wave structure arising from generation of vorticity at the chamber boundaries. Modifications of the classical acoustic stability analysis have been proposed that partially correct this defect by incorporating energy source/sink terms arising from rotational flow effects. One of these is Culick's *flow-turning* stability integral; related terms appear that are not found in the acoustic stability algorithm.

In the Task 3.3 work a more complete representation of the linearized motor aeroacoustics was utilized to determine the growth or decay of the system energy with *all* rotational flow effects accounted for. Significant changes in the motor energy gain/loss balance result; these help to explain experimental findings that are not accounted for in the present acoustic stability assessment methodology. In particular, the origins of several types of vortex-driven instabilities observed in in large solid propellant motors are illuminated.

Culick's papers on combustion instability[1-5] published in the early 1970's are the foundation for all stability prediction methods now in use.[6,7] His method is based on three crucial assumptions:

1. small amplitude pressure fluctuations superimposed on a low-speed mean flow,
2. thin, chemically reacting surface layer with mass addition, and
3. oscillatory flow-field represented by chamber acoustic modes.

The first assumption allows linearization of the governing equations both in the wave amplitude and the surface Mach number of the mean injected flow. The second causes all surface reaction effects, including combustion, to collapse to simple acoustic admittance boundary conditions imposed at the chamber surfaces. The last assumption oversimplifies the oscillatory gas dynamics by suppressing all unsteady rotational flow effects; the acoustic

representation is strictly irrotational. Concern for this omission was addressed partially by Culick in a paper in which he introduced his well-known rotational mean flow model.[2] Stability calculations based on this improved mean flow representation produced no significant changes in the system stability characteristics. On this basis, it has since been generally assumed that all vorticity (rotational flow effects), including the unsteady part, have negligible influence on combustion instability growth rate calculations.

Considerable progress has been made in the last decade in understanding both the precise source of the vorticity and the resulting changes in the oscillatory flow-field Analytical,[8-16] numerical,[17-22] and experimental investigations[23-26] have demonstrated that rotational flow effects play an important role in the unsteady gas motions in solid rocket motors. Much effort has been directed to constructing the required corrections to the acoustic model. This has culminated in a comprehensive picture of the unsteady motions that agrees with experimental measurements,[8-10] as well as numerical simulations.[11]

These models were used in carrying out three-dimensional system stability calculations,[8,9] in a first attempt to account for rotational flow effects by correcting the acoustic instability algorithm. In this process one discovers the origin, and the three-dimensional form, of the classical *flow-turning* correction; related terms appear that are not accounted for in the SSPP algorithm. In particular, a rotational correction term was identified that cancels the flow-turning energy loss in a full-length cylindrical grain. However, all of these results must now be questioned because they are founded on an incomplete representation of the system energy balance.

Culick's stability estimation procedure is based on calculating the exponential growth (or decay) of an irrotational acoustic wave; the results are equivalent to energy balance models used earlier by Cantrell and Hart.[27] In all of these calculations the system energy is represented by the classical Kirchoff (acoustic) energy density. Consequently, it does not represent the *full* unsteady field, which must include both acoustic and rotational flow effects. Kinetic energy carried by the vorticity waves is ignored. It will be demonstrated in this paper that the actual average unsteady energy contained in the system at a given time is about 25% larger than the acoustic energy alone. Furthermore, representation of the energy sources and sinks that determine the stability characteristics of the motor chamber must also be modified. Attempts to correct the acoustic growth rate model by retention of rotational flow source terms only,[8,9] preclude a full representation of the effects of vorticity generation and coupling.

In fact, there is a convincing body of evidence pointing to the existence of other aeroacoustic coupling mechanisms that are not incorporated in the current acoustic-stability theory. For example, the so-called parietal or surface vortex shedding (PVS) has been identified some years ago as a source of instability that eludes classic theory.[28] The corresponding phenomenon was first detected by numerical simulations of 1:5 subscale models of the French Ariane V P230 MPS booster[29-32] that was known to exhibit large amplitude oscillations.[33] This new type of instability was especially important in long, segmented rocket motors such as the Japanese H-II vehicle,[34] the Titan 34D SRM,[35] the Titan IV SRM/SRMU (upgrade),[36-39] the Shuttle Rocket Booster SRB,[40] and other elongated motors whose dimensionless lengths ranged from 15 to 25.

In order to compensate for the inability of classic theory[3,5,41-48] to explain the large pressure oscillations driven by so-called "crawling" vortices,[29] a number of dedicated studies have been carried out hoping to improve our understanding of the suspected mechanism.[28] Credit should be given, in that regard, to Vuillot, Avalon, Casalis,

Griffond, Lupoglazoff, Traineau, Dupays, Pineau, Tissier, Ugurtas and co-workers who have tried experimental,[28,49-52] numerical,[53-60] and theoretical avenues[61-64] to elucidate the origin of PVS coupling. It should also be noted that Casalis, Avalon, Pineau, and Griffond have based their theoretical study on linear instability theory introduced in 1969 by Varapaev and Yagodkin.[65] Their efforts have provided an alternate source of instability whose omission in classic analyses has led them to associate some of the unforeseen instabilities to the hydrodynamic evolution and inception of turbulence.[61,62] At the outset, their results have been limited in fully explaining the observed PVS-related mechanisms.

At the conclusion of these studies,[30-32,50-52] speculations that resonance-like pressure amplifications were caused only by vortex shedding at annular restrictors or inhibitor rings were laid to rest when similarly intense vorticity-generated oscillations were observed in unsegmented rocket motors. As noted by Ugurtas *et al.*,[66] two-dimensional compressible flow simulations of the Navier-Stokes equations by Lupoglazoff and Vuillot[29-31] have confirmed the measurements acquired from subscale firings; the collection of all available data points to the existence of a strong vorticity-driven coupling irrespective of whether inhibitor rings or other surface anomalies are present.

The main objective of the Task 3.3 work was construction of a more complete stability model that accounts for *all* of the system energy and correctly portrays all energy sources and sinks. This task is most readily accomplished by application of the energy balance approach. As is usually the case with energy analyses, an improved physical understanding of the results is achieved.

Considerable work was needed to implement these changes. The outcome is a stability algorithm that accounts fully for both the acoustic and vortical flow interactions. Significant differences between these new results and those presently utilized for rocket motor stability computations are demonstrated. The new model was tested by applying it to several solid propellant rocket motor designs. Despite significant changes in the mathematical formulation, it is not necessary to discard the current solid rocket motor stability estimation methodology; required modifications are readily accomplished by means of additions to the existing codes. A new energy source terms is identified that suggests a possible origin of the unexplained instabilities in large solid booster motors. This energy source, arising from production of unsteady vorticity, is comparable in size to the key pressure coupling term itself. It may also be related to velocity coupling effects, which cannot be fully represented in the context of irrotational acoustic instability theory.

Following the classical method of energy balance analysis, but including the evolution of the vortical as well as the acoustic system energy leads to the following expression for the rate of change of the complete time-averaged system energy:

$$\begin{aligned}\frac{\partial E}{\partial t} = \iiint_V \overbrace{\Big\langle -\nabla\cdot\left(\hat{p}\hat{\mathbf{u}}\right) - \tfrac{1}{2}M_b\left(\mathbf{U}\cdot\nabla\hat{p}^2\right) - M_b\left[\hat{\mathbf{u}}\cdot\nabla\left(\mathbf{U}\cdot\hat{\mathbf{u}}\right)\right]}^{\text{irrotational}} \\ +\delta_d^2\hat{\mathbf{u}}\cdot\nabla\left(\nabla\cdot\hat{\mathbf{u}}\right) + M_b\left[\hat{\mathbf{u}}\cdot\left(\hat{\mathbf{u}}\times\Omega\right) + \hat{\mathbf{u}}\cdot\left(\mathbf{U}\times\omega\right)\right] \\ \overbrace{-\tilde{\mathbf{u}}\cdot\nabla\hat{p} - M_b\begin{bmatrix}\tilde{\mathbf{u}}\cdot\nabla\left(\mathbf{U}\cdot\hat{\mathbf{u}}\right) + \hat{\mathbf{u}}\cdot\nabla\left(\mathbf{U}\cdot\tilde{\mathbf{u}}\right) + \tilde{\mathbf{u}}\cdot\nabla\left(\mathbf{U}\cdot\tilde{\mathbf{u}}\right) \\ -\tilde{\mathbf{u}}\cdot\left(\mathbf{U}\times\omega\right) - \tilde{\mathbf{u}}\cdot\left(\tilde{\mathbf{u}}\times\Omega\right)\end{bmatrix}}^{\text{rotational}} \\ +\delta_d^2\tilde{\mathbf{u}}\cdot\nabla\left(\nabla\cdot\hat{\mathbf{u}}\right) - \delta^2\left[\hat{\mathbf{u}}\cdot\left(\nabla\times\omega\right) + \tilde{\mathbf{u}}\cdot\left(\nabla\times\omega\right)\right]\Big\rangle dV\end{aligned} \tag{1}$$

The terms in the first part of the volume integral, the irrotational parts, form the basis for all presently used methods for the estimation of rocket motor stability. Included here are two rotational terms, $M_b\left[\hat{\mathbf{u}}\cdot\left(\hat{\mathbf{u}}\times\Omega\right)+\hat{\mathbf{u}}\cdot\left(\mathbf{U}\times\omega\right)\right]$the energy change due to rotational mean flow and the Culick "Flow Turning" effect. These are so placed because this is done in the Standard Stability Prediction Program, SSPP. Discussions of Culick's analyses leading to these two terms are found in Refs. 2,4,8, and 9. It is important to see that many additional terms appear when a complete energy balance is utilized.

Using this new formulation and following the standard method of analysis[1-7,27], one finds for the linear growth rate of the system:

The classical stability integrals are shown in the first line. The second line displays Culick's flow turning effect and additional terms that are not found in the classical irrotational analysis. All terms in the first two lines were deduced by Flandro (Refs. 8 and 9) by inclusion of rotational terms in the acoustic stability analysis. It is important to observe that the term labeled "5. Rotational Flow Correction," cancels the flow turning to the precision of the calculation. This result has led to considerable confusion and debate within the combustion stability establishment. For example, Brown[69] has questioned this result, and attempts to prove that term number 5 is " just another way to represent the flow turning . . ." (represented by term 4). However, it is clear that these two effects result from quite different flow interactions; they cannot possibly represent the same physical effect. Considering the results carefully, it becomes clear that this outcome should have been expected. Since only acoustic stability is represented in the classical approach, then no rotational interactions are represented. Attempting to account for them by including the rotational terms as demonstrated in Refs. 8 and 9 leads inevitably to the acoustic result; again, only acoustic (irrotational) stability is represented.

$$
\alpha_m=\frac{1}{E_m^2}\iiint_V
\Bigg\langle
\begin{array}{l}
\text{-------- ACOUSTIC/ MEAN FLOW ---------}\\
\underbrace{-\nabla\cdot\left(\hat{p}\hat{\mathbf{u}}\right)-M_b\left(\frac{1}{2}\mathbf{U}\cdot\nabla\hat{p}^2+\hat{\mathbf{u}}\cdot\nabla\left(\mathbf{U}\cdot\hat{\mathbf{u}}\right)\right)}_{\text{1. Pressure Coupling Nozzle Damping}}\quad\underbrace{+\delta_d^2\hat{\mathbf{u}}\cdot\nabla\left(\nabla\cdot\hat{\mathbf{u}}\right)}_{\text{2. Dilatational Viscous Damping }(\mathbf{a}/\mathbf{a})}\\
\text{------ ACOUSTIC/ VORTICAL/ MEAN FLOW ------}\\
\underbrace{+M_b\hat{\mathbf{u}}\cdot\left(\mathbf{U}\times\boldsymbol{\omega}\right)}_{\text{4. Culick's Flow Turning}}\quad\underbrace{-\tilde{\mathbf{u}}\cdot\nabla\hat{p}}_{\text{5. Rotational Flow Correction}}\quad-M_b\left[\begin{array}{l}\tilde{\mathbf{u}}\cdot\nabla\left(\mathbf{U}\cdot\hat{\mathbf{u}}\right)+\\+\hat{\mathbf{u}}\cdot\nabla\left(\mathbf{U}\cdot\tilde{\mathbf{u}}\right)\end{array}\right]\\
\underbrace{+\delta_d^2\tilde{\mathbf{u}}\cdot\nabla\left(\nabla\cdot\hat{\mathbf{u}}\right)}_{\text{Dilatational Viscous Damping }(\mathbf{a}/\mathbf{v})}\quad\underbrace{-\delta^2\hat{\mathbf{u}}\cdot\left(\nabla\times\boldsymbol{\omega}\right)}_{\text{Viscous Damping }(\mathbf{a}/\mathbf{v})}\\
\text{---------- VORTICAL/ MEAN FLOW ---------}\\
\underbrace{+M_b\tilde{\mathbf{u}}\cdot\left(\mathbf{U}\times\boldsymbol{\omega}\right)}_{\text{6. Surface ("Parietal") Vortex Shedding}}\quad\underbrace{-\delta^2\tilde{\mathbf{u}}\cdot\left(\nabla\times\boldsymbol{\omega}\right)}_{\text{7. Viscous Damping }(\mathbf{v}/\mathbf{v})}\quad-M_b\left[\tilde{\mathbf{u}}\cdot\nabla\left(\mathbf{U}\cdot\tilde{\mathbf{u}}\right)\right]
\end{array}
\Bigg\rangle
dV
\qquad (2)
$$

When all unsteady effects are included, as in Eq. (2), then a different picture emerges. We have demonstrated (see full discussions in Ref. 81) that there are new terms that introduce important changes in the stability energy balance. For example, term number 6 yields a destabilizing effect closely tied to the French parietal vortex shedding effect. Table 1 shows a comparison of the classical stability computations to one in which the new terms are accounted for.

Table 1. Comparison of Stability Estimates

	A_b	f (Hz)	$\alpha_{Standard}$ (s^{-1})	$\alpha_{Composite}$ (s^{-1})
Small Research Motor (Yang and Culick[7])	2.50	1227	32.1	145.4
Tactical Rocket (Typical Geometry)	1.2	360	-43.7	26.9
Space Shuttle SRM	1.0	19.5	-5.7	2.2

For example, the prediction that the Shuttle SRM motor should be expected to be unstable is in agreement with actual experience. All Shuttle motors have demonstrated longitudinal oscillations in the first few modes. As Table 1 shows, the SSPP calculation (standard stability, SSPP result) predicts stability. A major improvement has been made in the capability to predict motor behavior.

3.3.2 Interactions with Other Tasks

Effort was undertaken in Task 3.3 to include findings from related tasks. In particular, progress was made in incorporating the effects of turbulence in the stability modeling by modifying the transport properties in the unsteady flow field. A The problem is treated by combining realistic numerical solutions for the turbulent field with detailed analytical solutions for the organized oscillatory gas motions. The main influence of turbulence is modification of the transport properties and the mean chamber velocity profile. The results show that the organized vorticity waves that fill the entire chamber in the laminar case reduce to a thin acoustic boundary layer in the presence of strong turbulence. From the standpoint of vorticity production, this can be viewed as a transition from organized vorticity associated with the periodic wave structure to the wideband vorticity distribution of the turbulent field. This process is similar in many respects to the turbulent transition process in a flow without organized oscillations. In that case organized oscillations (*e.g.* Tollmein-Schlichting waves) appear naturally as an intermediate stage in the transition to a fully turbulent field. Despite the major impact of turbulence on the flow geometry, there is little change in linear acoustic stability gain/loss terms related to vorticity propagation. This reinforces the concept that the flow-turning interaction is not the result of viscous losses at the chamber boundaries.

However, it is clear that stochastic fluctuations can have a major influence on the flame zone dynamic behavior especially in the nozzle end of a long motor burning port where the flow becomes fully turbulent.

An approximate method for including the turbulence effects was developed. The field is decomposed into two elements. The first is a realistic numerical model of the mean flow which includes the corrections to the transport properties resulting from transition and growth of random turbulent eddies. The second is a detailed analytical model of organized unsteady motion consisting of the acoustic field and associated rotational waves created by production of vorticity at the chamber inflow boundaries. Information on the mean flow with turbulence is obtained from a detailed computational model by Yang and his coworkers.[19] Weidong Cai carried out the numerical determination of the flow properties for several typical solid rocket motor configurations. This provideds spatial distributions of the turbulence-modified flow field and associated transport properties. These were then employed in the analytical flowfield expressions to produce the corrected unsteady field. This procedure is approximate in that the direct interaction between the organized and turbulent fluctuations is neglected. It is believed that in most cases these are not strong interactions, so the main effect of turbulence on the organized oscillations comes from the changes in transport properties and the mean flow velocity distribution.

Results compare favorably to the complete unsteady simulations. In particular, as the nozzle end of the chamber is approached, the turbulence effects grow rapidly in importance. The organized vortical waves are more rapidly damped due mainly to increase in the effective coefficient of viscosity (eddy viscosity), and the motion can then truly be described as an acoustic boundary layer; the organized rotational effects are confined to a thin region near the burning surface. The unsteady vorticity distribution outside this boundary layer does not then contain components directly related to the irrotational acoustic field. Despite this major departure for the laminar description of the unsteady rotational flow, there is little change in the basic effects of vorticity production on the system stability characteristics. That is, important contributions to the system energy gain/loss balance such as the flow-turning loss are not strongly affected by turbulence. Direct interactions of the turbulent field with the combustion processes near the propellant were not considered in the present effort, but will be incorporated in developing flame zone models.

3.3.3 Recommendations for Future Work

There is need for continued research on the effects of realistic flow field features on the stability of oscillatory flows in rockets. In particular, it is clear that a fully numerical approach will be needed in implementing the improved stability algorithm. For example, there is a clear need to accommodate geometrical features (cononcyls, slots, submerged nozzles, ignitor cavities, etc.) that cannot be handled analytically in evaluating Eq. 2. However, the analytical models of the type demonstrated here will play a very important role in the validation of the full CFD stability modeling of the future.

References

1. Culick, F.E.C., "Acoustic Oscillations in Solid Propellant Rocket Chambers," *Astronautica Acta,* Vol. 12, No. 2, 1966, pp. 113-126.
2. Culick, F.E.C., "Rotational Axisymmetric Mean Flow and Damping of Acoustic Waves in a Solid Propellant Rocket," *AIAA Journal,* Vol. 4, No. 8, 1966, pp. 1462-1464.
3. Culick, F.E.C., "Stability of Longitudinal Oscillations with Pressure and Velocity Coupling in a Solid Propellant Rocket," *Combustion Science and Technology,* Vol. 2, No. 4, 1970, pp. 179-201.
4. Culick, F.E.C., "The Stability of One-Dimensional Motions in a Rocket Motor," *Combustion Science and Technology,* Vol. 7, No. 4, 1973, pp. 165-175.
5. Culick, F.E.C., "Stability of Three-Dimensional Motions in a Rocket Motor," *Combustion Science and Technology,* Vol. 10, No. 3, 1974, pp. 109-124.
6. Lovine, R.L., Dudley, D.P., and Waugh, R.D., "Standardized Stability Prediction Method for Solid Rocket Motors," Vols. I, II, III Rept. AFRPL TR 76-32, Aerojet Solid Propulsion Co., May 1976 1976.
7. Nickerson, G.R., Culick, F.E.C., and Dang, L.G., "Standardized Stability Prediction Method for Solid Rocket Motors Axial Mode Computer Program," AFRPL TR-83-017, Software and Engineering Associates, Inc., September 1983.
8. Flandro, G.A., "Effects of Vorticity on Rocket Combustion Stability," *Journal of Propulsion and Power,* Vol. 11, No. 4, 1995, pp. 607-625.
9. Flandro, G.A., "On Flow Turning," AIAA Paper 95-2530, July 1995.
10. Flandro, G.A., Cai, W., and Yang, V., "Turbulent Transport in Rocket Motor Unsteady Flow," *Solid Propellant Chemistry, Combustion, and Motor Interior Ballistics*, Vol. 185, AIAA Progress in Astronautics and Aeronautics, Washington, DC, 2000.
11. Majdalani, J., Flandro, G.A., and Roh, T.S., "Convergence of Two Flowfield Models Predicting a Destabilizing Agent in Rocket Combustion," *J. of Propulsion and Power,* Vol. 16, No. 3, 2000, pp. 492-497.
12. Majdalani, J., and Van Moorhem, W.K., "Improved Time-Dependent Flowfield Solution for Solid Rocket Motors," *AIAA Journal,* Vol. 36, No. 2, 1998, pp. 241-248.
13. Majdalani, J., "The Boundary Layer Structure in Cylindrical Rocket Motors," *AIAA Journal,* Vol. 37, No. 4, 1999, pp. 505-508.
14. Majdalani, J., "Vorticity Dynamics in Isobarically Closed Porous Channels. Part I: Standard Perturbations," *Journal of Propulsion and Power,* Vol. 17, No. 2, 2001, pp. 355-362.
15. Majdalani, J., and Roh, T.S., "Vorticity Dynamics in Isobarically Closed Porous Channels. Part II: Space-Reductive Perturbations," *Journal of Propulsion and Power,* Vol. 17, No. 2, 2001, pp. 363-370.
16. Majdalani, J., and Roh, T.S., "The Oscillatory Channel Flow with Large Wall Injection," *Proceedings of the Royal Society, Series A,* Vol. 456, No. 1999, 2000, pp. 1625-1657.
17. Vuillot, F., and Avalon, G., "Acoustic Boundary Layer in Large Solid Propellant Rocket Motors Using Navier-Stokes Equations," *Journal of Propulsion and Power,* Vol. 7, No. 2, 1991, pp. 231-239.
18. Roh, T.S., Tseng, I.S., and Yang, V., "Effects of Acoustic Oscillations on Flame Dynamics of Homogeneous Propellants in Rocket Motors," *Journal of Propulsion and Power,* Vol. 11, No. 4, 1995, pp. 640-650.
19. Yang, V., and Roh, T.S., "Transient Combustion Response of Solid Propellant to Acoustic Disturbance in Rocket Motors," AIAA Paper 95-0602, January 1995.
20. Vuillot, F., "Numerical Computation of Acoustic Boundary Layers in Large Solid Propellant Space Booster," AIAA Paper 91-0206, January 1991.
21. Baum, J.D., Levine, J.N., and Lovine, R.L., "Pulsed Instabilities in Rocket Motors: A Comparison between Predictions and Experiments," *Journal of Propulsion Power,* Vol. 4, No. 4, 1988.
22. Baum, J.D., "Investigation of Flow Turning Phenomenon; Effects of Frequency and Blowing Rate," AIAA Paper 89-0297, January 1989.
23. Glick, R.L., and Renie, J.P., "On the Nonsteady Flowfield in Solid Rocket Motors," AIAA Paper 84-1475, June 1984.
24. Brown, R.S., Blackner, A.M., Willoughby, P.G., and Dunlap, R., "Coupling between Acoustic Velocity Oscillations and Solid Propellant Combustion," *J. of Propulsion and Power,* Vol. 2, No. 5, 1986, pp. 428-437.
25. Shaeffer, C.W., and Brown, R.S., "Oscillatory Internal Flow Field Studies," AFOSR Contract Rept. F04620-90-C-0032, United Technologies, San Jose, CA, 1990.
26. Shaeffer, C.W., and Brown, R.S., "Oscillatory Internal Flow Studies," Chemical Systems Div. Rept. 2060 FR, United Technologies, San Jose, CA, Aug. 1992.

27. Cantrell, R.H., and Hart, R.W., "Interaction between Sound and Flow in Acoustic Cavities: Mass, Momentum, and Energy Considerations," *Journal of the Acoustical Society of America,* Vol. 36, No. 4, 1964, pp. 697-706.
28. Avalon, G., Casalis, G., and Griffond, J., "Flow Instabilities and Acoustic Resonance of Channels with Wall Injection," AIAA Paper 98-3218, July 1998.
29. Lupoglazoff, N., and Vuillot, F., "Numerical Simulations of Parietal Vortex-Shedding Phenomenon in a Cold-Flow Set-Up," AIAA Paper 98-3220, July 1998.
30. Lupoglazoff, N., and Vuillot, F., "Parietal Vortex Shedding as a Cause of Instability for Long Solid Propellant Motors. Numerical Simulations and Comparisons with Firing Tests," AIAA Paper 96-0761, January 1996.
31. Lupoglazoff, N., and Vuillot, F., "Numerical Simulation of Vortex Shedding Phenomenon in 2d Test Case Solid Rocket Motors," AIAA Paper 92-0776, Jan. 1992.
32. Prevost, M., Vuillot, F., and Traineau, J.C., "Vortex-Shedding Driven Oscillations in Subscale Motors for the Ariane 5 Mps Solid Rocket Motors," AIAA Paper 96-32471996.
33. Scippa, S., Pascal, P., and Zanier, F., "Ariane 5 Mps -Chamber Pressure Oscillations Full Scale Firings Results Analysis and Further Studies," AIAA Paper 94-3068, June 1994.
34. Fukushima, Y., "H-II Launcher Propulsion Experience," Proceedings of the 5th AAAF Symposium International on Propulsion in Space Transportation Paper 5.9-5.20, May 1996.
35. Brown, R.S., Dunlap, R., Young, S.W., and Waugh, R.C., "Vortex Shedding as a Source of Acoustic Energy in Segmented Solid Rockets," *Journal of Spacecraft and Rockets,* Vol. 18, No. 4, 1981.
36. Dotson, K.W., Koshigoe, S., and Pace, K.K., "Vortex Shedding in a Large Solid Rocket Motor without Inhibitors at the Segment Interfaces," *Journal of Propulsion & Power,* Vol. 13, No. 2, 1997, pp. 197-206.
37. Dotson, K.W., Murdock, J.W., and Kamimoto, D.K., "Launch Vehicle Dynamic and Control Effects from Solid Rocket Motor Slag Ejection," *Journal of Propulsion & Power,* Vol. 15, No. 3, 1999, pp. 468-475.
38. Dotson, K.W., Baker, R.L., and Sako, B.H., "Launch Vehicle Self-Sustained Oscillation from Aeroelastic Coupling Part 1: Theory," *Journal of Spacecraft & Rockets,* Vol. 35, No. 3, 1998, pp. 365-373.
39. Dotson, K.W., Baker, R.L., and Bywater, R.J., "Launch Vehicle Self-Sustained Oscillation from Aeroelastic Coupling Part 2: Analysis," *Journal of Spacecraft & Rockets,* Vol. 35, No. 3, 1998, pp. 374-379.
40. Nesman, T., "Rsrm Chamber Pressure Oscillations: Full Scale Ground and Flight Test Summary and Air Flow Test Results," 31st AIAA Joint Prop. Conf. Paper AIAA Solid Rocket Technical Committee, July 1995.
41. Hart, R.W., and McClure, F.T., "Combustion Instability: Acoustic Interaction with a Burning Propellant Surface," *The Journal of Chemical Physics,* Vol. 10, No. 6, 1959, pp. 1501-1514.
42. Hart, R.W., Bird, J.F., Cantrell, R.H., and McClure, F.T., "Nonlinear Effects in Instability of Solid Propellant Rocket Motors," *AIAA Journal,* Vol. 2, No. 7, 1964, pp. 1270-1273.
43. Hart, R.W., and McClure, F.T., "Theory of Acoustic Instability in Solid Propellant Rocket Combustion," *Tenth Symposium(International) on Combustion*, 1964, pp. 1047-1066.
44. Culick, F.E.C., "Non-Linear Growth and Limiting Amplitude of Acoustic Oscillations in Combustion Chambers," *Combustion Science and Technology,* Vol. 3, No. 1, 1971, pp. 1-16.
45. Culick, F.E.C., Burnely, V. S., and Swenson, G., "Pulsed Instabilities in Solid-Propellant Rockets," *Journal of Propulsion Power,* Vol. 11, No. 4, 1995.
46. Culick, F.E.C., "Some Recent Results for Nonlinear Acoustics in Combustion Chambers," *AIAA Journal,* Vol. 32, No. 1, 1994, pp. 146-168.
47. Culick, F.E.C., and Yang, V., "Prediction of the Stability of Unsteady Motions in Solid Propellant Rocket Motors," *Nonsteady Burning and Combustion Stability of Solid Propellants*, Vol. 143, edited by L. DeLuca, E.W. Price, and M. Summerfield, Prog. in Astronautics and Aeronautics, Washington, DC, 1992, pp. 719-779.
48. Culick, F.E.C., "Rotational Axisymmetric Mean Flow and Damping of Acoustic Waves in a Solid Propellant Rocket," *Journal of Propulsion and Power,* Vol. 5, No. 6, 1989, pp. 657-664.
49. Avalon, G., and Comas, P., "Simulative Study of the Unsteady Flow inside a Solid Propellant Rocket Motor," AIAA Paper 91-1866, June 1991.
50. Vuillot, F., "Vortex-Shedding Phenomena in Solid Rocket Motors," *Journal of Propulsion and Power,* Vol. 11, No. 4, 1995, pp. 626-639.
51. Traineau, J.C., Prevost, M., and Lupoglazoff, N., "A Subscale Test Program to Assess the Vortex Shedding Driven Instabilities in Segmented Solid Rocket Motors," AIAA Paper 97-3247, July 1997.
52. Vuillot, F., Traineau, J.C., Prevost, M., and Lupoglazoff, N., "Experimental Validation of Stability Assessment Methods for Segmented Solid Propellant Motors," AIAA Paper 93-1883, January 1993.
53. Couton, D., Doan-Kim, S., and Vuillot, F., "Numerical Simulation of Vortex-Shedding Phenomenon in a Channel with Flow Induced through Porous Wall," *International Journal of Heat and Fluid Flow,* Vol. 18, No. 3, 1997, pp. 283-296.

54. Morfouace, V., and Tissier, P.Y., "Two-Phase Flow Analysis of Instabilities Driven by Vortex Shedding in Solid Rocket Motors," AIAA Paper 95-2733, July 1995.
55. Tissier, P.Y., Godfroy, F., and Jacquemin, P., "Cfd Analysis of Vortex Shedding inside a Subscale Segmented Motor," AIAA Paper 94-2781, June 1994.
56. Tissier, P.Y., Godfroy, F., and Jacquemin, P., "Simulation of Three Dimensional Flows inside Solid Propellant Rocket Motors Using a Second Order Finite Volume Method - Application to the Study of Unstable Phenomena," AIAA Paper 92-3275, July 1992.
57. Traineau, J.C., Hervat, P., and Kuentzmann, P., "Cold-Flow Simulation of a Two-Dimensional Nozzleless Solid-Rocket Motor," AIAA Paper 86-1447, July 1986.
58. Vuillot, F., and Lupoglazoff, N., "Combustion and Turbulent Flow Effects in 2d Unsteady Navier-Stokes Simulations of Oscillatory Rocket Motors," AIAA Paper 96-0884, January 1996.
59. Vuillot, F., Dupays, J., Lupoglazoff, N., Basset, T., and Daniel, E., "2d Navier-Stokes Stability Computations for Solid Rocket Motors: Rotational, Combustion and Two-Phase Flow Effects," AIAA 97-3326, July 1997.
60. Ugurtas, B., Avalon, G., Lupoglazoff, N., and Vuillot, F., "Numerical Computations of Hydrodynamic Instabilities inside Channels with Wall Injection," AIAA Paper 99-2505, June 1999.
61. Casalis, G., Avalon, G., and Pineau, J.-P., "Spatial Instability of Planar Channel Flow with Fluid Injection through Porous Walls," *The Physics of Fluids,* Vol. 10, No. 10, 1998, pp. 2558-2568.
62. Griffond, J., Casalis, G., and Pineau, J.-P., "Spatial Instability of Flow in a Semiinfinite Cylinder with Fluid Injection through Its Porous Walls," *European Journal of Mechanics B/Fluids,* Vol. 19, 2000, pp. 69-87.
63. Griffond, J., and Casalis, G., "On the Dependence on the Formulation of Some Nonparallel Stability Approaches Applied to the Taylor Flow," *The Physics of Fluids,* Vol. 12, No. 2, 2000, pp. 466-468.
64. Griffond, J., and Casalis, G., "On the Nonparallel Stability of the Injection Induced Two-Dimensional Taylor Flow," *The Physics of Fluids,* Vol. 13, No. 6, 2001, pp. 1635-1644.
65. Varapaev, V.N., and Yagodkin, V.I., "Flow Stability in a Channel with Porous Walls," *Fluid Dynamics (Izvestiya Akademii Nauk SSSR, Meckanika Zhidkosti i Gaza),* Vol. 4, No. 5, 1969, pp. 91-95.
66. Ugurtas, B., Avalon, G., Lupoglazoff, N., Vuillot, F., and Casalis, G., "Stability and Acoustic Resonance of Internal Flows Generated by Side Injection," *Journal of Propulsion and Power,* Vol. x, No. x, 2001, pp. x-x.
67. Chu, B.-T., and Kovásznay, L.S.G., "Non-Linear Interactions in a Viscous Heat-Conducting Compressible Gas," *Journal of Fluid Mechanics,* Vol. 3, No. 5, 1957, pp. 494-514.
68. Morse, P.M., and Ingard, K.U., *Theoretical Acoustics*, McGraw Hill Book Co., New York, 1968, pp. 278-279.
69. Brown, R.S., private communication, t, 2000.
70. Barron, J., Van Moorhem, W.K., and Majdalani, J., "A Novel Investigation of the Oscillatory Field over a Transpiring Surface," *Journal of Sound and Vibration,* Vol. 235, No. 2, 2000, pp. 281-297.
71. Brown, R.S., Blackner, A.M., Willoughby, P.G., and Dunlap, R., "Coupling between Velocity Oscillations and Solid Propellant Combustion," AIAA 24th Aerospace Sciences Meeting Paper 86-0531, January 1986.
72. Kirchoff, G., *Vorlesungen Über Mathematische Physik: Mechanik*, 2nd ed., Teubner, Leibzig, 1877, pp. 311-336.
73. Beddini, R.A., and Roberts, T.A., "Turbularization of an Acoustic Boundary Layer on a Transpiring Surface," *AIAA Journal,* Vol. 26, No. 8, 1988, pp. 917-923.
74. Beddini, R.A., and Roberts, T.A., "Response of Propellant Combustion to a Turbulent Acoustic Boundary Layer," *Journal of Propulsion and Power,* Vol. 8, No. 2, 1992, pp. 290-296.
75. Thomas, H.D., Flandro, G.A., and Flanigan, S.N., "Effects of Vorticity on Particle Damping," AIAA Paper 95-2736, July 1995.
76. Dupays, J., Prevost, M., Tarrin, P., and Vuillot, F., "Effects of Particulate Phase on Vortex Shedding Driven Oscillations in Solid Rocket Motors," AIAA Paper 96-3248, July 1996.
77. Sabnis, J.S., de Jong, F.J., and Gibeling, H.J., "Calculation of Particle Trajectories in Solid-Rocket Motors with Arbitrary Acceleration," *Journal of Propulsion and Power,* Vol. 8, No. 5, 1992, pp. 961-967.
78. Culick, F.E.C., "Remarks on Entropy Production in the One-Dimensional Approximation to Unsteady Flow in Combustion Chambers," *Combustion Science and Technology,* Vol. 15, No. 4, 1977, pp. 93-97.
79. Blomshield, F.S., Crump, J.E., Mathes, H.B., Stalnaker, R.A., and Beckstead, M.W., "Stability Testing of Full-Scale Tactical Motors," *Journal of Propulsion and Power,* Vol. 13, No. 3, 1997, pp. 349-355.
80. Blomshield, F.S., Mathes, H.B., Crump, J.E., Beiter, C.A., and Beckstead, M.W., "Nonlinear Stability Testing of Full-Scale Tactical Motors," *Journal of Propulsion and Power,* Vol. 13, No. 3, 1997, pp. 356-366.
81. Flandro, G.A. and Majdalani, J., "Aeroacoustic Instability in Rockets," AIAA Paper No. 2001-3868, July 2001.

3.4 Pulsed Motor Firings (Blomshield)

For the last several years, the Naval Air Warfare Center Weapons Division (NAWCWD) has participated in an extensive effort to understand nonlinear-pulsed instability in tactical sized solid rocket motors. The purpose of this work was to broaden the knowledge of design factors that influence nonlinear axial mode combustion instability. . In this paper, combustion instability data are presented on ten tactical size motor firings.[1,3] Earlier papers have reported on previous NAWCWD work on this program.[4,5] The parameters investigated in these firings were the effects of pressure and pulse amplitude on nonlinear-pulsed instability. Each motor was pulsed two to three times during burn. The motors were instrumented with two or three high-frequency piezoelectric quartz pressure transducers. The motors with three transducers had them mounted at the forward, middle, and aft ends of the motor. Acoustic data are presented and compared with linear stability predictions made by the Standard Performance Prediction/Standard Stability Program (SPP/SSP) computer code. Included in the paper are laboratory response testing results. As previous studies indicated, results indicate a significant adverse effect on nonlinear stability as pressure is increased. Second, the stability boundary was determined by bracketing the pulse amplitude required to trigger a motor into high levels of combustion instability. Third, placement of three transducers mounted along the length of the motor determined the hard-to-obtain waveform and phase data of a motor undergoing combustion instability. Finally, results showed that it is possible to pulse a motor into nonlinear limiting amplitude oscillations, even when the propellant contains a stability additive.

3.4.1 Motor Firing Details

Two different propellants were used in the motor firings. Both were reduced smoke propellants. Propellant "A" consisted of 82% AP, 4% RDX, 12.5% HTPB, 0.5% carbon black and contained 1% ZrC stability additive with a pressure exponent of 0.36 and a burning rate of 0.68 cm/sec at 6.9 MPa.. Propellant "B" consisted of 86.5% AP, 13% HTPB and 0.5% carbon black with a pressure exponent of 0.39 and a burning rate of 0.88 cm/sec at 6.9 MPa.

Table 1 shows the testing matrix for the ten motor firings. All motors fired in the program were 12.7 cm in diameter and 170 cm in length. In addition, all motors were typically pulsed two to three times during burn. Motors No. 1 and 2 both failed during firing. Motors No. 3 through 5 were identical except for the nozzle throat size, which caused the chamber pressure to vary. These three used the reduced smoke propellant without additive, propellant "B," and were full cylinder geometries. The purpose of these motors was to look at the effect of pressure on non-linear pulsed instability. All three motors were pulsed with similar pulsing levels, three times during burn. Motors No. 6 through 9 were star aft motors loaded with propellant "A" given in Table 3. Motor No. 10 was a full cylinder motor containing propellant "B." The purpose of Motors No. 6 through 9 was to see what effect pulsing amplitude would have on the stability of the motors. Motors No. 6 and 7 were pulsed at 5 and 3% levels at 33 and 66% of the web burned. Motors No. 8 and 9 were pulsed at 10 and 6% levels. A pulse of 3% means that the desired pulse amplitude was to be 3% of the current chamber pressure in the motor. To look at effects of increasing motor pressure, motors No. 6 and 7, with the light pulses, were fired at mean chamber pressures of 6.9 and 10.3 MPa, respectively. Likewise, motors No. 8 and 9, with the hard pulses, had chamber pressures of 6.9 and 10.3 Mpa,

respectively, as well. The intent of motor No. 10 was to repeat the second firing of the previous year's motor firing, motor No. 4, but with added instrumentation.2,3

The standard NAWCWD pulsers were used on the firings.[1-5] By using the results of subscale testing and past motor firings, the pulsers were sized to give the desired pulse amplitude. The subscale results were scaled by knowing the motor volume and pressure and choosing a laboratory pulser baseline that was closest to the test conditions. The pulser was then fine tuned by adjusting the charge amount to motor pressure, gas density, and volume conditions.[5]

TABLE 1. Motor Test Matrix

Motor No.	Firing date	Pressure, MPa	Propellant	Geometry	Case hardware	Comments
1	1994	20.7	A	Star aft	Light	Motor failed
2	1995	20.7	A	Star aft	Light	Motor failed
3		3.45	B	Full cylinder	Heavy	
4	1996	10.3	B	Full cylinder	Heavy	Pressure effects
5		13.8	B	Full cylinder	Heavy	
6		6.90	A	Star aft	Light	Enhanced
7		10.3	A	Star aft	Light	instrumentation,
8	1997	6.90	A	Star aft	Light	stability additives,
9		10.3	A	Star aft	Light	pulsing magnitudes
10		10.3	B	Full cylinder	Heavy	and geometry effects

Each motor was instrumented with either two or three water-cooled Kistler 211B2 piezoelectric quartz gauge and one low-frequency strain gauge type pressure transducer. Also mounted on the motor were two or three pulsers and the igniter. All data were recorded at 20,000 samples per second with a 16-bit analog-to-digital converter with a 10,000-Hz anti-aliasing filter, recorded on frequency modulated (FM) Wide Band I tape with one channel per tape track at 60 inches per second (ips), and recorded on multiplexed FM tape. Additional details of the instrumentation can be found in ref. 2 and 3.

Motors No. 1 through 8 had two high-frequency Kistler gauges mounted in the forward closure. For motors No. 9 and 10, three identical Kistler gauges were mounted along the length of the motor. The first was located at the forward closure, like motors No. 1 through 8. The second was located at the middle of the motor, and the third was located very near the nozzle entrance at the aft end. The middle and aft gauges were installed by drilling a hole through the 4-cm case wall and on through the propellant. The propellant was then inhibited to prevent burning on the inside of the hole. The purpose of these gauges was to examine wave structure and phase relationships of the acoustic oscillations in the motor. This data was specifically requested by MURI researchers.

3.4.2 Firing Results and Analysis of Motors No. 3 Through 5

Motors No. 3 through 5 were fired in the summer of 1996. The principal intent of these motor firings was to examine the effect of increasing motor pressure on pulsed nonlinear combustion instability. Figure 1 shows the ballistic pressure traces of the three motors with the ballistic prediction (dashed line) for each motor. The predicted

pressures followed the experimental traces fairly well until the onset of instability. The instability results of each motor firing are described below.

Motor No. 3 was a low pressure 3.45-MPa motor that was pulsed three times as approximately 25, 50, and 75% of the web burned or at 1, 2, and 3 seconds. Each of the pulses decayed rapidly and no oscillations were sustained in the motor after the pulses. Movies and video taken of the motor firing showed flashes in the plume during each pulse. Also, there were two additional unplanned pulses due to debris passing out through the nozzle.

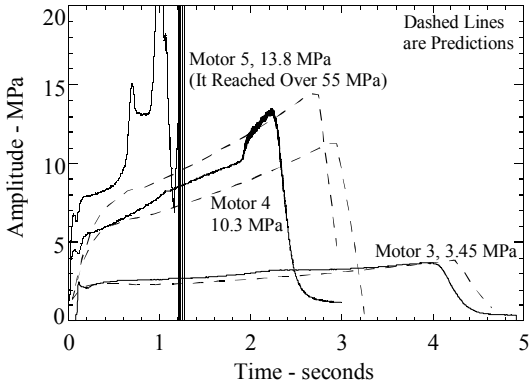

Figure 1. Ballistic Pressure of Motors 3-5 Compared to Predicted Pressure

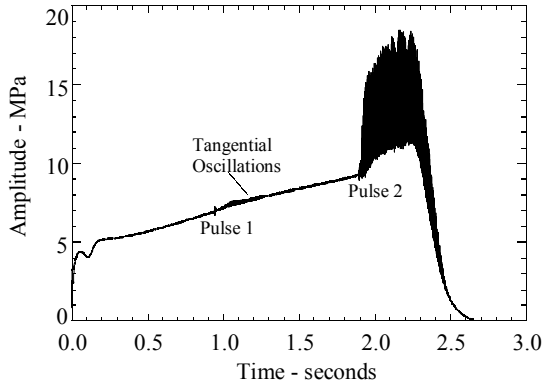

Figure 2. DC Coupled High-Frequency Ballistic Pressure Trace of Motor No. 4

Motor No. 4 was a higher-pressure motor whose pressure ranged from 5.5 to 11.7 MPa during a normal burn. It was pulsed twice, at 1 and 2 seconds, corresponding to 40 and 80% of the web burned. The pulse timing was incorrectly set so the third pulse was after burnout. Motor oscillations decayed after the first pulse and grew after the second pulse. Figure 2 shows the DC coupled high-frequency data of the firing. There are several interesting items shown in this figure. The first pulse, which decays, can be seen at around 1 second. Immediately after the decay, some tangential oscillations are observed. The motor is reasonably quiet until the second pulse, which triggers the motor into violent nonlinear combustion instability.

Figure 3 shows the first pulse whose nonlinear peaks match the first longitudinal mode of the motor, which is 320 Hz. There is a very interesting observation concerning the high-frequency content of the pulse. Besides showing the non-linearities of the pulse, it also corresponds to the first tangential mode of the case near the forward closure. These oscillations are observed in the traces of all pulses, both decaying and growing. Similar acoustic content was noted by Harris and others in recent work [6] At the forward end of the motor, the propellant stops 2.5 cm short of the closure containing the instrumentation and pulsers. The propellant face is inhibited. In this region of exposed case wall, the computed tangential mode is around 6,500 Hz. The first tangential mode is computed by:

$$Frequency = \frac{0.586 * (Gas\ Speed\ of\ Sound)}{Diameter\ of\ Chamber}$$

The second pulse is shown in Figure 4. An initial disturbance grows from an initial pulse of around 345 to 6,900 kPa in less than 10 cycles. In this figure the DC component of the signal has been taken out by digitally high passing the data above 80 Hz. This serves two purposes. First, the DC pressure level is changing very rapidly, making determination about the AC component difficult. Second, it eliminates some minor 60 Hz signal noise that can distort the true data. More details on the character and frequency content of these oscillations can be found in Ref. 3-5.

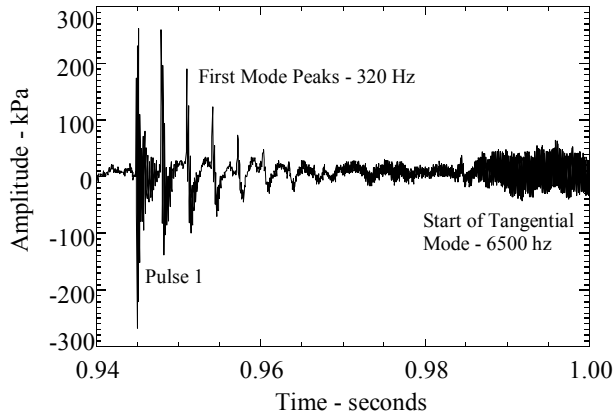

Figure 3. Details of Pulse 1 of Motor No. 4

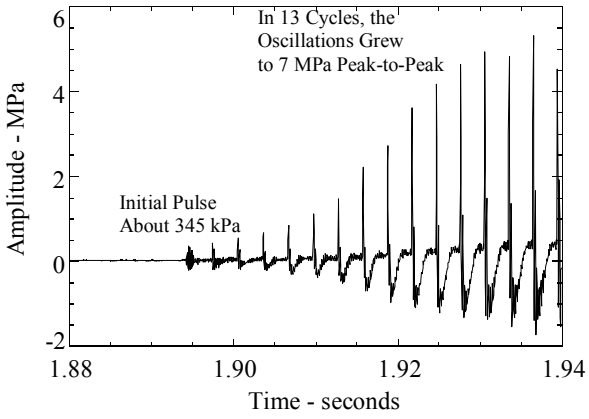

Figure 4. Details of Pulse 2 of Motor No. 4

Motor No. 5 was the highest-pressure motor with pressure ranging from 8.3 to 13.8 MPa during a normal burn. Although the motor was scheduled to be pulsed three times, spontaneous tangential oscillations prevented the analysis or detection of any of the pulses. The motor went spontaneously unstable at around 0.5 second and, after some acoustic gyrations, failed at just over a second of the planned 2-second burn. Figure 5 documents the probable series of events that led to failure. The oscillations quickly increased to 6.9 MPa peak-to-peak with a 13.8-MPa DC pressure shift. At this point, it is believed that the nozzle partially failed. The resultant nozzle assembly bounced around in the motor until it blocked the nozzle at about 0.95 second. The pressure then increased dramatically to 55 MPa. At this pressure the nozzle blockage was ejected along with the nozzle assembly, and the instantaneous large aft end opening with 55-Mpa chamber pressure caused the mean thrust of the motor to increase ten-fold to around 400 kilo-Newton (kN). A second possible scenario causing the massive over-pressurization deals with the fluid dynamics of the violent tangential mode oscillations. It is possible that these oscillations caused a “tornado” to form down the axis of the motor. This fluid dynamic vortex prevented the mean flow from escaping the motor through the nozzle due to a reduction of the effective nozzle diameter. The mean chamber pressure increased until the nozzle assembly was ejected from the motor. Like the previous scenario, the instantaneous large nozzle opening with 55-MPa chamber pressure increased the mean thrust of the motor to around 400 kN. Whatever the reason, the acoustic oscillations exceeded 21 MPa peak-to-peak and mean chamber pressure exceeded 55 MPa. The excessive thrust and violent oscillatory behavior sheared the four 16-mm grade-five bolts holding the motor to the test stand. The motor left the test stand and traveled about 150 meters up over a 15-meter high earthen berm and into the

surrounding desert. Amazingly, no damage was done to the test stand and the motor hardware except to the forward closure and instrumentation. The motor case and end caps were scratched but undamaged.

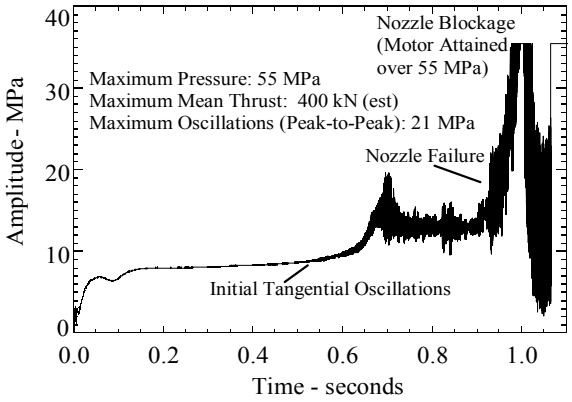

Figure 5. DC Coupled Ballistic Pressure of Motor No. 5

(a) Linear Stability

One thrust of the overall program was to develop an improved understanding of nonlinear (pulsed) combustion instability. Linear stability aspects were studied on this program because the nonlinear (pulsed) instability of a motor is believed to be related to its linear stability. The linear stability of a motor is characterized by its exponential decay (stability) or growth (instability) of pressure oscillations, $\hat{P} = P_0 e^{\alpha t}$. The rate of growth (or decay) is expressed in terms of the alpha in this equation. If a pressure perturbation in the motor is damped, the alpha is negative and the motor is linearly stable. If the perturbation excites a growth of pressure oscillations, the alpha is positive and the motor is linearly unstable. Nonlinear instability, on the other hand, deals with the response to large or finite-amplitude (nonlinear) types of disturbances.[7-11] The Solid Propellant Performance computer program (SPP) and the one-dimensional Standard Stability Prediction computer program (SSP) were used to predict the motor performance and linear stability of the motors.[12,13] The code's inputs include motor geometry, propellant ballistics, and the response of the propellant. The ballistic predictions shown in Fig. 1 were performed using the SPP code. Figure 6 shows the pressure coupled response of the two propellants at 6.9 MPa measured by the T-burner.[14,15] Figure 7 compares the predicted motor stability computed by the SPP/SSP program with the measured experimental data. The comparison is surprisingly good. The magnitudes of the total stability alphas produced by SPP/SSP and the trend of the data both agree with the predicted values. This type of comparison is similar to that seen in past studies.

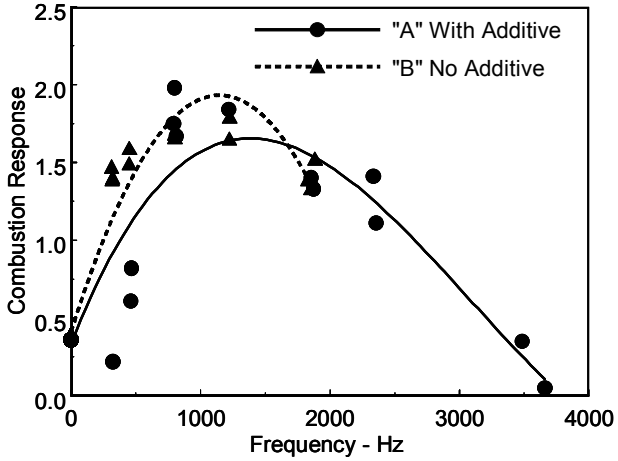

Figure 6. Combustion Response of Propellants

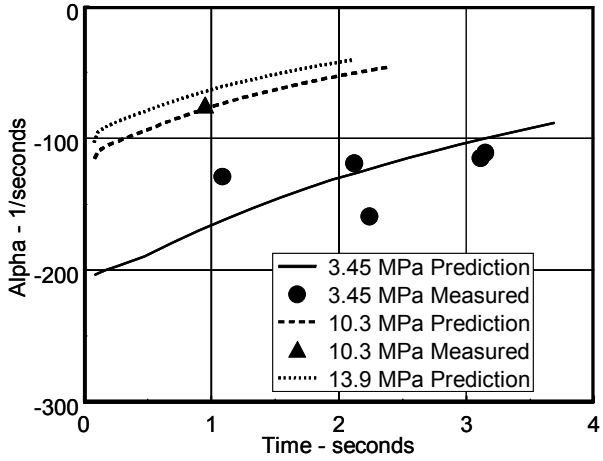

Figure 7. Stability Comparison of Stable Pulses

3.4.3 Firing Results and Analysis of Motors No. 6 Through 10

Motors No. 6 through 10 were successfully fired during August 1997. Motor No. 6, Figure 8, had a chamber pressure of 6.9 MPa and star aft geometry, and was loaded with propellant "A." It was pulsed twice lightly at 3.9 and 3.1% levels (276 and 205 kPa, respectively) and both pulses decayed, *i.e.* no oscillations resulted. Motor No. 7 had a chamber pressure of 10.3 MPa and star aft geometry, and was loaded with propellant "A." It was also pulsed twice lightly at 4.7 and 2.9% levels (442 and 220 kPa, respectively) and both pulses decayed. Motor No. 8, Fig. 9, had a chamber pressure of 6.9 MPa and star aft geometry, and was loaded with propellant "A." This motor was pulsed hard at 9.7% (689 kPa). The motor went into violent nonlinear longitudinal oscillations, *i.e.* the oscillations grew to a limiting amplitude and the chamber pressure was elevated. Motor No. 9 had a chamber pressure of 10.3 MPa and star aft geometry, and was loaded with propellant "A." This motor was pulsed hard at 10.2 percent (959 kPa). The motor went into violent nonlinear longitudinal oscillations. Motor No. 10 had a chamber pressure of 13.45 MPa and full cylinder geometry, and was loaded with propellant "B." This motor went spontaneously unstable before pulsing occurred, and experienced large DC pressure shifts and reached chamber pressures in excess of 41 MPa before the nozzle insert was ejected.

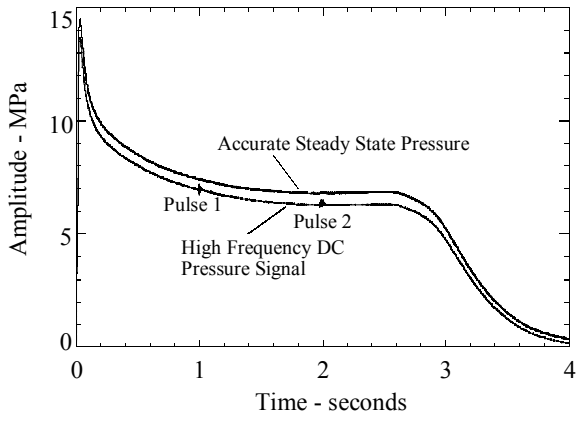

Figure 8. Motor No. 6

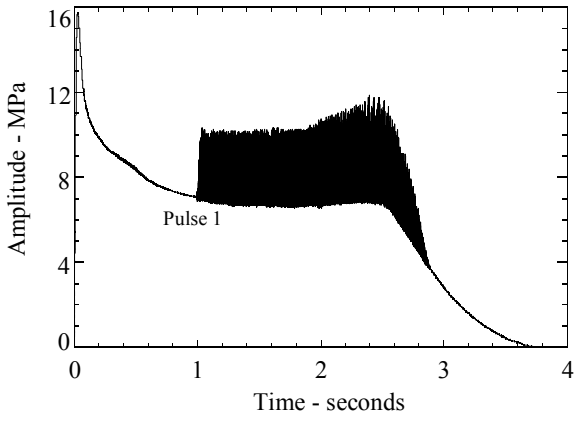

Figure 9. Motor No. 8

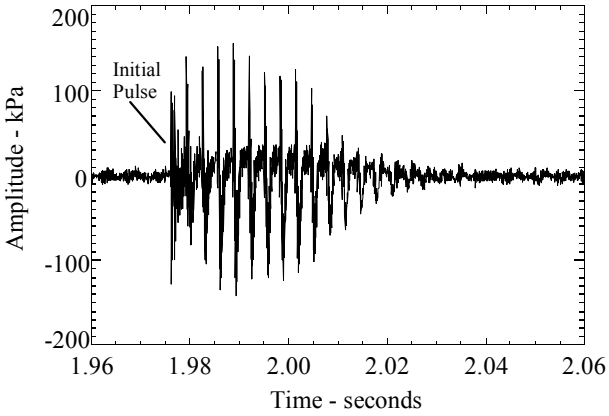

Figure 10 AC Data for Pulse 2 of Motor No. 6

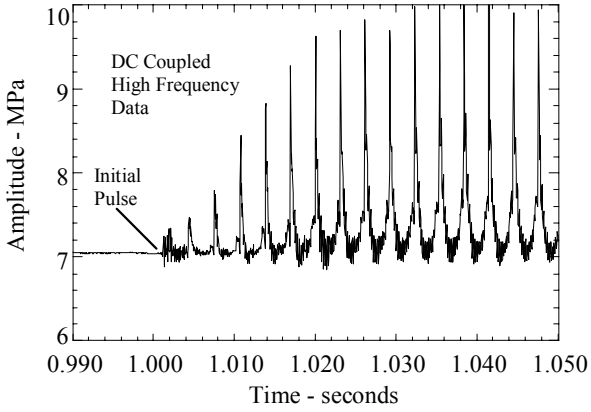

Figure 11 Pulse 1 of Motor No. 8, DC Coupled Data

Figure 10 shows the AC data for pulse 2 of motor No. 6. This was an interesting pulse, as it appeared that the motor almost went unstable. Figure 11 shows the DC data for pulse 1 of motor No. 8. The pulse and resultant oscillations are nonlinear and steep fronted. In approximately 11 cycles, the oscillations reached a limiting amplitude of around 3.5 MPa.

One aspect looked for in past motor firings was the pulsing level required to trigger a motor into non-linear instability. In motor No. 6, a 3.9% pulse did not trigger the motor. A 9.7% pulse in an identical motor No. 8 did. This behaviour was repeated in the higher-pressure motors No. 7 and 9, which had 4.7 and 10.2% pulses, respectively. Figure 12 shows this graphically by comparing the steady state gauge outputs for motors No. 6 and 8, and motors No. 7 and 9, respectively. The steady state strain gauge type transducer does not have the frequency response and, hence, the oscillatory levels shown by the gauge are much lower than they actually were, as was indicated in Figure 9. This type of data is very hard to obtain and will be very valuable in gaining understanding into the physics of combustion instability. A qualitative knowledge of what pulsing level is required to trigger a motor into limiting amplitude non-linear instability should provide insight into the mechanistic behaviour of this form of instability. Figure 13 shows real time photographs of motors No. 7 and 9 taken at the same time during burn after the onset of oscillation of motor No. 9. The difference is obvious.

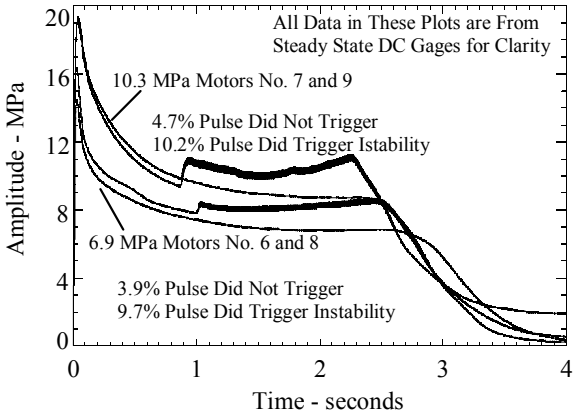

Figure 12. Examples of Pulsing Threshold

By installing three gauges along the axis of the motor, it was hoped to gain insight into the phase, waveform shape, and frequency content of the acoustic oscillations. Figure 14 shows some of this detail. The onset of oscillations is shown for motor No. 9 for all three high-frequency gauges. All three gauges were mounted very close to the motor cavity, with no loss in signal response at the 20-KHz sample rate. To allow more readable comparison of the signals, the middle signal in Figure 14 has an artificial offset of 3 MPa and the aft signal has an offset of 6 MPa. The gauges all use the identical time scale, making phase relationships possible. It is quickly noted that the aft gauge is 180 degrees out of phase with the forward gauge. The middle gauge is 90 degrees out of phase. The middle gauge also appears to have dominant harmonics at twice the frequency and half the amplitude, compared to the forward location. This is expected because the oscillatory wave passes the mid-point twice for each cycle of oscillation. Because most of the longitudinal acoustic energy is conserved for a cycle of oscillation, the energy level or amplitude is half of the amplitudes at the ends of the motor. Also seen in this figure is the relative noise level before the onset of oscillations. Typical noise levels were sometimes less than 7 kPa out of 35 MPa.

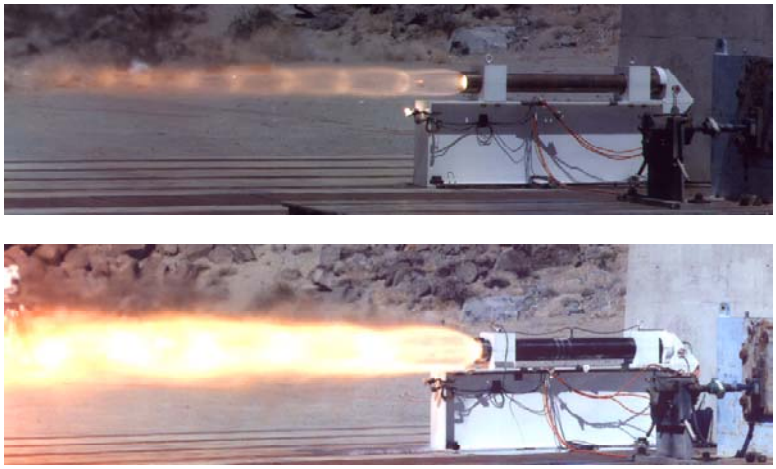

Figure 13. Comparison of Motors No. 7 and 9

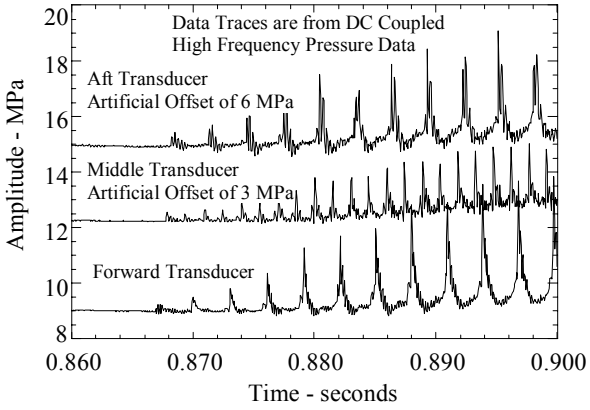

Figure 14. Waveshape Comparison for Motor No. 9

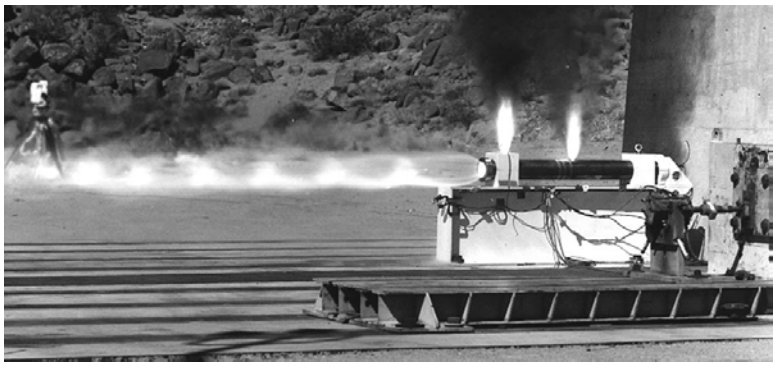

Figure 15. Motor No. 10 After Gauge Failure

Motor No. 10 was a 10.3-MPa full cylinder with a propellant containing no stability additive and was to be pulsed at 5 and 3% levels. Three high-frequency Kistler gauges were mounted at the forward, middle, and aft ends of the motor. This was supposed to be a repeat of motor No. 4 of the previous year in which the motor was stable to the first pulse and unstable to the second. The difference was enhanced instrumentation with the three gauges. Unfortunately, the motor went spontaneously unstable at about 1 second with the first tangential mode. This was followed by a DC shift in pressure to 41 MPa. At this elevated pressure, the nozzle insert was ejected and the middle and aft gauges blew off and were lost. However, good data were obtained up to this point. Figure 15 is a photograph taken during the firing, after the gauges were lost. Notice the two vertical plumes where the transducers were located.

3.4.4 Conclusions

The purpose of this study was to examine the stability of motors as a function of pulse amplitude, geometry, pressure and propellant formulation. Ten motors with extensive instrumentation to characterize their combustion instability behavior were carefully fired and pulsed. Several significant observations were made from the data. It is important to note that some of the following conclusions were not discussed in this paper. Ref. 1 through 3 have more complete motor firing analyses. It is hoped that the data provided here, and future and past data, will provide

other researchers acoustic oscillatory data for model validation purposes and insight into the physical mechanisms that cause this type of combustion instability.

(1) The susceptibility of a motor to go unstable with pressure was shown in a very clear and precise manner. As pressure was increased, it was easier to pulse a motor unstable. Also the inherent stability of the motors decreased with pressure.
(2) Comparisons with the predicted stability were performed with favorable results. Both the magnitude and trends in the data agreed with the theoretical predictions.
(3) Linear growth rates were observed for both the pulsed longitudinal and spontaneous tangential instabilities.
(4) The triggering level was bracketed between two pulse amplitudes for two sets of motor firings at different pressures.
(5) The function of additives to suppress triggered instability was questioned. It was possible to trigger two motors that used stability additives in their propellant. The motors that did go unstable showed lower than expected DC pressure shifts, which may be due to the additive. In addition, the DC shifts appeared to increase slightly as motor pressure increased.
(6) Detailed acoustic waveform measurements were performed by mounting transducers at three locations along the length of the motor. It showed the expected phase, frequency, and amplitude characteristics as a function of axial location along the motor. Details of these data are available. It should also be mentioned that the noise level for some of the data was less than 7 kPa out of 35 MPa (1 psi out of 5,000).
(7) Extensive frequency analysis was performed on the nonlinear, tangential, and background oscillations. One important conclusion reached here is that the dominant nonlinear oscillations appear to couple with whatever the local tangential modes happen to be.
(8) Detailed analysis was performed on motors No. 5 and 10, which failed. It was concluded that spontaneous tangential oscillations caused the over-pressurization in both motors.
(9) Another important lesson learned in this study is the destructive and potentially violent nature of a motor experiencing combustion instability. The motor tie downs for motor No. 5 were designed with a safety factor of 10 times the expected thrust of 35 kN. The actual thrust achieved reached over 400 kN, or nearly 12 times higher. The presence of instability made things even worse. If motor No. 5 had merely failed due to nozzle blockage, without combustion instability, it is most likely that the motor would merely have burned to completion after ejecting the blockage. The thrust oscillations acted like a jackhammer to cut the retaining bolts. Motor tie down hardware was redesigned with limits in excess of the absolute worst-case scenario.
(10) An added important result of this work has been a working knowledge of dealing with higher-pressure motors in terms of instrumenting, pulsing, and fabricating motor hardware to allow for detailed measurements.

References

1. F. S. Blomshield, C. J. Bicker, and R. A. Stalnaker. "High Pressure Pulsed Motor Firing Combustion Instability Investigations," AIAA Paper 97-3253 (July 1997).
2. F. S. Blomshield and R. A. Stalnaker. "Pulsed Motor Firings: Pulse Amplitude, Formulation and Enhanced Instrumentation," AIAA Paper 98-3557 (July 1998).
3. F. S. Blomshield, "Pulsed Motor Firings," NAWCWD TP-8444, Naval Air Warfare Center Weapons Division, China Lake, CA, August 2000.
4. F. S. Blomshield, J. E. Crump, H. B. Mathes, R. A. Stalnaker, and M. W. Beckstead. "Stability Testing of Full-Scale Tactical Motors," *AIAA J. Propulsion and Power*, Vol. 13, No. 3 (May-June 1997), pp. 349-355.
5. F. S. Blomshield, H. B. Mathes, J. E. Crump, C. A. Beiter, and M. W. Beckstead. "Nonlinear Stability Testing of Full-Scale Tactical Motors," *AIAA J. Propulsion and Power*, Vol. 13, No. 3 (May-June 1997), pp. 356-366.
6. P. G. Harris, A. Champlain, and C. Bourque. "Pulse-Triggered Nonlinear Instability in Solid Rocket Motors: An Experimental Study," AIAA Paper 97-3246 (July 1997).
7. W. G. Brownlee. "Nonlinear Axial Combustion Instability in Solid Propellant Motors," *AIAA J.*, Vol. 2 (February 1964), pp. 275-284.
8. Air Force Rocket Propulsion Laboratory. *Limiting Amplitude Analysis*, by R. C. Jensen and M. W. Beckstead, Hercules, Inc., Magna, UT. Edwards Air Force Base, California, July 1973. (AFRPL-TR-73-61, publication UNCLASSIFIED.)

9. J. D. Baum, J. N. Levine, and R. L. Lovine. "Pulse-Triggered Instability in Solid Rocket Motors," *AIAA J.*, Vol. 22, No.10 (October 1984), pp. 1413-1419.
10. J. D. Baum and J. N. Levine. "Modeling of Nonlinear Longitudinal Instabilities in Solid Rocket Motors," *Acta Astronautica,* Vol. 13, No. 6-7 (June-July 1984), pp. 339-348.
11. J. D. Baum, J. N. Levine, and R. L. Lovine. "Pulsed Instability in Rocket Motors: A Comparison Between Predictions and Experiments," *J. Propulsion and Power*, Vol. 4, No. 4 (July-August 1988), pp. 308-316.
12. Air Force Rocket Propulsion Laboratory. *A Computer Program for the Prediction of Solid Propellant Rocket Motor Performance (SPP), Vol. 5,* by R. W. Hermsen, J. T. Lamberty, and R. E. McCormick. Edwards Air Force Base, California, September 1984. (AFRPL-TR-84-03661, publication UNCLASSIFIED.)
13. Air Force Rocket Propulsion Laboratory. *Standard Stability Prediction Program for Solid Rocket Motors,* by G. R. Nickerson, F. E. C. Culick, and L. D. Dang. Edwards Air Force Base, California, September 1983. (AFRPL-TR-83-017, publication UNCLASSIFIED.)
14. Air Force Rocket Propulsion Laboratory. *T-Burner Testing of Metallized Solid Propellants,* by F. E. C. Culick. Edwards Air Force Base, California, October 1974. (AFRPL-TR-74-28, publication UNCLASSIFIED.)
15. Naval Weapons Center. "Combustion Instability in Minimum Smoke Propellants," by J. E. Crump. China Lake, CA, NWC, November 1977. (NWC TP 5936, publication UNCLASSIFIED.)

3.5 Pulsed Tests of Motors Using Bi-plateau Propellants (Blomshield)

IR&D work conducted by Thiokol Corporation resulted in the achievement of plateau ballistics in practical reduced smoke AP/HTPB propellants.[1] As part of the MURI Programs, this capability has been extended to aluminized AP/HTPB propellants.[2] The key to this development was understanding and exploiting the peculiar combustion characteristics of "wide-AP-distribution" propellants, then accommodating the formulations to aluminum addition in such a way that the aluminum does not disrupt the underlying mechanisms. Bi-plateau behavior in these propellants was achieved by the use of DDI curative; with IPDI or TMXDI curatives, plateaus appear only at high pressures. A variety of tailoring techniques enables a broad range of bum rates for the high pressure plateau; the range of bum rates on the low pressure plateau with DDI cure has been relatively small, and some of the tailoring techniques impair the low pressure plateau. High pressure plateaus can be tailored to occur at very high pressures (e.g., above 4000 psi), with accompanying high bum rates and without the use of expensive or undesirable ballistic modifiers, providing increased performance potential.

A successful test of a 15% aluminum bi-plateau propellant in a 13.6 Kg (30-pound) motor, showing boost-sustain operation (2250 and 480 psi), combustion stability, 92.3% specific impulse efficiency and low throat erosion was reported previously.[2] At the time, that motor was not pulsed (nonlinear stability was not verified), but pulse tests were carried out much later. A similar test was carried out with an 18% aluminum bi-plateau propellant (88% total solids) in which the motor was pulsed during both boost and sustain phases, described here.

PROPELLANTS

FORMULATION

The subject test propellant contains 68% AP (200μ/2μ = 53:47), 18% coarse aluminum (117μ), 2% TiO_2 ballistic modifier additive (0.5μ) and 12% HTPB binder (including 1.5% DOA plasticizer) cured with DDI. It differs from the 15% aluminum propellant in its replacement of 3% AP with aluminum and a small decrease in the AP coarse/fine ratio to accommodate the added aluminum. Reasons for adjusting the AP coarse/fine ratio and using coarse aluminum were discussed previously.[2] There had been concern about using coarse aluminum from the standpoint of combustion efficiency, but that concern was dispelled by the prior test.[2]

MECHANICAL AND BALLISTIC PROPERTIES

The test motor consisted of four segmented cylindrical grains (see below). Propellant to cast the motor was obtained from two 5-gallon mixes. End-of-mix viscosity average for the mixes was 4 Kp at 125°F.

Mechanical properties for the propellant were obtained at 75°F, 2 ipm strain rate, on Class C tensile specimens. Data were obtained on each of the 5-gallon mixes with good reproducibility. The average values of the properties are shown in Table 1, together with those reported previously for the 15% aluminum propellant. There was no attempt to optimize the mechanical properties.

TABLE 1. PROPERTIES OF ALUMINIZED BI-PLATEAU PROPELLANTS

Mechanical Properties (75°F, 2 ipm, Class C)	**15 Wt-% Al**	**18 Wt-% Al**
Modulus, psi	377	966
Maximum Corrected Stress, psi	116	164
Strain at Maximum Corrected Stress, %	36	26
Strain at Failure, %	42	29
Shore A	51	68
Ballistic Properties (80°F, 70-g C. P. Motors)		
High-Pressure Plateau Region, psi	1800 to 2300	1700 to 2300
High-Pressure Plateau Exponent	–0.22	–0.22
High-Pressure Rb, ips at 2000 psi	0.59	0.58
High-Pressure Plateau π_k , %/°F	0.04 (40°F to 135°F)	0.09 (20°F to 120°F)
Low-Pressure Plateau Region, psi	300 to 500	300 to 700
Low-Pressure Plateau Exponent	0.24	0.29
Low-Pressure Rb, ips at 400 psi	0.27	0.26
Low-Pressure Plateau π_k , %/°F	0.09 (40°F to 135°F)	0.09 (20°F to 120°F)

Ambient temperature strand and 70-g C.P. motor bum rate data for the propellant are shown in Table 1 and Figure 1. There is the typical bias between strands and motors at low pressures, the motors producing slightly higher bum rates, but the strands giving slightly higher rates along the high pressure plateau. Another bias (not shown) is that bum rates on the high pressure plateau were slightly higher from 1-gallon mixes. Reproducibility of bum rates and plateaus is very good; the largest variance tends to be at the start of the high pressure plateau, where there is a change in mechanism. Temperature sensitivity, π_k, was determined across the temperature range of 20 to 120°F; data yielding an average π_k of 0.09%/°F at both pressure levels are shown in Figure 2.

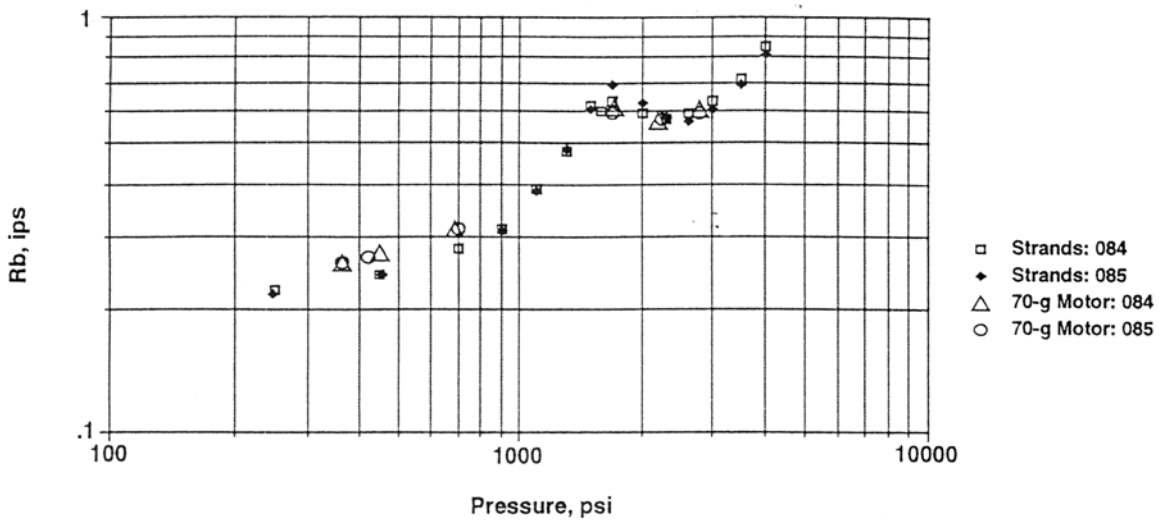

Figure 1. Ballistic Test Results for 18 Wt-% Aluminum Bi-plateau Propellant at 80°F from 5-Gallon Mixes.

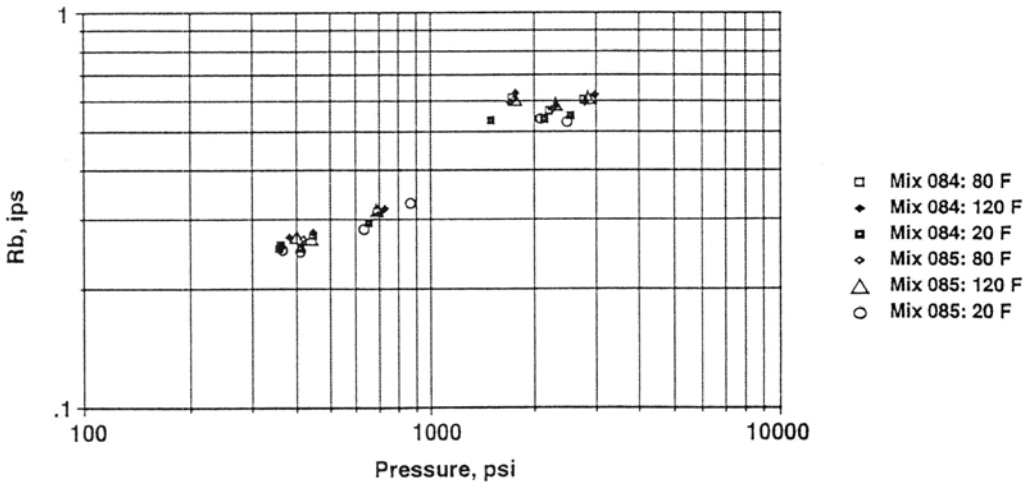

Figure 2. Propellant Temperature Sensitivity, 20°F to 120°F, 18 Wt-% Aluminum Bi-plateau Propellant from 5-Gallon Mixes.

PULSER DESIGN AND TESTING

A motor is said to be "linearly stable" if pressure oscillations are not excited by normally occurring small perturbations in the course of firing. That was the result of the previous test with the 15% aluminum bi-plateau propellant. However, a motor which is linearly stable may be "triggered" into instability by means of a finite-amplitude pulse-such as by debris being expelled from the motor. Such an instability is called a "nonlinear instability" because the initiating disturbance is large enough to invoke higher-order (nonlinear) effects. The standard method for testing the nonlinear stability of a motor is to impose a pressure pulse in accordance with established criteria, representative of pulses encountered from motor experience (e.g., Reference 3 and citations therein). Since the 15% aluminum propellant was linearly stable, it could be expected that the 18% aluminum propellant would also be linearly stable, so the purpose of this test was to acquire nonlinear stability (or instability) data as a part of its evaluation and for use on the MURI program.

The pulser was based on the USNAWC design described in detail in Reference 4. A pyrotechnic charge is used to introduce a pressure pulse into the motor. In order to introduce two pulses, two pulsers were mounted symmetrically about the igniter chamber. The effect of the off-centerline and slightly angled positioning of the pulsers is reported to be negligible regarding the desired one-dimensional pressure wave to be achieved. The pulsers were fabricated and composed for desired performance in accordance with USNAWC specifications. They were tested in chambers pressurized with helium and sized to represent the motor geometries at the times of actuation. It was desired to achieve a 50 psi pulse during boost (2.2% of motor pressure) and a 15 psi pulse during sustain (3.5% of motor pressure). A modification was necessary in order to reliably prevent leakage at the boost pressure level. A series of tests was performed to gain experience with this particular pulser and to quantify its design parameters (orifice size, charge weight, burst diaphragm thickness and insulation) for the desired results.

TEST RESULTS

BALLISTIC PERFORMANCE

Pressure-time data for the test are shown together with ballistic predictions in Figure 3. An unbond occurred or was encountered at 0.5 seconds into the test, which caused the pressure to rise suddenly from 2250 to 2550 psi. There was no high-frequency activity during this time as would assign the cause to combustion instability, and the first pulse had not yet fired. Inspection of post-fire hardware showed unusual erosion patterns consistent with non-bonded areas around the grain circumference. Guided by this scenario, a ballistic reprediction was able to match the observed pressure-time behavior. After the burning front passed though the non-bond region and its effect upon the grain burn pattern burned away, the pressure-time behavior returned to normal.

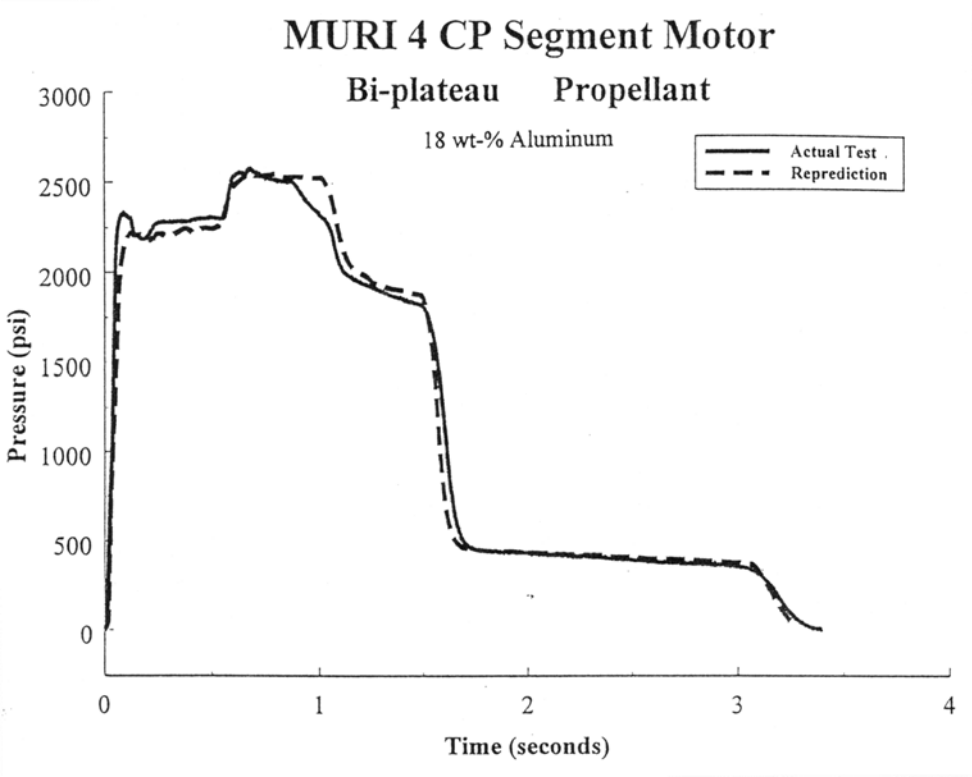

Figure 3. Actual and Predicted Pressure-Time Traces.

PULSE TESTS

Figures 4 and 5 show details of the pulses and pulse decays by two different signal processing methods. The "a" figures are for digital data over the range 100 Hz–110KHz at a sampling rate of 50 KHz. The "b" figures used a 200 Hz high pass to filter out an apparent transducer ringing and other high-frequency noise. These raise a question about the actual pulse magnitudes achieved. With the pulser configured from an "a" analysis of the helium test chamber data, the desired pulse magnitudes were achieved. But a "b" analysis would indicate that the actual pulse magnitudes were much lower, such that the pulsers would need to be strengthened in future tests.

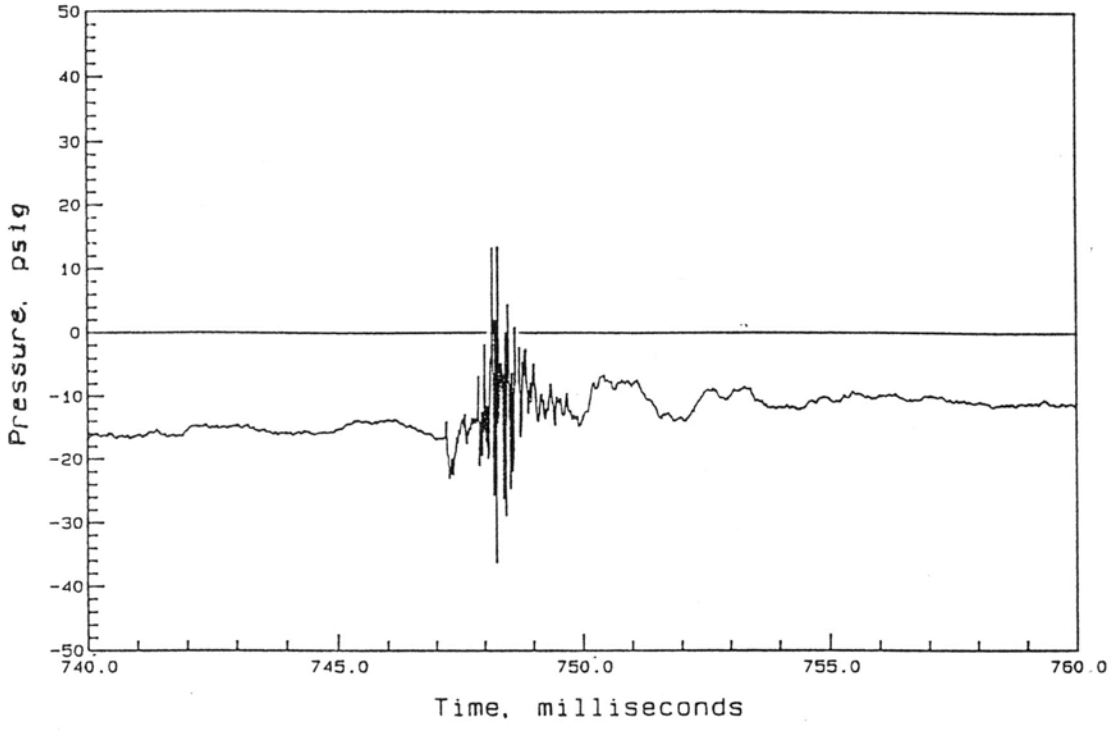

(a) Digital Data, 100 Hz - 10 KHz, 50 KHz Sampling

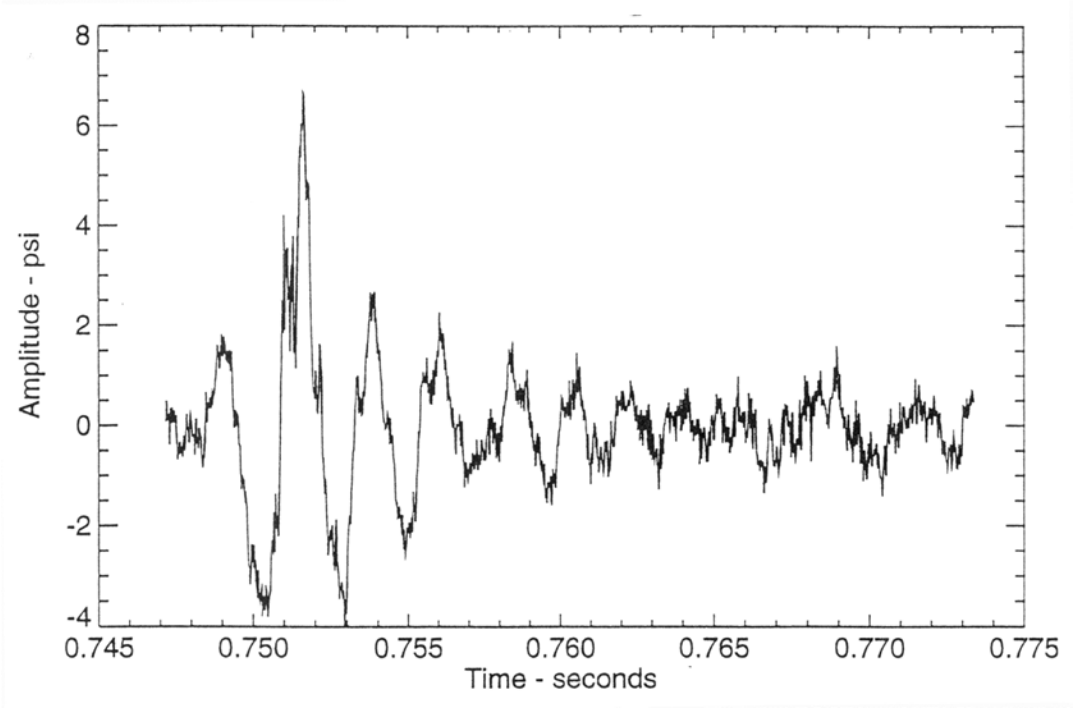

(b) 200 Hz High Pass

Figure 4. First Pulse AC Data, Forward Closure High-Frequency Gage.

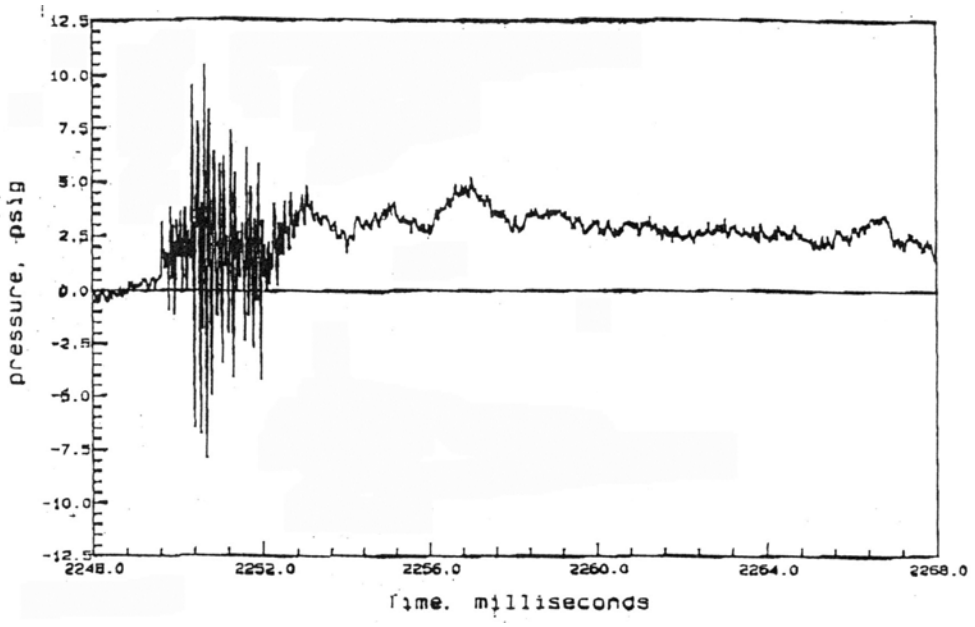

(a) Digital Data, 100 Hz – 10 KHz, 50 KHz Sampling

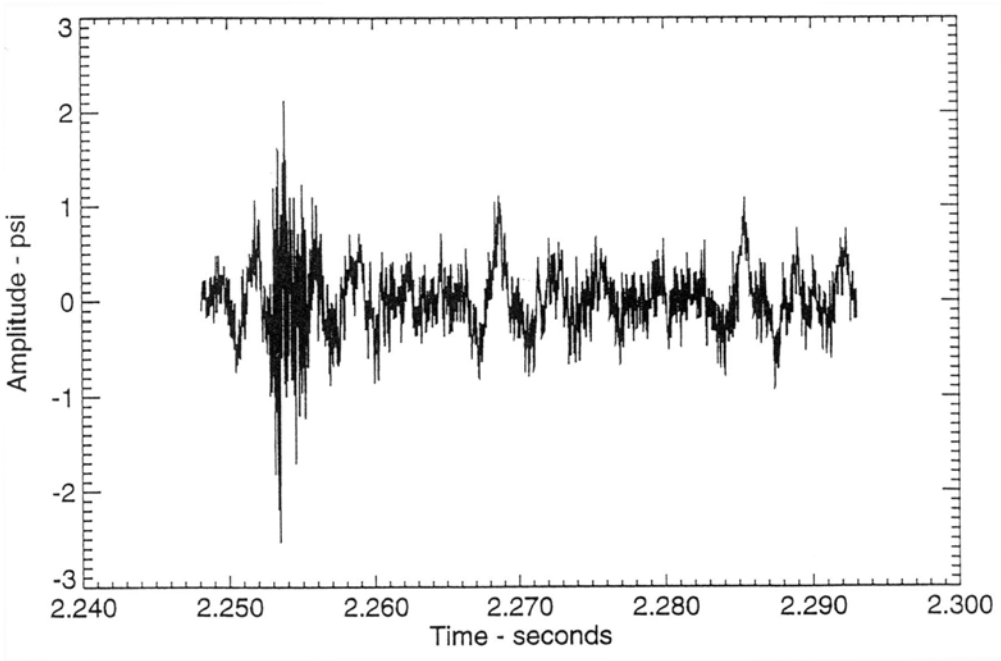

(b) 200 Hz High Pass

Figure 5. Second Pulse AC Data, Forward Closure High-Frequency Gage.

CONCLUSIONS

Aluminized bi-plateau propellants with up to 18 wt-% aluminum were successfully demonstrated in a 13.6 Kg (30-pound) class motor. Operation and transition between boost and sustain pressure modes were achieved with good specific impulse efficiency (92.3 % with 15 wt-% aluminum, 91.9% with 18 wt-% aluminum), acoustic stability and low nozzle throat erosion. Good combustion efficiency is still achieved with coarse aluminum at the 18 wt-% level. An advantage of plateau ballistics was confirmed by the motor response to a fortuitous propellant debond or non-bond which was encountered. The latest test incorporated pulsers to test for nonlinear stability during the boost and sustain phases. The decay of the first (boost) pulse showed a large margin of stability. It seems that the combustion response of the propellant is smaller than was expected, possibly because of the suppression of the fine AP that is a part of the proposed plateauing mechanism. It was not possible to quantify the decay of the second (sustain phase) pulse. This test information is available for use under the MURI program.

References

1. Hinshaw, C. J. and Cohen, N. S., "Achievement of Plateau Ballistics in AP/HTPB Propellants", 32"' JANNAF Combustion Meeting, Huntsville, AL, October 1995.
2. Hinshaw, C. J., Mancini, V. E., and Cohen, N. S., "Development and Demonstration of Aluminized AP/HTPB Propellants Having Plateau and Biplateau Ballistics", 1995 JANNAF Propulsion Meeting, Tampa, FL, December 1995.
3. Lovine, R. L., and Micheli, P. L., *Nonlinear Stability for Tactical Motors* (5 Volumes), AFRPL-TR-85-017, Aerojet Tactical Systems Co., Sacramento, CA, October 1985.
4. Blomshield, R. S., et al., "Nonlinear Stability Testing of Full-Scale Tactical Motors", *AIAA Journal of Propulsion and Power*, Vol. 13, No. 3, May–June 1997, pp 356–366.
5. Cohen, N. S. and Strand, L. D., "Combustion Response to Compositional Fluctuations", *AIAA Journal of Propulsion and Power*, Vol. 23, No. 5, May 1985, pp 760–767.
6. Cohen, N. S., "Why Negative Exponent Propellants Can Exhibit Combustion Instability", 30th JANNAF Combustion Meeting, November 1993.
7. Blomshield, F. S., et al., Stability Testing of Full–Scale Tactical Motors", *AIAA Journal of Propulsion and Power*, Vol. 13, No. 3, May–June 1997, pp 349–355.

ATTACHMENTS

Attachment A

MURI Propellants

Cohen Associates, Redlands, CA

PHASE 1 PROPELLANTS

Phase 1 propellants were a series of AP/HTPB formulations which exhibit plateau or bi-plateau ballistics, including variants designed to explore features and mechanisms of this behavior. The formulations are listed in Table 1. These propellants were furnished by the Thiokol Propulsion Division of Cordant Technologies (Thiokol).

The objective of the MURI program is to develop techniques and understandings that will assure the stability of future solid rocket motors containing advanced energetic propellants. That was the general guideline for selecting the propellants to be tested, but other constraints influenced the choices, including availability, cost, and contemporary views of program managers and advisors.

The plateau and bi-plateau propellants are a novel advanced form of AP/HTPB propellant. While they do not contain advanced energetic ingredients, the plateau property offers significant gains that are equivalent to energy gains from a design or systems standpoint. It is the first time that plateaus have been achieved in practical AP/HTPB propellants, both reduced-smoke and aluminized. Selection of these propellants for Phase 1 was endorsed by Dr. Dick Miller, ONR.

The purposes in testing these propellants are:

- to gain mechanistic understandings of the plateau behavior.
- to discern the stability implications of the plateau behavior or the combustion processes associated with it.
- to check out novel experimental techniques for the measurement of stability properties, *e.g.*, response functions, and apply them to this family of plateau propellants.
- to acquire a sequence of data from devices ranging from laboratory apparatus to sub-scale motors in order to develop and validate our understandings and models of stability from the standpoint of the combustion (propellant) and its coupling with the gasdynamics of the rocket motor chamber (motor).

PHASE 2 PROPELLANTS

There are two sets of Phase 2 propellants, one set furnished by Thiokol and the other by the Chemical Systems Division of United Technologies (CSD).

A) THIOKOL ADVANCED ENERGETIC BINDER FORMULATIONS

The Thiokol formulations are azido-oxetane binder systems representing an advanced energetic binder of interest. This is in keeping with the advanced energetic ingredient aspect of the MURI objective (approved by Dr. Dick Miller, ONR).

There are two sets of two formulations:

- "propellants" containing a conventional bi-modal distribution of AP, in a binder composed of BAMO-AMMO co-polymer plasticized with GAP, one reduced-smoke and one aluminized
- "binders", which are energetic monopropellants, one being the binder used in the above propellants and another in which polycaprolactone (PCP) is substituted for GAP

TABLE 1. MURI Propellant Formulations, Phase 1

MIX NUMBER CJH-1258-90- MIX SIZE	1a 1-Gal	1 5-Gal	2 1-Gal	4 5-Gal	5 1-Gal	6 1-Gal	6a 1-Gal	7a 1-Gal	8 1-Gal	9 1-Gal	10 1-Gal
Ingredient, wt%											
R45M	8.244	8.244	9.189	8.244	9.189	19.037	24.902	27.755	8.244	8.244	8.244
Tepanol	0.075	0.075	0.075	0.075	0.075	0.073	0.075	0.075	0.075	0.075	0.075
DOA	2.000	2.000	2.000	2.000	2.000	4.593	6.006	6.006	2.000	2.000	2.000
ODI	0.030	0.030	0.030	0.030	0.030	0.059	0.030	0.030	0.030	0.030	0.030
DDI	1.651	1.651	---	1.651	---	3.823	4.987		1.651	1.651	1.651
IPDI	---	---	0.706	---	0.706	---	---	2.134	---	---	---
TiO_2	2.000	2.000	2.000	2.000	2.000	4.177	6.000	6.000	2.000	2.000	---
AP (200u)	39.050	44.020	44.020	53.320	53.320	---	---	---	47.300	60.200	54.560
AP (2u)	31.950	26.980	26.980	32.680	32.680	68.238	58.000	58.000	38.700	25.800	33.440
AI (H-95)	15.000	15.000	15.000	---	---	---	---	---	---	---	---
Mix Number	AC 0304/0305	209-96- 065	AC 0189	209-96- 064	AC 0190	AC 0191	AC 0317	AC 0193	AC 0194	AC 0195	AC 0196
Total % AP	71	71	71	86	86	68.238	58	58	86	86	88
AP C/F	55:45	62:38	62:38	62:38	62:38	0:100	0:100	0:100	55:45	70:30	62:38
Total % Binder	12	12	12	12	12	27.585	36	36	12	12	12
Fine AP/Binder	2.66	2.25	2.25	2.72	2.72	2.47	1.61	1.61	3.22	2.15	2.79
Interstitial Space, u	0.37	0.47	0.47	0.37	0.37	0	0.12	0.12	0.25	0.52	0.36

Interstitial spacing calculations based on an assumed fine AP size of 1.7u for consistency with earlier calculations.
Equivalent weight differences between IPDI and DDI require different weight % for same NCO/OH (0.90).

The purposes in testing these formulations are:

- to acquire data with which to refine recent analytical models of the combustion of azido type binders and develop models of propellant combustion for such binders combined with AP.
- to discern the stability implications of using azido-type binders.
- to apply the novel experimental techniques for the measurement of stability properties.
- to acquire data in order to develop and validate our understandings and models of combustion instability, as applied to azido-type systems.

TABLE 2. MURI Propellant Formulations, Phase 2 (Thiokol)

	1”	2”	3”	6”
BAMO-AMMO	7.58	7.58	36.20	45.20
GAP	11.99	11.99	59.99	---
PCP	---	---	---	38.70
AP (200μ)	63.20	49.6	---	---
AP (20μ)	15.80	12.40	---	---
Aluminum (5μ)	1.00	18.00	---	---
curatives	0.43	0.43	3.81	16.10

NOTE: Formulations 3 and 5 were omitted due to high costs.

B) CSD AP/HTPB AND GAP PROPELLANTS

The CSD propellants represent more near-term interests, including a type of AP/HTPB formulation that was a basis for motivating the MURI program (approved by Dr. Len Caveny, BMDO).

There are a total of 5 propellants, all of which are aluminized. Four are AP/HTPB formulations, three of which vary AP size distribution and one replaces a portion of AP with HMX. The fifth is an AP/GAP binder formulation, using GAP as polymer rather than plasticizer.

The purposes in testing these formulations are:

- to apply the novel experimental techniques to measure stability properties
- to discern effects of AP particle size and HMX addition on stability properties
- since there is motor experience with this type of AP/HTPB propellant, to acquire data to develop and validate our understandings and models of stability from the standpoint of the combustion (propellant) and its coupling with the gasdynamics of the rocket motor chamber (motor)
- to further develop models of AP/GAP propellant combustion and discern their stability implications (more azido-type binder work)

TABLE 3. MURI Propellant Formulations, Phase 2 (CSD)

	2”	3”	4”	5”	6”
R-45 HTPB	7.14	7.14	7.14	7.14	---
DOA Plasticizer	3.00	3.00	3.00	3.00	---
GAP polymer	---	---	---	---	22.60
AP (200μ)	69.00	52.00	41.00	59.00	55.00
AP (2.8μ)	---	17.00	28.00	---	---
HMX (20μ)	---	---	---	10.00	---
Aluminum (17μ)	19.00	19.00	19.00	19.00	19.00
curatives & agents	1.86	1.86	1.86	1.86	2.40
additives	---	---	---	---	1.00

NOTE: Formulation 1 was unavailable during the test period.

PHASE 3 PROPELLANTS

Phase 3 propellants are based upon using a nitrato-type energetic binder of current interest for insensitive munitions (recommended by Dr. Dick Miller) and due to relatively low cost. It makes use of past experience and combustion research with nitrato-type chemistry. Both reduced-smoke and aluminized versions are of interest for a range of applications. The propellants were provided by Alliant Techsystems.

TABLE 4. MURI Propellant Formulations, Phase 3 (Alliant Techsystems)

	1*	2	3	4	5*	6	7
BuNENA-plasticized polyether (PE) binder	20	20	20	15	20	20	20
AP (size?)	50	50(s)	60	44	70	70(s)	80
AN (size?)	10	10	---	---	10	10	---
Aluminum (size?)	20	20	20	20	---	---	---
Bismuth Trioxide (size?)	---	---	---	21	---	---	---

The purposes in testing these formulations are similar to those given above for the Phase 1 and 2 propellants, but now involving a nitrato-type binder and AN. The propellant families of current interest (HTPB, azido, nitratoPE) are thereby given representation. Also, the choice of Alliant Techsystems as supplier established firm connections between the MURI programs and the three main U.S. suppliers of propellants.

Attachment B

Caltech-sponsored MURI Workshops

Workshops are a major means of achieving collaboration among the participants

- **1995 Workshops**

1995 October	Initial "Kick-Off" Meeting in Huntsville, AL (Caltech and UIUC separately)

- **1996 Workshops**

1996 January	General Reviews (Caltech and UIUC separately)
1996 April	Caltech General MURI Review following the BMDO/MURI Review
1996 November	General Caltech and UIUC Annual Review, JANNAF Combustion Meetings

- **1997 Workshops**

1997 January	Workshop on Bi-Plateau Propellant Testing, Reno, NV
1997 March	Review of Russian Propellant Chemistry Projects, Huntsville AL
1997 March	Workshop on Rocket Motor Combustion Instability and Flow Problems, China Lake, CA
1997 May	MURI Program Review, Washington DC
1997 June	Review of Russian Propellant Combustion Projects, Milan Italy
1997 June	Review of Russian Propellant Chemistry Projects, Karlsruhe, Germany
1997 July	Workshop on Bi-Plateau Propellant Testing, Seattle, WA
1997 July	Workshop on Rocket Motor Combustion Instability and Flow Problems, San Diego, CA
1997 October	MURI Program Review, West Palm Beach, FL
1997 October	Workshop on Bi-Plateau Propellant Testing, West Palm Beach, FL

- **1998 Workshops Conducted at the Aerospace Sciences Meeting, Reno, NV**

1998 January	Analysis of Motor Flow Field Dynamics
1998 January	Workshop on ADN
1998 January	Review of Russian Work (Contractors)
1998 January	Aluminum Agglomeration

- **1998 Workshops (Other)**

1998 June	Review Meeting with Russian Contractors (Moscow)
1998 July	Combustion of Aluminum, Joint Propulsion Meeting (Cleveland, OH)
1998 July	Response Measurements, Joint Propulsion Meeting (Cleveland, OH)
1998 July	Task 2 / Task 3 Interactions Workshop (Cleveland, OH)
1998 July	Informal Workshop on The Method of Spatial Averaging (NAWC and SEA, Inc.)
1998 August	MURI Review Meeting (Washington, DC)
1998 December	The MURI Program on Stability After Three Years: A Review (Held at the 35th JANNAF Combustion Meeting, Tucson, AZ)

- **1999 Workshops**

1999 May	MURI/Thiokol Workshop on Bi-Plateau Propellants
1999 February	MURI Workshop on Boundary Conditions (Caltech, Pasadena, CA)
1999 June	MURI Assessment & Planning Meeting (Caltech, Pasadena, CA)
1999 October	MURI Review Meeting (Held at the 36th JANNAF Combustion Meeting, Cocoa Beach, FL)

Attachment C

A Workshop Report:

Mechanisms for Plateau Behavior in AP/HTPB Propellants[*] (Cohen)

INTRODUCTION

The relatively recent achievement of plateau and bi-plateau ballistics in AP/HTPB propellants was incorporated into the MURI program by selecting a series of formulations for phase 1 experimental studies. They are considered to be an advanced form of conventional propellants having potential in the long term. Plateau ballistics (zero or negative pressure exponents) offer performance and cost advantages, and bi-plateau ballistics (plateaus at both high and low pressures) are attractive for boost-sustain applications.

The objectives of the Workshop were to discuss the mechanisms of the plateau and bi-plateau behavior, their implications for combustion stability and needs for additional work. Supporting experimental and analytical work provided the bases for these discussions.

BACKGROUND

The Foundational Work

It is agreed that these forms of plateau ballistics in AP/HTPB propellants are derived from abnormal burning characteristics which have been observed and studied since the 1960s. The phrase "abnormal burning" came about because the combustion behavior did not fit, and could not be explained by, contemporary models. The abnormality is characterized by a depressed burning (compared to what would be expected) and, in more extreme cases, by an inability to sustain burning at intermediate pressures ("intermediate pressure extinction").

Prior to the development of the plateau propellants, certain facts were known about abnormal burning. In monomodal AP propellants formulated for research purposes, abnormal burning is promoted by lower concentrations of finer particle size AP. Thus fuel-richness is thought to be a factor. It is also a strong function of binder composition: it is promoted by incorporating and increasing the concentration of plasticizer, it is affected significantly by polymer type and the type of curative used, and it can be eliminated by incorporating very fine particulate additives such as carbon black. Thus binder liquefaction and decomposition properties are also thought to be important. In bimodal AP propellants that are suitable for practical applications, the abnormality is promoted by using "wide AP size distributions": combinations of very fine and very coarse AP at certain coarse/fine ratios. Here, the thinking is that the bimodal propellant is formulated in a way that evokes the abnormal property of the fine AP/binder matrix component—the same as in the monomodal research formulations.

[*] This attachment was originally prepared as the report of the Caltech MURI Workshop held in 1999, jointly sponsored by Thiokol, Inc. The report was circulated to all interested parties.

Plateau Propellant Development

The plateau and bi-plateau ballistics were achieved by exploiting the abnormal burning property of wide-distribution propellants. It was found that incorporating various types of very fine particulate additives eliminated the depressed burning. They included a strong catalyst, a mild catalyst and non-catalysts, in terms of their known effects in normal-burning propellants. Plateaus were uniquely brought about by the addition of very fine titanium dioxide, which is a weak catalyst (at most small effects in normal-burning propellants). The forms taken by the plateaus suggested transitions between degrees of normal burning and depressed burning, as affected by the presence of the additive.

Plateau behavior was achieved with IPDI-cured HTPB, bi-plateau behavior was achieved with DDI-cured HTPB. The effect of curative was large, and the formulations contained plasticizer, consistent with what had been observed in the depressed burning studies of the research-type formulations. The propellant development included formulation variations to observe trends and limitations on the plateau behavior.

Trends and Limitations on Plateau Behavior

Work with the IPDI-cured HTPB binder established the following trends and limits upon the plateau behavior (variables & baseline values for the plateaus are underlined):

- increasing AP level from 86-88% resulted in increased burn rates and high exponent characteristic of fine AP propellants, without a plateau; reducing AP level to 85% resulted in decreased burn rates and a less pronounced plateau
- reducing coarse/fine ratio from 62/38 to 55/45 resulted in increased burn rates and high exponent characteristic of fine AP propellants, without a plateau; increasing the coarse/fine ratio to 70/30 resulted in decreased burn rates characteristic of coarse AP propellants, without a plateau
- increasing fine AP size from 2μ to 9μ resulted in decreased burn rates and a less pronounced appearance of the plateau; larger fine AP sizes did not produce a plateau
- increasing the coarse AP size from 200μ to 400μ had a small effect on the plateau
- increasing DOA plasticizer level from 2% - 3% resulted in a more pronounced plateau; decreasing it to 1% resulted in a less pronounced plateau
- reducing additive level from 2% to 1% resulted in decreased burn rates and a washing out of the plateau (much less pronounced)
- reducing additive particle size from 0.5μ to 0.02μ increased high pressure burn rates and pushed the plateau up to higher burn rates & pressures
- aluminum addition maintains plateau behavior provided that coarse aluminum is used and the AP coarse/fine ratio is adjusted downward

With DDI-cured HTPB binder:

- reducing AP level to 85% lowered burn rates, did not impair the low pressure plateau but made the high pressure plateau less vivid
- reducing coarse/fine ratio to 55/45 increased burn rates, impaired the low pressure plateau (higher exponent) but markedly accentuated the high pressure plateau; increasing it to 70/30 washed out the plateaus
- fine AP size was not varied in the DDI-cured system
- increasing the coarse AP size to 400μ lowered burn rates without impairing either of the plateaus
- increasing DOA plasticizer level lowered burn rates without impairing the plateaus

- reducing additive level to 1% lowered burn rates, did not impair the low pressure plateau but impaired the high pressure plateau to a small extent
- reducing additive particle size to 0.02μ increased the low pressure burn rates in such a way as to impair the low pressure plateau (higher exponent), and shifted the high pressure plateau upwards in the same way as with IPDI-cure
- aluminum addition maintains the bi-plateau behavior provided that coarse aluminum is used and the AP coarse/fine ratio is adjusted downward

EXPERIMENTAL RESEARCH ON PLATEAU MECHANISMS

The following experiments have been performed which help to elucidate the combustion mechanisms:

- burn rate as functions of pressure and conditioning temperature
- mass loss vs. temperature (thermogravimetric analysis, TGA, slow decomposition)
- heat absorbed vs. temperature (differential scanning calorimetry, DSC, slow decomposition)
- rates of decomposition (flash pyrolysis, fast decomposition)
- burn rate as a function of surface temperature (microthermocouple data, surface decomposition kinetics)
- liquefaction and melt fluidity (hot stage microscope, slow decomposition)
- viscosity measurements on fluid binder components, and effect of additives
- extinguished surface observations, AP/binder/AP sandwiches
- intermediate pressure extinguishment maps for model research formulations
- extinguished surface observations, propellants, as a function of pressure

Some of these experiments were performed on other programs but are included because of their relevance. A brief summary highlighting the essential facts will be given in this section, except that burn rate and extinguished propellant surface data will be combined with a discussion of mechanisms later. Also, the σp (burn rate vs. conditioning temperature) data will be deferred to a discussion of stability implications which will include response function and motor test data.

Decomposition Data

TGA data showed no difference between IPDI-cured and DDI-cured HTPB samples plasticized with DOA. It appeared that DOA volatility was the initial step in the mass loss process.

For HTPB samples, there was no effect of the presence of TiO_2 on TGA decomposition. For propellant samples (AP/HTPB), the presence of TiO_2 accelerated the decomposition in both TGA (slow) and flash pyrolysis (fast) methods.

DSC data showed no difference in the thermograms between IPDI-cured and DDI-cured HTPB samples, heated in an inert atmosphere. However, data in air showed exotherms that were more pronounced with IPDI.

Arrhenius plots from the microthermocouple data showed no discontinuity across plateau and non-plateau pressure regions as would indicate a change in surface decomposition mechanism.

Binder Liquefaction and Fluidity

DDI-cured HTPB liquefied instantly at 260 C and the melt was observed to be very fluid. IPDI- cured HTPB liquefied slowly beginning at 360 C and the melt was observed to be mildly fluid. The hot-stage decompositions were complete at 500 C, in agreement with TGA results.

The presence of TiO_2 in the hot-stage experiments stiffened the melts and left a residue upon completion of the binder decomposition.

Viscosity measurements were made on uncured R-45 pre-polymer on the theory that it would represent liquefied polymer. This theory, and that polymerization could be reversible, is controversial [formation of Diels-Alder adducts can provide reversibility]. The viscosities of DOA and IPDI are comparable and considerably below the viscosity of R-45. The viscosity of DDI is higher than that of IPDI and comparable to a representative mixture of R-45 & DOA.

The addition of fine or ultrafine TiO_2 to liquid R-45 increased the viscosity, more so with the ultrafine. But these increases were much less than with additions of other fine particulates having lower specific surfaces. Those other fine particulates produced normal-burning propellants.

Extinguishment Maps

Intermediate pressure extinction regions of model propellants were broadened by decreasing AP particle size, and were much broader with DDI-cure than with IPDI, in agreement with prior research reported in the literature.

Extinguished sandwiches showed evidence of a more fluid binder melt with DDI-cure than with IPDI. Lateral binder flow and coverage of the adjacent AP surface were more extensive with DDI.

DISCUSSION OF BASIC MECHANISMS

Effects of Curative and Plasticizer

The significant difference between DDI-cured HTPB and IPDI-cured HTPB is in their liquefaction and melt properties. Their kinetics and energetics of decomposition are the same in inert atmospheres, but can be different in oxidative environments. Oxidative environments introduce the possibility of gas phase reactions, which would confuse the decomposition issue but can be relevant to the overall combustion process.

DDI-cure yields a lower liquefaction temperature and a more fluid melt. The differences are large. A possible explanation is that DDI-cure produces a more symmetrical polymer structure which facilitates unzipping.

DOA plasticizer serves to lower the viscosity of liquefied binder as long as it is present in the liquid layer. Since it appears to volatize relatively early in the binder decomposition process, its rate of volatilization compared to other rates can be significant in its effect upon the combustion process as a function of pressure.

Depressed Burning

Depressed burning can come about by a combination of the fuel-richness of the fine AP/binder matrix and binder melt layer interference with the ability to establish the normal multiple flame structure about the fine AP. These are promoted by lower concentrations of finer AP in the matrix (finer AP spaced further apart), and a thicker and more fluid binder melt layer. A possible explanation is that the smothered fine AP decomposes in the condensed phase, and the gases bubble through to create a sort of low-energy energetic binder that does not contribute significantly to the rate of heat feedback to the matrix surface. The combustion is sustained primarily by the multiple flame structure or leading edge flame about the coarse AP particles.

Why does the depressed burning maximize at intermediate pressures? The fuel-richness of the matrix does not change with pressure. An explanation is that there is a trade-off between melt layer thickness, which decreases with increasing pressure (or increasing rates), and melt fluidity which increases with increasing pressure (or increasing temperature in the melt). At low pressure, the melt is thicker but too stiff; at high pressure, the melt is more fluid but too thin. An optimum combination arises at intermediate pressures. The point at which DOA volatility becomes significant may also be a factor in ending the depressed burning at higher pressures.

The fuel-richness of the matrix does not change with curative. DDI-cure produces a more extensive depressed burning because it facilitates binder liquefaction and yields a more fluid melt.

The depressed burning of pure monopropellant AP crystals at relevant pressures was considered as a possible mechanism and rejected. This depressed burning of the pure AP disappears when small amounts of fuel are present in pressed powders, and the depressed burning of propellants is so dependent upon binder composition and AP variables that it must be a propellant effect.

Effect of TiO_2

The presence of TiO_2 retards the fluidity of the binder melt. It has no effect on binder decomposition rates in inert atmospheres but accelerates the decomposition of AP/binder propellants. In decomposition experiments with propellants, as with oxidative environments, the possibility of gas phase reactions cannot be ruled out. However, TiO_2 is considered to be a weak catalyst in normal-burning propellants. For these reasons, plateau behavior is more likely brought about by effects of TiO_2 on the melt layer interference process than on reaction rates. It is complicated because it involves transitions between various degrees of normal and depressed burning.

TiO_2 seems to have a unique surface morphology because it produces relatively modest increases in the viscosity of uncured R-45 for its specific surface area. It is just right for plateau behavior. Other additives which produce larger viscosity increases restore normal burning such that there are no plateaus.

A question was raised about the proximity of the TiO_2 particles in the matrix. They are the smallest particles in the formulation (0.5μ), 1/6 the weight fraction of the binder in which they are situated. A pocket model calculation results in 4 particles within each pocket framed by the fine AP, and that the particles are spaced 1.5 diameters apart.

DISCUSSION OF PLATEAU MECHANISMS: BURNING RATE DATA AND EXTINGUISHED PROPELLANT SURFACE OBSERVATIONS

IPDI-Cured HTPB, No Additive

Burn Rate Data: [This was not one of the MURI formulations, but Thiokol had prepared it and acquired burn rate data as part of its developments.] For pressures < 2300 psi, r = 0.5 in/sec @ 1000 psi with n = 0.5. For pressures > 2300 psi, n rapidly increases with pressure to n > 1.

Extinguished Surfaces: No data.

Mechanistic Discussion: Burning is considerably depressed compared to what would be expected for this AP loading and size distribution, based upon combustion model calculations and data for unplasticized HTPB cured with TDI (r = 1.2 in/sec @ 1000 psi, n = 0.9). It appears that the data will merge with normal-burning expectations at a pressure of about 5000 psi.

It is agreed that the depressed burning is caused by binder melt layer interference with the fine AP such that a flame structure does not develop or, if it can develop, it is so fuel-rich and the flame temperature so low that the matrix burns at a slow rate. The propellant burning is driven and controlled mainly by the flame processes about the coarse AP particles.

Artificial combustion model calculations (turning off the fine AP) infer that the depressed burning maximizes at intermediate pressures, in agreement with the intermediate pressure extinction phenomenon. This maximal depression is believed to be due to a trade-off between melt layer thickness and fluidity, which achieves optimal combinations for interference at intermediate pressures. Model computations of melt layer thicknesses and propellant surface structures confirm the feasibility of binder melt layer interference with a 2μ AP size.

At high pressures, the binder melt is becoming too thin or too stiff to be able to interfere with the fine AP such that normal burning is quickly restored with increasing pressure. It is becoming too thin because of the higher rates, or too stiff because the DOA plasticizer may be volatizing more rapidly. The coupled flame structure complex involving the fine and coarse AP compensates for the fuel-richness of the matrix to achieve the normal higher burn rates. The rapid restoration of normal burning is manifested by the very high exponent (n).

DDI-Cured HTPB, No Additive

Burn Rate Data: At pressures < 2000 psi, rates and exponents are less than with IPDI-cure:

r = 0.3 in/sec @ 1000 psi with a plateau (n ~ 0) from 700-1700 psi. Note that there is a plateau region without the additive in the formulation. For pressures > 2000 psi, n rapidly increases with increasing pressure to n > 1.

Extinguished Surfaces: In the plateau region, there are burned-out or nearly burned-out coarse AP hollows burned into a relatively flat matrix surface. In the nearly burned-out hollows, the coarse AP surfaces are dished-down concave into the matrix. At higher pressures, above the plateau, the surface flattens out in that the coarse AP

surfaces are less recessed into the matrix or are level with the matrix. At still higher pressures, in the high exponent region well above the plateau, the coarse AP surfaces become raised relative to the matrix plane.

Mechanistic Discussion: The ability of the coarse AP particles to burn ahead of the matrix confirms the retardation of the matrix. In theory, for normal burning, the matrix should be burning much faster than the coarse AP. As pressure increases above the plateau region, the matrix progressively catches up to the coarse AP and is eventually able to burn ahead of the coarse AP.

The added retardation with DDI-cure relative to IPDI-cure is attributed to the lower liquefaction temperature and more fluid binder melt with DDI. Thus the binder melt is thicker and more mobile such that melt layer interference is more effective and extensive with DDI. This shows up as lower burn rates and a lower exponent than with IPDI. Discussion of the high-pressure behavior would be the same as with IPDI-cure, as above.

IPDI-Cured HTPB, with TiO_2

Burn Rate Data: At pressures below 1400 psi, the burn rate and pressure exponent are very close to what would be expected for normal burning: r = 1 in/sec @ 1000 psi with n = 0.9. A mesa region (negative exponent) occurs between 1400 and 2100 psi in which the burn rate falls by 15% in the well of the mesa. At pressures > 2100 psi, the exponent rapidly increases to n ~ 1.

Extinguished Surfaces: In the low-pressure, high-exponent region, well before the start of the mesa, the surface is flat - comparable to the DDI-cured, no-additive case above its plateau. The TiO_2 (confirmed by EDAX returns) appears as clusters on the surfaces of the coarse AP particles which are level with the matrix. At a pressure just below the start of the mesa, the surface is very different. The coarse AP is now raised significantly above the matrix, the matrix appearing as valleys or canyons between coarse AP particles which appear as boulders. In the well of the mesa, and at a pressure above the mesa (same burn rate as just before the mesa), the surface structure continues to have this lumpy appearance; no quantitative differences could be observed.

Mechanistic Discussion: By one view, the TiO_2 has increased the viscosity of the melt (stiffened the melt) so as to block the melt layer interference at low pressures and thereby restore normal burning. Another view is that the TiO_2 catalyzes the interaction between the fine AP and binder. Specifically, it is believed that the TiO_2 accelerates $HClO_4$ decomposition ($HClO_4$ is a product of AP decomposition) to cause an exotherm within the matrix so as to facilitate binder decomposition and establish the coupled flame structure complex. The progressive ability of the matrix to burn faster than the coarse AP as pressure increases is an expected result for normal burning.

There is a similar difference of opinion regarding the mesa. One view is that the melt layer becomes sufficiently fluid, even with the TiO_2 present, to cause some partial degree of suppressed burning. The melt is more fluid because the flames are situated closer to the surface so as to heat the melt to higher temperatures. That is the pressure-dependent process which drives the effect. However, in arriving at the lower burn rate in the mesa, the

melt layer thickens and cools (stiffens) where portions of the fine AP become suppressed so that there is a partial reversal in the melt response. An equilibrium balance is achieved at a lower burn rate.

The other view is that catalysis by TiO_2 becomes less effective at higher pressure because its time constant becomes longer than the time constant for the underlying reaction (either $HClO_4$ decomposition or its interaction with the binder). This mechanism is analogous to the loss of catalysis in double-base propellants (catalyzed by lead compounds), which produces plateaus and mesas in those propellants. The loss of catalysis by TiO_2 here allows some degree of matrix inhibition to set in from the binder melt layer.

The high exponent at high pressures manifests a restoration of normal burning, the same as without the additive. One possibility is that the melt becomes too thin to be an effective suppressant, no matter how fluid. The turnaround from the mesa results from the steepening temperature gradients due to the thinning flame zones, such that equilibrium begins to occur at higher burn rates. Another possibility is accelerated DOA volatility such that the melt stiffens.

DDI-Cured HTPB, with TiO_2, Baseline Coarse/Fine AP Ratio

Burn Rate Data: The "low pressure plateau" is actually a low-exponent region between 150 and

700 psi, with a burn rate of 0.3 in/sec @ 700 psi - similar to the result without additive. There is then a "transition region" between 800 and 1600 psi, which is a region of high exponent, whereby the burn rate reaches 0.6 in/sec ($n \sim 1$). This region corresponds to the plateau region in the no-additive analog. A weak mesa, more like a plateau ($n \sim 0$), follows from 1700 - 3000 psi. This is the "high pressure plateau". At pressures > 3100 psi, the exponent rapidly increases with pressure to $n > 1$.

Extinguished Surfaces: Results were similar to the no-additive analog. At low pressure, the surface is relatively flat and TiO_2 particles are observed to be clustered on the surfaces of the coarse AP particles. These clusters are believed to be residue deposits from the burning of the previous layer of interstitial matrix. In the transition pressure region, the coarse AP is raised relative to the matrix surface. This surface structure is maintained on the high-pressure plateau; no change could be distinguished. At higher pressure, above the plateau, the coarse AP is raised more significantly above the matrix surface. However, the more extreme lumpy surface observed with IPDI-cure was not observed here.

Mechanistic Discussion: TiO_2 has very little effect on the low pressure behavior in the case of DDI-cure. This is believed to be due to the superior liquefaction and fluidity of the binder with DDI, so that viscosity increases or catalytic effects from TiO_2 are not enough to bring about normal burning. The result is a low pressure plateau similar to the no-additive analog, quite different from the low pressure result with IPDI.

The occurrence of two plateaus with a transition region complicates the explanation. Something rather sudden happens to cause the high exponent transition. A likely explanation is that here is where DOA volatilization becomes significant. The effect is to raise the viscosity of the binder melt enough to make the TiO_2 more effective as a stiffener or as a catalyst to restore a degree of normal burning. From the viscosity experiments, the loss of DOA

with DDI would be more significant than with IPDI to raise the viscosity of the system. In propellants with TiO_2, the inferior liquefaction properties with IPDI are such that the loss of DOA does not matter so that normal burning occurs in any event with IPDI. With DDI, the loss of DOA does matter. The higher rate of loss can come about from higher temperatures in the melt at higher pressures.

The occurrence of the high-pressure plateau involves the tradeoffs between melt layer thickness and viscosity, or loss of catalysis due to comparative time constants, as discussed above. The plateau is not as dramatic as with IPDI because the burn rates never get as high and the tradeoffs are more balanced in this particular formulation.

If DOA volatilization becomes significant at lower pressures, and is responsible for the transition region, then the ending of the plateau with the subsequent high exponent behavior (restoration of normal burning) can be explained by the melt becoming too thin under the conditions prevailing. Another possibility is volatilization of the curative components, which are lower-viscosity ingredients, so that their loss (either DDI or IPDI) would stiffen the remaining R-45 melt. TGA experiments showed that binder gasification follows the loss of DOA, at higher temperatures.

DDI-Cured HTPB, with TiO_2, Lower Coarse/Fine AP Ratio

Burn Rate Data: The low-pressure data are similar to the baseline. There is a low exponent region between 250 and 600 psi ($n \sim 0.2$) with a burn rate of 0.3 in/sec @ 600 psi. This is the "low pressure plateau". From here on, the results differ dramatically from the baseline. The transition region is from 700 to 1500 psi, but is of higher exponent ($n > 1$) and reaches much higher burn rate (1.8 in/sec @ 1500 psi, the expected result for normal burning at this pressure). The mesa which follows is more like a cliff. Burn rates fall 60% in going from 1900 to 2600 psi, which is the well of the mesa. Above 3100 psi, burn rates rapidly increase with pressure such that $n > 1$.

Extinguished Surfaces: The surface in the transition region just before the start of the mesa looked to be very much the same as the lumpy topography of the IPDI formulation just before the start of its mesa. In the mesa, the surface was noticeably flatter. The more dramatic drop in the burning rate enabled this difference to be observed here. At higher pressure, well above the mesa, the surface was lumpy again.

Very high magnification views were obtained to try to distinguish mesa from post-mesa surface structures in the matrix. In the mesa, the surface appeared to be a knitted binder melt covering little bumpy AP particles. It is believed to be a uniform binder surface because there were no outlines of particles and no difference in shading between the smooth and bumpy areas as would distinguish AP from binder. In some views, there were small holes distributed in the melt which appeared to be vent holes - possibly due to subsurface AP gasifications that did not knit. The thickness of the binder melt could not be measured but appeared from the nature of the views to be about 1μ. A thickness of that order agrees with model calculations for that burning rate. At a pressure well above the mesa, the binder was pocked with little depressions of a size that could be associated with burned-out fine AP particles.

Mechanistic Discussion: Coarse/fine ratio is a very important variable. It affects the spacing between the fine AP particles and the fuel-richness of the matrix. We know from the propellant developments that there is a relatively narrow range for plateau behavior between the extremes of normal and depressed burning. The fuel-richness of the matrix can affect local flame temperatures. The particle spacing can affect the scope and consequences of binder melt mobility. Here, the lower coarse/fine ratio produced dramatic burn rate and surface structure changes that could be related to the ability of the matrix to burn ahead of the coarse AP. It increases potential flame temperatures in the matrix. A closer spacing of the fine AP can hold the binder melt in the form of a meniscus, so it does not interfere, but if it does happen to flow there is potential for a greater coverage of the fine AP.

The changes in fuel-richness or AP spacing were not enough to significantly affect the low-pressure plateau, but the transition region manifested a much greater degree of restoration of normal burning. The TiO_2 could be much more effective as a stiffener or catalyst with the closer spacing of the fine AP. The very pronounced mesa indicated that improved melt fluidity, once it set in, was much more effective with the closer spacing—or that loss of catalysis is more abrupt when the competing time constant decreases more rapidly. At higher pressure, the burning rate turned around to increase just as abruptly as the melt equilibrated too thin or became too stiff for the reasons discussed previously.

ALUMINIZED PROPELLANTS

In going from a reduced-smoke propellant to an aluminized propellant, aluminum replaces AP to maintain a constant total solids loading. Since aluminum is of higher density than AP, substantial quantities of aluminum enable the total solids to be increased for a constant volumetric solids loading. The reduced-smoke formulations contain 88% solids. Good bi-plateaus have been achieved with 20% aluminum, the highest attempted, at 90% solids. Subscale motor tests have been conducted with 15-18% aluminum at 88% solids. The aluminized formulations for the MURI experiments contained 15% aluminum at 88% solids.

Replacing AP with aluminum increases the fuel-richness of the AP/binder system. The AP/binder ratio goes from 7.2 in the baseline reduced-smoke formulation to 5.9 with 15% aluminum. It also increases the spacings between the AP particles. Which is more important to the plateau behavior? Model formulations made with monomodal fine AP and TiO_2 to represent the fuel-richness of the matrix and the particle spacing in the matrix indicated that a closer spacing was more important than increased fuel-richness to enhance the appearance of the depressed burning effect and thereby make the plateau more vivid.

The aluminized formulations are made with the view of minimizing the impact of the presence of aluminum on the matrix. First, a coarse aluminum (~100μ) is used in order to maximize the spacing between the aluminum particles in the propellant microstructure and minimize the possibility of aluminum agglomeration at the burning surface. Second, the coarse/fine AP ratio is adjusted downward, using pocket model calculations, to maintain the same spacing of the fine AP in the matrix as existed in the reduced-smoke analog. This approach successfully maintained the plateau and bi-plateau behavior.

High-speed microcinematography and videos of the aluminized MURI propellant showed very little (if any) agglomeration at the burning surface, ignition of the particles at the burning surface and what appeared to be excellent combustion of the particles in an extraordinarily bright combustion zone. It appears that the very fine TiO_2 particles enhance the radiant luminosity of the flame zone. Microscopic views of unburned propellant showed the aluminum particles to be spaced well apart, further apart than the coarse AP particles. Microscopic views of extinguished surfaces confirmed the absence of aluminum agglomeration.

The subscale motor tests indicated complete aluminum combustion as measured by c* efficiency and Isp efficiency. The mean residence time in the motors is 20 msec., indicating a particle burn time that is within that time frame. A burn time of less than 20 msec. for a 100μ particle is not out of line with results of aluminum particle burning studies. Thus coarse aluminum can be used without performance penalty.

STABILITY IMPLICATIONS

Experiments Applying Z-N Theory

Measurements of n, σp and surface temperatures enabled the application of Z-N theory to compute the pressure-coupled response function of bi-plateau propellants. Although Z-N theory is of questionable applicability to heterogeneous propellants, or where there are subsurface condensed phase reactions, it is considered to be a worthwhile exercise for general trends. However, the favorable stability properties computed for the bi-plateau propellants was colored by the use of values of n measured from steady-state data. This is a more serious deficiency of the method.

Under transient pressure conditions, such as oscillatory burning, it can be expected that there will be time lags in the surface processes that are responsible for the plateaus in steady-state. In the extreme, at sufficiently high frequencies, the surface will not change at all during the oscillations. This leaves the ordinary pressure-dependent processes, the gas phase reactions, to drive the oscillatory burning with their characteristic pressure exponents. The frequencies at which the surface time lags become important are unknown, but are expected to be low. Where they do become important, the characteristic exponents are more likely those from normal burning.

A more relevant favorable result is the low values of σp (burn rate temperature-sensitivity) that were measured in the plateau regions. Low σp tends to lower the pressure-coupled response. Mechanistically, extensive coverage of the burning surface by a binder melt layer can lower σp and that condition would prevail under oscillatory pressure conditions. It does not depend upon changing the surface. From a fundamental standpoint, increasing the enthalpy of the solid phase tends to reduce σp because changes in initial temperature become proportionally less significant. Since HTPB surface temperatures are higher than those of AP, and HTPB decomposition is endothermic, a surface layer that is mostly binder would be less sensitive to temperature changes.

T-Burner Data

Response function measurements at pressures and frequencies of interest were acquired in the T-burner. Results were encouraging in that response functions for the reduced-smoke formulation were low on its low-pressure plateau, and very low on its high-pressure plateau up to a frequency of about 600 Hz. For the aluminized formulation, response functions were very low on its low-pressure plateau but high on its high-pressure plateau.

The data for the aluminized formulation may be less reliable because of its high damping, in particular on the high-pressure plateau where the damping became very high. Where the damping is innately high, the errors in the pulsing technique can become large. Efficient combustion of the coarse aluminum, which yields the damping material, may be very pressure-dependent in the T-burner because it has a large volume for the amount of propellant used and is pre-pressurized with cold gas. In order to deduce a higher response at higher pressure, the damping after burnout has to increase more than the damping during burning. It is therefore possible that we were measuring an effect of distributed combustion which masked the low response function.

Subscale Motor Tests

The 15% aluminum bi-plateau propellant and an 18% aluminum bi-plateau propellant were each tested on both plateaus by the use of a boost-sustain segmented cylinder grain design containing 30 pounds of propellant, and with an axial mode frequency of 550 Hz. The 18% aluminum propellant was pulsed at both pressures. Both of the motors were stable. The measured pulse decays can be used in association with a motor stability analysis to deduce the response functions.

The 18% aluminum propellant developed an unbond during boost such that the pressure temporarily rose to a higher level before the first pulse was actuated. The higher pressure was still on the high-pressure plateau. Dynamic data confirmed that the pressure rise was not caused by a spontaneous instability. Post-test examination of the motor revealed erosion patterns consistent with an unbond. A ballistic analysis verified the benefit of the plateau in preventing the unbond from raising the pressure excessively. The pressure returned to the design level when the burning passed the localized unbond and the subsequent low-pressure operation proceeded normally.

The measured pulse dampings were greater than expected. Pre-test stability analysis computed

less stable margins based on response function calculations from a model assuming normal burn- ing (viz., no plateau effect). That the margins were measured to be more stable is evidence of lower response functions, as indicated by the T-burner results for this family of propellants, per- haps due to the abnormal burning mechanism responsible for the low values of σ_p.

RECOMMENDATIONS FOR FUTURE WORK

Plateau Mechanism Time Lags

Oscillatory burner experiments, using the ultrasound method for direct measurement of response functions, are planned over a range of frequencies that are expected to discern the time lags in the plateau mechanism. These frequencies are expected to be low, of the order of tens of Hz. We will be looking for the transition from the negative pressure exponent at zero frequency to a positive response function curve characteristic of normal burning. This has never been done be- fore, not even for the classical double-base family of plateau propellants.

Another benefit of working at low frequencies is that the data are expected to be of better quality and much more accurate. A complement of accurate data at low frequencies can have leverage as a basis for predicting the response function curve at higher frequencies (relevant to motors) with models. A range of 0-100 Hz should be enough to capture the time lags, the transition to normal behavior, and then the initial portion of the normal response function curve.

It was suggested that extinguished surfaces be obtained under oscillatory pressure conditions to look for effects of frequency on the surface structure as a part of the time lag studies.

Crossflow Effects on Plateau Behavior

A question arose about the ability of the plateau mechanism to hold up under the high crossflow conditions that are encountered in the initial stage of operation of high-performance designs. It is known that high crossflow can interfere with the stable establishment of plateau burning in the ignition of classical double-base and modern energetic binder plateau propellants.

Experimental erosive burning and acoustic erosivity studies have not been included in the MURI program as a considered judgment in view of limited resources and the need to study the basic combustion behavior of advanced forms of propellants. They are being treated analytically in the combustion and turbulence modeling in progress, making use of considerable data available for normal-burning propellants. However, they do not address the question of abnormal burning.

The subscale tests of the bi-plateau propellants did not encounter crossflow Mach numbers greater than 0.1. Ballistic test motors used to qualify propellant mixes also have very low Mach number crossflows. In contrast, crossflow Mach numbers in high-performance designs can reach 0.3 and even higher values are desirable to increase propellant loadings. Current designs are limited by erosive burning pressure spikes rather than grain structural properties.

A proper test of bi-plateau propellants combining pressures, crossflows and acoustic frequencies of interest would require in essence a full-scale motor. It is difficult to combine high crossflow with a constant high pressure in small-scale hardware, necessitating supplemental means to generate crossflow in experimental devices used for that purpose. In any case, the acoustic frequencies would not be representative and the tests that would be required are outside of the planned MURI scope of work.

The abnormal burning mechanism of the bi-plateau propellants depends upon a binder melt layer that has adhesive properties. In contrast, the plateau mechanism of the classical double-base and modern energetic binder plateau propellants depends upon forming a carbonaceous ash residue on the burning surface; it is an altogether different mechanism. It is expected that a binder melt layer would be much more resistant to crossflow than a

carbonaceous ash. Experimental verification can be deferred to a future program and would be a recommendation for follow-on work.

Uncured Propellants

In view of the importance of binder melt layers to the underlying abnormal burning mechanism, it was suggested that experiments be carried out with uncured propellants. This would retain a binder "melt" throughout the sample and at all pressures, having the thermal gradients and properties of the melt at the surface without the process of liquefaction. It would eliminate the effect of curative and enable a better focusing on the effect of plasticizer. Whether the results are similar to or different from the cured analog propellants, the comparisons would provide valuable information. It was also suggested that properties of the melt could be controlled by use of surfactants and surface tension modifiers as additives. At the least, a portion of a future propellant mix could be set aside to obtain burning rate data for uncured strands.

Analytical Combustion Modeling

Combustion modeling under the MURI program has been limited to normal-burning propellants, for which there has been much to do. These include improved representations of the heterogeneity of composite propellants for both steady-state and unsteady combustion, and models for the combustion of advanced energetic ingredients. In addition, there have been advancements in the modeling of diffusion flames, acoustic erosivity and distributed aluminum particle combustion. Integration of the combustion modeling efforts into the motor gasdynamics modeling is also in progress.

The limitations of the use of simplified Z-N theory are recognized. Therefore, response function modeling is proceeding with numerical solutions of the non-steady equations that will be applicable to non-linear as well as linear instability. Of special interest are the new methods for treating composite propellants, which are expected to yield better descriptions of the response behavior. It was recommended that numerical analysis of the condensed phase include subsurface reactions because solutions for the oscillatory burning of a homogeneous solid show large temperature fluctuations in the depth of the solid. Normally, the condensed phase reactions are lumped at the surface in the modeling due to their high temperature-dependence. However, these large temperature fluctuations in depth could increase the importance of subsurface reactions to affect the combustion response.

Modeling the mechanisms of plateau and bi-plateau behavior would be difficult at best, even for steady-state let alone the surface time lags under oscillatory burning. The description of mobile melt layers interacting with fine AP, as affected by pressure and the presence of TiO_2, would require a semi-empirical approach because we don't know enough about the details of this behavior. Thus far, the modeling has been used in the gross sense of artificially "turning off" portions of the fine AP to explain the data. Given the work that needs to be done with normal burning, the other types of MURI propellants to be studied which will be normal burning, and the nearer-term interests in normal-burning propellants, analytical modeling of abnormal burning can be deferred to a future program.

Further Propellant Developments with Advanced Energetic Binders

The Workshop included a presentation of more recent Thiokol propellant developments under Navy (ONR and NAWC) sponsorships. Plateau ballistics have been achieved with advanced energetic binders using the same approach as with HTPB, based upon the same mechanism. Advanced energetic ingredients are relevant to MURI objectives.

Plateaus analogous to IPDI-cured HTPB have been achieved with azido-oxetanes (AMMO and BAMO/AMMO), and bi-plateaus analogous to DDI-cured HTPB have been achieved with a nitrato-oxetane (NMMO). These binders are nitrato-plasticized and cured with N-100. Both reduced smoke and aluminized versions were successfully achieved. Plateaus were also achieved with nitrato-plasticized polyesters and polyethers.

Since energetic binder propellants are formulated with lower AP concentrations, it was necessary to reduce the coarse/fine ratio to maintain the same fine AP spacings as in the HTPB propellants. However, optimal fine AP spacings may vary somewhat with binder type in accordance with the liquefaction properties.

It is interesting that the plateau mechanisms were not defeated by the monopropellant quality of these energetic binders. Another interesting finding with these binders is that plateau behavior can also be achieved with 20μ fine AP. That was not possible with IPDI-cured HTPB, but suggests that DDI-cured HTPB should be re-visited for that purpose because it appears to result from superior binder melt properties (lower liquefaction temperatures, thicker and more fluid melts). Where lower burn rate plateaus are desirable, the 20μ fine AP enables smaller amounts of TiO_2 to be used because normal burning with 20μ AP is at lower rates and with lower exponents than with 2μ AP; there is more of a blending between the normal and abnormal burning rather than wide swings between the two.

The apparent new generality in being able to achieve plateau ballistics in AP composite propellants stems from a combination of wide AP size distributions with binders having superior melt properties, controlled by the use of TiO_2. Since other MURI propellants that will be studied will have similar types of binders, their potential for plateaus should be kept in mind in the course of future work and for possible follow-on work.

CONCLUDING REMARKS

A considerable degree of understanding of the mechanisms of plateau and bi-plateau behavior in AP/HTPB propellants has been achieved. While some uncertainty and disagreement remains as to details of the processes, it has been possible to progress to more advanced energetic binder propellants which exhibit this behavior.

An objective of the MURI program is to develop sufficient mechanistic understandings to assure the stability of future solid rocket motors containing advanced energetic propellants. It is under-stood that zero or negative pressure exponents are not a panacea for stability because of dynamic time lag effects, but low temperature-sensitivity has considerable benefit to lower combustion response functions. This has been shown analytically, and the low σp of the bi-plateau propellants may have been responsible for the very favorable T-burner data. The stable subscale motor tests are also encouraging. Another benefit of low σp combined with plateaus is higher motor design efficiency which can be worth many seconds of Isp or, in the alternative, lower costs by allowing simpler designs

and wider tolerances. These bode well for future applicability, enhancing the relevance of the MURI research to meet future needs.

The improved mechanistic understanding has not been reduced to a computerized mathematical model of the plateau behavior, but that would be difficult to accomplish at this point and was not an intended goal of the program. There is more interest in improved response function measurement techniques. The T-burner remains the most reliable and representative method at pressures and frequencies of interest, but the new ultrasound method shows promise for special purposes such as time lag measurements at low frequencies. Much thought and some effort is being given to ways to improve the T-burner in its mode of operation and by adding supplemental means for direct measurements of combustion response. Analytical combustion modeling for integration with the motor gasdynamics analysis is currently limited to normal-burning propellants that will comprise the remaining propellants for MURI research, and which are of greater interest for the nearer term.

Another objective of the MURI program is to develop a new generation of scientists and engineers. There has been much student involvement in this work and in its presentations, and initial graduates have moved on to relevant industry or post-doctoral work. It was also encouraging that the Workshop was attended by many of the young propellant and motor design specialists employed by Thiokol who hosted it. A broader scope of industrial involvement is anticipated as more propellants are acquired from other companies for the remaining experimental work to be accomplished. These participations will enhance the technology transfer of the MURI program accomplishments.

Attachment D

Thoughts on Oscillatory Vorticity Models Contributions to Combustion Stability of Solid Propellant Rocket Motors

R. S. Brown
Brown & Associates, Santa Clara CA.

SUMMARY

A number of experimental[1,2], numerical, and analytical[4,5,6,7,8,9] studies have addressed the effect of flow vorticity on the stability of the combustion chamber pressure in solid propellant rocket motors. These studies were motivated by the substantial difference in vorticity contributions predicted by the two "standard" stability prediction models. In one model, both the mean and oscillatory flow are assumed to be one-dimensional (*i.e.*, a rotational flow with finite vorticity in an infinitesimal volume at the wall)[10] while three-dimensional irrotational flows are assumed in the second model[11,12]. This difference in the flow environment produces a significant "flow turning" acoustic loss term in the one-dimensional stability model that does not appear in the conventional three-dimensional stability model. Additionally, the cold flow studies in full length cylindrical chambers[1,2] show that both the steady state and oscillatory flows are three-dimensional and rotational. Thus, there is substantial practical need for including vorticity contributions in three-dimensional stability predictions. These recent analytical studies[4-9] of these vorticity improvements have concluded the flow turning response function to be -1 (the sign signifying damping) when vorticity is included in the three-dimensional model. These same studies also indicate there is an additional source of acoustic energy which has not been included in either "standard" stability model.

These observations have significant implications for motor design and prompted a detailed review of these analytical results. Three primary conclusions result from this review. First, these studies correctly conclude the "flow turning response function" should be -1 for motors having full length grains with cylindrical ports. This value is also consistent with motor stability experience, both research motors[13] and operational motors. This value also supports the good agreement observed in comparing predicted and observed profiles for the axial oscillatory velocity one cold flow test. Second, the new energy source term is really an alternative statement for the flow turning loss. Third, the vorticity predictions cannot be extended to grains that are displaced from either end of the chamber. The "no-slip" boundary condition leads to step function changes in the velocity profiles which are physically unrealistic when the grain is displaced axially from the head-end.

DETAILED DISCUSSION

This review starts with the same basic linear equations of motion for small disturbances employed in references 4 thru 9:

$$ikM' + \nabla\left(\overline{M} \bullet M'\right) - M' \times \left(\nabla \times \overline{M}\right) - \overline{M} \times \left(\nabla M'\right) + \nabla\varepsilon' = 0 \tag{1}$$

and

$$ik\varepsilon' + \overline{M} \bullet \nabla\varepsilon' + \nabla \bullet M' = 0 \tag{2}$$

Note that the vorticity of both the mean and oscillatory flows have been retained in Eq. (1). By following the analytical path of previous three-dimensional models[11, 12], it can be shown[1] that the corresponding complex eigenvalue is

$$\left(k^2 - k_L^2\right)\int_V \in_L \in' dV = ik_L \int_S n \cdot \left(A_b + M_b\right) \in_L \in' dS + \int_V k_L^2 \left(\overline{M} \cdot M'\right) \in_L dV$$
$$- ik_L \int_V \in' \left(\overline{M} \cdot \nabla \in_L\right) dV - \int_V \nabla \in_L \cdot \left(\overline{M} \times \left[\nabla \times M'\right] + M' \times \left[\nabla \times \overline{M}\right]\right) dV \tag{3}$$

where $$k^2 = \left(2\pi f r_w / a\right)^2 - i\left(\alpha r_w / a\right)\left(2\pi f r_w / a\right)$$

The first term on the right-hand side is the classical surface integral characterizing the propellant combustion driving term* as well as conventional the nozzle loss term. The second and third terms on the right-hand side cancel since the velocity and pressure oscillations follow the classical motions. The term $M' \times \nabla \times \overline{M}$ is of order M_b^2 because the pressure gradient is primarily axial, the mean vorticity is azimuthal and of order M_b, and the oscillatory velocity is radial and of order M_b. Since the stability retains terms of order M_b and higher order terms are dropped, this term can also be neglected. However, the oscillatory vorticity term must be retained because both the experimental data[1,2] and the analytical results[4-9] indicate that the oscillatory vorticity is inversely related to M_b. Note also that if both the mean and oscillatory flows are irrotational (*i.e.*, have zero vorticity), the classical results reported in references 11 and 12 are recovered. With these simplifications, Eq. (3) becomes

$$\left(k - k_L^2\right)\int_V \left(\in_L\right)^2 dV = ik_L \int_S n \cdot \left(A_b + M_b\right)\left(\in_L\right)^2 dS - \int_V \nabla \in_L \cdot \left(\overline{M} \times \left[\nabla \times M'\right]\right) dV \tag{4}$$

A simplified analysis extending those reported in refs. 4-9, can be used to assess the magnitude of the vorticity term in Eq. (4). In those works, Eqs. (1) and (2) are separated into the solenoidal (rotational, constant dilatation) domain and the acoustic (compressible, irrotational) domain, as suggested by Chu and Kovasznay[14]. The oscillatory pressure and oscillatory velocity are thereby separated into two components

$$\in' = \hat{\in} + \widetilde{\in} \qquad M' = \hat{M} + \widetilde{M} \tag{5}$$

Setting $\nabla \times \hat{M} = 0$ yields the acoustical domain equations

$$ik\,\hat{\in} + \overline{M} \bullet \nabla \hat{M} = 0 \tag{6}$$

$$ik\hat{M} + \nabla\left(\hat{M} \bullet \overline{M}\right) - \hat{M} \times \left(\nabla \times \overline{M}\right) + \nabla\,\hat{\in} = 0 \tag{7}$$

Setting $\nabla \bullet \widetilde{M} = 0$ yields the corresponding vortical domain equations

* Note that Ab and Mb are written in the gas chamber coordinate system which is positive going outward from the centerline. Acoustic driving values are therefore negative.

$$ik\,\tilde{\in} + \overline{M} \bullet \nabla\,\tilde{\in} = 0 \tag{8}$$

$$ik\tilde{M} + \nabla\left(\overline{M} \bullet \tilde{M}\right) - \overline{M} \times \left(\nabla \times \tilde{M}\right) - \tilde{M} \times \left(\nabla \times \overline{M}\right) + \nabla\,\tilde{\in} = 0 \tag{9}$$

These prior studies assume that oscillatory pressure associated with the rotational flow field is zero. There is no doubt that zero pressure is a particular solution to Eq. (8), but it is clearly not a general solution. With this assumption, the basic set of equations for the vortical motion becomes

$$\nabla \bullet \tilde{M} = 0 \tag{10}$$

$$ik\tilde{M}_r + \partial\left(\overline{M}_r \tilde{M}_r\right)/\partial r + \overline{M}_z\,\partial\tilde{M}_r/\partial r = 0 \tag{11}$$

$$ik\tilde{M}_z + \partial\left(\overline{M}_z \tilde{M}_z\right)/\partial z + \overline{M}_r\,\partial\tilde{M}_z/\partial r + \tilde{M}_r \partial\overline{M}_z/\partial r = 0 \tag{12}$$

Inspecting Eqs. (10) to (12) shows these three equations have two unknowns; the radial and axial components of the oscillatory vortical domain velocity. This discrepancy in the number of equations vs. the number of unknowns indicates the mathematical analysis has over specified the physical problem. Note also these equations violate Newton's Laws of motion since there is no force term in either Eq. (11) or Eq. (12).

Inserting the well-known equations for the mean flow

$$r\overline{M}_r = M_b \sin\left(\pi r^2/2\right) \qquad \overline{M}_z = -\pi z M_b \cos\left(\pi r^2/2\right) \tag{13}$$

Eq. (11) becomes

$$\left[-\frac{ik}{\pi M_b} + \frac{\sin(\theta)}{\theta} - \cos(\theta)\right]\left(\tilde{N}_r\right) - \sin(\theta)\,\partial\left(\tilde{N}_r\right)/\partial\theta + z \bullet \cos(\theta)\,\partial\tilde{N}_r/\partial z = 0 \tag{14}$$

and Eq. (12) becomes

$$\left[-\frac{ik}{\pi M_b} + \cos(\theta)\right]\tilde{M}_z + z \bullet \cos(\theta)\,\partial\tilde{M}_z/\partial z - \sin(\theta)\,\partial\tilde{M}_z/\partial\theta - \pi z \bullet \sin(\theta)\tilde{N}_r = 0 \tag{15}$$

where

$$\tilde{N}_r = r\tilde{M}_r \qquad \theta = \pi\left(r^2\right)/2 \tag{16}$$

Following the suggestion that the last term in Eq. (15) is small[5], assuming a hard head-end wall, and letting

$$\tilde{M}_z = \sum (\pi z)^{n+1} \tilde{C}_n(\theta) \tag{17}$$

the first order linear axial momentum equation can be solved for each C_n. Using the "no-slip" boundary condition at the propellant surface and resonant acoustic oscillations, the solution is

$$\tilde{M}_z = \sum A_n (\pi z)^{n+1} \left(\sin(\theta)^{n+2}\right) \exp\left(\frac{-ik}{\pi M_b} \ln[\tan(\theta/2)]\right) \tag{18}$$

where

$$A_0 = i(2fL/a)(r_w/L) \qquad A_{n+2} = (2fL/a)^2 (r_w/L)^2 \, A_n/((n+2)(n+3)) \tag{19}$$

Figures 1 and 2 show the resulting predicted radial profile for the total oscillatory axial velocity profile (rotational plus acoustic) at several axial stations for the "Shuttle Motor" conditions (L/R = 50.14 and M_b = –0.0023)[5,9]. These plots agree closely with figure 7 of reference 5 and figures 4 and 5 of reference 9.

One can also derive the corresponding oscillatory radial component of the rotational velocity by differentiating Eq. (17) with respect to z, inserting the result into Eq. (10), and integrating with respect to θ. Figure 3 shows the predicted magnitude of the inward radial velocity for the "Shuttle Motor" conditions at z/L= 0.15 and duplicates Fig. 4c and Table 3 of ref. 8. Thus, the approximate analysis described above essentially predicts the same basic rotational flow behavior reported in the more detailed analyses reported previously[4-9].

Next, the predicted effect of oscillatory vorticity on stability can be examined. Note that the oscillatory vorticity is defined as $\partial M_r/\partial z - \partial M_z/\partial r$. Since the first term is of order M_b and can thereby be neglected, the oscillatory vorticity can be obtained directly by numerically differentiating Eq. (18). The result can then be substituted into Eq. (4) and appropriately integrated. For the "Shuttle Motor" condition's one finds the vorticity damping to be

$$\alpha_{ft} = 1.004 \; M_b \; a/r \tag{20}$$

This result agrees exactly (within the numerical accuracy) with the full length example results shown in Table 3 of reference 9 (Eq. (98)). Parametric studies show the factor of 1.004 is nearly independent of M_b. Note Eq. (20 predicts the flow turning damps the oscillations, as expected, since $M_b < 0$ for solid propellants. Furthermore, the factor 1.004 is almost exactly the flow turning response function of –0.1 derived in the one-dimensional stability analysis. It is also interesting that a value of one has often been found to provide the best comparisons between predicted and observed motor behavior[13]. Additionally, this term is proportional to $\int (\nabla \in_L)^2 dS$ which is equivalent in form to the flow turning term in the one-dimensional analysis[10].

One can also analyze the derivation of the "new" term using the splitting theorem approach. This analysis starts with Eqs. (6) and (7) for the acoustic motions for the "split" flow instead of Eqs.(1) and (2) since predicting the stability of the acoustic motions is the primary goal. Using the same analytical path and simplifications used in deriving Eq. (4), one obtains

$$\left(k^2 - k_L^2\right) \int_V (\in_L)^2 dV = ik_L \int_S n \cdot \left[\left(\tilde{A}_b + M_b\right) \in_L^2\right] dS \tag{21}$$

As expected, no vorticity term appears in Eq. (21) because the acoustic motions are assumed to be irrotational. The admittance term differs from the corresponding term in Eq. (4) since only part of the oscillatory combustion products go into the acoustic domain. The remainder goes into the vortical domain. Chu and Kovasznay[14] clearly note the sum of flows into the acoustic domain and the vortical domain is determined by the appropriate overall

mass balance at the chamber boundary. In other words, the surface mass balance means the total oscillatory flow from the burning propellant surface is the sum of the oscillatory flow into the acoustic domain and the oscillatory flow into the vortical domain. Thus

$$A_b \in_L = \widetilde{A}_b \in_L + \widetilde{M}_r \tag{22}$$

where the second term on the right-hand-side accounts for the oscillatory flow into the vortical motions. Substituting Eq. (22) into Eq. (21) yields

$$\left(k^2 - k_L^2\right)\int_V \left(\in_L\right)^2 dV = ik_L \int_S n \cdot \left[\left(A_b + M_b\right) \in_L^2 - \widetilde{M}_r \in_L\right] dS \tag{23}$$

The reader is reminded that the sign conventions for the velocity and admittance are positive values are outward from the chamber centerline. Thus the net effect of an inward flow into the vortical flow, such as that shown in figure 3, decreases the acoustic driving.

Separating out this additional term on the right-hand-side of Eq. (23) and calculating its value from Eqs. (10), (18), and (19) as outlined above, one eventually obtains

$$\alpha_{dv} = 1.045\ M_b\ a/r \tag{24}$$

for this damping contribution. Note this result is remarkably similar to Eq. (20) since M_b is negative for solid propellants.

At first, one is tempted to conclude initially that these two approaches yield identical results. However, closer inspection reveals a number objections to this initial conclusion. First, the solutions offered above are based entirely on solving Eqs. (10) and (12). As noted, Eqs. (10) to (12) constitute two equations in a set of three equations in two unknowns. One then wonders if the radial rotational velocity shown in Fig. 3 also satisfies the radial momentum equation, Eq. (11). To investigate this possibility, one can substitute

$$\widetilde{N}_r = \left[\left(2\theta/\pi\right)^{0.5}\right]\widetilde{M}_r = \sum \left(\pi z\right)^m \widetilde{R}(\theta) \tag{25}$$

into Eq. (11). One then finds that

$$\widetilde{N}_r(\theta) = \sum S_m \left(\pi z\right)^m \theta\left(\sin(\theta)\right)^{(m-1)} \exp\left(\frac{-ik}{\pi M_b} \ln\left[\tan\left(\theta/2\right)\right]\right) \tag{26}$$

Equations (18) and (26) can then be inserted into Eq. (10) to determine if is zero throughout the chamber and also to relate m to n and S_m to A_n. This substitution yields

$$\nabla \bullet \tilde{M} = \left[\pi \exp\left(\frac{-ik}{\pi M_b} \ln[\tan(\theta/2)] \right) \right]$$

$$\left[\sum A_n (n+1)(\pi z)^n (\sin(\theta))^{(n+2)} + \sum S_m \theta (\pi z)^m \left(\frac{-ik}{\pi M_b} + \frac{\sin(\theta)}{\theta} + (m-1)\cos(\theta) \right) \sin(\theta)^{m-2} \right] \tag{27}$$

Note that the functions which multiply A_n and S_m differ significantly. This difference prevents relating m to n and S_m. to A_n in a manner that makes Eq. (27) universally zero throughout the chamber. Thus, Eqs. (18) and (26) do not simultaneously satisfy Eqs. (10) to (12). This result is simply another manifestation of the basic dilemma with having three equations and two unknowns.

Another difficulty with the splitting approach is identified by examining Eq. (22). The coefficient 1.045 is basically proportional to $(\in_L)^2$, while the coefficient 1.004 in Eq. (20) is proportional to $(\nabla \in_L)^2$. These two proportionality factors are numerically identical for full length cylindrical grains, but can differ significantly for grains displaced from the head-end, the aft-end, or both ends. Since the predicted effects on stability should be identical, this discrepancy casts added doubts about using Eq. (23) as a basis of predicting motor stability.

As an additional minor point, references 4 through 8 suggest symmetry is a basic boundary condition that must be imposed on the flow conservation equations. This condition, in fact, is redundant since the basic flow equations already require the flow to be symmetric about the motor centerline. This behavior can be easily demonstrated by the simple transformation of variables in Eqs. (1) and (2) yielding

$$N_r' = rM_r' = F(z/L, \theta, t) \qquad M_z' = G(z/L, \theta, t) \qquad P' = H(z/Km\theta, t) \tag{28}$$

Thus, the radial velocity at radius -r is simply - the radial velocity at radius r, thus predicting the flow to be symmetric about the centerline.

The effect of displacing the grain axially reveals additional difficulties with the oscillatory vorticity predictions. When the grain starts at the head-end, the axial components of both the acoustic and rotational velocities are zero (hard-wall). When a grain is displaced axially ΔL from the head-end of the motor, the acoustic velocity at that the leading edge of the propellant grain will be approximately $i\sin(\pi\Delta L/L)$. The "no-slip" condition then requires the axial rotational velocity to be $-i\sin(\pi\Delta L/L)$ at this position resulting is substantial radial variations, as shown in Fig. 1, at the leading edge of the grain. However, there are no radial profiles just upstream of this leading edge. Thus, a direct consequence of the "no-slip" condition is a significant discontinuity in the total axial velocity at the upstream edge of the propellant grain.

ACKNOWLEDGMENT

The author wishes to express his sincerest thanks to Dr. R. H. W. Waesche for his many helpful suggestions and encouragement. Thanks are also expressed to the Office of Naval Research for their support provided by the MURI Grant No. N00014-95-1-1338 managed by Dr. Judah Goldwasser.

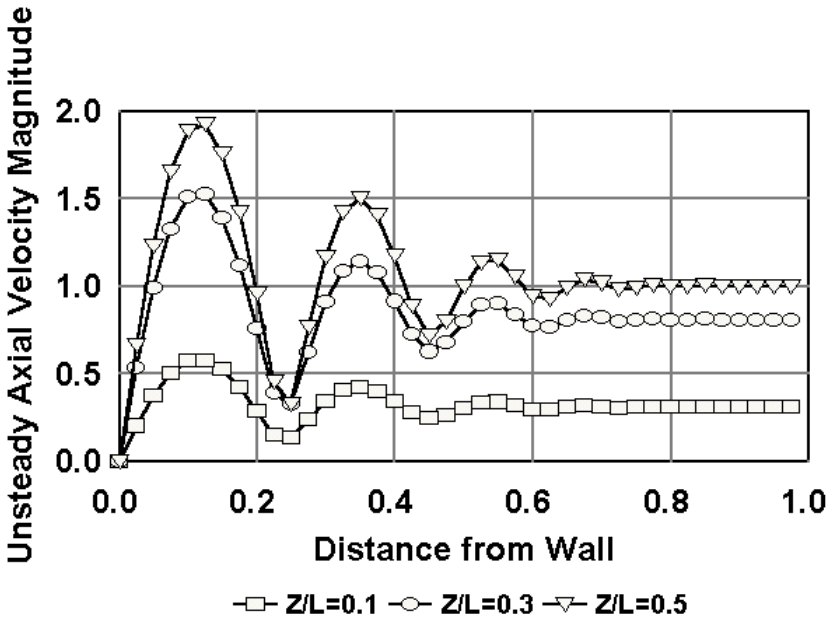

Figure 1. Total Axial Oscillatory Velocity ($0 \leq z/L \leq 0.5$)

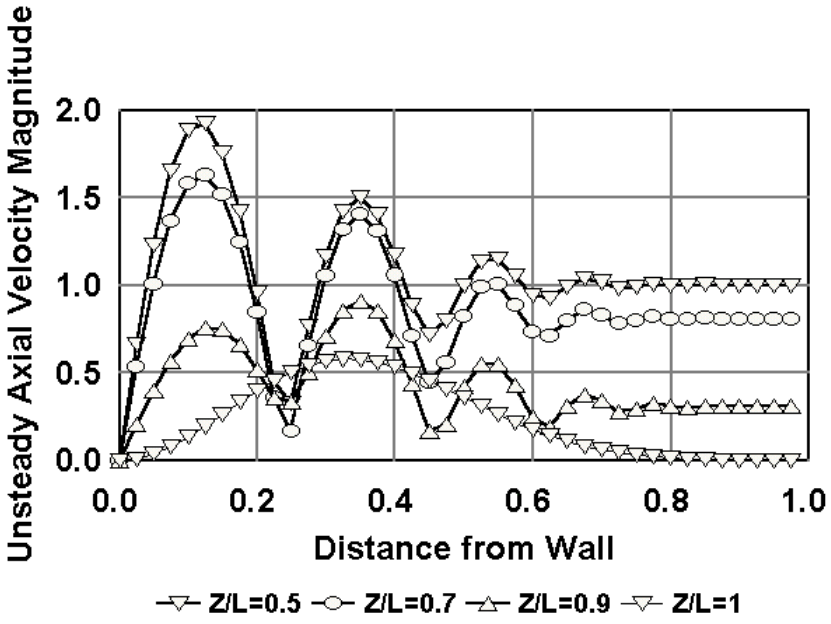

Figure 2. Total Axial Oscillatory Velocity ($0.5 \leq z/L \leq 1.0$)

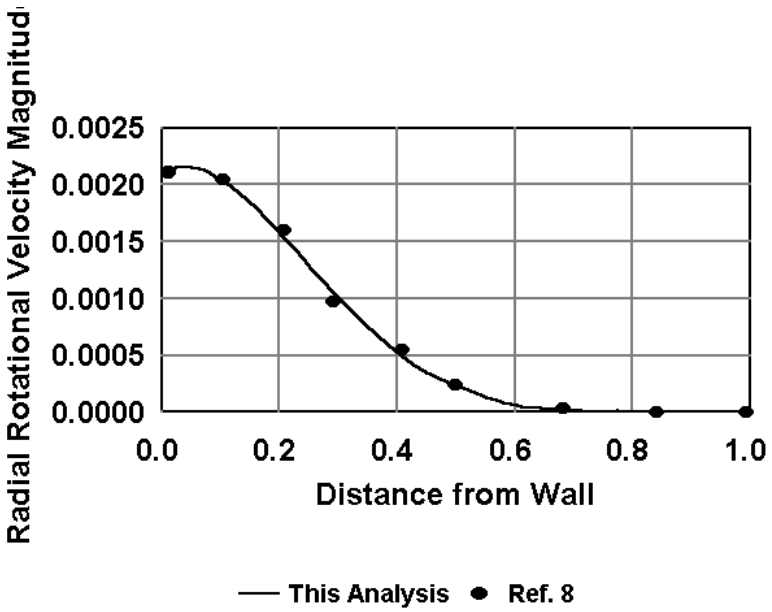

Figure 3. Radial Velocity Comparison

REFERENCES

1. Brown, R.S., Blackner, A.M.., Willoughby, P.G., and Dunlap, R., "Coupling Between Velocity Oscillations and Solid Propellant Combustion," AIAA Paper 86-0531, Jan. 1986. See also Final Report, AFOSR Contracts F49620-81-C-0027 and F49620-84-C-0081, 1984.
2. Shaeffer, C.W., and Brown, R.S., "Oscillatory Internal Flow field Studies," Final Report, AFOSR Contract F04620-90-C-0032, 1990.
3. Vuillot, F., Avalon, G., "Acoustic Boundary Layers in Solid Propellant Rocket Motors Using Navier Stokes Equations," *Journal of Propulsion and Power*, Vol. 7, No. 2, 1991, pp. 231-239.
4. Culick, F.E.C., "The Stability of One-Dimensional Motions in a Rocket Motor," *Combustion Science and Technology*, Vol. 7, No. 4, 1973, pp. 165-175.
5. Cantrell, R. H., and Hart, R.W., "Interaction Between Sound and Flow in Acoustic Cavities: Mass, Momentum, and Energy Considerations," *Journal of Acoustical Society of America*, Vol. 36, No. 4, 1964, pp. 697-706.
6. Culick, F.E.C., "Stability of Three-Dimensional Motions in a Rocket Motor," *Combustion Science and Technology*, Vol. 10, No. 3, 1974, pp. 109-124.
7. Majdalani, J., "Vortical and Acoustic Mode Coupling Inside a Two-Dimensional Cavity with Transpiring Walls," *Journal of Acoustical Society of America*, Vol. 106, No. 1, 1999, pp. 46-56.
8. Majdalani, J., Flandro, G., Roh, T.S., "Convergence of Two Analytical Flow Field Models Predicting a Destabilizing Agent in Rocket Combustion," *Journal of Propulsion and Power*, Vol. 16, No. 3, 2000, pp. 492-497.
9. Flandro, G., "Effects of Vorticity on Rocket Motor Combustion Stability," *Journal of Propulsion and Power*, Vol. 11, No. 4, 1995, pp. 607-625.
10. Culick, F.E.C., "The Stability of One-Dimensional Motions in a Rocket Motor," *Combustion Science and Technology*, Vol. 7, No. 4, 1973, pp. 165-175.
11. Cantrell, R.H., and Hart, R.W., "Interaction Between Sound and Flow in Acoustic Cavities: Mass, Momentum, and Energy Considerations," *Journal of Acoustical Society of American*, Vol. 36, No. 4, 1964, pp. 697-706.
12. Culick, F.E.C., "Stability of Three-Dimensional Motions in a Rocket," *Combustion Science and Technology*, Vol. 10, No. 3, 1974, pp. 109-124.
13. Blomshield, F.S., Crump, J.E., Mathes, H.B., Stainaker, R.A., and Beckstead, M.W., "Stability Testing of Full-Scale Tactical Motors," *Journal of Propulsion and Power*, Vol. 13, No.3, 1997, pp. 349-355.
14. Chu, B.T., and Kovasznay, L.S.C., "Non-linear interactions in a viscous heat-conduction compressible gas," *Journal of Fluid Mechanics*, Vol. 3, No. 5, 1988, pp. 494-514.

Attachment E

List of Caltech MURI Publications

BEDDINI

1. Beddini, R.A., The Role of Turbulence in Combustion Instability, *Proc. of the 34th JANNAF CS/PSHS/APS Joint Meeting*, CPIA Pub., West Palm Beach, FL, October 27-31, 1997.
2. Beddini, R.A., The Role of Turbulence Interactions in Solid Propellant Combustion Instability, *AIAA* Paper 98-3703, *34th AIAA/ASME/SAE/ASEE Joint Propulsion Conference*, July 1998.
3. Lee, Y., and Beddini, R. A., The threshold condition of propellant velocity response and its relation to local turbulent transition, 1998 JANNAF CS/PSHS/APS Joint Meeting, CPIA Pub., Tucson, AZ, December 7-11, 1998.
4. Lee, Y., and Beddini, R. A.: Acoustically–induced turbulent transition in solid propellant rocket chamber flowfields, AIAA paper no. 99-2508, AIAA/ASME/SAE/ASEE 35th Joint Propulsion Conference, Los Angeles, July 1999.
5. Beddini, R.A. and Lee, Y., Acoustically-Induced Turbulent Transition – A New Mechanism of Chamber Resonance, *36th JANNAF CS/PSHS/APS Joint Meeting*, CPIA Pub., Cocoa Beach, FL, October 19-22, 1999.
6. Beddini, R. A.: Acoustically Induced Turbulence and its Role in Propellant Velocity Response, Proceedings, International Workshop On Unsteady Combustion And Interior Ballistics Saint Petersburg, Russia, June 26 - 30, 2000.
7. Lee, Y., and Beddini, R. A.: Effect of solid rocket chamber pressure on acoustically–induced turbulent transition, AIAA paper no. 2000-3802, AIAA/ASME/SAE/ASEE 36th Joint Propulsion Conference, Huntsville, July 2000.
8. Beddini, R. A., and Lee, Y.: Visco-Acoustic and Resonant Interactions in Solid and Hybrid Propulsion Chambers, 2000 JANNAF CS/PSHS/APS Joint Meeting,, Monterey, CA, November 13-17, 2000.

BECKSTEAD

9. Erikson, W.W. and Beckstead, M.W., "A Numerical Model of Monopropellant Deflagration Under Unsteady Conditions," AIAA 96-0652, 1996.
10. Beckstead, M. W. and Erikson, W.W., "Solid Monopropellant Oscillatory Combustion Instability," Proceedings 2nd International Conference on Combustion Conversion and Environmental Problems of Energetic Materials, St. Petersburg, June 1966.
11. Beckstead, M.W. , Davidson, J.E. and Jing, Q., "A Comparison of Solid Monopropellant Combustion and Modeling," 4th Int'l Symposium on Special Topics in Chemical Propulsion, Stockholm, Sweden, 1966.
12. Beckstead, M. W., Tanaka, M., Jing, Q., and Jeppson, M. B., An Ammonium Perchlorate Model Based on a Detailed Kinetic Mechanism, 33rd JANNAF Combustion Meeting, 1996, Vol. II, CPIA #653, pp 21–34.
13. Lee, M. J., Blomshield, F. S., and Beckstead, M. W., Analysis of Initial Pressure Pulsing Amplitude for Triggering of Nonlinear Solid Rocket Combustion Instability, 33rd JANNAF Combustion Meeting, 1996, Vol. III, CPIA #653, pp 559–569.
14. Beckstead, M. W. and Erikson, W. W., Combustion Instability of Solid Monopropellants, 33rd JANNAF Combustion Meeting, 1996, Vol. II, CPIA No. 653, pp 145–157.
15. Blomshield, F. S., Stalnaker, R. A., and Beckstead, M. W., Solid Propellant Combustion Stability Additive Investigation, Combustion and Detonation, 1997, 28th Int'l Conf. of ICT, Karlsruhe, Germany, pp v6-1, 6-13.
16. Glotov, O. G., Zarko, V. E., Karasev, V. V., and Beckstead, M. W., Effect of Binder on the Formation and Evolution of Condensed Combustion Product of Metalized Solid Propellant, Combustion and Detonation, 1997, 28th Int'l Conf. of ICT, Karlsruhe, Germany, pp P75-1, 75-14.
17. Beckstead, M. W., Davidson, J. E., and Jing, Q., A Comparison of Solid Monopropellant Combustion and Modeling, AIAA 97-0586, 1997.
18. Erikson, W. W. and Beckstead, M.W., "Modeling Unsteady Monopropellant Combustion with Full Chemical Kinetics", 34th JANNAF Combustion Meeting, 1997, Vol. I, CPIA #662, pp. 302.
19. Jing, Q. and Beckstead, M.W., "Modeling of HMX Temperature Sensitivity", 34th JANNAF Combustion Meeting, 1997, CPIA No. 662, Vol. IV, pp. 249-261.
20. Jing, Q. Beckstead , M.W. and Jeppson, M.B., "Influence of AP Solid Phase Decomposition onTemperature Profile and Sensitivity", 34th JANNAF Combustion Meeting, 1997, CPIA No. 662, Vol. IV, pp. 99-108.

21. Liang, Y. and Beckstead, M.W., "Numerical Simulation of Single Aluminum Particle Combustion in Air", 34th JANNAF Combustion Meeting, 1997, CPIA No. 662, Vol. IV, pp. 197-208.
22. Beckstead, M. W. and Price, C.F., "A Computer User's Manual for KALCID (A Computer Program to Describe Kinetic Analysis of Laboratory Combustion and Ignition Data)", 1997, Brigham Young University, Provo, Utah.
23. Davidson, J. E. , and Beckstead, M.W., "A Mechanism and Model for GAP Combustion", 1997, AIAA 97-0592.
24. Erikson, W. W. and Beckstead, M.W., "Modeling Unsteady Monopropellant Combustion with Full Chemical Kinetics", 1998, AIAA 98-0804.
25. Jeppson, M. B. , Beckstead, M.W. and Jing, Q., "A Kinetic Model for the Premixed Combustion of a Fine AP/HTPB Composite Propellant", 1998, AIAA 98-0447, Reno, NV.
26. Liang, Y. and Beckstead, M.W., "Numerical Simulation of Unsteady Single Aluminum Particle Combustion in Air", 1998, AIAA 98-3825.
27. Widener, J. F. and Beckstead, M.W., "Aluminum Combustion Modeling in Solid Propellant Combustion Products", 1998, AIAA 98-3824.
28. Blomshield, F.S. , Stalnaker, R.A. and Beckstead, M.W., "Combustion Stability Additive Investigation", 35th JANNAF Combustion Meeting, 1998.
29. Erikson, W.W. and Beckstead, M.W., "Modeling Pressure and Heat Flux Responses of Nitramine Monopropellants with Detailed Kinetics", 35th JANNAF Combustion Meeting, 1998.
30. Erikson, W.W. and Beckstead, M.W., "Modeling Unsteady Monopropellant Combustion with Full Chemical Kinetics", 1998, AIAA 98-0804.
31. Glotov, O.G., Zarko, V.E., Karasev, V.V. and Beckstead, M.W., "Aluminum Agglomeration in Solid Propellants: Formulation Effects", 1998, AIAA-98-0449.
32. Jeppson, M.B., Beckstead, M.W. and Jing, Q., "A Kinetic Model for the Premixed Combustion of a Fine AP/HTPB Composite Propellant", 1998, AIAA 98-0447, Reno, NV.
33. Jing, Q. and Beckstead, M.W., "Influence of Condensed Phase Mechanism on HMX Temperature Sensitivity", 1998, AIAA-98-3222.
34. Jing, Q. Beckstead , M.W. and Jeppson, M.B., "Influence of AP Solid Phase Decomposition on Temperature Profile and Sensitivity", 1998, AIAA 98-0448.
35. Liang, Y. and Beckstead, M.W., "Numerical Simulation of Unsteady Single Aluminum Particle Combustion in Air", 1998, AIAA 98-3825.
36. Liang, Y. and Beckstead, M.W., "Numerical Simulation of Quasi-Steady Single Aluminum Particle Combustion in Air", 1998, AIAA 98-0254.
37. Blomshield, F.S., "Pulse Motor Firings," to appear in Journal of Propulsion And Power, November 1999.
38. Beckstead, M. W., "An Overview of Combustion Mechanisms and Flame Structure of Advanced Solid Propellants", Journal of Propulsion and Power, Special Issue on Solid Propellant and Combustion, 1999.
39. Erikson, W. W. and Beckstead M. W., "Modeling Pressure and Heat Flux Responses of Nitramine Monopropellants with Detailed Chemistry", AIAA 99-2498, 1999.
40. Widener, J. F. Liang Y. and Beckstead M. W., "Aluminum Combustion Modeling in Solid Propellant Environments", AIAA 99-0049, 1999.
41. Jing, Q. Beckstead M.W. and Erikson W.W., "Modeling Pressure Response of HMX Including a Condensed Phase Void Fraction", AIAA-2000-3192, *36th AIAA/ASME/SAE/ASEE Joint Propulsion Conference*, Huntsville, Alabama, July 2000.
42. Liang, Y. Beckstead M.W. and Pudduppakkam K., "Numerical Simulation of Unsteady, Single Aluminum Particle Combustion", *36th JANNAF Combustion Meeting*, Cocoa Beach, Florida, Oct. 1999,CPIA #691, Vol I, pp. 283-309.
43. Beckstead, M.W. Meredith, K. V. and Blomshield F.S., "Examples of Unstable Combustion, as Measured in T-Burners", *36th JANNAF Combustion Meeting*, CPIA #691, Vol I, 1999, pp. 539-555.
44. Beckstead, M.W. Meredith K.V. and Blomshield F.S., "Examples of Unstable Combustion, as Measured in T-Burners", *29th JANNAF Propellant Development & Characterization Meeting*, Cocoa Beach, Florida, May 2000.
45. Beckstead, M.W., " Modeling Condensed Phase Reactions in Energetic Solids", Gordon Conference on Energetic Materials, Tilton, New Hampshire, June 2000.
46. Beckstead, M.W. Meredith K. V. and Blomshield F. S., "Examples of Unstable Combustion, as Measured in T-Burners", *36th AIAA/ASME/SAE/ASEE Joint Propulsion Conference*, AIAA-2000-3696, Huntsville, Alabama, July 2000.

47. Beckstead, M.W., "An Overview of Combustion Mechanisms and Flame Structure of Advanced Solid Propellants", *29th JANNAF Propellant Development & Characterization Meeting*, CPIA #698, 2000, pp 371-397.
48. Beckstead, M.W., "An Overview of Combustion Mechanisms and Flame Structures of Advanced Solid Propellants", *36th AIAA/ASME/SAE/ASEE Joint Propulsion Conference & Exhibit*, AIAA-2000-3325 AIAA Joint Propulsion Conference, Huntsville, Alabama, July 2000.
49. Beckstead, M.W., "An Overview of Monopropellant Modeling Using Detailed Kinetics ", ONERA, Paris, France, an invited lecture, June 2000.
50. Beckstead, M.W., "Potential Combustion Mechanisms of Advanced Propellants", NATO DEA 5660 Meeting, Huntsville, Alabama, July 2000.
51. Beckstead, M.W., "Metal Combustion in the MURI Program", *36th AIAA/ASME/SAE/ASEE Joint Propulsion Conference & Exhibit*, Huntsville, Alabama, July 2000.
52. Beckstead, M.W., "Modeling Detailed Combustion Mechanisms and Flame Structure of Solid Propellants in the MURI Program", *36th AIAA/ASME/SAE/ASEE Joint Propulsion Conference & Exhibit*, Huntsville, Alabama, July 2000.

BLOMSHIELD, BREWSTER, FLANAGAN

53. Blomshield, F. (2000) "Summary of Multidisciplinary University research Initiative in Solid Propellant Combustion Instability," *36th AIAA/ASME/SAE/ASEE Joint Propulsion Conference & Exhibit*, AIAA Paper No. 2000-3172.
54. Brewster, M.Q. (2000) "Unsteady Combustion of Solid Propellants—Simplified Kinetics Modeling," *36th AIAA/ASME/SAE/ASEE Joint Propulsion Conference & Exhibit*, AIAA Paper No. 2000-3174.
55. Flanagan, J. (2000) "Fundamental Chemistry Studies: MURI – CIT & UIUC," *36th AIAA/ASME/SAE/ASEE Joint Propulsion Conference & Exhibit*, AIAA Paper No. 2000-3171.

BRILL

56. G. K. Williams and T. B. Brill, Thermal Decomposition of Energetic Materials 70. Kinetics of Organic Peroxide Decomposition Derived from the Filament Control Voltage of T-Jump/FTIR Spectroscopy, *Appl. Spectrosc.* 51, 423 (1997).
57. T. B. Brill, P. E. Gongwer and B. D. Budenz, Oxidizer-Binder Interactions from T-Jump/FTIR Spectroscopy Flash Pyrolysis, *Proc. 28th Int. ICT Conf.*, Karlsruhe, Germany, June 1997 p. 14-1.
58. Budenz, B.T. and Brill, T.B. "Effects of Burning-Rate Modifiers on the Pyrolysis Chemistry of AP-HTPB Mixtures" Gordon Research Conference on Energetic Materials, Holderness, NH, June 1998.
59. Roos, B.D. and Brill, T.B. "Development of T-Jump/Raman Spectroscopy as a Complement to T-Jump/FTIR Spectroscopy", Gordon Research Conference on Energetic Materials, Holderness, NH, June 1998.
60. Brill, T.B. "How Far Can We Go in Connecting Molecular Processes to Macro-Events?" Gordon Research Conference on Energetic Materials, Holderness, NH, June 1998.
61. Brill, T.B. and Williams, G.K. "Unusual Flash Thermolysis Behavior of Nitronitraminofurazans" 34th JANNAF Combustion Meeting, West Palm Beach, FL, October 1997.
62. Brill, T.B., Gongwer, P.E., and Budenz, B.T. "Flash Thermal Decomposition of Oxidizer-Binder Mixtures" 34th JANNAF Combustion Meeting, West Palm Beach, FL, October 1997.
63. T. B. Brill, P. E. Gongwer and B. D. Budenz, Condensed Phase Oxider-Binder Chemistry During Flash Pyrolysis, *34th JANNAF Combustion Meeting, CPIA Publ.* 662, 447 (1997).
64. T. B. Brill and G. K. Williams, Nitronitraminofurazans: Unusual Behavior Upon Flash Pyrolysis, *34th JANNAF Combustion Meeting, CPIA Publ.* 662, 457 (1997).
65. Arisawa, H. and Brill, T.B. "Thermal Decomposition of Energetic Materials 71. Structure-Decomposition Relationships in Flash Pyrolysis of Glycidyl Azide Polymer (GAP)" Combustion and Flame, 112, 533-544 (1998).
66. Williams, G.K. and Brill, T.B. "Thermal Decomposition of Energetic Materials 72. Unusual Behavior of Substituted Furazan Compounds upon Flash Pyrolysis", Combustion and Flame, 114, 569-576 (1998).
67. T. B. Brill and B. D. Budenz, Flash Pyrolysis of AP and HTPB and the Effect of TiO_2 and Melamine, *35th JANNAF Combustion Meeting CPIA publ.* 680, Dec. 1998, p. 617.
68. T. B. Brill and B. D. Budenz, Condensed-Phase Issues for AP-HTPB Pseudo-propellant and the Effect of Burning Rate Additives, *J. Propul. Power*, in press.

69. T. B. Brill, T. L. Zhang and B. C. Tappan, Thermal Decomposition of Energetic Materials 74. Volatile Metal Isocyanates from Flash Pyrolysis of Metal-NTO and Metal-Picrate Salts and an Application Hypothesis. *Combust. Flame*, in press.
70. T. B. Brill, T. L. Zhang, B. C. Tappan and R. W. Beal, Volatile Metal Salts a Combustion Stabilizers: Another Approach?, *36th JANNAF Combustion Meeting*.
71. T. B. Brill, T. L. Zhang, B. C. Tappan and R. W. Beal, IR Spectra and DFT Calculations on gaseous MNCO Molecules (M=Li, Na, K, Rb, Cs), *submitted*.
72. B. D. Roos and T. B. Brill, Thermal Decomposition of Energetic Materials 75. T-Jump/Raman Spectroscopy and the Application to Pyrolysis of High-Nitrogen Compounds, *submitted*.
73. Brill, T.B. "Azide Chemistry", MURI Workshop on Azide Decomposition/Combustion, Reno, NV, Jan. 1999, (organized and chaired workshop).
74. Brill, T.B. "Molecular Control of Burning Rates", JANNAF Workshop on Burning Rate Modifiers, Army Research Lab. Aberdeen, MD Sept. 1998, (invited).
75. Brill, T.B. and Budenz, B.T. "Flash Decomposition Characteristics of AP-HTPB with TiO_2 and Melamine", 35th JANNAF Combustion Meeting, Tucson, AZ, Dec. 1998.
76. Brill, T.B. and Budenz, B.T. Condensed phase issues for the AP-HTPB mixtures and the effect of burning rate additives, J. Propuls. Power, in press.
77. Brill, T.B. and Budenz, B.T. Flash pyrolysis of mixtures of AP and HTPB and the effect of TiO_2 and melamine additives, 35th JANNAF Combustion Meeting, Tucson AZ, Dec. 1998.
78. Brill, T.B. "High Nitrogen Compounds" Seminar, Los Alamos national Lab. Jan. 2000.
79. Roos, B.D. and Brill, T.B. " Flash Pyrolysis of GAP/RDX Mixture" Gordon Conference on Energetic Materials, Tilton NH, July 2000.
80. Tappan, B.C. and Brill, T.B., "Preparation and Properties of Mono- and Diavlent 5-Nitroaminotetrazole Complexes of Metal Ions," Gordon Conference on Energetic Materials, Tilton NH, July 2000.
81. Brill, T.B. and Roos, B.D., "Comparison of T-Jump/Raman and T-Jump/FTIR Spectroscopy for High-Nitrogen Compounds," Proc. Int. Conf. ICT, Karlsruhe, Germany, June 2000.
82. Brill, T.B., Ramanathan, H., and Beal, R.W., "Pyrolysis Studies of the Burning Mechanisms of High- Nitrogen Compounds", Proc. Int. Symp. Spec. Top. Combust. Stresa, Italy, June 2000.
83. Brill, T.B., Zhang, T.L., Tappan, B.C. and Beal, R.W., Volatile Metal Salts a Combustion Stabilizers. Another Approach? 36th JANNAF Combustion Meeting, Cocoa Beach, FL, Oct. 1999, in press.

CULICK

84. Culick, F.E.C., Modal Representation of Linear and Nonlinear Instabilities in Combustion Chambers, SIAM Mini-Symposium, 6th International Conference on Numerical Combustion, Analyses and Control of Combustion Instabilities, March 1996.
85. Culick, F.E.C. and Burnley, V., Some Dynamics of Acoustic Oscillations with Nonlinear Combustion and Noise, Proceedings, *4th International Symposium on Special Topics in Chemical Propulsion: Challenges in Propellants and Combustion 100 years after Nobel*," Stockholm, May 1996.
86. Culick, F.E.C., On the Roles of Approximate Methods of Analysis and Numerical Simulations for Investigation of Combustion Instabilities in Solid Propellant Rockets, Proceedings, *2nd International Conference on Combustion Conversion and Environmental Problems of Energetic Material*, Saint Petersburg, Russia, June 1996.
87. Culick, F.E.C. and Roh, T.-S., Applications of Various Methods of Analysis to Combustion Instabilities in Solid Propellant Rockets, 33rd JANNAF Combustion Meeting, CPIA #653, November 1996.
88. Culick, F.E.C., A Note on Ordering Perturbations and the Insignificance of Linear Coupling in Combustion Instabilities, *Combustion Science and Technology*, 1997.
89. Culick, F.E.C., Burnley, V. and Isella, G., Ordering and Nonlinear Problems of Combustion Instabilities, *International Workshop on Combustion Instabilities of Solid Rocket Propellants and Rocket Motors*; Politecnico di Milano, Italy, June 1997.
90. Culick, F.E.C. and Isella, G., Some Influences of Nonlinear Energy Transfer Between the Mean Flow and Fluctuations, *2nd International Seminar on Intra-Chamber Processes, Combustion, and Gas Dynamics of Dispersed Systems*, Saint Petersburg, Russia, June 1997.
91. Roh, T.S. and Culick, F.E.C., Transient Combustion Responses of Homogeneous Propellants to Acoustic Oscillations in Axisymmetric Rocket Motors, *33rd AIAA/ASME/SAE/ASEE Joint Propulsion Conference & Exhibit*, *AIAA* Paper No. 97-3325, Seattle, WA, July 1997.

92. Culick, F.E.C. and Roh, T.-S., Numerical Analysis of Transient Combustion Responses to Acoustic Oscillations in Axisymmetric Rocket Motors, *36th Aerospace Sciences Meeting*, *AIAA* Paper No. 98-0253.
93. Culick, F.E.C., Isella, G. and Seywert,C., Influences of Combustion Dynamics on Linear and Nonlinear Unsteady Motions in Solid Propellant Rockets, *AIAA* Paper No. 98-3704, *34th AIAA/ASME/SAE/ASEE Joint Propulsion Conference*, Cleveland, OH, July 1998.
94. Roh, T.S., Cohen, N.S., Beddini, R.A. and Culick, F.E.C., Stability Analysis and Combustion Modeling of AP Composite Propellants, *35th JANNAF Combustion Meeting*, Dec. 1998.
95. Culick, F.E.C. and Burnley, V., The Influences of Noise on Acoustic Instabilities, *34th JANNAF Combustion Meeting*, Tucson, AZ, May 1999.
96. Culick, F.E.C. and Isella, G., Some Influences of Nonlinear Energy Transfer Between the Mean Flow and Fluctuations, *34th JANNAF Combustion Meeting*, Tucson, AZ, May 1999.
97. Culick, F.E.C. and Roh, T.-S., Numerical Study of Acoustic Oscillations and Combustion Instabilities in Solid Propellant Rockets, *34th JANNAF Combustion Meeting*, Tucson, AZ, May 1999.
98. Culick, F.E.C., Roles of Bifurcations in Combustion Instabilities, *International Workshop on Status and Perspectives in Liquid Rocket Combustion Chamber Flow Dynamics*, CNES, Paris, France, 27-28 May 1999.
99. Roh, T.S., Cohen, N.S., Beddini, R.A. and Culick, F.E.C., Numerical Analysis of Solid Rocket Motor Instabilities with AP Composite Propellants, *AIAA* Paper 99-2804, *35th AIAA/ASME/SAE/ASEE Joint Propulsion Conference*, June 1999.
100. Culick, F.E.C. and Seywert, C., Some Influences of Noise on Combustion Instabilities and Combustor Dynamics, *36th JANNAF Combustion Meeting*, Cocoa Beach, FL, Oct. 18-21, 1999.
101. Culick F.E.C. and Isella, G.C., Modeling the Combustion Response Function with Surface and Gas Phase Dynamics, *36th JANNAF Combustion Meeting*, Cocoa Beach, FL, Oct. 18-21, 1999.
102. Malhotra, S. and Culick, F.E.C., On the Pathways of Energy Transfer in Combustion Chambers, *36th JANNAF Combustion Meeting*, Cocoa Beach, FL, Oct. 18-21, 1999.
103. Cohen, N.S. and Shusser, M., Combustion Modeling of AP Composite Propellants for Stability Analysis, *36th 1999 JANNAF Joint Meeting*, Cocoa Beach, FL, Oct. 18-21, 1999.
104. Culick, F.E.C., "Influence of Nonlinear Energy Transfer and Internal Geometry on Motor Combustion Instability," to appear in *Journal of Propulsion and Power*, November 1999.
105. Culick, F.E.C. and Burnley, V., "Comment on 'Triggering of Longitudinal Combustion Instabilities in Rocket Motors: Nonlinear Combustion Response'", *J. of Propulsion and Power*, 16(1), 164-165, March-April 2000.
106. Cohen, N.S., Shusser, M., Culick, F.E.C. and Beddini, R.A., "Combustion Modeling of AP Composite Propellants for Stability Analysis", 36th JANNAF Combustion Meeting, Cocoa Beach, FL, 18–22 Oct 1999.
107. Malhotra, S. and Culick, F.E.C., "On the Pathways of Energy Transfer in Combustion Chambers", 36th JANNAF Combustion Meeting, Cocoa Beach, FL, 18–22 Oct 1999.
108. Malhotra, S. and Culick, F.E.C., "On the Pathways of Energy Transfer in Combustion Chambers" 36th AIAA/ASME/JAE/ASEE Joint Propulsion Conference, July 16–19, 2000, Huntsville, AL, Paper No. AIAA-2000-3328.
109. Pun, W., Palm, S.L., and Culick, F.E.C., "PLIF Measurements of Combustion Dynamics in a Burner under Forced Oscillatory Conditions", 36th AIAA/ASME/SAE/ASEE Joint Propulsion Conference and Exhibit, AIAA 2000-3123, July 16–19, 2000, Huntsville, AL, to be published, *Combustion Science and Technology* (2002).
110. Seywert, C. and Culick, F.E.C., "Some Influences of Noise on Combustion Instabilities and Combustor Dynamics", 36th JANNAF Combustion Meeting, Cocoa Beach, FL, 18–22 Oct 1999.
111. Seywert, C. and Culick, F.E.C., "Some Influences of Noise on Combustion Instabilities and Combustor Dynamics", Fifth International Symposium on Special Topics in Chemical Propulsion, Stresa, Italy, 18–22 June 2000.
112. Shusser, M., Culick, F.E.C. and Cohen, N.S., "Combustion Response of Ammonium Perchlorate", 36th AIAA/ASME/SAE/ASEE Joint Propulsion Conference & Exhibit, July 16–19, 2000, Huntsville, AL, Paper No. AIAA 2000-3694, accepted for publication in *AIAA Journal*, 2001.
113. Culick, F.E.C. and Burnley, V. S., "Triggering of Longitudinal Combustion Instabilities in Rocket Motors: Nonlinear Combustion Response", *Journal of Propulsion and Power*, 1999.
114. Culick, F.E.C. and Isella, G., "Modeling the Combustion Response Function with Surface and Gas Phase Dynamics" *38th Aerospace Sciences Meeting & Exhibit*, AIAA Paper No. 2000-0310.
115. Culick, F.E.C. and Isella, G., "Modeling the Effects of Velocity Coupling on the Global Dynamics of Combustion Chambers" *36th AIAA/ASME/SAE/ASEE Joint Propulsion Conference & Exhibit*, July 16–19, 2000, Huntsville, AL, Paper No. AIAA 2000-3187.

116. Culick, F.E.C., Combustion Instabilities: Mating Dance of Chemical, Combustion, and Combustor Dynamics, *36th AIAA/ASME/SAE/ASEE Joint Propulsion Conference & Exhibit* July 16–19, 2000, Huntsville, AL., Paper No. AIAA 2000-3178.
117. M. Shusser, N.S. Cohen and F.E.C. Culick, "Combustion response of AP composite propellants," 37th JANNAF Combustion Meeting, Monterey, CA, 13-17 November 2000, (submitted to *AIAA J. Prop. and Power*).
118. Shusser, M. and Culick, F.E.C., "Analytical Solution for Composite Solid Propellant Response Function," 37th AIAA Joint Propulsion Conference, Salt Lake City, UT, 8-11 July 2001, submitted to *AIAA Journal* 2001.
119. Shusser, M., Culick, F.E.C. and Cohen, N.S., "Pressure Exponent of a Composite Solid Propellant," submitted to *AIAA Journal*, 2001.
120. Shusser M., Cohen N.S., "Effect of Variable Thermal Properties of the Solid Phase on Composite Solid Propellant Combustion," submitted to *Astronautica Acta*, 2001.

FREDERICK

121. Miyata, K., Frederick, R.A., "Combustion Mechanisms of Fuel-Rich Ammonium Nitrate-Based Propellants," *AIAA Journal of Propulsion and Power.*
122. Chiyyarath, K., Frederick, R. A., Jr. and Moser, M. D., "Ballistic Characterization of Bi-Plateau Solid Propellants," *CPIA Pub* 662, Vol. IV, p73-81, October 1997.
123. Rasmussen, B., Lengelle, G. and Frederick, R.A., Jr., "Pressure-Coupled Frequency Response Models of Solid Propellants," *CPIA Pub* 662, Vol. II, p263-274, October 1997.
124. Rochford, E. E., Moser, M.D., and, Frederick, R. A., Jr. "Ballistic Characterization of MURI Propellants," *35th JANNAF Combustion Meeting*, Dec. 1998.
125. Rasmussen, B., Frederick, R. A., Jr., Moser, M. D., and Lengelle, G., "A Theoretical Pressure-Driven Response Function for Composite Solid Propellants," *CPIA Pub* 675, Vol. I, p69-78, July 1998.
126. DiSalvo, R., Frederick, R.A., Jr., and Moser, M. D., "Experimental Determination of Solid Propellant Combustion Response Function," *AIAA* Paper No. 98-3553, July 1998.
127. DiSalvo, R and Frederick, R.A., Jr., and Moser, M.D., "Experimental Determination of Pressure Coupled Response Functions." 1998 JANNAF Combustion Meeting.
128. McQuade, W., Dauch, F., Moser, M. D, and Frederick, R.A., Jr., "Determination of the Ultrasonic Burning Rate Technique Resolution," *AIAA* Paper No. 98-3555, July 1998.
129. Miyata, K., and Frederick, R.A., "An Engineering Model for Temperature Sensitivity of AP Composite Propellants," *AIAA* Paper No. 98-3221, July 1998.
130. Rochford, E. E., R. DiSalvo, R., Frederick, R. A., Jr., and Moser, M.D., "Transient Ballistic Measurements in a Solid Motor," *CPIA Pub* 675, Vol. III, p109-188, July 1998.
131. DiSalvo, R., Frederick, R.A., Jr., and Moser, M.D., "Experimental Determination of Solid Propellant Combustion Response Function, " AIAA Paper No. 98-3553, July 1998.
132. Edmund Rochford, Temperature Sensitivity Measurements of Solid Rocket Propellants, Defense: February 18, 1999, Chairman: Marlow Moser.
133. McQuade, W., Dauch, F., Moser, M.D, and Frederick, R.A., Jr., "Determination of the Ultrasonic Burning Rate Technique Resolution," AIAA Paper No. 98-3555, July 1998.
134. Moser, M.D., McQuade, W. and Dauch, F., "Surface Roughness Effects on Ultrasonic Burning Rate Measurements," planned for *ASME Meeting.*
135. Rasmussen, B., An Intrinsic Heterogeneous Model of Composite Solid Propellant Combustion, Defense, December 17, 1998, Chairman: Robert A. Frederick, Jr.
136. Rasmussen, B., and Frederick, R.A., Jr., "A Nonlinear Heterogeneous Model of Composite Solid Propellant Combustion." AIAA Paper No. 99-2228, 35th AIAA/ASME/SAE/ASEE Joint Propulsion Conference Joint Propulsion Conference, Los Angeles, CA, June 20-23, 1999.
137. Rasmussen, B., Frederick, R.A, Jr., and Moser, M.D., "Issues in Non-Linear, Non-Steady Solid Combustion Modeling." 1998 JANNAF Combustion Meeting.
138. Rasmussen, B., Frederick, R.A., Jr., Moser, M. D., and Lengelle, G., "A Theoretical Pressure-Driven Response Function for Composite Solid Propellants," CPIA Pub 675, Vol. I, p69-78, July 1998.
139. Rochford, E., Dauch, F., and Moser, M.D., "Uncertainty Assessment of Ultrasonic Measurement of Propellant Burning Rate," AIAA Paper No. 99-2224, 35th AIAA/ASME/SAE/ASEE Joint Propulsion Conference Joint Propulsion Conference, Los Angeles, CA, June 20-23, 1999.

140. Rochford, E.E., Moser, M.D., and, Frederick, R.A., Jr. "Ballistic Characterization of MURI Propellants," 1998 JANNAF Combustion Meeting.
141. Rochford, E.E., Moser, M.D., and, Frederick, R.A., Jr. "Ballistic Characterization of MURI Propellants", JANNAF Combustion Meeting, 1998.
142. Boxx, D, Frederick, R.A., Jr., Moser, M. D., and Cohen, N., "SEM Analysis of Extinguished Propellant Surfaces," *AIAA* Paper No. 99-2222, *35th AIAA/ASME/SAE/ASEE Joint Propulsion Conference*, Los Angeles, CA, June 20-23, 1999. Submitted to *AIAA Journal of Propulsion and Power*.
143. DiSalvo, R., Frederick, R. A., Jr., and Moser, M., "Direct Ultrasonic Measurements of Solid Propellant Combustion Transients," *AIAA* Paper No. 99-2223, *35th AIAA/ASME/SAE/ASEE Joint Propulsion Conference*, Los Angeles, CA, June 20-23, 1999.
144. Dauch, F., and Moser, M. D., Frederick, R. A., Jr., and Coleman, H. W., "Uncertainty Assessment of Ultrasonic Measurement of Propellant Burning Rate," *AIAA* Paper No. 99-2224, *35th AIAA/ASME/SAE/ ASEE Joint Propulsion Conference*, Los Angeles, CA, June 20-23, 1999. Submitted to *AIAA Journal of Propulsion and Power*.
145. Rasmussen, B., and Frederick, R. A., Jr., "Direct Numerical Simulation of Heterogeneous Solid Combustion." *AIAA* Paper No. 99-2228, *35th AIAA/ASME/SAE/ASEE Joint Propulsion Conference*, Los Angeles, CA, June 20-23, 1999.
146. Moser, M. D., Dauch, F. and McQuade, W. W., "Surface Roughness effects on Ultrasonic Burning Rate Measurements," *1999 National Heat Transfer Conference*, Paper NHTC99-0285, August 1999.
147. Frederick, R. A., Jr., and Traineau, J. C., "Survey of Ultrasonic Instrumentation for Burning Rate Measurement," *36th JANNAF Combustion Meeting*, October 1999.
148. Di Salvo, R., Dauch, F, Frederick, R. A. Jr., and. Moser M. D, "Direct Ultrasonic Measurement of Solid Propellant Ballistics" *Review of Scientific Instruments*, Vol. 70, No. 11, November, 1999.
149. Di Salvo, R., Frederick, R.A., Jr., and Moser, M., "Effect of Oxidizer Size Distribution on Propellant Response Function," AIAA Paper 2000-3799, 36th AIAA/ASME/SAE/ASEE Joint Propulsion Conference and Exhibit, July 16-19, 2000.
150. Smith, M.D., Moser, M.D., and Frederick, R.A., Jr. "Temperature Sensitivities of Energetic Binder Propellants," AIAA Paper No. 2000-3319, 36th AIAA/ASME/SAE/ASEE Joint Propulsion Conference and Exhibit, July 16-19, 2000.
151. Frederick, R.A., Jr., "Ballistic Studies of Wide Distribution Propellants," AIAA Paper 2000-3318, 36th AIAA/ASME/SAE/ASEE Joint Propulsion Conference and Exhibit, July 16-19, 2000.
152. Frederick, R.A., Jr., Traineau, J-C, and Popo, M., "Review of Ultrasonic Technique for Steady State Burning Rate measurements," AIAA Paper 2000-3801, 36th AIAA/ASME/SAE/ASEE Joint Propulsion Conference and Exhibit, July 16-19, 2000.

FLANDRO

153. Flandro, G. A., "Stability Prediction with Rotational Flow Effects," *31st JANNAF Combustion Meeting*, San Jose, CA, October 1994.
154. Flandro, G. A., "On Flow Turning," *31st AIAA Joint Propulsion Conference*, July 1995, *AIAA Journal*.
155. Thomas, H. D., Flandro, G. A. and Flanagan, S. N., "Effects of Vorticity on Particle Damping," *31st AIAA Joint Propulsion Conference*, July 1995, *AIAA Journal*.
156. Flanagan, S. N., Flandro, G. A. and Thomas, H. D., "A New Approach to Velocity Coupling," *31st AIAA Joint Propulsion Conference*, July 1995, *AIAA Journal*.
157. Flandro, G. A., "Effects of Vorticity on Rocket Combustion Stability," *Journal of Propulsion and Power*, Vol. 11, No. 4, July-August 1995.
158. Flandro, G. A., "Interpretation on Nonlinear Rocket Instability Test Data," *32nd JANNAF Combustion Meeting*, Huntsville, AL, October 1995.
159. Flandro, G. A. and Garza, D. M., "Nonlinear Combustion Instability Data Reduction," AIAA Paper 96-3251, *32nd AIAA Joint Propulsion Conference*, Orlando, FL, July 1996.
160. Flandro, G.A., Garza, D.M., "Nonlinear Combustion Instability Data," *AIAA Journal*.
161. French, J. C., Flanagan, S. N. and Flandro, G. A., "A New Method for Combustion Instability Mode Shape and Frequency Computation," *Proceedings of the 33rd JANNAF Combustion Meeting*, Monterey, CA, September 1996.
162. Flandro, G. A., "Flow Processes in Combustion Instability," MURI Motor Flow Field Workshop, NAWC China Lake, 25 March 1997.

163. Malhotra, S. and Flandro, G. A., "On the Origin of the DC Shift," AIAA Paper 97-3249, *33rd AIAA Joint Propulsion Conference*, Seattle, WA, July 1997.
164. Malhotra, S. and Flandro, G. A., "On Nonlinear Combustion Instability," AIAA Paper 97-3250, *33rd AIAA Joint Propulsion Conference*, Seattle, WA, July 1997.
165. Flandro, G. A., "Nonlinear Unsteady Combustion of a Solid Propellant," *34th JANNAF Combustion Meeting*, West Palm Beach, FL, October 1997.
166. Flandro, G. A., "Analysis of Nonlinear Unsteady Combustion," Invited Paper, *SIAM Combustion Symposium*, York, England, March 1998.
167. Flandro, G. A., "Rotational Flow Effects in Rockets," Invited Paper *ONERA, Rocket Flow Field Symposium*, Chatillon, France, June 1998.
168. Majdalani, J., Flandro, G. A. and Roh, T. S., "Implications of Unsteady Analytical Flow Fields on Rocket Combustion Instability," AIAA Paper 98-3698, *34th AIAA Joint Propulsion Conference*, Cleveland, OH, July 1988.
169. Flandro, G. A., "Nonlinear Unsteady Solid Propellant Flame Zone Analysis," AIAA Paper 98-3700, *34th AIAA Joint Propulsion Conference*, Cleveland, Ohio, July 1998.
170. Flandro, G. A., "Origins of Linear Velocity Coupling," *35th JANNAF Combustion Meeting*, Tuscon, AZ, December 1998.
171. Majdalani, J. and Flandro, G. A., "Generalized Solution for the Oscillatory Pipe Flow Driven by Wall Injection of the Berman Type," *Journal of Fluid Mechanics*, 1999 (in press).
172. Flandro, G. A., "Flame Zone Coupling in Combustion Instability with Parallel Wave Incidence," *36th JANNAF Combustion Meeting*, Cocoa Beach, FL, October 1999.
173. Flandro, G. A., Majdalani, J. and Roh, T. S., "Convergence of Two Analytical Flowfield Models Predicting a Destabilizing Agent in Rocket Combustion," *Journal of Propulsion and Power*, Vol. 16, No. 3, May-June 2000.
174. Flandro, G. A., "Turbulent Transport in Rocket Motor Unsteady Flowfield," to appear in *Journal of Propulsion and Power*, November 1999.
175. Flandro, G. A., Cai, W., and Yang, V., "Turbulent Transport in Rocket Motor Unsteady Flow Field," Chapter 3.3 in *Solid Propellant Chemistry, Combustion, and Motor Interior Ballistics, AIAA Progress in Astronautics and Aeronautics*, Vol. 185, July 2000.
176. Flandro, G. A., Brown, R. S., Rudy, T. P., "Generation of Forces and Torques in Nonlinear Instability," *37th JANNAF Combustion Meeting*, Monterey, CA, November 2000.
177. Flandro, G. A., Cai, W., and Yang, V., "Effect of Turbulence on Combustion Zone Dynamics," 37th JANNAF Combustion Meeting, Monterey, CA, November 2000.
178. Flandro, G. A. and Majdalani, J., "Aeroacoustic Instability in Rockets," AIAA-2001-3868, *37th AIAA Joint Propulsion Conference & Exhibit*, Salt Lake City, UT, July 2001.
179. Majdalani, J. and Flandro, G. A., "The Oscillatory Pipe Flow with Arbitrary Wall Injection," accepted for publication by The Royal Society of London, *Proceedings: Mathematical, Physical, and Engineering Sciences*, 2001.

LIN

180. Hsu, C.-C., Kristyan, S., Lin, M.C., "Ab Initio Study of the Isomerization and Decomposition of Hydrogen Nitroxide and Hydroxyl Amino Radicals," *Journal of Chemical Physics*.
181. Kristyan, S., Lin, M.C., "Thermal Rate Constant for the HCN => HNC Isomerization Reaction Comparison of the Reversible RRKM and Reaction Dynamic Simulation Results," *International Journal of Chemical Kinetics*.
182. Kristyan, S., Lin, M.C., "A Theoretical Study of the H + C_2H_4 => C_2H_5 Reaction: Effects of Temperature, Pressure, and Quantum Mechanical Tunneling," *International Journal of Physical Chemistry*.
183. Kristyan, S., Lin, M.C., "The Application of Energy Transfer and Tunneling Reactions of Interest to Propellant Decomposition: Reactions of C_2H_4 with H and CH_3 Radicals," 25th Southeastern Theoretical Chemistry Association Conference, Florida State University, Tallahassee, Florida, May 1996.
184. Kristyan, S., Lin, M.C., "The Application of Energy Transfer and Tunneling Reactions of Interest to Propellant Decomposition: Isomerization and Decomposition of H_2NO and HNOH," 1996 Gordon Conference on Energetic Materials, New Hampton, NH, June 1996.

185. Kristyan, S., Klippenstein, S. J., and Lin, M. C., Study of the NH + NO reaction: Potential Surface, VRRKM rate, Master Equation Treatment and Branching Ratio, 26th Southeastern Theoretical Chemistry Association Conference, Univ. of Alabama, Birmingham, AL, May 15–17, 1997.
186. M. C. Lin, C.- C. Hsu, S. Kristyan and C. F. Melius, "Theoretical Study of the Isomerization and Decomposition of H_2NO Radical," *Procs. 1996 JANNAF Combustion Meeting*, *CPIA Publication* No. 653, Vol. II, pp 419-426, Laurel, MD, 1997.
187. M. C. Lin and J. Park, "Kinetic Modeling of the Decomposition of Sublimed ADN under Low-Pressure Conditions," *1997 JANNAF Joint Meeting*, West Palm Beach, FL, Oct. 27-31, 1997.
188. M. C. Lin, S. Kristyan and S. J. Klippenstein, "Theoretical Calculations for the Kinetics of the NH + NO Reaction," *1997 JANNAF Joint Meeting*, West Palm Beach, FL, Oct. 27-31, 1997.
189. J. W. Boughton, S. Kristyan and M. C. Lin, "Theoretical Study of the Reaction of Hydrogen with Nitric Acid: Ab Initio MO and TST/RRKM Calculations," *Chem. Phys*., **214**, 219 (1997).
190. A. M. Mebel and M. C. Lin, "Reactions of NO_x with Nitrogen Hydrides," *Int. Rev. Phys. Chem*. **16**, 249 (1997).
191. C.-C. Hsu, J. W. Boughton, A. M. Mebel and M. C. Lin, "Theoretical Study of HONO Reactions with H, OH, NO and NH_2 Radicals," in *Challenges in Propellants and Combustion: 100 Years after Nobel*, Begell House, Inc., New York, pp. 48-57, Aug. 1997.
192. Chakraborty, D. and Lin, M.C. "Ab initio MO/statistical calculations of the NH + NO2 rate constant and product branching ratios", 27th Southeastern Theoretical Chemistry Conference, May 28-30, 1998, Florida State University, Tallahassee, FL.
193. Chakraborty, D. and Lin, M.C. "Theoretical studies of the CH2N radical reactions: ab initio MO/statistical calculations of the CH2N + N2O and NO2 processes", Gordon Research Conference on Energetic Materials, Holderness School, New Hampshire, June 14-19, 1998.
194. Lin, M.C. and Musin, R.N. "Novel bimolecular initiation reactions in the thermal decomposition of ammonium nitrate", CPIA Publication no. 662, vol. II, pp.377-388, CPIA, Columbia, MD, 1998.
195. R. N. Musin and M. C. Lin, "Novel Bimolecular Reactions Between NH_3 and HNO_3 in the Gas Phase," *J. Phys. Chem.* A **102**, 1808-14 (1998).
196. D. Chakraborty, J. Park and M. C. Lin, "Theoretical Study of the OH + NO_2 reaction: formation of nitric acid and the hydroperoxyl radical," *Chem. Phys*. **231**, 39-49 (1998).
197. S. J. Klippenstein, D. L. Yang, T. Yu, S. Kristyan and M. C. Lin, "A Theoretical and Experimental Study of the CN + NO Association Reaction," *J. Phys. Chem. A*, **102**, 6973 (1998).
198. Lin, M.C., Kristyan, S. and Klippenstein, S.J. "Theoretical calculation for the kinetics of the NH + NO reaction", CPIA Publication no. 662, Vol. II, pp. 407-414, CPIA, Columbia, MD, 1998.
199. S. Kristyan and M. C. Lin, **"**Theoretical calculations for the kinetics of the HN+NO reaction," *Chem. Phys. Lett*. **29**, 200 (1998).
200. J. Park and M. C. Lin, "Kinetic Applications of the Pulsed Laser Photolysis/Mass Spectrometric Technique," *Recent Research Development in Physical Chemistry*, Transworld Research Network, 2, 965-979 (1998).
201. V. Yang, Y. -C. Liau, M. C. Lin, J. Park, "Analysis of ADN Combustion with Detailed Chemistry," *35th JANNAF Joint Meeting*, Tucson, AZ, Dec. 7-11, 1998.
202. M. C. Lin, D. Chakraborty, "Theoretical Studies of Methyleneamino (CH_2N) Radical Reactions: Rate Constants for the Direct and Indirect Metathetical Reactions of CH_2N with N_2O," *35th JANNAF Combustion Meeting*, Tucson, AZ, Dec. 7-11, 1998.
203. M. C. Lin, D. Chakraborty, "Theoretical Study of the Thermal Decomposition of a Model GAP Compound," *36th JANNAF Combustion Meeting*, Cocoa Beach, FL, Oct. 18-21, 1999.
204. V. Yang, Y.-C. Liau, J. Park, M. C. Lin, "An Improved Model of Ammonium Dinitramide (ADN) Combustion with detailed Chemistry," *36th JANNAF Combustion Meeting*, Cocoa Beach, FL, Oct. 18-21, 1999.
205. D. Chakraborty and M.C. Lin, "Gas Phase Chemical Kinetics of [C,H,N,O]-Systems Relevant to the Combustion of Nitramines in Their Early Stages," *J. Propul. Power*, (invited review), in press.
206. W. S. Xia, D. Chakraborty and M. C. Lin, "The Multifacet Mechanism of the OH + HNO_3 Reaction: An ab Initio MO Study," *J. Phys. Chem*. A, submitted.
207. X. Lu, R. N. Musin, and M.C. Lin, "Gas-phase reactions of HONO with HNO and NH_3: An ab initio and TST study," *J. Phys. Chem*. A, submitted.
208. Chakraborty, D. and Lin, M.C., "Theoretical Studies of Methyleneamino (CH2N) Radical Reactions: (I) Rate Constant and product Branching for the CH2N + N2O Process by ab initio MO/Statistical Theory calculations," J. Phys. Chem. A. 103, 601 (1999).

209. Chakraborty, D., Hsu, C.-C. and Lin, M.C. "Theoretical Studies of Nitroamino Radical Reactions: Rate Constants for the Unimolecular Decomposition of HNNO2 and Related Bimolecular Processes," J. Chem. Phys. 109, 8887 (1998).
210. Chakroborty, D. and Lin, M.C. Gas phase kinetics of [C,H,N,O]-systems relevant to the combustion of nitramines in their early stages, J. Propuls. Power, in press.
211. Chakroborty, D. and Lin, M.C. Theoretical calculations for the kinetics of the NH+NO reaction, Chem. Phys. Lett., 297, 200 (1998).
212. Chakroborty, D. and Lin, M.C. Theoretical studies of the methyleneamino radical reactions: Rate constants and product branching ratios for the CH2N+N2O processes by ab initio MO/statistical theory calculations. J. Phys. Chem. A, 103, 601 (1999).
213. Park, J. and Lin, M.C. "Kinetic Applications of the Pulsed Laser Photolysis/Mass Spectrometric Technique" Recent Research Development in Physical Chemistry, Transworld Research Network, 2 (1998).
214. Park, J., Chakraborty, D. and Lin, M.C. "Thermal Decomposition of Gaseous ADN: Kinetic Modeling of Product Formation with ab initio MO/RRKM Calculations" *Proc. 27th Int. Symposium on Combustion*, pp. 2231-57, Boulder, CO, August 2-7, 1998.
215. Park, J., Chakroborty, D. and Lin, M.C. Thermal decomposition of gaseous ammonium dinitramide at low pressure: Kinetic modeling of the product formation with ab initio MO/cVRRKM calculations, Proc. 27th Int. Symp. Combust. 2351 (1998).
216. Lin, M.C. "Ab Initio MO Studies of CH2N Radical Reactions and Model Azide Decomposition Reactions" MURI Workshop on Azide Decomposition/Combustion, Jan. 14 1999, Reno, NV. (organized by T. B. Brill).
217. Lin, M.C. "Ab Initio MO Studies of Combustion and Propulsion Processes" Invited talk, at the Symposium on "In the Frontiers of Quantum Chemistry & Chemical Reactions", May 21 and 22, 1999, Emory University, Atlanta, Ga.
218. Lin, M.C. "Experimental and Theoretical Studies of Elementary Combustion Processes: NOx Removal and Incipient Soot Formation Reactions" Invited talk, at 'Workshop on Combustion and Atmospheric Chemistry', Institutue of Atomic and Molecular Sciences, June 24, 1999, Taipei, Taiwan.
219. Lin, M.C. "Recent Progress in Studies of Elementary Reactions Important to NH3 deNOx and Soot Formation Processes" Invited lecture, 15th Int. Symposium on Gas Kinetics, Bilbao, Spain. Sep. 6-10, 1998.
220. Lin, M.C. "Theoretical Studies of Elementary Processes Relevant to RDX Decomposition Reaction" MURI Workshop on the Mechanism of RDX Decomposition Reaction, Jan.30, 1999, Rock Hall, MD. (organized by M. W. Beckstead and R. S. Miller).
221. Lin, M.C., Park, J., Gilles, N.D., Moore, J. "A Comprehensive Kinetic Modeling of the Thermal Reactions of NO2 with H2" 1998 JANNAF 35th Combustion Subcommittee and Propulsion Systems Hazards Subcommittee Joint Meeting, Tucson, AZ, Dec. 7-11, 1998.

LITZINGER

222. Fetherolf, B.L., Lee, Y.J.and Litzinger, T.A. "Study of the Gas-Phase Chemistry of RDX: Experiments and Modeling," *Journal of Propulsion & Power*, V. 11 No. 4. 1995 July-August. p. 698.
223. Fetherolf, B.L.; Litzinger, T.A. CO2 Laser-induced Combustion of Ammounum Dinttramide (ADN)., Combustion and Flame v 114 n 3-4 Aug-Sep 1998 p 515-530.
224. Lee, Y.J.; Tang, C.-J. ; Kudva, G.; Litzinger, T.A. Thermal Decompostion of 3,3 -Bis-Azidomethyl-Oxetane, Journal of Propulsion and Power v 14 n 1 Jan-Feb 1998 p 37-44.
225. Lee, Y., C.-J. Tang, G. Kudva and T. Litzinger, "Thermal Decomposition of BAMO and RDX/BAMO Pseudo-propellants," *33rd JANNAF Combustion Meeting*, Monterey, CA. 1996.
226. Tang, C., Y. Lee, G. Kudva and T. Litzinger, "A Study of the Combustion Response of HMX Mono-propellant to Sinusoidal Laser Heating," *33rd JANNAF Combustion Meeting*, Monterey, CA. 1996.
227. Tang, C., Lee, Y., Kudva, G., and Litzinger, T., "A Study of the Combustion Response of HMX Mono-propellant to Sinusoidal Laser Heating," *Proceedings of Fall Technical Meeting of the Eastern States Section of the Combustion Institute*, Hilton Head, SC, 1996, 4 pp.
228. Tang, C. J., Y. J Lee,., and T. A. Litzinger, The Chemical and Thermal Processes of GAP/Nitramine Pseudo-propellants under CO_2 Laser Heating, 34th JANNAF Combustion Meeting, November 1997.
229. Lee, Y. J., C. J. Tang and T. A. Litzinger, Comparison of Laser-driven and Acoustically-driven Combustion of HMX, 34th JANNAF Combustion Meeting, November, 1997.
230. Lee, Y. J., C. J. Tang and T. A. Litzinger, An Experimental Study of Acoustically-driven Combustion Instabilities of Solid Propellants, 34th JANNAF Combustion Meeting, November, 1997.

231. Lee, Y.J., Tang, C.-J., and Litzinger, T. A., A Triple Quadrupole Mass Spectrometer System for Studies of Gas-Phase Combustion Chemistry of Energetic Materials, *Measurement Science and Technology* v. 9, 1576-1586 (1998).
232. Lee, Y., C.-J. Tang, G. Kudva and T. Litzinger, The Thermal Decomposition of 3,3'-Bis-Azidomethy-Oxetane, *Journal of Propulsion and Power*. 14: 37-44 (1998).
233. Lee, Y. J., G. Kudva and T. Litzinger, Development of a Thrust Response Measurement System for Pressure-driven Combustion Studies, 35th JANNAF Combustion Meeting, Tucson, AZ, December 1998.
234. Kudva, G., Y. J. Lee, and T. Litzinger, Comparison of Laser and Pressure-driven Thrust Measurements in the Combustion of MURI Propellants, 35th JANNAF Combustion Meeting, Tucson, AZ, December 1998.
235. Litzinger, T. A., Y. Lee and C.-J. Tang, An Experimental Study of Nitramine/Azide Propellant Combustion, *Journal of Propulsion and Power*, Special Issue Solid Propellant Combustion, Chemistry and Interior Ballistics, (1999).
236. Tang, C.-J., Y. Lee, G. Kudva and T. Litzinger, A Study of the Gas-phase Chemical Structure during Laser-assisted Combustion of HMX, *Combustion and Flame* v. 117, p. 170-188 (1999).
237. Tang, C.-J., Y. Lee, G. Kudva and T. Litzinger, Simultaneous Species and Temperature Measurements during Laser-assisted Combustion of GAP, *Combustion and Flame* v. 117, 244-256 (1999).
238. Lee, Y., C.-J., Tang and T. Litzinger, A Study of the Chemical and Physical Processes Governing the CO_2 Laser-induced Pyrolysis and Combustion of RDX, *Combustion and Flame*, 117:600-628 (1999).
239. Lee, Y. J., C.-J. Tang and T. Litzinger, Thermal Decomposition of RDX/BAMO Pseudo-Propellants, *Combustion and Flame*, 117: 795-809 (1999).
240. Lee, Y. J., G. Kudva, and T. Litzinger, Thermal Decomposition of BAMO/AMMO Co-polymer, AIAA Joint Propulsion Conference, Los Angeles, CA, July 1999.
241. Kudva, G., Y. J. Lee and T. Litzinger, Comparison of Laser and Pressure-driven Thrust Measurements of HMX, AIAA Joint Propulsion Conference, Los Angeles, CA, July 1999.
242. Lee, Y. J., G. Kudva and T. Litzinger, "Thermal Decomposition of BAMO/AMMO and BAMO/AMMO/TiO_2," 36th JANNAF Combustion Meeting, 18-22 October 1999.
243. Kudva, G., Y. J. Lee and T. Litzinger, Comparison of Laser and Pressure-driven Thrust Measurements in the Combustion of an AP/Energetic Binder Propellant," 36th JANNAF Combustion Meeting, 18-22 October, 1999.
244. Lee, Y., G. Kudva, and T. Litzinger, An Apparatus for Measurement of Pressure-driven Combustion Response, accepted for *Measurement Science and Technology*, 1999.
245. Tang, C.-J., Y. Lee, G. Kudva and T. Litzinger, Self-Oscillatory Combustion of HMX during CO_2 Laser-assisted Combustion, *Journal of Propulsion and Power,* Vol. 15, No.2, 296-303 (1999).
246. Litzinger, T.A. "Gas-phase Structure of Nitramine/Azide Propellants," Gordon Research Conference on Energetic Materials, Tilton, NH, July 5, 2000.

SIGMAN & PRICE

247. Sigman, R.K., Price, E.W., Chakravarthy, S.R., and Zachary, E.K., "Subignition Heating Tests for Flake and Powdered Aluminum," *33rd JANNAF CS/PSHS/APS Joint Meeting*, CPIA Pub. 653, Vol. 2, pp 459–470, Monterey, CA, November 1996.
248. Chakravarthy, S.R., Price, E.W., and Sigman, R.K., "Studies of Quenched Biplateau Propellant Burning Surfaces," MURI Meeting, Seattle, WA, July 9, 1997 (unpublished).
249. Sigman, R.K., Zachary, E.K., Chakravarthy, S.R., Freeman, J.F., and Price, E.W., "Preliminary Characterization of the Combustion Behavior of ALEX™ in Solid Propellants", Proceedings of the *34th JANNAF Combustion Meeting*, CPIA Pub. 662, Vol. IV, pp. 209–223, West Palm Beach, FL., October 1997.
250. Price, E.W., Chakravarthy, S.R., Freeman, J.M., and Sigman, R.K., "Surface Features of BiPlateau AP Composite Propellants," Proceedings of the *34th JANNAF Combustion Meeting*, CPIA Pub. 662, Vol. IV, pp. 45–72, West Palm Beach, FL., October 1997.
251. Price, E.W. "Surface Accumulation of Aluminum on MURI Thiokol and CSD Propellants'" Presented at MURI Workshop, Cleveland, OH, July 15, 1998 (unpublished).
252. Price, E.W., "Combustion of MURI Propellants," Presented at the MURI Workshop, Cleveland, OH, July 1998 (unpublished).
253. Freeman, J.M., Price, E.W., and Sigman, R.K., "Effect of Matrix Variables on Bimodal Propellant Combustion," Proceedings of the *35th JANNAF Combustion Meeting,* Tucson, AZ, Dec. 1998.

254. Freeman, J.M., Price, E.W., Chakravarthy, S.R., and Sigman, R.K., "Contribution of Monomodal AP/HC Propellants to Bimodal Plateau-Burning Propellants, AIAA Paper # 98-3388, *34th AIAA/ASME/SAE/ASEE Joint Propulsion Conference and Exhibit*, July 13-15, 1998.
255. Price, E.W., "Burning Surface Features of Four Bimodal AP Plateau Propellants (as inferred from dp/dt quench samples for four pressures), presented at an ONR/MURI Workshop in Reno, NV, Jan. 1999 (unpublished).
256. Price, E.W., Freeman, J.M., Jeenu, R., Chakravarthy, S.R., Sigman, R.K., and Seitzman, J.M., "Plateau Burning of Ammonium Perchlorate Propellants," AIAA Paper # 99-2364, *35th AIAA/ASME/SAE/ASEE Joint Propulsion Conference and Exhibit*, June 20-24, 1999.
257. Seitzman, J.M., Price, E.W., Freeman, J.M., Jeenu, R , and Sigman, R.K., "Quenched Surface Studies of Plateau Burning Propellants," ," Proceedings of the *35th JANNAF Combustion Meeting,* Tucson, AZ, Dec. 1998.
258. Sigman, R.K., Lillard, R.P., Price, E.W., Seitzman, J.M., and Dokhan, A., "Size Distribution of Residual Oxide Droplets from MURI Propellants," Proceedings of the *36th JANNAF Combustion Subcommittee Meeting*, CPIA Pub. 691, Volume III, pp. 227-248, Cocoa Beach, FL, Oct. 1999.
259. Price, E.W., and Sigman, R.K., "Combustion of Aluminized Solid Propellants," Proceedings of the *36th JANNAF Combustion Subcommittee Meeting*, CPIA Pub. 691, Volume I, pp. 227-248, Cocoa Beach, FL, October 1999.
260. Sigman, R.K., Jeenu, R., and Price, E.W., "A Small-Scale Solid Propellant Mixer and Vacuum Degasser", Proceedings of the *36th JANNAF Combustion Subcommittee*, CPIA Pub. 691, Volume I, pp. 189-194, Cocoa Beach, FL, October 1999.
261. Sigman, R.K., and E.W. Price, "Behavior of Metals in Combustion Instability", Annual MURI Review, Cocoa Beach, FL Oct. 1999 (unpublished).
262. Price, E.W. and Sigman, R.K., "Combustion of Aluminized Solid Propellants", Chapter 219 in *Solid Propellant Chemistry, Combustion, and Motor Interior Ballistics,* editors: Yang, V., Brill, T. B., and Ren, Wu-Zhen, 2000 AIAA Progress in Aeronautics and Astronautics Series, Vol. 185, pp. 663-687; accepted for publication in the *AIAA Journal of Propulsion and Power*, Jan/Feb. 2000.
263. Sigman, R.K., Dokhan, A., Price, E.W., Lillard, R.P., and Seitzman, J. M., "Size Distribution of Residual Oxide in Aluminized Propellants," Proceedings of the *37th JANNAF Combustion Subcommittee Meeting*, Monterey, CA, November, 2000.
264. Dokhan, A., Price, E. W., Sigman, R. K., and Seitzman, J. M., "The Effects of Al Particle Size on the Burning Rate and Residual Oxide in Aluminized Propellants", AIAA Paper 2001-3581, *37th AIAA/ASME/SAE/ASEE Joint Propulsion Conference and Exhibit*, Salt Lake City, UT, 8–11 July 2001.

YANG

265. Chu, W.W. and V. Yang, "Dynamic Responses of Diffusion Flames to Acoustic Oscillations in a Simulated Solid Rocket Motor," AIAA Paper 96-0883, presented at 34th Aerospace Sciences Meeting, January 1996.
266. Yang, V., Modeling of Combustion Instabilities in Solid Propellant Rocket Motors, SIAM Mini-Symposium, 6th International Conference on Numerical Combustion, Analyses and Control of Combustion Instabilities, March 1996.
267. Yang, V., "Interactions Between Unsteady Flows and Combustion of Energetic Materials," 1996 Gordon Conference on Energetic Materials, New Hampton, NH, June 1996.
268. Roh, T.S. and Yang, V., Numerical Analysis of Combustion Instabilities of Homogeneous Propellants in Axisymmetric Rocket Motors, *AIAA* Paper 96-2623, *32nd AIAA/ASME/SAE/ASEE Joint Propulsion Conference*, July 1996.
269. Wicker, J.M., W.D. Greene, S.I. Kim, and V. Yang, "Triggering of Longitudinal Combustion Instabilities in Rocket Motors: Nonlinear Combustion Response," Journal of Propulsion and Power, Vol. 12, pp. 1148-1158, 1996.
270. Liau, Y.C. and V. Yang, "An Improved Model of Laser-Induced Ignition of RDX Monopropellants," Proceedings of the 33rd JANNAF Combustion Meeting, November 1996.
271. Chu, W.W. and V. Yang, "Combustion of AP/HTPB Composite Propellant in a Rocket Motor Flow Environment," Proceedings of the 33rd JANNAF Combustion Meeting, November 1996.
272. Liau, Y.C. and V. Yang, "On the Existence of Dark-Zone Temperature Plateau in RDX Monopropellant Flame," Proceedings of the 33rd JANNAF Combustion Meeting, November 1996.

273. Cai, W.D. and Yang, V., Particle Dynamics in a Simulated Rocket Motor with Acoustic Oscillations, 33rd JANNAF Combustion Meeting, November 1996.
274. Chu, W.W. and V. Yang, "Oscillatory Combustion of AP-Based Composite Propellant in a Rocket Motor Flow Environment," AIAA Paper 96-2885, presented at 32nd AIAA/ASME/SAE/ASEE Joint Propulsion Conference, July 1996.
275. Liau, Y.C. and V. Yang, "On the Existence of Dark-Zone Temperature Plateau in RDX Monopropellant Flame," AIAA Paper 97-0589, presented at 35th AIAA Aerospace Sciences Meeting, January 1997.
276. Cai, W. and V. Yang, "Two-Phase Turbulent Flow Interactions in a Simulated Rocket Motor with Acoustic Waves," Proceedings of the 34th JANNAF Combustion Meeting, October 1997.
277. Liau, Y.C., S.T. Thynell, and V. Yang, "Analysis of RDX/GAP Propellant Combustion with Detailed Chemistry," Proceedings of the 34th JANNAF Combustion Meeting, October 1997.
278. Apte, S. and V. Yang, "Numerical Simulation of Turbulent Flowfields in Solid-Propellant Rocket Motors," Proceedings of the 34th JANNAF Combustion Meeting, October 1997.
279. Yang, V. and S.T. Thynell, "Recent Advances in Modeling of RDX Propellant Ignition and Combustion," *U.S. Army Workshop on Solid-Propellant Ignition and Combustion Modeling*, M.S. Miller, R.W. Shaw, and D.M. Mann (eds.), Army Research Laboratory ARL-TR-1411, 1997, pp. 34-49.
280. Cai, W. and V. Yang, "Two-Phase Flow Interactions in a Rocket Motor," AIAA Paper 98-0161, presented at the 36th Aerospace Sciences Meeting, January 1998.
281. Yang, V., "Combustion and Ignition of Nitramine/Azide-Polymer Propellants," presented at the US-France DEA Meeting on Internal Ballistics and Combustion Instability of Solid Propellant Rocket Motors, Paris, France, June 1998.
282. Yang, V., "Recent Advances in Numerical Analysis of Solid-Propellant Rocket Motor Internal Flows," presented at the US-France DEA Meeting on Internal Ballistics and Combustion Instability of Solid Propellant Rocket Motors, Paris, France, June 1998.
283. Roh, T.S., S. Apte, and V. Yang, "Transient Combustion Response of Homogeneous Solid Propellant to Acoustic Oscillation in a Rocket Motor," Proceedings of 27th Symposium (International) on Combustion, The Combustion Institute, August 1998, pp. 2335-2341.
284. Apte, S. and V. Yang, "Effects of Acoustic Oscillations on Turbulent Flowfield in a Simulated Rocket Motor," Proceedings of 35th JANNAF Combustion Meeting, December 1998.
285. Liau, Y.C., V. Yang, M.C. Lin, and J. Park, "Analysis of Ammonium Dinitramide (ADN) Combustion with Detailed Chemistry," Proceedings of 35th JANNAF Combustion Meeting, December 1998.
286. Liau, Y.C., V. Yang, and S.T. Thynell, "Analysis of RDX/GAP Pseudo-Propellant Combustion with Detailed Chemistry," Proceedings of 35th JANNAF Combustion Meeting, December 1998.
287. Cai, W. and V. Yang, "Combustion of AP/HTPB Composite Propellant in a Turbulent Flow with Acoustic Oscillations," Proceedings of 35th JANNAF Combustion Meeting, December 1998.
288. Apte, S. and V. Yang, "Effects of Acoustic Oscillations on Turbulent Flowfield in a Porous Chamber with Surface Transpiration," AIAA Paper 98-3219, presented at the 34th AIAA/ASME/SAE/ASEE Joint Propulsion Conference, July 1998.
289. Liau, Y.C. and V. Yang, "An Improved Model of Ammonium Dinitramide (ADN) Combustion with Detailed Chemistry," Proceedings of 36th JANNAF Combustion Meeting, October 1999.
290. Yang, R. and V. Yang, "Thermal Decomposition and Combustion of Ammonium Dinitramide: A Review," Proceedings of 36th JANNAF Combustion Meeting, October 1999.
291. Apte, S. and V. Yang, "Combustion Dynamics of Double-Base Homogeneous Propellant in a Solid Rocket Motor," Proceedings of 36th JANNAF Combustion Meeting, October 1999.
292. Cai, W. and V. Yang, "Flame Structure of AP/HTPB Composite Propellant and its Response to an Acoustic Oscillation," Proceedings of 36th JANNAF Combustion Meeting, October 1999.
293. Liau, Y.C. and V. Yang, "Modeling of RDX/GAP Propellant Combustion with Detailed Chemical Kinetics," Proceedings of 36th JANNAF Combustion Meeting, October 1999.
294. Yang, V, "Effect of Turbulence on Acoustic Response of Homogeneous Solid Propellant Combustion in a Rocket Motor," to appear in Journal of Propulsion and Power, November 1999.
295. Apte, S., and Yang, V., "Combustion Dynamics of Double-Base Homogeneous Propellant in a Solid Rocket Motor," *Proceedings of the 36th JANNAF Combustion Meeting*, October 1999.
296. Apte, S., and Yang, V., "Combustion Dynamics of Double-Base Homogeneous Propellant in a Solid Rocket Motor," presented at 36th JANNAF Combustion Meeting, October 1999.
297. Apte, S., and Yang, V., "Large Eddy Simulation of Internal Flowfield in Porous Chamber with Surface Mass Injection," AIAA Paper 200-0709, 38th Aerospace Sciences Meeting, January 2000.

298. Apte, S., and Yang, V., "Large Eddy Simulation of Internal Flowfield in Porous Chamber with Surface Mass Injection," presented *at* 38th Aerospace Sciences Meeting, January 2000.
299. Apte, S., and Yang, V., "Turbulent Combustion Dynamics of Double-Base Homogeneous Propellant in a Solid Rocket Motor," *Proceedings of the 11th Annual Symposium on Combustion*, Propulsion Engineering Research Center, Pennsylvania State University, November 1999.
300. Apte, S., and Yang, V., "Turbulent Combustion Dynamics of Double-Base Homogeneous Propellant in a Solid Rocket Motor," presented at 11th Annual Symposium on Combustion, Propulsion Engineering Research Center, Pennsylvania State University, November 1999.
301. Cai, W.D., and Yang, V., "A Model of AP/HTPB Composite Propellant Combustion," AIAA Paper 2000-0311, 38th Aerospace Sciences Meeting, January 2000.
302. Cai, W.D., and Yang, V., "A Model of AP/HTPB Composite Propellant Combustion," presented at 38th Aerospace Sciences Meeting, January 2000.
303. Cai, W.D., and Yang, V., "Flame Dynamics of AP/HTPB Composite Propellant and its Response to Acoustic Oscillations," *Proceedings of the 36th JANNAF Combustion Meeting*, October 1999.
304. Cai, W.D., and Yang, V., "Flame Dynamics of AP/HTPB Composite Propellant and its Response to Acoustic Oscillations," presented at 36th JANNAF Combustion Meeting, October 1999.
305. Liau, Y.C., Yang, V., and Thynell, S.T., "Modeling of RDX/GAP Propellant Combustion with Detailed Chemical Kinetics," *Proceedings of the 36th JANNAF Combustion Meeting*, October 1999.
306. Liau, Y.C., Yang, V., and Thynell, S.T., "Modeling of RDX/GAP Propellant Combustion with Detailed Chemical Kinetics," presented at 36th JANNAF Combustion Meeting, October 1999.
307. Liau, Y.C., Yang, V., Lin, M.C., Park, J., "An Improved Model of Ammonium Dinitramide (ADN) Combustion with Detailed Chemistry," *Proceedings of the 36th JANNAF Combustion Meeting*, October 1999.
308. Liau, Y.C., Yang, V., Lin, M.C., Park, J., "An Improved Model of Ammonium Dinitramide (ADN) Combustion with Detailed Chemistry," presented at 36th JANNAF Combustion Meeting, October 1999.
309. Yang, R.J., and Yang, V., "Thermal Decomposition and Combustion of Ammonium Dinitramide: A Review," *Proceedings of the 36th JANNAF Combustion Meeting*, October 1999.
310. Yang, R.J., and Yang, V., "Thermal Decomposition and Combustion of Ammonium Dinitramide: A Review," presented at 36th JANNAF Combustion Meeting, October 1999.
311. Yang, V., "Combustion Dynamics of Solid Rockets," presented at *36th AIAA/ASME/SAE/ASEE Joint Propulsion Conference & Exhibit*, AIAA Paper No. 2000-3177, July 2000.

The following is a list of students whose thesis works were partly or wholly supported by MURI funding.

BYU — Beckstead

Qibo Jing, "1-D Modeling of Solid Propellant Combustion with Detailed Kinetics (From Steady-State to Unsteady-State)", Ph.D. Thesis, Brigham Young University, Provo, Utah, 2001

Brian Newbold, "A Quantitative Study of Acoustic Growth Rates in a Characterized Rijke Burner With Particle Combustion", Ph.D. Thesis, Brigham Young University, Provo, Utah, 2000

Bill Erikson, "Modeling the Unsteady Combustion of Solid Propellants with Detailed Chemistry", Ph.D. Thesis, Brigham Young University, Provo, Utah, 1999.

Jeff Widener, "Computer Modeling of Aluminum Particle Heat-Up and Combustion Under Rocket Motor Conditions", M.S. Thesis, Brigham Young University, Provo, Utah, 1998

Mike Jeppson, "A Kinetic Model for the Premixed Combustion of a Fine AP/HTPB Composite Propellant", M.S. Thesis, Brigham Young University, Provo, Utah, 1998

Jeff Davidson, "Combustion Modeling of RDX, HMX and GAP with Detailed Kinetics", Ph.D. Thesis, Brigham Young University, Provo, Utah, 1997

Caltech — Culick

Burnley, Victor, "Nonlinear Combustion Instabilities and Stochastic Sources," Ph.D. Thesis, California Institute of Technology, Pasadena, CA, January 1996.

Seywert, Claude, "Combustion Instabilities: Issues in Modeling and Control," Ph.D. Thesis, California Institute of Technology, Pasadena, CA, February 2001.

Isella, Giorgio, "Modeling and Simulation of Combustion Chamber and Propellant Dynamics and Issues in Active Control of Combustion Instabilities," Ph.D. Thesis, California Institute of Technology, Pasadena, CA, February 2001.

Malhotra, Sanjeev, "On Combustion Instability," Ph.D. Thesis, California Institute of Technology, Pasadena, CA, 2002.

UIUC — Beddini
Lee, Yongho, "Instability of Oscillatory Flow in Ducts and Application to Solid Propellant Rocket Aeroacoustics," Ph. D. Thesis, University of Illinois at Urbana-Champaign, Urbana, IL, May 2002.

UDEL — Brill
Budenz, Brandon T., "Oxidizer-Binder Interactions in the Ammonium Perchlorate Hydroxyl-Terminated Polybutadiene Pseudopropellant," Master of Science Thesis, University of Delaware, Newark, DE, Spring 1999.

Roos , Brian D., "Pyrolysis Studies of Energetic Materials by T-Jump/Vibrational Spectroscopy," Ph.D. Thesis, University of Delaware, Newark, DE, Summer 2002.

UTSI — Flandro
Garza, D. M., "Investigation of the Composite Amplitude in Solid Rocket Motor Combustion Chamber Pressure Oscillations," Master of Science Thesis, University of Tennessee, UTSI, Knoxville, TN, August 1994.

Flanagan, S. N., "A New Method for the Prediction of Combustion Instability," Doctoral Dissertation, University of Tennessee, UTSI, Knoxville, TN, December 1997.

UAH — Frederick
Chiyyarath, Kairali, Ballistic Characteristics of Bi-Plateau Solid Propellants, Master of Science in Engineering, University of Alabama, Huntsville, Defense October 27, 1998, Chairman: Robert A. Frederick, Jr.

Dauch, Frederic, Uncertainty Analysis of the Ultrasonic Technique Applied to Solid Propellant Burning Rate," Master of Science in Engineering, March 22, 1999, Advisor: M.D. Moser.

Edmund Rochford, Temperature Sensitivity Measurements of Solid Rocket Propellants, Defense: February 18, 1999, Chairman: Marlow Moser.

Rasmussen, B., An Intrinsic Heterogeneous Model of Composite Solid Propellant Combustion, Defense, December 17, 1998, Chairman: Robert A. Frederick, Jr.

PSU — Litzinger
Lee, YoungJoo, A Study of the Chemical and Physical Processes Governing the CO_2 Laser-induced Pyrolysis and Combustion of RDX, BAMO, and RDX/BAMO Pseudo-propellants, Ph.D. Thesis, The Pennsylvania State University, University Park, PA, 1996.

Tang, Ching-Jen, A Study of the Chemical Structure of HMX Propellants and Combustion Response to Oscillatory Radiant Heat Flux, Ph.D. Thesis, The Pennsylvania State University, University Park, PA, 1997.

Kudva, Gautam K., A Study of the Laser and Pressure-driven Response Measurements of Propellants at Low Pressure, Ph.D. Thesis, The Pennsylvania State University, University Park, PA, 2000.

PSU — Yang
Y. C. Liau, "A Comprehensive Analysis of RDX Propellant Combustion and Ignition with Two-Phase Subsurface Reactions," May 1997.

W. W. Chu, “Dynamic Responses of Combustion to Acoustic Waves in Porous Chambers with Transpiration,” December 1999.

S. Apte, “Unsteady Flow Evolution and Combustion Dynamics of Homogeneous Solid Propellant in a Rocket Motor,” December 2000.

E. S. Kim, “Modeling and Simulation of Laser-Induced Ignition of RDX Monopropellant and Steady-State Combustion of HMX/GAP Pseudo Propellant,” December 2000.

W. D. Cai, “Two-Phase Flow Interactions and Combustion of AP/HTPB Composite Propellants in Rocket Motors with Acoustic Oscillations,” May 2001.

GIT — Price/Sigman
Elizabeth K. Zachary, M.S. in A.E., 1998.

Robert Lemoyne (special graduate student – no degree).

Allan Dokhan, “Collection of Al Residue from UTP-3001 Propellant,” MS in AE, Georgia Institute of Technology, Atlanta, GA, December, 2000.

Emory — Lin
No students funded